Advances in Silicon Science 4
Series Editor: J. Matisons

Michael J. Owen
Petar R. Dvornic *Editors*

Silicone Surface Science

Springer

Advances in Silicon Science

ADVANCES IN SILICON SCIENCE

VOLUME 4

Series Editor:

JANIS MATISONS
Gelest Inc., 11 East Steel Road, Morrisville, PA 19067, USA

Advances in Silicon Science is a book series which presents reviews of the present and future trends in silicon science and will benefit those in chemistry, physics, biomedical engineering, and materials science. It is aimed at all scientists at universities and in industry who wish to keep abreast of advances in the topics covered.

Series Editor

Prof. Janis Matisons
Senior R & D Manager
Gelest Inc
11 East Steel Road
Morrisville
Pennsylvania 19067
USA
jmatisons@gelest.com

Volume 4

Silicone Surface Science

Volume Editors

Michael J. Owen
Petar R. Dvornic
Michigan Molecular Institute
Midland, MI
USA

For further volumes:
www.springer.com/series/7926

Michael J. Owen • Petar R. Dvornic
Editors

Silicone Surface Science

Springer

Editors
Michael J. Owen
Michigan Molecular Institute
Midland, MI
USA

Petar R. Dvornic
Michigan Molecular Institute
Midland, MI
USA

ISSN 1875-3108
ISSN 1875-3086 (electronic)
Advances in Silicon Science
ISBN 978-94-007-3875-1
ISBN 978-94-007-3876-8 (eBook)
DOI 10.1007/978-94-007-3876-8
Springer Dordrecht Heidelberg New York London

Library of Congress Control Number: 2012939196

Printed on acid-free paper

Springer is part of Springer Science+Business Media (www.springer.com)

Preface

God made the bulk; surfaces were invented by the devil
Wolfgang Pauli[1]

It is somewhat surprising, in our opinion, that this book, to the best of our knowledge, is the first to be devoted to the surface properties and behavior of silicone polymers. The situation is all the more perplexing when one considers that surface-related applications have consistently accounted for the major part of the commercial success of silicones since the establishment of this industry in the early 1940s.

The importance of surfaces and interfacial phenomena cannot be overemphasized. When any two materials are brought together it is their surfaces that initially matter and their interfacial interactions that need to be studied and understood first. Therefore, in order to contribute to this, in this book we attempt to present a broad overview of the state-of-the-art of silicone surface science by a group of widely recognized experts in their fields summarizing both the historical development and the current progress in each selected area. With almost 70 years of scientific and technological interest in silicones we can hardly claim to be rigorously comprehensive, but we are sure that the most exciting developments in this field today are covered in this volume.

Much of the content of this book deals with polydimethylsiloxane (PDMS) since it has been the mainstay of the silicone industry from its very beginnings to the present day. Furthermore, looking into the future, while anticipating continued interest in and development of other polymers derived from organosilicon entities, there is no reason not to believe that the science and applications of PDMS and related organosiloxane polymers will continue to grow and play as important a role as they have in the past.

As is common in the field of silicon-containing polymers, we use the term silicone to describe polymers whose backbone is siloxane, i.e. alternating arrangement of silicon and oxygen atoms, with pendent organic groups attached to that backbone. Consequently, polyhedral oligomeric silsesquioxanes (POSS), which certainly meet

[1] Quoted in "*Growth, Dissolution and Pattern Formation in Geosystems*" (1999) by Bjorn Jamtveit and Paul Meakin, p. 291.

the "alternating siloxane bonds" requirement, are not usually considered "silicones", because of their insufficient molecular weights and fundamentally different macroscopic properties. Nevertheless, we consider these oligomers to be a proper subject for inclusion in this volume because of their critical importance to silicone surface science as explained in detail in two chapters dealing with POSS derivatives.

What might appear to some to be a somewhat capricious chapter order is based on our attempt to marry two seemingly "incompatible" concepts: (i) a progressive shift from fundamentals to more applied topics, and (ii) a development from "pure" PDMS to other important, surface-active silicones such as fluorosilicones and modified materials such as surfactants and coupling agents. The book opens with a general introduction to silicone surfaces with an emphasis on the surface properties of PDMS. Following this, in Chap. 2 Ahn and Dhinojwala describe the sum frequency generation vibrational spectroscopy of silicone surfaces and interfaces, a relatively recently introduced technique that has provided considerable new insight into surface structure and most notably to buried interfaces as well. Genzer and co-workers have made great strides in creating different functionalities on silicone surfaces and their contributions are reviewed in Chap. 3. Superhydrophobic surfaces have featured strongly in the last decade, and McCarthy et al. review their silane/siloxane studies of this topic in Chap. 4. Chapters 5 and 6 deal with fluorine-containing silicones where Ganachaud and Ameduri and their colleagues review structure/property relationships in fluorosilicones and Tuteja and Mabry contribute a chapter on fluoro-POSS materials which are highly relevant to the earlier topic of superhydrophobicity, respectively. Our strong interest in fluorosilicones derives from their potential to produce significantly lower surface energies than conventional PDMS surfaces.

Langmuir trough investigations of silicones have been of interest since surface studies of silicones began. In Chap. 7 Esker and Yu provide a summary of this topic with an update of recent works that offers another facet of the growing importance of POSS compounds to organosilicon surface science today. A topic of high-interest to current siloxane science with considerable surface-related implications is the interaction of proteins and silicon-based materials which is the subject of Chap. 8 by Clarson and co-workers. This is followed by a review of silicone surfactant fundamentals and applications by Snow and Petroff in Chap. 9, while Matisons' Chap. 10 deals with the adsorption of polymeric siloxanes on glass surfaces and their coupling behavior as well as with more conventional silane coupling agents. Surface treatments such as plasma and corona have been widely exploited in silicone surface modification. These are summarized in Chap. 11 by Hillborg and Gedde (see also Chap. 3 which deals with aspects of this topic).

Analytical techniques are self-evidently central to understanding of silicone surface behavior. A review of these studies with emphasis on X-ray photoelectron spectroscopy (XPS), secondary ion mass spectrometry (SIMS), scanning electron microscopy (SEM) and scanning probe microscopy (SPM) is provided by Leadley, O'Hare and McMillan in Chap. 12. Finally, we close with an outline of some important surface applications of silicones relating to both the science and technology of silicone surfaces. Some of these applications are also included in several of the earlier chapters, underlining a dominant theme of this book, the relationship between

the structure and surface properties of silicones and their utilization in various everyday as well as more sophisticated applications.

A variety of authors contributed different perspectives to this work, including academic and industrial specialists from Europe and North America. We sincerely thank all of them for their impressive contributions and their patience and perseverance throughout the process of bringing this book to fruition. We are particularly grateful to our publishing editor, Dr. Sonia Ojo and her Springer colleagues for their expert help during the preparation of the manuscript and to Donatas Akmanavičius of VTeX UAB in the realization of this finished work.

Midland, MI, USA

Michael J. Owen
Petar R. Dvornic

Contents

Contributors

Dongchan Ahn Dow Corning Corporation, Midland, MI, USA

Bruno Ameduri Institut Charles Gerhardt, Equipe "Ingénierie et Architectures Macromoléculaires", UMR5253 CNRS, ENSCM, Montpellier Cedex, France

Stephen J. Clarson Department of Chemical and Materials Engineering and the Polymer Research Center, University of Cincinnati, Cincinnati, OH, USA

Julie A. Crowe-Willoughby Department of Chemical & Biomolecular Engineering, North Carolina State University, Raleigh, NC, USA; College of Textiles, North Carolina State University, Raleigh, NC, USA

Ali Dhinojwala Department of Polymer Science, The University of Akron, Akron, OH, USA

Petar R. Dvornic Michigan Molecular Institute, Midland, MI, USA

Kirill Efimenko Department of Chemical & Biomolecular Engineering, North Carolina State University, Raleigh, NC, USA

Alan R. Esker Department of Chemistry (0212), Virginia Tech, Blacksburg, VA, USA

Alexander Y. Fadeev Polymer Science and Engineering Department, University of Massachusetts, Amherst, MA, USA

Kathy Gallardo Department of Chemical and Materials Engineering and the Polymer Research Center, University of Cincinnati, Cincinnati, OH, USA

François Ganachaud Institut Charles Gerhardt, Equipe "Ingénierie et Architectures Macromoléculaires", UMR5253 CNRS, ENSCM, Montpellier Cedex, France; IMP@INSA, UMR5223 CNRS, INSA-Lyon, Villeurbanne Cedex, France

Lichao Gao Polymer Science and Engineering Department, University of Massachusetts, Amherst, MA, USA

Ulf W. Gedde Fibre and Polymer Technology, School of Chemical Science and Engineering, Royal Institute of Technology, Stockholm, Sweden

Jan Genzer Department of Chemical & Biomolecular Engineering, North Carolina State University, Raleigh, NC, USA

Larry Grazulis University of Dayton Research Institute, Dayton, OH, USA

Siska Hamdani-Devarennes Institut Charles Gerhardt, Equipe "Ingénierie et Architectures Macromoléculaires", UMR5253 CNRS, ENSCM, Montpellier Cedex, France; Ecole des Mines d'Alès, CMGD, Alès, France

Henrik Hillborg Fibre and Polymer Technology, School of Chemical Science and Engineering, Royal Institute of Technology, Stockholm, Sweden; Corporate Research, ABB AB, Västerås, Sweden

Joseph W. Krumpfer Polymer Science and Engineering Department, University of Massachusetts, Amherst, MA, USA

Stuart Leadley Dow Corning Europe, Seneffe, Belgium

Claire Longuet Ecole des Mines d'Alès, CMGD, Alès, France

Joseph M. Mabry Space and Missile Propulsion Division, Air Force Research Laboratory, Edwards AFB, CA, USA

Janis G. Matisons Gelest Inc., Morrisville, PA, USA

Thomas J. McCarthy Polymer Science and Engineering Department, University of Massachusetts, Amherst, MA, USA

Christopher McMillan Dow Corning Corporation, Midland, MI, USA

Lesley-Ann O'Hare Dow Corning Corporation, Midland, MI, USA

Michael J. Owen Michigan Molecular Institute, Midland, MI, USA

Ali E. Őzçam Department of Chemical & Biomolecular Engineering, North Carolina State University, Raleigh, NC, USA

Cedric Pasquet Institut Charles Gerhardt, Equipe "Ingénierie et Architectures Macromoléculaires", UMR5253 CNRS, ENSCM, Montpellier Cedex, France; IMP@INSA, UMR5223 CNRS, INSA-Lyon, Villeurbanne Cedex, France

Siddharth V. Patwardhan Department of Chemical and Process Engineering, University of Strathclyde, Glasgow, UK

Lenin J. Petroff Dow Corning Corporation, Midland, MI, USA

Steven A. Snow Dow Corning Corporation, Midland, MI, USA

Anish Tuteja Department of Materials Science and Engineering, University of Michigan, Ann Arbor, MI, USA

Hyuk Yu Department of Chemistry, University of Wisconsin, Madison, WI, USA

Chapter 1
General Introduction to Silicone Surfaces

Michael J. Owen and Petar R. Dvornic

1.1 Introduction

Surface properties of silicones have been exploited from the start of the silicone industry and continue to be dominant today. According to Warrick [1] one of the most useful early applications was the treatment of glass fibers using hydrolyzed silanes to create a water-repellent product. Other early silicone products include hydrophobic greases to seal aircraft ignition systems and antifoam agents for petroleum oils. We conservatively estimate that 70 % of the current market for silicones result from their surface properties and behavior. For more information on silicone applications see Chap. 13.

The term "silicone" is not a precise one. We use it to describe polymeric materials based on a silicon-oxygen backbone with organic groups attached directly to silicon atoms. These organic groups can be inert or reactive so our definition encompasses not only polydimethylsiloxane $-[Si(CH_3)_2O]_n-$ (PDMS), which continues to hold the dominant position in the silicone industry, but also other polysiloxanes such as fluorosilicones and hydrolyzed silane coupling agents. This definition does not include, nor does this volume address except in passing, other organosilicon polymers such as polycarbosilanes, polysilanes and polysilazanes. With its inorganic backbone and organic pendant groups, PDMS and other silicone polymers belong to the class of "semi-inorganic" [2] or "organo-inorganic" polymers. Superficially, the surface properties of PDMS might be expected to be an average of these two dissimilar constituents but this is not the case. For example, the surface energy and hydrophobicity of PDMS are much more akin to hydrocarbons such as paraffin wax than they are to silica. The explanation lies in two general rules, namely, the second

M.J. Owen (✉) · P.R. Dvornic
Michigan Molecular Institute, 1910 W. St. Andrews Rd., Midland, MI 48640, USA
e-mail: michaelowen01@chartermi.net

P.R. Dvornic (✉)
e-mail: dvornic@mmi.org

M.J. Owen, P.R. Dvornic (eds.), *Silicone Surface Science*, Advances in Silicon Science 4,
DOI 10.1007/978-94-007-3876-8_1,

law of thermodynamics and Langmuir's principle of the independence of surface action [3].

The second law of thermodynamics can be expressed in numerous ways. One common form is that systems will change spontaneously in the direction of minimum total free energy. Hence, for a polymer like PDMS containing both polar and non-polar entities it is axiomatic that the low-surface-energy methyl groups will accumulate in the surface and dominate surface behavior. Langmuir's principle takes this expectation a step further. It postulates that one can conceive of separate surface energies for each of the different parts of complex molecules and that the surface energy of a material made of such molecules is determined by the composition and orientation of the outermost groups independent of the underlying components. This is the principle on which Zisman [4] based his quantification of the surface energy of hydrocarbon and fluorocarbon groups showing that their contributions to the total surface energy of the material decrease in order: $–CH_2– > CH_3– > –CF_2– > –CF_3$. The principle is not absolute, but is a very good first approximation. Most measurements of solid surface energy by contact angle determination (discussed later in this chapter) attribute only a small polar component that would arise from the Si–O chain backbone to the surface energy of PDMS. Another example of particular relevance to fluorosilicones is the somewhat surprising longer range effect exhibited by the uncompensated dipole that arises at the junction of fluorocarbon and hydrocarbon entities.

Before considering surface properties of silicones in general and PDMS in particular, it is pertinent to consider the fundamental characteristics of PDMS that account for its pre-eminent position in the ranks of organo-inorganic polymers. These include:

- Low intermolecular forces between pendant methyl groups [$p^* = 341$ J cm^{-3}]
- Compact size of the methyl group [van der Waals radius = 200 pm]
- High siloxane backbone flexibility [$T_g = 150$ K]
- High siloxane bond energy [445 kJ mol^{-1}]
- Partial ionic nature of the siloxane bond [*ca* 40 % ionic]

Here p^* is the characteristic pressure obtained from the Shih and Flory equation of state [5] and it is a measure of intermolecular energy per unit volume, which has a reasonable correlation with surface energy, and T_g is the temperature of the glass transition. The first three of the above characteristics together explain much of the surface and bulk physical behavior of PDMS with the other two accounting for the chemical consequences of environmental exposure in use [6]. In principle, all applications of silicones can be directly linked to combinations of these five factors, an exercise that is the subject of Chap. 13. The use of "high" and "low" as descriptors in this list is in qualitative comparison to other organic polymers in general. For example, when considering the intermolecular forces between polymer chains or segments, the range is from strongly polar hydrophilic materials such as polyacrylamide to low-surface-energy aliphatic fluoropolymers. PDMS lies low on this scale in the region between hydrocarbons such as polypropylene and fluoropolymers such as polytetrafluoroethylene.

Table 1.1 Glass transition temperatures of selected polysiloxanes and other polymers

Polymer	T_g (K)
Polypentamethylcyclopentasiloxane (PD_5)	122 [7]
Polydiethylsiloxane	134 [8]
Polymethylhydrogensiloxane	135 [8]
Polymethylethylsiloxane	138 [8]
Co-poly(CF_2CF_2–O–CF_2O)	140 [9]
Polyethylene	148 [10]
Polydimethylsiloxane	150 [10]
Polydimethylsilmethylene	173 [10]
Polymethylnonafluorohexylsiloxane	198 [11]
Polyisobutylene	200 [10]
Polymethyltrifluoropropylsiloxane	203 [10]
Polyoxyhexafluoropropylene	207 [10]
Polydimethylphosphazene	227 [12]

A low T_g of a polymer segment reflects pronounced backbone chain flexibility (low energy barrier for rotation around the Si–O main chain bonds) although other factors, such as pendant group size also have an effect. PDMS benefits from both the compact size of the methyl groups (the smallest possible alkane substituent; only an atom such as hydrogen or fluorine is smaller) and the intrinsic flexibility of the siloxane backbone (the most flexible chain of atoms known to polymer science [13]). The architecture of the backbone, consisting of alternating small, unsubstituted oxygen atoms and larger, substituted silicon atoms also plays a part. Table 1.1 lists T_g values of selected polymers to put the PDMS value in perspective. Note that PD_5 is a polymer of D_5H, pentamethylcyclopentasiloxane reported by Kurian and co-workers [7] that consists of cyclopentasiloxane rings linked by siloxane linkages. Note also that the lowest reported fluoropolymer glass transition is for the fluoroether copoly(oxytetrafluoroethylene-oxydifluoromethylene), which has no pendant groups, only fluorine atoms.

The most important surface property of any polymer is its surface energy which arises directly and inevitably from the imbalance of intermolecular forces between the polymer molecules at any phase boundary. By surface energy we mean the surface free energy being the change in total surface free energy per unit change in surface area brought about by an expansion of the surface at constant temperature, pressure and number of moles of substance in the surface. In principle, these conditions can be met for a liquid polymer. The free energy per unit area is then numerically and dimensionally identical to the surface tension, expressed as a force per unit length in the surface. The SI unit for surface energy is $mJ\,m^{-2}$. Provided the viscosity is not too high, the liquid surface tension of a polymer can be directly measured, giving an unambiguous value if both the temperature of the measurement and the molecular weight of the sample are specified. The latter information is necessary as liquid surface tension of polymers is usually a function of molecular weight due

primarily to end-group effects. Surface tension values of liquids are usually quoted in $mN\,m^{-1}$, numerically equal to cgs dyne cm^{-1} units. For solid surfaces it is conventional to speak of surface energy (in $mJ\,m^{-2}$) rather than surface tensions. These two quantities are numerically equal. Both σ and γ are used as the symbols for surface tension and surface energy, but in this volume we choose the latter symbol.

For a solid polymer the situation is much more complex. The surface area cannot generally be changed at constant chemical potential to allow an equal number of moles to be present before and after expansion of a solid surface. Moreover, elastic forces complicate the issue and the surface state after extension can be far from equilibrium. Therefore, indirect approaches are usually resorted to for the determination of the surface energy of a solid. Historically, and still to a very great extent today, investigators resort to methods based on contact angle determinations most commonly using either a sessile drop or Wilhelmy plate configuration. In the sessile drop approach a liquid drop is simply placed upon a smooth, flat sample of the solid under investigation. In the Wilhelmy plate method a thin plate of the sample is partially immersed in a chosen liquid. A variety of liquids may be chosen to probe the surface and there is also a variety of semi-empirical equations available to convert the obtained contact angle data into surface energy values. The consequence of this is that the literature contains a variety of conflicting values for solid surface energy and the task of selecting a preferred value is challenging.

One way out of this dilemma is to resort to contact mechanics. Using methodology such as the Johnson, Kendall and Roberts (JKR) approach [14], one can obtain objective values of polymer surface energy. However, relatively few polymers have been characterized so far in this manner, but, fortunately, PDMS is among these, thanks primarily to the studies of Chaudhury and co-workers [15] and the fortuitous situation that its bulk properties are ideal for contact mechanics investigations. For all the above described reasons, in this chapter we first discuss the liquid surface tension of PDMS, then the contact angle of water on solid PDMS, followed by the determination of solid surface energy by contact angle and contact mechanics approaches. Langmuir trough studies are also briefly reviewed.

1.2 Liquid Surface Tension

Figure 1.1 [16] shows liquid surface tension (γ_{LV}) at 20 °C as a function of boiling point for low molecular weight linear PDMS and poly(oxyhexafluoropropylene) as well as *n*-alkanes and *n*-fluoroalkanes which can be viewed as oligomers of polyethylene (PE) and polytetrafluoroethylene (PTFE). At first glance these curves seem to parallel the familiar order, established half a century ago by Zisman and coworkers [4] for solids by contact angle study, where the CF_3– group has the lowest surface energy, followed by the –CF_2– group and the CH_3– group, with the –CH_2– group being the least surface active of these four entities. However, it appears that the PDMS and *n*-fluoroalkane curves might cross if higher liquid fluoroalkanes were available. There is also the impression that the oligomers with a flexibilizing oxygen linkage have a flatter slope than the alkanes and fluoroalkanes. A lower coefficient of property change with temperature is a familiar situation with PDMS, often at-

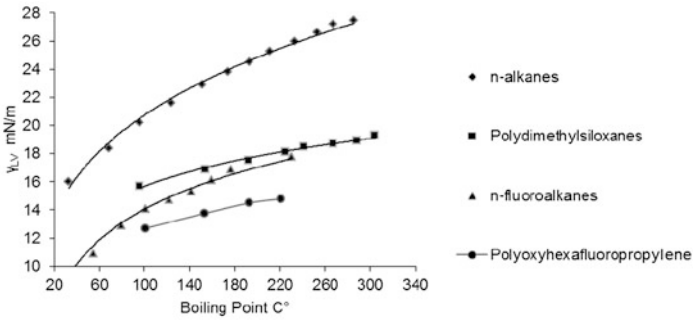

Fig. 1.1 Dependence of surface tension at 20 °C on boiling point for a variety of hydrocarbon- and fluorocarbon-containing compounds. Reprinted from Ref. [16] with kind permission of © The American Chemical Society (1980)

Table 1.2 Surface tensions and their temperature coefficients of selected liquids

Polymer	γ_∞ (mN m^{-1})	Temp. (°C)	$-\delta\gamma/\delta T$ (mN {m K}$^{-1}$)
Poly(oxyhexafluoropropylene)	18.4	25	0.059
n-fluoroalkanes (PTFE)	25.8	20	0.053
PDMS	21.3	20	0.048
PMTFPS	24.4	25	–
n-alkanes	36.9	20	0.060

tributed to its backbone flexibility but in this case possibly also a function of the varying end-groups of these four sets of oligomers.

The best way to remove complications of end-group, density and volatility effects is to extrapolate the data to infinite molecular weight. The LeGrand and Gaines equation [17] Eq. (1.1) offers a convenient way of doing this. Here γ_{LV} is again the surface tension of any given liquid polymer sample (LV indicating the value at the liquid (L)/vapor(V) interface) and γ_∞ is the extrapolated value at $1/M_n^{2/3} = 0$, where M_n is the number average molecular weight, and K is a constant. The extrapolation to zero reciprocal molecular weight is short, yielding convincing values shown in Table 1.2 together with the temperature (T) at which the measurements were made and the coefficient of surface tension change with temperature, $\delta\gamma/\delta T$.

$$\gamma_\infty = \gamma_{LV} - K/M_n^{2/3} \tag{1.1}$$

It can be seen from this table that γ_∞ for both the *n*-fluoroalkanes and polymethyltrifluoropropylsiloxane (PMTFPS) is higher than that of PDMS. For PMTFPS we can rationalize that the two CH_2 groups of higher intrinsic surface energy than CH_3 must more than outweigh the effect of the lower surface energy CF_3 group. The CF_3 group is insufficiently stable when directly attached to silicon for one to test this idea by dispensing with the ethylene bridge in PMTFPS and attempting to study $[Si(CH_3)(CF_3)O]_n$. The temperature coefficient values are not

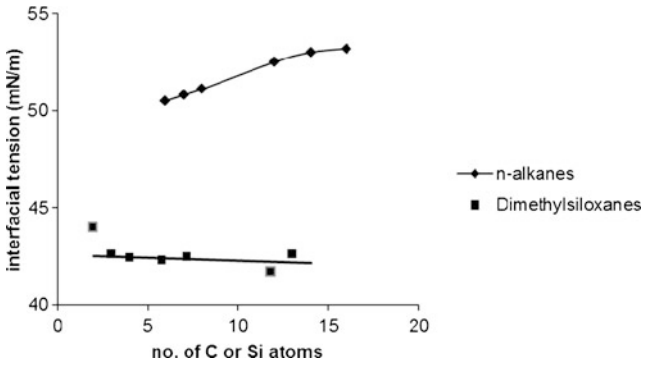

Fig. 1.2 Interfacial tensions of *n*-hydrocarbons and polydimethylsiloxane oligomers against water

at infinite molecular weight since insufficient data are available. Instead, the values chosen are for the highest molecular weight available. More details are given in the original citation [18]. Surface tensions of polymers vary linearly with temperature with $-\delta\gamma/\delta T$ values typically in the 0.05 to 0.08 range and the PDMS value being the lowest value reported. These values are somewhat lower than the temperature coefficients for non-polymeric liquids an effect that is attributed to conformational restrictions of long-chain molecules. Generally, increasing surface tension correlates weakly with increasing temperature coefficient, although this is not evident from the limited selection made in Table 1.2.

The interfacial tension between liquids can also be measured directly (see also Chap. 5, Appendix A.1). Water is usually the other phase of interest and Fig. 1.2 shows the interfacial tension between water and PDMS oligomers and *n*-alkanes [19]. Once again the lower slope of the silicone curve compared to the hydrocarbon one can be seen, but more noticeable is the distinct difference in values: the interfacial tensions for PDMS are much lower than those for the *n*-alkanes, around 42.6 mN/m except for hexamethyldisiloxane, which is higher: at 44 mN m^{-1}. These significantly lower values can be attributed to the interaction of water molecules with the oxygen atoms in the siloxane bonds, facilitated by the pronounced flexibility of the siloxane backbone chain.

The literature also contains reports of a number of studies of interfacial tension between two different polymers (γ_{12}). Table 1.3 gives examples where PDMS was one of the components, taken from Kuo's compilation [20]. It can be seen that the temperature coefficients for interfacial tension are much lower than for surface tension, which results from the smaller density difference between two polymers compared to the individual polymer densities. Generally, the more polar the polymer, the larger is the interfacial tension with PDMS although there is no numerical equality between the interfacial tension and the difference of the two surface tensions (Antonow's rule [21]).

Note that in this table, for purposes of comparison, values are quoted at room temperature. As most polymers other than PDMS are solid at this temperature (melting point of PDMS is between −40 and −35 °C) the data presented are extrapo-

Table 1.3 Interfacial tension at 20 °C between various polymers and PDMS

Polymer	γ_{12} (mN m^{-1})	$-\delta\gamma/\delta T$ (mN {m K}$^{-1}$)
Polypropylene	3.2	0.002
Poly(*t*-butyl methacrylate)	3.6	0.003
Polyisobutylene	3.9	0.016
Polybutadiene	4.2	0.009
Poly(*n*-butyl methacrylate)	4.2	0.004
Polyethylene	5.3	0.002
Polystyrene	6.1	*ca* 0
Polytetrahydrofuran	6.3	0.0004
Polyoxytetramethylene	6.4	0.001
Polychloroprene	7.1	0.005
Poly(vinyl acetate)	7.4	0.008
Polyoxyethylene	9.9	0.008

lations from higher temperature studies so although the temperature coefficient is small, the data are not as absolute as might be imagined. Interfacial tension should change discontinuously at the crystal/melt transition and continuously at the glass transition with discontinuous $\delta\gamma/\delta T$. Wu [22] has shown that extrapolation is usually adequate as semi-crystalline polymers generally have amorphous surfaces when cooled from the melt.

1.3 Water Contact Angle Studies

The contact angle θ of a liquid on a solid is the angle between the liquid and the solid at the three-phase (liquid, solid, vapor) point of contact measured through the liquid phase (see also Chap. 5, Appendix A.3). The advancing angle θ_a is that for a liquid contacting a previously unwetted surface whereas the receding angle θ_r relates to a liquid that has already wetted the surface in question. Figure 1.3 illustrates this situation. If the drop is held stationary and the sample and stage moved to the left as shown, it is clear that the left hand side of the drop is in contact with previously wetted sample surface whereas the right hand side of the drop contacts unwetted surface.

The difference between the advancing and receding angles is called the contact angle hysteresis. Contact angle hysteresis is very common. Its diverse causes include surface roughness, chemical heterogeneity, surface reorganization, swelling, extraction of leachable species and chemical reaction. As a general rule, surfaces that exhibit little contact angle hysteresis are likely to be freer of these complications than more hysteretic surfaces.

There is a great variety of wetting studies of PDMS by water described in the literature which report a rather surprising broad range of advancing contact angles (θ_a) extending from 95° to 120°. These investigations deal with three broad classes

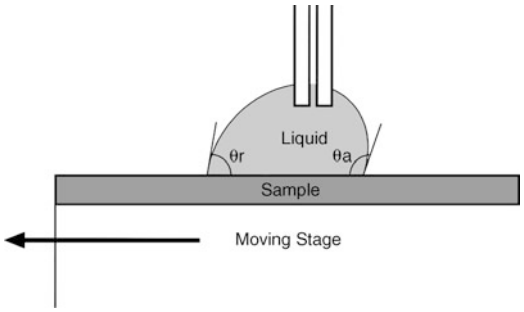

Fig. 1.3 Contact angle hysteresis. θ_r is the receding contact angle; θ_a is the advancing contact angle. Reprinted from Ref. [23] with kind permission of © The American Chemical Society (2003)

Table 1.4 Selected water contact angle data

Polymer cure	Authors	Contact angle method	θ_a (°)	θ_r (°)
Peroxide	Kennan et al. [27]	Sessile drop	111	57
Hydrosilylation	Kennan et al. [27]	Sessile drop	114	60
Peroxide	Kennan et al. [27]	Captive bubble	120	70
Hydrosilylation	Kennan et al. [27]	Captive bubble	122	73
Hydrosilylation	Wynne et al. [28]	Wilhelmy plate	118/108	83/87
End-grafted	She et al. [29]	Sessile drop	118	92
PHMS/PDMS	She et al. [29]	Sessile drop	108	105

of PDMS surfaces (a) PDMS fluids baked or otherwise adsorbed onto solids such as glass or metals, (b) cross-linked polymers on flexible substrates such as paper or plastic, and (c) PDMS elastomer surfaces. Given the propensity of PDMS to remain liquid to high molecular weights, these three classes essentially represent different strategies for immobilizing the surface sufficiently for contact angle study. One widely quoted value for the advancing contact angle of water on PDMS is 101° from the seminal studies of Zisman and co-workers [4]. It is an example of the first class of studies but is now regarded as a somewhat low value. Values in the 110° to 120° range are now considered more realistic—see Table 1.4. Gordon and Colquhoun's study [24] of PDMS release liners for pressure-sensitive adhesives and Chaudhury and Whitesides' [25] characterization of elastomeric PDMS are classic examples of the other two classes.

Part of the variation in results obtained surely derives from neglect of many pitfalls inherent to contact angle measurement. For example, using water of insufficient purity would lower its surface tension and result in reduction of the contact angle. The effect of surface roughness is to increase the contact angle which cautions against favoring the higher values as probably uncontaminated. Other drawbacks are unique to each class of measurement. For instance, when a PDMS film is adsorbed onto a rigid glass or metal substrate, the maximum hydrophobic effect is not initially evident and a thermal baking treatment is required to develop the familiar, high water repellency. This phenomenon was first documented by Hunter et al. [26] over 60 years ago but is still not fully understood. It could be that residual bound water is thermally removed during the baking allowing for more immobiliz-

ing siloxane/surface interactions but residual or surface-catalyzed creation of silanol groups on the polymer that can condense with surface hydroxyls or cross-link with each other are probably also involved. Hunter's initial water contact angles on films formed on glass by dipping in benzene solution were as low as 50° and heat treatment to 200 °C was required to obtain values in excess of 100°.

These difficulties are much less pronounced in the other two classes of measurement where adequate cross-linking is ensured but micro-roughness effects become more evident, both from fillers present in the underlying substrates and from the elastomer surface texture themselves. Morphological differences in coating surfaces resulting from how the coatings are formed (e.g. solvent cast, emulsion based or neat), are also a factor. Although not so important for water studies, the propensity of organic liquids to swell PDMS also plays a role. This is a particular problem with *n*-alkanes which are the preferred contact angle test liquids for determining the Zisman critical surface tension of wetting (γ_C) and other surface energy measurement approaches for low energy polymer surfaces.

There are surprises that arise even where care is taken to eliminate experimental artifacts. In a study by Kennan and co-workers [27] medical-grade silicone elastomers cross-linked in two different ways, by peroxide cure and by hydrosilylation cure, were subjected to accelerated aging in saline solution to verify the hydrolytic stability. Both advancing and receding contact angles of pure water were measured, using two different methods of measurement, the sessile drop method and the captive bubble method. These and other related data are shown in Table 1.4.

An even greater surprise emerges from a third method of measuring contact angle, the Wilhelmy plate approach. Wynne and co-workers [28] studied hydrosilylation cured PDMS coatings that are analogs of biomedical silicone materials. One type of PDMS was a commercial divinyl-terminated PDMS, while the other, a low polydispersity version, was synthesized in the laboratory. They found for both materials that an initial wetting/dewetting cycle of the Wilhelmy plate gave higher advancing contact angle and a lower receding contact angle than was the case for the second and subsequent wetting/dewetting cycles of the Wilhelmy plate. These data are also included in Table 1.4 as initial values/subsequent values. The authors [28] attributed this difference to contamination of the water by the PDMS sample although the nature of this contamination was not unambiguously identified. The presence of low molecular weight linear and cyclic oligomers is common in PDMS and a molecule like hexamethyldisiloxane could certainly be leached out into the aqueous phase. However, in many studies including the Kennan data (Table 1.4), the materials studied have been rigorously extracted and unlikely to be contaminated in this manner. Furthermore, contamination is not the only conceivable explanation. It is also possible that the siloxane backbone becomes hydrated on contact with water and that the higher advancing contact angle is that of the unhydrated state and the lower value corresponds to the hydrated situation.

She et al. [29] attempted to create a PDMS surface that did not suffer from the drawbacks of the three classes of studies described above. Working from the premise that what is required is a very thin film of un-filled PDMS attached by a well-understood, low-temperature chemistry to a very smooth, rigid substrate, they

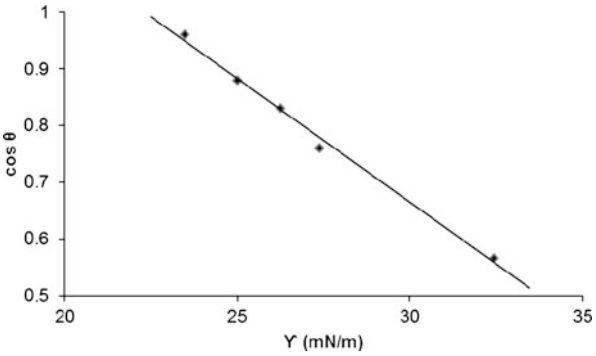

Fig. 1.4 Zisman plot of PDMS. Reprinted from Ref. [29] with kind permission of © The American Chemical Society (2000)

began with carefully cleaned silicon wafers that had been lightly plasma-oxidized to produce a thin silanol-functional, silica layer. A self-assembled monolayer of undecenyltrichlorosilane ($Cl_3Si(CH_2)_9CH{=}CH_2$) was then formed on this surface and SiH-functional PDMS polymers grafted onto this surface by platinum catalyzed hydrosilylation. Two types of polymer were used, monofunctional linear polymers of varying chain length, and a polydimethylsiloxane/polymethylhydrogensiloxane (PDMS/PHMS) copolymer ($Me_3Si(OMe_2Si)_{145}(OSiMeH)_{20}OSiMe_3$). Any unreacted polymer chains were removed by solvent extraction. The data of She et al. for the longest grafted chain and the copolymer are also shown in Table 1.4. Note how little contact angle hysteresis is exhibited by these two surfaces.

1.4 Solid Surface Energy Determination

The oldest approach to quantifying solid polymer surface energies is that of Zisman and co-workers [4]. They found that when the cosines of the contact angles of a series of liquids placed on the solid are plotted against their surface tensions, an almost linear plot is obtained. A PDMS example is shown in Fig. 1.4. The extrapolation of this line to $\cos\theta = 1$, i.e. zero contact angle, is known as the critical surface tension of wetting of that solid. It is the surface tension of the hypothetical liquid that just wets the polymer and as such has correctly, and perhaps pedantically, units of mN/m rather than mJ/m^2. Note that it is not equal to the solid surface free energy because it ignores the possible interfacial tension between the liquid and the solid. Using this approach Shafrin and Zisman [29] developed the order of the impact of substituent groups in polymers on surface energy referred to in Sections 1.1 and 1.2. Critical surface tension of wetting values, γ_C, from Shafrin and Zisman and She et al. for PDMS are shown in Table 1.5.

Surface and interfacial energies are related to the contact angle by the Young equation:

$$\gamma_{SV} - \gamma_{SL} = \gamma_{LV}\cos\theta \tag{1.2}$$

where the subscripts SV, LV, and SL refer to the solid/vapor and liquid/vapor surfaces, and the solid/liquid interface, respectively. Obviously, to use this equation to

Table 1.5 A summary of solid surface energy data for PDMS

Quantity	Authors	Value
γ_C (mN m^{-1})	Shafrin and Zisman [30]	24
γ_C (mN m^{-1})	She et al. [29]	22.7
γ_{JKR} (mJ m^{-2})	Chaudhury [15]	22.6
γ_{SV} ($\gamma_{SV}^d + \gamma_{SV}^p$) (mJ m^{-2})	Owens and Wendt [33]	22.8 (21.7 + 1.1)
γ_{SV}^d (mJ m^{-2})	She et al. [29]	21.3

derive surface energies, liquids that form a finite contact angle and do not spread on the substrate must be selected. This equation was first described in 1805 but was not experimentally verified until 1971 when Johnson, Kendall and Roberts [14] introduced their contact mechanics approach to surface and interfacial energies independent of contact angle measurement. The Young equation can be combined with the Dupré equation for W_{SL}, the thermodynamic work of adhesion of a liquid to a solid:

$$W_{SL} = \gamma_{SV} + \gamma_{LV} - \gamma_{SL} \tag{1.3}$$

Combining Eqs. (1.2) and (1.3) gives

$$W_{SL} = \gamma_{LV}(1 + \cos\theta) \tag{1.4}$$

Girifalco and Good [31] proposed that W_{SL} could be expressed in a geometric mean form of the surface energies of the liquid and solid phases as

$$W_{SL} = 2\Phi\,(\gamma_{SV}\gamma_{LV})^{0.5} \tag{1.5}$$

where Φ is a correction factor for intermolecular interactions that equals unity if the intermolecular forces acting across the interface are alike. This is a reasonable approximation for n-alkanes on the predominantly non-polar PDMS surface, so it follows that by combining these equations with $\Phi = 1$ one obtains

$$\gamma_{SV} = \gamma_{LV}(1 + \cos\theta)^2/4 \tag{1.6}$$

also known as the Girifalco, Good, Fowkes, Young (GGFY) equation. It provides a useful way of estimating surface energy, or at least the dispersion force component, of apolar polymers from their contact with one liquid, usually n-hexadecane as it is the highest surface tension n-alkane at room temperature. This equation, using the data of She et al. [29], gives a value of 21.3 mJ/m^2 for PDMS (see Table 1.5).

Fowkes [32] suggested that the surface energy of a solid is made up additively of components that correspond to intermolecular interactions. As many as seven terms have been suggested but a common simplification is to consider only two: the component resultant from electrodynamic London dispersion forces common to all matter, known as the dispersion force component (γ_{SV}^d), and the so-called polar component (γ_{SV}^p) that incorporates all other interfacial interactions. One of the most frequently used two-component methods is that of Owens and Wendt [33] shown in Eq. (1.7):

$$\gamma_{LV}(1 + \cos\theta) = 2\left(\gamma_{LV}^d\gamma_{SV}^d\right)^{0.5} + 2\left(\gamma_{LV}^p\gamma_{SV}^p\right)^{0.5} \tag{1.7}$$

The two unknowns, γ^d and γ^p, of the solid require two contact angle liquids. Water and methylene iodide (diiodomethane) are a common choice, the former being predominantly polar and the latter primarily nonpolar, with both liquids having a high surface tension conducive to forming finite contact angles on a given solid. There are sound reasons to suppose that dispersion forces interact in a geometric mean fashion but this is certainly not so for polar interactions so this approach is only semi-empirical. PDMS data from Owens and Wendt are included in Table 1.5.

Also included in Table 1.5 is a JKR contact mechanics value that is further discussed in the next section. Table 1.5 is a very limited, personal selection from a much greater body of data, however, the relative closeness of these values obtained in very different ways is comforting but perhaps illusory.

1.5 Contact Mechanics Approach

Contact mechanics, as the name implies, is concerned with the behavior of solids in contact under the action of an external load. From the perspective of silicone surface science, the great interest in this topic in recent decades is driven by the realization that it offers an alternative way of measuring surface energies free from the vagaries inherent in contact angle approaches. Hertz in 1882 was the first to address this topic. However, he took no account of interfacial interactions considering only frictionless, non-adhering surfaces of perfectly elastic solids. This neglect is more obvious for relatively small particles contacting each other on a flat surface when it is evident that contact deformations are larger than those predicted by the Hertz theory.

Johnson, Kendall and Roberts [14] reasoned that these excess deformations were the result of attractive forces. They assumed that the attractive forces were confined within the area of contact and used an energy balance approach to develop a general expression for the contact deformation as a function of the surface and elastic properties of solids, now widely known as the JKR theory. However, this theory is not the only one accounting for contact between solids. The so-called DMT theory introduced by Derjaguin et al. [34] assumes that all the attractive forces lie outside the area of contact which is under compression as described by the Hertzian strain profile and makes significantly different predictions from those of the JKR theory. As a consequence, there has been considerable discussion in the literature concerning the relative merits of these two theories which have since been shown to describe different limiting cases of a more general situation. There is now general agreement that the DMT approach is most suitable for hard, low-surface-energy materials with small radii of curvature, whereas the JKR approach is most suited to soft materials with relatively high surface energies and large radii of curvature. In practice, it transpires that the JKR theory correctly accounts for the contact behavior of soft polymeric materials, including low-surface-energy silicones, and it is, therefore, the only approach that is considered in this chapter.

The application of the JKR approach to silicone surfaces was pioneered by Chaudhury and Whitesides [15, 25]. As pointed out by them, PDMS is an ideal

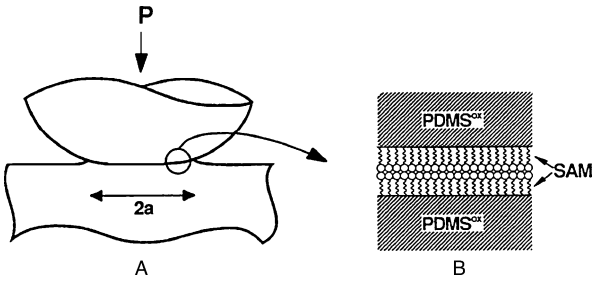

Fig. 1.5 Contact between a semi-spherical lens and flat sheet of PDMS. Both surfaces have been modified with an alkoxysilane self-assembled monolayer (SAM)

substrate for such studies. The surface of the deformable component must be very smooth and homogeneous and this has been shown to be the case for PDMS by electron microscopy. No structural inhomogeneity is evident even at a resolution of 20–30 nm. Of course, it must be possible to cast the material into spherical or semi-spherical shapes and this is readily achieved with liquid, cross-linkable silicone formulations by forming drops on an ultra-low energy surface such as a fluorinated self-assembled monolayer (SAM) prior to cross-linking of the PDMS network A further advantage of PDMS substrates is that by plasma oxidation of the surface followed by SAM modification, the surface properties can be varied without affecting bulk physical properties.

The original approach of Chaudhury and his co-workers was to bring a semi-spherical lens and a flat sheet of PDMS into contact and measure the resulting contact deformation under controlled loads. This was then extended to other flat surfaces, notably silicon wafers modified by a variety of self-assembled monolayers [35]. They have also extended the sample geometry to a cylinder rather than a sphere [36] and used rolling contact mechanics to study adhesion hysteresis at the interface of plasma-oxidized PDMS elastomer rolling on a PDMS film grafted to a silicon wafer. It should be also noted that other geometries are amenable to JKR analysis and that Chaudhury's group is not the only one using the JKR approach to investigate polymer surfaces. The surface forces apparatus (SFA) originally developed by Tabor and Winterton [37] is used in this way. In this apparatus thin polymer film samples coated onto molecularly smooth thin mica sheets, often in a crossed cylinder configuration, are brought into contact. Tirrell and co-workers [38, 39] in particular have used the SFA to characterize a variety of polymer substrates.

When a deformable semi-spherical solid with radius of curvature R and a flat plate are brought into contact the result is the formation of a circular region of contact of radius "a" whose size depends on the surface forces and the external applied load P. A diagram of this geometry is shown as A in Fig. 1.5. The enlargement of the interfacial contact area shown as B in Fig. 1.5 illustrates how the surfaces may be modified by a self-assembled monolayer (SAM). The $PDMS^{OX}$ layer is a thin silica-like layer produced by plasma oxidation of the PDMS surface [35].

For this sphere on plate geometry, Johnson, Kendall and Roberts [14] showed that

$$a^{3/2}/R = (1/K) \cdot \left(P/a^{3/2}\right) + (6\pi \mathrm{W}/\mathrm{K})^{1/2} \tag{1.8}$$

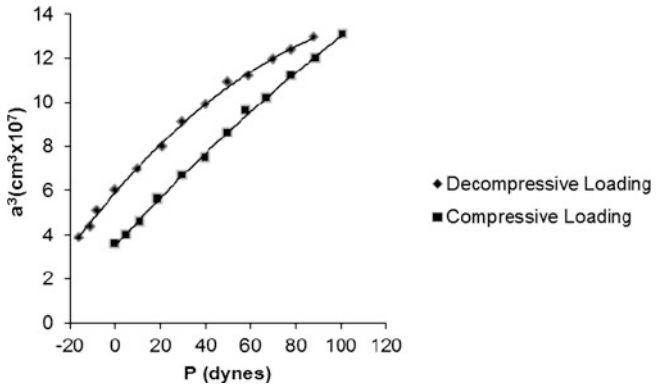

Fig. 1.6 JKR plot for PDMS against a fluoroalkylsiloxane monolayer. Reprinted from Ref. [40] with kind permission of © The American Chemical Society (1993)

Table 1.6 Comparison of surface energies derived from JKR and contact angle data [35]

Silane SAM head-group	γ_{JKR} (mJ m^{-2})	γ_{SV}^{d} (mJ m^{-2})	γ_{SV}^{p} (mJ m^{-2})	γ_{SV} (mJ m^{-2})
$-CF_3$	16.0	15.0	0.8	15.8
$-CH_3$	20.8	20.6	0.1	20.7
$-OCH_3$	26.8	30.8	6.4	37.2
$-CO_2CH_3$	33.0	36.0	6.4	42.4
–Br	36.8	37.9	1.7	39.6
Polyethylene	33	32.0	1.1	33.1

where K is the composite elastic modulus and W is the thermodynamic work of adhesion. Since for two identical surfaces W is simply $2\gamma_{SV}$, the solid surface energy, γ_{JKR}, can be derived by contacting two of the same surfaces. A typical plot of the applied load P against $a^{3/2}$ for PDMS against a fluoroalkylsiloxane monolayer is shown in Fig. 1.6. The curves follow different paths as the applied load is increased or decreased thus showing hysteresis in a similar manner as do advancing or receding contact angles. Because of the action of the attractive forces across the interface, a finite tensile force is required to separate the surfaces from adhesive contact. Johnson, Kendall and Roberts showed that this "pull-off" force, P_S, is given by

$$P_S = 3\pi W R/2 \tag{1.9}$$

Chaudhury's [15] value of 22.6 mJ m^{-2} for γ_{JKR} of PDMS is given in Table 1.5. Table 1.6 lists his results from a study of the surface free energy of alkylsiloxane monolayers supported on elastomeric PDMS [35] as shown in B of Fig. 1.5. The value for polyethylene is also included so that it can be seen that the surface energy follows the order first described by Zisman and co-workers, $CF_3- <$

Table 1.7 Selected values of JKR interfacial tension between various polymers and PDMS [38]

Polymer	γ_{12} (mN m^{-1})
Poly(vinyl cyclohexane)	3
Poly *p*-*t*-butylstyrene	9
Polystyrene	10
Poly *p*-phenylstyrene	11
Poly(vinyl benzyl chloride)	12
Polyacrylonitrile	20

CH_3- < $-CH_2-$, but note that a γ_{JKR} value for $-CF_2-$ has not been reported yet to the best of our knowledge. Contact angle values of γ_{SV} derived using Eq. (1.7) with water and methylene iodide (except for the $-CF_3$ surface where perfluorodecalin was used instead of methylene iodide) are included in Table 1.6 for comparison. Agreement is quite close for the non-polar substrates but not so good for the polar entities.

The literature also contains reports on some polymer interfacial tension studies involving PDMS determined by the JKR contact mechanics approach. Some pertinent data are shown in Table 1.7 [38]. It can be seen that only one polymer pair, PDMS/polystyrene, replicates any data listed in Table 1.3. However, the JKR solid/solid interfacial energy value of 10 mJ m^{-2} is quite different from the melt extrapolation value of 6.1 mN m^{-1} in Table 1.3. Coincidence of these two different quantities is not to be expected. As with the melt studies, there is a trend for higher surface energy, more-polar polymers to have a higher interfacial energy with PDMS.

1.6 Langmuir Trough Studies

Being of low surface-energy and insoluble in water but also having a polar backbone to interact with the water surface, PDMS and some other silicone polymers are able to spread over water surfaces thus making it possible to study the behavior of their surface pressure/surface area isotherms by the Langmuir trough technique. An example of such behavior is given in Fig. 1.7 [41]. From this figure it can be seen that the isotherm has essentially four regions; an initial low surface-pressure region (A_1–A_2) followed by a rise in surface pressure (A_2–B) which leads to a plateau region (B–C) followed by a final small rise and a very small plateau before reaching the collapse point. Chapter 7 of this book covers Langmuir trough behavior of silicones but the subject is briefly reviewed here for the sake of completeness.

There has been much varied interpretation of these PDMS isotherms over the years. For a long time a model introduced by Fox et al. [42] was accepted, according to which at low surface-pressure every siloxane bond was envisioned in contact

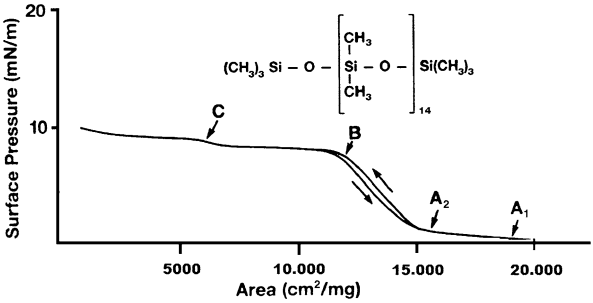

Fig. 1.7 Langmuir trough isotherm for PDMS. This material is reproduced from Ref. [41] with kind permission of © John Wiley & Sons, Inc. (1971)

with the water surface and all the methyl groups were assumed to be oriented outwards towards the air phase. At higher surface pressures the spread monolayer was supposed to transition to a six-unit helical coil whose axis is parallel to the water surface. The considerable reduction in surface area caused by this transition was used to explain the characteristic plateau in the PDMS isotherm in the 8–10 mN m^{-1} surface pressure region. More than a decade later, Noll and co-workers [41] suggested a modification of this model involving hydration of the polymer backbone and squeezing out of the water molecules as the film is compressed in the low-surface-pressure region.

In 1989, Granick and co-workers [43] questioned the helical coiling concept when they found that cyclic PDMS with as few as 20 monomer units also showed this plateau. Later Mann et al. [44] challenged the implied homogeneous monolayer assumption of the original model by demonstrating the co-existence of domains of different surface density at very low surface-pressures using Brewster angle microscopy. Most recently Kim et al. [45] applied the sum frequency generation technique (see Chap. 2) to this problem and concluded that in the initial low-surface-pressure region the methyl groups do not all point outwards to the air phase. Their results indicated either a totally random orientation of the methyl groups or one where one of the methyl groups is pointing directly out and the other is pointing inwards to the water. The first of these possibilities would seem to be the most likely. Neutron reflectivity studies suggest a PDMS layer thickness of *ca.* 15 Å in the dilute region, twice that of a single spread monolayer, consistent with a disordered, freely rotating chain concept. The rising surface pressure region up to the plateau seems to involve PDMS chains lying at the interface with both methyl groups pointing towards the air with one closer normal to the surface and the other closer to the interface. The results for the plateau region are more consistent with a horizontal chain folding geometry than with contraction into helices. The horizontal chain folding idea was first proposed by Kalachev et al. [46] based on surface potential studies.

At present, we doubt that we have heard the last of explanations of Langmuir trough behavior of PDMS and related polymers. The technique has been applied to a variety of other silicones including, cyclo-linear polysiloxanes [47] where up to seven plateaus were observed, polar-group substituted siloxanes such as amino and quaternary ammonium functional polymers [48], and poly(amidoamine-organosilicon) dendrimers [49].

Table 1.8 Surface tension of polysiloxanes other than PDMS

Polymer	Viscosity (cS)	Surface tension ($mN\,m^{-1}$)
Polymethylphenylsiloxane [50]	500	28.5
Polydiethylsiloxane [51]	Unknown	25.7
Polymethyltrifluoropropylsiloxane [18]	Infinite	24.4
Polymethylhydrogensiloxane [52]	30	20
Polydimethylsiloxane [18]	Infinite	20.9

Table 1.9 Surface energies of selected fluoropolymers

Polymer	γ_C ($mN\,m^{-1}$)	γ_{SV} ($mJ\,m^{-2}$)	γ_∞ ($mN\,m^{-1}$)
Polydimethylsiloxane	22.7	22.8	21.3
Polymethyltrifluoropropylsiloxane	21.4	13.6	24.4
Polymethylnonafluorohexylsiloxane	16.3	9.5	19.2
Polytetrafluoroethylene	18.5	14.0	25.9
Polyhexafluoropropylene	16.2	12.4	–
Polyoxyhexafluoropropylene	–	–	18.4

1.7 Other Silicones

Although they are extensively used in surface modification, very little systematic information has been reported concerning the surface energy of silicone polymers with functional entities in the pendant side-groups. A major reason for this is that silicones with polar functionalities such as aminofunctional PDMS incorporate the polar entity to enhance substantivity to substrates while maintaining PDMS surface properties. Consequently, they are usually copolymers with PDMS whose surface energy behavior is dominated by the PDMS component.

Even among the silicone homopolymers other than PDMS there is a paucity of reported surface energy data in the literature. Some liquid surface tension values are available and a selection of such data for the commercially more important homopolymers is given in Table 1.8. No temperature dependence data have been reported and in most cases insufficient data are available to extrapolate to infinite molecular weight as can usefully be done for PDMS. Not surprisingly, however, the exception to this is the fluorosilicones as they offer the only prospect of improving on the already considerable low surface energy of PDMS (see Table 1.9, Chap. 5).

The polymethylphenylsiloxane has an expectedly higher surface tension than PDMS because of the aromatic ring current. Polydiethylsiloxane is included in this list because of growing interest in the West. It has long been a favorite silicone in Russia but only recently has much attention been paid to it in Europe and the USA. The higher PMTFPS value than that for PDMS is briefly discussed in Section 1.2. The polymethylhydrogensiloxane measurement was made at 37 °C. A similar viscosity PDMS at this temperature would have a very comparable liquid surface

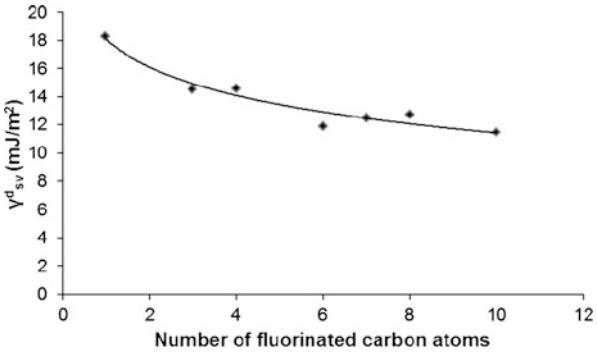

Fig. 1.8 Dispersion force component of surface energy versus fluorinated side-chain length for fluorosilicones

tension of 20.5 mN m^{-1}, implying that the SiH entity has a similar intrinsic surface energy to CH_3.

Table 1.9 summarizes the more complete surface property data available [18] for PMTFPS and polymethylnonafluorohexylsiloxane (PMNFHS). Also included for comparative purposes are polytetrafluoroethylene (PTFE), polyhexafluoropropylene (PHFP) and polyoxyhexafluoropropylene (POHFP). Critical surface tensions were all determined using *n*-alkanes and the solid surface tensions were obtained by the Owens/Wendt approach [33] using water and methylene iodide so data in each column can be usefully compared. Note that with PMNFHS a fluorosilicone is available that has a lower surface energy than PDMS in all three of these surface properties.

Figure 1.8 presents some further data on silicone polymers of the same structure as PMTFPS, that is to say, those that retain one methyl group on every silicon atom. This structure has process benefits in that it expands the range of possible solvents and also encourages chain extension over formation of cyclics but it does hinder the attainment of very low surface energies. These data are from the work of Doeff and Lindner [53] and one of us [54] using Eq. (1.6) with *n*-hexadecane as the contact angle liquid. The figure shows the feature that is typical for all fluoropolymers, namely a decrease in surface energy with the lengthening of the fluoroalkyl pendant group. This is usually explained as a consequence of burying the transient dipole that occurs at the fluorocarbon/hydrocarbon chain junction. The fluorocarbon groups also polarize the adjacent $–CH_2–$ groups making them rather acidic which may also be the explanation. It is not completely clear why the effect persists to quite a depth, *ca.* six fluorinated atoms being required before the plateau of 11–12 mJ m^{-2} is reached. However, this does suggest that there would be little advantage in pursuing longer fluorocarbon side-chains, particularly with the bio-accumulation concerns of such entities. Note also that Thanawala and Chaudhury [55] have reported a surface energy of 7.5 mJ m^{-2} for a $F[CF(CF_3)CF_2O]_7CF(CF_3)CONHCH{=}CH_2$ modified PDMS surface also using *n*-hexadecane and the GGFY equation. The lowest surface energies for fluorosilicones are found with the fluorocarbon-substituted polyhedral oligomeric silsesquioxanes which contain no methyl groups. These are the subject of Chapter 6; other fluorosilicone polymers are reviewed in Chapter 5.

1.8 Concluding Remarks

Silicones, particularly PDMS, are widely exploited for their surface properties and behavior. In this chapter we have sought to establish the structure/property relationships of silicone surface science in order to set the stage for the elaboration of important topics pertaining to this field and comprising the contents of the following chapters.

The central position of PDMS in the silicone industry is a consequence of its structure. The combination of small methyl side-groups arrayed along the uniquely flexible siloxane backbone and exhibiting low inter-segmental attractive forces results in a polymer whose low surface energy can be equaled or bettered by relatively few other polymers. Moreover, it has the added bonus of greater thermal and oxidative stability than most comparable organic polymers. Smaller, pendant entities than the methyl group are not forthcoming. Likely atoms such as hydrogen or fluorine are reactive when directly linked to the silicon atom. Larger groups would dilute the special qualities such as extreme chain flexibility that the siloxane backbone confers. As a consequence, PDMS is used for its special surface properties in a wide variety of applications, some important examples of which are further considered in the final chapter of this book. The principal drawbacks of PDMS in this arena are its susceptibility to cleavage of the siloxane bond at extremes of pH and its oleophilicity. The former is shared by all polymers that have different alternating atoms in their backbone, while the solution to oleophilicity-causing difficulties is to turn to the more solvent-resistant fluorosilicones.

Nearly 20 years ago one of us [56] was bold enough to make a variety of predictions concerning silicone surface science and technology. Some of these predictions materialized but one in particular has failed so far to do so: the anticipated exploitation of more flexible backbones and new low-surface-energy pendant groups. Both polyphosphazenes and fluoroethers have expanded their scope but no new polymer backbone with significant greater flexibility than the siloxane chain has appeared. Nor has a lower surface energy substituent based on anything other than aliphatic fluorocarbon been found. Maybe current work with the SF_5–moiety might change this circumstance [57].

References

1. Warrick EL (1990) Forty years of firsts. McGraw-Hill, New York
2. Mark JE (1978) Macromolecules 11:627
3. Langmuir I (1916) J Am Chem Soc 38:2221
4. Zisman WA (1964) In: Fowkes FM (ed) Contact angle, wettability and adhesion. Adv Chem Ser, vol 43. Amer Chem Soc, Washington, p 1
5. Shih H, Flory PJ (1972) Macromolecules 5:758
6. Owen MJ (2000) Surface properties and applications. In: Jones RG, Ando W, Chojnowski J (eds) Silicon-containing polymers. Kluwer, Dordrecht, pp 213–231
7. Kurian P, Kennedy JP, Kisliuk A, Sokolov A (2002) J Polym Sci, Part A, Polym Chem Ed 40:1285

8. Dvornic PR (2000) Thermal properties of polysiloxanes. In: Jones RG, Ando W, Chojnowski J (eds) Silicon containing polymers. Kluwer, Dordrecht, pp 185–212
9. Schiers J (1997) Perfluoroethers: synthesis, characterization and applications. In: Schiers J (ed) Modern fluoropolymers. Wiley, New York, pp 435–485
10. Lee WA, Rutherford RA (1975) In: Brandrup J, Immergut EH (eds) Polymer handbook, 2nd ed. Wiley, New York, pp 111–139
11. Kobayashi H, Owen MJ (1990) Macromolecules 23:4929
12. Nielson RH, Hani R, Wisian-Nielson P, Meister JJ, Roy AK, Hagnauer JL (1987) Macromolecules 20:910
13. Dvornic PR, Jovanovic JD, Govedarica MN (1993) J Appl Polym Sci 45:1497
14. Johnson KL, Kendall K, Roberts AD (1971) Proc R Soc London A 324:301
15. Chaudhury MK, Whitesides GM (1991) Langmuir 7:1013
16. Owen MJ (1980) Ind Eng Chem Prod Res Dev 19:97
17. LeGrand DG, Gaines GL (1969) J Colloid Interface Sci 31:162
18. Falsafi A, Mangipudi S, Owen MJ (2006) Surface and interfacial properties. In: Mark JE (ed) Physical properties of polymers handbook 2nd ed. Am Inst Phys, New York. Chap 59
19. Kanellopoulos AG, Owen MJ (1971) Trans Faraday Soc 67:3127
20. Kuo ACM (1999) Polydimethylsiloxane. In: Mark JE (ed) Polymer data handbook. OUP, New York, pp 411–435
21. Antonow GN (1907) J Chim Phys 5:372
22. Wu S (1982) Polymer interface and adhesion. Dekker, New York
23. Owen MJ (2003) Surface energy. In: Brady RF (ed) Comprehensive desk reference of polymer characterization and analysis. Am Chem Soc, New York. Chap 15
24. Gordon DJ, Colquhoun JA (1976) Adhes Age 19(6):21
25. Chaudhury MK, Whitesides GM (1992) Science 255:1231
26. Hunter MJ, Gordon MS, Barry AJ, Hyde JF, Heidenreich RD (1947) Ind Eng Chem 39:1389
27. Kennan JJ, Peters YA, Swarthout DE, Owen MJ, Namkamisorn A, Chaudhury MK (1997) J Biomed Mater Res 36:487
28. Wynne KJ, Lambert JM (2004) Silicones. In: Encyclopedia of biomaterial and biomedical engineering. Dekker, New York, pp 1348–1362
29. She H, Chaudhury MK, Owen MJ (2000) In: Clarson SJ, Fitzgerald JJ, Owen MJ, Smith SD (eds) ACS Symp Ser, vol 729, pp 322–331
30. Shafrin EG, Zisman WA (1960) J Phys Chem 64:519
31. Good RJ, Girifalco LA (1960) J Phys Chem 64:561
32. Fowkes FM (1964) Ind Eng Chem 56:40
33. Owens DK, Wendt RC (1969) J Appl Polym Sci 13:1741
34. Derjaguin BV, Muller VM, Toporov YP (1975) J Colloid Interface Sci 53:314
35. Chaudhury MK (1993) J Adhes Sci Technol 7:669
36. She H, Malotky D, Chaudhury MK (1998) Langmuir 14:3090
37. Tabor D, Winterton RHS (1969) Proc R Soc London Ser A 312:435
38. Mangipudi VS, Tirrell M, Pocius AV (1995) Langmuir 11:19
39. Li L, Mangipudi VS, Tirrell M, Pocius AV (2001) In: NATO Science Series II, Mathematics, Physics and Chemistry, vol 10, pp 305–329
40. Chaudhury MK, Owen MJ (1993) Langmuir 9:29
41. Noll W, Steinbach H, Sucker C (1971) J Polym Sci, Part C 34:123
42. Fox HW, Taylor PW, Zisman WA (1947) Ind Eng Chem 39:1401
43. Granick S, Kuzmenka DJ, Clarson SJ, Semlyen JA (1989) Macromolecules 22:1878
44. Mann EK, Henon S, Langevin D, Meunier J (1992) J Phys II (France) 2:1683
45. Kim C, Gurau MC, Cremer PS, Yu H (2008) Langmuir 24:10155
46. Kalachev AA, Litvinov VM, Wegner G (1991) Makromol Chem, Macromol Symp 46:365
47. Fang J, Dennin M, Knobler CM, Godovsky YK, Makarova NN, Yokoyama H (1997) J Phys Chem B 101:3147
48. Mehta SC, Somasundaran P, Maldarelli C, Kulkarni R (2006) Langmuir 22:9566
49. Dvornic PR, De Leuze-Jallouli A, Perz SV, Owen MJ (2000) Mol Cryst Liq Cryst 353:223

50. http://www.clearcoproducts.com. Accessed 23 March 2011
51. http://www.accudynetest.com. Accessed 23 March 2011
52. Schurch S, Georke J, Clements JA (1976) Proc Natl Acad Sci USA 73:4698
53. Doeff M, Lindner E (1989) Macromolecules 22:2951
54. Kobayashi H, Owen MJ (1995) Trends Polym Sci 3:330
55. Thanawala SK, Chaudhury MK (2000) Langmuir 16:1256
56. Owen MJ (1993) Surface chemistry and applications. In: Clarson SJ, Semlyen JA (eds) Siloxane polymers. Prentice Hall, New York, pp 309–372
57. Kostov G, Ameduri B, Sergeeva T, Dolbier WR Jr., Winter R, Gard GL (2005) Macromolecules 38:8316

Chapter 2
Sum Frequency Generation Vibrational Spectroscopy of Silicone Surfaces & Interfaces

Dongchan Ahn and Ali Dhinojwala

2.1 Introduction

Silicone materials such as polydimethylsiloxane (PDMS) exhibit very unusual surface properties that arise from the unique flexibility, bond energy, partially ionic nature of the siloxane (Si-O) backbone, and low intermolecular forces [1, 2]. These molecular features are manifested in bulk properties such as low surface energy, heat stability, low temperature flexibility, dielectric strength, inertness, hydrophobicity, optical clarity and ease of crosslinking by a variety of mechanisms that have allowed silicones to grow from a research concept in the early 20th century to a virtually ubiquitous material set used in a remarkably diverse variety of industries and applications [3]. For example, Dow Corning Corporation, which was established in 1943, has grown to a $6 billion company in 2010, based largely on silicones going into over 6,000 products spanning nearly every major commercial industry. In particular, the unique range of surface and interfacial properties attainable in a facile manner through the versatility of organosilicon chemistry positions silicones well for even greater future prominence as products and processes leverage structural control over ever-diminishing length scales.

Paramount to the effective development of micro- or nano-engineered materials are the structural and compositional insights from characterization of the interfaces. Despite remarkable advances in surface analysis techniques, elucidating direct structural information from interfaces remains difficult for a variety of reasons. Perhaps the most common challenge in surface science is the scarcity of the interface relative to large background signals from the 'bulk' that tend to result in poor sensitivity. Sum-frequency generation vibrational (SFG) spectroscopy offers

D. Ahn (✉)
Dow Corning Corporation, Midland, MI 48686, USA
e-mail: d.ahn@dowcorning.com

A. Dhinojwala (✉)
Department of Polymer Science, The University of Akron, Akron, OH 44325, USA
e-mail: ali4@uakron.edu

M.J. Owen, P.R. Dvornic (eds.), *Silicone Surface Science*, Advances in Silicon Science 4,
DOI 10.1007/978-94-007-3876-8_2,

intrinsic advantages in this regard, because the output is based on nonlinear optical selection rules that render it sensitive only to regions of a material where inversion symmetry is broken. In the majority of materials that are isotropic and homogeneous in the bulk, the technique is ideal for studying surfaces and buried interfaces non-invasively. The resulting output is an infrared (IR) vibrational spectrum that offers the same richness of molecular information and bonding with nearly unparalleled surface sensitivity.

While several general reviews of the applications of SFG appear in the literature, none have focused specifically on the application of SFG to silicones [4–10]. The reader is directed to these cited references for additional background and details on the technique and its use with other classes of materials. The unique and somewhat dichotomous surface properties of silicones, and their ever-increasing use in surface and interface-dependent applications such as lubricants, adhesives, microfluidic materials, sensors and matrices or scaffolds for nanocomposites, calls for increased fundamental understanding that has motivated the use of SFG analysis. The intent of this chapter is to focus specifically on the combination of this uniquely surface sensitive tool to study applications using PDMS and other silicone-based materials. We distinguish silicones from silicates and silanes by focusing on materials that have a flexible polymeric -Si-O-Si- backbone. For example, the body of references on SFG characterization of silane-based self-assembled monolayers or modified silica surfaces falls outside the scope of this review. We briefly overview the technique, then illustrate its utility in studying a number of important interfacial phenomena involving silicone-based materials by way of examples from the literature. Because the interpretation of SFG spectra can be quite complex, many of these examples highlight how SFG can be coupled with complementary techniques to provide a more complete understanding of interfacial effects. Lastly, we conclude by providing a summary of strengths, limitations and potential future opportunities for application of SFG and complementary techniques to silicone-based materials.

2.2 Fundamentals

2.2.1 Theory of Surface-Sensitive SFG

The theory of SFG has been explained in published works [11–14] and is not presented here at the same level of detail. The following background is sufficient for enabling the reader not familiar with SFG to understand the examples and case studies presented in the text [15].

When light interacts with a medium the polarization is expressed using the electric-dipole approximation as follows:

$$\mathbf{P} = \varepsilon_0(\chi^{(1)}:\mathbf{E} + \chi^{(2)}:\mathbf{EE} + \cdots) \tag{2.1}$$

Here, $\mathbf{P}$ is the polarization vector, $\mathbf{E}$ is the electric field vector, and $\boldsymbol{\chi}^{(1)}$ and $\boldsymbol{\chi}^{(2)}$ are the first- and second-order electric susceptibility tensors of the medium (higher-order susceptibilities are not shown and are usually negligible in magnitude). Also,

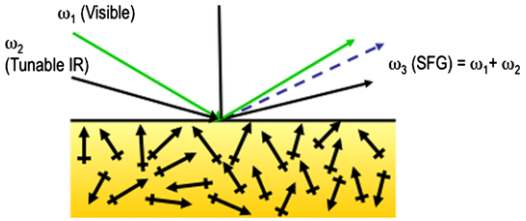

Fig. 2.1 Schematic diagram (not to scale) of a copropagating, external-reflection (ER) geometry used for SFG. The beams of frequencies ω_i are as follows: $i = 1$, S- or P-polarized visible; 2, S- or P-polarized IR; and 3, SFG. The SFG signal is detected after passing through a polarizer and filters

it is assumed that the medium does not have a permanent polarization (true for most organic materials). The second- and higher-order terms in the polarization equation are experimentally observed only when the medium is subjected to high electric field using a high intensity pulsed lasers. In infrared-visible SFG experiments, the medium is simultaneously subjected to two intense electric fields; then the induced polarization is as follows:

$$\mathbf{P} = \varepsilon_0\left(\boldsymbol{\chi}^{(1)}:(\mathbf{E}_1 + \mathbf{E}_2) + \boldsymbol{\chi}^{(2)}:(\mathbf{E}_1\mathbf{E}_2 + \mathbf{E}_2\mathbf{E}_1) + \cdots\right) \tag{2.2}$$

The meaning of $\mathbf{P}$, $\mathbf{E}_i$, and, $\boldsymbol{\chi}^{(j)}$ are the same as, or analogous to, those in (2.1).

When the source of electric fields is laser light as in Fig. 2.1, $\mathbf{E}_1 = \mathbf{E}_1^0\cos(\omega_1 t)$ and $\mathbf{E}_2 = \mathbf{E}_2^0\cos(\omega_2 t)$; therefore, it is easily seen with a trivial trigonometric rearrangement that the term containing $\boldsymbol{\chi}^{(2)}$ in (2.2) will have a sinusoidal component of frequency $\omega_1 + \omega_2$ which shows that $\boldsymbol{\chi}^{(2)}$ is responsible for SFG. The $\boldsymbol{\chi}^{(1)}$ term is responsible for linear optical-processes such as Raleigh and Raman scattering; however, unlike such scattering, the nonlinear SFG generates a coherent signal in the form of a collimated beam in a predictable direction. From symmetry arguments it can be shown that the third-rank tensor, $\boldsymbol{\chi}^{(2)}$, has a value of 0 in centrosymmetric media if it can be assumed that only electric-dipole mechanisms are responsible for $\boldsymbol{\chi}^{(2)}$, and the contributions from higher-order multipoles and magnetic dipoles are negligible (a usually good approximation). This is why SFG is forbidden in the bulk of most substances, but it is allowed at the interface between bulk phases where there can be no centrosymmetry.

Figure 2.1 shows a simple geometry for SFG that is commonly used. Here, the visible and IR beams are moving in the same direction along the x axis (copropagating), and all three beams are in the same plane, the plane of incidence. The ω_1 and ω_2 beams are either S- or P-polarized; S means the electric field of the light beam is perpendicular to the plane of incidence (along the y axis), and P means the field is in the plane of incidence (the xz plane). The signal-beam polarization is also set to S or P by the polarizer before the beam reaches the detector. The combination of polarizations of all three beams is given by a sequence of three letters, each being S or P (e.g., SSP), with the letters having the following meaning: polarization of the SFG beam, visible beam, and IR beam, respectively. The polarization settings

in SFG play an important role in selectively probing different components of $\boldsymbol{\chi}^{(2)}$ (discussed below).

If $I(\omega_i)$ is the intensity of a beam at frequency ω_i (see Fig. 2.1), then the SFG-signal intensity depends on the probing visible- and IR-beam intensities as follows [14]:

$$I(\omega_3 = \omega_1 + \omega_2) \propto \left|\chi_{\text{eff}}^{(2)}\right|^2 I(\omega_1) I(\omega_2) \tag{2.3}$$

Here, $\chi_{\text{eff}}^{(2)}$ (or χ_{eff} for simplicity) is an effective, second-order, nonlinear susceptibility of the interface; it is a sum of terms in which each term contains a single component of the second-order susceptibility tensor, $\boldsymbol{\chi}^{(2)}$, of the interface; the components are $\chi_{ijk}(\omega_2)$ (or χ_{ijk} for simplicity), where $i, j, k = x, y, z$ (x, y, and z are the lab axes in Fig. 2.1, and, from here on, the indices ijk appearing together will have this meaning). For an interface with azimuthal, or x–y, isotropy (such as all the interfaces described below) only seven combinations of ijk, in χ_{ijk}'s, out of the 27 possibilities are nonvanishing, and only four are independent: $\chi_{xxz} = \chi_{yyz}$, $\chi_{xzx} = \chi_{yzy}$, $\chi_{zxx} = \chi_{zyy}$, and χ_{zzz}.

The combination of χ_{ijk}'s that comprises χ_{eff} depends on the beam polarizations: for example, χ_{eff} in SSP polarization consists of just one term containing a single χ_{ijk}.

$$\chi_{\text{eff, SSP}} \propto \chi_{yyz}(\omega_2) \tag{2.4}$$

The constant of proportionality in Eq. (2.4) has a weak dependence on ω_2, and this dependence is often neglected. This equation shows that in SSP the χ_{yyz} component of the $\boldsymbol{\chi}^{(2)}$ tensor is probed.

The χ_{ijk}'s are each a sum of one nonresonant term and Q resonant terms, one for each vibrational mode of each interfacial species.

$$\chi_{ijk}(\omega_2) = \chi_{ijk}^{\text{NR}} e^{i\Phi} + \sum_{q=1}^{Q} \frac{\chi_{ijk,\,q}}{\omega_2 - \omega_q + i\Gamma_q} \tag{2.5}$$

where $\chi_{ijk,q}$, ω_q, and Γ_q are the line strength, frequency, and line width, respectively, of the resonance q, and Φ is the relative phase of the nonresonant term with respect to the resonant terms. The SFG spectra are usually normalized for the variation in $I(\omega_1)$ and $I(\omega_2)$ Eq. (2.3). Often, spectra are then fit to Eq. (2.5), and the $\chi_{ijk,q}$'s obtained from the fit are then adjusted by any proportionality constant, such as in Eq. (2.4).

The $\chi_{ijk,q}$'s have their origins in the molecular hyperpolarizability-tensor ($\boldsymbol{\beta}$) components, which are as follows:[1]

$$\beta_{lmn}(\omega_2) = \sum_{q=1}^{Q} \frac{\beta_{lmn,q}}{\omega_2 - \omega_q + i\Gamma_q} \quad \text{where } l, m, n = a, b, c \tag{2.6}$$

[1] In Eq. (2.6), and the subsequent expressions that follow, we have assumed that all the vibrational modes, q, belong to a single type of molecular species or moiety. Although this is usually not true, the extension for the case of multiple types of species is trivial. The more general treatment would unnecessarily increase the complexity of the notation.

Here, a, b, and c are axes of the Cartesian frame-of-reference that is fixed to the molecule; c is conventionally taken to coincide with the axis (or one of the axes) of highest symmetry of the molecule. $\beta_{lmn,q} = A_{lm,q} M_{n,q}$, where $A_{lm,q}$ is the lm component of the Raman tensor and $M_{n,q}$ is the n component of the transition-dipole-moment vector [16]. Therefore, only those vibration modes that are both Raman- and IR-active contribute to the hyperpolarizability tensor—i.e., only such modes are SFG-active.

The $\beta_{lmn}(\omega_2)$ (or β_{lmn}'s for simplicity) can be projected on the lab axes (xyz), given the orientation of the abc axes with respect to the xyz axes. This orientation is conveniently expressed using the Euler angles $(\chi, \theta, \phi) = \Omega$ [11]. Knowing Ω, the 27×27 projection coefficients $U_{ijk:lmn}(\Omega)$ can be determined and applied to obtain per-molecule components of $\boldsymbol{\beta}$ in the xyz frame as follows:

$$\beta_{lmn}(\omega_2, \Omega) = \sum_{l,m,n=a,b,c} U_{ijk:lmn}(\Omega)\beta_{lmn}(\omega_2) \tag{2.7}$$

The resonant portion of Eq. (2.5) is then a summation of the ijk component of hyperpolarizability for all interfacial molecules:

$$\begin{aligned} \sum_{q=1}^{Q} \frac{\chi_{ijk,q}}{\omega_2 - \omega_q + i\Gamma_q} &= \sum_{\text{molecules}} \beta_{ijk}(\omega_2, \Omega) \\ &= N\langle \beta_{ijk}(\omega_2, \Omega) \rangle \\ &= N \int \beta_{ijk}(\omega_2, \Omega) f(\Omega)\, \mathrm{d}\Omega \end{aligned} \tag{2.8}$$

Here, N is the total number of such molecules, $\langle\rangle$ indicates an ensemble average, and $f(\Omega)$ is the probability distribution function of the molecular orientation. θ, the tilt of the molecular c-axis from the surface normal (z axis), is of particular significance because often the molecules at the interface can be assumed to have azimuthal isotropy (randomly distributed in χ and ϕ); in such cases, Ω in Eq. (2.8) can be replaced by θ (we shall assume this in what follows).

Substituting from Eqs. (2.7) and (2.6) in Eq. (2.8) gives

$$\chi_{ijk,q} = N \int \left[\sum_{l,m,n=a,b,c} U_{ijk:lmn}(\theta)\beta_{lmn,q} \right] f(\theta)\, \mathrm{d}\theta \tag{2.9}$$

$f(\theta)$ is usually assumed to be a Gaussian distribution, and clever methods to estimate the above integral have been devised [17]. Equation (2.9) shows the intimate connection between the components of the macroscopic susceptibility tensor, $\boldsymbol{\chi}^{(2)}$, and its molecular counterpart, the microscopic hyperpolarizability tensor, $\boldsymbol{\beta}$, of the molecular species that make up the interface. Herein lies the ability of SFG to determine the orientation of interfacial species; with a knowledge of $\chi_{ijk,q}$ (obtained from SFG spectra), $\beta_{lmn,q}$ (obtained from linear spectroscopies or computational methods), and a solution to Eq. (2.9), it is often possible to determine the tilt of molecular species, θ, at the interface by taking ratios of appropriate $\chi_{ijk,q}$'s, and eliminating N; in some cases, the ratio of $\chi_{ijk,q}$'s is independent of $\beta_{lmn,q}$'s, and it is possible to obtain θ without knowing any $\beta_{lmn,q}$.

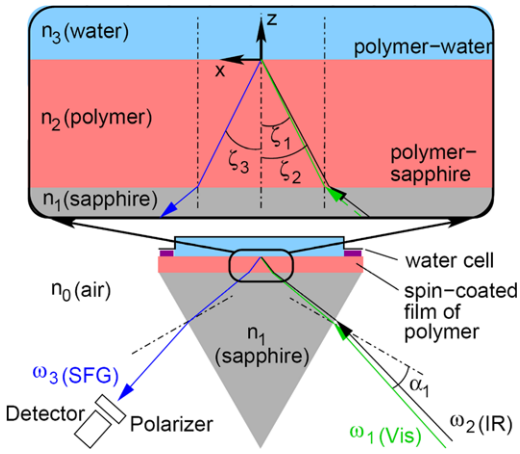

Fig. 2.2 Schematic diagram (not to scale) of a TIR geometry used for SFG of a polymer–polymer interface. The beams of frequencies ω_I have the same meaning as in Fig. 2.1. The mediums of refractive indices n_i are as labeled. The interfaces formed at the boundaries of these mediums are as follows: A and D, sapphire–air; B, polymer 1–sapphire; C, polymer 1–polymer 2. The incident angles (ω_1 and ω_2 beams) and the reflected/refracted angles (ω_3 beam) at these interfaces are denoted by $\phi_{\text{interface}}$

Figure 2.2 shows another commonly used geometry for SFG measurements, called the total-internal-reflection (TIR) geometry; the figure shows an example of a polymer–polymer interface being probed by SFG. Here, one face of an equilateral, sapphire prism has two films of different polymers coated on it. The prism is then mounted on a cell (not shown) of an appropriate construction, and the incoming laser beams (at ω_1 and ω_2) are aligned as shown. The angle α_1 and α_2 are selected so that the incident and reflected angles at the polymer 1–polymer 2 (C) interface—$\zeta_{C,1}$, $\zeta_{C,2}$, $\zeta_{C,3}$—are close to the critical angles for the visible, IR, and SFG frequencies at this interface. This set of ζ_C's greatly enhances the SFG signal from the C interface, while reducing any interfering signal from the polymer 1–sapphire (B) or polymer 2–air (D) interface [18, 19]. Therefore, proper choice of α_A's allows the selective probing of the C interface, but by choosing other values of α_A's, it is possible to selectively probe the B and the D interfaces, too. The setup shown here is for a polymer–polymer interface, but by replacing polymer 2 by a liquid (e.g. water) or gas (e.g. air), the polymer–liquid and polymer–gas interfaces can also be probed by appropriate selection of α_A's. Hence, we can appreciate the versatility of the TIR geometry.

2.2.2 Experimental Set-up and Sample Considerations

The study of silicone surfaces and interfaces requires either spin coating or dip coating a thin film on a solid substrate. The silicone films are cured by one of

the chemistries described below. In external-reflection geometry, the visible and infrared laser beams are incident on the films and the reflected SFG beam is collected (Fig. 2.1) and analyzed. In this external geometry, the SFG signal is generated at two interfaces, polymer-air and polymer-solid interfaces. The separation of the signal from these two interfaces is not trivial and requires solution of the linear and nonlinear Fresnel equations. By using different film thickness it is possible to find a range of film thickness where the SFG signals will be higher for either polymer-air or polymer-solid interfaces. This approach to separate the signals from both the interfaces has been demonstrated using polystyrene films [20]. In general, the signals from the polymer-solid interfaces are weak and are difficult to measure using external-reflection geometry [21]. However, the contributions from the solid interfaces cannot be known without any prior knowledge of the relative strength of the signals from both these interfaces. The use of plasma or UV to destroy or alter the SFG contribution from the polymer-air interface has been also used to confirm the relative contributions to the SFG spectra from both these interfaces [22].

The internal-reflection geometry described in Fig. 2.2 can be used to separate the contributions of the polymer-air and polymer-solid interfaces by changing the incident angle of the laser beams [23]. This geometry involves spin coating or dip coating polymer films on a sapphire prism. As a simple approximation, Snell's law can be used to determine the incident angles where the polymer-air and polymer-solid spectra can be collected. This technique was first demonstrated for polystyrene (PS) films and the orientation of the phenyl groups was shown to be very different for polystyrene in contact with air or sapphire substrate [23]. This approach was further extended to study polymer-polymer and polymer-liquid interfaces [15, 18, 24, 25]. The internal-reflection geometry was also used to study confinement of liquids between polymer in contact with sapphire or other polymer surfaces [26, 27]. The use of this geometry to study friction will be discussed later. The complete model for analyzing SFG spectra in internal-reflection geometry for polymer systems has been published recently [28]. This model highlights the conditions needed to use the internal-reflection geometry to obtain spectra for polymer-air (or liquid) or polymer-solid interfaces.

Both the internal and external geometry for SFG experiments are suitable for kinetic and temperature studies. The sample cells can be heated and the SFG spectra can be collected as a function of time and temperature. This technique has been used to study glass temperatures of thin films [29, 30], melting of molecules at interfaces [23, 31], kinetics of plasma treatment [32], and kinetics of rearrangements at polymer-liquid interfaces [10, 25, 33–35]. The collections of SFG spectra take from 5–20 minutes depending on the laser systems. This restricts the time scale for kinetic measurements. If the changes can be monitored without scanning the whole frequency range and instead can be monitored by changes in the peak intensity, changes on the time scale of seconds can be monitored as a function of time. With recent developments in femtosecond lasers coupled with CCD camera detection systems, the SFG spectra can be collected in milliseconds [36]. SFG is also very well suited to measure long time changes and in some recent work changes on the PDMS surfaces were monitored over a period of years [37].

2.2.3 Simulation

The intensity of the SFG signals can be related to the orientation of the molecules at the interface. Equation (2.9) describes the relationship between the macroscopic susceptibility and the orientation distribution of the molecules at the interface. Therefore, molecular models are often needed to interpret SFG spectra. A variety of known modeling approaches may be utilized depending on the complexity of the problem at hand. For well-defined systems such as self-assembled monolayers, the distribution can be assumed to be a Gaussian function with a very narrow width of tilt angles. One can model the polymer systems also using a Gaussian distribution and the average tilt angles and width of the distribution can be determined from the SFG spectra. However, the definition of the interface is often complicated for liquids and solids. The interface is not atomically flat and interfaces are not one molecular layer thick. Because of these complications, computational modeling and simulations are important complementary tools in understanding the SFG spectra. Naturally, it is important to select a tool that balances computational expense with a suitable level of structural detail at relevant length and time scales. In cases of phenomena such as wetting, interfacial tension, and chain orientation at complex interfaces, more extensive techniques such as molecular dynamics (MD) simulations are needed to ensure proper interpretation of SFG results.

The first comparison of MD and SFG results for polymers was done for PS films in contact with air [38]. The MD results provide information on the orientation and density of molecular units of polymer chains. The cosine average of tilt angle $\langle \cos\theta \rangle$ is important in determining the intensity of the SFG signals. The maximum value is one when all the molecules are oriented at a tilt angle of zero with respect to the surface normal. The value of $\langle \cos\theta \rangle$ is zero when the distribution of tilt angles is random or disordered. The MD simulations of PS showed that the orientation of phenyl groups is random in the center of the film and the symmetry is broken at the interface. The phenyl rings at the surface are facing outwards with tilt angle close to zero. The orientation of the methylene groups of the PS main chains are weaker than that of the phenyl groups and these results are in excellent agreement with the SFG results. The MD also revealed that the SFG signal does not originate from phenyl groups in the immediate vicinity of the surface. Instead the phenyl rings in the region as thick as 1 nm have non-zero $\langle \cos\theta \rangle$ and they also contribute to the SFG signals. In addition, the SFG intensity is proportional to the product of the number density and $\langle \cos\theta \rangle$, and both these quantities are important in determining the strength of the SFG signals.

The MD results for PDMS films on glass substrate clearly showed that there is a break down in symmetry of the methyl groups in contact with air [39, 40]. Because of layering of molecules, using simple Gaussian models is incorrect. One needs to understand the average contributions of all these layers. For PDMS the analysis revealed that the methyl groups next to the solid surface are responsible for the strong SFG signals for PDMS in contact with sapphire coated with self-assembled monolayers. The consequences of these conclusions in the context of friction will be discussed later. The combination of MD and SFG is extremely important in understanding the orientation and density of molecules at complex surfaces or interfaces.

2.2.4 Silicone Cure Systems

Many of the best known applications of silicones, such as sealants, adhesives, coatings and rubbers, involve PDMS in its cross-linked, or 'cured', elastomeric form. The versatility and convenience of organosilicon chemistry is evident in the variety of cross-linking mechanisms (or cure systems) that can be used to convert PDMS and other silicone polymers into solids with the aforementioned unique surface and bulk properties. A more detailed discussion is deferred to references on organosilicon chemistry and silicone rubber technology [1, 41, 42], but we briefly describe two of the most common general curing schemes for PDMS because both the static and dynamic surface properties of silicone elastomers can be influenced by the cure system. Additionally, this serves to denote key functional groups that can be observed by SFG to monitor the effects of surfaces and interfaces on curing reaction kinetics and stoichiometric balance.

First, consider an addition cured PDMS such as the widely studied Sylgard® 184 elastomer. The cross-linking occurs through a hydrosilylation reaction between the elastically active vinyl (Vi) terminated PDMS chain ends with a multifunctional silicon hydride (SiH) cross-linker to form an end-linked network with no leaving groups or by-products. In addition, additives such as fillers, adhesion promoters and cure modifiers may introduce Vi or SiH functional groups to ensure their incorporation into the network.

Hydrosilylation requires a catalyst, typically a Pt or Rh complex, and is accelerated by heat, making it well suited for rapid continuous assembly or coating applications. Hence, this is a very widely used system for curing silicone rubbers and coatings. In this chapter, silicone elastomers can be assumed to be cross-linked by this chemistry unless otherwise noted. The cure rate can be modified by a variety of additives to achieve a desired working time, or pot life, after the various components are combined. However, inadvertent cure inhibition can occur by the presence of certain additives, substrates, or even atmospheres that contain other catalyst-coordinating compounds such as those containing S, P, Sn, or N. Because cross-linkers, catalysts and additives are typically small molecules or oligomers, they are prone to interface segregation resulting in composition gradients near surfaces and interfaces [43, 44]. The consequence of segregation is to alter the effective stoichiometric balance in these regions and the resulting properties. The ability of SFG to detect the infrared spectrum from interfaces makes it a useful tool to track the fate of reactive groups involved in curing or adhesion. Common IR fingerprint regions for functional groups of interest in hydrosilylation curing silicone matrices include SiH (2100–2200 cm^{-1}) and Si-Vi (1600 cm^{-1}), which can be compared against the characteristic C-H stretching from Si-methyl groups on a PDMS backbone (2960 cm^{-1} asymmetric and 2910 cm^{-1} symmetric) [45].

Another common class of cure systems is based upon hydrolysis and condensation of hydrolysable silicone polymers. Variants generally involve combinations of linear polymers capped by either –OH or alkoxysilyl terminal groups that react with cross-linkers that are typically organosilanes multifunctional in alkoxysilane or

other hydrolysable groups capable of undergoing condensation. While many variants exist, the most common condensation cure systems are catalyzed by organotitanium or organotin compounds and are often controlled by the in-diffusion of moisture and out-diffusion of alcohol or acidic leaving groups. In reality, the organometallic compounds are not classic catalysts because they may participate as reactants and are incorporated into the network [46]. These cure systems are commonly utilized to cross-link silicone sealants and caulks used in household and construction applications. In some cases, such as acetoxy-cured sealants that give off the familiar vinegar scent while curing, the reaction is driven forward by the formation and subsequent evaporation of acidic leaving groups on exposure to moisture, requiring relatively low organometallic catalyst loadings. Because cross-linking is typically performed at ambient conditions and is generally slower than heated addition cure systems, concentration gradients can be even larger in condensation cured materials [47–49]. Additionally, both the leaving groups and the unreacted residual groups can have very significant implications on adhesion because of their polarity. Useful IR fingerprints regions for functional groups of interest in condensation curing silicone matrices include Si-O-CH_3 (2830–2850 cm^{-1}), SiOH (broad 3700–3800 cm^{-1} and 3200–3450 cm^{-1}), and for acetoxy-cured silicones, –C=O (1750 cm^{-1}) [45].

2.3 Applications of SFG to Silicone Surfaces and Interfaces

2.3.1 Silicone Surface Orientation and Rearrangement

A number of unique surface properties of siloxanes are often attributed to the unusual backbone flexibility and mobility of their polymer chains. PDMS surfaces are often reported to be quite dynamic, and terms such as rearrangement, restructuring, reorganization or hydrophobic recovery are used to describe these changes with limited insights to the mechanisms and underlying chain conformations. Highlighted below are examples where SFG has been used to probe these effects at the molecular level.

2.3.1.1 Silicone/Air and Silicone/Water Interfaces

The siloxane backbone is very flexible, and the glass temperature of high molecular weight PDMS is typically observed near 150 K. The flexibility of PDMS chains can result in two potential conformations and could either expose methyl groups at the surface or more polar oxygen atoms. The low surface energy of PDMS surface could favor either of these two conformations because the methyl groups could face the air interface. However, PDMS also shows unusually high water contact angles that are very stable with time. Because the chains are very flexible and mobile they could potentially restructure to expose the more polar oxygen groups at the PDMS-water

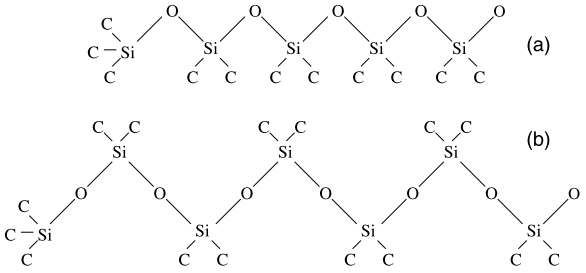

Fig. 2.3 A schematic showing the two possible orientations of PDMS chains. Hydrogen atoms are not shown for clarity. Reprinted from Ref. [39] with kind permission of © The American Institute of Physics (2003)

interface, as shown in Fig. 2.3(a). However, the stable high water contact angles suggest that the structure in Fig. 2.3(b) is more preferred. The Si-O-Si bonds are not planar as suggested in this two-dimensional picture and the structure (b) provides the least steric constraints in packing of the bulky methyl groups. The molecular dynamics simulation results show that the methyl groups cover the surface of PDMS in contact with air [39]. In contact with water, the simulation results show sharpening of the orientation of the methyl groups [50]. While subtle changes in orientation, such as 'flattening' of the average methyl group bond angle away from water surface have been reported experimentally [51], no large scale cooperative reorganization events such as the complete inversion of structure as shown in Fig. 2.3(a) were observed in the simulations. This explains the stable water contact angles even though the chains are flexible and have the mobility to restructure and adopt different conformations. Other observations of dynamic contact angle changes of PDMS/water are attributed to chemical changes from process by-products [52] or side reactions involving small numbers of reactive groups such as cross-linker molecules [53]. The simulation results also showed a small amount of hydrogen bonding between water and silicon atoms. These simulation results are consistent with the SFG results that show methyl groups at the PDMS-air [40], PDMS-water [51], and also PDMS in contact with polymer surfaces [54, 55]. We note that the presence of methyl groups of PDMS at the water interface has important consequences in adhesion of cells, bacteria, and biocompatibility [56, 57].

2.3.1.2 High Energy Surface Treatment Effects

Various forms of high energy treatment of PDMS are often used to render PDMS surfaces more hydrophilic for applications in microfluidics, bioengineering and lithography. The most common of these surface treatment methods are based upon exposure to various types of plasma, long wavelength ultraviolet (UV) or short wavelength UV-ozone (UVO) sources (see also Chap. 3). All three methods have been studied by a variety of conventional surface analytical techniques that indicate that under appropriate exposure conditions, the exposed silicone surface is oxidized to various extents into a silsesquioxane or silicate layer through a complex set of potential free radical- and anion- promoted oxidation mechanisms [2, 58–62]. However, optimization of these techniques is largely empirical because of limited understanding of the physico-chemical processes at the surface and near-surface regions. Additionally, these treated surfaces are often reported to be time dependent,

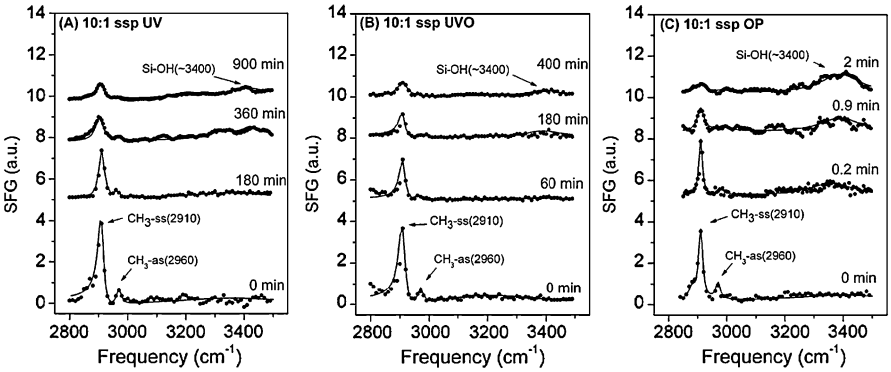

Fig. 2.4 SFG spectra showing surface chemical changes of Sylgard® 184 silicone elastomer induced by various exposure times to (**A**) UV, (**B**) UV-ozone and (**C**) oxygen plasma treatments. Reprinted from Ref. [58] with kind permission of © The American Chemical Society (1996)

with contact angles that can rapidly increase with aging time in air after the treatment, a phenomenon called hydrophobic recovery. Many studies indicate that this recovery originates from migration of low surface energy siloxane oligomers that are created by chain scission of PDMS [2]. This effect can obscure the interpretation of data from post-mortem techniques that cannot be conducted in situ or under ambient conditions. Hence, the surface sensitivity and relatively rapid acquisition in ambient conditions make SFG an excellent complement to develop the better mechanistic understanding needed to optimize these methods. Ye et al. used SFG to study the effects of treatment time by oxygen plasma (OP), UV and UVO treatments on Sylgard® 184 prepared at two different crosslinking stoichiometries (10:1 vs. 4:1 base to curing agent mix ratios) [58]. In the case of UV and UVO, the SFG spectra were obtained in situ. All three techniques resulted in a decrease in $–CH_3$ and $–CH_2–$ groups, and the formation of Si–OH groups, which is consistent with increased hydrophilicity caused by silicate formation (Fig. 2.4). The loss of surface $–CH_3$ groups was reported to follow first order kinetics, with OP providing the fastest response, followed by UVO and UV. The OP also resulted in virtually complete removal of $–CH_3$ within 2 min, unlike UVO and UV. The persistence of residual $–CH_3$ at the surface is consistent with a higher proportion of radical-based chain scission events in the UV techniques. Such experiments illustrate the power of SFG to provide mechanistic insights needed for more precise surface modification by high energy techniques

2.3.2 Friction and Lubrication

Mechanical contact between two soft solids, particularly polymers, is of fundamental importance in the areas of friction, adhesion, and contact mechanics. Although there have been numerous studies on measurements of adhesion and friction using

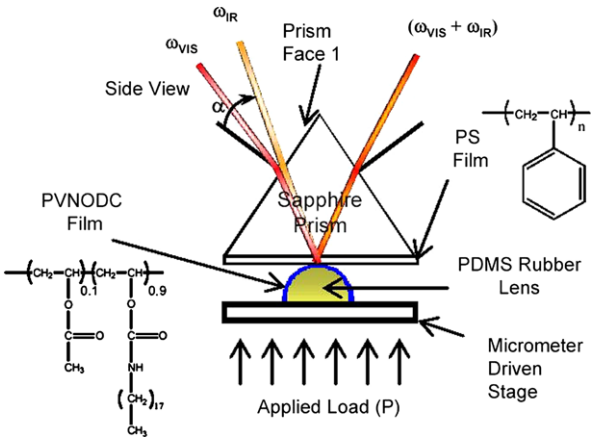

Fig. 2.5 Schematic of the experimental geometry used to probe the mechanically formed contact interface between two polymer surfaces using TIR-SFG. One polymer film is coated on the sapphire surface and the other on top of a deformable elastomeric lens. In this case, the lens is coated with poly(vinyl *n*-octadecyl carbamate-co-vinyl acetate) (PVNODC). Reprinted from Ref. [63] with kind permission of © Taylor & Francis Group (2005)

macroscopic and microscopic contact areas, there have been no direct measurements of interfacial structure during mechanical contact between two polymer surfaces. In order to understand adhesion hysteresis, friction, and mechanisms of energy dissipation at interfaces, it is important to study the structure of polymer surfaces upon mechanical contact.

2.3.2.1 Probing Contact Interfaces

SFG in internal-reflection geometry was used to directly probe the contact interface between an elastomeric lens and a solid surface [63]. The soft elastomeric semispherical PDMS lens provides a uniform and smooth contact area for studying friction and adhesion in conjunction with SFG (Fig. 2.5). The size of the contact area can be easily controlled by varying the normal force and the radius of curvature of the PDMS lens. Moreover, by depositing films of different polymers on the elastomeric lens, this geometry can be used to study the interface between many different polymers and can be easily adapted to incorporate in situ friction and adhesion force measurements. The usefulness of this geometry was first demonstrated by studying the mechanical contact of a comb polymer with PS films [63]. The structure of the interface upon mechanical contact was very different from the interface after annealing.

The ability of SFG to study the contact or buried interfaces was used to study PDMS in contact with solid surfaces [40]. Figure 2.6 shows SFG spectra in SSP polarization for various PDMS surfaces in contact with sapphire or sapphire surfaces coated with hydrophobic self-assembled monolayers. Figures 2.6A and 2.6B are SFG spectra for octadecyltrichlorosilane (OTS) and crosslinked-PDMS surfaces before contact. No differences in the SFG spectra were observed for crosslinked and oligomeric PDMS surfaces. Figure 2.6A is a typical spectrum for a well-packed OTS monolayer with ordered methyl groups. The methylene peaks are absent for an all-trans conformation. In Fig. 2.6B, the two main peaks are assigned to the

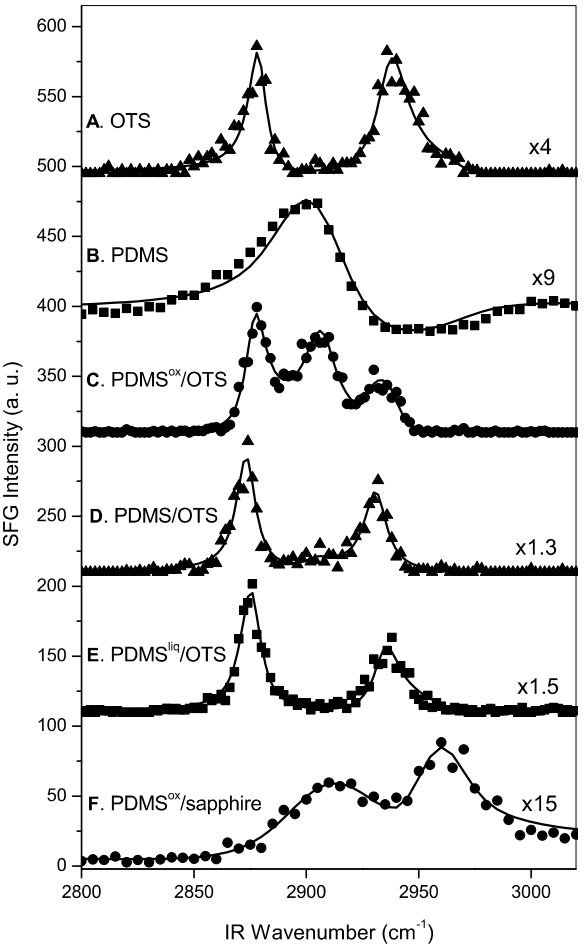

Fig. 2.6 SFG spectra of (**A**), OTS; (**B**), PDMS; (**C**), PDMSox/OTS; (**D**), PDMS/OTS; (**E**), PDMSliq/OTS; and (**F**), PDMSox/sapphire. The *solid lines* are fits to the square of the sum of the Lorentzian functions Eq. (2.1). (**B**) and (**F**) are taken with a broader wavenumber resolution (full width half maximum (fwhm) ~20 cm^{-1}) to improve the signal-to-noise ratio. The SFG spectra were offset along *y*-axis by an arbitrary amount and were scaled for clarity. In (**C**) and (**D**) for OTS, the methyl Fermi band is slightly red shifted and the ratio of the symmetric methyl and methyl Fermi intensity has changed upon contact. This effect is reversible as the spectra before and after contact are indistinguishable. Reprinted from Ref. [40] with kind permission of © The American Chemical Society (2005)

methyl groups bonded to silicon (symmetric vibration at 2906 cm^{-1} and asymmetric vibration at 2962 cm^{-1}). In the case of PDMS surface treated with short oxygen plasma treatment (PDMSox), the oxygen plasma treatment oxidizes the surface and the SFG spectrum from 2800–3200 cm^{-1} does not have any resolvable features. Figure 2.6C shows the spectrum for PDMSox-OTS interface. The silicone methyl peak is extremely strong at this interface. Since the PDMSox surface before contact has no methyl peaks, this indicates a significant interfacial reconstruction. The presence of PDMS chains after interfacial reconstruction is also evident in the adhesion experiments that show reduced hysteresis. For the PDMSox/OTS contact, once the highest load is reached the reconstruction is completed and the unloading proceeds with an equilibrium interface. The strain energy release rate on unloading is equal to 43 mJ/m^2. This value is similar to that expected for the thermodynamic work of adhesion, which between PDMS and OTS is around 40–45 mJ/m^2. These adhesion measurements of PDMS/OTS and PDMSox/OTS are consistent with the SFG

results. A strong adhesion and adhesion hysteresis is observed for PDMS/sapphire contact due to the formation of hydrogen bonds between the hydroxyl and silicon groups. The adhesion hysteresis decreases significantly at the PDMSox/sapphire interface due to the enrichment of the interface in low molecular weight PDMS chains, thus forming a weak boundary layer (less energy dissipation due to reduced chain pull-out). Consequently, based on the adhesion results, the PDMSox/sapphire interface has reconstructed with the diffusion of short PDMS chains.

2.3.2.2 Long term Aging Effects

PDMS is widely used as a model elastomer to study adhesion and friction. Because of the robustness of the platinum catalyst used for crosslinking, hydrophobicity, transparency, and nanometer-smooth surfaces, it is used in the areas of soft lithography, release coatings, biomaterial, and medical implants. However, it was shown recently by Kurian et al. [37] that the surface of PDMS is not stable with time. The friction and adhesion of PDMS lenses in contact with a glassy methacrylate polymers, showed an unusually high adhesion hysteresis and friction for PDMS lenses that were stored for an extended period of time (aged lenses) as compared to those that were prepared and used within a week (fresh lenses). This effect was very reproducible, and these results could not be explained by contamination of the lenses during storage or by the generation and segregation of short oligomeric PDMS chains upon aging. Additionally, the authors did not observe any differences between the aged and fresh samples using x-ray photoelectron spectroscopy (XPS) and contact angle measurements.

To understand the effect of aging, Kurian et al. [37] studied the contact interface between PDMS lenses and poly(*n*-propyl methacrylate) (PPMA)-coated sapphire prisms using the SFG spectroscopy in the TIR geometry. They observed no differences between the aged and unaged lenses at the PDMS/PPMA interface in static contact, even though there were striking differences in adhesion and friction properties. Interestingly, the biggest differences were observed only after sliding PDMS lenses on the PPMA-coated surface. The SFG intensity of the PDMS Si-CH_3 symmetric peak increases by almost three orders of magnitude upon sliding the aged lens on the PPMA (Fig. 2.7). This dramatic increase in SFG signal could only be due to alignment of PDMS chains at the contact interface. These measurements were conducted on aged lenses after extracting them in toluene to remove the short oligomeric chains and this ruled out the possibilities of short oligomeric chains affecting the SFG results. The nearly identical nature of the surface of aged and unaged lenses suggests that the differences due to aging are very subtle and indistinguishable in a static contact. The authors postulated that aging results in chain scission that disrupts the cross-linking and increases the density of the surface anchored chains with one free end. These surface anchored chains are stretched during sliding as postulated by the earlier theories in the area of rubber friction by Schallamach [64]. The authors also postulated that the stretching of chains also leads to

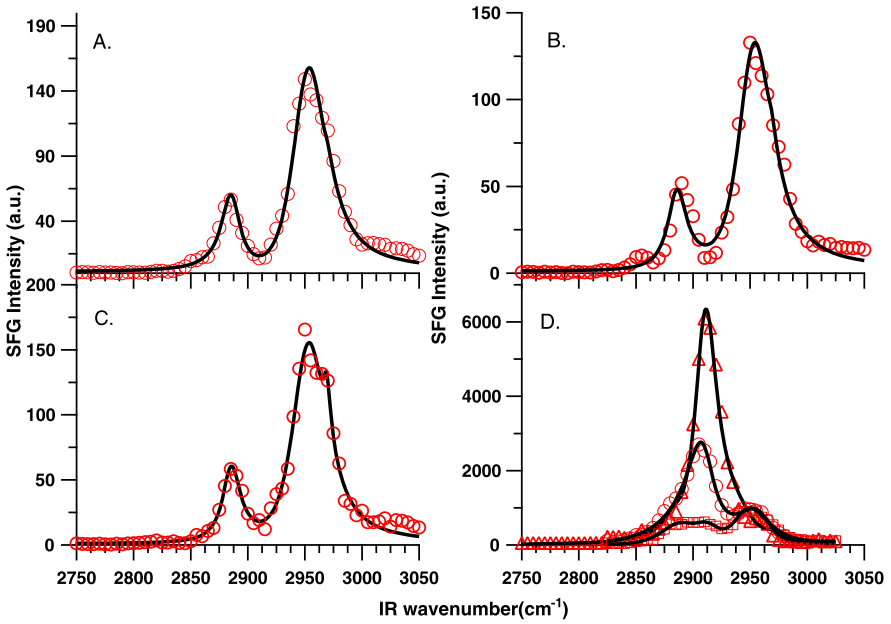

Fig. 2.7 SFG spectra in SSP polarization of a fresh PDMS lens/PPMA interface in contact (**A**) and after sliding (**B**). The spectrum remains unchanged for fresh lens after friction experiment. SFG spectra of aged lens/PPMA interface in contact (**C**, 18 month aged lens) and after sliding (**D**, aging time: 4 months (*box*), 8 months (O), and 18 months (*triangle*)). The data for 4 and 8 months in (**D**) are scaled by 7 times for clarity. The solid lines are the fits to the data using a Lorentzian equation. Significant enhancement in 2910 cm^{-1} peak, as a function of aging time, is observed upon sliding of aged PDMS lens. Reprinted from Ref. [37] with kind permission of ©The American Chemical Society (2010)

ordering of these molecules at the interface. Interestingly, the ordering is not permanent and the surface structure relaxes after stopping the sliding. These relaxation time constants are much higher than those expected based on bulk viscosity.

2.3.2.3 Probing Acid-Base Interactions

The molecular interactions at interfaces govern the wetting, adhesion, friction, chemical reactions, and many other material and biological phenomena at interfaces. Techniques such as heat of mixing in dilute solutions are employed to determine the strength of the donor–acceptor interactions. Kurian et al. [65] have used SFG to directly determine the strength of the donor-acceptor interactions by probing the shift in the vibrational peaks at buried interfaces. The authors have demonstrated the application of this spectroscopic technique to determine the interaction energies of various polar and nonpolar polymers in contact with the sapphire substrate. Because SFG does not require dilute solutions or the use of common solvents, it is widely applicable for determining interaction energies for many other solid–solid interfaces

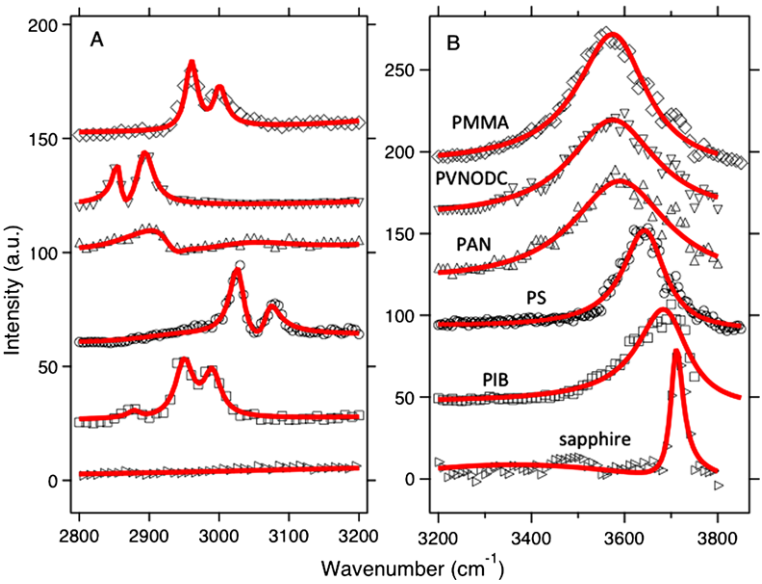

Fig. 2.8 (**A**) SFG spectra of hydrocarbon region for interface of sapphire with air (*right triangle*), PIB (*box*), PS (*circles*), PAN (*triangle-up*), PVNODC (*triangle-down*), and PMMA (*diamond*). (**B**) Hydroxyl region interfacial SFG spectra for the interfaces reported in (**A**). All the spectra were collected at room temperature using P-polarized input and SFG beams. The *solid lines* in (**A**) and (**B**) are the fits using the Lorentzian equation. Reprinted from Ref. [65] with kind permission of © The American Chemical Society (2010)

that are important in the areas of adhesion, tribology and wetting. The application of this direct spectroscopic technique to determine the interaction energies of various polar and nonpolar polymers in contact with the sapphire substrate was demonstrated. The SFG spectra in PPP polarization for these polymers in contact with the sapphire substrate are shown in Fig. 2.8. The interaction energies determined from the shift do not correlate with water-contact angles which clearly demonstrates the importance of molecular rearrangement in contact with the sapphire substrate. For example, the octadecyl side chain polymer poly(vinyl *n*-octadecyl carbamate–co–vinyl acetate) (PVNODC) exhibits a very high water contact angle (110°, similar to polyisobutylene (PIB)). However, the interaction energies of PVNODC with the sapphire substrate are closer to the ester interaction of poly(methyl methacrylate) (PMMA). These differences are due to the molecular rearrangement of the octadecyl side chains in contact with the sapphire substrate which increases the interactions of the polar groups (carbonyl or N–H) with the surface OH. This rearrangement is also observed in the differences in the orientation of the methyl and methylene groups. Another interesting example is that of poly(acrylonitrile) (PAN) in contact with sapphire. Even though PAN has the lowest water contact angle (60°) among the five polymers studied, the interaction energies are not as high as PMMA (water contact angle of 73°). This is due to the strong affinity between the CN–CN groups (within the polymer) compared to the CN-surface OH interactions. Lachat et al.

have also observed a shift in the CN peak due to the interactions of the CN group with the surface OH groups [34]. PIB is the most hydrophobic polymer Kurian et al. [65] have studied and the small red shift of 30 cm^{-1} is similar to that of sapphire in contact with nonpolar pentadecane. PS is in between the more polar PMMA and PIB due to the interaction of the phenyl groups with the sapphire substrate. While silicone systems were not studied in this work, the technique to determine subtle non-covalent molecular interactions such as acid-base interactions has obvious relevance for better understanding of interfacial contributions to silicone lubrication, release and adhesion.

2.3.2.4 SFG Studies of Lubricated Sliding

Liquids confined between two solid surfaces are important in understanding friction and wear of lubricated surfaces. Tires on roads, windshield wipers, movements of human joints are some examples where flexible-rigid contact interfaces are experienced. There has been a long standing discussion on whether the structure of liquids confined between two surfaces is different from that in the bulk. Experiments by Robert and Tabor using rubber lenses in contact with glass substrates concluded that the bulk viscosity of confined liquids were similar to those in the bulk for thicknesses as small as 25 nm [66]. Due to surface roughness, Tabor's experiments were inconclusive for a thickness less than 25 nm. Using atomically smooth mica surfaces, Israelachvili and coworkers have studied nanometer thin films and have shown that oscillatory force profiles are observed for a variety of liquids due to layering of molecules under confinement [67]. These results are supported by results from computer simulations. As a consequence of layering, the Newtonian liquids show solid-like response under confinement. Nanjundiah et al. studied confinement effects of small linear alkanes trapped between PDMS and sapphire substrate using SFG [26]. This novel approach of using flexible elastomeric lenses that deform against flat solid surfaces to confine molecules offsets the need to have perfectly parallel surfaces.

Nanjundiah et al. [26] measured the SFG spectra of confined hexadecane and pentadecane above and below the bulk melting points (Fig. 2.9). The SFG spectra upon confinement are different from unconfined hexadecane and pentadecane in contact with sapphire substrate. The confinement-induced ordering can be inferred from the higher SFG signals (3 times higher than liquid spectra), and the presence of methyl symmetric mode and weak methylene symmetric mode. Both the confined and bulk pentadecane liquid spectra have strong methyl asymmetric signals, which indicates methyl groups are on average tilted with respect to the surface normal. Pentadecane confined crystal/sapphire interface is dominated by the presence of a strong methylene symmetric peak at 2840 cm^{-1} along with the methyl symmetric and methyl Fermi resonance modes. The SFG intensity for confined pentadecane crystal is higher than that of confined pentadecane/sapphire interface. The presence of strong methylene symmetric mode is surprising and suggests that the structure of the confined crystal structure is very different from bulk pentadecane

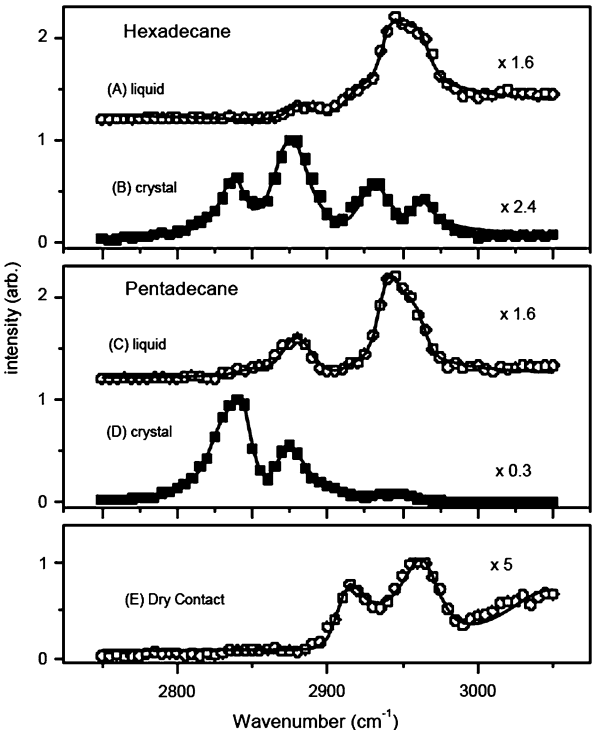

Fig. 2.9 SFG (SSP) spectra of hexadecane (**A**) and pentadecane (**C**) confined liquid/sapphire interfaces at 295 K. The SSP spectra for confined hexadecane (**B**) and pentadecane (**D**) crystal/sapphire interfaces were taken at 287 and 279 K, respectively. The dry PDMS/sapphire SFG spectrum is shown in (**E**). Reprinted from Ref. [26] with kind permission of © The American Physical Society (2005)

crystal/sapphire interface. The strong methylene intensity in confined crystal cannot be accounted for by the presence of gauche defects as in the case of liquid alkane/sapphire interfaces. Nanjundiah et al. [26], with the help of a simple model, postulated that the confined pentadecane chains are crystallizing with the chains lying flat next to the sapphire substrate. These results have important implications in our understanding of friction and lubrication in confined geometry.

Nanjundiah et al. [27] showed that the confinement of water between PDMS and sapphire substrate was very different from that of alkanes. The sliding of the PDMS lens in the presence of water shows lower friction than dry sliding. The frictional forces for wet sliding were much higher than those expected for lubricated sliding. The authors proposed that the water is not expelled from the contact spot with regions where the PDMS is in direct contact with the sapphire substrate which can explain the higher friction coefficient than that expected from lubricated contact. Roberts and Tabor have also observed higher friction for a rubber sliding on a glass surface in the presence of water [66]. They concluded that the higher friction was due to asperity contact rather than higher viscosity of confined water, as depicted in Fig. 2.10. The SFG results agree with the hypothesis of the PDMS sliding on wet sapphire surface with asperity contacts. The asperity contacts are where the PDMS methyl groups are coming in direct contact with the surface hydroxyls on the sapphire substrate.

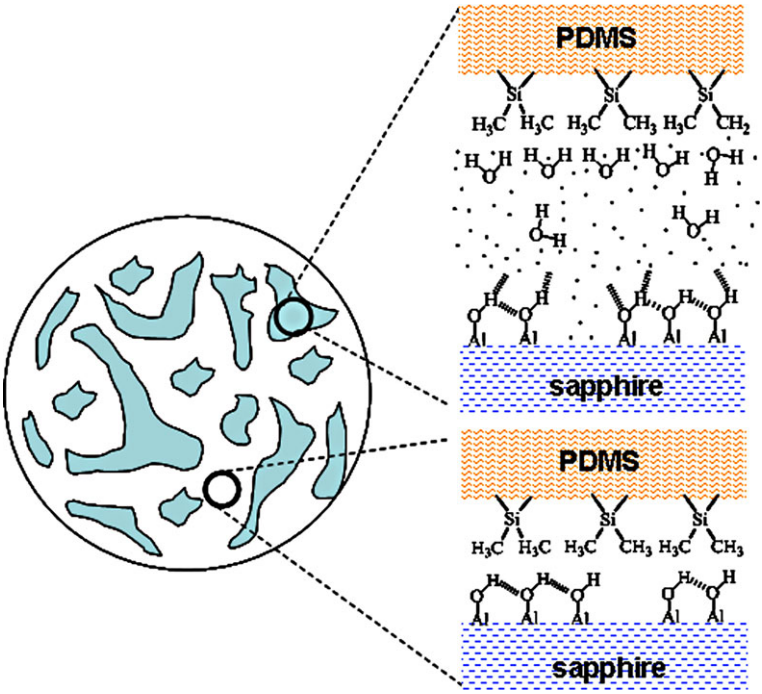

Fig. 2.10 A sketch of the contact region formed between the PDMS lens and the sapphire surface in the presence of confined water. A tentative physical picture of the molecular structure in these two types of contact region are also shown on the right. The relative size of those two regions cannot be quantified from these results and the area and size selected in the sketch are only for visual aid. Reprinted from Ref. [27] with kind permission of © The American Institute of Physics (2009)

2.3.3 Adhesion

Pressure-sensitive adhesives (PSAs) and release coatings differ considerably from curable adhesives and sealants in their mechanism of adhesion. Therefore, we present these topics separately. A key difference is that PSA materials rely upon non-covalent interactions across the interface that are coupled multiplicatively by bulk energy dissipation mechanisms to give the measured adhesion or release profile. Mathematically, this can be expressed concisely for any type of elastomeric adhesive by the following empirical relationship based upon the form proposed first by Gent and Schulz [68, 69]:

$$\mathcal{G} = W\left[1 + \Phi(a_T v)\right] \tag{2.10}$$

Here, $\mathcal{G}$ is the energy release rate, the practical adhesion energy measured by some adhesion or release test, W is the thermodynamic work of adhesion, and Φ is a bulk viscoelastic loss function which is dependent on the crack growth velocity (v), which is in turn governed by the rate of testing, reduced by the Williams–Landel–

Ferry (WLF) shift factor for time-temperature superposition (a_T) [70].[2] For our purposes this empirical relation captures the essential physics of practical adhesion, the key feature being the multiplicative interplay of W and Φ. It is important to emphasize that Φ is usually the dominant term with most elastomers, often causing $\mathcal{G}$ to be many orders of magnitude larger than W. However, this can only be so when W is sufficiently high that the mechanisms of bulk dissipation can be invoked to raise the product to an appreciable value, a fact that is borne out mathematically in the limit where W approaches zero. In other words, no matter how optimally "lossy" the bulk properties of the adhesive are, this cannot overcome an inherently weak interface; adhesion always starts with the interface. As shown by the aforementioned recent studies of acid-base interactions [65], SFG allows one to study both non-covalent and covalent interfacial interactions responsible for W.

2.3.3.1 Pressure-sensitive Adhesion and Non-covalently Bonded Interfaces

To this point commercial silicone pressure-sensitive adhesives and release coatings have not been studied by SFG. However, Roan has used SFG to gain insights on the interfacial segregation of certain functional groups in hydrocarbon-resin tackified acrylic PSA's [71]. Further, as discussed in the preceding section, SFG has been coupled with the interfacially sensitive Johnson, Kendall and Roberts (JKR) adhesion test method (see also Chap. 1) to probe the origins of adhesion hysteresis in contact interfaces between surface-modified PDMS elastomers and solid substrates, which is fundamentally relevant to mechanisms of adhesion and release [40]. It is noteworthy that the hydrosilylation cure chemistry used for cross-linking the lenses is the relevant system for both silicone PSAs and release coatings, the majority of which are addition cured. Therefore, significant opportunities remain to enhance current state of understanding of silicone release coatings and PSAs that is based largely on bulk measurements [72–74] by using SFG to study interface structure and composition.

2.3.3.2 Curable Adhesives and Reactive Interfaces

Curable silicone adhesives differ considerably from PSAs in that they are dispensed in place as an uncured, flowable composition that undergoes one or more reactions to crosslink into a gelled solid with adhesion to the substrate. Examples of curable silicone adhesives range from moisture-cured construction sealants and caulks to heat-cured adhesives for microelectronics or medical devices. These applications typically require durable, irreversible adhesion to the substrate that preferably develops simultaneously during the curing process through chemical coupling reactions with the substrate surface. While primers or surface pre-treatments may be used, it is generally more desirable to use a self-priming, or primerless, adhesive to eliminate

[2] Although Eq. (2.10) is valid only at thermodynamic equilibrium, it can be generalized to accommodate non-equilibrium conditions by substituting for W some inherent value of adhesion G_o usually regarded as rate-independent.

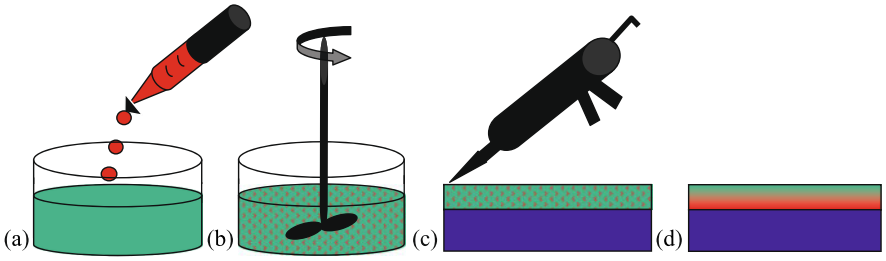

Fig. 2.11 Idealized representation of key steps in the preparation of a self-priming adhesive: (**a**) addition of adhesion promoter (*red*) to a curable silicone elastomer formulation (*green*), (**b**) mixing of the formulation, (**c**) dispensing of the adhesive onto a substrate (*blue*), and (**d**) curing of the adhesive in which the adhesion promoter migrates to the substrate interface

the additional time and cost associated with pre-treatment. In essence, the ideal adhesive is one in which a low concentration of adhesion promoters is homogeneously blended into the uncured silicone composition but selectively migrates to the substrate interface during the curing process to effectively form a primer layer in situ, as depicted in Fig. 2.11.

In some cases, the coupling chemistry may involve the same groups as crosslinking, but often the reactions must be completely different to accommodate different types of substrate. Because of the drastic change in physical properties that occur and the complex array of competing reaction-diffusion events that ultimately determine the interface structure and composition, the mechanisms of adhesion are difficult to ascertain. In cases where strong adhesion develops, the interface by definition cannot be separated readily for study by conventional surface analytical techniques. Hence, the molecular sensitivity and ability of SFG to study buried interfaces nondestructively has motivated several SFG studies of curable silicone adhesives.

2.3.3.2.1 Silane Orientation at Amorphous Polymer Interfaces

Perhaps the most common class of adhesion promoters, or coupling agents, for self-adherent curable adhesives is the alkoxysilanes [75]. These react under mild conditions with a variety of substrates and do not generally interfere with Pt cure catalysts. Despite their wide use, there remain many unanswered questions regarding their mechanisms of adhesion, particularly to plastics and other non-metallic substrates lacking an obvious reactive site. Chen et al. took the first step in understanding such effects by studying the orientation of neat silane coupling agents in contact with various plastics [76]. Both the nature of the tri-functional silane 'headgroup' (trimethoxysilyl vs. trichlorosilyl) and the organo-functional tail (octadecyl vs. aminopropyl), and their resulting interactions with the polymer substrates, were found to profoundly influence the interfacial orientation of the coupling agents on PS or PMMA substrates. To eliminate background signals from the substrates, they used deuterated PS (d-PS) and PMMA (d-PMMA) to study the silane orientation, and saw large spectral differences (Fig. 2.12a) that could be interpreted qualitatively by the schematics in Fig. 2.12b.

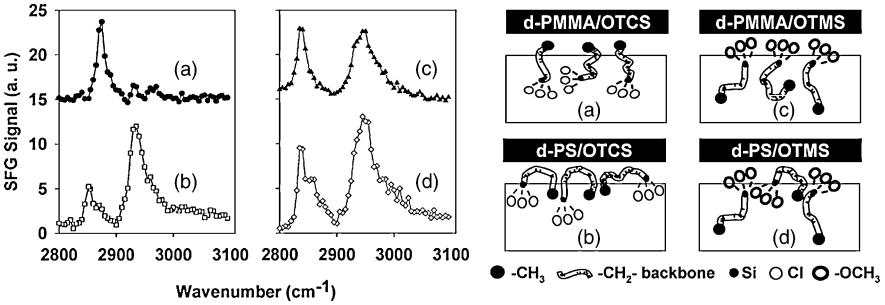

Fig. 2.12 (*Left*) Summaries of SFG spectra (SSP) collected from various polymer/silane interfaces: (**a**) d-PMMA/octadecyltrichlorosilane, (**b**) d-PS/ octadecyltrichlorosilane, (**c**) d-PMMA/octadecyltrimethoxysilane, (**d**) d-PS/octadecyltrimethoxysilane. (*Right*) Corresponding schematic representations of silane orientation deduced from these spectra. Reprinted from Ref. [76] with kind permission of ©The American Chemical Society (2003)

Chen et al. [76] also studied the response of the non-deuterated PMMA side of the interface. By monitoring the 2955 cm^{-1} peak signal characteristic of the symmetric stretch of the ester methyl group of PMMA, they found that exposure to the aminopropyltrimethoxysilane (ATMS) caused a time-dependent loss of signal that indicated a complete loss of interfacial order after about 100 s of contact. In contrast, the PMMA interfaces with octadecyl trichlorosilane (OCTS) and octacdecyltrimethoxysilane (OTMS) retained a stable, finite signal after initial exposure.

2.3.3.2.2 Aminosilane Diffusion into Polymer Films

Further studies of the dynamics of aminosilane/PMMA interfaces by Chen et al. confirmed that the transient loss of SFG signal was due to diffusion of the silane into the polymer substrate [77]. By testing against d-PMMA films of different thicknesses, they were able to use SFG to monitor the structure of the silane diffusion front and estimate a diffusion coefficient of approximately 4×10^{-13} $cm^2\,s^{-1}$, several orders of magnitude smaller than most other small molecules (Fig. 2.13). Further, they observed rapid diffusion of the aminosilane into PS thin films in a bilayer experiment. This experiment demonstrates the power of SFG to simultaneously study both the structure and dynamics of very slow diffusional processes that would be very difficult and time consuming to study by conventional means such as attenuated total reflectance infrared (ATR-IR) spectroscopy. Such a technique could be further exploited to understand the interplay between the diffusional processes that control interfacial self-assembly of coupling agents and any concurrent bulk and interfacial reactions, and may yield new mechanistic insights on penetrant/polymer interactions.

2.3.3.2.3 Silane Adhesion Promoters for Pt-Cured Silicone Elastomers

Because of their effectiveness as penetrants into glassy polymer surfaces and fast reactivity with moisture, aminosilanes can serve as effective adhesion promoters

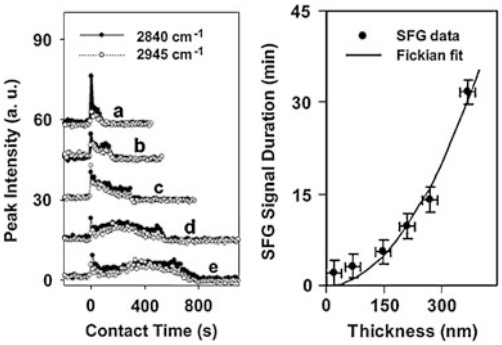

Fig. 2.13 (*Left*) Time-dependent SFG peak intensities (SSP) at 2840 and 2945 cm^{-1} that follow the diffusion of N-(2-aminoethyl)-3-aminopropyltrimethoxysilane through d-PMMA films of thicknesses (**a**) 20, (**b**) 70, (**c**) 150, (**d**) 210 and (**e**) 269 nm. (*Right*) SFG signal duration vs. film thickness showing the fit of a Fickian diffusion model. Reprinted from Ref. [77] with kind permission of © The American Chemical Society (2004)

in moisture-cured silicone sealants and adhesives. Unfortunately, amine groups are known to inhibit the Pt-catalyzed hydrosilylation crosslinking reactions commonly used for heat-cured silicone elastomers such as Sylgard® 184. Such addition cured materials are preferred in fast assembly processes that require a fast controllable cure with no volatile products, such as found in potting and lid sealing of automotive electronic modules or in the attachment of dies and heat sinks on microprocessors. A more commonly used system for promoting adhesion in Pt-cured elastomers utilizes a combination of 3-glycidoxypropyltrimethoxysilane (γ-GPS) and a methylvinylsiloxane diol oligomer (MVS) [78, 79]. Just 1–3 wt.% of this combination of additives mixed into a silicone elastomer can enable good primerless adhesion to a variety of metals and some polar plastics found in electronics applications such as polyesters or FR-4 fiberglass-epoxy composites used in circuit boards when cured at a suitable temperature. Recent studies with this system serve to further illustrate how SFG can be used to shed light and advance fundamental understanding of important and complex problems in adhesion promotion.

The general design concept behind such adhesion-promoting systems combines the reactivity of the γ-GPS to various substrates with the ability of the MVS to couple to the curing silicone elastomer through hydrosilylation of the pendant vinyl groups, and to the γ-GPS through condensation of the silanol ends with the alkoxysilane headgroup of γ-GPS by the following scheme: –SiOH (MVS) + –SiOR (γ-GPS) → –Si–O–Si– + ROH. However, because of the number of potential competing reactions among the additives, substrate and matrix, and the limited sensitivity of conventional surface analytical techniques to study small concentrations of silane additives against a strong bulk siloxane background, further detailed mechanistic understanding of bonding is limited. For instance, one can question whether epoxy ring opening is necessary for adhesion, or whether it merely serves as a driver for interfacial segregation of the γ-GPS through limiting the miscibility of GPS in the PDMS matrix. A number of studies of silane coupling agents on porous surfaces suggest that an interpenetrating resinous silsesquioxane network

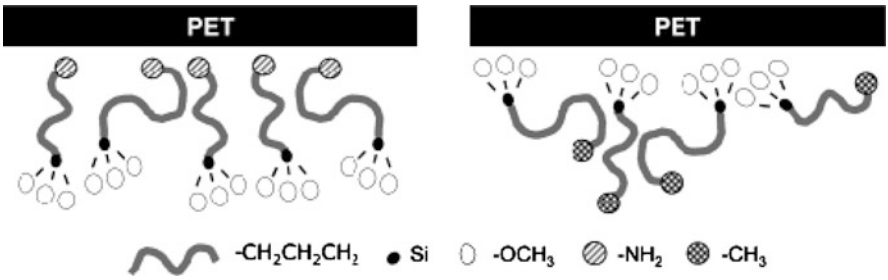

Fig. 2.14 Schematic representations of the conformations of the silane molecules at the PET/ATMS (*left*) and PET/BTMS (*right*) interfaces. Reprinted from Ref. [83] with kind permission of © The American Chemical Society (2004)

can form at the adhesive/substrate interface, or more appropriately 'interphase', as the result of diffusion into the substrate surface followed by auto-condensation of the silane headgroups [80, 81]. Of course, this can only occur in cases where the substrate is sufficiently porous or penetrable by the silanes. For amorphous glassy polymers such as PS or PMMA, SFG studies by Loch et al. indicate that significant diffusion of γ-GPS can occur, to the point where the thin films are, respectively, swollen or altogether dissolved, within an hour of ambient exposure [82].

2.3.3.2.4 H-Bonding Between Silane Adhesion Prometers and Polar Substrates

Many commercially important engineering plastics such as polyesters and polyamides are semi-crystalline and therefore less penetrable by adhesion promoters, presenting more stringent challenges to primerless adhesion. In studies using polyethylene terephthalate (PET) thin films as a model semi-crystalline substrate, Loch et al. observed the formation of stable interface signals between PET and aminopropyltrimethoxysilane (ATMS) and butyltrimethoxysilane (BTMS) due to the absence of silane diffusion [83]. A substantial shift in the –C=O peak stretch of PET at the PET/ATMS interface (1715 cm^{-1}) relative to its original position of 1725 cm^{-1} at the PET/air, PET/γ-GPS and PET/BTMS interfaces gave direct evidence of hydrogen bonding between PET and the $–NH_2$ tail of ATMS. Further, by preparing PET films on a fused silica substrate with a nonresonant TiO_2 interlayer, they compared the interface signals from the PET/ATMS surface against the PET/BTMS and deduced that ATMS oriented strongly to maximize favorable contacts between the $–NH_2$ tail and the PET surface, in contrast to BTMS which takes on an opposite net orientation at the PET surface (Fig. 2.14).

2.3.3.2.5 Adhesion Promoter Segregation

The aforementioned adhesion-promoting mixtures of γ-GPS and MVS were studied in various ratios against PET with perdeuterated glycol units (d-PET) [84]. It was found that the methoxy peak at 2835 cm^{-1} and a peak at 2950 cm^{-1} became stronger as the γ-GPS was effectively diluted by blending with MVS

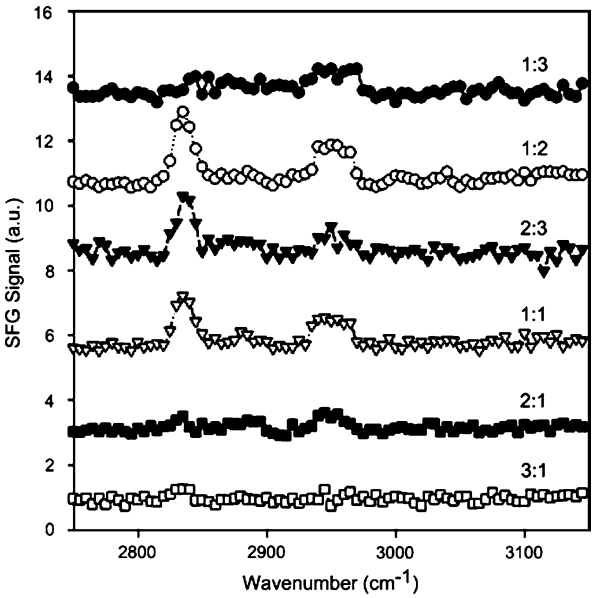

Fig. 2.15 Stable SFG spectra (SSP) collected from the interfaces between d-PET and mixtures comprising different γ-GPS/MVS ratios. Reprinted from Ref. [84] with kind permission of © The American Chemical Society (2006)

(Fig. 2.15). If either component were diluted beyond 1:2 or 2:1 ratios, the SFG signal strength became notably weaker at these positions, suggesting that MVS plays a role in enhancing the net orientational order of γ-GPS at the interface. Comparisons at 1:1 ratios of γ-GPS to dimethylsiloxanol oligomer of similar chain length and to octamethyltrisiloxane show spectral features and intensity to 1:1 γ-GPS:MVS, indicating this silane order-enhancing effect can be generalized to other siloxane oligomers. However, when MVS was studied in mixtures with two non-adhesion-promoting silanes, *n*-octadecyltrimethoxysilane and (tridecafluoro-1,1,2,2-tetrahydrooctyl)-trimethoxysilane, no enhancement in the order of the silane was observed [85]. Interestingly, a γ-GPS:MVS ratio close to 1:1 (w/w) is often used in practice because it generally gives the best adhesion. Therefore, these results motivate further studies to understand whether this observation is simply coincidental or whether interfacial silane ordering is a pre-requisite condition for adhesion.

2.3.3.2.6 Cure Temperature Effects on Primerless Silicone Adhesives

Having established feasibility of interrogating adhesion promoter-polymer interactions through SFG, we proceed to the more complex problem of seeking correlations between practical adhesion and the interfacial concentration, ordering and reactivity of adhesion promoters diluted within a primerless silicone adhesive matrix. Loch et al. showed that even at just 1–2 wt.% of γ-GPS blended into uncured Sylgard® 184, SFG could detect a peak at 2840 cm^{-1} characteristic of the methoxysilane

headgroup after curing against PET [86, 87]. Hence, as in the case of oligomeric siloxanes, it appears that the presence of a siloxane matrix helps induce enrichment and/or ordering of the silane at the substrate interface.

It should be noted that the development of adhesion in Pt-cured silicone elastomers to most substrates depends strongly upon temperature. Generally, a higher temperature is needed to develop adhesion than to merely cure the material for a given time. This effect can be studied easily by using a linear thermal gradient hotplate such as that developed by Meredith et al. for high throughput and combinatorial studies of polymers [88]. Ahn et al. developed a methodology to study the effects of cure temperature on the adhesion of Pt-cured adhesives by curing a peel test specimen on the thermal gradient hot plate [44]. Because any position on the sample can be precisely mapped to a cure temperature, this approach allows one to probe correlations between thermal history (which is directly given by interface position), peeling behavior and interface composition through surface analysis in a continuous fashion. A peel test can be performed by initiating an interfacial crack at the originally cool end of the sample, which is then allowed to propagate along the temperature gradient, to expose an interface of linearly increasing cure temperature history. As the critical temperature (T_{CF}) needed for adhesion is reached, the crack arrests at a position where the failure mode switches from interfacial failure to cohesive failure within the adhesive. One can then study either side of the exposed interface by a variety of conventional surface analytical techniques to determine how the interface composition and/or structure evolves as T_{CF} is reached asymptotically. Conveniently, this technique can also yield the temperature needed to cure (T_{Cure}) the sample by simple measurement of the position where the adhesive transforms from a liquid to a solid.

For instance, Sylgard® 184 elastomer containing 1.5 wt.% γ-GPS cures in 1 h at $T_{Cure} = 50\,°C$ but has to be heated to nearly 150 °C to develop adhesion to PET in the same time. The addition of an additional 1.5 wt.% of MVS can reduce the thermal requirement for adhesion significantly ($T_{CF} = 86\,°C$), while also raising the T_{Cure} to 81 °C.[3] Hence, one can infer that adhesion is an activated process that differs from crosslinking, but the molecular origins of this activation energy have not been elucidated. To this end, the thermal gradient testing protocol has been applied in conjunction with SFG to give insights to the buried interface composition and structure at temperatures even above the transition to cohesive failure where conventional techniques are insensitive. Vasquez et al. showed that when samples are cured at temperatures above T_{CF} on d-PET there is actually a decrease in the methoxy stretch (2835 cm^{-1}) from the γ-GPS headgroups, rather than an enhancement as observed for the aforementioned cases [87]. This result is consistent with a mechanism in which the adhesion to PET depends on reactivity of the alkoxysilane groups near T_{CF}. However, further studies are needed to establish whether these two events are directly correlated, and whether the origin of the signal loss is truly due to reaction of the methoxy groups, rather than diffusion (interface broadening) or

[3]The increase in cure temperature arises from mild Pt catalyst inhibition due to complexation between the Pt catalyst complex and the electron-rich adjacent vinyl groups of MVS.

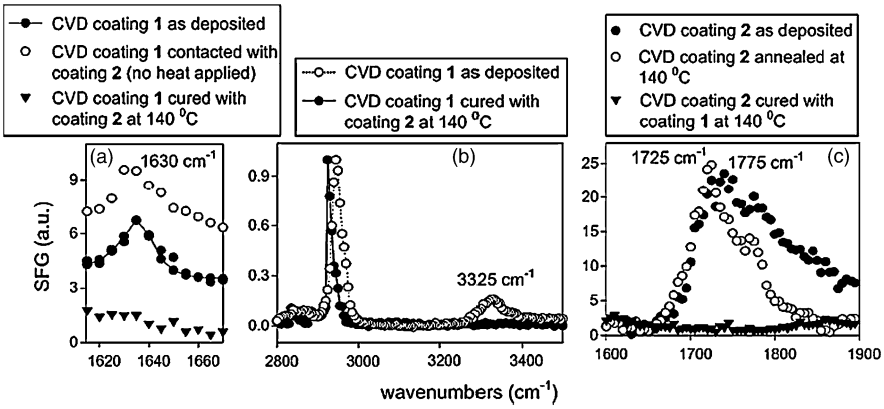

Fig. 2.16 SFG spectra (SSP) of CVD-deposited poly(*p*-xylylenes) before and after bonding. Coating 1 is a primary amine PPX and Coating 2 is an aldehyde-functional PPX. (**a**) The NH_2 bending peak at 1635 cm^{-1} before bonding, which disappears after bonding with coating 2. (**b**) The characteristic N-H stretching peak at 3325 cm^{-1} before bonding, which disappears after bonding. (**c**) –C=O stretching before bonding, and its disappearance after bonding. Reprinted from Ref. [89] with kind permission of ©The American Chemical Society (2008)

randomization near the interface. In particular, it would be particularly enlightening to develop sufficient signal strength to resolve the relatively weak epoxy ring C-H vibrations which so far have been gone undetected at these low concentrations of γ-GPS.

2.3.3.3 Adhesion of CVD-deposited films

Chen et al. studied the adhesion of cured Sylgard® 184 substrates that had been surface modified by CVD deposition of poly(*p*-xylylenes) (PPX) for microfluidic devices. By CVD-treating one substrate with amine-functional PPX and the second substrate with aldehyde-functional PPX then co-joining them at 140 °C, they observed strong adhesion resulting in cohesive failure of the silicone substrates [89]. As shown in Fig. 2.16, SFG was used to show the disappearance of amine (1635 cm^{-1} and 3325 cm^{-1}) and aldehyde (1725 cm^{-1}) bands upon heating, providing evidence consistent with reactive coupling via imine bond formation at the interface between the opposing substrates. Spectral information regarding the interface between the PPX and silicone substrates was not reported.

2.3.4 Sensors

Sensors for chemical detection are another area where surface properties have strong impact on performance. The high gas permeability of siloxanes makes them quite useful matrices for sensors for gases and vapors. Selectivity and sensitivity to various analytes require incorporation of specific functional groups, whose structure

and proximity to the surface can presumably affect response strength and dynamics. Hartmann-Thompson et al. prepared a variety of coatings comprising hydrogen-bond acidic functional polyhedral oligosilsesquioxane (POSS) resins dispersed in siloxane or polycarbosilane matrices for chemical detecting surface acoustic wave sensors [90]. SFG studies of the free surfaces of these coatings spin coated onto quartz substrates indicated different levels of ordering of POSS at the free surface depending on loading in the matrix and upon the specific structure of the organofunctional groups decorating the vertices of the POSS cage. In the case where one of the vertices comprised an aliphatic hexafluoroalcohol group, a hydrogen-bonded OH band was observed at 3470 cm^{-1} in SSP mode.

2.4 Conclusions and Future Directions

This chapter provides an overview of SFG vibrational spectroscopy and its use to study a variety of phenomena involving silicone surfaces and interfaces. We highlighted several examples of applications where SFG was used to provide unique insights to important problems related to the surface and interfacial behavior of silicones. However, SFG is still in its infancy as an analytical technique and perhaps somewhat under-utilized relative to other surface analysis techniques (see Chap. 12). This is in part due to limited awareness in the general materials research community of its capabilities coupled with the relatively limited number of available instruments and potential complexity of interpretation. As a nonlinear optical method, there are physical limits to the types of material, geometries and testing conditions that can be accommodated by SFG. It remains a highly specialized technique that is unlikely to surpass workhorse materials characterization techniques such as ATR-IR or contact angle goniometry in volume. However, from the standpoints of materials, instrumentation and analysis, we believe there remain many opportunities to increase utilization of SFG with silicone-based materials because of its unique surface sensitivity. Below are a number of topics where, to our knowledge, SFG has not yet been utilized but perhaps could be leveraged in the future to generate better understanding of phenomena relevant to silicones and siloxanes.

2.4.1 Materials

(i) *Dispersed interfaces, filled systems* Many commercial silicone products contain fillers, pigments and other additives that introduce dispersed interfaces within the bulk of the silicone. In cases such as thermally or electrically conductive silicones, the structure of these dispersed interfaces can be critical to bulk performance. Even with adhesives and sealants, a reinforcing silica filler can act to absorb significant quantities of adhesion promoters designed to go to the substrate interface. In general, filled systems create difficulties for SFG analysis because the fillers tend to reduce transmission of IR and visible beams, and because they typically present non-uniform interfaces where inversion

symmetry is broken, generating an SFG signal which may or may not average to zero. For example, work with polymer-metal interfaces has been restricted to planar continuous interfaces [91]. However, there may be opportunities to test limits of SFG with dispersed interfaces in well characterized nanoparticle filled silicone elastomers where transparency is not sacrificed and where the particles have sufficient shape uniformity to behave isotropically in the bulk. Another example where SFG analysis could yield useful insights include correlations between filler surface chemistry, structure and alignment of aniosotropic fillers with performance of thermally or electrically conductive silicones. Other areas of interest include characterization of particulate siloxanes and hybrid silicone-silicate materials. Intrinsically anisotropic materials such as Janus particles or rough surfaces in general are difficult to characterize by conventional means. For example, while the anisotropy of a densely packed array of Janus particles should generate differences in the signal from each hemisphere, structural inferences such as bond angle distributions would be obscured by the spherical surfaces. These considerations suggest SFG microscopy in conjunction with fast acquisition protocols might be useful in studying heterogeneous surfaces with micron-size surface topology.

(ii) *Silicone surfactants* As discussed elsewhere in this volume (see Chap. 9), silicone surfactants are a powerful class of commercially important surfactants that can offer a rich variety of phase behavior. To our knowledge there has not been a systematic application of SFG to study and test correlations between surfactancy and molecular organization of functional groups in various architectures of silicone surfactants at air/water, oil/air and oil/water interfaces. We believe SFG may offer complementary insights to the current understanding and accelerate the 'smart' design of new silicone surfactants.

(iii) *Crystalline and semi-crystalline siloxanes* The literature is predominantly focused on PDMS which is amorphous at ambient temperature and above. However, pure PDMS will crystallize around −50 °C, and many other siloxanes such as polydiethylsiloxane and polydiphenyl siloxane exhibit higher melting transitions. While bulk crystallization can be conveniently studied by x-ray techniques, the effects of surfaces and interfaces on controlling crystallinity of siloxanes is much less understood than in, say, polyolefins. We speculate that SFG may shed light on the effects of surfaces and interfaces on localized chain orientation in semi-crystalline siloxanes and liquid crystalline oligosiloxanes [92, 93].

(iv) *Biological systems* We have not discussed the literature on silicone-biological interfaces in this chapter, as the applications of SFG have been limited to only a few studies involving silicones and silicone-modified organic copolymers such as polyurethane-PDMS block copolymers [56, 57]. Because of its inertness and stability in water, PDMS-based elastomers are widely used as substrates in biomedical devices and research in cellular biology. The development of microfluidic devices has spurred a number of studies of cell proliferation on PDMS elastomers modified by a variety of techniques to render the surface more hydrophilic and 'cell-friendly' [53, 94]. To our knowledge these studies

have not applied SFG to probe the molecular origins of the effects of surface modification on cell-polymer interactions.

2.4.2 Instrumentation and Techniques

(i) *Turnkey SFG spectrometers* There have been considerable advances in SFG instrumentation over the last twenty years. The most critical element in the instrumentation is generation of a tunable high intensity infrared laser. Twenty years ago, the optical parametric amplifiers (OPA) were home built and there were very few laboratories equipped to do these measurements. In the last ten years many companies offered fully automated OPA and there are several companies who offer turnkey SFG systems [95]. In addition, we now have femtosecond systems based on Ti-sapphire lasers that can generate IR pulses ranging from 25 to 150 femtoseconds. With these advances the use of this technique is growing rapidly.

(ii) *Dynamics and kinetics* With the introduction of the femtosecond laser systems in conjunction with CCD camera to detect SFG pulses it has become possible to acquire SFG spectra within msec [96]. This capability has opened the possibility to follow kinetics of diffusion and changes in the structure during frictional sliding. In addition, the pump-probe with femtosecond pulses offers possibilities of studying dynamics of PDMS chains at interfaces.

(iii) *Extreme conditions* Most of the experiments with silicones to date have been conducted under ambient laboratory conditions. However, the transient behavior of many of the materials is strongly dependent on temperature and humidity. SFG instruments equipped with more sophisticated environmental controls to allow in situ studies of interface evolution with environmental conditioning should provide important insights on degradation mechanisms and suggest means to improve materials reliability.

(iv) *Extension with high throughput or combinatorial methods* The thermal gradient experiments discussed above [44, 97] offer a glimpse at the possibility of combining a simple high throughput adhesion test method with SFG spectroscopy. Heightened interest and development of high throughput and combinatorial analytical methods over the past decade has yielded useful advances in automated sample processing and analysis that could be integrated with some aspects of SFG spectroscopy to make experimentation more efficient and analysis more informative.

(v) *SFG mapping or imaging/microscopy* Industrial applications of polymers often involve blending of at least two polymers, block copolymers, small molecules, or composites. These systems are often phase separated and heterogeneous. The combination of SFG with microscopy could be valuable in studying such systems. Some initial progress has been reported in the literature on combining SFG with microscopy [98] and offers future possibility of combining this approach to study problems related with adhesion, friction, and wetting.

Acknowledgements The authors would like to acknowledge helpful discussions with Professor Zhan Chen (DA) and support from Dow Corning Corporation (DA) and the National Science Foundation (AD, DA).

References

1. Noll W (1968) Chemistry and technology of silicones. Academic Press, New York
2. Kim J, Chaudhury MK, Owen MJ (1999) Hydrophobicity loss and recovery of silicone HV insulation. IEEE Trans Dielectr Electr Insul 6:695
3. Warrick EL (1990) Forty years of firsts: recollections of a Dow Corning pioneer. McGraw-Hill, New York
4. Shen YR (1996) A few selected applications of surface nonlinear optical spectroscopy. Proc Natl Acad Sci USA 93(22):12104–12111
5. Chen Z, Shen YR, Somorjai GA (2002) Studies of polymer surfaces by sum frequency generation vibrational spectroscopy. Annu Rev Phys Chem 53(1):437–465
6. Miranda PB, Shen YR (1999) Liquid interfaces: a study by sum-frequency vibrational spectroscopy. J Phys Chem B 103(17):3292–3307
7. Lambert AG, Davies PB, Neivandt DJ (2005) Implementing the theory of sum frequency generation vibrational spectroscopy: a tutorial review. Appl Spectrosc Rev 40(2):103–145
8. Morita A, Ishiyama T (2008) Recent progress in theoretical analysis of vibrational sum frequency generation spectroscopy. Phys Chem Chem Phys 10(38):5801–5816
9. Gracias DH, Chen Z, Shen YR, Somorjai GA (1999) Molecular characterization of polymer and polymer blend surfaces. Combined sum frequency generation surface vibrational spectroscopy and scanning force microscopy studies. Acc Chem Res 32:930–940
10. Chen Z (2010) Investigating buried polymer interfaces using sum frequency generation vibrational spectroscopy. Prog Polym Sci 35(11):1376–1402
11. Hirose C, Akamatsu N, Domen K (1992) Formulas for the analysis of the surface SFG spectrum and transformation coefficients of Cartesian SFG tensor components. Appl Spectrosc 46(6):1051–1072
12. Hirose C, Akamatsu N, Domen K (1992) Formulas for the analysis of surface sum frequency generation spectrum by CH stretching modes of methyl and methylene groups. J Chem Phys 96(2):997–1004
13. Shen YR (ed) (1984) The principles of nonlinear optics. Wiley, New York
14. Zhuang X, Miranda PB, Kim D, Shen YR (1999) Mapping molecular orientation and conformation at interfaces by surface nonlinear optics. Phys Rev B 59(19):12632
15. The theory section was reproduced with permission from Rangwalla H, Dhinojwala A (2004) J Adhesion 80:37–59
16. Watanabe N, Yamamoto H, Wada A, Domen K, Hirose C, Ohtake T, Mino N (1994) Vibrational sum-frequency generation (VSFG) spectra of *n*-alkyltrichlorosilanes chemisorbed on quartz plate. Spectrochim Acta, Part A, Mol Biomol Spectrosc 50(8–9):1529–1537
17. Simpson GJ, Rowlen KL (1999) An SHG magic angle: dependence of second harmonic generation orientation measurements on the width of the orientation distribution. J Am Chem Soc 121(11):2635–2636
18. Harp GP, Gautam KS, Dhinojwala A (2002) Probing polymer/polymer interfaces. J Am Chem Soc 124(27):7908–7909
19. Löbau J, Wolfrum K (1997) Sum-frequency spectroscopy in total internal reflection geometry: signal enhancement and access to molecular properties. J Opt Soc Am B 14(10):2505–2512
20. Wilson PT, Briggman KA, Wallace WE, Stephenson JC, Richter LJ (2002) Selective study of polymer/dielectric interfaces with vibrationally resonant sum frequency generation via thin-film interference. Appl Phys Lett 80(17):3084–3086

21. Wang J, Chen C, Buck SM, Chen Z (2001) Molecular chemical structure on poly(methyl methacrylate) (PMMA) surface studied by sum frequency generation (SFG) vibrational spectroscopy. J Phys Chem B 105(48):12118–12125
22. Gautam KS, Dhinojwala A (2001) Molecular structure of hydrophobic alkyl side chains at comb polymer-air interface. Macromolecules 34(5):1137–1139
23. Gautam KS, Dhinojwala A (2002) Melting at alkyl side chain comb polymer interfaces. Phys Rev Lett 88(14):145501
24. Harp GP, Rangwalla H, Yeganeh MS, Dhinojwala A (2003) Infrared-visible sum frequency generation spectroscopic study of molecular orientation at polystyrene/comb-polymer interfaces. J Am Chem Soc 125(37):11283–11290
25. Harp GP, Rangwalla H, Li G, Yeganeh MS, Dhinojwala A (2006) Coupling of interfacial motion at polystyrene–alkane interfaces. Macromolecules 39(22):7464–7466
26. Nanjundiah K, Dhinojwala A (2005) Confinement-induced ordering of alkanes between an elastomer and a solid surface. Phys Rev Lett 95(15):154301
27. Nanjundiah K, Hsu PY, Dhinojwala A (2009) Understanding rubber friction in the presence of water using sum-frequency generation spectroscopy. J Chem Phys 130(2):024702
28. Li G, Dhinojwala A, Yeganeh MS (2011) Interference effect from buried interfaces investigated by angular-dependent infrared—visible sum frequency generation technique. J Phys Chem C 115(15):7554–7561
29. Schwab AD, Dhinojwala A (2003) Relaxation of a rubbed polystyrene surface. Phys Rev E 67(2):021802
30. Oh-e M, Hong S-C, Shen YR (2002) Orientations of phenyl sidegroups and liquid crystal molecules on a rubbed polystyrene surface. Appl Phys Lett 80(5):784–786
31. Prasad S, Hanne L, Dhinojwala A (2005) Thermodynamic study of a novel surface ordered phase above the bulk melting temperature in alkyl side chain acrylate polymers. Macromolecules 38(7):2541–2543
32. Zhang D, Dougal SM, Yeganeh MS (2000) Effects of UV irradiation and plasma treatment on a polystyrene surface studied by IR—visible sum frequency generation spectroscopy. Langmuir 16(10):4528–4532
33. Rangwalla H, Schwab AD, Yudumakan B, Yablon DG, Yeganeh MS, Dhinojwala A (2004) Molecular structure of an alkyl-side-chain polymer-water interface: origins of contact angle hysteresis. Langmuir 20:8625–8633
34. Lachat V, Varshney V, Dhinojwala A, Yeganeh MS (2009) Molecular origin of solvent resistance of polyacrylonitrile. Macromolecules 42(18):7103–7107
35. Li G, Dhinojwala A, Yeganeh MS (2009) Interfacial structure and melting temperature of alcohol and alkane molecules in contact with polystyrene films. J Phys Chem B 113(9):2739–2747
36. Wilson PT, Richter LJ, Wallace WE, Briggman KA, Stephenson JC (2002) Correlation of molecular orientation with adhesion at polystyrene/solid interfaces. Chem Phys Lett 363(1–2):161–168
37. Kurian A, Prasad S, Dhinojwala A (2010) Unusual surface aging of poly(dimethylsiloxane) elastomers. Macromolecules 43(5):2438–2443
38. Clancy TC, Jang JH, Dhinojwala A, Mattice WL (2001) Orientation of phenyl rings and methylene bisectors at the free surface of atactic polystyrene. J Phys Chem B 105(46):11493–11497
39. Tsige M, Soddemann T, Rempe SB, Grest GS, Kress JD, Robbins MO, Sides SW, Stevens MJ, Webb E (2003) Interactions and structure of poly(dimethylsiloxane) at silicon dioxide surfaces: electronic structure and molecular dynamics studies. J Chem Phys 118(11):5132–5142
40. Yurdumakan B, Harp GP, Tsige M, Dhinojwala A (2005) Template-induced enhanced ordering under confinement. Langmuir 21(23):10316–10319
41. Brook MA (2000) Silicon in organic, organometallic and polymer chemistry. Wiley, New York
42. Skeist I (ed) (1990) Handbook of Adhesive, 3rd edn. Van Nostrand Reinhold, New York

43. Ahn D, Lipp ED, McMillan CS (2003) Improved self-priming silicone adhesives through selective interfacial enrichment. In: Proceedings 26th annual meeting of the adhesion society. Adhesion Society, Blacksburg, pp 430–432
44. Ahn D, Shephard NE, Olney PA, McMillan CS (2007) Thermal gradient enabled XPS analysis of PDMS elastomer adhesion to polycarbonate. Macromolecules 40(11):3904–3906
45. Smith AL (ed) (1991) The analytical chemistry of silicones. Wiley-Interscience, New York
46. Zhou X, Hu S, Shephard NE, Ahn D (2003) Diffusion-controlled titanate-catalyzed condensation of alkoxysilanes in nonpolar solvents. In: Synthesis and properties of silicones and silicone-modified materials. ACS symposium series, vol 838, pp 375–387
47. Comyn J, de Buyl F, Comyn TP (2003) Diffusion of adhesion promoting and crosslinking additives in an uncured silicone sealant. Int J Adhes Adhes 23(6):495–497
48. Comyn J, de Buyl F, Shephard NE, Subramaniam C (2002) Kinetics of cure crosslink density and adhesion of water-reactive alkoxysilicone sealants. Int J Adhes Adhes 22(5):385–393
49. Gordon GVL, Loren D (2008) A generalized cure model for one-part RTV sealants and adhesives. In: Proceedings of the annual meeting of the adhesion society, pp 298–300
50. Ismail AE, Grest GS, Heine DR, Stevens MJ, Tsige M (2009) Interfacial structure and dynamics of siloxane systems: PDMS-vapor and PDMS-water. Macromolecules 42(8):3186–3194
51. Chen CY, Wang J, Chen Z (2004) Surface restructuring behavior of various types of poly(dimethylsiloxane) in water detected by SFG. Langmuir 20:10186–10193
52. Lee SH, Ruckenstein E (1987) Surface restructuring of polymers. J Colloid Interface Sci 120(2):529–536
53. Park JY, Ahn D, Choi YY, Hwang CM, Takayama S, Lee SH, Lee S-H (2011) Surface chemistry modification of PDMS elastomers with boiling water improves cellular adhesion. Manuscript submitted for publication
54. Kurian A, Prasad S, Dhinojwala A (2010) Unusual surface aging of poly(dimethylsiloxane) elastomers. Macromolecules 43:2438–2443
55. Yurdumakan B, Nanjundiah K, Dhinojwala A (2006) Origin of higher friction for elastomers sliding on glassy polymers. J Phys Chem C 111(2):960–965
56. Ye S, Majumdar P, Chisholm B, Stafslien S, Chen Z (2010) Antifouling and antimicrobial mechanism of tethered quaternary ammonium salts in a cross-linked poly(dimethylsiloxane) matrix studied using sum frequency generation vibrational spectroscopy. Langmuir 26(21):16455–16462
57. Chen Z, Ward R, Tian Y, Eppler AS, Shen YR, Somorjai GA (1999) Surface composition of biopolymer blends biospan-SP/phenoxy and biospan-F/phenoxy observed with SFG, XPS, and contact angle goniometry. J Phys Chem B 103(15):2935–2942
58. Ye H, Gu Z, Gracias DH (2006) Kinetics of ultraviolet and plasma surface modification of poly(dimethylsiloxane) probed by sum frequency vibrational spectroscopy. Langmuir 22(4):1863–1868
59. Ouyang M, Yuan C, Muisener RJ, Boulares A, Koberstein JT (2000) Conversion of some siloxane polymers to silicon oxide by UV/ozone photochemical processes. Chem Mater 12(6):1591–1596
60. Schnyder B, Lippert T, Kötz R, Wokaun A, Graubner V-M Nuyken O UV-irradiation induced modification of PDMS films investigated by XPS and spectroscopic ellipsometry. Surf Sci 532–535, 1067–1071 (2003)
61. Graubner V-M, Jordan R, Nuyken O, Schnyder B, Lippert T, Kötz R, Wokaun A (2004) Photochemical modification of cross-linked poly(dimethylsiloxane) by irradiation at 172 nm. Macromolecules 37(16):5936–5943
62. Efimenko K, Wallace WE, Genzer J (2002) Surface modification of Sylgard-184 poly(dimethyl siloxane) networks by ultraviolet and ultraviolet/ozone treatment. J Colloid Interface Sci 254(2):306–315
63. Harp GP, Dhinojwala A (2005) Direct probe of interfacial structure during mechanical contact between two polymer films using infrared visible sum frequency generation spectroscopy. J Adhes 81(3–4):371–379
64. Schallamach A (1963) A theory of dynamic rubber friction. Wear 6(5):375–382

65. Kurian A, Prasad S, Dhinojwala A (2010) Direct measurement of acid-base interaction energy at solid interfaces. Langmuir 26(23):17804–17807
66. Roberts AD, Tabor D (1971) The extrusion of liquids between highly elastic solids. Proc R Soc London, Ser A 325(1562):323–345
67. Israelachvili JN (1991) Intermolecular & surface forces, 2nd edn. Academic Press, San Diego
68. Andrews EH, Kinloch AJ (1973) Proc R Soc London, Ser A 332:385
69. Gent AN, Schultz J (1972) J Adhes 3:281
70. Ferry JD (ed) (1980) Viscoelastic properties of polymers, 3rd edn. Wiley, New York
71. Roan GA (2003) Advances in acrylic hybrid technology. Adhes Sealants Industry 2003:36–40
72. Schmidt RG, Gordon GV, Dreiss CA, Cosgrove T, Krukonis VJ, Williams K, Wetmore PM (2010) A critical size ratio for viscosity reduction in poly(dimethylsiloxane)-polysilicate nanocomposites. Macromolecules 43(23):10143–10151
73. Gordon GV, Schmidt RG, Quintero M, Benton NJ, Cosgrove T, Krukonis VJ, Williams K, Wetmore PM (2010) Impact of polymer molecular weight on the dynamics of poly(dimethylsiloxane)-polysilicate nanocomposites. Macromolecules 43(23):10132–10142
74. Gordon GV, Perz SV, Tabler RL, Stasser JL, Owen MJ, Tonge JS (1998) Silicone release coatings: a closer look at release mechanisms. www.dowcorning.com/content/publishedlit/26-016.pdf. Dow Corning Corporation, Midland, MI
75. Plueddeman EP (ed) (1991) Silane coupling agents, 2nd edn. Plenum Press, New York
76. Chen C, Loch CL, Wang J, Chen Z (2003) Different molecular structures at polymer/silane interfaces detected by SFG. J Phys Chem B 107:10440–10445
77. Chen C, Wang J, Loch CL, Ahn D, Chen Z (2004) Demonstrating the feasibility of monitoring the molecular-level structures of moving polymer/silane interfaces during silane diffusion using SFG. J Am Chem Soc 126(4):1174–1179
78. Mine K, Nishio M, Sumimura S (1977) Heat curable organopolysiloxane compositions containing adhesion additives. US Patent 4,033,924, July 5
79. Schulz JR (1978) Self-adhering silicone compositions and preparations thereof. US 4,087,585, May 2
80. Gellman AJ, Naasz BM, Schmidt RG, Chaudhury MK, Gentle TM (1990) Secondary neutral mass spectrometry studies of germanium-silane coupling agent-polymer interphase. J Adhes Sci Technol 4(7):597–601
81. Gentle TE, Schmidt RG, Naasz BM, Gellman AJ, Gentle TM (1992) Organofunctional silanes as adhesion promoters: direct characterization of the polymer/silane interphase. In: Mittal KL (ed) Silanes and other coupling agents. VSP, Utrecht, pp 295–304
82. Loch CL, Ahn D, Vazquez AV, Chen Z (2007) Diffusion of one or more components of a silane adhesion-promoting mixture into poly(methyl methacrylate). J Colloid Interface Sci 308(1):170–175
83. Loch CL, Ahn D, Chen C, Wang J, Chen Z (2004) Sum frequency generation studies at poly(ethylene terephthalate)/silane interfaces: hydrogen bond formation and molecular conformation determination. Langmuir 20:5467–5473
84. Loch CL, Ahn D, Chen CY, Chen Z (2006) Sum frequency generation vibrational spectroscopic studies on a silane adhesion promoting mixture at a polymer interface. J Phys Chem B 110:914–918
85. Vázquez AV, Boughton AP, Shephard NE, Rhodes SM, Chen Z (2009) Molecular structures of the buried interfaces between silicone elastomer and silane adhesion promoters probed by sum frequency generation vibrational spectroscopy and molecular dynamics simulations. ACS Appl Mater Interfaces 2(1):96–103
86. Loch CL, Ahn D, Chen Z (2005) Polymer-silane interactions probed by sum frequency generation vibrational spectroscopy. J Adhes 81:319–345
87. Vázquez AV, Shephard NE, Steinecker CL, Ahn D, Spanninga S, Chen Z (2009) Understanding molecular structures of silanes at buried polymer interfaces using sum frequency generation vibrational spectroscopy and relating interfacial structures to polymer adhesion. J Colloid Interface Sci 331(2):408–416
88. Meredith JC, Karim A, Amis EJ (2000) High-throughput measurement of polymer blend phase behavior. Macromolecules 33(26):5760–5762

89. Chen H-Y, McClelland AA, Chen Z, Lahann J (2008) Solventless adhesive bonding using reactive polymer coatings. Anal Chem 80(11):4119–4124
90. Hartmann-Thompson C, Keeley DL, Dvornic PR, Keinath SE, McCrea KR (2007) Hydrogen-bond acidic polyhedral oligosilsesquioxane filled polymer coatings for surface acoustic wave sensors. J Appl Polym Sci 104(5):3171–3182
91. Lu X, Li D, Kristalyn CB, Han J, Shephard N, Rhodes S, Xue G, Chen Z (2009) Directly probing molecular ordering at the buried polymer/metal interface. Macromolecules 42(22):9052–9057
92. Tschierske C (1998) Non-conventional liquid crystals-the importance of micro-segregation for self-organisation. J Mater Chem 8(7):1485–1508
93. Yoon H, Agra-Kooijman DM, Ayub K, Lemieux RP, Kumar S (2011) Direct observation of diffuse cone behavior in de Vries smectic-A and -C phases of organosiloxane mesogens. Phys Rev Lett 106(8):087801
94. Park JY, Hwang CM, Lee S-H (2008) Effective methods to improve the biocompatibility of poly(dimethylsiloxane). BioChip J 2(1):39–43
95. Smith JP, Hinson-Smith V (2004) Product review: SFG coming of age. Anal Chem 76(15):287 A-290
96. Richter LJ, Petralli-Mallow TP, Stephenson JC (1998) Vibrationally resolved sum-frequency generation with broad-bandwidth infrared pulses. Opt Lett 23(20):1594–1596
97. Vazquez AV, Shephard NE, Steinecker CL, Ahn D, Spanninga S, Chen Z (2009) Understanding molecular structures of silanes at buried polymer interfaces using sum frequency generation vibrational spectroscopy and relating interfacial structures to polymer adhesion. J Colloid Interface Sci 331(2):408–416
98. Hernandez M, Chinwangso P, Cimatu K, Srisombat L-O, Lee TR, Baldelli S (2011) Chemical imaging and distribution analysis of mono-, bi-, and tridentate alkanethiol self-assembled monolayers on gold by sum frequency generation imaging microscopy. J Phys Chem C 115(11):4688–4695

Chapter 3
Creating Functional Materials by Chemical and Physical Functionalization of Silicone Elastomer Networks

Jan Genzer, Ali E. Őzçam, Julie A. Crowe-Willoughby, and Kirill Efimenko

3.1 Introduction

Silicones or polysiloxanes represent unique polymeric materials comprising an inorganic Si-O-Si backbone with two pendant functional groups attached to each silicon atom. Polydimethylsiloxane (PDMS) is the most commonly utilized silicone which possesses two methyl groups anchored to the backbone silicon atom. The exceptional mechanical properties of PDMS arise from the high backbone flexibility, asymmetric Si-O-Si bond angles, longer bond length and low energy barriers for rotation as compared to their hydrocarbon counterparts [1]. The aforementioned properties lead to a very low glass transition temperature (T_g) ($\approx$150 K) rendering silicones a liquid at room temperature with a high degree of flexibility. For instance, due to attractive/repulsive interactions, the methyl groups on the Si-O-Si backbone will orient themselves to the surface at an air-interface, yet they will get buried under the polymer backbone at a water-interface to allow the macromolecule to adopt the lowest surface energy conformation. These conformational changes take place rapidly due to the polymer's low T_g. Silicones can be cross-linked chemically to form silicone elastomer networks (SEN) with an elastic modulus ranging from $\approx$0.05 to 1 MPa while maintaining the liquid-like nature of the parent individual polymer chains between the cross-link junctions. Due to the presence of two stable methyl groups, PDMS also possesses a high chemical resistance.

Silicones are employed in numerous applications ranging from electronics to personal care, automotive, biomedical, and construction industries. Among these application areas, PDMS is especially important for biomedical science since it is

J. Genzer (✉) · A.E. Őzçam · J.A. Crowe-Willoughby · K. Efimenko
Department of Chemical & Biomolecular Engineering, North Carolina State University, Raleigh, NC 27695-7905, USA
e-mail: Jan_Genzer@ncsu.edu

Present address:
J.A. Crowe-Willoughby
College of Textiles, North Carolina State University, Raleigh, NC 27695-7103, USA

M.J. Owen, P.R. Dvornic (eds.), *Silicone Surface Science*, Advances in Silicon Science 4,
DOI 10.1007/978-94-007-3876-8_3,

biocompatible. For instance, PDMS is utilized as a material for contact lenses and for human implants [2]. The past few years witnessed enormous activity in using SENs (PDMS being the primary example) in the micro and nanotechnology area, specifically, in soft lithography [3, 4], fabrication of microfluidic systems [5], and a variety of novel functional devices [6, 7]. In addition to employing SENs as functional materials that can be molded to assume any size and shape, the mechanical flexibility of SENs has been utilized in devices and structures whose function and properties stem from the soft nature of the network [8–12]. Generation of stretchable, deformable devices or substrates with topographical corrugations represents examples of such activities.

Many applications of SENs demand that their surfaces are hydrophilic or can be modified to attach various chemical moieties. Most commercial SENs, at least those that have been utilized most widely, are inherently hydrophobic and are difficult to alter chemically. For instance, the exceptional stability of the hydrophobic PDMS surfaces prevents them from being modified by routine chemical means. Application of strong acidic or basic agents, which work for most other hydrophobic polymeric materials, is not an option as those treatments lead to uncontrollable and non-uniform decomposition of SEN due to hydrolytic cleavage of the Si-O bond. In spite of some exceptions reported recently [13–16], the most widely applied method to turn PDMS hydrophilic employs some type of physical treatment.

Over the past years, modification of PDMS surfaces was carried out using various physical modification techniques including plasma, corona, ultraviolet (UV), UV/Ozone (UVO), electron and ion beams [17–22]. Among these techniques, oxygen plasma treatment has been utilized widely to impart the PDMS surface more hydrophilic via introduction of various polar, oxygen-containing groups. Previous research has shown that plasma treatment propagates several hundred nanometers below the surface causing irreversible chemical changes to the base material in the near-surface region and produces a brittle silica-like layer at the material surface, which differs significantly in mechanical properties from the elastomer bulk [23]. The thickness of the silica layer is a function of treatment time, power of the plasma, chamber pressure, and gas chemical composition. During treatment, the surface of silicone rubber gets decorated with microscopic cracks within the silica-like layer [24, 25] that facilitates the diffusion of uncross-linked PDMS oligomers to the surface; this alters the initial hydrophilic state and results in recovering the original hydrophobic nature of material (so-called "hydrophobic recovery") [26–29].

In addition to plasma treatment, UVO has also been employed to increase the hydrophilicity of PDMS surfaces [22, 30–32]. The UVO treatment involves a photosensitized oxidation process in which the molecules of the treated material are excited and/or dissociated by the absorption of short-wavelength UV radiation and atomic oxygen. Atomic oxygen is generated simultaneously when molecular oxygen is dissociated by $\lambda_1 = 184.9$ nm and ozone by $\lambda_2 = 253.7$ nm. Additionally, the radiation at these wavelengths is absorbed by most hydrocarbon compounds. The organic products of this excitation react with atomic oxygen to form simpler, volatile molecules, which desorb from the surface. When both wavelengths are present,

atomic oxygen is generated continuously, and ozone is continually formed and destroyed. Compared to plasma treatment, the UVO treatment represents a milder type of physical modification with similar surface changes but with approximately an order of magnitude increase in processing time.

Even though it is more controlled than the plasma modification, the UVO treatment of PDMS still causes uncontrollable and irreversible changes to the surface of SENs. At short modification times a variety of hydrophilic groups are formed including hydroxyls, carboxyls, aldhehydes, peroxides, and other hydrophilic groups [30]. Long UVO treatments of PDMS lead to the formation of a silica-like layer on the surface of the PDMS which hardens considerably the originally soft surface of SENs [31–33]. While most UVO-modification studies involving SENs have been carried out with PDMS, Efimenko and coworkers reported on UVO treatment of polyvinylmethylsiloxane (PVMS), whose higher susceptibility to the UVO reduces the UVO treatment time and increases the chemical tailorability to obtain hydrophilic SENs without significant changes in the mechanical properties of the interfacial region [34]. Efimenko et al. provided experimental evidence that only brief UVO treatment times (seconds to a few minutes) are sufficient to form highly hydrophilic PVMS surfaces compared to the UVO treatment of PDMS, which renders the PDMS surface hydrophilic only after prolonged UVO treatment times [34].

Unlike the case of PDMS, which owns its exceptionally high chemical stability to the presence of two methyl groups, chemical tailorability of PVMS is accomplished more readily due to the vinyl functionality, which can be modified via: (1) chemical oxidation resulting in formation of either alcohol or carboxylic acid-containing moieties with subsequent chemical grafting at the newly generated "active" sites, or (2) direct attachment of the desired functionality through addition reactions such as hydrosilylation, hydrosulfidation, hydrophosphination, epoxidation, and alkyl halide addition reactions. Therefore, PVMS represents a unique class of SENs that provides the same multiple functions of PDMS with the additional ability to tune the chemical nature of PVMS via vinyl-based reactions. We have utilized this chemical moiety to attach various reactive groups to the PVMS backbone.

In this chapter we provide a synopsis of decade-long activities in our group aimed at preparing functional materials from SENs. We commence with providing an overview of simple physical modification methods that employ UVO treatment of PDMS and PVMS and subsequent chemical functionalization of such hydrophilized SENs. We document that judicious choice of the physico-chemical modification in tandem with mechanical deformation of the substrates offers new avenues towards creating coatings with unprecedented functionality. We also outline methods of employing UVO treatment in generating substrates with topographical corrugations to show how one can control the properties, i.e., sizes, orientation, of the surface protrusions. We further demonstrate the capability of PVMS as a novel material for creating functional substrates by performing chemical reactions on the reactive vinyl group. This process facilitates generating responsive/"smart" SENs whose surfaces alter depending on the environmental stimulus. We also document that PVMS can serve as a general organic precursor for manufac-

turing functional coatings with tailored mechanical properties and chemical compositions.

3.2 Physical Modification of SEN Surfaces

As pointed out in Sect. 3.1, plasma or corona treatment has been utilized quite widely in converting the originally hydrophobic SEN surface into a hydrophilic layer. Multiple examples in the literature describe this modification process. Williams and coworkers performed a detailed study of plasma modification of silicone rubbers [35] in the presence of argon, oxygen, nitrogen, or ammonia gases. A substantial increase in wettability was observed in specimens treated with O_2 and Ar plasmas; in addition, a brittle silica-like layer formed on top of the SENs. The presence of this dense silica-like layer slowed down the "hydrophobic recovery" during 1 month aging in air. Additionally, the aging in phosphate-buffered saline (PBS) showed a considerable decrease in "hydrophobic recovery". Samples modified with N_2 and NH_3 plasmas showed an increase in hydrophobicity and a "hydrophobic recovery" compared to that observed in the O_2 and Ar plasma modified SENs. Williams and coworkers also reported on different degrees of biocompatibility for those specimens. While the O_2- and Ar-plasma treated samples exhibited decreased haemocompatibility, the N_2 and NH_3 plasma modification produced specimens with longer blood-contacting times without platelet activation and coagulation than untreated PDMS. The researchers pointed out that in addition to the various surface compositions achieved during the various plasma conditions, the biocompatibility may also be affected by surface topography and surface morphology. Because the plasma/corona treatments are rather harsh and not very easy to control, researchers have turned to other physical modification methods that cause less dramatic and better controlled alterations of the SEN surfaces.

Compared to plasma or corona treatment, the UVO modification is considered generally to be much milder for physical modification of polymer surfaces [36, 37]. This is largely due to the smaller radiation dosage that gets delivered to the sample surface resulting in slower chemical alternations of the material and longer processing times. The degree of magnitude reduction in UVO exposure time (generally, minutes) relative to plasma/corona (seconds to tens of seconds, depending on the power) allows for better control over the surface chemical composition and consequently the degree of wettability. Yet another advantage of the UVO treatment relative to the plasma and corona techniques is that the sample temperature during the treatment raises only slightly, thus avoiding any non-desirable combined chemico-physical-thermal treatment effects.[1] The time needed to convert from a hydrophobic to hydrophilic SEN surface depends not only on the processing conditions but also on the chemical nature of the parent SEN material. To illustrate this point, in Fig. 3.1

[1] In a typical set up, a dose of 8.2 mW cm^{-2} causes the temperature of a sample to raise to a maximum of 70° [Őzçam AE, unpublished data].

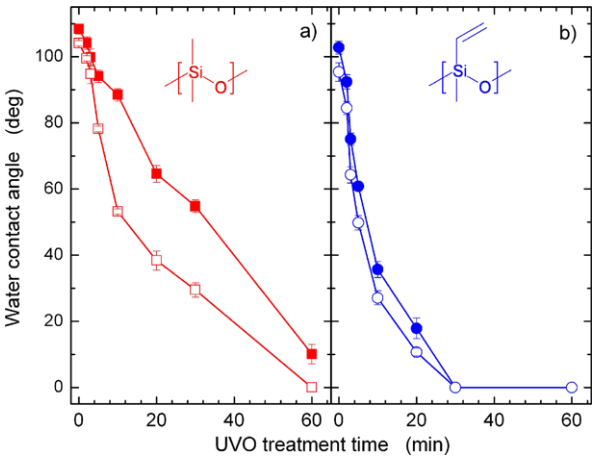

Fig. 3.1 Dependence of the advancing (*closed symbols*) and receding (*open symbols*) contact angles of deionized water on the UVO modification of PDMS (**a**) (*squares*) and PVMS (**b**) (*circles*). The *lines* are guides to the eye

we plot water contact angles collected from UVO-modified PDMS (squares) and PVMS (circles) samples. In both instances, the average molecular weight between the cross-links in the network was approximately 30 kDa. A few important observations can be made from the data. The hydrophobicity of the parent PDMS is higher than that of PVMS. This is due to the presence of the slightly more hydrophilic vinyl group present in PVMS relative to the more hydrophobic two methyl units in PDMS. Secondly, the rate of hydrophilization is much faster for PVMS compared to PDMS. This behavior is associated with different chemical changes inside the two SENs during the UVO radiation [33, 34]. Finally, the presence of two chemically stable methyl groups minimizes the modification of PDMS initially; only the prolonged UVO treatment causes dramatic changes in the SEN material [33]. While still under investigation [38], the primary sites in the PDMS SEN that get modified first appear to be the cross-link points.[2] The vinyl groups are less stable than methyls and more susceptible to UVO modification, as discussed elsewhere [34]. Therefore the PVMS SENs undergo more rapid modification relative to PDMS. After about 10 minutes of UVO exposure the PVMS specimens are hydrophilic.

UVO treatment causes not only changes in wettability of SENs but also leads to modification of mechanical properties. We already mentioned earlier that plasma and corona treatments produce rather thick, silica-like layers resting on top of the unmodified SEN base. UVO leads to densification of the SEN and eventual chemical modification that may propagate deeper into the substrate. Because detailed published of this topic has been discussed previously [33, 34] and will be reported also in our subsequent work [38], we restrict ourselves here to only a brief account. UVO treatment times up to 5–10 min (depending on the UVO dosage) only lead to relatively small changes in surface wettability and do not affect dramatically the

[2]We infer this from our initial observation that PDMS SENs with lower molecular weight, i.e., higher degree of cross-linking, get modified to a larger degree than PDMS SENs made by cross-linking higher molecular weight PDMS chains.

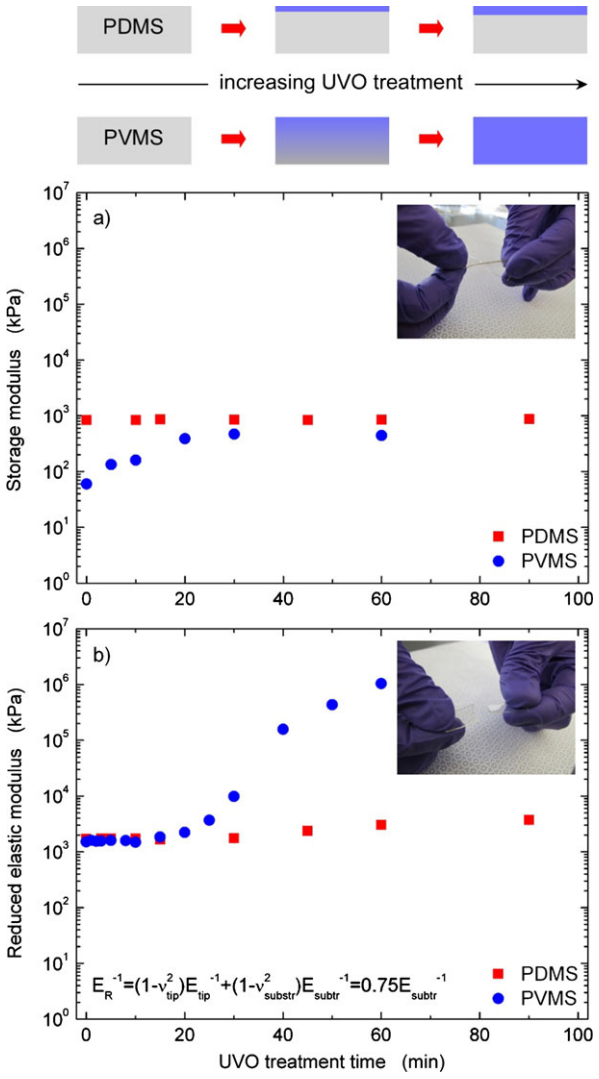

Fig. 3.2 (*Top*) Schematic illustration of the proposed UVO modification of PDMS and PVMS. The base material (*grey*) gets converted into a silica-layer structure (*blue*) with increasing UVO exposure time. (**a**) Bulk storage modulus and (**b**) surface reduced elastic modulus of PDMS (*squares*) and PVMS (*circles*) as a function of the UVO treatment time. The photographs in the insets depict the response of the UVO-modified PDMS and PVMS networks to mechanical stretching

mechanical properties of the PDMS SEN. Extensive exposure to UVO results in the formation of a ≈5 nm thick silica-like layer (50 % density of silica, as determined by x-ray reflectivity [33]). These changes in mechanical properties of PDMS with increasing UVO exposure can be followed conveniently with mechanical measurements. In Fig. 3.2 we plot the storage and elastic modulus determined by dynamic mechanical thermal analysis (DMTA) and nanoindentation, respectively. While the storage modulus remains virtually unchanged for all UVO times studied, there is a small increase in the elastic modulus. These data support the x-ray reflectivity studies indicating the formation of a thin rigid layer formed on top of PDMS SEN. This layer is not being sensed by the storage modulus measured by DMTA, which

probes the properties of the entire specimen, but is detected by the elastic modulus established from surface-sensitive nanoindentation. The mechanical properties of UVO-modified PVMS SEN are quite different from those of PDMS. While a brief exposure of PVMS to UVO (2–5 min) only causes chemical changes in the PVMS surfaces, extended UVO treatment results in a dramatic variation of the base material. After ≈20 mins, the PVMS sample hardens considerably; this hardening occurs not only on the surface but propagates throughout the entire specimen, as documented by the bulk (storage) and surface (elastic) moduli plotted in Fig. 3.2. As a consequence, prolonged UVO treatment converts the originally flexible SEN into a glass-like material [38]. The schematic on top of Fig. 3.2 depicts pictorially the different mechanisms for UVO modification of PDMS and PVMS SENs.

Upon UVO exposure, the SEN undergoes dramatic changes in chemical composition, as discussed earlier [33, 34]. While the actual chemical composition varies depending on the sample, UVO dosage, and other environmental conditions present during the treatment and may also involve post-modification reactions among the generated functional species, it suffices to state that a large number of reactive, and relatively stable functional polar groups are generated. These moieties can be employed in post-UVO chemical modification with various reactive species. Typical examples of the latter represent organosilanes that tend to chemisorb onto hydroxyl-contaning substrates. We have previously studied the attachment of semifluorinated organosilanes based on $F(CF_2)_8(CH_2)_2$- (F8H2) functional groups having two different head-group chemistries, i.e., 1H,1H,2H,2H-perfluorodecyldimethylchlorosilane ($F(CF_2)_8(CH_2)_2Si(CH_3)_2Cl$, m-F8H2) and 1H,1H,2H,2H-perfluorodecyltrichlorosilane ($F(CF_2)_8(CH_2)_2SiCl_3$, t-F8H2) to UVO-pretreated PDMS and PVMS substrates [34]. While m-F8H2 adsorbs directly to the substrate, t-F8H2 has the capability of both anchoring to the support as well as forming in-plane networks that further stabilize the resulting self-assembled monolayer (SAM). In Fig. 3.3 we plot the near-edge x-ray absorption fine structure (NEXAFS) spectroscopy data collected at the carbon K-edge from UVO-treated PDMS (Fig. 3.3a, Fig. 3.3b) and PVMS (Fig. 3.3c, Fig. 3.3d) supports that have been exposed to m-F8H2 (Fig. 3.3a, Fig. 3.3c) and t-F8H2 (Fig. 3.3b, Fig. 3.3d). The results demonstrate that on the PDMS-UVO substrates, dense m-F8H2 SAMs form only after extended UVO treatment time (>5 min) while t-F8H2 SAMs deposit at moderate densities on PDMS exposed to UVO for only a few minutes. In contrast, due to the high degree of modification of PVMS during the UVO treatment, stable and dense SAMs from both the mono- and tri- functional species are deposited only after 30 s of UVO treatment to the base SEN. These results document that chemical changes occurring on top of PVMS substrates exposed to UVO are dramatic with functional groups capable of acting as reaction sites for organosilanes regardless of their head-group chemistry. Due to the higher resistance of PDMS to UVO, only a small fraction of hydrophilic groups is generated on top of PDMS at short UVO times. This leads to imperfect SAMs made from m-F8H2 while relatively high coverage can be formed with t-F8H2 due to their ability to form in-plane cross-links among neighboring t-F8H2 groups. Figure 3.4 depicts the proposed structures of the m-F8H2 and t-F8H2 SAMs on PDMS and PVMS substrates treated for relatively short UVO times.

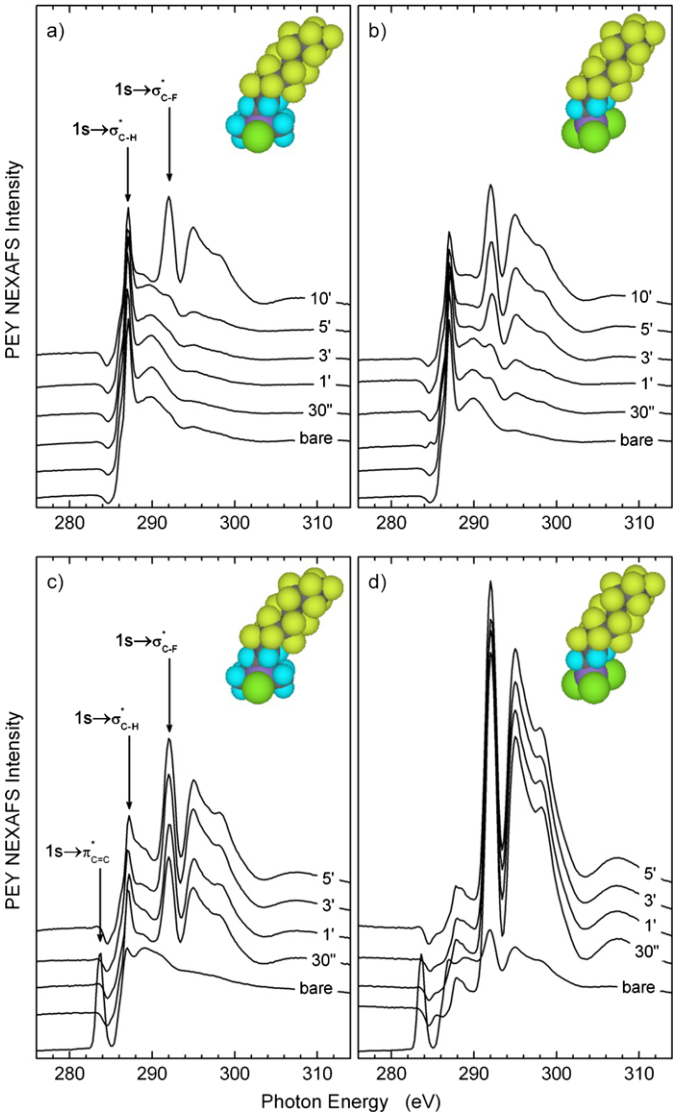

Fig. 3.3 Partial energy yield NEXAFS spectra at the carbon K-edge collected from (**a**) m-F8H2 and (**b**) t-F8H2 SAMs deposited on PDMS network films ($M_n = 39{,}000$), and from (**c**) m-F8H2 and (**d**) t-F8H2 SAMs deposited on PVMS network films ($M_n = 39{,}000$) that were previously treated for various UVO treatment times. The arrows indicate the positions of the characteristic NEXAFS transitions. Also shown are cartoons illustrating the molecular structure of m-F8H2 and t-F8H2. Reproduced from Ref. [34] with kind permission of © Elsevier (2005)

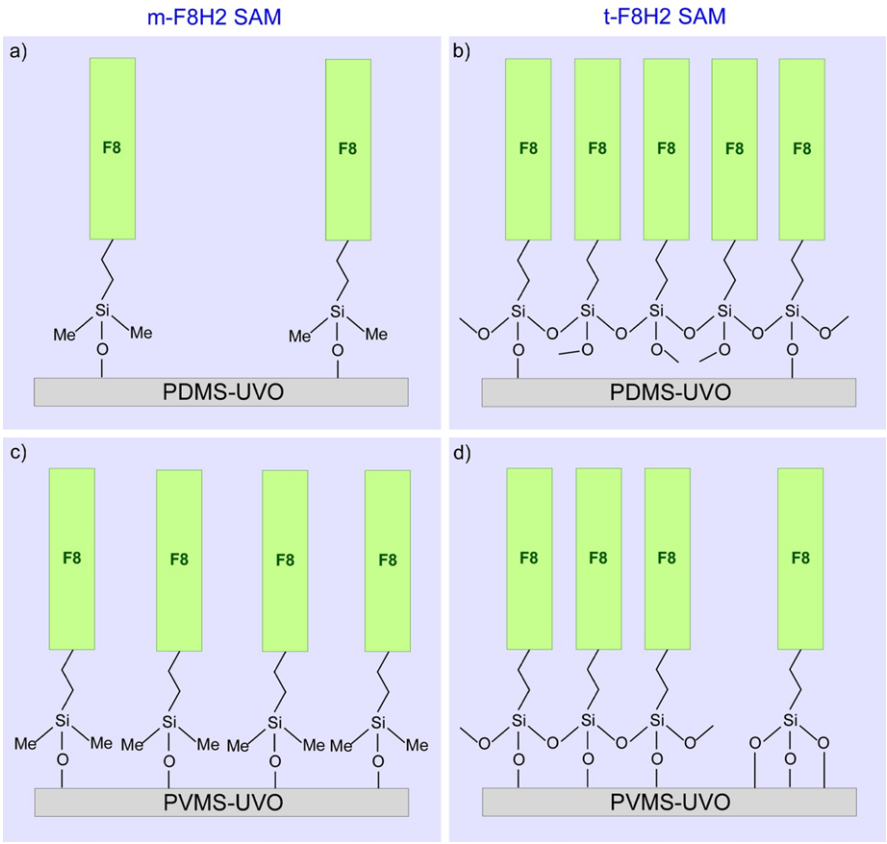

Fig. 3.4 Schematic of the organization of (**a**), (**c**) m-F8H2 and (**b**), (**d**) t-F8H2 molecules on (**a**), (**b**) PDMS and (**c**), (**d**) PVMS substrates after a brief expose of the substrate to short UVO treatment

3.3 Controlling Molecular and Macromolecular Packing Using SENs

As pointed out previously, longer UVO treatment times are required to modify the PDMS surface to achieve a higher number of hydrophilic sites for subsequent chemical grafting. But even at relatively short UVO times, a high enough number of grafting sites exists that are capable of attaching trichlorosilane-based moieties. Moreover, exposing PDMS to short UVO times does not compromise the mechanical characteristics of the underlying SEN support (cf. Fig. 3.2). As a result, PDMS samples exposed to relatively low UVO dosages maintain their mechanical flexibility and concurrently feature a sufficient density of hydrophilic sites available for chemical modification. We have capitalized on the flexibility of PDMS substrates and their ability to attach functional groups at low UVO dosages to demonstrate that the wettability of SAMs and their stability depend on the interplay between the chemical functionality of the parent SAM molecules and molecular packing on the

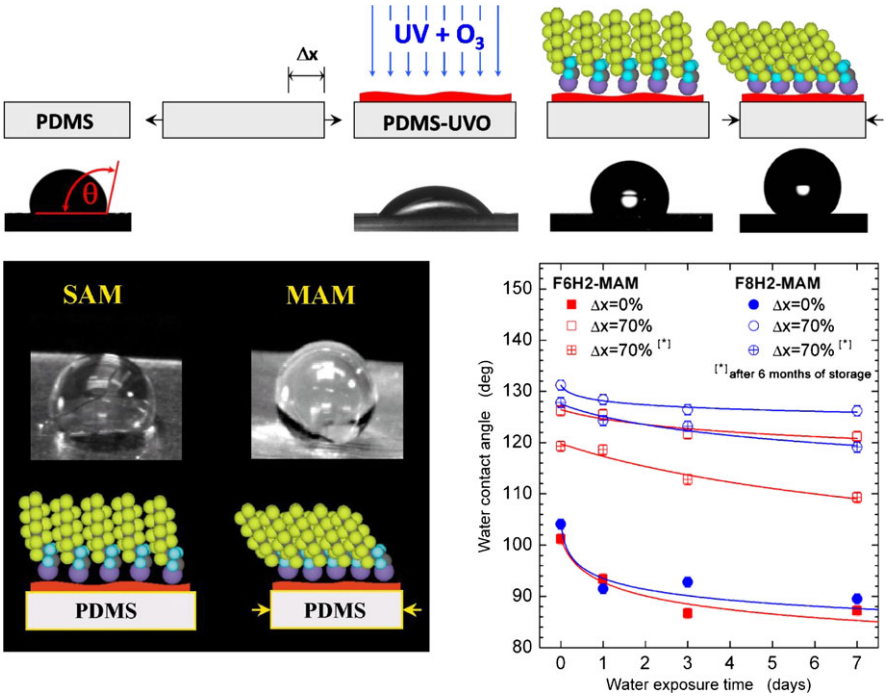

Fig. 3.5 (*Top*) Schematic illustration of the mechanism of increasing packing density of a self-assembled monolayer after mechanically stretching the substrate. (*Bottom left*) Representation showing the higher water contact angle (θ) mechanically-assembled monolayers (MAMs) on PDMS vs. self-assembled monolayers (SAMs) on PDMS (*bottom right*) Water contact angles for MAMs made of semifluorinated alkanes on PDMS SENs. Reproduced from Ref. [39] with kind permission of ©The American Association for the Advancement of Science (2000)

substrate [39]. Specifically, we have developed a simple method leading to the formation of so-called assembled monolayers (MAMs) by stretching mechanically a slab of PDMS SEN (thickness ≈0.5 mm), exposing it to a brief UVO treatment and depositing a semifluorinated SAM made of t-F8H2 (or t-F6H2) by vapor treatment. After forming the semifluorinated SAM, we release the strain from the sample allowing it to return to its original size forcing the organosilane molecules to pack tightly on the substrate (see Fig. 3.5). We have explored the organization of the packed organosilane molecules with NEXAFS and contact angle measurements. Both techniques provided evidence that tight packing of the molecules resulted in robust stable layers deposited on the underlying support. In Fig. 3.5 we plot the contact angle data from t-F8H2 and t-F6H2 MAMs prepared on PDMS substrates elongated originally (Δx) by 70 %, after modification and after aging for six months in a humid environment. The as-prepared specimens exhibited a high degree of hydrophobicity (corresponding to the maximum hydrophobicity one can achieve by chemical modification without using topography [40]). Importantly, there was only a small loss of hydrophobicity after prolonged exposure to moisture. The t-F8H2 specimens performed better because they could form more closely packed MAMs

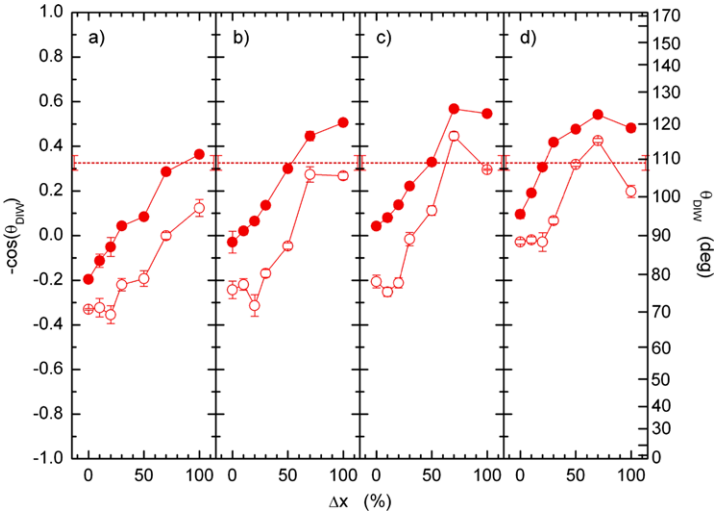

Fig. 3.6 Advancing (*closed symbols*) and receding (*open symbols*) contact angles, θ, of DI water on H8-MAMs prepared by vapor deposition of *n*-octyltrichlorosilane (OTS) as a function of the stretching of the PDMS substrate, Δx. After stretching, the PDMS was exposed to the UVO treatment for 15 minutes and such PDMS-UVO substrates were exposed to a vapor of OTS for: (**a**) 10, (**b**) 20, (**c**) 30, and (**d**) 60 min. The error bars correspond to uncertainties based on measurement from 3 different samples. The dashed lines denote the values of θ for a crystalline array of $-CH_3$. Reproduced from Ref. [41] with kind permission of © the Materials Research Society (2002)

relative to the t-F6H2-based samples. The effect of packing on monolayer stability was evident by comparing the data to t-F8H2 and t-F6H2 SAMs prepared on UVO-treated PDMS supports without pre-stretching. Thus the high hydrophobicity and stability of the surfaces resulted from close packing of the semifluorinated groups on the surface that hindered the motion of the surface-grafted molecules.

In addition to MAMs made of semifluorinated organosilanes, we prepared similar structures by assembling hydrocarbon-based organosilanes [41]. Specifically, we fabricated hydrocarbon MAMs from short ($H(CH_2)_8SiCl_3$, H8) and long ($H(CH_2)_{16}SiCl_3$, H16) organosilanes. Considering that short hydrocarbon species assume liquid-like conformations while longer counterparts form semi-crystalline like domains, with the transition around 10–12 methylene units [42–44], we intended to evaluate how chain packing during the MAM formation process influences the organization and stability of the resulting MAM surfaces. Grafting densities of the alkane-based organosilanes were varied by stretching the PDMS substrate to different elongations (Δx) prior to the UVO treatment. In accord with the experiments performed on semifluorinated MAM, we expected the packing density of alkanes to increase with increasing the substrate elongation. If the alkane chains were indeed densely packed on the PDMS surface, neighboring chains should restrict their mobility even if the alkane chain lengths were shorter than 10–12 methylene units needed for a stable crystalline array [42–44]. In Fig. 3.6 we plot the water contact angle data on H8-MAM substrates prepared by vapor deposition of *n*-octyltrichlorosilane (OTS) for various times on PDMS substrates pre-stretched

by Δx and exposed to UVO for 15 min. The data document that there is an increase in the contact angle with increasing OTS deposition time and Δx, accompanied for $\Delta x < 70$ % by a decrease in the contact angle hysteresis (CAH), i.e., difference between the advancing (solid circles) and receding (open circles) contact angles. This behavior documents close packing of the chains in the MAMs. Increasing Δx beyond 70 % resulted in higher CAH, which was associated with increased roughening of the surface due to overcrowding of the alkane chain moieties. We have also studied the stability of the H-MAMs and shown that these structures possess excellent barrier properties towards water due to close chain packing. NEXAFS experiments were carried out on the H8-MAM samples with the aim of establishing chain orientation and thus a possible semi-crystalline order in H8-MAM. As expected, no chain orientation was detected at $\Delta x = 0$ % (i.e., H8-SAMs). However, several H8-MAMs samples prepared on PDMS-UVO pre-stretched to $0\ \% < \Delta x < 30\ \%$ and exposed to OTS for 30 minutes revealed a non-negligible orientational order within the H8-MAM. Detailed analysis of the NEXAFS data revealed that the chains were tilted on average approximately 40–50° away from the sample normal [45]. While more experiments need to be carried out to confirm these findings, these results may provide indication that the "liquid"-to-"solid"-like transition in alkanes anchored to substrates can be fine-tuned by tailoring the molecular packing density.

While MAMs allow chain packing with unprecedented degree, these do not allow for tailoring the thickness of the coatings and limit the chemical composition to that of the chains that are deposited. A logical solution to this issue is thus to replace the short chain molecules with macromolecular assemblies. Grafting of polymers to substrates has grown into a mature field primarily due to the various polymerization techniques and a broad range of chemical compositions of monomers that constitute the grafted polymer layer [46, 47]. There are two general methodologies that lead to the formation of surface-tethered polymers. In the so-called "grafting onto" technique, polymers are synthesized in bulk and grafted chemically to the substrate via a reactive end. While easy to carry out, the method's primary limitation is insufficient grafting density of the polymer anchors on the substrate. This limitation can, in principle, be overcome by synthesizing polymers directly on the surface. In the so-called "grafting from" method, polymerization initiators are immobilized chemically on the substrate, which then serve as center points, from which polymers grow. While this method removes the primary limitation of the "grafting onto" approach, it possesses an upper limit of grafting densities because of large number of terminating chains close to the substrate [48, 49]. The methodology described earlier in preparing MAMs can, in principle, overcome this limitation. The scheme in Fig. 3.7 depicts the technological steps involved in the so-called "mechanically assisted polymerization assembly" (MAPA) method [50]. We first pre-stretched a slab of PDMS SEN, activated its surface with UVO and deposited chlorosilane-based polymerization initiators. Surface-initiated polymerization of acrylamide following the atom transfer radical polymerization (ATRP) [51–53] resulted in macromolecular polyacrylamide (PAAm) grafts. After polymerization the original strain was removed from the SEN support, which, in turn, returned to its original size. The last step provided further densification of the grafted

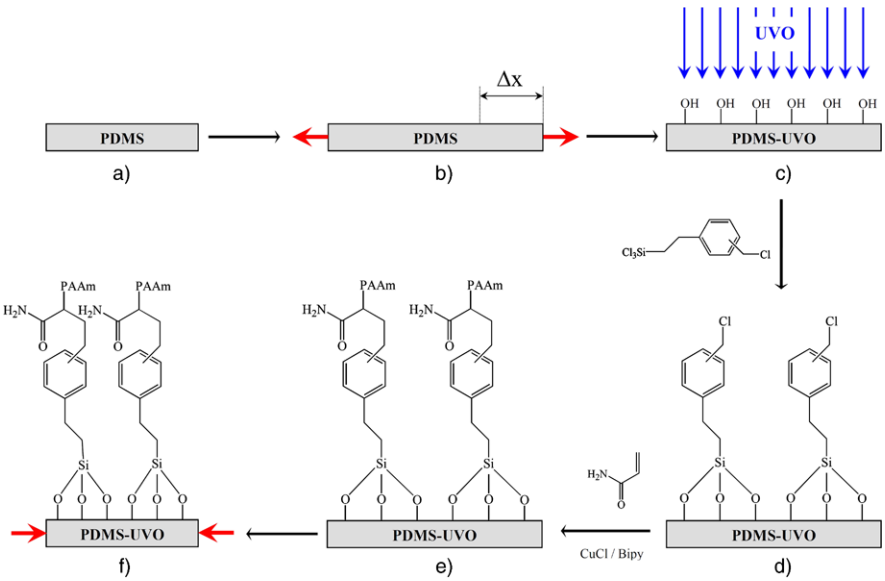

Fig. 3.7 Schematic illustrating the principle of preparing high-density polyacrylamide bushes using MAPA ("mechanically assisted polymer assembly"). A slab of PDMS (**a**) is mechanically elongated (**b**) and exposed to a brief UVO treatment (**c**). The latter provides attachment points for chlorosilane-based initiator that forms monolayers after chemisorptions (**d**). Polymerization from the initiator center results in macromolecular grafts (**e**). Upon releasing the strain from the substrates the density of the polymeric assemblies increases (**f**) proportionally to the initial degree of stretching of the bare substrate, Δx. Reproduced from Ref. [50] with kind permission of © The American Chemical Society (2001)

polymer assemblies, as documented in our original publication [50]. Thus, by controlling the degree of stretching on the elastomeric substrate, one can adjust conveniently the density distribution of the polymer chains on the substrate. There are obviously many different variants of this method that enable further adjustment of grafting densities of the polymer grafts on the substrate. Those will not be discussed here, however.

The MAM technology can also be employed for controlling spatial distribution of molecular grafts [54]. The first method we describe leads to molecular wettability gradients with tunable steepness. Here we combine the substrate stretching/UVO activation with a chemical vapor deposition of organosilanes developed by Chaudhury and Whitesides [55]. The technological process, described schematically in the upper portion of Fig. 3.8, involves pre-stretching the PDMS substrate and UVO activation, as described before. The molecular gradient is then prepared by letting short organosilanes evaporate for controlled periods of time in a closed vessel. The width of the gradient depends on the evaporation time of the molecules, as described elsewhere [56, 57]. However, further tuning of the width of the molecular gradient can be achieved by varying the strain on the PDMS sample before the gradient formation. The water wettability profiles on molecular gradients made of OTS are plotted

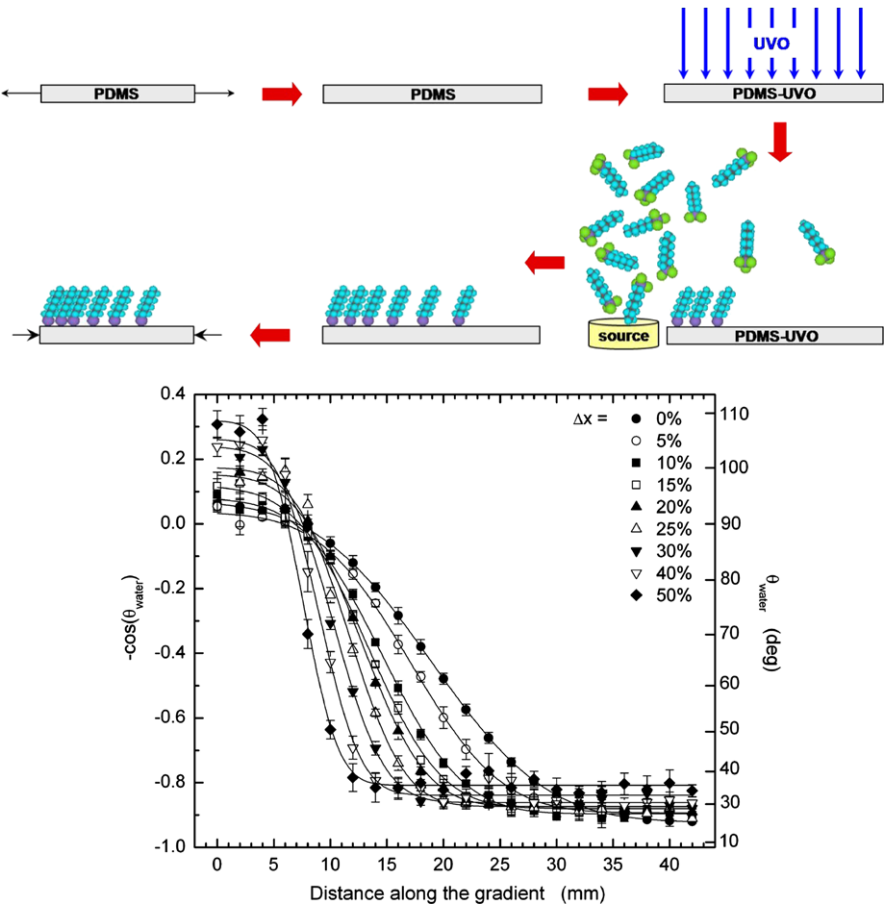

Fig. 3.8 (*Top*) Schematic illustration of the formation of molecular gradient with tunable steepness. (*Bottom*) Contact angles of deionized water along gradient substrates prepared on PDMS network films that were previously extended by Δx for 0 % to 50 % and treated with UVO for 30 min. The gradients were deposited from a vapor source exposed to the substrates for 5 min. Reproduced from Ref. [54] with kind permission of ©John Wiley and Sons (2001)

in Fig. 3.8 for various degrees of pre-stretching of the SEN substrate before the gradient formation. The abscissa denotes the distance along the PDMS substrate, 0 mm being the closest point to the evaporating source of organosilanes. Inspection of the data shows a steeper concentration profile at ≈5 mm that plateaus at constant wetting angle at ≈12 mm. In this method, the majority of hydrophobic OTS molecules were packed in the 0–15 mm region in contrast to a more gradual distribution of hydrophobic moieties in the unstretched samples.

While the density of MAMs can be tailored by simply adjusting the applied strain, more complex density profiles of the grafted chemical modifiers can be achieved by varying the shape of the original PDMS SEN substrate [58]. Figure 3.9

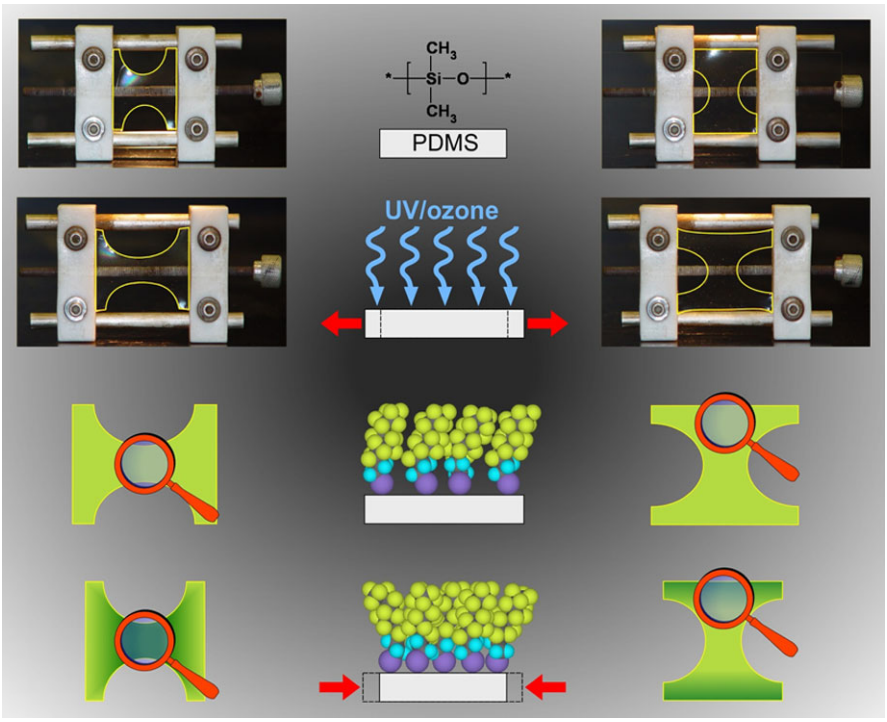

Fig. 3.9 Photographs of PDMS sheets with a "bone-like" shape clamped in the stretching apparatus before stretching (*top*) and after imposing the 40 % uniaxial strain (*bottom*) in two different sample orientations. The cartoons in the bottom portion of the figure represent the concentration of semifluorinated SAMs (*top*) and HAMs (*bottom*); the latter one formed after removing the strain from the specimens

depicts the sample shape and stretching apparatus employed in our study. Specifically, a PDMS slab having a "bone-like" shape was inserted in the apparatus in two different orientations. The sample deformation after mechanical stretching differs depending on the sample orientation. Specifically, the portion of the specimen that is continuous between the stretching clamps gets elongated most, while the remaining parts of the sample exhibit only a small degree of mechanical deformation. After UVO activation of the elongated PDMS sample, a t-F8H2 SAM was deposited uniformly onto the sample and the strain was relaxed from the sample. Due to the different spatial distribution of strain in the stretched sample, the degree of packing of the t-F8H2 molecules in the relaxed sample state varied spatially; it was higher in the regions that were stretched continuously decreasing gradually to the remaining portions of the specimen. Clearly, the degree of packing depended on the strain imposed on the PDMS substrate after stretching. Combinatorial NEXAFS spectroscopy [59] was employed to determine the in-plane t-F8H2 concentration on the PDMS substrates.

3.4 Turning Flat SENs into Topographically Corrugated Surfaces

The techniques described in Sect. 3.2 of this chapter all benefited from the rather high chemical stability of PDMS SENs. While a brief UVO treatment created a relatively small number of hydrophilic groups, it did not compromise the mechanical characteristics of the PDMS substrates. We already pointed out earlier in Sect. 3.2 that prolonged UVO treatment of PDMS resulted in the formation of ≈5 nm thick top silica-like layer resting on the unmodified flexible PDMS support. Mechanical deformation of this bilayer (either in tension or in compression) gives rise to interfacial instabilities that result in the formation of buckles/wrinkles [60, 61] with a characteristic wavelength of the wrinkles (λ) thus formed given by

$$\lambda = 2\pi h \left[\frac{(1-\nu_B^2)E_S}{3(1-\nu_S^2)E_B} \right]^{1/3} \tag{3.1}$$

In Eq. (3.1) h is the thickness of the top skin (S), E_S and E_B are the elastic moduli of the skin and the elastic base (B), respectively, and ν_S and ν_B are the Poisson ratios of the skin and the base, respectively. The mechanism of buckle formation is as follows. The UVO treatment densifies the upper surface of the PDMS skin and leads to an equilibrium (strain-free) configuration of the skin that resides on top of the flexible substrate, which is still under tensile strain. When the strain is relieved from the specimen, the substrate attempts to contract back to its strain-free configuration. However, the mismatch between the equilibrium strains of the stiff skin and the soft substrate prevents this from happening uniformly throughout the depth of the material. The competition between the bending-dominated deformations of the skin and the stretching/shearing-dominated deformations of the substrate causes the skin to wrinkle in response to the relaxation of the applied strain [60].

While Eq. (3.1) holds for small strains (a few percent), it does not describe quantitatively situations that involve stretching to much larger extensions. As is described below, imposing large strains on sample results in the formation of buckles with multiple wavelength generations (and amplitudes) that are organized in a hierarchical fashion. The combination of mechanical deformation and UVO treatment, depicted schematically in Fig. 3.10, may thus result in surfaces with two very different surface topographies.

In order to investigate the effect of strain on the formation of the silica-like/PDMS bilayer, PDMS was strained mechanically to 30–70 % while being exposed to UVO for prolonged periods of time [62]. Optical microscopy and atomic force microscopy (AFM) experiments confirmed that the surfaces were originally flat even in the presence of strain. After the UVO treatment, the strain was removed from the specimen, which exhibited buckles oriented in the direction perpendicular to the strain. A detailed analysis of the buckled surface with AFM and profilometry uncovered that the buckling patterns were hierarchical. In Fig. 3.11 we show representative microscopy images depicting the various buckle generations. Buckles with smaller wavelengths (and amplitude) rested parallel to and within larger

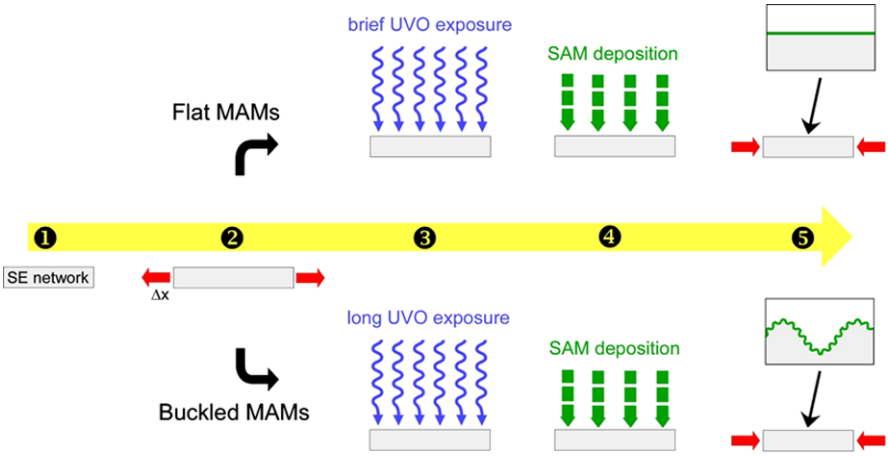

Fig. 3.10 Schematic representation of the response of silicone elastomer networks (SENs) to strain and UVO treatment. A SEN (1) is stretched mechanically (2) and exposed to UVO radiation (3) for various times (i.e., dosages of the UVO). The stretched and UVO-modified substrates are exposed to a vapor of fluorinated chlorosilanes (4). Depending on the UVO dosage, upon release of the initial strain the samples comprise either flat fluorinated topographies (low UVO dosage) or produce hierarchically-corrugated fluorinated buckles (high UVO dosage)

buckles, forming a nested structure. Figure 3.11e summarizes the AFM and profilometry results of the buckle periods. Specifically, the data in Fig. 3.11e reveal that at least five distinct buckle generations (G) are present: the wavelengths of the generations (λ) are G1: ≈50 nm, G2: ≈1 μm, G3: ≈5 μm, G4: ≈50 μm, and G5: ≈0.4 mm. Using experimentally established E_S/E_B (≈15 and ≈87 for PDMS specimens treated with UVO for 30 and 60 min, respectively) and h (≈5 nm for UVO times >60 min) by means of nanoindentation and x-ray reflectivity, respectively, we estimated $\lambda \approx 12$ and ≈22 nm, respectively, for the two UVO treatment times. From the data in Fig. 3.11, the estimated λ corresponds to the experimentally measured periods of the first generation of buckles (G1).

As stated earlier, the basic driving force behind wrinkling is the mismatch in the equilibrium states of the skin and the substrate due to the competition between bending of the skin, which penalizes short-wavelength buckles, and stretching the unmodified substrate base, which penalizes long wavelengths [60]. This sets the stage for the amplitude of the primary wrinkles to grow as the applied strain is further relieved. Eventually the amplitude saturates owing to nonlinear effects in stretching and shearing the substrate. The composite of the wrinkled skin and the stretched substrate leads to the formation of an "effective skin" that is now thicker and much stiffer than the original one. Further release of the applied strain results in additional effective compression; consequently, the composite skin buckles on a much larger length scale, creating a hierarchical buckled pattern (see Fig. 3.11e). The formation of higher generation buckles continues until the strain is removed completely from the substrate. In an infinite system there is clearly no limit to this hierarchical patterning. Even in this finite system, up to five generations of these

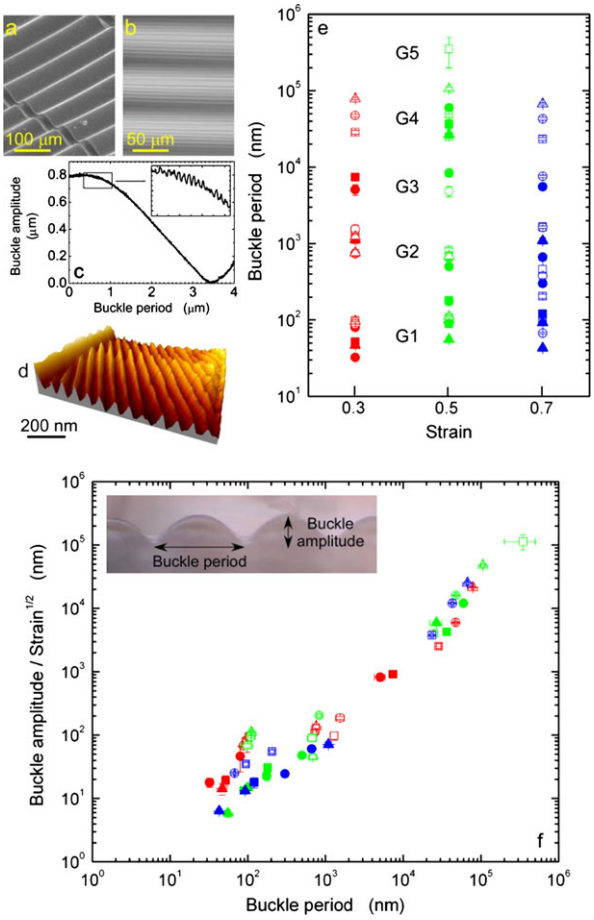

Fig. 3.11 (**a**) Scanning electron microscopy image of a buckle on PDMS substrate revealing the G4 generation of buckles. (**b**) Optical microscopy image in the transmission mode of G3 and G4 generations of buckles. (**c**) Topography profile collected with profilometry on G2 (*inset*) and G3 (main figure) generations of buckles. (**d**) Scanning force microscopy image revealing the structure of G1 buckles. (**e**) Buckle period as a function of the strain imposed on the samples before the UVO treatment lasting for 30 (*squares*), 60 (*circles*), and 90 (*up-triangles*) minutes as measured by scanning force microscopy (filled symbols) and profilometry (*open symbols*). (**f**) Ratio of the buckle amplitude to the square root of the strain plotted as a function of the buckle period on a log–log plot. The data collapse onto a straight line consistent with the prediction of Eq. (3.1). Reproduced from Ref. [62] with kind permission of © Nature Publishing Group (2005)

hierarchical buckles are arranged in a nested manner; each buckle generation represents a scaled-up version of the primary buckle (see Fig. 3.11f). The smallest buckles possess wavelengths of a few nanometers while the largest ones are almost a millimeter in size, thus spanning nearly five orders of magnitude in dimension. Cerda and Mahadevan established that the amplitude of a wrinkle (ζ) scales as $\zeta = \lambda\varepsilon^{1/2}$, where ε is the implied strain [63]. Using this relation the scaled experimental buckle

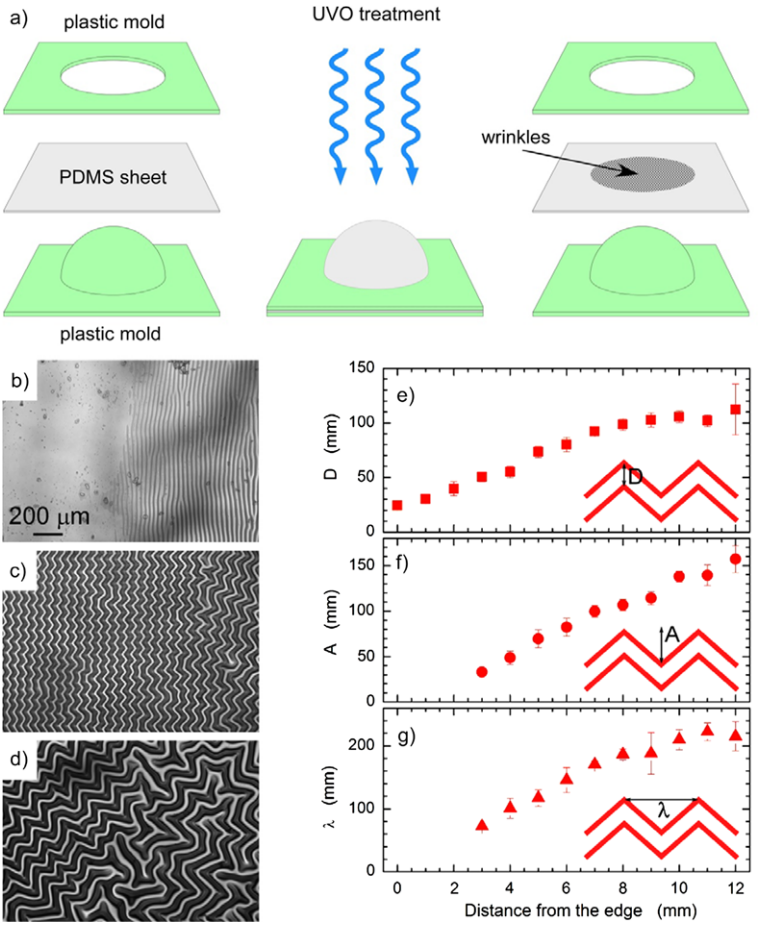

Fig. 3.12 (**a**) Schematic illustration of the formation and properties of biaxial hierarchically-wrinkled surface topologies (bHWST). (**b**)–(**d**) Optical micrographs of the bHWST taken at different locations along the sample ((**b**): close to the edge, (**c**): half way between the edge and the center, and (**d**): center). (**e**)–(**g**) variation of the wrinkle geometrical features (defined in the insets) as a function of the position along the substrate (0: edge, 12.5 mm: center). The scale bars in (**c**) and (**d**) are identical to that in (**b**). Reproduced from Ref. [66] with kind permission of © The American Chemical Society (2009)

amplitudes $\zeta/\varepsilon^{1/2}$ as a function of λ plotted in Fig. 3.11f all collapse roughly on a master curve.

The orientation of buckles does not have to always follow the parallel geometry and can be altered by various means [61]. Perhaps the easier method leading to non-parallel buckle morphology involves varying the direction of strain imposed on the SEN support before the UVO treatment. For instance, specimens bearing biaxial wrinkle topographies can be generated by the method depicted in Fig. 3.12. Here, a flat sheet of PDMS was stretched over a support containing a hemispherical tem-

plate. After extensive UVO treatment, the substrate was removed from the assembly; the wrinkling pattern was present in a circular area with a diameter of ≈25 mm. In this biaxial stretching geometry the surface topography comprises three wrinkling/buckling patterns. While close to the sample periphery the buckles/wrinkles are aligned parallel to the edge (see Fig. 3.12b), in the center of the sample the wrinkles adopt a disordered orientation (see Fig. 3.12d). Wrinkles that reside between the uniaxial and disordered geometries adopt chevron-type patterns (see Fig. 3.12c) that have been reported earlier [64, 65]. Figures 3.12e–3.12g represent the variation of the sizes of the three structural characteristics of the chevrons as a function of the position of the distance from the edge of the wrinkling pattern. The biaxial strain was estimated to be ≈50 %.

We conclude this section by commenting briefly on possible applications of wrinkled substrates. Due to space limitation we keep this discussion very succinct. In our original publication, we have demonstrated that hierarchically wrinkled substrates may provide a convenient platform for separating objects, such as particles, of various sizes from multicomponent mixtures by means of selective sedimentation [62]. We have also used surfaces with hierarchically wrinkled topographies as marine antifouling release coatings. In our recent work we have provided evidence that the presence of hierarchically organized topographies in combination with fluorinated chemistries provides a convenient platform for minimizing adhesion of barnacles [66]. More work is currently underway that aims at understanding the combined role of surface topography and chemical composition of buckled surfaces on controlling the adhesion of some biological species, such as barnacle cyprids [67]. Many other examples of buckle applications can be found throughout the literature [61, 68–70].

3.5 SEN as a Material Platform for Creating Responsive/“Smart” Materials

From the previous discussion it is evident that plasma, corona, UVO (or other, not specifically mentioned) treatments are capable of changing the hydrophobic nature of SEN into hydrophilic. The degree of modification depends on the chemical nature of the SEN combined with the characteristics and dosage of the modifying radiation. Two of the biggest advantages of these techniques are their simplicity and ability to modify just about any type of SEN, including the most hydrophobic and chemically resistant PDMS. The major drawbacks represent the inability to endow the newly created materials with well-defined chemical groups and controlling the penetration depth into which the radiation propagates and causes irreversible chemical and physical changes of the parent SEN material. While the latter does not represent typically a problem for the applications described thus far, it limits the opportunities functionalized SEN offer for creating surfaces with tailored characteristics, including so-called responsive/“smart” materials.

Responsive materials have recently gained their market share as novel dynamic structures that exhibit multiple physico-chemical functionalities, which can be triggered through changes in some external stimulus, i.e., electrical, chemical, thermal or mechanical [71]. The two key parameters that define the functionality (and ultimately application) of any responsive surface are (1) the degree of change of the surface properties after the external trigger was applied, and (2) the rate at which these changes occur. Hence a "supreme" responsive surface is one that responds instantaneously to changes in its environment with a measurable property change. In most cases, the responsiveness of the surface is a result of the rearrangement of the various chemical functionalities present close to or directly at the surface. The required degree of control over these characteristic changes is dependent on the end-use for the surface. Surfaces may respond to the changes in the outside environment in several ways. Various chain constituents can either be delivered to the surface from the bulk or, when already present at or close to the surface, they can rearrange locally. In the former case, surface segregation occurs due to disparities between the surface energy of the monomers (or parts of the polymers such as end-groups), polymer flexibility, tacticity and molecular weight. This is a rather slow process and not very suitable for creating responsive surfaces with fast response time. The presence of a chemical moiety, different from the rest of the chain, may influence local chain rearrangements in the latter case. This process is faster than surface segregation, however, it still occurs on time scales of minutes or even longer depending on the nature of the matrix from which the chain ends segregate. While some of the most powerful stimuli-responsive materials have been formed from surface-anchored polymer macromolecules [71–75], polymer networks, including specialty SENs, have also shown great promise. We have shown that SENs indeed represent an attractive platform for creating effective responsive materials. Their low T_g ($\approx$150 K for PDMS) depending on the chemical structure, endows them with exceptional mobility even at room temperature. As will be demonstrated later, the ability to attach just about any functional group facilitates anchoring functional moieties with a variety of chemical structures and functions.

We have introduced PVMS earlier as a functional alternative to the more widely used PDMS. The presence of two different functional groups attached to the Si atom, i.e., methyl and vinyl, which exhibit different surface energies, endows PVMS with inherent surface responsiveness. Our initial observation of reversible PVMS siloxane surfaces was demonstrated by water contact angle measurements [34]. As the vinyl group possesses a slightly higher surface energy than the methyl group, it hides beneath the surface when exposed to hydrophobic environments, such as air. Exposure to water leads to rearrangement of the two moieties at the surface as the preferred state in hydrophilic environments is dominated by the vinyl groups at the surface. As contact angle measurements are sensitive to just the first $\approx$5 Å of the polymer surface, the rearrangement of functional groups on the surface can be observed by tracking contact angle changes over time [76].

In order to further accentuate the difference in surface energy between the two groups, one can modify selectively the vinyl groups through direct covalent attachment of various functional groups via addition reactions, i.e., hydrosilylation,

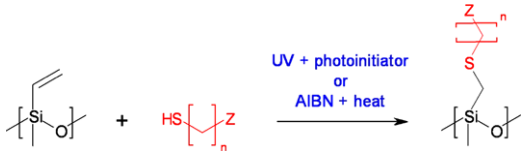

Fig. 3.13 Schematic of thiol-ene addition to PVMS. Z denotes an end-functional group (i.e., -COOH, -OH) on the alkanethiol

hydrosulfidation (thiol-ene), hydrophosphination, epoxidation, metathesis or alkyl halide addition [77–82]. We have opted for thiolene modification [83] by following the successful demonstration of this reaction by others [84]. The reaction scheme, shown schematically in Fig. 3.13, involves activation of the –SH group on a functional thiol by either UV or by heat (either with or without an addition of a photoinitiator, such as commercial Darocur®, or a more common free radical initiator, i.e., azobisisobutyronitrile, AIBN). We have performed a series of experiments implementing the thiol-ene addition reaction to PVMS. In an early study, modifying PVMS substrates with 3-mercaptopropionic acid and 11-dodecanethiol led to PVMS-S-$(CH_2)_2COOH$ and PVMS-S-$(CH_2)_{11}CH_3$, respectively. In both instances, the addition to the vinyl bond was confirmed via the elimination of the C=C peaks at 960, 1407 and 1587 cm^{-1} in ATR-FTIR spectroscopy. When the PVMS-S-$(CH_2)_2COOH$ SEN was exposed to air, the methyl groups populated the substrate/air interface while the carboxy-terminated pendent group resided underneath the surface. Exposing the substrate to water repelled the methyl groups from the surface as the preferred energy state was to maximize the polar interactions at the water-carboxy interface. The opposite situation was seen for PVMS-S-$(CH_2)_{11}CH_3$. Here alkyl chains longer than methyl populated the substrate/air interface but would "hide" beneath the surface when exposed to water, thus allowing the shorter and less hydrophobic methyls to occupy the sample surface region (see Fig. 3.14). More details pertaining to the behavior of the two systems can be found elsewhere [85]. We only comment here on the responsive behavior of PVMS-S-$(CH_2)_2COOH$, which exhibited a large changes ($\approx 40°$) in water contact angle when exposed to a drop of water in 20 s, demonstrating the fastest observed responsiveness rate of $\approx 2° \, s^{-1}$ in any polymeric material.

In order to comprehend completely the effect of chain length on the rearrangement kinetics, PVMS sheets were modified with three different mercaptoalkanols: $HS(CH_2)_2OH$, $HS(CH_2)_6OH$, and $HS(CH_2)_{11}OH$, leading to PVMS-S-$(CH_2)_2OH$, PVMS-S-$(CH_2)_6OH$, and PVMS-S-$(CH_2)_{11}OH$, respectively, [85–87]; their chemical structures are shown in the upper right section of Fig. 3.15. We have employed dynamic contact angle (DCA) measurement to access wettability changes in the specimens in 10 subsequent runs. After each run, the sample was dried with a nitrogen gas purge. Repeatability testing was done on three independent samples to insure consistent results. The initial cycle of DCA measurements performed for each substrate agreed with the static contact angle results [85]. The left panel in Fig. 3.15 depicts the DCA results from (top to bottom) PVMS, PVMS-S-$(CH_2)_2OH$, PVMS-S-$(CH_2)_6OH$, and PVMS-S-$(CH_2)_{11}OH$, illustrating the restructuring of the modified mercaptoalkanol substrates between wet and dry states. The response rate to wettability changes was very fast for the first three samples and decreased for

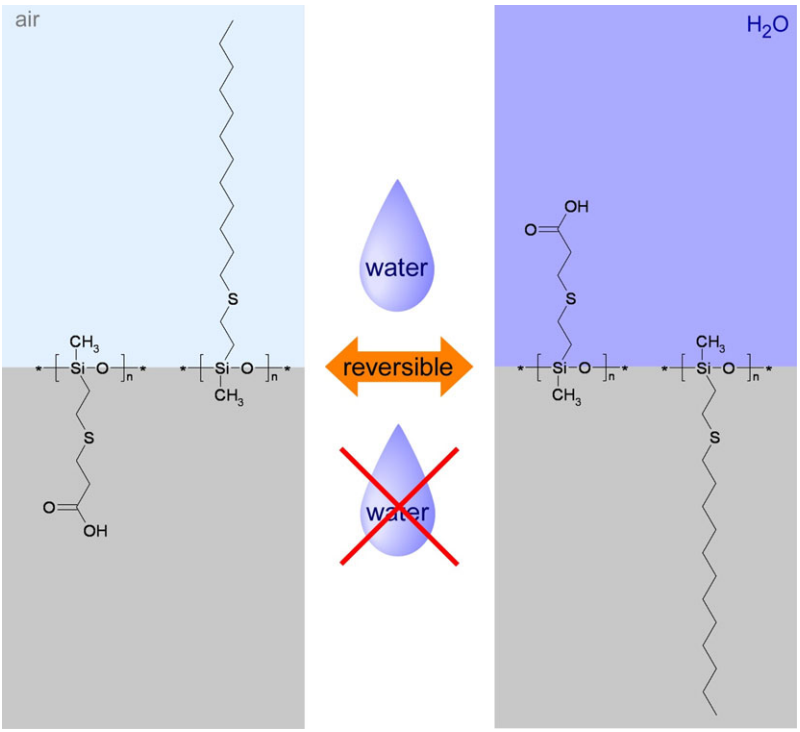

Fig. 3.14 Schematic illustration of the molecular orientation of PVMS modified with 3-mercaptopropionic acid ($HS(CH_2)_2COOH$) and 11-dodecanethiol ($HS(CH_2)_{11}CH_3$) at the SEN/air and SEN/water interfaces

PVMS-S-$(CH_2)_{11}$OH. Further insight regarding chain reorganization on the PVMS and mercaptoalkanol-modified PVMS surfaces was obtained from monitoring the CAH, $\Delta\theta$, with the DCA experiments. The plot in the bottom right portion of Fig. 3.15 presents the $\Delta\theta$ for all substrates over the 10 repeating wettability cycles. The most responsive surface, PVMS-S-$(CH_2)_2$OH, possesses the largest observed hysteresis of $\approx$75°, which is consistent with its repeatable and reversible state between a polar and non-polar environment.

The sluggish reconstruction rate observed in PVMS-S-$(CH_2)_{11}$OH was attributed to ordering of the –$(CH_2)_{11}$– alkanes due to inter-chain van der Waals interactions. The resulting semi-crystalline nature of –$(CH_2)_{11}$– prevented the rapid reconstruction observed in PVMS-S-$(CH_2)_2$OH and PVMS-S-$(CH_2)_6$OH, which remained in a flexible liquid-like state, allowing continued oscillations for at least 10 cycles. The semi-crystalline nature of PVMS-S-$(CH_2)_{11}$OH was supported with three independent measurements: (1) the level of opaqueness, (2) a change in the storage modulus (G′), and (3) ATR-FTIR results (see Fig. 3.16). PVMS, PVMS-S-$(CH_2)_2$OH and PVMS-S-$(CH_2)_6$OH were transparent, elastic, and tacky. In contrast, the PVMS-S-$(CH_2)_{11}$-OH specimens were opaque, rigid, and non-adhering. Upon immersion into hot water ($\geq$70 °C), PVMS-S-$(CH_2)_{11}$-OH turned transparent

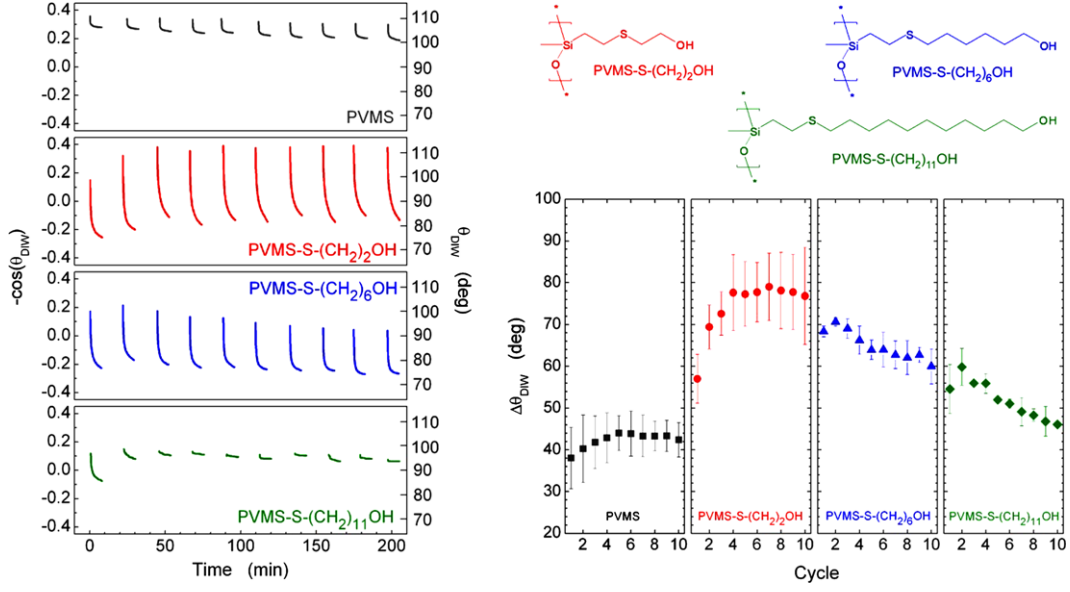

Fig. 3.15 (*Upper right*) Structures of alkanethiols used in the study. (*Upper left*) Time dependence of the DI water wettabilities for PVMS-S-$(CH_2)_n$OH surfaces measured by dynamic contact angle. The error for θ_{DIW} is $\pm 1.5°$. Contact angle hysteresis ($\Delta\theta = \theta_{advancing} - \theta_{receding}$) for a dynamic contact angle cycle depicted the upper left portion of the figure for: PVMS (*squares*), PVMS-S-$(CH_2)_2$OH (*circles*), PVMS-S-$(CH_2)_6$OH (*triangles*), and PVMS-S-$(CH_2)_{11}$OH (*diamonds*). Reproduced from Ref. [85] with kind permission of © John Wiley and Sons (2009)

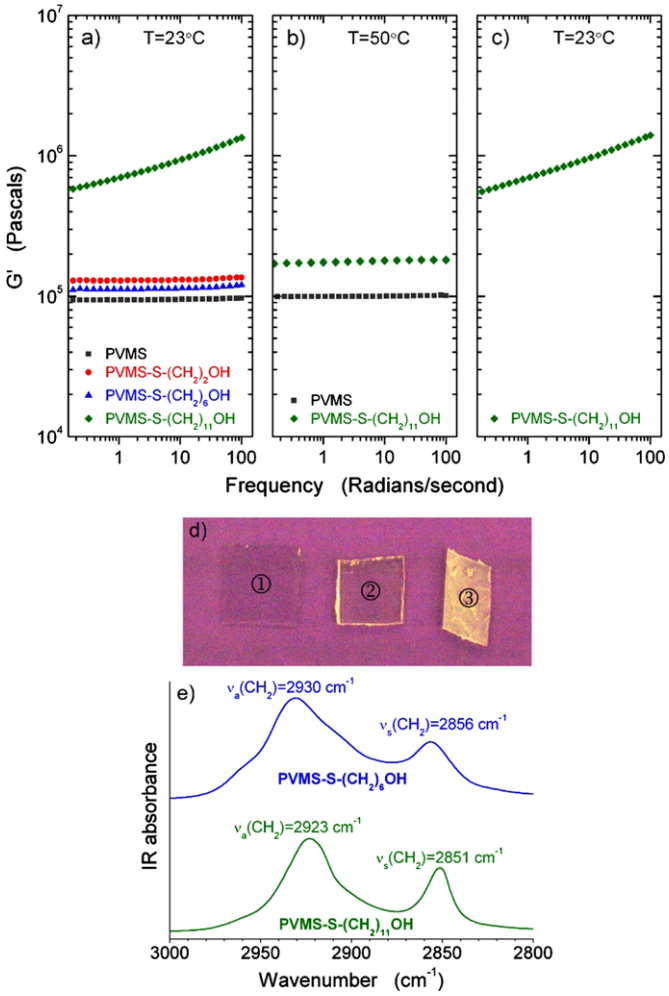

Fig. 3.16 Dynamic rheology on PVMS and mercaptoalkanol-modified PVMS substrates. Runs performed at sequential operational temperatures (T): (**a**) 23 °C, (**b**) 50 °C, and (**c**) 23 °C. The average standard deviation of data is ±33 kPa. (**d**) Photographs of mercaptoalkanol-modified PVMS substrates in front of an opaque background; (1) PVMS, (2) PVMS-S-$(CH_2)_6$OH and (3) PVMS-S-$(CH_2)_{11}$OH. The opaqueness is indicative of crystallization. (**e**) ATR-FTIR for the PVMS-S-$(CH_2)_6$OH and PVMS-S-$(CH_2)_{11}$OH substrates; the lower frequencies for the methylene asymmetric and symmetric stretches in PVMS-S-$(CH_2)_{11}$OH are a signature of a semi-crystalline structure. Reproduced from Ref. [85] with kind permission of © John Wiley and Sons (2009)

but became opaque upon cooling. When quenched to room temperature water immediately after the hot water treatment, the surface 'froze' at a water contact angle of ≈80°. When these same samples were allowed to slowly cool the methyl groups had more time to rearrange to the surface as indicated by the water contact angle in-

creasing to >95°. Dynamic mechanical testing revealed that while PVMS, PVMS-S-$(CH_2)_2$OH and PVMS-S-$(CH_2)_6$OH were quite soft, the storage modulus, G′, of PVMS-S-$(CH_2)_{11}$OH was about 10-fold higher (see Fig. 3.16a). Upon heating at 50 °C, i.e., above the melting point of 11-mercaptoundecanol (33 ∼ 37 °C [88]), the G′ of PVMS-S-$(CH_2)_{11}$OH decreased and became frequency independent, indicating that the network had reached a near-perfect elasticity (see Fig. 3.16b). When cooled down, however, the mechanical response of PVMS-S-$(CH_2)_{11}$OH recovered to the values detected before heating (see Fig. 3.16c). Thus the ordered alkane chains were acting as filler-like reinforcers at room temperature disrupting the elastic nature of the siloxane network. Finally, we performed a detailed ATR-FTIR analysis to provide further evidence supporting our claims that the 11-mercapto-1-undecanol modified PVMS surface had undergone a phase transition with the formation of semi-crystalline domains. The FTIR spectra for PVMS-S-$(CH_2)_6$OH and PVMS-S-$(CH_2)_{11}$OH substrates shown in Fig. 3.16e exhibit characteristic asymmetric and symmetric C-H stretches of the methylene group. While liquid methylene chains feature stretching vibrations at 2930 cm^{-1} and 2856 cm^{-1}, in crystalline methylene chains those occur at 2923 cm^{-1} and 2851 cm^{-1}. The downward shift in both symmetric and asymmetric C–H stretches observed in the latter specimen, which is consistent with earlier reports [43, 44] reinforcing our earlier findings, namely, that while PVMS-S-$(CH_2)_6$OH remains completely flexible at room temperature, PVMS-S-$(CH_2)_{11}$OH contains a large number of semi-crystalline domains. Detailed temperature-dependent FTIR experiments enabled us to follow the transition from semi-crystalline to liquid states in PVMS-S-$(CH_2)_{11}$OH [85].

More insight into the observed surface responsive behavior has been gained recently by combining a palette of experimental methods including dynamic mechanical testing, differential scanning calorimetry and dielectric relaxation spectroscopy [87]. These methods provided information about pendant and PVMS-backbone relaxations in the stimulus-responsive PVMS SENs. The glass transition of PVMS was not affected by SEN formation but increased significantly with introduction of the -S-$(CH_2)_2$-based pendant groups. For instance, for PVMS-S-$(CH_2)_2$-CH_3 and PVMS-S-$(CH_2)_2$-OH we measured the change in T_g of +40 K and +25 to +40 K, respectively, relative to PVMS ($T_g \approx 145$ K). While ΔT_g of PVMS-S-$(CH_2)_6$-OH was similar to that of PVMS-S-$(CH_2)_2$-OH, the T_g increased considerably ($\Delta T_g \approx 130$ K) for PVMS-S-$(CH_2)_{11}$-CH_3 and PVMS-S-$(CH_2)_{11}$-OH. Thus the T_g of the network changed as a result of the presence of different groups constraining the siloxane backbone to differing degrees, indicating that network dynamics can be tuned markedly by adjusting the size, shape, and polarity of the pendant groups. Importantly, the wettability macroscopic response time and amplitude measured previously by DCA correlated well with the observed changes in T_g glass transition temperatures, providing evidence that these two effects likely arise from the same source; namely, the increased interactions between pendant groups increase the rigidity of the entire system.

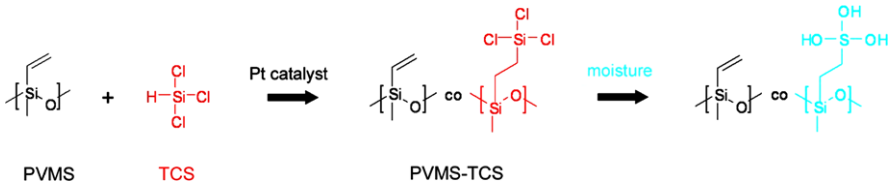

Fig. 3.17 Coupling of trichlorosilane (TCS) molecule to vinyl groups of PVMS via the hydrosilylation reaction

3.6 A Quest Towards Universal Coating Layers

In the final section of this chapter we present a brief account of a new technology to modify surfaces of SENs that differs from those described previously. To recall, we have outlined physical and chemical methods using which surfaces of SENs can be altered to achieve desired functionality. We have also pointed out advantages and disadvantages of those methodologies. The approach described below offers an exciting new opportunity to decorate surfaces of just about any SEN by depositing functional surface coatings.

SENs, just like most other polymeric materials, are inherently hydrophobic. Physical modification methods can be employed commonly to alter these surfaces but they come at a cost of losing some functionality or lead to irreversible (and often hard to control) changes of the base material. Methods based on plasma/corona/UVO treatments do not allow one to control properly the chemical composition of the surface and also the depth into which they modify the original support. Metallization, often utilized in many solid state materials, may also not solve the problem completely as delivering a layer of metal (or any non-polymeric substance) via sputtering or evaporation would likely result in composites that posses some degree of buckling (given the soft nature of the polymeric substrate) [89–93]. This leaves one with a possible alternative, namely, coating the substrate with a soft layer made of a functional polymer. Accomplishing this task is not easy, however, given that, as stated earlier, polymers are typically hydrophobic and assuring a sufficient level of adhesion between the support and the new coating layer is not straightforward. We have recently developed a simple method capable to delivering the desired functionality of just about any support materials, i.e., polymeric or non-polymeric, by means of depositing a highly tailored top SEN-based coating.

The presence of the vinyl group in PVMS allows for relatively simple chemical modifications of the parent material. We couple trichlorosilane (TCS) to the PVMS backbone via hydrosilylation reaction in the presence of a platinum catalyst, as shown in Fig. 3.17. The coupling reaction results in the formation of silicone random copolymers comprising the parent (VMS) and modified (VMS-TCS) units. When exposed to a minute amount of moisture, the chlorosilane groups get converted quickly and quantitatively into silanols (Si-OH), which can then either condense with each other (resulting in a relative stable network) or attach to hydrophilic functionalities on surfaces. We benefit from both functions of the Si-OH groups and

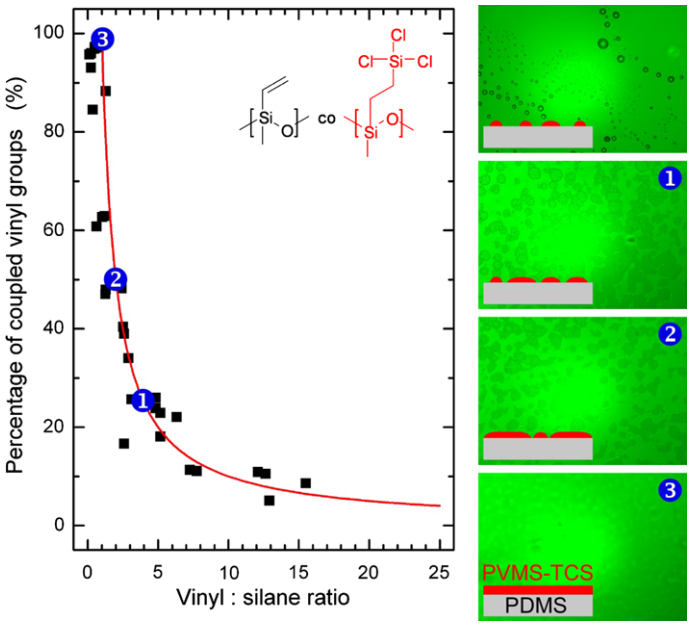

Fig. 3.18 (*Left*) The percentage of reacted vinyl groups with the TCS molecules as a function of the vinyl:TCS ratio. (*Right*) Optical images of PVMS-TCS coated PDMS network with PVMS-TCS that has different percentages of the coupled vinyl groups. The numbers in the images correspond to the concentration indicated on the plot on the left. The inset cartoons depict the suggested structure of the PVMS-TCS/PDMS bilayer

stabilize the thin PVMS-TCS layers on solid substrates via cross-linking during the spin-coating process and attachment to the underlying substrate.

The PVMS-TCS platform offers unique opportunities for tailoring both physical and chemical characteristics of the coating. The chemical composition of the copolymer, reflecting the extent of coupling between PVMS and TCS, can be tuned by varying the concentration of TCS. We demonstrate this by generating bilayers comprising PVMS-TCS coatings resting on top of PDMS supports. We prepared functional PVMS-TCS coatings by altering the ratio of the vinyl to silane (i.e., TCS) in the reaction medium. The vinyl:TCS ratio was determined with FTIR by monitoring the area under the vinyl peaks of PVMS; C=C twist/=CH_2 wagging ($\approx$960 cm^{-1}), =CH_2 scissors ($\approx$1407 cm^{-1}) and C=C stretch ($\approx$1587 cm^{-1}). In Fig. 3.18 we plot the percentage of the coupled vinyl groups as a function of the vinyl:silane ratio along with the theoretical values (solid line) calculated based on complete coupling (quantitative reaction) of vinyl:TCS groups of PVMS. As shown by the data, the experimental extents of reaction were in accord with the theoretical values confirming the quantitative nature of TCS coupling to the vinyl groups of PVMS. We then deposited PVMS-TCS layers having a different vinyl:silane content onto PDMS substrates made of commercial Sylgard-184 kit. The thicknesses of the spin-coated layers were below $\approx$50 nm, as measured via ellipsometry for films deposited onto silicon wafers. Coating PDMS-UVO with pure PVMS resulted

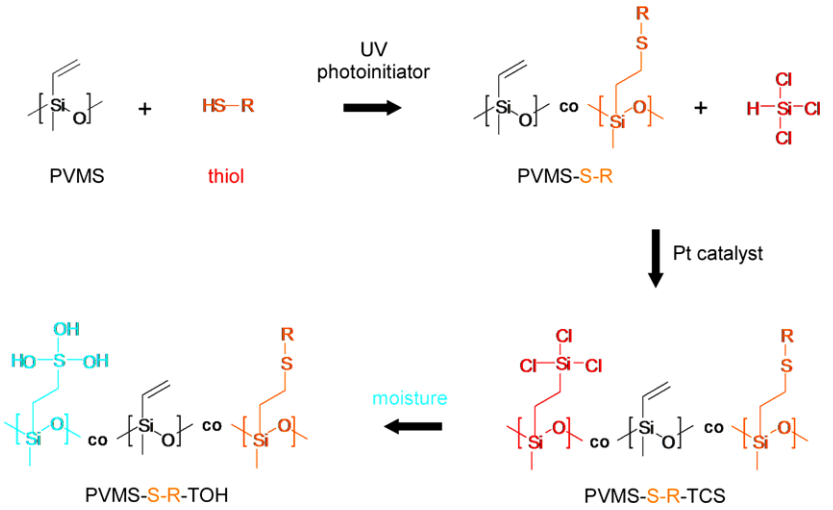

Fig. 3.19 Reaction scheme depicting the pre-modification of PVMS-TCS coating. PVMS is reacted with a thiol via UV-induced thiol-ene reaction. Hydrosilylation of a fraction of the remaining vinyl groups leads to the formation of functional PVMS-TCS material. Exposure to a minute amount of moisture converts the chlorosilane groups into hydroxysilanes

in dewetting of the top film, due to both the thermodynamic incompatibility between PVMS and PDMS and autophobicity due to the presence of the PDMS network. Spin-coating PVMS-TCS copolymers onto PDMS SENs revealed that the stability of top PVMS-TCS layer increased with increasing the extent of TCS coupling to the vinyl groups of PVMS. Optical micrographs of spin-coated layers of PDMS/PVMS and PDMS/PVMS-TCS along with the representative cartoons are depicted in Fig. 3.18. Relative to pure PVMS that exhibited islands on the substrates, the dewetted patterns comprised holes when PVMS-TCS with 25 % of TCS coupling was deposited via spin-coating on top of PDMS network substrates. The sizes of the holes decreased with increasing the extent of TCS coupling. The spin-coated layers become completely defect free and stable when all the vinyl groups in PVMS were consumed for the coupling reaction. A stable PVMS-TCS copolymer layer is formed when the rate of cross-linking exceeds the rate of dewetting during spin-coating process. Cross-linking (even partial) of the PVMS-TCS stabilizes the film by decreasing chain mobility, which, in turn, reduced the tendency of film to dewet from the PDMS support. Mechanical properties of the functional coating, such as the Young modulus, can also be tailored by varying the chemical composition (i.e., vinyl:silane content) and/or the thickness of the coating; the latter can be adjusted conveniently by varying the concentration of the copolymer in the spin-coating solution [94].

Further chemical modification can be achieved by thiol-ene coupling onto the remaining unreacted vinyl groups of the PVMS-TCS copolymer, as shown schematically in Fig. 3.19. This additional chemical treatment results in functional coatings that can provide protein-resistance, self-cleaning, scratch resistance, and other

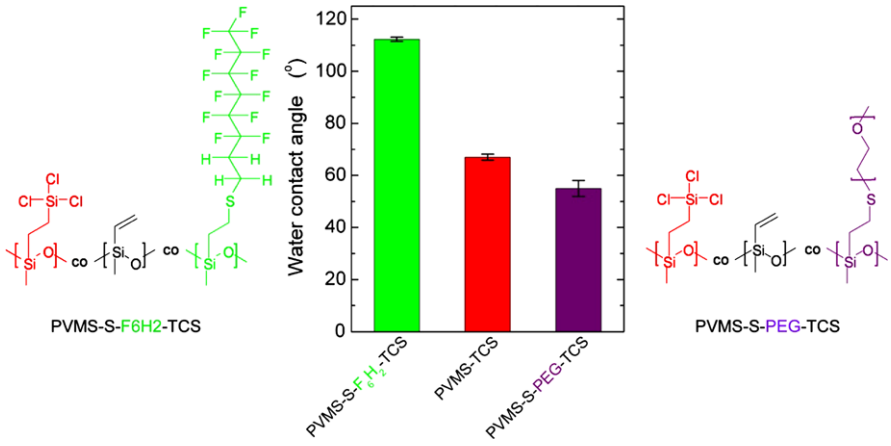

Fig. 3.20 Chemical structure of functional coatings and their corresponding wettabilities

characteristics. For instance, the PVMS chains were modified initially via thiol-ene addition reaction and then the TCS molecules were coupled to the remaining vinyl groups to introduce cross-linkable points. Two different thiol molecules, semifluorinated thiol (F6H2-SH) and thiol-terminated PEG (PEG-SH) were utilized for these reactions to generate hydrophobic and hydrophilic/protein-resistant surfaces respectively. The chemical structures and the water contact angles of the functional copolymer layers spin-coated onto silicon wafers are shown in Fig. 3.20. The F6H2 mesogens attached to the coating rendered the surface hydrophobic with a WCA of 112.3°± 0.8°. The PEG oligomers rendered the surface hydrophilic with a WCA of 55.1°± 3.1°. Chemical changes occurring on the surface of the coating were confirmed with ATR-FTIR.

PVMS-TCS copolymer coatings can be utilized to generate buckles on a variety of samples. For instance, truly biaxial buckles can be formed on the substrates that can swell in solvents. Coating the swollen polymeric substrates with PVMS-TCS, exposing the coating to moisture and following solvent removal will lead to biaxial buckles on the substrate surface provided that a modulus difference exists between the coating and the substrate. As discussed earlier, biaxial buckles on PDMS network films can be formed after prolonged UVO treatment of PDMS. It is hard to obtain truly biaxial strain over large areas on the substrates; therefore only a small portion of the resulting sample bears "real" biaxial buckles. However, homogeneous swelling of the substrates in a solvent can eliminate this problem. The tunability of the PVMS thickness and modulus would facilitate alteration of the formed buckles' wavelength. For example, a piece of PDMS network can be swollen in toluene and immersed in PVMS-TCS copolymer solution. After removing the PVMS-TCS/PDMS specimen from the copolymer solution, exposing it to moisture causes cross-linking of the top layer, which increases its modulus. Subsequent drying of PVMS-TCS/PDMS results in biaxial buckles over large area, as shown in Fig. 3.21. Combining buckle formation with the aforementioned PVMS-

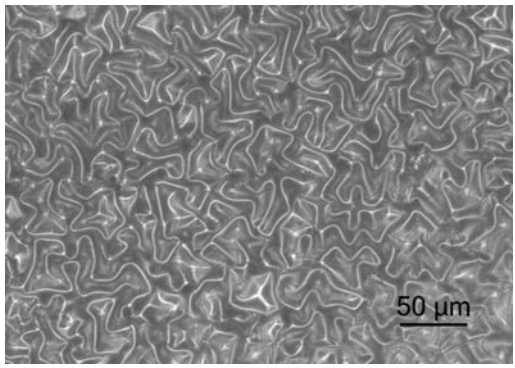

Fig. 3.21 Biaxial buckles formed on PDMS network via immersion of swollen PDMS network in PVMS-TCS copolymer solution

TCS pre-modification routes would allow facile generation of topographically corrugated surfaces.

3.7 Conclusions

This chapter provides an overview of the extensive "flexibility" of silicone elastomeric surfaces. By utilizing mechanical and chemical techniques we have manipulated SENs to comprise tunable chemical, mechanical, topographical, and dynamic characteristics. By evaluating systematically the chemical structure of two physically treated SENs, i.e., PDMS and PVMS, we have demonstrated the fundamental differences of UVO-modification processes to each type of SEN. We capitalized on the flexibility of the silicone backbone to create mechanically assembled monolayers (MAMs) on SENs via mechanically stretching the network and applying the UVO treatment. This allowed full exposure of the SEN substituents to radiation for efficient conversion to the polar moieties. The polar moieties served as reactive sites for subsequent organosilane modification. Performing chemical changes on the SEN in the stretched state allowed the "grafting to" molecules accessibility to the reactive sites. Once the tension was released from the elastomer, the grafted molecules packed densely on the SEN surface creating a superhydrophobic surface with minimal surface mobility preventing rearrangement thus generating the ultimate stable surface. Throughout our work of physical modification of these unique elastomeric substrates we observed surface wrinkling, which took place due to the mismatch of elastic properties between the modified "skin" and the bulk of the elastomer. Understanding the fundamental aspects of the wrinkling phenomenon elucidated mechanisms to systematically control topography of a surface. This understanding enabled the establishment of a "biomimetic" self-cleaning surface and was employed for establishing truly surface-cleaning biomimetic surfaces.

The diversity of SENs was further demonstrated with our studies that sought the opposite of our "long-lived" superhydrophobic surfaces. Specifically, we utilized the surface energy differences between the methyl and vinyl substituents to demonstrate surface responsiveness. Combining the flexibility of the silicone backbone with the

capability to modify the vinyl substituent with a high surface energy moiety resulted in extreme surface responsiveness, at room temperature, of the SEN network. This surface restructuring was the fastest observed response rate of any polymeric system studied to date. We also demonstrated that cycling between wet and dry states showed minimal hysteresis or dampening of the hydrophilic–hydrophobic responses. The fundamental mechanisms of the chain interactions were elucidated with an investigation of the molecular origins of the responsiveness, namely the interactions among side chains and the substituents terminal end-group.

Recognizing that PVMS is a convenient platform to maximize the attributes of reactive addition chemistry on a flexible polymeric substrate, we developed functional PVMS substrates by grafting "sticky" groups based on trichlorosilane. This chemistry offered a wide flexibility for additional substituents through chemical tailoring of the properties of the substrate. As alcohol compounds are very diverse, there is no limit to the type of chemical functionalization we can achieve on silicone substrates. Silicone substrates can be used in diverse applications ranging from electronic to biomedical; their future in surface science is bright with no significant boundaries on their use.

Acknowledgements We acknowledge gratefully the financial support from the National Science Foundation and the Office of Naval Research. We are also grateful for the gift of PJ Fluid from the Dow Corning Corporation. Finally, we thank our many colleagues around the world for fruitful collaboration on various SEN-related projects over the past several years. Specifically, we thank William Wallace, Daniel Fischer (both NIST), L. Mahadevan (Harvard University), Evangelos Manias (Penn State University), Laura Clarke (NC State University), Manoj Chaudhury (Lehigh University), Dwight Schwark (Cryovac SealedAir), Jan Groenewold (University of Twente), Russell Gorga (NC State University), Simon Lappi (NC State University) and others.

References

1. Jershow P (2001) Silicone elastomers, smithers rapra technology, vol 12. Report 137
2. Nicolson PC, Vogt J (2001) Soft contact lens polymers: an evolution. Biomaterials 22:3273–3283
3. Xia Y, Whitesides GM (1998) Soft lithography. Angew Chem, Int Ed Engl 37:550–575
4. Xia Y, Whitesides GM (1998) Soft lithography. Annu Rev Mater Sci 28:153–184
5. Wong I, Ho C-M (2009) Surface molecular property modifications for poly(dimethylsiloxane) (PDMS) based microfluidic devices. Microfluid Nanofluid 7:291–306
6. Fudouzi H, Xia Y (2003) Photonic papers and inks: color writing with colorless materials. Adv Mater 15:892–896
7. So J-H, Qusba A, Hayes GJ, Lazzi G, Dickey MD (2009) Reversibly Deformable and Mechanically Tunable Fluidic Antennas. Adv Funct Mater 19:3632–3637
8. Plass KE, Filler MA, Spurgeon JM, Kayes BM, Maldonado S, Brunschwig BS, Atwater HA, Lewis NS (2009) Flexible polymer-embedded Si wire arrays. Adv Mater 21:325–328
9. Wang Y, Yang R, Shi Z, Zhang L, Shi D, Wang E, Zhang G (2011) Super-elastic graphene ripples for flexible strain sensors. ACS Nano 5:3645–3650
10. Görrn P, Lehnhardt P, Kowalsky W, Riedl T, Wagner S (2011) Elastically tunable self-organized organic lasers. Adv Mater 23:869–872
11. Ahmed S, Yang YK, Őzçam AE, Efimenko K, Weiger MC, Genzer J, Haugh JM (2011) Poly(vinylmethylsiloxane) elastomer networks as functional materials for cell adhesion and migration studies. Biomacromolecules 12:1265–1271

12. Sochol RD, Higa AT, Janairo RRR, Li S, Lin L (2011) Unidirectional mechanical cellular stimuli via micropost array gradients. Soft Matter 7:4606–4609
13. Qian T, Li Y, Wu Y, Zheng B, Ma H (2008) Superhydrophobic poly(dimethylsiloxane) via surface-initiated polymerization with ultralow initiator density. Macromolecules 41:6641–6645
14. Tugulu S, Klok H-A (2009) Surface modification of polydimethylsioxane substrates with non-fouling poly(poly(ethyleneglycol)methacrylate) brushes. Macromol Symp 279:103–109
15. Ouellet R, Yang CWT, Lin T, Yang LL, Lagally E (2010) Novel carboxyl-amine bonding methods for poly(dimethylsiloxane)-based devices. Langmuir 26:11609–11614
16. Yang L, Li L, Tu Q, Ren L, Zhang Y, Wang X, Zhang Z, Liu W, Xin L, Wang J (2010) Photocatalyzed surface modification of poly(dimethhylsiloxane) with polysaccharides and assay of their protein adsorption and cytocompatibility. Anal Chem 82:6430–6439
17. Duffy DC, McDonald JC, Schuller OJA, Whitesides GM (1998) Rapid prototyping of microfluidic systems in poly(dimethylsiloxane). Anal Chem 70:4974–4984
18. Owen MJ (2005) Plasma/corona treatment of silicones. Australian J Chem 58:433–436
19. Zhou J, Ellis AV, Voelcker NH (2009) Recent developments in PDMS surface modification for microfluidic devices. Electrophoresis 31:2–16
20. Wong I, Ho C-M (2009) Surface molecular property modification for poly(dimethylsoloxane) (PDMS) based microfluidic devices. Microfluid Nanofluid 7:291–306
21. Huszank R, Szika D, Simon A, Szilasi SZ, Nagy IP (2011) $^4He^+$ ion beam irradiation induced modification of poly(dimethylsiloxane). Characterization by infrared spectroscopy and ion beam analytical techniques. Langmuir 27:3842–3848
22. Fu Y-J, Qui H-Z, Liao K-S, Lue SJ, Hu C-C, Lee K-R, Lai JY (2010) Effect of UV-ozone treatment on poly(dimethylsoloxane) membranes: Surface characterization and gas separation performance. Langmuir 26:4392–4399
23. Hillborg H, Ankner JF, Gedde UW, Smith GD, Yasuda HK, Wikström K (2000) Crosslinked polydimethylsiloxane exposed to oxygen plasma studied by neutron reflectometry and other surface specific techniques. Polymer 41:6851–6863
24. Kim J, Chaudhury MK, Owen MJ (1999) Hydrophobicity loss and recovery of silicone HV insulation. IEEE Trans Dielectr Electr Insul 6:695–702
25. Kim J, Chaudhury MK, Owen MJ (2000) Hydrophobic recovery of polydimethylsiloxane elastomer exposed to partial electrical discharge. J Colloid Interface Sci 226:231–236
26. Kim J, Chaudhury MK, Owen MJ, Orbeck T (2001) The mechanisms of hydrophobic recovery of polydimethylsiloxane elastomers exposed to partial electrical discharges. J Colloid Interface Sci 244:200–207
27. Kim J, Chaudhury MK, Owen MJ (2006) Modeling hydrophobic recovery of electrically discharged polydimethylsiloxane elastomers. J Colloid Interface Sci 293:364–375
28. Hillborg H, Gedde UW (1998) Hydrophobicity recovery of polydimethylsiloxane after exposure to corona discharges. Polymer 39:1991–1998
29. Meincken M, Berhane TA, Mallon PE (2005) Tracking the hydrophobicity recovery of PDMS compounds using the adhesive force determined by AFM force distance measurements. Polymer 46:203–208
30. Hillborg H, Gedde UW (1999) Hydrophobicity changes in silicone rubbers. IEEE Trans Dielectr Electr Insul 6:703–717
31. Egitto FD, Matienzo LJ (2006) Transformation of poly(dimethylsiloxane) into thin surface films of SiO_x by UV/Ozone treatment. Part I: Factors affecting modification. J Mater Sci 41:6362–6373
32. Egitto FD, Matienzo LJ (2006) Transformation of poly(dimethylsiloxane) into thin surface films of SiO_x by UV/Ozone treatment. Part II: Segregation and modification of doped polymer blends. J Mater Sci 41:6374–6384
33. Efimenko K, Wallace WE, Genzer J (2002) Surface modification of Sylgard-184 poly(dimethyl siloxane) networks by ultraviolet and ultraviolet/ozone treatment. J Colloid Interface Sci 254:306–315
34. Efimenko K, Crowe JA, Manias E, Schwark DW, Fischer DA, Genzer J (2005) Rapid formation of soft hydrophilic silicone elastomer surfaces. Polymer 46:9329–9341

35. Williams RL, Wilson DJ, Rhodes NP (2004) Stability of plasma-treated silicone rubber and its influence on the interfacial aspects of blood compatibility. Biomaterials 25:4659–4673
36. Huck WTS, Bowden N, Onck P, Pardoen P, Hutchinson JW, Whitesides GM (2000) Ordering of spontaneously formed buckles on planar surfaces. Langmuir 16:3497–3501
37. Ouyang M, Yuan C, Muisener RJ, Boulares A, Koberstein JT (2000) Conversion of some siloxane polymers to silicon oxide by UV/ozone photochemical processes. Chem Mater 12:1591–1596
38. Őzçam AE, Efimenko K, Genzer J, in preparation
39. Genzer J, Efimenko K (2000) Creating long-lived superhydrophobic polymer surfaces through mechanically assembled monolayers. Science 290:2130–2133
40. Nishino T, Meguri M, Nakamae K, Matsushita M, Ueda Y (1999) The lowest surface free energy based on $–CF_3$ alignment. Langmuir 15:4321–4323
41. Efimenko K, Genzer J (2002) Tuning the surface properties of elastomers using hydrocarbon-based mechanically assembled monolayers. Mater Res Soc Symp Proc 710:DD10.3.1–DD10.3.6
42. Allara DL, Parikh AN, Judge E (1994) The existence of structure progressions and wetting transitions in intermediately disordered monolayer alkyl chain assemblies. J Chem Phys 100:1764–1767
43. Chaudhury MK, Owen MJ (1993) Correlation between Adhesion Hysteresis and Phase State of Monolayer Films. J Phys Chem 97:5722–5726
44. Snyder RG, Strauss HL, Elliger CA (1982) C-H Stretching Modes and the Structure of n-Alkyl Chains. 1. Long, Disordered Chains. J Phys Chem 90:5623–5630
45. Efimenko K, Genzer J, Fischer DA unpublished results
46. Brittain W, Advincula R, Rühe J, Caster K (eds) (2004) Polymer Brushes. Wiley, New York
47. Brittain WJ, Minko S (2007) A Structural Definition of Polymer Brushes. J Polym Sci A Polym Chem 45:3505–3510
48. Genzer J (2006) In silico polymerization: computer simulation of controlled radical polymerization in bulk and on flat surfaces. Macromolecules 39:7157–7169
49. Turgman-Cohen S, Genzer J (2010) Computer simulation of controlled radical polymerization: Effect of chain confinement due to initiator grafting density and solvent quality in "grafting from" method. Macromolecules 43:9567–9577
50. Wu T, Efimenko K, Genzer J (2001) Preparing high-density polymer brushes by mechanically assisted polymer assembly. Macromolecules 34:684–686
51. Huang XY, Doneski LJ, Wirth MJ (1998) Surface-confined living radical polymerization for coatings in capillary electrophoresis. Anal Chem 70:4023–4029
52. Huang XY, Doneski LJ, Wirth MJ (1998) Make ultrathin films using surface-confined living radical polymerization. Chemtech 28:19–25
53. Huang X, Wirth MJ (1999) Surface initiation of living radical polymerization for growth of tethered chains of low polydispersity. Macromolecules 32:1694–1696
54. Efimenko K, Genzer J (2001) How to prepare tunable planar molecular chemical gradients. Adv Mater 13:1560–1563
55. Chaudhury MK, Whitesides GM (1992) How to Make Water Run Uphill. Science 256:1539–1541
56. Genzer J, Efimenko K, Fischer DA (2006) Formation mechanisms and properties of semifluorinated molecular gradients on silica surfaces. Langmuir 22:8532–8541
57. Douglas JF, Efimenko K, Fischer DA, Phelan FR, Genzer J (2007) Propagating waves of self-assembly in organosilane monolayers. Proc Natl Acad Sci USA 104:10324–10329
58. Genzer J, Fischer DA, Efimenko K (2003) Fabricating two-dimensional molecular gradients via asymmetric deformation of uniformly-coated elastomer sheets. Adv Mater 15:1545–1547
59. Genzer J, Fischer DA, Efimenko K (2003) Combinatorial near-edge x-ray absorption fine structure: Simultaneous determination of molecular orientation and bond concentration on chemically heterogeneous surfaces. Appl Phys Lett 82:266–268
60. Allen HG (1969) Analysis and design of structural sandwich panels. Pergamon, New York
61. Genzer J, Groenewold J (2006) Soft matter with hard skin: From skin wrinkles to templating and material characterization. Soft Matter 2:310–323

62. Efimenko K, Rackaitis M, Manias E, Vaziri A, Mahadevan L, Genzer J (2005) Nested self-similar wrinkling patterns in skins. Nat Mater 4:293–297
63. Cerda E, Mahadevan L (2003) Geometry and physics of wrinkling. Phys Rev Lett 90:074302
64. Chen X, Hutchinson JW (2004) A family of herringbone patterns in thin films. Scr Mater 50:797–801
65. Mahadevan L, Rica S (2005) Self-organized origami. Science 307:1740
66. Efimenko K, Finlay J, Callow ME, Callow JA, Genzer J (2009) Development and testing of hierarchically wrinkled coatings for marine antifouling. ACS Appl Mater Interfaces 1:1031–1040
67. Efimenko K, Aldred N, Genzer J, Clare A, in preparation
68. Hendricks TR, Wang W, Lee I (2010) Buckling in nanomechanical films. Soft Matter 6:3701–3706
69. Chung JY, Nolte AJ, Stafford CM (2011) Surface wrinkling: a versatile platform for measuring thin-film properties. Adv Mater 23:349–368
70. Crosby AJ (2010) Themed issue "The physics of buckling". Soft Matter 6:5647–5818
71. Cohen Stuart M, Huck W, Genzer J, Müller M, Ober CK, Stamm M, Sukhorukov G, Szleifer I, Tsuktruk V, Urban M, Winnik F, Zauscher S, Luzinov I, Minko S (2010) Stimuli-responsive polymer materials for sensors, actuators, coatings, and delivery systems. Nat Mater 9:101–113
72. Luzinov I, Minko S, Tsukruk VV (2004) Adaptive and responsive surfaces through controlled reorganization of interfacial polymer layers. Prog Polym Sci 29:635–698
73. Minko S (2006) Responsive polymer brushes. Prog Chem 46:397–420
74. Minko S (ed) (2006) Responsive Polymer Materials: Designs and Applications. Wiley, Ames
75. Luzinov I, Minko S, Tsukruk VV (2008) Responsive brush layers: from tailored gradients to reversibly assembled nanoparticles. Soft Matter 4:714–725
76. Bain CD, Whitesides GM (1988) Depth sensitivity of wetting—Monolayers of omega-mercapto ethers on gold. J Am Chem Soc 110:5897–5898
77. Boutevin B, Guida-Pietrsanta F, Ratsimihety A (2000) Side group modified polysiloxanes. In: Chojnowski (ed) Silicone-containing polymers. Kluwer Academic, Dordrecht, pp 79–112
78. Bauer J, Husing N, Kickelbick G (2001) Synthesis of new types of polysiloxane based surfactants. Chem Comm 137–138
79. Bauer J, Husing N, Kickelbick G (2002) Preparation of functional block copolymers based on a polysiloxane backbone by anionic ring-opening polymerization. J Polym Sci A Polym Chem 40:1539–1551
80. Cai GP, Weber WP (2002) Synthesis and chemical modification of poly(divinylsiloxane). Polymer 43:1753–1759
81. Marciniec B, Pietraszuk C (2010) Functionalisation of vinylsubstituted (poly)siloxanes and silsesquioxanes via cross-metathesis and silylative coupling transformations. In: Draguta V, Demonceau A, Dragutan I, Finkelshtein ES (eds) Green metathesis chemistry: great challenges in synthesis catalysis and nanotechnology. Springer, Berlin
82. Zak P, Skrobanska M, Pietraszuk C, Marciniec B (2009) Functionalization of vinyl-substituted linear oligo- and polysiloxanes via ruthenium catalyzed silylative coupling with styrene. J Organomet Chem 694:1903–1906
83. Crowe JA, Efimenko K, Genzer J, Schwark DW (2006) Responsive siloxane-based polymeric surfaces. In: Minko S (ed) Responsive polymer materials: design and applications. Blackwell, Oxford, pp 184–205
84. Chojnowski J, Cypryk M, Fortuniak W, Rozga-Wijas K, Scibiorek M (2002) Controlled synthesis of vinylmethylsiloxane-dimethylsiloxane gradient, block and alternate copolymers by anionic ROP of cyclotrisiloxanes. Polymer 43:1993–2001
85. Crowe-Willoughby JA, Genzer J (2009) Formation and properties of responsive siloxane-based polymeric surfaces with tunable surface reconstruction kinetics. Adv Funct Mater 19:460–469
86. Crowe JA, Genzer J (2005) Creating responsive surfaces with tailored wettability switching kinetics and reconstruction reversibility. J Am Chem Soc 127:17610–17611

87. Crowe-Willoughby JA, Stevens DR, Genzer J, Clarke LI (2010) Investigating the molecular origins of responsiveness in functional silicone elastomer networks. Macromolecules 43:5043–5051
88. http://www.sigmaaldrich.com/catalog/search/ProductDetail/ALDRICH/
89. Woo PJ, Park SY, Suh KY, Lee HH (2002) Physical self-assembly of microstructures by anisotropic buckling. Adv Mater 14:1383–1387
90. Woo PJ, Park SY, Kwon SJ, Suh KY, Lee HH (2003) Microshaping metal surfaces by wave-directed self-organization. Appl Phys Lett 83:4444–4446
91. Kwon SJ, Yoo PJ, Lee HH (2004) Wave interactions in buckling: Self-organization of a metal surface on a structured polymer layer. Appl Phys Lett 84:4487–4489
92. Yoo PJ, Lee HH (2003) Evolution of a stress-driven pattern in thin bilayer films: Spinodal wrinkling. Phys Rev Lett 91:154502
93. Yoo PJ, Suh KY, Kang H, Lee HH (2004) Polymer-elasticity-driven wrinkling and coarsening in high temperature buckling of metal-sapped polymer thin films. Phys Rev Lett 93:034301
94. Őzçam AE (2011) PhD thesis, NC State University

Chapter 4
Using Surface-Attached Organosilanes to Control and Understand Hydrophobicity and Superhydrophobicity

Joseph W. Krumpfer, Lichao Gao, Alexander Y. Fadeev, and Thomas J. McCarthy

4.1 Introduction

The preparative aspects of three different, but overlapping research programs are reviewed in this chapter. Silane monolayers prepared using monofunctional silanes and random covalent attachment reactions are described that implicate molecular topography and flexibility as important issues in wetting. Surfaces prepared using multifunctional methylchlorosilanes are discussed. Samples similar to those prepared in the 1940s are shown to be the most hydrophobic (superhydrophobic) ever prepared. The chemical reactions of linear trimethylsilyl-terminated polydimethylsiloxanes with the surface of oxidized silicon are described. These reactions lead to covalently attached polydimethylsiloxane polymer chains and to hydrophobized inorganic surfaces. Linear silicones of this type (silicone oils) are generally not considered to be reactive with inorganic oxide surfaces.

This chapter is a review of the preparative aspects of our research on wetting that was carried out from the late-1990s until recently. This topic has involved the preparation of covalently attached monolayers as well as what can be called grafted layers on silicon surfaces. This work was carried out with the objectives of correlating surface chemical structure with wetting and developing tools to control wetting behavior using rational chemistry. While this review is focused on preparative work, we cannot completely ignore a second topic that is more fundamental. This topic involves analysis of wetting from a different perspective than the commonly used surface physics one. These preparative and analytical topics overlap in various ways and overlapped significantly during the years in which the experiments were conducted. In fact the second topic was born from wrestling with data that were produced in the first. Central to all of this work is contact angle analysis of wetting, but we do not begin this chapter with a discussion of wetting and contact angle. We

J.W. Krumpfer · L. Gao · A.Y. Fadeev · T.J. McCarthy (✉)
Polymer Science and Engineering Department, University of Massachusetts, Amherst, MA 01003, USA
e-mail: tmccarthy@polysci.umass.edu

M.J. Owen, P.R. Dvornic (eds.), *Silicone Surface Science*, Advances in Silicon Science 4,
DOI 10.1007/978-94-007-3876-8_4,

have reviewed this topic in detail elsewhere [1] and try to minimize it here. This may seem unusual to some readers, but in fact this is the way that the research was carried out. We learned our perspective of contact angle from wrestling with data of the type that we present here.

We began this work in the late-1990s after over a decade of research on polymer surface modification [2].[1] There were (and are) obvious advantages of inorganic surfaces (over polymers) to the study of interface science issues, in particular for preparing surfaces with defined chemistry. Silicon was the obvious substrate to use as the advantages were apparent, multiple and include the facts that molecularly smooth silicon wafers were available and inexpensive and that, because of the technology of silane coupling reagents [3–5], more was known about the chemistry of the silica surface than that of any other substrate. Self-assembled monolayers (SAMs) were "in vogue" and Sagiv [6–8] and Whitesides [9] had advanced silicon-supported SAMs to the state that it was an obvious choice for us to make. There was one issue with SAMs that we did not care for—self-assembly. At a first glance this technique looks very attractive—the molecules do the work for you. But after closer inspection one realizes that the molecules do whatever they want and that one is not necessarily in control. We chose to study monofunctional silanes [10] because of the potential to exert control. We also studied [11] difunctional and trifunctional silanes, but these are significantly more complicated and this chemistry is not reviewed here except to show some interesting examples. In particular, these multifunctional reagents are capable of polymerization with water as a co-monomer which can lead to complex product structures on surfaces. We discuss two examples of this complexity in the section of this chapter on superhydrophobicity. We also discuss chemistry that occurs with non-functional silanes. This work was based on the surprising results of control experiments.

4.2 Monofunctional Silanes: Molecular Topography and Flexibility Contribute to Contact Angle Hysteresis

The reaction between surface silanols and monofunctional silanes (see Reaction Scheme 4.1) had a substantive literature when we began this work and in many senses the chemistry was well understood. Most of this work, however, had been carried out on porous surfaces (often to prepare chromatography stationary phases) and in contrast to the work on alkyltrichlorosilane-derived SAMs [6–9], very little had been reported on monofunctional silanes on single surfaces. The effects of temperature, solvent, reaction conditions and leaving group had not been studied in any detail nor had the kinetics of the reaction. There were notable inconsistencies

[1] Reference [2] is a leading reference to our reports on polymer surface modification and involves the surface chemistry of poly(ethylene terephthalate). Other polymers that we studied include poly(ether ether ketone), polychlorotrifluoroethylene, poly(vinylidene fluoride) and polytetrafluoroethylene.

Scheme 4.1 Reaction between surface silanols and monofunctional silanes

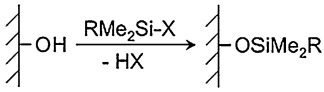

Table 4.1 Water contact angle data for Me_3Si surfaces prepared from Me_3SiNMe_2 at room temperature using different reaction times

Reaction time, h	θ_A/θ_R (°)
0.1	80/35
0.5	93/82
1	99/93
2	99/93
2.5	100/97
3	102/95
4	102/94
15	103/94
24	104/95
48	105/96
72	105/96
196	105/96

in the literature; for example, there were conflicting reports of the effect of chain length (R in Scheme 4.1) on water contact angle of *n*-alkyldimethylsilyl monolayers. Some groups reported that contact angle increased with increasing chain length [12, 13], one group reported that contact angles decreased slightly [14], one group reported data that were independent of chain length [15] and minima in plots of contact angle versus chain length were also described [16, 17]. Advancing and receding water contact angles for trimethylsilyl monolayers on quartz, silica and glass plates had been reported, but they varied widely from one report to another and included the values: $\theta_A/\theta_R = 113°/52°$ [16], 72°/35° [18], 75°/63° [19], and 89°/89° [20].[2]

Therefore, our first experiments were directed at preparing reproducible trimethylsilyl monolayers on silicon wafers. These wafers were rigorously cleaned with oxidizing acid, rinsed with pure water and dried [10]. We studied reactions with various leaving groups (X in Scheme 4.1), different solvents and catalysts, compared vapor phase versus solution phase reactions and studied the kinetics of several different systems.

In Table 4.1 we present kinetics data for only one system, the reaction of Me_3SiNMe_2 with silicon wafers in toluene at room temperature. The table shows water contact angle data for silicon wafers that had been treated with Me_3SiNMe_2 in toluene at room temperature for various time periods. It can be seen that significant

[2]For a more complete list of various reported water contact angles for trimethylsilyl monolayers, see Table 1 of Ref. [9].

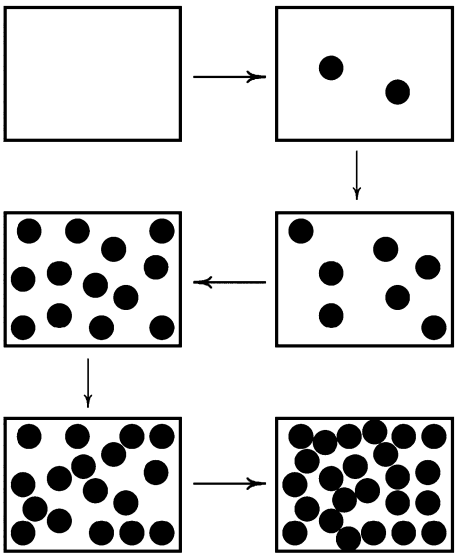

Fig. 4.1 Graphic representation of what could either be trimethylsilyl groups reacting at random with surface silanols on a silicon wafer or velcro ball darts being thrown at a fabric target. The surface is initially rapidly filled, but the rate of filling (reaction or ball dart attachment) slows significantly in the later stages. This figure also indicates that there is not a unique "complete monolayer" for a random covalent attachment, but that many different ones could form depending on reaction conditions

hydrophobization occurs within minutes (θ_A/θ_R changes from 5°/0° to 80°/35° after six minutes and to 99°/93° after 1 h), but also that the reaction continues over days and is not complete until 2 or 3 days. Noteworthy (and discussed below) is that minimum hysteresis ($\theta_A - \theta_R$) does not correlate with the maximum extent of reaction or maximum contact angle: the hysteresis is 3° ($\theta_A/\theta_R = 100°/97°$) for the sample prepared using a 2.5 h reaction time and increases markedly to 8°–11° for samples reacted longer than a day. We emphasize the differences between this reaction to form chemically grafted monolayers and that of alkyltrichlorosilanes, in which self-assembly occurs causing maximum surface density very quickly [6–9]. The late stages of the reaction with the monofunctional silane are very slow and reaction can only occur when surface-attached groups adopt conformations that expose unreacted surface silanols. This reaction can be described as a random covalent attachment and we use an analogy of "velcro ball darts" to explain certain issues of this process.

Figure 4.1 shows what can represent either trimethylsilyl groups reacting randomly with surface silanols on a silicon wafer or velcro ball darts being thrown at a fabric surface. The surface is rapidly filled initially but the rate of filling (reaction or ball dart attachment) slows significantly in the later stages. This figure also points out that there is not just one possible "complete monolayer" in a randomly attached monolayer, but that surfaces with many different densities can be prepared. This suggests that reaction conditions, including solvent identity and temperature, can play an important role in determining monolayer structure. In research not discussed here, we took advantage of this process to prepare binary mixed monolayers. The rather large silane, tris(trimethylsiloxy)chlorosilane, was used to prepare complete monolayers and in subsequent reactions, smaller silanes were introduced in the "holes" between the bulky covalently attached groups [21].

Table 4.2 Water contact angles (θ_A/θ_R) for *n*-alkyldimethylsilyl monolayers prepared under different reaction conditions

Alkyl groups in alkyldimethylchlorosilane	Toluene, EDIPA, 60–70 °C	Toluene, EDIPA, Room Temp.	Vapor phase, 60–70 °C
CH_3	105/91	105/96	108/96
C_2H_5	104/91	108/96	110/98
C_3H_7	103/91	104/93	104/93
C_4H_9	104/92	105/93	105/93
C_8H_{17}	103/91	106/93	106/99
$C_{10}H_{21}$	104/92	106/92	106/95
$C_{12}H_{25}$	104/92	105/93	106/99
$C_{18}H_{37}$	103/91	107/95	–
$C_{22}H_{45}$	104/91	106/93	–

Several reproducible reaction conditions were identified and numerous reactions were carried out using various trialkylchlorosilanes (primarily alkyldimethylchlorosilanes) with silicon wafers and three reaction conditions: reaction in toluene with ethyldiisopropylamine (EDIPA) at room temperature for 72 h, reaction in toluene with EDIPA at 60–70 °C for 72 h, and reaction in the vapor phase at 60–70 °C for 72 h. We point out that kinetics were not determined for reactions in the vapor phase and a reaction time of 72 h was chosen somewhat arbitrarily. The data offer convincing evidence that reactions are complete after this time, but they may be complete after much shorter time periods.

A series of nine *n*-alkyldimethylchlorosilanes with alkyl groups varying in chain length from 1 to 22 C atoms was used to prepare chemically grafted monolayers on silicon wafers using the three conditions described above. Water contact angle data for these surfaces are summarized in Table 4.2.

Reactions in the vapor phase with the C_{18} and C_{22} chlorosilanes were not successful under these conditions. Duchet et al. [15] reported the modification of a silica surface using $C_{18}H_{35}Me_2SiNMe_2$ in the vapor phase at higher temperatures and found $\theta_A/\theta_R = 95°/93°$. We note five trends in the data of Table 4.2: (1) The wettability of the surfaces is almost independent of alkyl chain length; this is true for all three series prepared using different conditions. These results indicate that inconsistencies in the earlier literature data are due to reaction conditions. This independence is discussed in more detail below. (2) The contact angles are higher for surfaces silanized in the vapor phase than for surfaces silanized in the liquid phase. The vapor phase method appears to be the cleanest and easiest to obtain high yield surface modification with these reagents. It is limited by the fact that it cannot be applied for reactions with silanes with low vapor pressures. (3) The surfaces prepared in toluene at room temperature exhibit advancing and receding water contact angles that are very similar to those of the samples prepared in the vapor phase at 60–70 °C. This procedure is likely the most versatile one for silanization of silicon wafers. (4) The reactions in toluene at elevated temperature give products with both

advancing and receding contact angles that are consistently lower than those obtained using the other two sets of conditions. We point out that this is not due to kinetic limitations, but is inherent to the reaction conditions. (5) The contact angle hysteresis in most of these surfaces is high (11–14°) and independent of the preparative method; two surfaces (the C_8 and C_{12} exhibited lower hysteresis (7°)). We discuss below that this hysteresis is not due to the presence of the residual silanol groups.

We also studied reactions of branched alkyldimethylsilanes to gain insight into the chemical factors that control wetting and found that vapor phase reactions gave the most complete monolayers. Table 4.3 shows water, methylene iodide and hexadecane contact angle data for samples prepared in the vapor phase. Two straight chain alkyl groups are included for comparison.

The data presented in Tables 4.1–4.3 and attempts to rationalize the often subtle differences in contact angles led to a significant understanding of wetting. We point out seven issues with these data that are worthy of note: (1) Careful analysis of the contact angle data presented in Table 4.1 for the trimethylsilyl surface shows that the hysteresis reaches a minimum after 2.5 h of reaction and then increases with increasing monolayer density. This tendency is reproducible and we have also observed it with other silanes, notably *tert*-butyldimethylchlorosilane. We interpret this low hysteresis in terms of molecular flexibility. At the "optimum" bonding density the trimethylsilyl groups can rotate freely and exhibit a liquid-like surface. These types of surfaces have inherent low hysteresis and this is discussed in more detail later in this chapter. (2) The hysteresis for the isobutyl surface (Table 4.3) is significantly greater than for either the more symmetrical *n*-butyl or *tert*-butyl surfaces. The *n*-butyl groups are mobile and they can adjust conformations to form a low energy smooth surface and the *tert*-butyl groups are rigid and pack to form a smooth surface, but the isobutyl groups, having less ability to pack or adjust conformation, expose two methyl groups and a hydrogen and project a rough surface. (3) The isopropyl surface is similarly rougher than the *n*-propyl surface. (4) The 1,1,2-trimethylpropyl (*t*-hexyl) surface has a relatively low bonding density as indicated by the low water contact angles, but also exhibits low hysteresis. This behavior is similar to that discussed above for trimethylsilyl surfaces of intermediate bonding density. (5) The 3,3-dimethylbutyl surface shows pronounced hysteresis and unusual water contact angle behavior. The surface contains *tert*-butyl groups that are separated from silicon by two carbons; these groups are evidently flexible enough to adopt a conformation that projects an extremely rough surface at the molecular level. The surface that water interacts with is chemically very similar to the *tert*-butyl surface but the advancing contact angle is 14° higher (118°) and the hysteresis is 20° as opposed to 6°. The hexadecane advancing contact angle (22°) of this surface is low, indicating that hexadecane penetrates this layer to access methylene groups and perhaps silanols. (6) The triisopropylsilyl, *n*-octyldiisopropylsilyl and octadecyldiisobutylsilyl surfaces exhibit contact angles that are significantly lower than *n*-alkyldimethylsilyl surfaces. The bonding density is lower in these sterically congested surfaces and probe fluids access the surface silanols. (7) The bicyclic alkyl surfaces show interesting contact angle behavior: water contact angles are high, but

Table 4.3 Wettability of monolayers composed of silanes with branched alkyl groups

Surface group	Water θ_A/θ_R (°)	CH_2I_2 θ_A/θ_R (°)	$C_{16}H_{34}$ θ_A/θ_R (°)
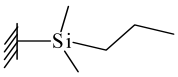	104/93	66/55	22/15
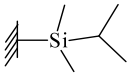	108/96	67/54	26/15
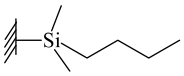	105/94	64/60	26/20
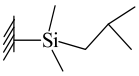	109/95	67/54	17/7
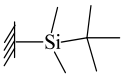	104/98	60/57	26/21
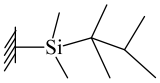	83/72	61/59	24/21
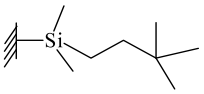	118/98	67/53	22/10
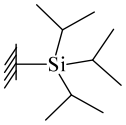	80/63	55/40	12/5
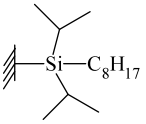	73/55	52/40	14/5
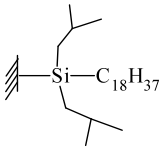	77/59	51/44	5/0
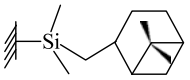	97/91	55/47	5/0
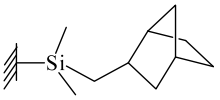	100/79	51/40	7/0

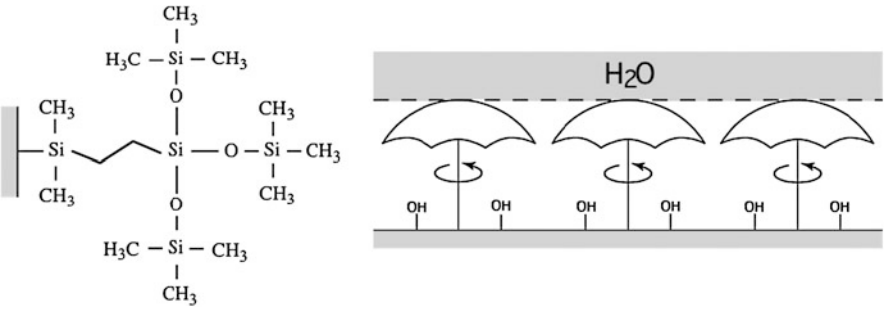

Fig. 4.2 Structure of the tris(trimethylsiloxy)silylethyldimethylsilane monolayer

CH_2I_2 and $C_{16}H_{34}$ contact angles are low. This indicates that CH_2I_2 and $C_{16}H_{34}$ penetrate the monolayers and interact with surface silanols, but that water does not.

These seven issues may seem like an extreme overanalysis of contact angle data and we were certainly conscious of the fact that this might be most people's opinion while we were trying to interpret these data. Saying that "molecular topography", for instance a *tert*-butyl group sticking out in a monolayer, or "molecular flexibility", for instance the bond rotations in trimethylsilyl groups, were contributing (and controlling) macroscopic contact angles was controversial, but our arguments have held up as appropriate interpretations of the data. In fact, we designed and prepared a monofunctional silane to test our interpretations and succeeded in preparing a surface with essentially no hysteresis. A covalently attached monolayer of tris(trimethylsiloxy)silylethyldimethylsilane (see Fig. 4.2) exhibits water contact angles of $\theta_A/\theta_R = 104°/103°$, and sessile water drops slide very easily on this surface. This monolayer can be regarded as an array of "molecular umbrellas" that rotate at room temperature. The "umbrellas" move the 3-phase contact line (solid-liquid-vapor) of the sessile drop. When a contact line moves, it either advances or recedes—this motion is responsible for the lack of hysteresis. We have discovered a simpler method of preparing surfaces that exhibit this wetting behavior (negligible hysteresis) and discuss this below.

4.3 Methylchlorosilanes React to Form Superhydrophobic Surfaces

In the late 1990s there were multiple reports of surfaces that exhibit anomalously high water contact angles [22] and in the first decade of the current millennium a "field of research" on superhydrophobicity developed. We have published perspective articles on this subject [1, 23] and pointed out in 1999 [22] that the then recent reports of high contact angles neglected to reference the work that was carried out 50–60 years prior to these publications. The hydrophobic nature of certain natural solids and the hydrophobization of solids that are not naturally hydrophobic were topics of chemical research interest in the 1940s. In 1944, Fogg reported [24] the

unusual contact angle behavior of mustard and wheat leaves. Cassie and Baxter commented [25] on this report in 1945 and described the mirror like reflection of the broccoli leaf–water interface and that the advancing and receding contact angles of duck feathers are "both around 150°". Imparting water repellency to textiles in ways to retain the fabric's permeability to air and water vapor was an active research field in the 1940s [26–28].

In 1940, a "direct" route to methylchlorosilanes (Me_nSiCl_{4-n}) was discovered by Eugene Rochow at the General Electric Company and this reaction has had a profound impact on science, technology, etc.—life as we know it—and amongst numerous other applications its products are used widely today to control interface chemistry in a diverse range of situations. Winton Patnode, working with Rochow, noticed that mixtures of methylchlorosilanes, prepared by the "direct process" [29, 30] produced water-repellent surfaces by vapor-solid contact reaction. This led to a 1942 patent [31] that claimed the treatment of cotton, glass, sheet materials, paper, cotton fabric, articles of manufacture and solid bodies with the vapors of mixtures of methylchlorosilanes. This patent did not claim mixtures of $SiCl_4$ and methylchlorosilanes as hydrophobizing agents, and it was only later when Norton [32] (also at GE) recognized that a particular one of these is special and claimed the mixture of $(CH_3)_3SiCl$ and $SiCl_4$, which form a minimum-boiling azeotrope which boils at 54.5 °C, i.e., ~3 °C below the two pure components, and reacts with a variety of solids as a vapor mixture to impart water repellency. This was a surprising result. Norton commented [32] that "although pure silicon tetrachloride does not itself confer water-repellent properties to surfaces treated therewith and, of all the known organosilicon halides, pure trimethylsilicon chloride is probably the least effective in so far as this property is concerned, compositions containing both of these chlorosilanes do confer excellent water repellency to surfaces".

In 2005, we began to look at reactions of silicon wafers with controlled composition mixtures of Me_nSiCl_{4-n} ($n = 0$–3), some of which must closely recreate the work done at General Electric in the 1940s. We studied reactions of silica surfaces (polished silicon wafers) under a variety of solution, vapor, catalyzed, uncatalyzed, competitive and sequential conditions involving thousands of experiments. That many different surface topographies should form from these reactive monomers and water as a co-monomer is intuitive: $SiCl_4$ and CH_3SiCl_3 polymerize to form 3-D structures, $(CH_3)_2SiCl_2$ polymerizes to form linear (and liquid) segments, $(CH_3)_3SiCl$ is a chain terminator. A number of these mixtures under certain conditions created surfaces with extremely high advancing and receding contact angles. In some cases the measured receding contact angles were higher than the measured advancing ones! Me_3SiCl and Me_2SiCl_2 when reacted individually with silicon wafers as pure silanes under a variety of conditions created surfaces with contact angles that were never higher than 108°. However, surfaces prepared with certain mixtures with $MeSiCl_3$ under certain conditions exhibited contact angles that were higher than 170°. Analysis of these data prompted us to carefully study the reaction conditions for $MeSiCl_3$, and to refine the work of Norton [32] on the $(CH_3)_3SiCl/SiCl_4$ azeotrope.

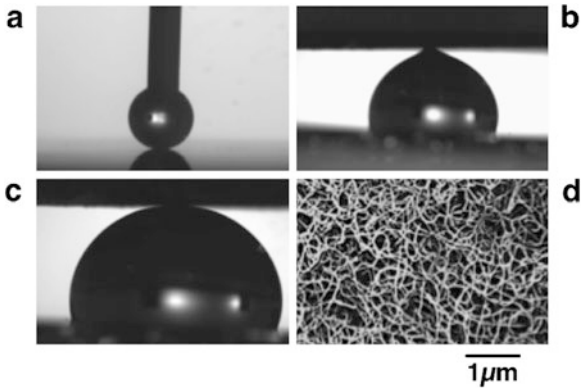

Fig. 4.3 (**a**) A receding water droplet on a silicon wafer modified with $MeSiCl_3$, (**b**) a surface that exhibits $\theta_A/\theta_R = 178°/176°$ being detached from a water droplet, **(c)** a $MeSiCl_3$-derived surface ($\theta_A/\theta_R = 180°/180°$) in contact with a water droplet, (**d**), an SEM image of the $MeSiCl_3$-derived surface on a silicon wafer. Partly reproduced from Ref. [32] with kind permission of © The American Chemical Association (2006)

4.3.1 Methyltrichlorosilane and a Perfectly Hydrophobic Surface [32]

Silicon wafer sections (cleaned by oxygen plasma treatment) were submerged in 1.0 M $MeSiCl_3$ in anhydrous toluene at 25 °C for 3 h, removed, rinsed with copious toluene, ethanol, ethanol-water (1:1) and water, and then dried at 120 °C for 10 min. Reaction vessels were closed to air during the reaction, but exposed (RH = 60–65 %) during solution and sample introduction. Important details of this reaction included using the correct volume of toluene/$MeSiCl_3$, trapping the correct volume of air (containing water that reacted completely) and using the correct reaction vessel. Using commercial scintillation vials that are purchased closed (clean rooms in bottles) was a "secret" technique developed in our group and eventually disclosed at a Faraday Discussion [33].

Water droplets do not come to rest on these surfaces but move spontaneously in various directions when gently released from a syringe onto horizontal surfaces. Figure 4.3a shows a receding droplet, pinned on a syringe tip, just before it detaches from the surface ($\theta_R = 180°$). The droplet can be "pushed onto" the surface and finite advancing contact angles ($\theta_A = \sim 176°$) can be measured, but the droplet distorts from a sphere under the conditions of the measurement. To prove that this surface in fact exhibited perfect hydrophobicity ($\theta_A/\theta_R = 180°/180°$), a method for testing perfect hydrophobicity was devised. A droplet of water was placed on a surface that exhibits $\theta_A/\theta_R = 120°/110°$ and surfaces to be examined were lowered onto this droplet. Droplets were contacted and squeezed while recording video. Surfaces with contact angles less than 180° exhibited affinity of water for the surface both during attachment and release of the droplet. Figure 4.3b shows a droplet, just before detachment from a surface on which we measured contact angles of

$\theta_A/\theta_R = 178°/176°$. It is clearly not perfectly hydrophobic as affinity for the surface is evident. Figure 4.3c, however, shows a $MeSiCl_3$-derived surface, to which the droplet shows no affinity for the surface during attachment, compression or release. The modified silicon wafers are highly reflective and indistinguishable by eye from unmodified wafers; there are no micron-scale topographical changes. Atomic force microscopy (AFM) and scanning electron microscopy (SEM) (Fig. 4.3d) images indicate the presence of a network of cylindrical fibers with diameters of ~20 nm. The average thickness of the modified layer is ~20 nm by ellipsometry. The conditions used for this modification (hydrated silica and a volume of air providing limited water) promote "vertical polymerization" [11] of $MeSiCl_3$ into a toluene-swollen 3-D methylsiloxane network until the water is exhausted. This network is cross-linked with and covalently attached to the wafer surface at many sites. Upon removing the toluene using ethanol, phase separation occurs to form the fibrillar network.

4.3.2 The $(CH_3)_3SiCl/SiCl_4$ Azeotrope [34]

The vapor phase reactions of $(CH_3)_3SiCl$ and $SiCl_4$ as individual reagents have been studied in some detail. $SiCl_4$ reacts with silicon wafers to form hydrophilic and reactive silica [35]. Silica can be "grown" in a controlled step growth manner by cyclic exposures to air and $SiCl_4$. $(CH_3)_3SiCl$ vapor reacts with silicon wafers by the random covalent attachment discussed in Sect. 4.2 and unknown to Norton (see Sect. 4.3), slows significantly in the later stages to yield a monolayer with water contact angles of $\theta_A/\theta_R = 108°/96°$ [10]. We carried out vapor phase reactions with a mixture of these two compounds (50:50 vol. %, 52.6/47.4 mol %) under various humidity conditions at room temperature. Humidity was controlled in a glove bag using an open container of aqueous sodium chloride. Optimized (for maximum contact angle) conditions were determined to be 40–45 % relative humidity at ~23 °C. Exposure time was controlled by introducing and removing silicon wafer samples to and from a covered crystallizing dish containing an open vial of the mixture of $(CH_3)_3SiCl$ and $SiCl_4$. Samples were rinsed with copious amounts of water and dried in air. After 2 min of exposure, samples exhibited contact angles of $\theta_A/\theta_R \geq 176°/\geq 176$. The thickness of the deposited layer increased with reaction time and was ~20 nm after 10 min exposure to the azeotrope vapor. Water droplets do not come to rest on these surfaces (sliding angle is 0°) and move spontaneously in every direction off the horizontal samples.

Figure 4.4 shows SEM images of modified silicon wafers that were exposed to the $(CH_3)_3SiCl/SiCl_4$ azeotrope vapor for different times. Contorted filaments with diameters of ~30 nm grow in an apparent one-dimensional chain growth fashion from nucleation sites that are visible after 30 sec of exposure to the azeotrope vapor. Titanium surfaces (containing a native oxide) were exposed to the $(CH_3)_3SiCl/SiCl_4$ azeotrope vapor in an effort to determine the stoichiometry of the reaction and gain insight into the mechanism of filament growth. Surfaces with the same wettability characteristics were obtained. X-ray photoelectron spectroscopy

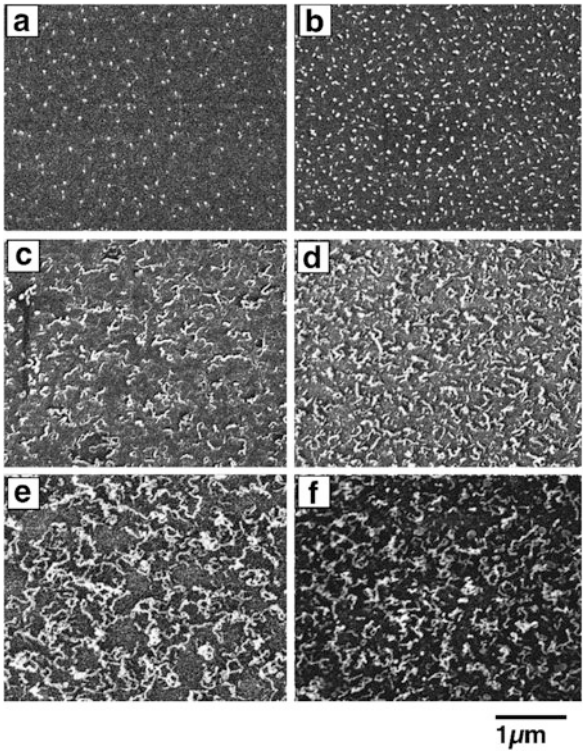

Fig. 4.4 SEM images of silicon exposed to the $(CH_3)_3SiCl/SiCl_4$ azeotrope for 30 s (**a**), 1 min (**b**), 2 min (**c**), 4 min (**d**), 6 min (**e**) and 10 min (**f**). Partly reproduced from Ref. [34] with kind permission of © The American Chemical Association (2008)

(XPS) of a sample reacted for 10 min revealed a Si:C ratio of 3.7. This indicates that $SiCl_4$ and $(CH_3)_3SiCl$ react in a ratio of ~10:1. This ratio is likely biased low because any contamination would contain carbon and not silicon and because of the exponential decay of sensitivity of XPS with depth: the contact angle data indicate that trimethylsilyl groups must be present at the outermost surface of the filaments and that few silanols are exposed.

We propose the following explanation for the one-dimensional growth of the filaments: $SiCl_4$ and $(CH_3)_3SiCl$ react with water and surface silanols to form covalently attached solid particles (Fig. 4.4a). $SiCl_4$ can polymerize with water and grow in three dimensions, but $(CH_3)_3SiCl$ terminates the polymerization and the trimethylsilyl groups inhibit further reaction near them on the surface of the particle. The resulting trimethylsilylated silica particles must have surfaces that are mostly unreactive toward $SiCl_4$ and its hydrolyzed derivatives ($HOSiCl_3$, $(HO)_2SiCl_2$, $(HO)_3SiCl$, $Si(OH)_4$), but reactive defects must be present in small numbers. Growth from such defects causes a loss of symmetry and particles become elongated and form short filaments (Fig. 4.4b, c). $(CH_3)_3SiCl$ more effectively terminates growth at the sides of the filaments than it does at the ends due to the relative curvature. Surface silanols are more exposed at the ends of filaments because the trimethylsilyl groups are splayed due to the curvature. The relative rates of reaction of hydrolyzed derivatives of $SiCl_4$ and $(CH_3)_3SiCl$, their relative concentra-

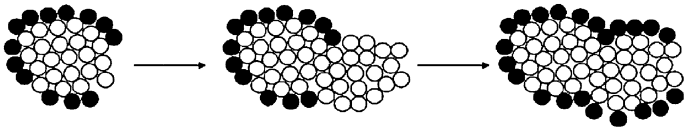

Fig. 4.5 Description for the mechanism of fiber growth in the $(CH_3)_3SiCl/SiCl_4$ azeotrope reaction. The open circles indicate $SiCl_4$-derived centers and the closed circles represent trimethylsilyl groups

tion (controlled by the azeotrope composition) and the relative reactivity of silanols between trimethylsilyl groups as a function of curvature control the resulting morphology. As discussed in Sect. 4.2, monofunctional silanes (e.g. $(CH_3)_3SiCl$) form complete, but not close-packed monolayers that contain defects of various cross sectional areas smaller than the silane. It is reasonable to expect that curvature should affect reactivity. Figure 4.5 shows a schematic of this process.

We reported the water contact angle behavior of the surfaces prepared from this azeotrope vapor as $\theta_A/\theta_R \geq 176°/\geq 176°$. The contact/compression/release analysis described above was performed many times on these azeotrope-derived surfaces. Some samples in some locations exhibited perfect hydrophobicity as defined in Sect. 4.3.1 and were indistinguishable (by this technique) from perfectly hydrophobic surfaces. Most of the samples, however, exhibited a very slight affinity for water during release. Figure 4.6 shows selected frames of a video of a contact/compression/release analysis of a surface exposed for 10 min. An azeotrope-derived surface was lowered onto and raised from a sessile droplet. Defects cause a small amount of receding contact line pinning (Fig. 4.6g). We do not label these surfaces "perfectly hydrophobic", but they are very close. This vapor phase reaction is much more convenient and much less condition-dependent than the methyltrichlorosilane solution phase reaction.

We wanted to make a surface with 180° water contact angles for largely egotistical/competitive reasons. After we had convinced ourselves that we had succeeded, we asked ourselves why would anyone need a surface with 180° contact angles? Would not a material that could be fabricated by the acre [36] and exhibit $\theta_A/\theta_R = 170°/165°$ be good enough? This led us to ideas about frictionless motion and lubrication and then to experiments involving vehicles with inverted sessile drop wheels driving on perfectly hydrophobic roads. However, the most obvious practical problem (that the wheels evaporate) led us to ionic liquid wetting behavior [37, 38]. We carried out a number of experiments on low friction motion and two of these are described in Figs. 4.7 and 4.8.

Figure 4.7a shows a silicon wafer that was patterned with hydrophilic circles that were 1 mm in diameter and spaced (hexagonally) by 4 mm. It was dipped in water to form an array of sessile drops. A perfectly hydrophobic sled (a quartz slide treated with methyltrichlorosilane as described above) was allowed to slide down this surface while a video was recorded. The sled moved at constant velocity down a 3° incline (Φ) (Fig. 4.8a). The friction was due to the quartz sled needing to depress the sessile drops (Fig. 4.7b) in order to move. The experiment was redesigned and

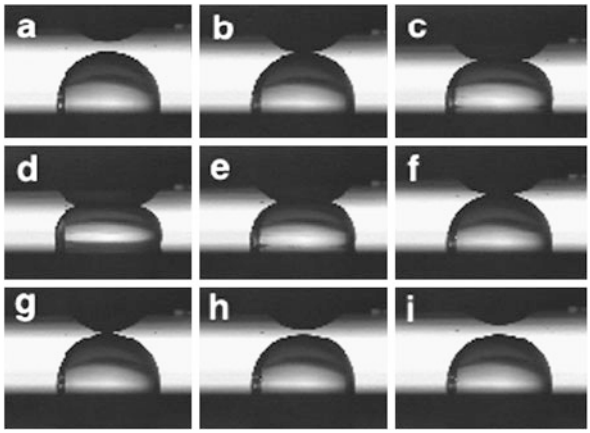

Fig. 4.6 Selected frames in chronological order of a video of a $(CH_3)_3SiCl/SiCl_4$ azeotrope—derived surface (*top*) contacting, compressing and being released from a sessile water droplet. The reflection of the sessile droplet defines the surface of the silicon wafer. Partly reproduced from Ref. [34] with kind permission of © The American Chemical Association (2008)

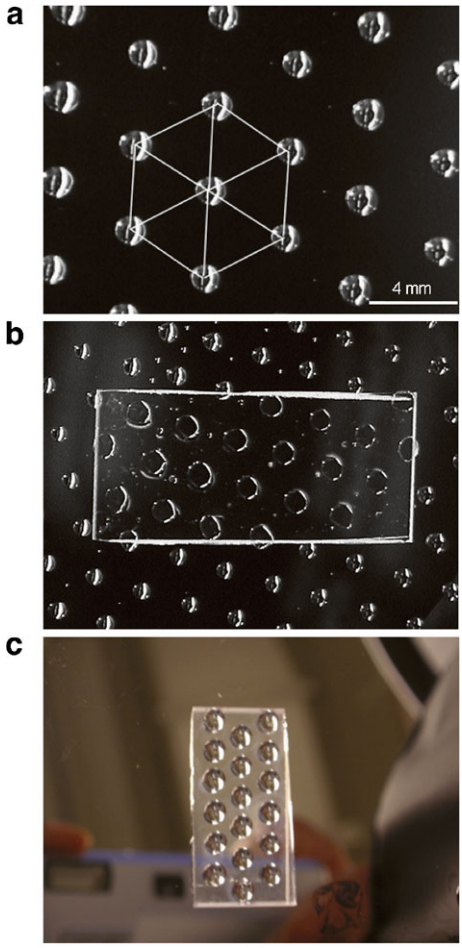

Fig. 4.7 (**a**) An array of sessile drops on 1 mm hydrophilic spots spaced by 4 mm. (**b**) A perfectly hydrophobic quartz sled on the surface described in (**a**). (**c**) A quartz sled with 18 sessile drop "wheels"

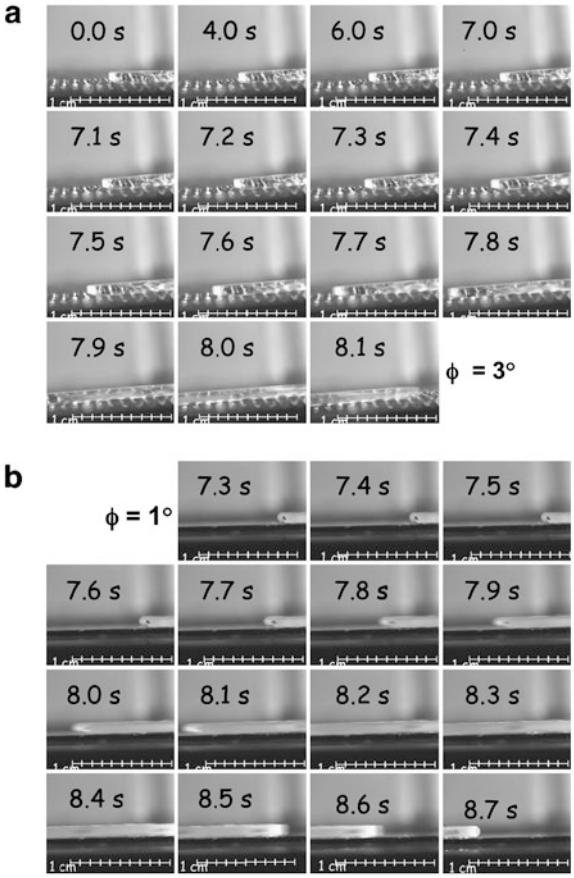

Fig. 4.8 (**a**) Frames of a video of a perfectly hydrophobic quartz sled sliding down an array of sessile drops held 3° from the horizontal. (**b**) Frames from a video of the vehicle shown in Fig. 4.7c sliding down a perfectly hydrophobic surface

the "wheels" were put on the vehicle (Fig. 4.7c). This vehicle accelerated down a perfectly hydrophobic ramp inclined 1° from the horizontal (Fig. 4.8b).

4.4 "Unreactive" Silicones React with Inorganic Surfaces

After spending more than 10 years preparing modified silicon surfaces using reactive silanes we made a surprising discovery: linear trimethylsilyl-terminated polydimethylsiloxanes (PDMS) react with the surfaces of oxidized silicon, titanium, aluminum and nickel [33, 39].

We began this work based on the results of control experiments that were carried out during studies of the reactions of hydridomethylsiloxane polymers and copolymers of dimethylsiloxane and hydridomethylsiloxane with titania surfaces. This can be considered a simple extension of the work we reported using low molecular weight alkylhydridosilanes [40]. The control experiments were with trimethylsilyl-terminated PDMS (with no Si–H bonds) and we expected to observe no reactivity.

Table 4.4 Contact angles and ellipsometric thicknesses for silicon wafer samples modified with PDMS^{2000}

Time (h)	Temp (°C)	Contact angles (θ_A/θ_R)			Thickness (nm)
		H_2O	CH_2I_2	$C_{16}H_{34}$	
24	25	94/80	71/61	37/30	0.67
24	60	102/93	72/65	37/34	0.72
24	100	104/102	76/74	36/35	1.15
24	150	105/102	75/72	37/33	3.1
1	100	91/71	71/60	35/29	1.1
6	100	98/85	74/69	36/34	1.22
24	100	104/102	76/74	36/35	1.15

Our expectation demonstrates a faulty understanding of silicone reactivity. We focused our efforts on silicon because we have experience with and data on silicon-supported monolayers.

Silicon wafer sections, after oxygen plasma-cleaning, were wet with a liquid silicone in a small screw-top vial that was then capped and heated in an oven. After the desired time at the desired temperature, the wafers were removed from the vial using tweezers and cleaned with solvents. These silicones are easily removed from these surfaces using solvent rinsing shortly after they are applied at room temperature. There are no solvent, catalyst or by-products in this reaction. There is only excess silicone that is easily rinsed away leaving only the oxide surface and any covalently attached (M–O–Si) silicone. The covalently grafted silicones were not removable by prolonged (1 week) exposure to toluene. This simplicity is in sharp contrast to other surface modification procedures, which depend on a host of variables and conditions that can often not be reproduced, even by researchers in the same group or by the same researcher when the relative humidity changes.

Table 4.4 shows advancing and receding contact angle data obtained using three probe fluids as well as ellipsometric thickness data for samples of silicon modified with PDMS (Mw $\sim$ 2000) at different temperatures (for 24 h) and for different times (at 100 °C). The 24 h/100 °C data are repeated to facilitate comparisons. Without reaction with PDMS, clean Si/SiO_2 is wet ($\theta_A/\theta_R = \sim 0°/\sim 0°$) by all three of these solvents: water, diiodomethane and hexadecane. The contact angles make it obvious that significant amounts of reaction occur in all cases, rising from values of $\theta_A/\theta_R = \sim 0°/\sim 0°$ to 90–105°/70–102° (H_2O), 70–75°/60–72° (CH_2I_2) and $\sim 35°/\sim 30°$ ($C_{16}H_{34}$). Examination of the receding contact angle data and hysteresis indicates that there are significant differences between these samples and that both temperature and time are important (contribute to reaction as evidenced by increasing contact angles and decreasing hysteresis). Careful analysis of the kinetics was not pursued, but it is clear that this is a thermally activated reaction and not a self-assembly or an adsorption process. At 100 °C the contact angles for all three liquids rise from 1 to 6 to 24 h and the thickness of the layer assessed by ellipsometry is 1.1–1.2 nm for samples prepared at each of the times. The 24 h/100 °C

reaction has been carried out dozens of times and we have used this surface for low hysteresis studies [33]. Values of $\theta_A/\theta_R = 104.0° \pm 0.7°/102.4° \pm 1.4°$ (H_2O), $75.5° \pm 0.6°/73.9 \pm 0.8°$ (CH_2I_2) and $36.1° \pm 0.5°/34.8° \pm 0.5°$ ($C_{16}H_{34}$), indicate that surfaces prepared with this simple procedure exhibit hysteresis that is indistinguishable from the lowest hysteresis dimethylsiloxane surfaces that we have prepared [11, 22, 41]. The vapor phase reaction of dimethyldichlorosilane with silicon wafers yields surfaces with contact angles of $\theta_A/\theta_R = 104°/103°$ (H_2O), 73°/69° (CH_2I_2) and 36°/34° ($C_{16}H_{34}$), respectively [11]. Sessile droplets of these liquids slide easily on tilted samples. We have not done a Cassie or Israelachvili analysis on the surfaces reacted for shorter times, but the presence of residual silanols that pin the receding contact line is apparent. We have reported this type of analysis on a similar surface [11]. Samples prepared at lower temperatures, 25 and 60 °C, for 24 h contain thinner (~0.7 nm) layers of PDMS and exhibit depressed contact angles that indicate the presence of silanols. Samples prepared at 150 °C have significantly greater ellipsometric thicknesses of their PDMS layers (~3 nm) than those prepared at 100 °C, however, the hysteresis exhibited is slightly greater.

Experiments were carried out (24 h at 100 °C) that indicate that the molecular weight of the silicone controls the PDMS thickness: $PDMS^{2000}$, $PDMS^{9430}$ and $PDMS^{116,000}$ (the superscripts are the molecular weights) formed covalently attached polymer layers with ellipsometric thicknesses of 1.15, 5.05 and 12.48 nm, respectively. Four additional silicones that were commercially available (Gelest) were reacted with silicon wafer sections for 24 h at 100 °C. A copolymer of phenylmethylsiloxane and dimethylsiloxane (48–52 % phenylmethylsiloxane) reacted to render a sample with water contact angles of $\theta_A/\theta_R = 95°/87°$. A π–π^* shake-up peak was evident in the high resolution C_{1s} XPS spectrum. A copolymer of aminopropylmethylsiloxane and dimethylsiloxane (6–7 % aminopropylmethylsiloxane) yielded a sample with water contact angles of $\theta_A/\theta_R = 99°/86°$. A N_{1s} peak was observed in the XPS spectrum. Polymethyltrifluoropropylsiloxane (homopolymer) reacted to yield a surface with an XPS F:C atomic ratio of 0.76 (the theoretical ratio is 0.75) and water contact angles of $\theta_A/\theta_R = 100°/89°$. Poly(dimethylsiloxane-*block*-ethylene oxide) (80–85 % non-siloxane, $M_w \sim 3600$) formed a modified silica surface that showed an ellipsometric thickness of ~2.0 nm and exhibited water contact angles of $\theta_A/\theta_R = 56°/36°$. These data suggest that this reaction is general for silicones.

We implicate water as being important to this reaction. Silica, which is present as a native oxide layer of ~2 nm thickness dissolves in water (silicic acid equilibrium—Fig. 4.9). Silicones are also known to react with water, although this is not often directly addressed in the chemical literature. For example, steam causes silicone rubber to degrade and lose mechanical stability [42, 43] and small molecule silanols and siloxanes reach true equilibrium (with water) in alcohols. However, these studies [44–46] involve either acid or base catalysis. The equilibration of polydimethylsiloxane with either acid or base catalysis is well known and has been used for silicone preparation since the 1940s; the mechanisms of these reactions were detailed in a 1954 publication [47]. We quote from a monograph that is an historical account [48] of the discovery of silicones during World War II regarding John Speier: "*In his work on mono-tri resins, Speier also discovered that many*

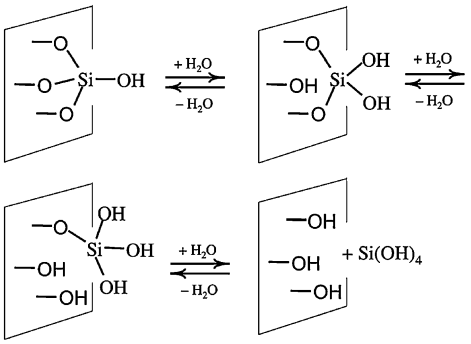

Fig. 4.9 Stages in the equilibration of silica and water

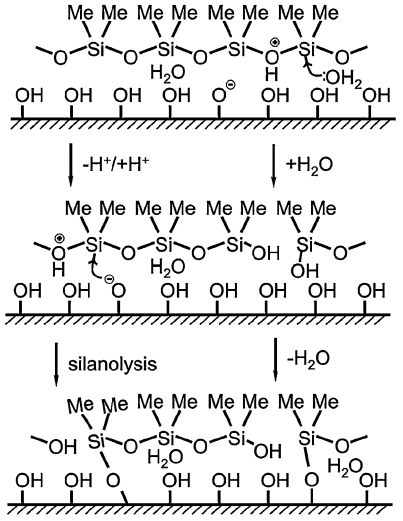

Fig. 4.10 Water-assisted equilibration of surface silanols and siloxane bonds in PDMS. An acid-catalyzed silanolysis, using the silica as the acid and a silanolate as the nucleophile, is shown on the *left*; hydrolysis followed by condensation is shown on the *right*

agents would react with the siloxane bond (Si–O–Si) that forms the backbone of all silicones. For example Speier found that water, ethanol and hydrochloric acid molecules would readily react and insert themselves into the siloxane bond" and "*Up to this time, it was a commonly held belief that the Si–O–Si backbone was too strong to be broken*."

Based on (i) the reactivity of both silica and silicones with water, (ii) that these reactions are equilibria, and (iii) that the products (grafted monolayers prepared from end-functional polymers) are stable, the equilibration of silicone chains with silica surface silanols should not be unexpected. We interpret the results described above in these now obvious terms. The molecular weight dependence of the grafted layer thickness suggests that the equilibration of grafted silicones is slow relative to the co-equilibration of silicones and surface silanols. Figure 4.10 shows two possible mechanisms: hydrolysis of PDMS followed by condensation with a surface silanol and direct silanolysis of PDMS by a surface silanol (acid catalyzed). There are reports [49, 50] of the use of naturally occurring minerals (montmorillonite, kaolite)

that can function as heterogeneous catalysts for silicone equilibration. In fact the reaction of silicones and glass was known, or at least suspected in the 1940s: In a 1947 paper [51], authors from Dow Chemical, Corning Glass Works, Dow Corning and Bell Telephone Laboratories reported tests of dozens of silanes applied to different types of glass to form silicone films. These authors report: "*In contrast to wax films, the dimethylsiloxane film is fixed when cured at high temperatures, probably by surface reaction; after that it is resistant to solvents and only slightly injured by elevated temperatures short of 500 °C*."

4.5 Closing Comments

All of the research described here was carried out with the objectives stated in the title of this chapter. Using the preparative chemistry described we were able to control and develop a better understanding of wetting of hydrophobic and superhydrophobic surfaces. Papers were published with titles of *The Lotus Effect Explained* [52], *Contact Angle Hysteresis Explained* [41], *How Wenzel and Cassie Were Wrong* [53] and *An Attempt to Correct the Faulty Intuition Perpetuated by the Wenzel and Cassie "Laws"* [54]. We refer readers to the paper, *Wetting 101°* [1] for a review of the contact line perspective that we developed on wetting.

Acknowledgements We thank the Materials Research Science and Engineering Center (DMR-0213695) and Center for Hierarchical Manufacturing (CMMI-0531171) at the University of Massachusetts for support as well as 3M, Henkel, and Shocking Technologies for unrestricted funding. We also acknowledge the American Chemical Society for permission to reproduce figures.

References

1. Gao L, McCarthy TJ (2009) Langmuir 25:14105
2. Chen W, McCarthy TJ (1998) Macromolecules 31:3648
3. Plueddemann EP (1982) Silane coupling agents. Plenum, New York
4. Mittal KL (ed) (1992) Silanes and other coupling agents. VSP, Utrecht
5. Leyden DE (1986) Silanes, surfaces and interfaces. Gordon and Breach, New York
6. Maoz R, Sagiv J (1984) J Colloid Interface Sci 100:465
7. Maoz R, Sagiv J (1987) Langmuir 3:1034
8. Maoz R, Sagiv J (1987) Langmuir 3:1045
9. Wasserman SR, Tao Y-T, Whitesides GM (1989) Langmuir 5:1074
10. Fadeev AY, McCarthy TJ (1999) Langmuir 15:3759
11. Fadeev AY, McCarthy TJ (2000) Langmuir 16:7268
12. Horr TJ, Ralston J, Smart R (1995) Colloids Surf A, Physicochem Eng Asp 97:183
13. Korosi G, Kováts E (1981) Colloids Surf 2:315
14. Fadeev AY, Soboleva OA, Summ BD (1997) Colloid J 59:273
15. Duchet J, Chabert B, Chapel JP, Jerard JF, Chovelon JM, Jaffrezic-Renault N (1997) Langmuir 13:2271
16. Park J-M, Andrade JD (1988) In: Andrade JD (ed) Polymer Surface Dynamics. Plenum Press, New York, pp 67–68
17. Park J-M, Kim JH (1994) J Colloid Interface Sci 168:103

18. Drelich J, Miller JD, Good RJ (1996) J Colloid Interface Sci 179:37
19. Lakowski J, Kitchener JA (1969) J Colloid Interface Sci 29:670
20. Trau M, Murray BS, Grant K, Grieser F (1992) J Colloid Interface Sci 148:182
21. Fadeev AY, McCarthy TJ (1999) Langmuir 15:7238
22. Chen W, Fadeev AY, Hsieh MC, Oner D, Youngblood J, McCarthy TJ (1999) Langmuir 15:3395
23. Gao L, McCarthy TJ, Zhang X (2009) Langmuir 25:14100
24. Fogg GE (1944) Nature 154:515
25. Cassie ABD, Baxter S (1945) Nature 155:21
26. Schuyten HA, Reid DJ, Weaver JW, Frick JG (1948) Tex Res J 18:396
27. Schuyten HA, Reid DJ, Weaver JW, Frick JG (1948) Tex Res J 18:490
28. Bartell FE, Purcel WR, Dodd CG (1948) Discuss Faraday Soc 3:257
29. Rochow EG (1945) J Am Chem Soc 67:963
30. Rochow EG U.S. Patent 2,380,995, Aug. 7, 1945
31. Patnode WI U.S. Patent 2,306,222, Dec. 22, 1942
32. Gao L, McCarthy TJ (2006) J Am Chem Soc 128:9052
33. Krumpfer JW, McCarthy TJ (2010) Faraday Discuss 146:103
34. Gao L, McCarthy TJ (2008) Langmuir 24:362
35. Jia X, McCarthy TJ (2003) Langmuir 19:2449
36. Gao L, McCarthy TJ (2006) Langmuir 22:5998
37. Gao L, McCarthy TJ (2007) J Am Chem Soc 129:3804
38. Gao L, McCarthy TJ (2007) Langmuir 23:10445
39. Krumpfer JW, McCarthy TJ (2011) Langmuir 27:11514
40. Fadeev AY, McCarthy TJ (1999) J Am Chem Soc 121:12184
41. Gao L, McCarthy TJ (2006) Langmuir 22:6234
42. Kole S, Srivastava SK, Tripathy DK, Showmick AK (2003) J Appl Polym Sci 54:1329
43. Lai SK, Batra A, Cohen C (2005) Polymer 46:4204
44. Scott DW (1946) J Am Chem Soc 68:2294
45. Patnode W, Wilcock DF (1946) J Am Chem Soc 68:358
46. Hyde JF U.S. Patent 2,567,110, September 4, 1951
47. Kantor SW, Grubb WT, Ostoff RC (1954) J Am Chem Soc 76:5191
48. Warrick EL (1990) Forty years of firsts. McGraw-Hill, New York, p 71
49. Bageli NN, Bryk MT (1981) Ukr Khim Zh 47:409
50. Xu S, Lehmann RG, Miller JR, Chandra G (1998) Environ Sci Technol 32:1199
51. Hunter MJ, Gordon MS, Barry AJ, Hyde JF, Heidenreich RD (1947) Ind Eng Chem 39:1389
52. Gao L, McCarthy TJ (2006) Langmuir 22:2966
53. Gao L, McCarthy TJ (2007) Langmuir 23:3762
54. Gao L, McCarthy TJ (2009) Langmuir 25:7249

Chapter 5
Comparison of Surface and Bulk Properties of Pendant and Hybrid Fluorosilicones

Cedric Pasquet, Claire Longuet, Siska Hamdani-Devarennes, Bruno Ameduri, and François Ganachaud

5.1 Introduction

The explosion of the US space shuttle Challenger in the late-1980s was provoked by the break-up of a polysulfide O-ring that had shrunk the night before the launch, because of the extreme low temperature in Cape Canaveral (−30 °C) [1]. Since that dramatic accident, silicone elastomers have systematically been chosen, owing to their wide range of temperature specifications, as the best performing materials particularly in the fields of aeronautics and automotive industry. These polymers are also good candidates for many other applications, including foam stability, paper release and so on. However, despite their exceptional properties, e.g. low surface tension, dielectric resistance, gas permeation or physiological inertness, they suffer from too large a swelling rate in solvents or oils which is disqualifying for O-rings applications. For this reason, the market for fluorosilicones in high-tech applications is gradually expanding, and the recent announcement of the joint venture between Dow Corning and Daikin [2] makes one believe that the panel of applications will go on growing.

The most common fluorosilicone polymer commercialized to date is the poly(methyl-3,3,3-trifluoropropylsiloxane) (PMTFPS) (Structure 5.1), which has

C. Pasquet · S. Hamdani-Devarennes · B. Ameduri (✉) · F. Ganachaud (✉)
Institut Charles Gerhardt, Equipe "Ingénierie et Architectures Macromoléculaires", UMR5253 CNRS, ENSCM, 8 rue de l'Ecole Normale, 34296 Montpellier Cedex, France
e-mail: bruno.ameduri@enscm.fr

F. Ganachaud (✉)
e-mail: francois.ganachaud@enscm.fr

C. Pasquet · F. Ganachaud
IMP@INSA, UMR5223 CNRS, INSA-Lyon, Bâtiment Jules Verne, 17, avenue Jean Capelle, 69621 Villeurbanne Cedex, France

C. Longuet · S. Hamdani-Devarennes
Ecole des Mines d'Alès, CMGD, 6 Avenue de Clavières, 30100 Alès, France

M.J. Owen, P.R. Dvornic (eds.), *Silicone Surface Science*, Advances in Silicon Science 4,
DOI 10.1007/978-94-007-3876-8_5,

first been described in the late-1950s [3] and then commercialized by Dow Corning in the 1960s [4, 5]. The two methylene groups separating the CF_3 moiety from the silicon atom were chosen both for the sake of synthesis and for stability (i.e. to avoid HF elimination). This polymer is referred to in the rest of this chapter as the "conventional" fluorosilicone. However, although the synthesis and formulation of PMTFPS is nowadays very well controlled, the low content of perfluorinated groups in the polymer (36.5 wt.%) still does not fulfill the requirements of some niche applications, particularly when swelling properties or degradation at high temperatures are concerned. A number of strategies, at first mainly in the academic domain, have, therefore, been applied to increase the number of fluorine atoms in the fluorosilicone polymers. One elegant way of preparing such materials is to introduce into the silicone chain perfluorinated groups of increasing size (typically C_6 or higher), either as pendant groups or inside the siloxane backbone. Here, we refer to silicones with perfluorinated chains introduced as side groups as "pendant silicones" (Structure 5.2) whereas those carrying fluorine atoms in the main backbone are called "hybrid silicones" (Structure 5.3). For the sake of simplicity, we will consider those polymers bearing fluorinated groups both in the main chain and in the pendant groups as "hybrid copolymers".

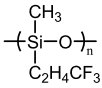

Structure 5.1

$$(2 \leq x \leq 8;\ y = 2, 3)$$

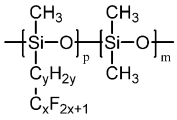

Structure 5.2

$$(2 \leq x \leq 8;\ y = 2, 3, n = 1, 2, 3)$$

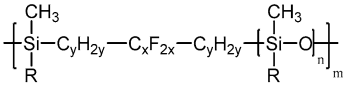

Structure 5.3

The syntheses of both types of polymer have been described in the literature [6–8]. Here, we briefly review the most conventional synthesis techniques. On the other hand, the properties of such fluorosilicones and their equivalent (cross-linked) elastomers have not been reviewed so far, apart from the surface properties that were described by Owen et al. [9]. A comparison of the above mentioned two classes of polymers in terms of mechanical, swelling and thermal properties, especially for the hybrid fluorosilicones synthesized mostly at Dow Corning or in our Laboratory for the last thirty years, was lacking and is now fulfilled here.

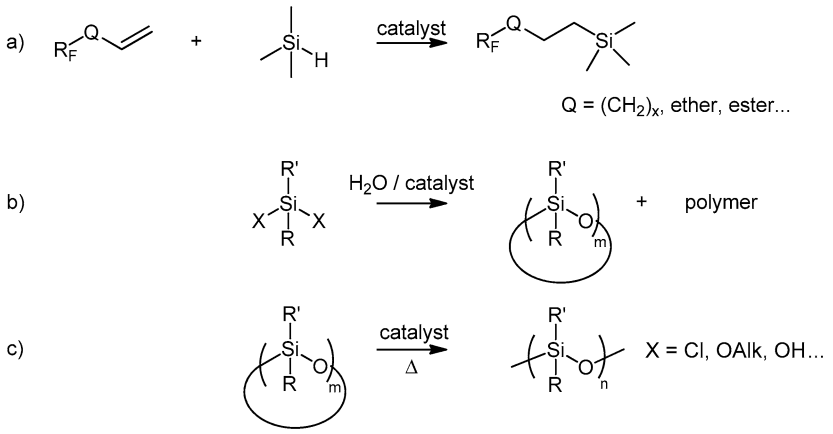

Scheme 5.1 Main methods for silicone synthesis and modification: (**a**) hydrosilylation; (**b**) condensation; (**c**) ring opening polymerization

Complex formulations used in industry to prepare elastomers with good mechanical properties will not be primarily considered here. Instead, this chapter focuses on structure/property relationships obtained by simple and comparable processing of various fluorosilicones. Furthermore, the properties of silicone/non-silicone copolymers are not surveyed here, although a concise description of the most promising materials is given at the end of this chapter. In all main sections, the properties of pendant fluorosilicones are reviewed first, starting from linear PMTFPS (often compared with polydimethylsiloxane (PDMS)), then copolymers with PDMS, and then cross-linked elastomers of homo and copolymers. Following this, a description of hybrid silicone properties using the same degree of complexity is given, where available. In each subsection, an intermediate conclusion succinctly compares both classes of polymers with respect to the considered property.

5.2 Some Insights on Fluorosilicone Synthesis

Silicone chemistry is unique and quite versatile so that chains with complex chemical microstructure can be constructed at will through different pathways. There are basically three types of reactions in the toolbox of the silicone chemist (see Scheme 5.1): (a) hydrosilylation between ≡SiH and ene moieties, (b) condensation of various reactive groups (alkoxysilane, chlorosilane and/or silanol) and (c) ring opening polymerization (ROP) of cyclic siloxanes. Hydrosilylation reaction is catalyzed either by initiators used in radical polymerizations (e.g. peroxides or azo-containing molecules) or by late transition metal complexes, in particular platinum derivatives. There is basically no distinction between the reactivity of simple or fluorinated olefins. The originality here, mainly shown in patents, is the nature of the Q group between the double bond and the fluorinated part of the reagent

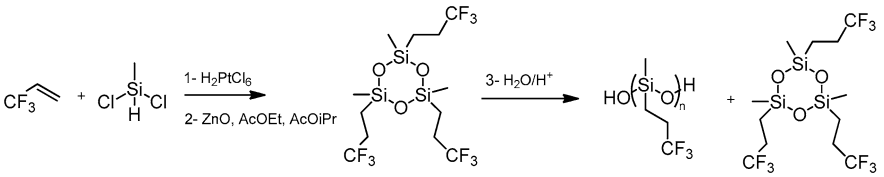

Scheme 5.2 Synthesis of PMTFPS

(Scheme 5.1). Due to the electropositive nature of the silicon atom, fluorination on the α or β position leads to polymers of poor stability and silicones are thus fluorinated on the γ position. Difunctional silanes (mostly dichloro and dimethoxysilanes) are hydrolyzed via either a basic or acidic catalyst to generate a mixture of linear oligomers and cyclic species. The same catalysts, e.g. tetramethylammonium hydroxide ($(CH_3)_4N^+OH^-$), KOH or H_2SO_4, promote the ROP of trimeric or tetrameric cyclics, if these are not systematically isolated. In the case of hybrid silicones, where cyclization is not likely, polycondensation generates exclusively chains of maximum molecular weights of about 15,000. A combination of these three methods can be used to generate fluorosilicones in the most straightforward way. The following sections describe the basic principles of the syntheses of pendant and hybrid fluorosilicones; readers are directed to more specialized reviews for complementary information [6–8].

5.2.1 Synthesis of Pendant Fluorosilicones

5.2.1.1 Homopolymers

The synthesis of PMTFPS was first reported by Pierce and Kim [10] in 1971 (see Scheme 5.2). Via a complex hydrosilylation process (trifluoropropene is gaseous), the generated bischlorosilane was condensed through a zinc catalyzed reaction to generate mostly the cyclic trimer 1,3,5-trimethyl-1,3,5-tris(3′,3′,3′-trifluoropropyl)cyclotrisiloxane (generally abbreviated F_3), which then polymerized into an open polymer chain by ROP. Using an acid catalyst (e.g. trifluoromethanesulfonic acid [11]), the average molecular weights obtained were in the range of 6,000, with a small quantity of cyclosiloxanes [12]. With basic catalysts, polymerizations were carried out in THF using *n*-butyl lithium, [13] sodium or lithium silanolate, [14, 15] KOH [15] or recently trimethylsilylmethyllithium in the presence of cryptands [16]. Industrially, either the last-mentioned catalyst or a mixture of H_2O/phosphazene bases is preferred, since they polymerize the trimer so fast that the final conversion and the molecular weights of the polymer are controlled by the kinetics (the polymer/cyclic thermodynamic equilibrium is typically of a 1/6 ratio).

The protocol described above also applies to fluorosilicones with larger perfluorinated substituents, starting from $HSiCl_2R$ where $R = CH_2CH_2QR_F$, Q = O, COO,

Scheme 5.3 Synthesis of fluorinated copolysiloxanes by polycondensation

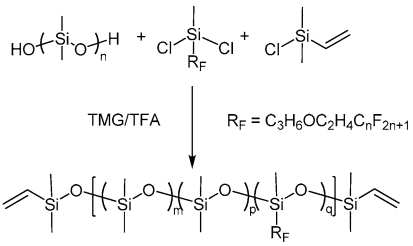

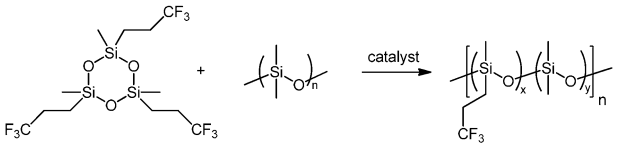

Scheme 5.4 Synthesis of fluorinated copolysiloxanes by ROP/redistribution reactions

CONH, SO_2NR, OCONH [6, 7, 17] and R_F is typically C_4F_9 [18]. Furukawa et al. [19] catalyzed the polymerization of $[F_9C_4\text{-}C_2H_4\text{-}Si(CH_3)O]_3$ by NaOH at temperatures between 150 and 200 °C, and showed that only the corresponding tetramer and few oligomers were produced. On the other hand, at temperatures between 0 and 20 °C, the viscosity of the reaction mixture passed through a maximum, reflecting the kinetic control of the polymerization. In contrast to this, the polymerization of F_3 at 150 °C with *n*-butyllithium produced polymer with a high average degree of polymerization (270) and a low polydispersity (∼1.18) [20].

5.2.1.2 Copolymers

5.2.1.2.1 By Polycondensation

Various fluorosilicone copolymers were synthesized via polycondensation of α,ω-hydroxy PDMS, a bischlorosilane bearing a perfluorinated chain and a monochlorosilane bearing a vinyl group as a chain end-linker terminator (see Scheme 5.3) [21, 22]. Addition of another bischlorosilane, bearing various types of acrylic group, yielded polymers that cross-link under UV irradiation [23–26].

5.2.1.2.2 By ROP

Fluorinated copolysiloxanes were also prepared by ROP/equilibration reactions of F_3 and PDMS catalyzed by potassium silanolate [27] (see Scheme 5.4). ROP of F_3 and cyclic dimethylsiloxy trimer (D_3) or tetramer (D_4) in the presence of trifluoroacetic anhydride produced polymers that contained both side and end-functionalities [28, 29]. Copolymerization of F_3 and the equivalent trimer bearing C_4F_9 groups led to an "all-fluorinated" silicone copolymer with high molecular weights.

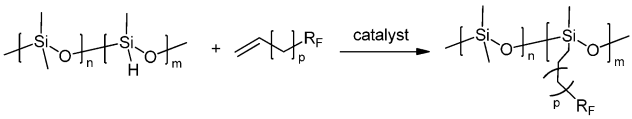

Scheme 5.5 Addition of fluorinated groups onto a PDMS-co-PMHS backbone by hydrosilylation reaction

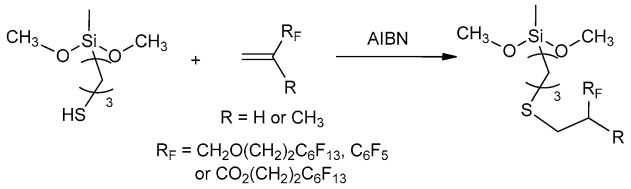

Scheme 5.6 Addition of fluorinated groups to a diethoxysilane by thiol-ene addition

5.2.1.2.3 By Hydrosilylation

An extended series of patents from Dow Corning [30–34] and General Electric [35] claimed the modification of hydrido-containing polysiloxanes with fluorinated groups. In academia also, some authors introduced long conventional alkyl [18, 36, 37], alkyl ether [38–43], alkyl ester [44–46] and aryl ester [47] perfluorinated chains [38–41, 48–51] by hydrosilylation onto poly(methylhydridosiloxane) (PMHS) and PDMS-co-PMHS copolymers (see Scheme 5.5). In most cases, the Speier catalyst (H_2PtCl_6), was used except for the aryl ester-based molecule [47] where a cobalt complex gave higher yield. In most cases, only the conventional β addition was observed. However, in one specific study [52], an exchange reaction occurred between the H of the silane and the fluorine atom on the α position of the double bond. In supercritical CO_2 [53] the extent of hydrosilylation reached 50 % yielding higher molecular weight products.

Furukawa and Kotera [54] hydrosilylated fluorinated precursors bearing (methyl) urea groups as structuring spacer agents. Varying the content of fluorine in these copolymers had an important impact on thermal properties (see below) [55]. When carrying out a hydrosilylation step with vinyltrichlorosilane, they could attach the polymer to a glass surface more effectively, thus significantly affecting the water contact angle and surface free energy. By post-hydrosilylating acryl-containing allylic molecules, Boutevin et al. [56–58] cross-linked the resulting material using a UV sensitive initiator to generate novel membranes for pervaporation applications.

5.2.1.2.4 Via Thiol-ene Addition

Functional fluorosilanes can be obtained by a radical addition of a fluorinated thiol onto a vinylsilane [59–61] or by addition of a mercaptosilane to a thiosilane [62] (as shown in Scheme 5.6).

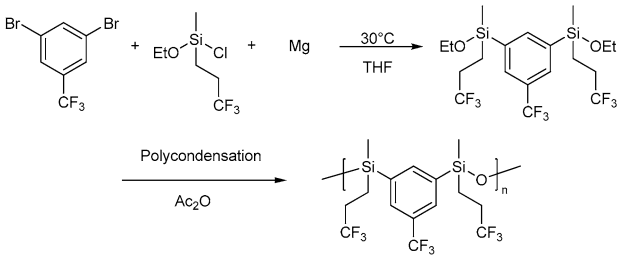

Scheme 5.7 Proposed synthesis of fluorosilicones by Grignard reaction followed by polycondensation

According to the principle of telomerization [63, 64], different adducts can be obtained: for instance, starting from a silylated thiol as a telogen, such as 3-mercaptopropyldimethoxymethylsilane (or its dichlorinated equivalent) [65], an allylic or vinylic fluorinated olefin gives a monoadduct [66] whereas a perfluorinated methacrylate or styrene oligomerizes to up to 10 units. These silanes can then be used in polycondensation reactions [65].

5.2.2 Synthesis of Hybrid Fluorosilicones

5.2.2.1 With Aromatic Structures

5.2.2.1.1 By Grignard Reaction

Most of these syntheses involve some alkoxy and/or chloro-functional silane and a halogenated (bromo or chloro) aromatic compound. For example, Grindahl [67] used the 3,5-dibromo-1-trifluorobenzene as a precursor to the corresponding bis(silylfluoroalkyl)ethoxysilane which was then subjected to polycondensation by an acidic catalyst (see Scheme 5.7).

Wu [68] claimed precursors with benzyl groups bearing one [66], two or four [68, 69] fluorine atoms (see Scheme 5.8). Either dichlorosilanes (R = Cl) [70] or bisethoxysilanes (R = OEt) [71] were first hydrolyzed under acidic conditions into silanols which were then polycondensed using a basic catalyst. Poly(*p*-fluorophenylmethylsiloxanes) with molecular weights between 44,000 and 74,000 were thus prepared. The bisfluorinated precursor, namely the 3,5-difluorobromobenzene, gave only polymers of 15,000 [72] maybe since the first hydrolysis was carried out under basic conditions (H_2O/Na_2CO_3).

Giori and Zerlaut [73] carried out such a synthesis using the pentafluorobromobenzene on tetraethoxysilane (TEOS). By polycondensation of the bis(pentafluorophenyl)diethoxysilane and the pentafluorophenyltriethoxysilane, derived through Grignard synthesis from pentafluorobromobenzene and TEOS [74], they reached a polymer with a large molecular weight ($M_n = 65{,}000$).

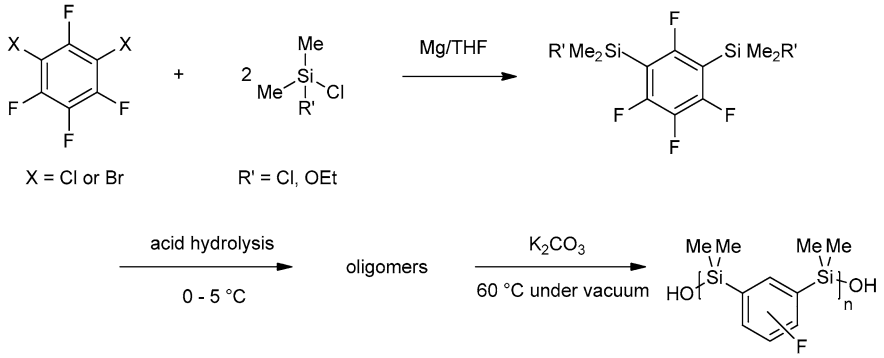

Scheme 5.8 Synthesis of hybrid fluorosilicones using fluorobenzene derivatives as precursors

5.2.2.1.2 By Polyhydrosilylation

An interesting recent study by Cassidy and co-workers [75, 76] considered novel poly(silanes-siloxanes) bearing hexafluoroisopropylidene groups. The hydrosilylation reaction, in the presence of Pt/divinyltetramethyldisiloxane, Karstedt catalyst, was performed in supercritical CO_2 (see Scheme 5.9). The molecular weights of these hybrid copolymers were notably higher than those synthesized in organic solvents, such as benzene. They also exhibited high thermal stability (10 % weight loss at 360 °C in air). Further hydrolysis and thermal treatment of these polymers led to materials with higher molecular weights which retained low glass temperature (T_g) values [76].

5.2.2.2 With Fluoroalkyl Groups

The first step in the preparation of fluorinated hybrid silicones deals with the preparation of telechelic non-conjugated dienes containing fluoroalkene groups of the formula shown in Structure 5.4, based on vinylidene fluoride (VDF), tetrafluoroethylene (TFE) and hexafluoropropylene (HFP) and represented by $H_2C{=}CH\text{-}R_F\text{-}CH{=}CH_2$ in the following text.

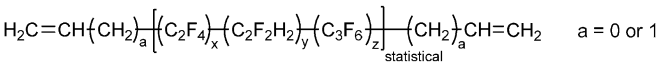

Structure 5.4

The dienes can be synthesized by one of the following two-step reactions, depending on the nature of the ene bond (see Scheme 5.10) [77, 78].

Kim et al. [79] pioneered the synthesis of such compounds using TFE as fluoroalkene (Structure 5.4, $a = y = z = 0$, $x = 8$), in 1977. Since then, to the best of our knowledge, no product from this series has been commercialized. Several years ago, different fluoroalkenes [80, 81] were inserted by telomerization reactions

Scheme 5.9 Synthesis of hybrid aromatic fluorosilicones by a hydrosilylation process

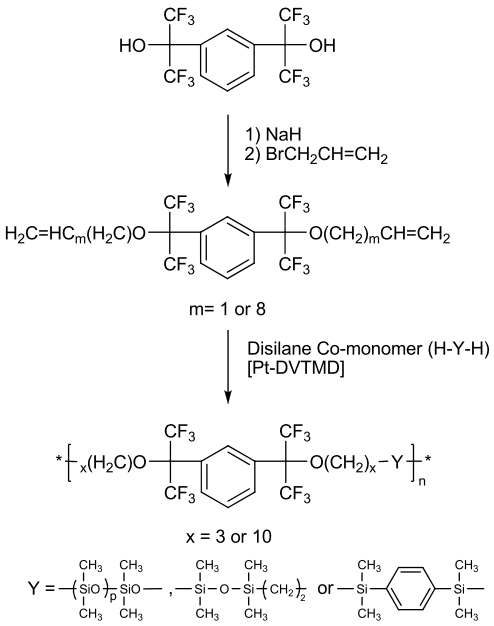

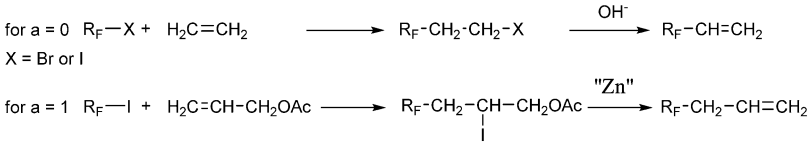

Scheme 5.10 Syntheses of fluoroalkyl dienes as precursors of hybrid fluorosilicones

[82] starting from I-C_nF_{2n}-I (with $n = 2, 4, 6$) to eliminate the crystallization of the resulting oligomers. Loree et al. [80] also synthesized interesting nonconjugated dienes with VDF units by the telomerization of VDF (revisited later by Modena et al. [83]) which, surprisingly, did not undergo any dehydrofluorination.

Hybrid fluorosilicones were prepared from these nonconjugated dienes, typically by two strategies: (i) hydrosilylation with a hydridochlorosilane to generate the bischloro intermediates which were further hydrolyzed/condensed or co-condensed with a bissilanol-terminated oligomer [84]; or (ii) polyhydrosilylation between the diene and a bishydrido terminated oligomer [85]. Since the siloxane units confer the softness, their number must be carefully adjusted in the polymer, if it is desired to lower as much as possible the T_g without decreasing the high temperature resistance to degradation that arises by cyclics production from intramolecular reactions at high temperatures [86]. Typically, oligosiloxane sequences with less than five silicon atoms, with the last two linked to a carbon atom to avoid any formation of cyclosiloxanes, were obtained by co-condensation.

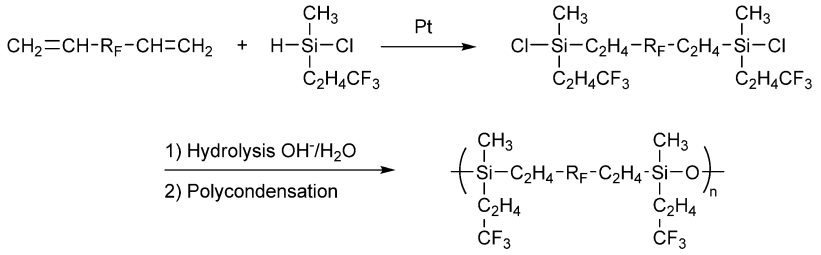

Scheme 5.11 Suggested synthesis of fluorosilicones by hydrosilylation/condensation reactions

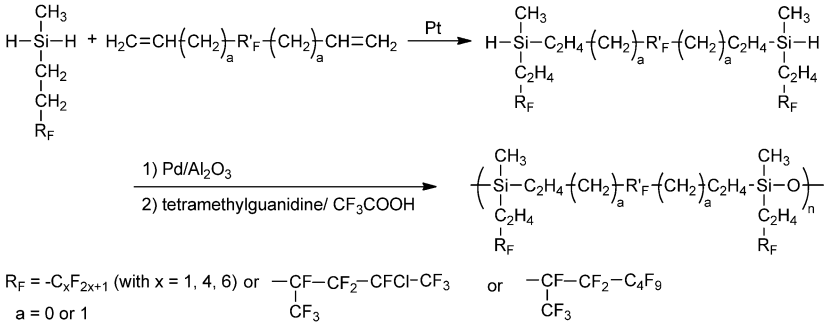

Scheme 5.12 Another pathway to synthesize fluorosilicones by hydrosilylation/Si-H end-groups' hydrolysis and polycondensation

5.2.2.3 With Both Pendant and Main-Chain Fluorinated Groups

The chemistry for preparation of these polymers typically follows the precepts given above, albeit starting from more expensive precursors. Kim [80, 87] proposed the synthesis of a hybrid fluorosilicone which begins with hydrosilylation, as shown in Scheme 5.11. The fluorinated side group, $–CH_2CH_2CF_3$, was required to avoid any crystallization which occurs when $R_F = C_8F_{16}$, and is unfavorable where the goal is to obtain elastomers. The chlorosilane precursor was obtained by the disproportionation of the dihydrido and dichlorosilane derivatives. The equilibrium was shifted toward the reactants when the length of the R_F group was increased (i.e., from CF_3 to C_6F_{13}) and the separation of the products (by distillation) became much more difficult.

To avoid such drawbacks, we investigated [88–90] a different pathway (see Scheme 5.12) which involved: (i) direct hydrosilylation of the bishydrido molecule with complex dienes, where R'_F represents a fluorinated group based on TFE, VDF, and hexafluoropropylene (HFP) units; followed by (ii) hydrolysis of Si-H end-groups into silanols using Pd/Al_2O_3 catalyst; and (iii) polycondensation of these silanols using the tetramethylguanidine/trifluoroacetic acid complex salt.

5.3 Surface Properties

The structural requirements for low surface energy polymers are well known (see for example, Chap. 1). These polymers should be very flexible in order to enable perfluoroalkyl chains to protrude towards the interface [9]. The number of hydrophobic pendant groups should be in sufficient proportions, and the spacer located between the silicon and the hydrophobic group should not confer any undesirable interaction. It follows from these requirements, set by Owen's group [91], that PDMS with its remarkable elasticity ($T_g = -123\,°C$) and low polarity (introduced by the adjacent methyl groups) is a suitable candidate for the purpose. Indeed, it is often used in blends with other polymers for its remarkable ability to deliver surface hydrophobicity, even at low contents. Only fluoropolymers give lower surface energies, except PMTFPS, for reasons that will be discussed later. Consequently, academic and industrial researchers and engineers have focused on fluorosilicones with longer perfluorinated chains than the CF_3 group.

The values of the surface tension, even for very apolar surfaces such as those of fluorosilicones, depend on the technique used (see also Chap. 1). In Appendix A of this chapter, along with a definition of surface tension, we give a description of two techniques employed to assess these values of liquid polymers (by means of a tensiometer) or on solid polymer surfaces (via contact angle measurements). The exact calculations of various surface tension components are also supplied.

5.3.1 Surface Tension of Pendant Fluorosilicones

5.3.1.1 Oils

5.3.1.1.1 Homopolymers

It is well known that many properties of polymers strongly depend on their average molecular weight, particularly below 10,000, because of the strong influence of oligomer chain ends. According to Legrand and Gaines [92], the surface tension of a liquid polymer can be expressed as a function of its number average molecular weight M_n by the following equation:

$$\gamma = \gamma_\infty - (K/M_n)^{2/3} \tag{5.1}$$

where γ_∞ and K, respectively stand for the surface tension of a polymer of "infinite" molecular weight and a constant which depends on the polymer studied.

Figure 5.1 shows linearized plots of Eq. (5.1) for PDMS and PMTFPS, using experimental values from different sources, and by different techniques (such as the Du Nouy ring and sessile drop techniques). Above an average molecular weight of about 3,000, some authors consider that the variation in surface tension is within the experimental error, i.e. less than 1 $mN\,m^{-1}$ [93]. This is confirmed by the data of Fig. 5.2, for both PDMS and fluorosilicones of increasing pendant perfluorinated

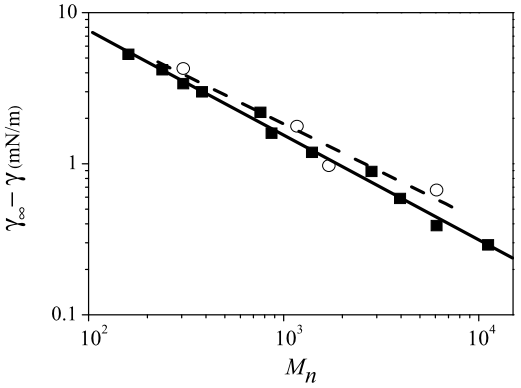

Fig. 5.1 Linearized plots of the Legrand/Gaines equation for PDMS (■) and PMFTPS (○) homopolymers

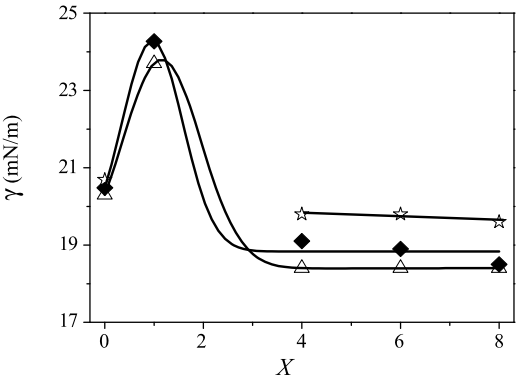

Fig. 5.2 Surface tensions of fluorosilicones with increasing pendant perfluorinated chainlengths ($x = 0$: PDMS). (♦) M_n about 7,000; (△) M_n 20 to 30,000; (☆) copolymer of PMFTPS and PDMS ($m/n = 0.55$, $y = 2$, Structure 5.2)

chain lengths, where surface tensions of homopolymers with molecular weights of about 7,000 and 50,000 are compared. Figure 5.2 also shows that the length of the perfluorinated sequence has almost no influence on the liquid surface tension [92, 94].

The surface tension for PDMS (see also Chap. 1) is below the value found for PMTFPS. Such a result has been explained [36, 95] on the basis of the hydrophobicity of the constituents of the pendant groups which decreases in the order $CF_3 > CH_3 > CH_2$. The spatial conformation of the trifluoropropyl group, as well as the relatively low proportion of perfluorinated units in it, would explain the relatively high liquid surface tension value of PMTFPS. However, this effect is rapidly screened with increasing x, and it would be of particular interest to measure the surface tension of fluorosilicones with $x = 2$, a study which, to our knowledge, has not yet been reported.

5.3.1.1.2 Copolymers

The influence of the length of the perfluorinated group in silicones on the liquid surface tension was studied for a model copolymer of fluorosilicone and PDMS

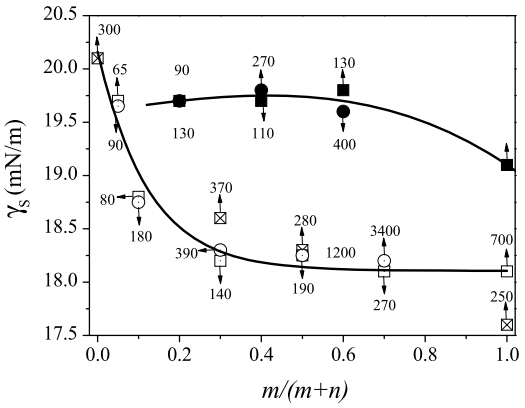

Fig. 5.3 Surface tensions of fluorosilicone copolymers according to reference [37] (*plain symbols*) and [55] (*open symbols*). (■, □, ⊠) $x = 4$, $y = 2$ (Structure 5.2); (○, ●) $x = 8$, $y = 3$ (Structure 5.2). All data were measured by the Wilhelmy plate technique at 25 °C, except for ⊠ measured at 20 °C [18]. Numbers on the graph indicate M_n of the polymers

$((x, y) = (3, 1), (5, 1), (7, 2), n/m = 0.55$, Structure 5.2) and the results are reported in Fig. 5.2 [96]. Apart from PDMS and PMTFPS homopolymers, all copolymers with $x \geq 4$ exhibit almost constant values of γ.

The influence of the content of dimethylsiloxane units on the surface tension is less straightforward, as illustrated in Fig. 5.3, where the discrepancy between two sets of data is marked. Both curves show a plateau over a large composition range, which would indicate that the surface tension is dictated either by the PDMS or fluorosilicone units in the polymer. The difference in surface tensions does not seem to depend significantly on the conditions of measurement, such as the temperature. We pointed out above that average molecular weights have a certain influence on the liquid surface tension, but viscosities of the different samples (see Fig. 5.3) do not differ significantly from one set of data to the other [18, 37, 55]. Rather, possible differences in the microstructure of these copolymers, i.e. random or multi-block, may explain the observed variation of the results. Kobayashi and Owen [37] reported that their fluorosilicones, obtained from hydrosilylation of PDMS-*co*-PMHS polymer, had mostly a random structure. Given so, it can be assumed that the behavior of dimethylsiloxy groups dominates their surface properties, the fluorinated groups being "diluted" inside the silicone chains. In the other study [55], a multi-block copolymer was obtained from the ring opening copolymerization of D_4 and F_3; here instead, patches of fluorosilicone segments may contribute to low surface tension of the copolymer, even at low fluorine contents.

5.3.1.2 Waxes and Gums

5.3.1.2.1 Homopolymers

The highly fluorinated homopolymer ($x = 8$, $y = 3$, Structure 5.2) is solid at ambient temperature, and could not be compared to its homologues through tensiometry measurements (see the data missing in Fig. 5.3, for $m/(m + n) = 1$). Therefore, this polymer and others, depicted below, were characterized by contact angle measurements on a solid polymer film.

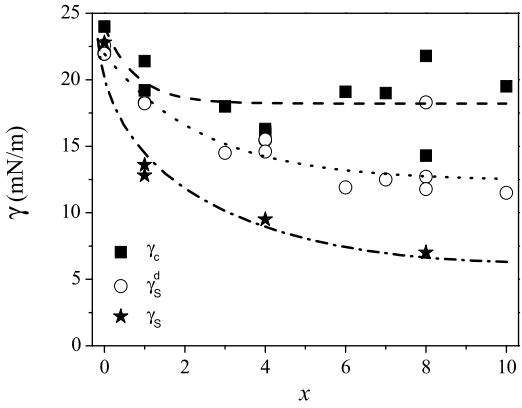

Fig. 5.4 Critical (■), dispersive (○) and overall (★) surface tensions of homofluorosilicones of increasing perfluorinated chain-lengths x, as determined by contact angle measurements ($x = 0$: PDMS, see Structure 5.2)

The authors generally report three types of surface tension, depending on the solvents used for measuring contact angles and on the chosen equation (see Appendix A for relevant equations and definitions of these surface tensions): (i) the critical surface tension, γ_c, is deduced by interpolation using a set of alkanes of increasing chain length [42]; (ii) the dispersive component, γ_S^d is calculated only from hexadecane contact angle measurement; and (iii) an overall surface tension γ_S is calculated from a combination of γ_S^d and γ_S^p determined from water and diiodomethane contact angles. From several different references in the open literature [9, 11, 37, 42, 45, 50, 97–99], the variation of these three components for homopolymers of increasing perfluorinated chain lengths (x in Structure 5.2) have been recalculated and are shown in Fig. 5.4.

The trends are similar regardless of how the surface tensions were calculated, i.e. there is a constant decrease of the surface tension with increasing perfluorinated chain lengths. This is, however, truly different from what was observed before by the Wilhelmy plate measurements, particularly for PMTFPS and is another confirmation that these two techniques cannot be compared.

Different calculations of surface tensions give similar values for PDMS, whereas for fluorosilicones, surface tensions level off for $x = 6$ at 18.2, 12.5 and 8 mN m^{-1} for γ_c, γ_S^d and γ_S, respectively. It is well known that the critical surface tension is generally higher than the dispersive surface tension for a given oleophobic solid such as fluorosilicones. The large deviation seen in the γ_c values in Fig. 5.4 was explained by some absorption of alkanes into the tested film, which distorted the extrapolation curve. In comparison, values obtained from hexadecane measurements are very reproducible from one publication to another, and the obtained γ_S^d values are in perfect agreement with values given for other fluorinated elastomers [91]. Besides, the overall surface components derived from the two liquids, water and diiodomethane, including both dispersive and polar surface tension components, are quite low. The ability of polymer chains to reorganize on the surface in the presence of the liquid drop [50] artificially changes the dispersive component and, *per se*, the overall surface tension. This can be better described by considering the contact angle hysteresis that was studied mainly for fluorosilicone resins and rubbers (see below).

5.3.1.2.2 Copolymers

The copolymers of PDMS and fluorosilicones ($x = 4, y = 2, m/(m + n) = 0.5$, Structure 5.2) gave similar contact angles to the corresponding fluoro-homopolymers [50]. In this study, contact angle measurements on films aged at 100 °C for one day showed little variation of the contact angle with time. Another study focused on the effect of the support on which the polymer was cast, namely a glass surface [55]. Segments with few $SiCl_3$ pendant groups were incorporated into the fluorosilicone copolymer prepared by polycondensation to induce a linking reaction between the Si-OH groups of the glass surface and the polymer. It was found that the solid surface tension decreased sharply (from 37 to 16.8 $mN\,m^{-1}$) with increased number of $SiCl_3$ side groups from 1 to 5 units per chains. Most likely, the glass surface repels the fluorinated groups to the air-polymer interface; in addition, the grafting reaction decreases the mobility of the chains and may induce some rugosity to the surface that could be responsible for superhydrophobicity (see Chap. 4) also known as "Lotus effect". Such hypothesis was not checked out by AFM in the paper.

5.3.1.3 Rubbers, Elastomers and Coatings

The formulation of silicone materials is often quite complex, since it includes at least, a silicone polymer, silica filler nanoparticles, and a catalyst for cross-linking reactions. The examples given below are intended to extract general tendencies rather than to try to explain all subtleties of the industrial know-how.

5.3.1.3.1 Homopolymers

Surface tensions of silicone homopolymers bearing phenylsiloxy groups with increasing degree of fluorination, and cross-linked via silanol/TEOS polycondensation, were examined by Patwardhan et al. (see Table 5.1) [70]. Silicones bearing simple phenyl side groups are less hydrophobic than PDMS, mainly because the rigidity of the phenyl groups disturbs the reorganization on the surface, with the $Si-CH_3$ groups protruding at the interface. The functionalization of the phenyl groups with one or two fluorine atoms improves the surface hydrophobicity and lipophobicity, but to a much smaller extent than PMTFPS does. These results preclude the use of phenylsilicones for low surface energy applications.

5.3.1.3.2 Copolymers

Hamada et al. [100] reported the preparation of two- or three-dimensional fluorosilicone networks cross-linked by platinum-catalyzed hydrosilylation. Contact angles of 110°, 83° and 41° with water, diiodomethane and hexadecane, respectively, were

Table 5.1 Contact angles and calculated surface tensions for (fluoro)phenyl functionalized silicone networks, compared to PDMS and PMTFPS [70]

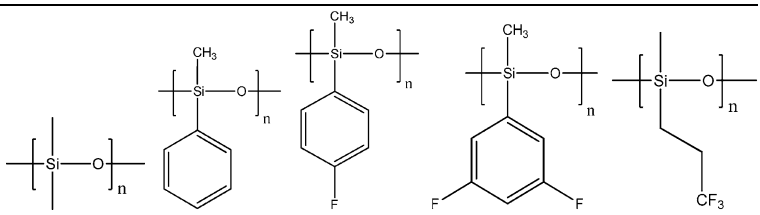

θ_{H_2O} (°)	100	83	105	104	104
$\theta_{CH_2I_2}$ (°)	68	/	77	76	90
γ_S (mN m^{-1})	23.5	33.2	18.7	19.1	13.6

lower than those measured for the equivalent copolymers with $R_F = C_8F_{17}$ side chains (121°, 105° and 72°, respectively). Kobayashi et al. [101] mixed linear fluorosilicones with a PDMS base containing silica, and cross-linked by radical, hydrosilylation or hydrolysis/condensation reactions. Similar contact angles were obtained regardless of the catalyst system, with contact angles varying from 106–119° with water to 20–28° with hexadecane, depending on the overall fluorine content of the formulation. The best results were obtained for mixed copolymers of PDMS, fluoroakyl esters and poly(ethylene oxide) and poly(propylene oxide) units (Structure 5.5).

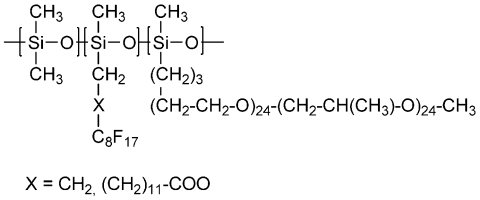

Structure 5.5

Copolymer silicone resins were prepared by Kobayashi and Masatomi [102, 103], with perfluorinated alkyl units of increasing x values (Structure 5.2). Fluorinated resins showed water repelling value close to that of PDMS networks (water contact angle of 105–110° relative to 101–104°), but striking differences were seen in oil staining (hexadecane contact angle of 48–66° *versus* 32–34°). The contact angle hystereses of fluorinated silicones were generally lower than those of PDMS networks (21–25° relative to 36°, respectively). A rather intriguing result was observed while introducing an aminosilane as an additive in the formulation (Structure 5.6) where it seems that a specific nanostructuring of the final material was responsible for the best oil and water repellencies observed in this patent (θ_{water} = 107–109° and $\theta_{hexadecane}$ = 59–66°, $\omega \sim 23°$).

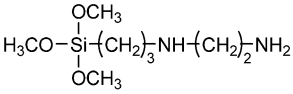

Structure 5.6

Grunlan et al. [95] studied the surface properties of copolymers cross-linked through an epoxide-amine reaction, using trifluoropropyl functionalized comonomers (see Structures 5.7 and 5.8).

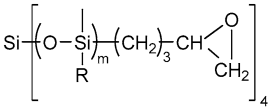

R = CH_3 , $CH_2CH_2CF_3$

Structure 5.7

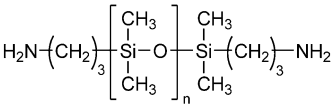

Structure 5.8

They measured static, advancing and receding contact angles and compared them as a function of PDMS molecular weights, fluorosilicone contents, and pretreatment of the star polymer, i.e. removal of small molecular weight residues before condensation. First, most of the static contact angles were lower than the advancing ones, showing a reorganization of the surface during the drop deposit. Second, static contact angles of water with PDMS networks were greater than those observed for fluorinated ones (107–128° *vs.* 99–117°), for similar reasons as those mentioned earlier for the poor water repellency of CH_2 compared to CH_3 groups [94]. Third, for both types of polymer, the difference in advancing and receding contact angles did not change with the chain-length of the amino-PDMS used. However, the receding contact angles for fluorosilicones were clearly above those for PDMS networks, which were emphasized by the contact angle hysteresis, which ranged from 7–23° and 23–41° for fluorinated and non-fluorinated silicones, respectively [95]. Kobayashi and Masatoni [102, 103] ascribed such an effect to the slower mobility of water molecules in the presence of fluoroalkyl groups than in the presence of methyl ones.

5.3.1.4 Supramolecular Architectures

Significant improvement of surface properties can be achieved by nanostructuring the polymer film, preferably by supramolecular self-assembly (compare with Chaps. 4 and 6). The fact that low substitution of PDMS by fluorinated

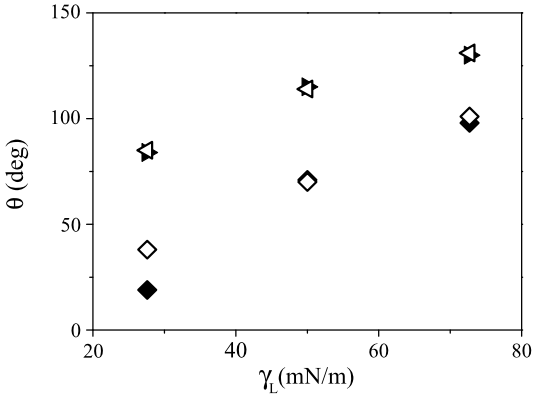

Fig. 5.5 Contact angles (θ, deg) versus surface tensions of test liquids (γ_L, mN m^{-1}) for supramolecular perfluorinated polymer of Structure 5.9 with 50 % (►) and 100 % (◁) complexation, compared to the original aminosilicone (◇) and a conventional PDMS (◆) [104]

groups is enough to dramatically affect the surface properties has recently been shown on *pseudo* fluorinated copolymers [104]. The copolymers were prepared by supramolecular assembly of low amino content silicone oils with perfluorododecanoic acid (Structure 5.9). The films were solvent-cast, stored in water to remove the excess of perfluorinated acids, and further cross-linked by curing at 120 °C for one day before carrying out contact angle measurements.

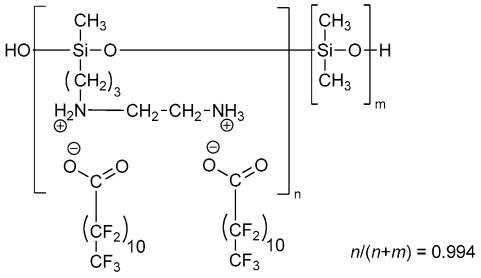

Structure 5.9

The fluorinated groups induced great changes in the contact angles of the three test liquids, hexadecane, water and diiodomethane, compared to the original aminated PDMS (see Fig. 5.5), with values higher than those found for a perfluorinated octyl group ($\theta_{H_2O} = 121°$, $\theta_{CH_2I_2} = 105°$, $\theta_{HD} = 72°$). In addition, the fluorine content (namely 4.58 and 8.76 wt.%) did not alter the surface properties, consistent with an organization of the fluorinated chains at the surface controlling their properties. X-ray photoelectron spectroscopy (XPS) measurements confirmed that the content of fluorine atoms on the surface was five times higher than the level expected from the bulk polymer.

Another example shows the influence of a structuring spacer, such as methylurea group, between the silicone backbone and the perfluorinated groups, on the surface properties. Furukawa and Kotera [54] prepared this novel type of fluorosilicone (co)polymers and studied their anti-stain properties in textile coating. Only qualitative results were given, noting the hydrophobicity and lipophobicity on scales

of 0–100 and 0–8, respectively. The best results were obtained for a homopolymer functionalized with an amido group, with values as high as 90 and 7, respectively. Such properties were ascribed to the alignment of the perfluorinated groups on the textile surface, aided by the H-bonding of the amido groups. This insight was confirmed by replacing the amido group with N-methylated ones, which resulted in a copolymer that did not behave better (hydrophilicity of 60 and lipophilicity of 2) than the copolymer without the structuring spacer (hydrophilicity of 80 and lipophilicity of 2).

5.3.2 *Surface Tension of Hybrid Fluorosilicones*

To our knowledge, few studies on the surface properties of hybrid silicones have been reported. For example, Bertolucci et al. [105] studied a copolymer with an interesting structure, between those of pendant and hybrid fluorosilicones (Structure 5.10). This polymeric backbone is an alternation of siloxy and carbosilane units, but the fluorinated groups are located on the side groups of the polymer, not inside the backbone.

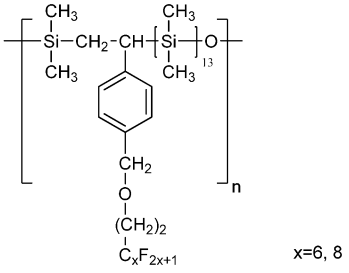

Structure 5.10

Table 5.2 summarizes different contact angles obtained with water and isopropanol as test liquids. The copolymer with the shortest perfluorinated chains showed smaller advancing contact angles, but also a lower hysteresis, than both PDMS and copolymer with $x = 8$ (Structure 5.10). A hindrance to the most preferable chain conformation at the surface was proposed, as shown previously for methylphenylsiloxane. Whereas isopropanol totally wets the PDMS, this hybrid silicone is capable of sustaining a solvent drop. These results correlate quite well with what has been observed previously for pendant fluorosilicones.

Takago et al. [106] studied the surface properties of "true" hybrid silicones, starting from building blocks such as those of Structure 5.3, where the perfluorinated chain R_F is either a perfluoroether, $CF(CF_3)OC_2F_4OCF(CF_3)_2$, or a perfluorinated alkane, C_6F_{12}. The Si-H functions incorporated at the end of the blocks reacted with a mixture of divinyl terminated PDMS and tetramethyltetravinylcyclotetrasiloxane (D_4^V) to form a solid rubber. The fluorosilicones with perfluoroether groups were found to exhibit higher hydrophobicity (111°) than the fluoroalkyl (107°) and

Table 5.2 Contact angles of water and isopropanol for polymers of Structure 5.10 [105]

	PDMS		$x = 6$		$x = 8$	
	θ_{adv} (°)	θ_{rec} (°)	θ_{adv} (°)	θ_{rec} (°)	θ_{adv} (°)	θ_{rec} (°)
Water	118	81	114	93	122	82
Isopropanol	0	0	–	–	64	44

PDMS-co-PMHS ones (103°). The contact angle of a silicone oil was similar for the two perfluorinated blocks (17°), whereas the PDMS was fully wetted. Inomata et al. [107] prepared filled vulcanizates using a mixture of the perfluorinated blocks given above and silica, $CaCO_3$ and $MgCO_3$. Contact angle with water did not change significantly (110° and 105°), whereas values for lubricating oil (ASTM n°3) were slightly lower than those found for hexadecane (53° and 51°).

5.3.3 Conclusions to Sect. 5.3

A definite improvement of anti-staining properties is obtained when fluoroalkyl groups are incorporated into the siloxane chains, if they are bigger than one CF_3 unit. The water repellency of these materials is less striking compared to that of PDMS, but still exists. The location of the fluorinated groups, randomly distributed either in the backbone or as a side group, seems to have little effect on the surface tension of these polymers. A further improvement was achieved by nanostructuring the surface, for instance by introducing a functional spacer between the silicone chain and the perfluorinated group, which can auto-associate *via* physical bonds to facilitate crystallization of the fluorinated groups. The extremely low interfacial tension values of PDMS and fluorinated copolymers, compared to a conventional perfluorinated oil ($C_{21}F_{44}$, $\gamma = 21.2$ mN m^{-1}), make these materials of great value for surface applications, such as in coatings or cosmetics.

5.4 Thermal Properties of Fluorosilicones

Silicone polymers exhibit lower glass temperatures than conventional organic polymers, making them the materials of choice for elastomer formulations. The inclusion of perfluorinated groups into, or pendant to, the silicone backbone stiffens the chains to an extent that must be controlled, as presented in this section. PDMS is also well known for its excellent thermal stability. However, under certain conditions (in acid and base media or at high temperatures), it depolymerizes by chain scission and production of cyclic oligomers. The chain ends greatly influence the thermal resistance of silicones and this phenomenon dramatically increases in the presence of silanol end groups (as recently reviewed [108]). In the last decades, hybrid silicones containing fluorinated groups have been developed to overcome this limitation.

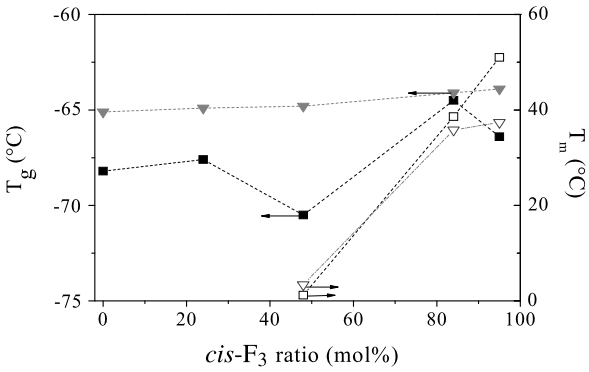

Fig. 5.6 Evolution of thermal transitions of PMTFPS oils and networks as a function of the *cis*-F_3 ratio [109, 110]: T_g PMTFPS (■), T_g cross-linked PMTFPS (▽), T_m PMTFPS (□), T_m cross-linked PMTFPS (▽)

5.4.1 Pendant Fluorosilicones

5.4.1.1 Thermal Transitions

Two main studies have reported on the effect of the conformation of a PMTFPS homopolymer [109, 110], synthesized by anionic ring-opening polymerization of the cis or trans-F_3 monomer, on its thermal transitions. The polymer was also cross-linked by hydrosilylation of Si-vinyl end-groups with tetrakis-(dimethylsiloxy)-silane in order to compare the T_g and the melting temperature T_m of the obtained materials with those of the intermediate polymer (Fig. 5.6). Crystallinity of the polymers and the corresponding networks increased as the amount of *cis*-D_3^F increased. Polymers and elastomers made from pure *trans*-F_3 or a small amount of *cis*-F_3 did not show any melting point. Depending on the amount of *cis*-F_3, the lengths of the isotactic segments were long enough for crystallization to occur in the polymer chains and the corresponding networks. The T_gs of cross-linked elastomers did not change much compared to those of the original linear polymers.

The length of the pendant perfluorinated group dramatically influences the thermal properties of pendant fluoro-homopolysiloxanes [94] (see Table 5.3). T_gs of these materials increase from −75 °C to −58 °C with increase in x of Structure 5.2 whereas for hydrogenated silicones T_gs increase from −123 °C to −92 °C. Perfluorinated pendant chains containing at least 8 carbon atoms lead to crystalline materials. For the allylic derivative [52] ($R = C_3H_6C_8F_{17}$) the melting temperature of the oligomer (Structure 5.2, $p = 25$; $m = 0$) rises to 20.5 °C.

5.4.1.2 Thermal Resistance

High temperature stability of these fluorinated homopolymers was monitored by thermogravimetric analysis (TGA) [94] and the results are shown in Fig. 5.7. In air and in inert atmosphere, the weight loss of four fluorinated polysiloxanes started between 200 and 300 °C, a little earlier than for PDMS which is stable to above

Table 5.3 Thermal transitions of fluorosilicones of Structure 5.2 ($m = 0$) as a function of the nature of pendant group R [94]

R	CH_3 (PDMS)	$C_2H_4C_6H_{13}$	$C_2H_4CF_3$	$C_2H_4C_4F_9$	$C_2H_4C_6F_{13}$	$C_2H_4C_8F_{17}$
T_g (°C)	−123	−92	−71	−75	−58	–[a]
T_c (°C)	−82	/	/	/	/	−0.3
T_m (°C)	−41	/	/	/	/	12.6

[a]Not reported

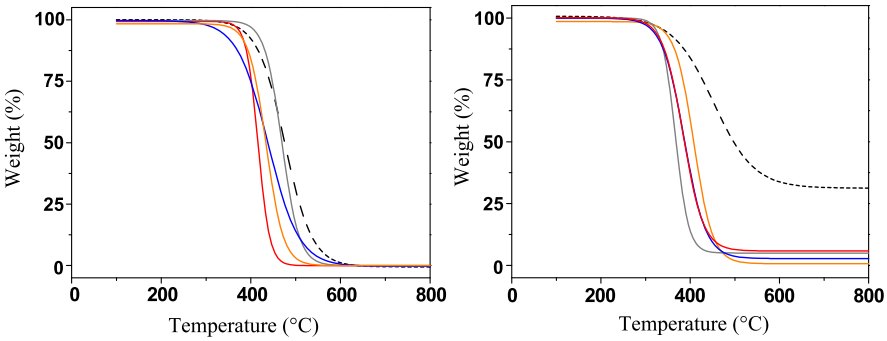

Fig. 5.7 Weight losses as a function of temperature, as measured by TGA [94] in nitrogen (*left*) and in air (*right*), of polydimethylsiloxane (PDMS, R = CH_3, *dash black*), polymethyl-3,3,3-trifluoropropylsiloxane (PMTFPS, R = $C_2H_4CF_3$, *red*), polynonafluorohexylmethylsiloxane (PNFHMS, R = $C_2H_4C_4F_9$, *gray*), polytridecafluorooctylmethylsiloxane (PTDFOMS, R = $C_2H_4C_6F_{13}$, *blue*), polyheptadecylfluorodecylmethylsiloxane (PHDFDMS, R = $C_2H_4C_8F_{17}$, *orange*)

300 °C. In air, the difference of thermal resistance between PDMS and fluorosilicones is more substantial. The amount of residues left over above 600 °C in air atmosphere decreases with increasing fluorine content.

5.4.2 Hybrid Fluorosilicones

5.4.2.1 Homopolymers

5.4.2.1.1 Thermal Transitions

Linear perfluorinated groups Different structural parameters influence the behavior of these materials at low temperatures, including the spacer and the nature of the pendant groups (Structure 5.3). The presence of a perfluorinated group of any type in the polymer skeleton noticeably leads to a loss of flexibility and to an increase of T_g, because of the stiffening effect of the fluoralkyl chains. For instance,

Table 5.4 Thermal transition temperatures of fluorosilicones with varying R and R' groups and the methylene spacer length y of Structure 5.3 ($n = 1$)

R	R′	M_n	y	T_g (°C)	T_c (°C)	T_m (°C)	Ref.
CH_3	C_6F_{12}	10,000	1	−53	−11	26	[111]
CH_3	C_6F_{12}	10,000	2	−40	−27	25	[111]
$C_2H_4CF_3$	C_6F_{12}	40,000	1	−28	/	/	[89]
$C_2H_4CF_3$	C_6F_{12}	14,000	2	−18	/	/	[89]
$C_2H_4C_4F_9$	C_6F_{12}	30,000	1	−42	/	/	[89]
$C_2H_4C_4F_9$	C_6F_{12}	12,000	2	−29	/	/	[89]
CH_3	C_6H_{12}	–[a]	1	−76	−31	−8	[90]
CH_3	C_6F_{12}	–[a]	1	−53	/	/	[90]

[a]Not given

Table 5.5 T_g values for hybrid fluorosilicones with fluorinated units of varying lengths in the skeleton [79, 90][a]

R′	T_g (°C)	Ref.
C_6F_{12}	−29	[90]
C_2F_4	−26	[79]
$(CF_2)_3O(CF_2)_2$	−39	[79]
$(CF_2)_2O(CF_2)_2O(CF_2)_2$	−40	[79]
$(CF_2)_2O(CF_2)_5O(CF_2)_2$	−52	[79]
$CF(CF_3)O(CF_2)_5O(CF_3)CF + (CF_2)_4(O(CF_3)CF)_2$	−47	[79]

[a]See Structure 5.3, with $x = 1$, $R = C_2H_4CF_3$, $n = 1$

Boutevin et al. [89, 90, 111] studied the influence of the number of CH_2 groups in the spacer between the silicon atom and the fluorinated internal chain (Table 5.4), and found that the longer the spacer, the higher the T_g. Moreover, compared to the equivalent fluorosilicone, the corresponding hydrogenated homopolymer exhibits a crystallization and a melting temperature. Boutevin et al. also demonstrated that the substitution of a CH_3 pendant group by a $C_2H_4CF_3$ group on the α position of the silicon atom results in a substantial increase of the T_g [10, 89, 111].

The influence of the length of the linear fluorinated group of a fluorosilicone homopolymer on the glass transition temperature is given in Table 5.5 [79, 89]. Riley et al. [79] obtained homopolymers that exhibit higher T_gs compared to those of the conventional fluorosilicones but lower than those prepared by Boutevin et al. [89]. This was probably due to the presence of the perfluorinated ether groups which enhance the flexibility of these structures. Concerning the homopolymers bearing $C_2H_4CF_3$ pendant groups and a linear fluoroalkyl hybrid group [89], it appears that the T_g does not vary substantially with hybrid group length.

Branched Perfluorinated Groups The same study also reported hybrid segments containing hexafluoropropylene (HFP) [88, 89] (-CF(CF_3)-CF_2-), with a CF_3

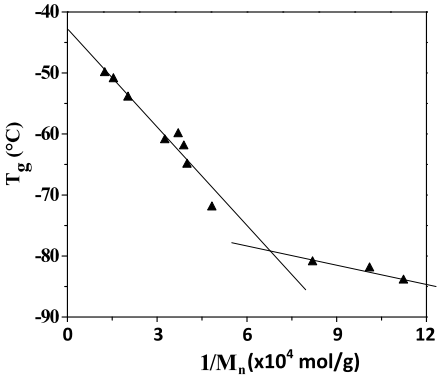

Fig. 5.8 Dependence of T_g on the inverse molecular weight of HFP hybrid fluorosilicones of Structure 5.11 [85]

pendant group. When R_F was HFP-C_4F_8-HFP in Structure 5.11, the T_gs were fairly similar to those obtained with linear perfluorinated hybrid homopolymers. Whatever the nature of the hybrid group, when the number of fluorine atoms was nine, the T_g values seemed to decrease. This tendency would be worth checking by measuring T_gs of fluorosilicones that contain at least ten fluorine atoms.

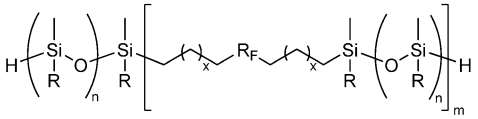

Structure 5.11

These authors also varied the molecular weight of these HFP-functionalized polymers [85, 112] and found that chain lengths correlate with T_g according to the Fox–Flory equation [113, 114] (5.2):

$$T_g = T_{g\infty} - \frac{A}{M_n} \tag{5.2}$$

where T_g is the glass temperature of the homopolymer, $T_{g\infty}$ the maximum T_g value that could be obtained at a theoretical infinite molecular weight, A an empirical constant for a given polymer and M_n, the number average molecular weight. Plotting the values of T_g as a function of $1/M_n$ showed that an increasing polymer chain length decreased the flexibility of the fluorosilicones as revealed by a strong increase in T_g (Fig. 5.8).

A patent similar to this study described the use of different types of branched hybrid group (Structure 5.11) [85] with obtained T_g values summarized in Table 5.6. These different studies all agreed on the fact that the addition of SiO units decreases the polymer T_g, providing an added flexibility to the polymer backbone. As shown previously, chain elongation leads to an increase of T_g due to the losses of chain flexibility and chain mobility.

Aromatic Core Fluorinated Hybrid More complex fluorinated hybrid units containing aromatic core groups (Structure 5.12) have been reported [76]. For the same

Table 5.6 T_g values of hybrid fluorosilicones [85][a]

R_F	R	n	m	T_g (°C)
HFP-C_4F_8-HFP	CH_3	2	4,2	−67
HFP-C_4F_8-HFP	CH_3	1	3,4	−62
HFP-C_4F_8-HFP	CH_3	1	6,7	−54
HFP-C_4F_8-HFP	CH_3	1	11	−50
$(VDF)_{4,6}$-$(C_3F_6)_2$-C_4F_8	CH_3	1	15	−39
HFP-C_4F_8-HFP	C_4F_9	1	12	−40
TFE-VDF-HFP	C_4F_9	1	13	−45

[a] n and m values from Structure 5.11; HFP = -CF(CF_3)CF_2-, VDF = -CF_2CH_2- and TFE = -CF_2CF_2-

number of SiO units (1 or 3), and against all expectations, T_g decreased with molecular weight (from −53 to −67 °C for $n = 1$ and from −48 to −59 °C for $n = 3$) whatever the number of CH_2 units, x. On the other hand, while keeping an equivalent molecular weight, a decrease of T_g was observed when the number of CH_2 units increased (from 3 to 10), which is the opposite to what was observed with the fluorosilicone hybrids that did not contain any aromatic core groups.

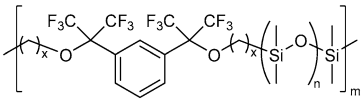

Structure 5.12

Rizzo and Harris [115] prepared fluorosilicones containing perfluorocyclobutane rings (PFCB) and studied both para (1,4)- and meta (1,2)-catenated (co)polymers. The incorporation of the rigid PFCB units into the siloxane backbone significantly enhanced thermal stability. The T_g of the para-catenated polymer shown in Structure 5.13 ($y = 0$) was strongly dependent on M_n up to approximately 50,000 (Fig. 5.9). The T_g of 27 °C appeared to be independent of M_n beyond this point. Meta-catenated polymer had a T_g of −12 °C for $M_n = 48{,}000$. This indicates that the meta-catenation reduced the T_g by nearly 40 °C. The addition of a SiO unit also decreases T_g. Even with relatively high T_gs for elastomers, these fluorosilicones seem to have the benefit of high thermal resistance (see Section 5.4.2.1.2).

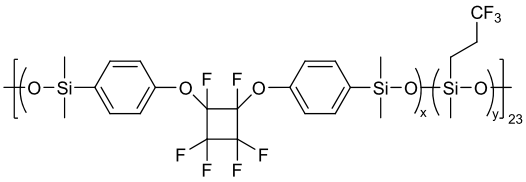

Structure 5.13

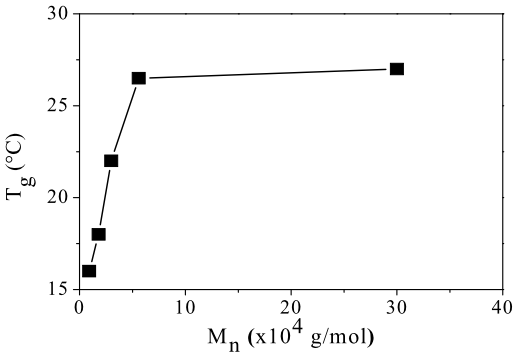

Fig. 5.9 Dependence of T_g of para-catenated perfluorocyclobutane-silicone copolymers of Structure 5.13 ($y = 0$) as a function of M_n [115]

5.4.2.1.2 Thermal Resistance

Linear and Branched Fluorinated Groups The influence of the nature of the fluorinated group R_F of Structure 5.11 on the properties of these hybrid polymers at high temperatures was assessed by TGA (see Fig. 5.10) [10, 79]. In air, whatever the R_F unit, PDMS exhibited slightly better thermal resistance than these hybrid silicones. The addition of in-chain fluoro groups in hybrid structures, however, improved silicone thermal stability in inert atmosphere.

Other factors such as the molecular weight of the polymer [112], the number of methylene groups in the spacers [111], the variation of fluorinated pendant group size, and different natures of R_F units were also correlated with the thermal resistance [88]. As mentioned above for T_g values, thermal resistance is extensively influenced by molecular weight variation [112] (in both air and N_2) (Fig. 5.11). The influence of chain ends is obvious for short chain polymers [116]. Degradation at 10 % weight loss occurs in inert atmosphere at around 160 °C for small oligomers while this temperature goes up to 360 °C for longer chain polymers (M_n above about 2,700). The degradation temperature corresponding to 50 % weight loss is noticeably less dependent on molecular weight

Furthermore, an increase of the methylene spacer number x results in a reduction of thermal stability of fluorosilicones in air [88], but this phenomenon is not observed in nitrogen atmosphere (see Table 5.7). In addition, a comparison of polymers with identical R pendant groups clearly revealed that hybrids containing linear R_F groups (from C_1 to C_6) are thermally more stable than those containing branched R_F groups.

Aromatic Core Fluorinated Groups A similar study was carried out on fluorosilicones containing both fluorinated and aromatic core units [76] (Structure 5.12) and the results obtained are summarized in Table 5.8. Unlike previous results and probably due to this particular backbone, an increasing SiO spacer length did not significantly affect the thermal properties. However, these materials were noticeably less resistant than both linear and branched hybrids and thus not amenable for uses requiring higher thermal resistance.

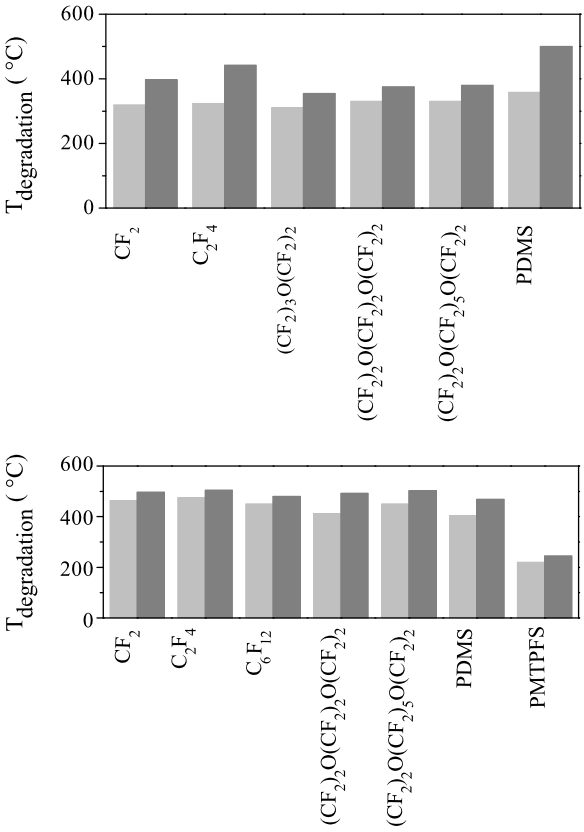

Fig. 5.10 Thermal resistances of hybrid fluorosilicones (Structure 5.11 with $R = C_2H_4CF_3$ and $n = 0$) [10, 79] in air (*upper figure*) and in nitrogen (*lower figure*): degradation temperatures for 10 % ($T_{10\,\%}$) (*light gray*) and 50 % ($T_{50\,\%}$) (*heavy gray*) weight loss

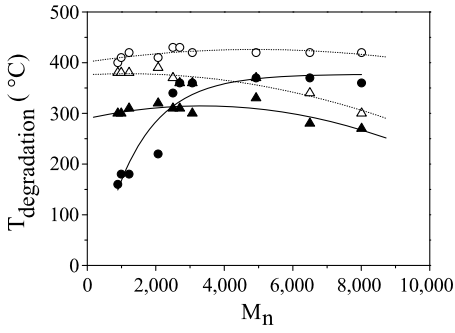

Fig. 5.11 Thermal resistances of hybrid silicones (Structure 5.10 with $R = CH_3$, R_F = HFP-C_4F_8-HFP, $n = 1$), TGA in air (▲) and in N_2 (●). $T_{degradation}$: temperature for 10 % weight loss (*full symbols*) and 50 % weight loss (*empty symbols*)

Due to the rigidity of PFCB units, fluorosilicones containing these rings [115] (see Structure 5.13) display very high thermal resistance. Temperatures for 5% weight loss are typically 385 ± 5 °C and 422 ± 17 °C in both air and nitrogen, independent of the nature of the polymer. These homopolymers are thermally more stable than PMTFPS (340 °C and 385 °C, respectively). To compete with this structure, Shoichet's group [117] synthesized similar hybrid fluorosilicones containing

Table 5.7 Thermal degradation of hybrid fluorosilicones (Structure 5.11) in inert atmosphere and in air as a function of the nature of the hybrid segment and the pendant group [89]

R_F	R	x[a]	M_n	T_{50} in air (°C)	T_{50} in N_2 (°C)
C_6F_{12}	CH_3	1	17,000	380	470
C_6F_{12}	CH_3	2	10,000	330	465
HFP/C_4F_8/HFP	CH_3	2	10,000	300	435
C_6F_{12}	$C_2H_4CF_3$	1	40,000	410	480
C_6F_{12}	$C_2H_4CF_3$	2	14,000	360	465
HFP/C_4F_8/HFP	$C_2H_4CF_3$	2	30,000	310	445
C_6F_{12}	$C_2H_4C_4F_9$	1	30,000	360	490
C_6F_{12}	$C_2H_4C_4F_9$	2	12,000	310	470
HFP/C_4F_8/HFP	$C_2H_4C_4F_9$	2	50,000	320	450
TFE/VDF/HFP	$C_2H_4C_4F_9$	2	9,000	315	420

[a] x value from Structure 5.11; HFP = -CF(CF_3)CF_2-, VDF = -CF_2CH_2-

Table 5.8 Thermal stability of polymers of Structure 5.12 [76]

N	1	1	3	3
X	3	10	3	10
M_n	2,700	5,900	4,900	5,100
T_{10} in air (°C)	249	314	317	307
T_{10} in N_2 (°C)	265	376	350	354

PFCB rings but with no oxygen between them and the aryl rings. Unfortunately, the thermal stability of these polymers was found to be lower than that of the polymers of Structure 5.13.

5.4.2.2 Copolymers

A variety of copolymers has been studied, particularly copolymers of hybrid fluorosilicones with siloxanes containing fluoroalkyl pendant groups. Various parameters can be changed in these copolymers such as the nature of both conventional fluorosilicones [89] and hybrid fluorosilicones [89, 118, 119] and the proportions of each monomer unit [76], to name a few.

5.4.2.2.1 T_g variations

T_gs of copolymers of Structure 5.14 (where s denotes spacer group) are summarized in Table 5.9 [89] according to the nature of pendant groups and the copolymer structure [89]. The presence of a branched perfluorinated pendant group (HFP) induces a slight decrease in T_g but this difference from linear perfluorinated pendant

Table 5.9 T_gs of copolymers of Structure 5.14 [89]

R	R′	R″	Structure	x/y	M_n	T_g (°C)
$C_2H_4CF_3$	CH_3	$C_2H_4C_6F_{13}$	Random	1.47	10,000	−40
$C_2H_4CF_3$	$C_2H_4CF_3$	$C_2H_4C_6F_{13}$	Random	1.54	8,900	−42
$C_2H_4CF_3$	CH_3	C_2H_4-HFP-C_4F_9[a]	Random	1.59	9,200	−44
$C_2H_4CF_3$	CH_3	C_2H_4-HFP-$CF(Cl)CF_3$[a]	Random	1.67	9,300	−46
$C_2H_4CF_3$	$C_2H_4CF_3$	CH_3	Alternating	1.00	22,000	−35
$C_2H_4CF_3$	$C_2H_4CF_3$	$C_2H_4C_6F_{13}$	Alternating	2.00	28,000	−31
$C_2H_4C_4F_9$	$C_2H_4C_4F_9$	$C_2H_4C_4F_9$	Alternating	0.50	11,000	−59

[a]HFP = -$CF(CF_3)CF_2$-

group seems not too meaningful. It clearly appears that increasing SiO unit number leads to lower T_g values, due to the gain of flexibility. The alternating copolymer $(BAB)_n$ of $x/y = 0.5$, which has the higher number of SiO units, has consequently the lowest T_g value.

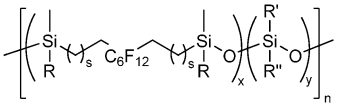

Structure 5.14

A hybrid silicone containing a fluoroalkyl fragment with an aromatic core unit was cross-linked by hydrolysis/condensation of ethoxysilane pendant groups disseminated along the polymer backbone (Structure 5.15) [76]. The cross-linking was achieved by curing in vacuum at 135 °C for 48 h. The dependence of T_gs on molecular weight is summarized in Fig. 5.12. As previously shown, an increased content of SiO units leads to a decrease in T_g values, while an increase in molecular weight does not have a net influence on the T_g. Whatever the molecular weight value, the T_g remains virtually constant, ranging between −60 and −45 °C.

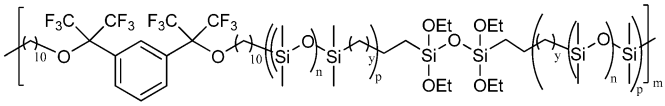

Structure 5.15

Kim and Riley [120] evaluated a hybrid fluorosilicone cross-linked with a tetrafunctional (T) silicone via hydrosilylation reaction (see Structures 5.16 and 5.17). The cross-linking did not influence the T_g values significantly, since these remained around −40 °C, compared to −30 °C for the linear precursor. The variation of the number of pendant fluorosilicone groups within the copolymer as well as the variation of the chain length were also considered. The reduction of the number of PMTFPS units resulted in an increase of T_g whatever the additive ratio (T). This

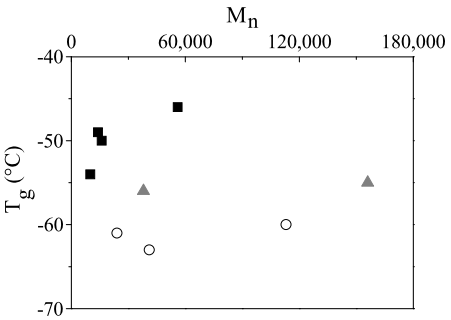

Fig. 5.12 Effect of molecular weight, number of SiO units and methylene spacer length on T_g of hybrid silicones of Structure 5.15, with $(n, y, p) = (1, 0, 1)$ (■), (3, 0, 1) (○) and (1, 1, 2) (▲) [76]

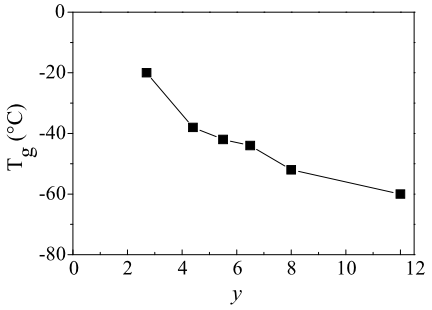

Fig. 5.13 Dependence of T_g on the number of SiO units, y, in polymers of Structure 5.13

was due to the reduction in the number of SiO units (when y decreased) which are responsible for chain flexibility and thus for T_g decrease.

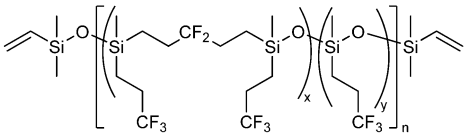

Structure 5.16

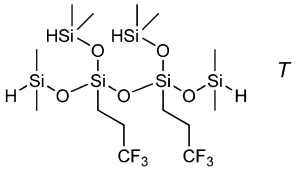

Structure 5.17

Copolymerization of fluorosilicones containing PFCB rings [115] with pure fluorosilicone as described in Structure 5.13 led to interesting results. The authors varied the y parameter, i.e. the number of SiO units, to assess its influence on thermal transitions. Results are plotted in Fig. 5.13. The T_gs of the para-catenated copolymers linearly decreased from −20 to −60 °C as the content of fluorinated units increased. A similar tendency was also observed with the meta-catenated copolymer.

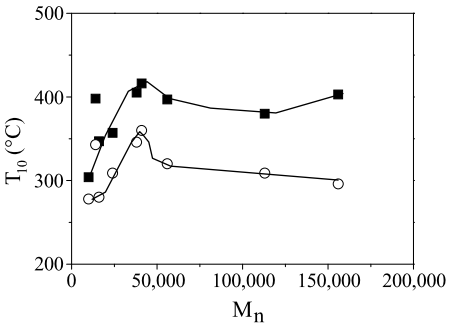

Fig. 5.14 Effect of M_n on temperature for 10 wt.% loss (T_{10}) of hybrid fluorosilicones of Structure 5.15 in air (*empty symbols*) and in nitrogen (*full symbols*) [89]

5.4.2.2.2 Thermal Resistance

The stability of fluorosilicones has been studied, varying different parameters such as the nature of pendant groups and the number of methylene spacers in the hybrid units in the backbone [88, 89]. Two studies have been reported: the first one on copolymers of random structure and the second one on alternating copolymers (see Structure 5.14). If these results are compared to those obtained for hybrid homopolymer, a loss of resistance to high temperature is observed since most polymers show a 50 wt.% loss at 470 ± 5 °C (homopolymer resists up to 490 °C) [88]. Alternating copolymers showed the same thermal resistances as that of the random and simple block copolymers. If the siloxane ("y" in Structure 5.14) is in majority ($y \gg x$), the thermal resistance is distinctly reduced to 330 °C. The influence of spacers can also be seen in addition to the influence of fluoroalkyl pendant or internal groups [118]. A sharp decrease in temperature for 50 % weight loss (from 475 °C to 330 °C) occurred when a significant quantity of fluorosilicone was introduced. The best thermal resistance was obtained for a copolymer made of hybrid block (expressed as "x" in Structure 5.14) and a PDMS fragment.

For fluorosilicones of Structure 5.15, both the spacer and the number of SiO units influenced the thermal decomposition temperatures. Results are summarized in Fig. 5.14. In comparison with the homopolymer, an improvement in thermal stability was clearly observed both in air and in nitrogen. An increase in molecular weight tends to significantly increase the thermal stability in nitrogen, and to a lesser extent in air. The addition of PDMS segments surprisingly improved the thermal resistance of the material. As expected, hydrogenated hybrid silicones had distinctly lower thermal resistance than fluorosilicones. For the polymer containing an organic hybrid fragment (C_6H_{12}, with $M_n = 40{,}000$), the degradation temperature for 10 % weight loss was 340 °C in air, compared to 380 °C for the corresponding fluorinated polymer (although with a lower M_n).

Copolymers containing PFCB groups [115] with varying number of SiO units (parameter y in Structure 5.13) were characterized by TGA. They were significantly more stable than the PMTFPS ($\Delta T \sim 50$ °C), but their thermal stability decreased slightly when the fluorosilicone content $x : y$ reached about 1 : 12. Nevertheless, the copolymer still underwent significantly less weight loss than a fluorosilicone when heated above 250 °C. The degradation would initiate at the chain ends and

proceed through cyclic formation until a perfluorocyclobutane unit is encountered, where it slows down or completely stops. Shoichet et al.'s poly(PFCB-*co*-PDMS) copolymers [117] were again less thermostable than the ones described above.

5.4.3 Conclusions to Sect. 5.4

All fluorinated polymers reviewed in this section exhibit higher T_gs than PDMS, with a gap of about +70 °C. On the other hand, their thermal resistance is similar to that of PDMS, or even better, and distinctly superior to those of conventional fluorosilicones. Only the hybrids containing aromatic groups do not follow this rule and behave similarly to the conventional fluorosilicones. The analysis of hybrid-*co*-conventional fluorosilicone copolymers indicated that the increase in conventional fluorosilicone level results in decreasing T_g values. The highest thermal resistance is obtained from poly(PDMS-*co*-fluorosilicone) hybrid copolymers.

5.5 Swelling Properties of Fluorosilicones

In high tech applications including aeronautics, elastomers should not be swollen by either polar or apolar oils and solvents. Fluorine and silicon atoms bring to a given polymer both hydrophobicity and lipophobicity and often provide solutions for such applications sought by the end-user. This section describes the solvent resistance as a function of the chemical structure of fluorosilicone polymers. The definitions of solvency, solubility parameters, Hildebrand parameters and description of PDMS swelling are given in Appendix B. In this section, we only focus on solubility parameters of fluorosilicone networks, and not on those of fluid, noncross-linked materials.

5.5.1 Pendant Fluorosilicones

5.5.1.1 Homopolymer Networks

Figure 5.15 shows the volume swell as a function of solvent solubility parameters for PMTFPS. It can be seen that polar solvents show a higher swelling tendency compared to non-polar solvents of identical solubility parameter. This fact arises from the polarity of the pendant $C_2H_4CF_3$ group which generates dipolar interactions with solvents such as ethers, esters and ketones. Gomez et al. [121] demonstrated that the polar grafted group brings about an increase in the solubility parameter through the δ_p component ($\delta_{\text{PMTFPS}} = 9.6\ \text{cal}^{1/2}\,\text{cm}^{-3/2}$). Unlike PDMS, PMTFPS is expected to display higher interaction force, and higher chain rigidity because of more restricted rotations around the siloxane backbone. A complementary study

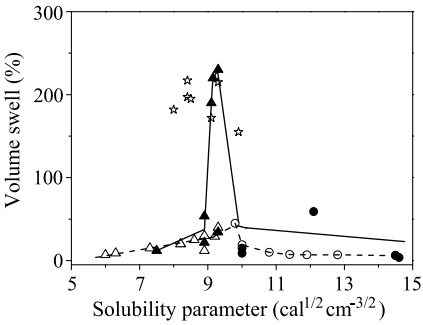

Fig. 5.15 PMTFPS volume swell as a function of solubility parameters of solvents with weak (△), strong (○), and moderate (☆) electrostatic interactions (see Appendix B for details). Values measured at 22 °C after 48 h exposure (*empty symbols*) and at 23 °C after 170 h (*full symbols*) for weak and strong solvents

Table 5.10 PMTFPS swelling resistance to oils, fuels, acids and base[a]

Solvent	Exposure time (days)	Exposure temp. (°C)	Volume swell (%)
ASTM n°1, oil	3	150	0
Crude 7 API, oil	14	135	5
JP-4, fuel	3	25	10
ASTM, fuel B	3	65	10
HCl (10 %)	7	25	0
HNO_3 (70 %)	7	25	5
NaOH (50 %)	7	25	5

[a]ASTM n°1 = heavy paraffinic distillates + solvent refined residual oils (petroleum); ASTM Fuel B = isooctane, JP-4 = aliphatic + aromatic hydrocarbons. Crude 7 API = crude oil

was carried out varying the exposure time [122] but only in solvents with weak and strong electrostatic interactions (see Fig. 5.15, full symbols). It appears that a long exposure time leads to an exacerbated swelling of PMTFPS with superior contributions of δ_d and δ_H.

Another study was performed by mixing PMTFPS with commercially available oils to check its swelling resistance [91]. Results are summarized in Table 5.10. It was found that PMTFPS is more sensitive to aromatic than aliphatic hydrocarbon solvents, while its swelling in aggressive acid and basic media is quite similar and low.

5.5.1.2 Cross-linked Copolymer Gels and Elastomers

The influence of cross-linking density on the volume swell of different PMTFPS copolymers has been studied [123] varying the content of methylvinylsiloxy units in the starting polymer (Fig. 5.16). As expected, an increase in the cross-linking density resulted in a decrease in the volume swell. This study also clearly emphasized the benefit conferred by the fluorinated group: compared to the volume swell of PDMS, it was found that PDMS with 50 mol. % of vinyl units had the same

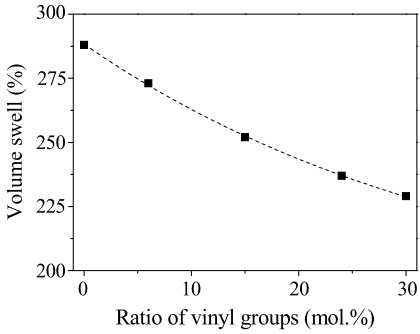

Fig. 5.16 Volume swell in ethyl acetate of PMTFPS as a function of the ratio of vinyl groups in the polymer

volume swell as the PMTFPS with only 25 mol.% vinyl units (i.e. volume swell in ethyl acetate of 235 vol.%).

PDMS-*co*-PMTFPS copolymers were synthesized varying both the fluorosilicone content and the nature of the chain ends (containing fluorinated side groups or not) and tested in the presence of different additives (neutral PDMS oil, phenyl oil or paraffin) [124]. In the presence of Fuel B, the increase in volume swell was inversely proportional to the fluorosilicone content of the copolymer. The same trend was observed in the presence of mineral oil [124] and without additives, even if the volume swellings were lower. The addition of phenyl groups increased the volume swell compared to the addition of PDMS. Long alkanes, such as paraffin, slightly increased the swelling, but in a less remarkable way than the fluorine groups. An industrial study was also carried out on PMTFPS/PDMS blend [125] with a binary filler system composed of potassium aluminosilicate (muscovite) and fumed silica. Two formulations were tested for the volume swell in a 50 : 50 mixture of toluene and 2,2,5-trimethylpentane (75 vol.%) and in methanol (25 vol.%). The laminar structure of the structuring filler, such as muscovite, helps to create a uniform pore structure in the cured matrix which leads to lower permeation of liquids and a slight decrease of the volume swell (from 34 vol.% to 27.3 vol.% and from 70 vol.% to 64 vol.%, respectively).

5.5.2 Hybrid Fluorosilicones

5.5.2.1 Homopolymer Networks

Although various examples of hybrid fluorosilicone homopolymers can be found in the literature, we focus here on four hybrid fluorosilicone polymers which illustrate a general trend. Yerrick and Beck [126] reported a study of fluorosilicones containing PFCB rings (Structure 5.13, $y = 1$ and 8) in different solvents, to vary the range of solubility parameters (Fig. 5.17).

This study revealed two interesting features. First, the PFCB groups in the polymer did not shield the hydrocarbon portions of the network since Fig. 5.17 shows that the maxima of these curves are quite large and in the low range of solubility

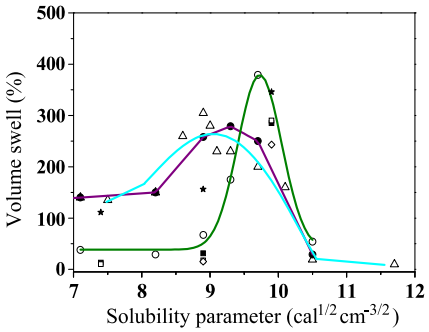

Fig. 5.17 Volume swells of the following polymers in different solvents after 22 h exposure to ambient temperature: homopolymer with PCFB of Structure 5.13 (△, *blue curve*), copolymer of PCFB with PMTFPS ($y = 1$) (△), with $y = 8$ (○); Kim's polymers of Structure 5.18: $R = CH_3$, $R' = C_2H_4CF_3$ (★), $R = R' = CH_3$ (■), $R = R' = C_2H_4CF_3$ (◇) and PMTFPS (□)

parameters. Second, volume swells tend to lower while decreasing the solubility parameter, but do not come back to nil values. This fluorosilicone presents a maximum volume swell for a solubility parameter of 8.9 $cal^{1/2}\,cm^{-3/2}$ (Fig. 5.17, blue curve), which matches that of toluene. Notice that this material showed a very good resistance to high solubility parameter solvents.

A similar study was carried out by Pierce and Kim [10] on hybrid fluorosilicone polymers of Structure 5.18 but with fewer solvents, namely acetone ($\delta = 9.9$ $cal^{1/2}\,cm^{-3/2}$), heptane ($\delta = 7.4$ $cal^{1/2}\,cm^{-3/2}$) and toluene ($\delta = 8.9$ $cal^{1/2}\,cm^{-3/2}$).

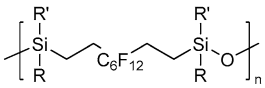

(R/R' : CH_3/CH_3, $CH_3/C_2H_4CF_3$ and $C_2H_4CF_3/C_2H_4CF_3$)

Structure 5.18

The polymer without fluorinated pendant groups and just a hybrid segment exhibited poor solvent resistance whereas the polymer with $C_2H_4CF_3/C_2H_4CF_3$ pendant groups had a similar behavior to PMTFPS (see Fig. 5.17). Comparing these two polymers, it seems that the hybrid segment did not have any substantial influence on the volume swell. The observation that two trifluoropropyl groups on the polymer skeleton were needed to significantly decrease swelling properties agrees with the PCFB-containing fluorosilicone behavior, where pendant trifluoromethyl groups [121] allowed less than 20 % volume swell in hydrocarbon solvents [91].

Complementary measurements [10] were performed to study the effect of the length of the hybrid segment in the polymers of Structure 5.18. For the fluorosilicone without pendant fluorinated groups, volume swell is shown as a function of the length of the perfluorinated in-chain group in three different solvents (acetone, toluene and heptane) in Fig. 5.18. Clearly, these polymers showed pronounced affinity to acetone, since in this solvent the volume swells were in all cases higher than

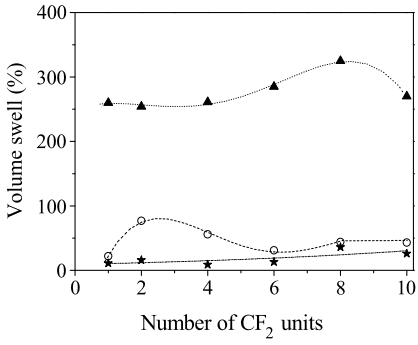

Fig. 5.18 Volume swells as a function of the number of CF_2 groups in polymers of Structure 5.18 in acetone (▲), toluene (○), and heptane (★) [10]

250 vol.%. Nevertheless, it can also be noted that volume swells are not so much connected to the fluorine content since only minor variations with the increase in the number of CF_2 groups were observed.

5.5.2.2 Copolymer Networks and Materials

Yerrick and Beck [126] copolymerized the PFCB hybrid with PMTFPS to form a new fluorosilicone shown in Structure 5.13. According to Fig. 5.17, when $y = 1$, the maximum volume swell was obtained for a solubility parameter of 9.3 $cal^{1/2}\,cm^{-3/2}$ (which corresponds to chloroform). Except with chlorinated solvents, this copolymer displays a slightly better solvent resistance relative to the corresponding hybrid homopolymer. Increasing the number of MTFPS units enhanced the solvent resistance. For $y = 8$, the copolymer showed a maximum swelling for $\delta = 9.7$ $cal^{1/2}\,cm^{-3/2}$ which was close to that of the pure PMTFPS ($\delta = 9.6$ $cal^{1/2}\,cm^{-3/2}$) [125] although the volume swell was higher for the fluorosilicone containing PFCB groups. Moreover, all other values were distinctly lower than those of the homopolymer and the maximum peak was narrower than that of the homopolymer.

In Fig. 5.19 volume swells of these hybrid fluorosilicone copolymers are plotted as a function of their fluorosilicone contents in order to understand the minimum quantity of PMTFPS necessary to obtain satisfactory hydrocarbon resistance. It appears that approximately 75 wt.% of fluorosilicone (fluorine content = 33.3 mol.%) is required to match the solvent resistance of PMTFPS.

Pierce and Kim [10] performed the copolymerization of the polymer of Structure 5.18 (R=CH_3, R′=$C_2H_4CF_3$) with PMTFPS to study mechanical and thermal properties. They observed a volume swell close to that of the homopolymer with R=R′=$C_2H_4CF_3$ in acetone and a significant swelling resistance in heptane. Increasing the content of trifluoropropyl groups increased the polarity of the polymer chains and the volume swells increased in polar solvents and decreased in non-polar ones.

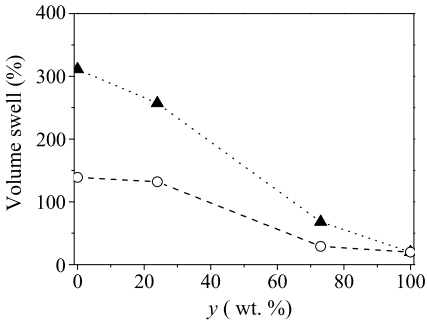

Fig. 5.19 Volume swells in toluene (▲), and isooctane (○) of the copolymer of Structure 5.13 as a function of the MTFPS content (y expressed here as wt.%) [126]

As for applications of such hybrid fluorosilicones, membranes designed for rechargeable lithium-ion batteries were produced from three types of unsaturated hybrid polyfluorosilicone precursor (see Structures 5.19, 5.20 and 5.21) [127]. Polymer 5.19 is composed of branched perfluorinated groups, whereas Polymers 5.20 and 5.21 differ in the length of the linear fluorinated groups.

$$ViSiMe_2O\text{-}[(SiMe_2C_3H_6\text{-}(C_2H_2F_2)_{2,3}CF_2CF(CF_3)C_5F_{10}CF(CF_3)(C_2H_2F_2)_{2,3}\text{-}C_3H_6SiMe_2O)_{50}\text{-}(SiMeViO)]_n\text{-}SiMe_2Vi$$

Structure 5.19

$$Vi\ SiMe_2O\text{-}\{(SiMe_2C_2H_4C_6F_{12}C_2H_4SiMe_2O)_{6,5}\text{-}(SiMeViO)_{2,2}\text{-}(SiMe_2O)_2SiMe_2\text{-}[C_2H_4C_6F_{12}C_2H_4(SiMe_2O)_2Si]_{3,5}\text{-}O\}_n\text{-}SiMe_2Vi$$

Structure 5.20

$$ViSiMe_2O\,[SiMe_2C_2H_4C_8F_{16}C_2H_4SiMe_2O)_{4,84}(SiMeViO)_{2,2}(SiMe_2C_2H_4C_6F_{12}C_2H_4SiMe_2O)_{2,2}(SiMe_2O)_2SiMe_2(C_2H_4C_6F_{12}C_2H_4SiMe_2OSi)_{3,5}]_nSiMe_2Vi$$

Structure 5.21

Cross-linked networks were prepared from these precursors using three different concentrations of Varox® catalyst (2,5-bis(*tert*-butylperoxy)-2.5-dimethyl-hexane): 0.3, 0.45 and 0.6 wt.% in order to obtain different cross-linking densities. The resulting membranes were then exposed to swelling in three different categories of electro-conductive solvents: those with a weak dielectric constant (diethyl carbonate (DEC) and dimethyl carbonate (DMC)), a strong dielectric constant (propylene carbonate (PC) and γ-butyrolactone (γBL)), and a very strong dielectric constant (ethylene carbonate (EC)). As shown in Fig. 5.20, in mixtures with a high content of strong dielectric constant solvent (and thus a higher solubility parameter) the membranes showed a decrease in the volume swell. This is consistent with the fact that fluorosilicones of low polarity have a low affinity towards high polarity solvents used for lithium-ion batteries. The authors also studied the swelling ability of these hybrid fluorosilicones by varying the EC/DEC mixture ratio (Fig. 5.20). They found that an increase of EC resulted in a strong decrease of the volume swell at 70 °C, while this did not happen at 20 °C, indicating a substantial influence of temperature on this important behavior.

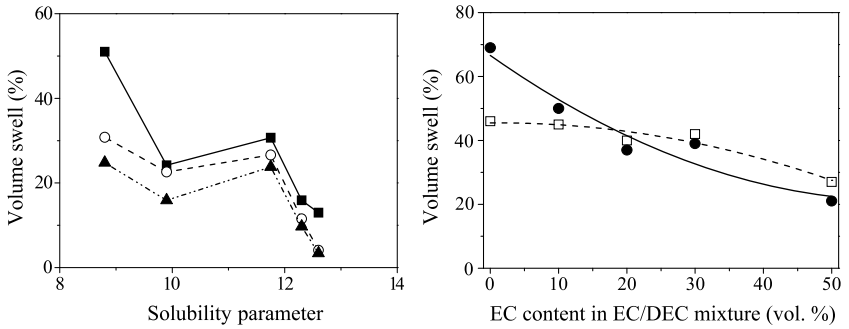

Fig. 5.20 (*Left*) Volume swells of membranes based on Polymer 5.19 (■), 5.20 (○) and 5.21 (▲), cross-linked with 0.6 wt.% catalyst after 24 h at 20 °C in selected 1M anhydrous electrolytic solutions. (*Right*) Volume swells of some of these membranes as a function of EC content in EC/DEC mixtures at two temperatures: 20 (□) and 70 °C (●) [127]

5.5.3 Conclusions to Sect. 5.5

In any kind of solvent, fluorosilicones show lower swelling than PDMS. Their most unfavorable solvents are polar ones. However, their solvent resistance can be improved by incorporating fillers into the cross-linked formulations, by increasing the loading content of the cross-linking groups, such as methylvinylsiloxy, or by increasing the content of fluorinated pendant groups. The comparison of conventional and hybrid fluorosilicones shows that the lowest swelling rates are obtained for materials composed of hybrid fluorosilicones bearing fluorinated pendant groups on their backbone, or copolymerized with conventional fluorosilicones.

5.6 Mechanical Properties of Fluorosilicones

Many techniques are available to determine various mechanical properties of fluorosilicone elastomers. Among these, the literature particularly focuses on hardness, tear and tensile strengths, elongation modulus and percent elongation (measured at defined time and temperature). The formulation, the cross-linking method and ageing also drastically affect the mechanical properties of materials.

5.6.1 Pendant Fluorosilicones

5.6.1.1 Homopolymers

5.6.1.1.1 Influence of Cross-linking Density

Formulations of vulcanizable elastomers usually contain PMTFPS, fumed silica, other fillers and/or additives and cross-linking agents. Each of these components

Table 5.11 Mechanical properties of PMTFPS elastomers [128][a]

	Hardness (Shore A)	Tensile strength (MPa)	Elongation (%)	Tear strength (kN m^{-1})	Compression set (%)
M_n^H press-cured[b]	34	8.09	346	9.86	24.2
M_n^H post-cured[c]	39	9.93	347	13.55	21.0
M_n^L press-cured[b]	59	5.52	83	4.75	11.1
M_n^L post-cured[c]	62	5.35	79	4.93	9.4

[a]H and L refer to high and low molecular weight polymers, respectively (see text for details). Formulation: 100 wt.% hydroxyl endblocked polytrifluoropropyl(methyl)siloxane + $0.76^L/2.2^H$ wt.% methylvinyldi(N-methylacetamido)silane + 2 wt.% dimethylvinylsiloxy endblocked copolymers (78 mol.% dimethylsiloxane units + 22 mol.% methylvinylsiloxane units) + 13 wt.% hydroxyl endblocked methyl(trifluoropropyl)polysiloxane + 33 wt.% fumed silica (250 m^2g^{-1}) + 1 wt.% (50 wt.% ceric hydrate dispersed in a polydimethylsiloxane gum) + 1 wt.% of 50 wt.% 2,5-bis(*tert*-butylperoxy)-2,5-dimethylhexane

[b]Press-cured: 10 min at 171 °C

[c]Post-cured: 2 h at 200 °C

may have a noticeable influence on the mechanical properties of the final materials. In one study showing the effect of cross-linking density [128], the authors used two PMTFPS polymers with M_n of ~31,000 and ~12,500, respectively. Those two were condensed with methylvinyldi(N-methylacetamido)silane to lengthen the chains and to introduce vinyl groups along the polymer chain for subsequent cross-linking (0.76 and 2.2 wt.% for the high and low molecular weight polymers, respectively). The resulting polymers had number average molecular weights M_n of 1.55×10^6 and 5.4×10^5, respectively. The mechanical properties of the cross-linked materials are summarized in Table 5.11. The elastomer with the higher content of cross-linking sites (2.2 wt.% chain extender) showed higher hardness but poorer elastic properties (tensile strength, elongation, tear strength and compression values). This was expected since elastomeric properties generally require long polymer chains and low cross-linking density.

Singh et al. [129] characterized materials obtained either from room temperature vulcanization (RTV) formulation or at high temperature via a peroxide cure (2,5-bis(*tert*-butylperoxy)-2,5-dimethylhexane). A hydroxy-terminated PMTFPS with a viscosity of 40 cP was mixed with treated fumed silica (9.2 wt.%), antioxidant Fe_2O_3 (5.7 wt.%) and a cross-linking system consisting of an oligomeric fluorosilicone functionalized with alkoxy end-groups (8 wt.%) and dibutyl tin diacetate (0.5 wt.%). After curing, the obtained material showed inferior properties to the formulation obtained by peroxide cures. The elongation was only 162 %, the tensile strength was 2.01 MPa and the modulus at 100 % strain was 0.37 MPa.

Table 5.12 Mechanical properties of PMTFPS vulcanizates as a function of different silica treatments [129, 130]

Silica treatment[a]	Viscosity (cSt)	Hardness (Shore A)	Tensile Strength (MPa)	Elongation (%)	Modulus (MPa)[b]	Hysteresis loss (%)[b]
I	500	33	2.45	183	0.48	9.1
II	200	34	0.66	85	0.49	12.8
III	1300	49	2.00	136	0.94	42.7

[a]I: Base: 100 wt.% hydroxy-terminated PMTFPS + 0.98 wt.% water + 1.52 wt.% hexamethyldisilazane + 13.70 wt.% amorphous silica 400 $m^2\ g^{-1}$, mixed for 1 h at 160 °C. Then 100 wt.% of this PMTFPS base was mixed with 72.0 wt.% dry methylethylketone and 22.1 wt.% vinyltris(methylethylketoxime)silane
II: 6.4 wt.% amorphous silica 400 $m^2\ g^{-1}$ dispersed in toluene + 0.46 wt.% water + 0.71 wt.% hexamethyldisilazane, heated for 3 h at 23 °C. Toluene and residual ammonia were evaporated (air drying for 16 h and heated at 150 °C for 3 h) and then added to formulation containing 100 wt.% hydroxy-terminated PMTFPS + 39.5 wt.% methylethylketone and 12 wt.% dry methylethylketone
III: Pre-treatment of the silica: 0.46 wt.% water + 0.71 wt.% hexamethyldisilazane+: 6.4 wt.% amorphous silica 400 $m^2\ g^{-1}$, combined for 3 h, residual ammonia were removed (heated at 150 °C for 16h), and then the pretreated silica was directly introduced into 46.7 wt.% hydroxy-terminated PMTFPS and then added to formulation containing 100 wt.% hydroxy-terminated PMTFPS + 39.5 wt.% methylethylketone and 12 wt.% dry methylethylketone

[b]At 50 % extension

5.6.1.1.2 Effect of Fillers

Silica used to fill siloxane elastomers often undergoes different surface treatments to make it readily dispersible within the silicone matrix [130, 131]. The surface of the silica is modified either by a pre-treatment or by an in situ treatment, both with hexamethyldisilazane (HMDS). A cross-linked product based on PMTFPS displayed different properties depending on the silica treatment (see Table 5.12). The hysteresis loss of a cured elastomer is an expression of its tendency to retain resiliency after repeated stressing. Compared to the formulation containing silica treated in situ, the formulation containing pre-treated silica had higher hardness, elasticity and hysteresis loss.

Maxson et al. [131] evaluated the effect of filler on the mechanical properties of vulcanizates based on PMTFPS mixed with treated fumed silica and metallic oxides such as Fe_2O_3 or TiO_2. They used two different moisture cure systems, one with a mixture of methyltriacetoxysilane/ethyltriacetoxysilane and the other with vinyltris(methylethyl-ketoxime) (Table 5.13). They noted that Fe_2O_3, which is a well-known antioxidant used in silicone formulations, generally improved the mechanical properties better than TiO_2. An exception was the hardness, which was better with TiO_2.

5.6.1.1.3 Mechanical Properties as a Function of Temperature

Pierce and Kim [10] studied the influence of temperature on the properties of a PMTFPS elastomer ($M_w \sim 6{,}000$). From measurements of tensile strength, elonga-

Table 5.13 Mechanical properties of vulcanizates filled with Fe_2O_3 and TiO_2 [131][a]

	Hardness (Shore A)	Tensile strength (MPa)	Elongation (%)	Tear strength (kN m^{-1})
Acetoxy[b]/Fe_2O_3	35	7.8	402	27.5
Acetoxy[b]/TiO_2	38	6.2	342	19.8
Oxime[c]/Fe_2O_3	42	7.2	320	19.6
Oxime[c]/TiO_2	37	5.1	312	15.4

[a]Formulation: (base: 100 wt.% hydroxyl-endblocked trifluoropropylmethylpolysiloxane + 1.8 wt.% water + 11.5 wt.% di(trifluoropropyl)tetramethyldisilazane + 25 wt.% fumed silica) + 7.4 wt.% Fe_2O_3 or 10 wt.% TiO_2

[b]100 wt.% Base + 4.6 wt.% mixture (50 wt.% methyltriacetoxysilane + 50 wt.% ethyltriacetoxysilane) + 0.35 wt.% trimethoxysilane + 0.025 wt.% stannane dimethyl bis(1-oxoneodecyl)oxy (Formez UL-28)

[c]100 wt.% Base + 5 wt.% vinyltris(methoxyethylketoxime)

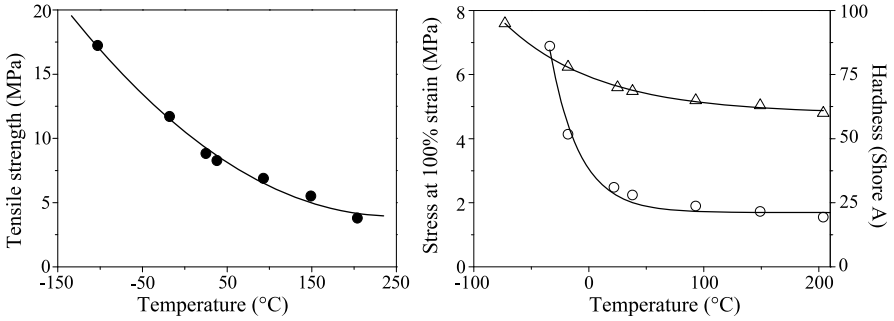

Fig. 5.21 Tensile strengths (●) (*left*) and hardnesses (○) and strains at 100 % elongation (△) (*right*) of PMTFPS as functions of temperature [10] (formulation as given in the reference: PMTFPS ($M_w \sim 6{,}000$) + fumed silica + peroxide vulcanizing agent and additives for heat stability (Fe_2O_3))

tion modulus and hardness at different temperatures (Fig. 5.21), they found that the material proportionally lost tensile strength with increasing temperature. Between −80 °C and −40 °C, both hardness and modulus at 100 % elongation decreased with increasing temperature.

5.6.1.1.4 Effect of Aging

In the same study, Pearce and Kim [10] also examined the aging of PMTFPS for a fixed period of time at different temperatures (Table 5.14). The increase in temperature induced further cross-linking which resulted in both elongation and tear strength decreases. Conversely, material hardness increased with temperature.

Table 5.14 Mechanical properties of PMTFPS elastomer after thermal aging for 70 h [10][a]

Aging	Hardness (Shore A)	Tensile strength (MPa)	Elongation (%)	Tear strength (kN m^{-1})
None	52	8.6	500	46.6
100 °C	53	8.7	470	45.8
150 °C	53	8.7	450	37.0
170 °C	54	7.6	400	30.8

[a]Formulation as reported in [10]: PMTFPS ($M_w \sim 6{,}000$) + fumed silica + peroxide vulcanizing agent and additives for heat stability (Fe_2O_3)

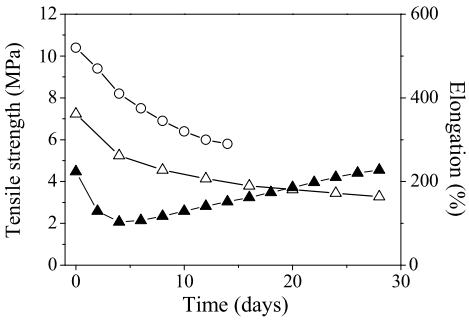

Fig. 5.22 Effect of aging of PMTFPS based sealant at 260 °C as a function of time on tensile strength (△), elongation (○) and (▲) tensile strength measured in the presence of JP-4 at 260 °C [10] (formulation as given in the reference: PMTFPS ($M_w \sim 6{,}000$) + fumed silica + peroxide vulcanizing agent and additives for heat stability (Fe_2O_3))

The authors also carried out a complementary study on PMTFPS varying either temperature or exposure time at high temperature (Fig. 5.22). While the tensile strength decreased for about ten days and then stabilized to become relatively unchanged, the elasticity progressively decreased between 0 and 5 days. The aging of this PMTFPS material was also studied in solvent (JP-4 type fuel) to determine its solvent resistance. Immersion in JP-4 drastically modified the tensile strength which passed through a minimum after five days and nearly recovered its initial value after 28 days.

5.6.1.2 Copolymers

5.6.1.2.1 Effect of the Type and Content of the Fluorinated Group

Evans [123] studied the effect of the content of fluorinated units in the PDMS-*co*-PMTFPS copolymers (50 mol.% ≤ PMTFPS ≤ 66 mol.%), after aging 4–6 h at 135–145 °C, on their mechanical properties. The increase of PMTFPS content in the copolymer, particularly worsened the compression set (increasing from 12.7 to 25 %) and the hardness (decreasing from 57 to 51 Shore A), whereas the other mechanical properties remained unchanged (tear strength ~18.7 kN m^{-1}, tensile strength 7.3 MPa, elongation ~430 %). Furukawa et al. [19] compared materials

Table 5.15 Comparison of mechanical properties of materials prepared from a commercially available PMTFPS and a PMTFPS-*co*-PNFHMS copolymer [19][a]

	Hardness (Shore A)	Tensile strength (MPa)	Elongation (%)	Compression set (%)
PMTFPS	72	8.0	310	20
PMTFPS-co-PNFHMS	45	8.9	350	25

[a]100 wt.% PMTFPS (or PMTFPS-*co*-PNFHMS) formulated with 33 wt.% Silica (Aerosil 300, BET Surface areas of 300 $m^2\,g^{-1}$) + 1.5 wt.% ceric hydroxide + 1 wt.% (2,5-dimethyl-2,5-di(*t*-butylperoxy)hexane. The composition was press-cured for 10 min at 170 °C and post-cured for 4 h at 200 °C

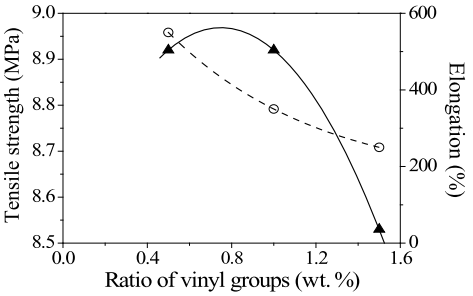

Fig. 5.23 Effect of vinyl group content on elongation (○) and tensile strength (▲) of elastomers made from PMTFS-*co*-PNFHMS copolymers described in the text (formulation: 100 wt.% PMTFPS (or PMTFPS-co-PNFHMS) with 33 wt.% Silica (Aerosil 300, BET Surface areas of 300 $m^2\,g^{-1}$) + 1.5 wt.% ceric hydroxide + 1 wt.% (2,5-dimethyl-2,5-di(t-butylperoxy)hexane. The composition was press-cured for 10 min at 170 °C and post-cured for 4 h at 200 °C)

made of a PMTFPS-*co*-PNFHMS (polynonafluorohexylmethyl-siloxane) copolymer and PMTFPS homopolymer. As shown in Table 5.15, the copolymer exhibited improved elongation and tensile strength properties.

5.6.1.2.2 Effect of Cross-linker

Furukawa et al. [19] also found that the content of vinyl groups in (PMTFPS-co-PNFHMS) copolymers (Fig. 5.23) did not immediately influence the tensile strength whereas elongation decreased progressively. Vinyl group content higher than 1 mol.% led, however, to a dramatic deterioration of mechanical properties. Nevertheless, this value is superior to the corresponding one for PDMS (0.1 mol.%) or for PMTFPS homopolymer (0.5 mol.%).

Chaffee [128] analyzed the effect of vinyl units incorporated into the formulation through a chain extender. They studied a complex blend containing PMTFPS-*co*-PMVS, PDMS-*co*-PMVS, PMTFPS, fumed silica, cross-linking agent and peroxide, and obtained results summarized in Fig. 5.24. Hardness and tensile strength showed

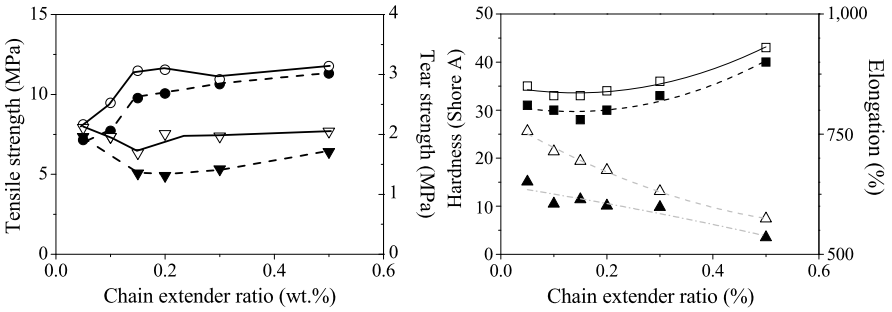

Fig. 5.24 Effect of the chain extender content (wt.%) on the properties of vulcanizates made from PMTFPS-*co*-PMVS, PDMS-*co*-PMVS, PMTFPS, fumed silica, filler and peroxide: hardness (□), elongation (△), tensile strength (○) tear strength (▽), after the first cure at 171 °C for 10 min (*full symbols*) and after a post-cure at 200 °C for 2 h (*empty symbols*) [128] (formulation: 100 wt.% hydroxyl endblocked polydiorganosiloxane (99.4 mol.% 3,3,3-trifluoropropylmethylsiloxane units + 0.6 mol.% methylvinylsiloxane units) + chain extender methylvinyldi(N-methylacetamido)silane + 3 wt.% dimethylvinylsiloxy endblocked copolymer (78 mol.% dimethylsiloxane units + 22 mol.% methylvinylsiloxane units) + 13 wt.% hydroxyl endblocked methyl(trifluoropropyl)polysiloxane + 40 wt.% fumed silica (400 $m^2\ g^{-1}$))

an increase with the chain extender content but did not significantly change after curing. In contrast to this, elongation decreased in both cases while the tear strength improved with the post-cure treatment. Subsequently, the authors repeated this study introducing from 1.5 to 4.5 wt.% of vinyl groups to determine the effect of excessive amounts of chain extender on these properties. The hardness increased from 50 to 60 Shore A and the tensile strength decreased from 13.1 to 11.6 MPa. After curing, there was almost no change in elongation and tear strength, indicating the limitation of incorporating chain extenders to improve mechanical properties.

The nature of the cross-linker also has a substantial influence on mechanical properties of vulcanizates. For example, Maxson [132] used a silanol-terminated PMTFPS-*co*-PMVS with reinforcing silica treated with both fluorine-containing silica agent (silanol-ended PMTFPS, called D_1) and fluorine free agent (silanol-ended PDMS, called D_2). The cross-linking was carried out by hydrosilylation using a platinum catalyst (hexachloroplatinic acid in this case) and trimethylsiloxy-terminated polyorganohydridosiloxane, and also with a peroxide catalyst (ditertiary butyl peroxide). As shown in Table 5.16, it was found that the use of the platinum catalyst with 1 wt.% of the silanol-ended PMTFPS-*co*-PMVS significantly enhanced mechanical properties relative to the peroxide-cured material, except for the hardness which remained roughly the same.

The same author [131, 132] also evaluated formulations containing varying content of a tri-functional SiH functional cross-linking agent (Structure 5.22) which reacted with vinyl groups contained in the base polymer. Compared with the previous example, this 3D cross-linking improved almost all mechanical properties of the resulting vulcanizates: elongation (from 505 to 650 %), tensile strength (from 7.1 to 8.4 MPa) and tear strength (from 22.3 to 35.5 $kN\,m^{-1}$), except for hardness which remained the same. An increase in the 3D additive expectedly led to an increase

Table 5.16 Effect of the cross-linking type on mechanical properties of copolysiloxane formulations described in the text. Materials were cured at 171 °C for 10 min and post-cured at 200 °C for 4 h [132]

Cross-linker	Silica treating agent	Hardness (Shore A)	Tensile Strength (MPa)	Tear strength ($kN\,m^{-1}$)	Elongation (%)
Peroxide[a,b]	D_1/D_2	47	7.0	21.7	575
Pt + 1 % of PMTFPS-*co*-PMVS[a,c]	D_1/D_2	49	8.1	36.7	607
Pt + 1.5 % of PMTFPS-*co*-PMVS[a,c]	D_1/D_2	51	7.8	31.0	535
Pt + 1 % of PMTFPS-*co*-PMVS[a,c]	D_1	42	6.3	25.9	–
Pt + 1 % of PMTFPS-*co*-PMVS[a,c]	D_2	51	6.4	14.1	–

[a]Base: 100 wt.% silanol terminated polydiorganosiloxane (99.4 mol.% 3,3,3-trifluoropropylmethylsiloxane units + 0.6 mol.% methylvinylsiloxane) + 25.1 wt.% dimethylvinylsiloxy-terminated polydimethylsiloxane (0.142 mol.% methylvinylsiloxane units) + 25.1 wt.% dimethylvinylsiloxy-terminated polydimethylsiloxane + 43.9 wt.% fumed silica ($350\ m^2\,g^{-1}$) + silica treating agent: D1 (10.5 wt.% silanol-terminated PMTFPS) or D2 (4.6 wt.% silanol-terminated PDMS)

[b]Peroxide cure: 100 wt.% base + 1.0 wt.% of 2,5-dimethyl-2,5-di(*t*-butylperoxy)hexane

[c]Hydrosilylation cure: 100 wt.% base + 0.15 wt.% of reaction product of hexachloroplatinic acid and tetramethyldivinyldisiloxane

of hardness and a decrease in all other properties (the highest values were obtained with 0.75 wt.% cross-linker).

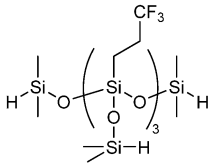

Structure 5.22

5.6.1.2.3 Effect of Silica Filler

The effect of the treatment of silica filler on the mechanical properties of vulcanizates from PMTFPS-co-PNFHMS base polymer is shown in Fig. 5.25 [19]. A high content of F_3 (used to treat silica) resulted in a large increase of tensile strength and elongation (the maximum value was reached for 19–20 wt.% of F_3) because of a better dispersibility of filler particles in the matrix. Above about 20 wt.% of F_3 loading, which corresponded to treating 60 mol.% of the silanol groups initially present on the silica surface, there was almost no change in mechanical properties.

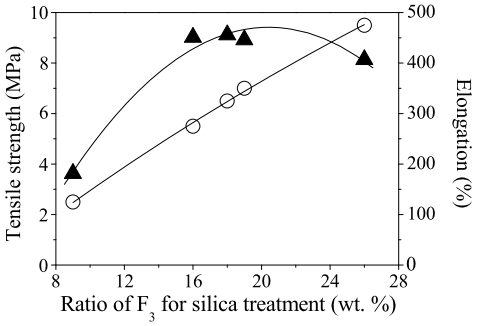

Fig. 5.25 Effect of silica treatment by F_3 on elongation (○) and tensile strength (▲) [19] (formulation: 100 wt.% PMTFPS (or PMTFPS-*co*-PNFHMS) formulated with 33 wt.% Silica (Aerosil 300, BET Surface areas of 300 $m^2\,g^{-1}$) + 1.5 wt.% ceric hydroxide + 1 wt.% (2,5-dimethyl-2,5-di(*t*-butylperoxy)hexane. The composition was press-cured for 10 min at 170 °C and post-cured for 4 h at 200 °C)

The authors also studied the influence of polymer intrinsic viscosity on mechanical properties. For treated silica they found that longer polymer chains improve both the elongation and the tensile strength of the resulting vulcanizates.

In another study [132] the silica was treated either by a fluorine free agent (D_2), or a fluorine-containing agent (D_1). The best values of mechanical properties were obtained when the silica treating agent did not contain any fluorinated group (see Table 5.16), although the authors did not give sufficient elongation test results to definitively state on this point. They also used silicas of different particle sizes in elastomer formulations containing a hydroxyl end-terminated PMFTPS-*co*-PMVS, with 0.2–1.2 wt.% of vinyl substitution in the silicone backbone. These results, summarized in Table 5.17, indicate that it is necessary to use fumed silica with the largest specific surface area to obtain the necessary reinforcement of the polymer and enhance elasticity as well as tensile and tear strengths.

5.6.1.2.4 Effect of Aging

Matsushita and Shigehisa reported the synthesis and application of terpolymers PMTFPS-*ter*-PDMS-*ter*-PMVS [133] in which the contents of both vinyl and fluorinated groups were varied. They also added to the formulation fumed silica (with a specific surface of 200 $m^2\,g^{-1}$), hydroxy-terminated PDMS, silanol-terminated PMVS and various additives. These compositions were then cured at 170 °C for 10 min before aging in mineral oil at 150 °C for 70 h. In all cases, they observed a drop of hardness before and after oil immersion from around 75 to about 53 Shore A. The material obtained from the most fluorinated terpolymer had the best resistance to aging (71 Shore A). On the contrary, the material with only non-fluorinated units exhibited the worst resistance to aging.

Table 5.17 Mechanical properties of a formulation based on fluorosilicone containing silica with different specific surfaces [132][a]

Specific surface area of SiO_2 ($m^2\ g^{-1}$)	Hardness (Shore A)	Tensile strength (MPa)	Tear strength ($kN\ m^{-1}$)	Elongation (%)	Modulus at 100% strain (MPa)	Compression set (%)
90	37	9.0	15.9	368	1.3	13
200	43	6.9	22.2	360	1.3	23
250	42	11.9	27.3	389	1.5	20

[a]Formulation: 100 wt.% hydroxyl end-terminated polymethylvinyl-(methyl-3,3,3-trifluoropropyl)siloxane having about 0.2 to 1.2 mol.% pendant vinyl substituted on silicon + 0.3 wt.% methylvinyldi(N-methylacetamido)silane + 2.0 wt.% hydroxyl end-terminated polydimethylsiloxane having about 1.0 to 6.0 mol.% pendant vinyl substituted on silicon + 5.1 wt.% hydroxyl end-terminated polymethyl(3,3,3-trifluoropropyl)siloxane fluid where the terminal hydroxyl substitution comprises about 3 to 10 wt.% of the fluid + 1.0 wt.% hydroxyl end-terminated polydimethylsiloxane having about 9 to 12 wt.% pendant vinyl substituted on silicon + 28.0 wt.% reinforcing silica

5.6.1.3 Formulation with Fluorocarbon Polymer

Fluororubbers are well known for both their high heat and oil resistances as well as for their excellent mechanical strength. Several groups have investigated the addition of fluorocarbon polymers into fluorosilocone polymers in order to improve the mechanical properties of the latter. Kobayashi's team used polytetrafluoroethylene (PTFE) [134] and a copolymer of vinylidene fluoride-co-hexafluoropropylene (poly(VDF-*co*-HFP)) [135] and obtained the results shown in Table 5.18. The most interesting features were obtained by cross-linking with peroxides, and when the PDMS end-capped with vinyl groups was mixed with a silicone carrying pendant perfluorinated groups. As for the addition of poly(VDF-*co*-HFP) copolymer to a finished vinyl PDMS-*co*-PMVS copolymer, the obtained material showed both improved tensile strength (from 10.8 to 11.8 MPa) and tear strength (from 21.6 to 23.5 $kN\ m^{-1}$) [136].

5.6.2 Hybrid Fluorosilicones

Pierce and Kim [10] reported a comprehensive study of hybrid silicones, with a wide range of in-chain $R_F = (CF_2)_x$ ($x = 1$ to 10) hybrid segments, as shown in Structure 5.23.

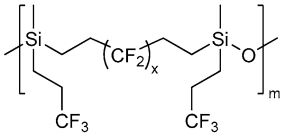

Structure 5.23

Table 5.18 Mechanical properties of vulcanizates from different polymers and PTFE cross-linked with the indicated type of cross-linking agent [134][a]

Cross-linking catalyst	Polysiloxane	Hardness (Shore A)	Tensile strength (MPa)	Elongation (%)	Tear strength (kN m^{-1})
Pt	$C_8F_{17}C_2H_4$-ended PDMS[b]	53	10.3	550	24.5
Peroxide cured 4 h at 200 °C	$C_8F_{17}C_2H_4$-ended PDMS[c]	52	9.7	480	23.5
	PNFHMS-*co*-PDMS[d]	54	8.8	390	22.6
	PHDFDMS-*co*-PDMS + vinyl-ended PDMS[e]	55	10.8	670	24.5

[a]*Base 1:* 100 wt.% diorganopolysiloxane (99.5 mol.% dimethylsiloxane units + 0.5 mol.% methylvinylsiloxane units) + 1 wt.% polytetrafluoroethylene resin fine powder (average size distribution of 0.2–0.3 μm) + 1 wt.% of organopolysiloxane $F(CF_2)_8C_2H_4SiMe_2O(Me_2SiO)_x$-$SiMe_2C_2H_4(CF_2)_8F$ (x required to provide a viscosity of 50 cP) + 35 wt.% fumed silica (200 m^2 g^{-1}). The base is heated for 2 h at 120 °C
Base 2: 100 wt.% diorganopolysiloxane (99.5 mol.% dimethylsiloxane units + 0.5 mol.% methylvinylsiloxane units) + 5 wt.% polytetrafluoroethylene resin fine powder (average size distribution of 0.3 μm) + 0.6 wt.% $Me_3SiO(C_4F_9C_2H_4SiMeO)_y(Me_2SiO)_zSiMe_3$ ($y : z = 1 : 1$) + 30 wt.% fumed silica (110 m^2 g^{-1})
Base 3: 100 wt.% diorganopolysiloxane (99.7 mol.% dimethylsiloxane units + 0.3 mol.% methylvinylsiloxane units) + 2 wt.% polytetrafluoroethylene resin fine powder (average size distribution of 0.2–0.3 μm) + 8 wt.% dimethylpolysiloxane terminated dimethylvinylsiloxane + 35 wt.% fumed silica (300 m^2 g^{-1}) + 0.8 wt.% Me_3Si-$O(F(CF_2)_8C_2H_4SiMeO)_y(MeSiO)_z$ $SiMe_3$ ($y : z = 1 : 5$)

[b]100 wt.% Base 1 + 1 wt.% methylhydrogenpolysiloxane (trimethylsiloxy-terminated) + 0.05 wt.% complex chloroplatinic acid and divinyltetramethyldisiloxane

[c]100 wt.% Base 1 + 0.5 wt.% 2,5-dimethyl-2,5-di(*tert*-butylperoxy)hexane

[d]100 wt.% Base 2 + 0.5 wt.% 2,5-dimethyl-2,5-di(*tert*-butylperoxy)hexane

[e]100 wt.% Base 3 + 0.5 wt.% 2,5-dimethyl-2,5-di(*tert*-butylperoxy)hexane

Hardness, tensile strength and elongation were studied as functions of the number of fluorine atoms in the hybrid segment. The authors compared the behavior of materials obtained using three different treatments: an initial cure for 8 h at 200 °C, followed by either a post-cure for 24 h at 250 °C in air or for 24 h at 250 °C in a sealed tube. Results of these experiments are summarized in Fig. 5.26. The polymer containing the smallest number of CF_2 groups ($x = 1$) in the fluorocarbon segment suffered the most from thermal oxidation and exhibited the worst mechanical properties. The post-cure treatment (either in the presence or absence of oxygen) led to better mechanical properties, except for elongation which was higher for the sample that underwent initial cure only. Post-cure in a sealed tube noticeably "homogenized" mechanical properties. While hardness and elongation proportionally increased with the length of the perfluorinated unit, tensile strength reached its maximum at $R_F = C_6F_{12}$. This study underlined that both hardness and tensile strength improved in hybrids containing at least one CF_2 group in the R_F unit compared

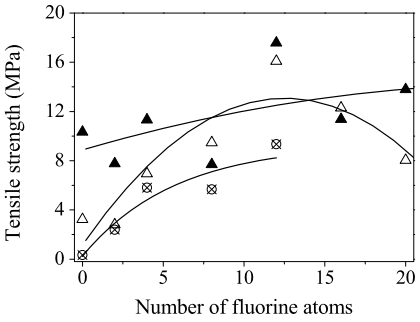

Fig. 5.26 Mechanical properties of hybrid fluorosilicones as a function of the length of the R_F segment in polymers of Structure 5.23. Curing for 8 h at 200 °C (▲) followed by 24 h at 250 °C in air (△) or in sealed tubes (⊗) [10] (formulation as given in the reference: PMTFPS ($M_w \sim 6{,}000$) + fumed silica + peroxide vulcanizing agent and additives for heat stability (Fe_2O_3))

to fluorosilicones with only pendant fluorinated groups. No conclusion is possible regarding elongation because of molecular weight variations.

A complementary study of two fluorosilicones of Structure 5.18 containing a few vinyl units necessary to achieve further cross-linking [80] focused on mechanical properties of these materials, with similar formulations: fumed silica, ferric oxide and peroxide (see Table 5.19). The fluorosilicone with R = CH_3 and R′ = $C_2H_4CF_3$ had better mechanical properties than the fluorosilicone with both fluorinated side groups being $C_2H_4CF_3$. Unlike conventional fluorosilicones this elastomer also maintained its physical properties even at very high temperature.

Some hybrid fluorosilicones have also been used as chain extenders (Structure 5.24) or cross-linking agents (Structure 5.25) through redistribution reactions [106]. R_F groups can be either a simple perfluorinated group or a grafted perfluorinated alkyl group or even a perfluorinated polyether. In any case, the chain extended material showed the same hardness (∼40 shore A), elongation (∼300 %), tensile strength (∼4.9 MPa) and tear strength (∼12 kN m^{-1}). When R_F was a perfluorinated polyether, the elasticity was significantly higher (450 %) than for the other materials, whereas the other properties did not change much. On the other hand, when a copolymer such as PMTFPS-*co*-PMVS [137] was added to the formulation, enhancements of all mechanical properties were observed: elongation (500 %), hardness (60 shore A), tensile strength (12.7 MPa), tear strength (ranging between 40 to 62 kN m^{-1}).

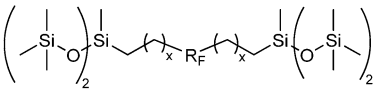

Structure 5.24

Table 5.19 Mechanical properties of PMTFPS and two hybrid fluorosilicones of Structure 5.18 [80]

Aging	Hardness (Shore A)			Tensile strength (MPa)			Elongation (%)
	8 h 200 °C	24 h 200 °C 2nd test	24 h 250 °C after the 2nd test	8 h 200 °C	24 h 200 °C 2nd test	24 h 250 °C after the 2nd test	8 h 200 °C
PMTFPS[a]	45	/	27	10.3	/	0.3	350
$CH_3/C_2H_4CF_3$[b]	68	56	56	13.0	10.00	3.4	360
$C_2H_4CF_3/C_2H_4CF_3$[c]	66	/	/	4.6	/	/	175

[a] 100 wt.% hydroxyl-endblocked copolymer containing 99.5 mol.% PMTFPS + 0.5 mol.% $CF_3C_2H_4Si(CHCH_2)O$ + 40 wt.% fumed silica + 17 wt.% $CF_3CH_2CH_2(CH_3)SiO$ (plasticizer) + 2 wt.% ferric oxide (stabilizer) + 0.5 wt.% di-*tert*butyl peroxide (catalyst)

[b] 100 wt.% hydroxyl-endblocked copolymer containing 99.5 mol.% $CH_3/C_2H_4CF_3$ + 0.5 mol.% $CF_3C_2H_4Si(CHCH_2)O$ + 40 wt.% fumed silica + 17 wt.% $CF_3CH_2CH_2(CH_3)SiO$ + 2 wt.% ferric oxide + 0.5 wt.% di-*tert*butyl peroxide

[c] 100 wt.% hydroxyl-endblocked copolymer containing 98 mol.% $C_2H_4CF_3/C_2H_4CF_3$ + 2 mol.% $CF_3C_2H_4Si(CHCH_2)O$ + 40 wt.% fumed silica + 17 wt.% $CF_3CH_2CH_2(CH_3)SiO$ + 2 wt.% ferric oxide + 0.5 wt.% di-*tert*butyl peroxide

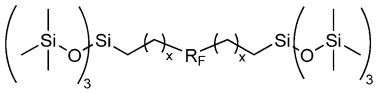

Structure 5.25

5.6.3 Conclusions to Sect. 5.6

The comparison of mechanical properties of conventional and hybrid fluorosilicones reveals exciting potentials of the latter for uses where the material undergoes thermal aging. Both hybrid perfluorinated chains and the introduction of vinyl groups enhance the mechanical properties to a certain threshold (reached at 0.1 wt.% for the PMTFPS). Addition of fillers also improves these properties, particularly fillers with high surface area.

5.7 New Avenues in Fluorosilicone Elastomer Synthesis

In the preceding sections we described selected synthetic pathways and properties of some of the most conventional fluorosilicones. In this section, we focus on more recent research and some possible future trends and synthetic alternatives. The basic molecular design idea here is to combine long sequences of silicones and (fluoro)organic polymers to enhance their immiscibility and achieve new materials properties by nanostructure/phase demixing.

5.7.1 Random Copolymers

5.7.1.1 Copolymers with Pendant Fluorinated Groups

Ten years ago, Vaidya and Chaudhury [138] reported the synthesis of a PDMS bearing perfluoropolyether pendant groups. Recently, a new pathway to obtain fluoropendant silicones was reported consisting of the ROP of D_4 in the presence of a fluorinated trimethoxysilane (Scheme 5.13) [139]. An emulsion of the modified polysiloxane was used for the treatment of polyester fabrics and it showed excellent surface activity not affecting the shade of color of the dyes and improving the handle of fabrics and providing excellent water repellency. Tang et al. [140] photocross-linked epoxide-pendant polysiloxanes bearing fluorinated groups. The combination of fluorine and silicone in the same copolymer increased thermal and water resistances, as well as surface properties of the coatings and decreased their surface energy.

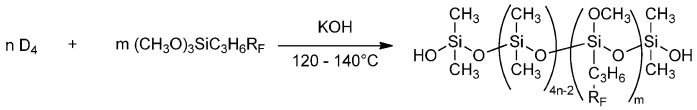

$R_F = C_3H_6CF(C_2F_5)CH(CF_3)_2$

Scheme 5.13 Ring-opening polymerization of D_4 in the presence of a fluorinated trimethoxysilane

5.7.1.2 Copolymers with Pendant Siloxane Chains

A reverse approach to fluorocarbon siloxane polymers, suggested by a Japanese group [141] consists of coupling a PDMS end-functionalized with an epoxy group and a poly(CTFE-*ter*-*t*BuA-*ter*-HEAE) terpolymer (where CFTE is chlorotrifluoroethyl, *t*BuA is *tert*-butyl acetate and HEAE is 2-hydroxyethyl allyl ether). This terpolymer, provided by Central Glass Co., is composed of 43 CTFE units, 43 *t*BuA units, 14 HEAE units and a PDMS graft chain as shown in Structure 5.26.

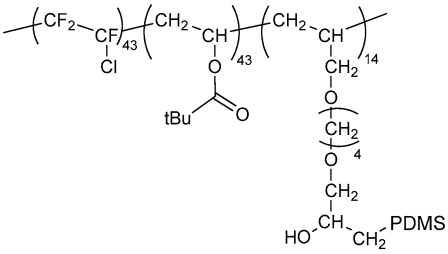

Structure 5.26

In a similar work, Baradie et al. [142] grafted polysiloxane chains onto a fluorinated copolymer backbone to prepare fluorosilicone copolymer networks (as shown in Scheme 5.14). They achieved the condensation of a monofunctional or telechelic bis(isocyanate) PDMS on fluorinated copoly(TFE-*co*-vinyl alcohol) prepared by radical copolymerization of tetrafluoroethylene (TFE) and vinyl acetate in supercritical CO_2, followed by hydrolysis.

5.7.1.3 Copolymers with Pendant Fluorinated and Siloxane Groups

Another recent strategy led to copolymers bearing both siloxane and fluorocarbon chains as pendant groups on the same polymer backbone (Scheme 5.15) [143, 144]. It was shown that these copolymers were surface-segregated and that in-depth segregation (ca. 5 nm) depended upon the chemical structure of the copolymer. A relatively small amount (i.e. 5 wt.%) of these copolymers in blends was sufficient to saturate the outermost surface in fluorine content. The chemical composition of the surface-segregated nanostructure of films was also affected by the external environment (e.g. water).

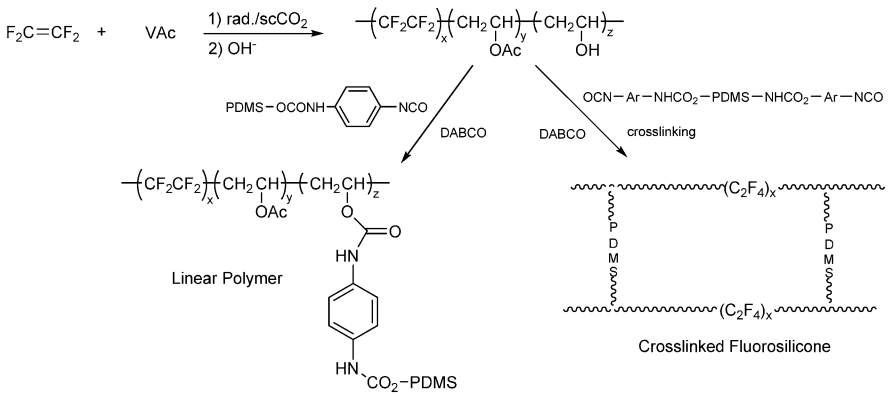

Scheme 5.14 Fluorosilicone copolymers and networks bearing PDMS side-chains

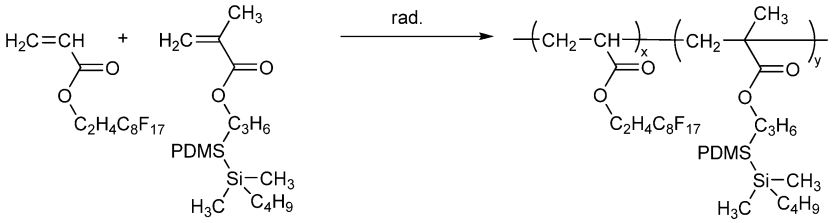

Scheme 5.15 Recent strategy of synthesizing copolymers with pendant fluorinated and silicone side-groups

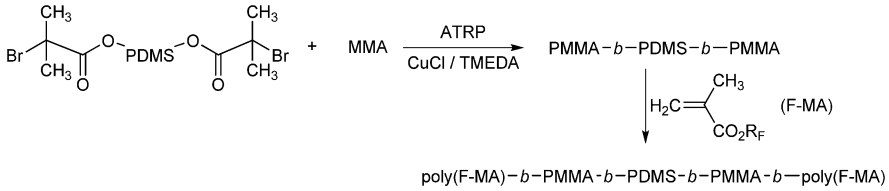

Scheme 5.16 Pentablock copolymers prepared by ATRP

5.7.2 Block Copolymers

5.7.2.1 Linear Copolymers

Liang et al. [145] synthesized poly(F-methacrylate)-*b*-PMMA-*b*-PDMS-*b*-PMMA-*b*-poly(F-methacrylate) pentablock copolymers by sequential atom transfer radical polymerization (ATRP) of MMA and fluorinated acrylate, as shown in Scheme 5.16, with properties that were better than those of a PDMS-*b*-PMMA-*b*-poly(F-methacrylate) triblock copolymer [146].

Zhang et al. [147] reported the synthesis of a copoly[(meth)acrylate], with both long perfluorinated groups and PDMS moieties, as surface modifiers for coatings (see Structure 5.27). A high concentration of this additive in a PDMS coating decreased the oleophobicity of the film via micellar aggregation (as observed by light scattering).

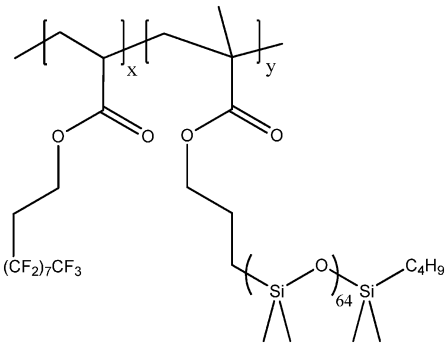

Structure 5.27

Recently we synthesized [148] a series of novel hybrid fluorosilicones based on poly(VDF-*co*-PMVE) copolymer prepared from the iodine transfer copolymerization of vinylidene fluoride (VDF) with perfluoromethyl vinyl ether (PMVE) [149], as depicted in Scheme 5.17. This reaction scheme highlights two pathways to create hybrid fluorosilicones starting from the same vinylsiloxane precursors: polyaddition of a hydrido terminated PDMS by hydrosilylation or ethoxyfunctionalization to generate cross-linked materials.

5.7.2.2 Block Copolymer Networks

Darras et al. [150] reported interpenetrating polymer networks from PDMS cross-linked by polyaddition of telechelic diol with polyfunctional isocyanate in the presence of dibutyltin dilaurate (DBTDL) and cross-linked by fluorinated diacrylate free radicals, as shown in Scheme 5.18. The network exhibited a water contact angle of 114° (compared to 108° for PDMS).

5.7.2.3 The Case of Perfluoroether-Based Copolymers

Perfluoropolyethers (PFPEs) have exceptionally low T_g and high thermal stability [151]. Daikin, DuPont, Nippon Mekktron, and Solvay-Solexis, are currently marketing four main commercially available PFPEs, i.e. Demnum®, Krytox®, Aflunox®, and Fomblin®, respectively. For most of them, the control of the functionalization of their chains is not easy and, in spite of much research, few studies have led to industrial development of fluorosilicones based on perfluoroethers. As a notable exception, the Shin-Etsu Company recently started marketing, under the trade name

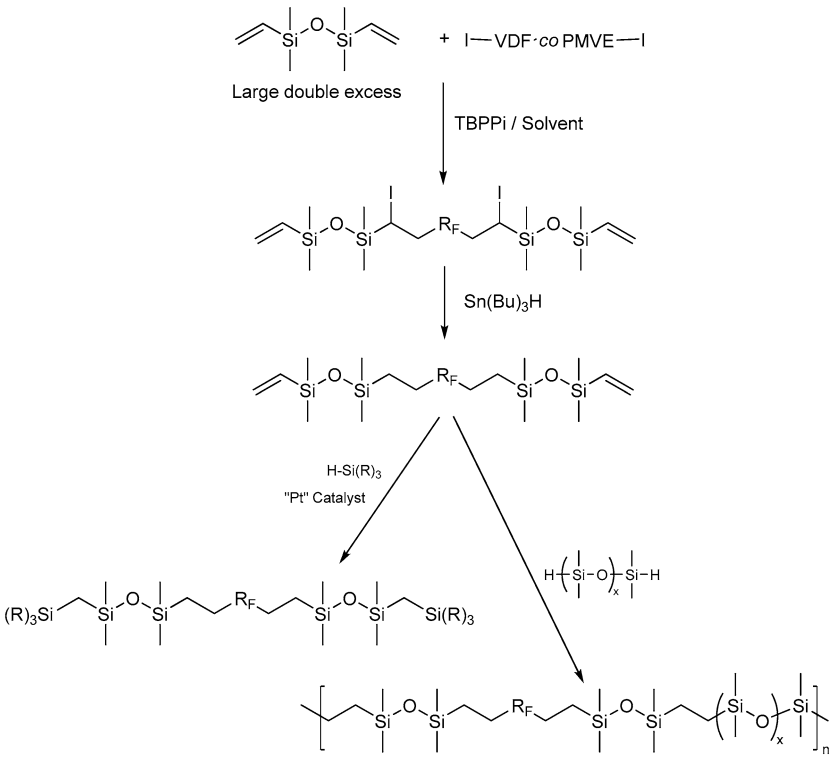

Scheme 5.17 Synthesis of poly(VDF-co-PMVE) copolymers by iodine tranfer polymerization technique and post-functionalization

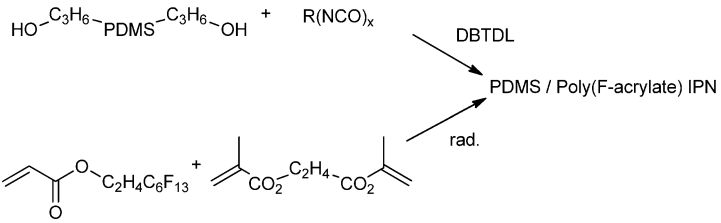

Scheme 5.18 Pathway to prepare interpenetrating polymer networks of PDMS and a perfluorinated polyacrylate

Sifel® (per)fluorinated polyethers cross-linked with short length siloxanes [152]. Conceptually, the synthesis involves a hydrosilylation polyaddition of telechelic dienes containing a fluorinated polyether and fluorinated or non-fluorinated compounds possessing at least two Si-H end-groups (Scheme 5.19).

Shin-Etsu [153] claimed both linear perfluorinated polymers (Structure 5.28) and cross-linkers (Structures 5.29 and 5.30). The early cross-linking agents were synthesized by cohydrolysis of a perfluorinated trichlorosilane and tetramethyldisiloxane. The latter variety seems to contribute to the improvement of properties at high tem-

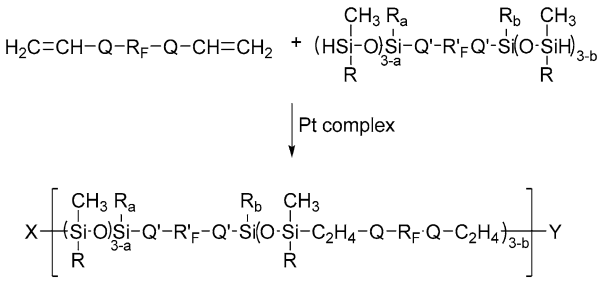

Scheme 5.19 Sifel® elastomer synthesis

peratures (as explained by Uritani [154]) thanks to the presence of C_2H_4-Si≡ rather than O-Si≡ moieties as linking groups.

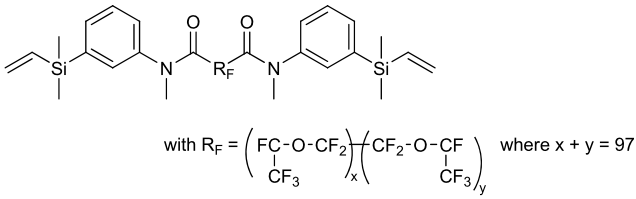

Structure 5.28

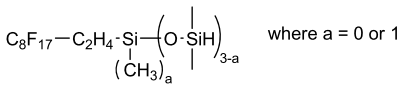

Structure 5.29

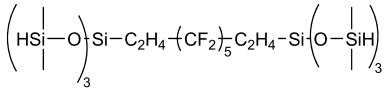

Structure 5.30

The inventors insisted on the need to prepare elastomers in three steps in order to obtain very good properties. They compared Sifel® with commercially available Viton® E, high-performance Viton® GLT, and a fluorosilicone. Sifel® showed better performance over competitors, with regard to T_g (ca. −60 °C), the non-swelling properties in various polar and non-polar solvents (less than 20 % volume swell in most conventional solvents, including MEK and gasoil), acid and base resistances (it does not decompose in concentrated nitric acid, sodium hydroxide or butylamine) and overall mechanical properties (tensile strength ≈9 MPa, elongation ≈250 %, tear strength ≈18 kN m^{-1}) including compression set (19 % after 24 hr at 200 °C).

Other elastomers based on PMTFPS, functional fluorinated silanes and perfluoropolyether oils have recently been claimed by the DuPont de Nemours Company as transparent, adhesive, scratch resistant coatings [155].

5.8 Conclusions

The tremendous amount of work that has been carried out in the area of fluorinated siloxane polymers (either block or graft) is driven by the need for high-performance elastomers. Here, the term "high performance" implies the ability to withstand very low temperatures ($T_g \leq -60\,°C$), to preserve elastomeric properties in the space environment and to retain stability at high application temperatures [156]. For example, at speeds ranging from Mach 2.05 (as for Concorde) to Mach 2.4, these materials should retain good thermal stability from 110 °C to 177 °C for 60,000 hrs (i.e., 6 years and 10 months). In addition, they also have to possess good mechanical properties (elastic strain and return) and excellent swelling resistance, whatever the nature of the solvent used (polar or non polar).

Meeting such challenges is not a trivial task and although numerous investigations have been carried out in this field, results are not yet conclusive so that several decades might still be needed to reach a satisfactory goal. Clearly, the Sifel® product is presently the most effective material for the purpose in view of the range of its temperature stability, mechanical resiliency, and solvent and acid/base resistance. One major drawback, however, is its price, because of the complex chemistry required to prepare both the core fluorinated polymers and the cross-linking agents.

Future technologies may be based on the controlled radical polymerization of fluoroolefins, enabling preparations of interesting fluorinated polymer segments. The most appealing method seems to be the living radical (co)polymerization (LRP) of fluorinated alkenes (such as vinylidene fluoride, perfluoromethyl vinylether, hexafluoropropylene or their combinations with other fluorinated alkenes) via the iodine transfer (co)polymerization (ITP) in which the iodine atoms act as reversible transfer sites. The versatility of ITP has already enabled several companies involved in fluorine chemistry (e.g., Daikin, DuPont, Ausimont-now Solvay-Solexis) to produce novel thermoplastic elastomers with combinations of soft and hard segments.

Appendix A: Definition and Measurements of Surface Tension for Soft Polymers

A.1 Definition of Surface Tension

Surface tension is the force per unit length necessary to minimize the surface area between two immiscible media. This contraction force results from the propensity

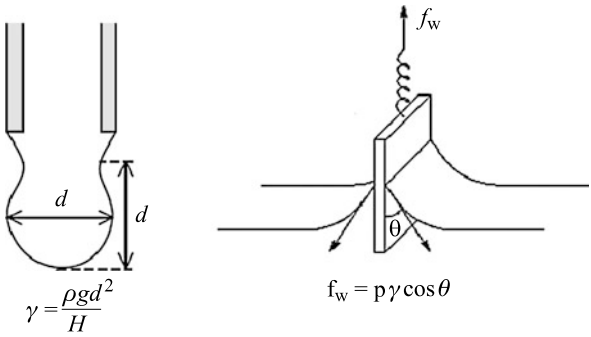

Fig. 5.27 Sessile drop (*left*) and Wilhelmy plate (*right*) techniques to measure liquid surface tension

of bulk liquid molecules to attract those at the interface to ensure cohesion between them. For a liquid, the measurement of this parameter is easy and reliable, since an equilibrium state between the liquid and the surrounding gas or liquid can always be reached. For solid surfaces, the elastic force between that surface and a drop of liquid may not be at equilibrium, and the surface energy of the solid acts as an attractive force opposing contraction of the liquid. Consequently, liquid and solid surface tensions cannot be compared.

A.2 Measurement of Liquid Surface Tensions

Two techniques are used to measure the surface tension of liquid polymers; the pendant drop technique and the Wilhelmy plate technique (equations (5.3) and (5.4) and Fig. 5.27). The former is not frequently used in the papers reviewed in this chapter, since it requires an apparatus calibration component and the shape of the drop may not be perfectly round for viscous polymers. The Wilhelmy plate technique consists of measuring the pulling force on the plate introduced into the liquid. The simplest case is when a meniscus forms between the plate and the liquid where the contact angle is $\theta = 0$, and the surface tension is calculated knowing the perimeter of the plate, i.e. horizontal length and thickness (5.4). Note that a correction for the liquid buoyancy is avoided by performing the force measurement when the edge of the plate is at the same level with the liquid surface.

$$\gamma = \frac{\rho g d^2}{H} \tag{5.3}$$

$$f_w = p\gamma\cos\theta \tag{5.4}$$

In these equations γ is surface tension of the liquid; ρ is density; g is specific gravity; H is a coefficient calibrated on the apparatus; f_w is the pulling force; and p is the plate perimeter.

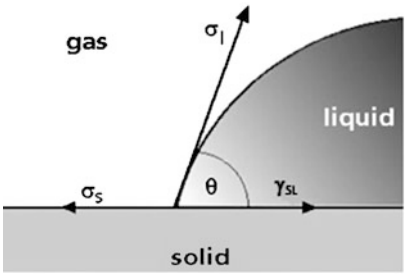

Fig. 5.28 Contact angle of a standard liquid drop on a flat (polymer) surface. By definition, if θ is less than 90°, the liquid wets the solid surface

A.3 Measurement of Solid Surface Tensions

Solid surface tensions are almost exclusively determined using a contact angle technique as illustrated in Fig. 5.28. When a drop of a liquid is deposited on the polymer substrate the contact angle between the liquid, air and solid is given by Young's equation:

$$\gamma_L \cos\theta = \gamma_S - \gamma_{SL} \tag{5.5}$$

where γ_L, γ_S and γ_{SL} are the liquid/air, solid/air and solid/liquid surface tensions, respectively. Since in this equation only γ_L and θ are known, this requires one to use semi-empirical equations to deduce the surface tension of the solid γ_S.

Surface tensions can be divided into two components, a dispersive one (γ_S^d) and a polar one (γ_S^p), according to (5.6):

$$\gamma_S = \gamma_S^d + \gamma_S^p \tag{5.6}$$

Based on this, Owens and Wendt [157] derived equation (5.7) using a geometric approximation:

$$\gamma_L(1+\cos\theta) = 2(\gamma_S^d \gamma_L^d)^{1/2} + 2(\gamma_S^p \gamma_L^p)^{1/2} \tag{5.7}$$

Generally, two model liquids are necessary to determine both components. To determine the dispersive component, test liquids with no polar surface tension component, such as hexadecane, are chosen, while the polar component can be obtained from a polar liquid, typically water.

Another method of solid surface tension determination is given by the Girifalco–Good–Fowkes–Young equation [158, 159]:

$$\cos\theta = 2(\gamma_S^d)^{1/2}(\gamma_L)^{-1/2} - 1 \tag{5.8}$$

The so-called Zisman technique consists of determination of the surface tension by plotting $\cos\theta$ versus γ_L for a series of liquid alkanes and extrapolating to cos $\theta = 1$; where $\gamma_S^d = \gamma_L$. This surface tension is referred to in this chapter as the dispersive critical surface tension, γ_c. The technique is believed to give solid surface tensions which depend little on the test liquids, although it was recently observed that short alkanes may partly swell the fluorosilicones.

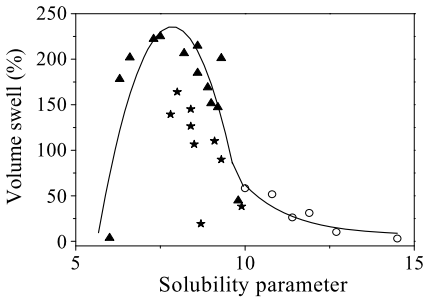

Fig. 5.29 Volume swells of PDMS elastomer as a function of solvent solubility parameters, for solvents with weak (▲), strong (○), and moderate (★) electrostatic interactions

One can also perform dynamic measurement of the contact angle: in this case the advancing angle (θ_A) is close but not similar to the one obtained by static measurements, i.e. "at equilibrium", whereas the receding angle (θ_R) is measured after dewetting the surface (experimentally performed by sucking back a part of the liquid to decrease the droplet volume). The contact angle hysteresis (ω), i.e. the difference between the advancing and the receding contact angles, gives an indication either of the chemical rearrangement of the surface upon contact with the liquid, or of the surface roughness.

Appendix B: Swelling Measurements, Solubility Parameters and PDMS Case

A solvent is generally a liquid that dissolves another liquid, solid or gaseous solute, resulting in a uniform mixture called solution. Two substances are miscible if they show the same cohesion energy, c (cal cm^{-3}). Since true solution requires complete separation of individual molecules, a cross-linked polymer can never dissolve but an appropriate solvent is likely to be absorbed by the network to give a swollen gel similar to a very viscous solution. The amount of swelling of the polymer depends on the competition between: (i) the free energy of the mixture on insertion of solvent molecules to solvate polymer segments; and (ii) the elastic retraction force acting opposite to the distortion, caused by the chain elongation in the swollen cross-linked network. Equilibrium of these two forces leads to an optimal volume swell.

Hildebrand solubility parameters δ (cal$^{1/2}$ cm$^{-3/2}$) describe interactions between different solvents and solutes. Swelling will be at maximum when the solubility parameter of the solvent δ_s and the polymer δ_p are numerically similar: $\delta_s \cong \delta_p$. Many theoretical models of the solvent-polymer pairing have been proposed to explain their intrinsic interactions. However, the theories are limited because of the large variety of solvents available and their different chemical properties. In some studies, the solubility parameters are often divided into three components, describing hydrogen bonding, polarity and dispersive behavior of solutes; these theories are not considered here.

By definition, the solubility parameters do not include any hypothesis with regard to the association, the polarity, the solvation and the hydrogen bonding between solvent and polymer. However, Yerrick and Beck [126] classified solvents

according to their electrostatic interactions with solutes into three categories: those inducing weak interactions (aliphatic, aromatic, fluorocarbon, chlorinated solvents); moderate (dipole–dipole) interactions (esters, ketones, ethers, nitriles); and strong (hydrogen bonding) interactions (aliphatic alcohols). For instance, the swelling of PDMS networks in different solvents is shown in Fig. 5.29 [126]. It can be seen from this figure that while hydrocarbon and chlorinated solvents have the same solubility parameter, chlorinated solvents tend to increase swelling while the hydrocarbons do not. Ethers, esters and ketones show reduced swelling abilities. In these solvents, interactions are mainly due to permanent dipole moments that tend to increase the efficient molecular volume and consequently to decrease their swelling ability. Plotting the volume swell as a function of the Hildebrand parameter yields the solubility parameter of PDMS ($\delta_{PDMS} = 7.5$ cal$^{1/2}$ cm$^{-3/2}$), as the maximum in the resulting curve. This value is in the range of earlier data in the literature (7.3 to 7.7 cal$^{1/2}$ cm$^{-3/2}$) [160–162] and is consistent with weak interaction forces characteristic for this polymer.

References

1. Report of the presidential commission on the space shuttle challenger accident, available through the web: http://history.nasa.gov/rogersrep/genindex.html
2. http://www.daikin.com/press/2005/050414/index.html
3. Holbrook GW, Brown PL (1959) US Pat US 2915544
4. Holbrook GW (1966) US Pat US 3269983
5. Steward O (1965) GB Pat GB 1014156
6. Boutevin B, Pietrasanta Y (1985) Prog Org Coat 13(5):297
7. Ameduri B, Boutevin B (2005) J Fluorine Chem 126:221
8. Guida-Pietrasanta F, Boutevin B (2005) Adv Polym Sci 179:1
9. Owen MJ (1990) Adv Chem Ser 224:705
10. Pierce OR, Kim YK (1971) Rubber Chem Technol 41:1350
11. Kobayashi H, Owen MJ (1990) Polym Prepr 31(1):334
12. Kobayashi H (1992) Eur Pat EP 535597
13. Lee CL (1970) Ger Offen., DE 1963523
14. Yuzhelevskii YA, Kagan EG, Fedoseeva NN (1970) Vysokomol Soedn A 12(7):1585
15. Miyake H, Shintani S, Furukawa Y (1988) Japan Pat, JP 6327530
16. Boileau S (1993) Makromol Chem 73:177
17. Boileau S, Boutevin B, Pietrasanta Y (1987) Polym Mater Sci Eng 56:384
18. Furukawa Y, Shin-Ya Y, Miyake Y, Kishino H, Yamada M, Kato H, Sato M (2001) J Appl Polym Sci 82(13):3333
19. Furukawa Y, Shin-Ya S, Saito M, Narui SI, Miyake H (2002) Polym Adv Technol 13:60
20. Lee CL (1969) US Pat US 2026446
21. Kaufmann R, Braunsperger K, Wegehaupt KH, Von A (1986) US Pat US 4577040
22. Boutevin B, Youssef B (1989) Makromol Chem 190:277
23. Abdellah L, Boutevin B, Youssef B (1991) Eur Polym J 27(8):821
24. Abdellah L, Boutevin B, Youssef B (1991) Eur Polym J 27:695
25. Boutevin B, Abdellah L, Dinia NM (1995) Eur Polym J 31(11):1127
26. Boutevin B, Youssef B, Abdellah L, Dinia NM (1996) Eur Polym J 32(6):701
27. Kobayashi H, Nishiumi W (1993) Makromol Chem 194(5):1403
28. Szendrey JP (1969) US Pat US 3560436
29. Szendrey JP (1969) US Pat US 3560437

30. Talcott TD (1961) US Pat US 3006878 (Dow Corning)
31. Holbrook GM, Steward OW (1966) Ger Offen DE 1445324 (Dow Corning)
32. Brown E (1965) US Pat US 3179619 (Dow Corning)
33. Lentz CW (1967) US Pat US 3328349 (Dow Corning)
34. Brown ED (1967) Fr Pat FR 1499082 (Dow Corning)
35. Evans ER (1981) Fr Pat FR 2464276 (General Electric)
36. Kobayashi H, Owen MJ (1990) Macromolecules 23:4929
37. Kobayashi H, Owen MJ (1993) Makromol Chem 194:259
38. Boutevin B, Pietrasanta Y, Youssef B (1986) J Fluorine Chem 31:57
39. Boutevin B, Pietrasanta Y, Youssef B (1986) J Fluorine Chem 34:167
40. Boutevin B, Youssef B (1989) J Fluorine Chem 45:355
41. Boutevin B, Youssef B (1991) Macromolecules 24:629
42. Chu EY, Pearce EM, Kwei TK, Yeh TF, Okamoto Y (1991) Makromol Chem, Rapid Commun 12:1
43. Höpken J, Möller M, Boileau S (1991) New Polymer Mater 2(4):339
44. Beyou E, Babin P, Benneteau B, Dunoguès J, Teyssié D, Boileau S (1994) Colloid Polym Sci 32:1673
45. Beyou E, Babin P, Benneteau B, Dunoguès J, Teyssié D, Boileau S, Corpart JM (1995) Polym Int 38:237
46. Boileau S, Beyou E, Babin P, Benneteau B, Dunoguès J, Teyssié D (1996) Eur Coat J 7–8:508
47. Atherton JH (1973) Ger Offen DE 2311879
48. Chujo Y, Mc Grath JE (1983) Polym Prep 24:47
49. Chujo Y, Mc Grath JE (1995) J Macromol Sci, Part A, Pure Appl Chem 32(1):29
50. Doeff M, Lindner E (1989) Macromolecules 22:2951
51. Wilczek L (1993) US Pat US 5233071 (Dupont)
52. Furukawa Y, Kotera M (2002) Colloid Polym Sci 40:3120
53. Mera AE, Morris RE (2001) Macromol Rapid Commun 22:513
54. Furukawa Y, Kotera M (2003) J Appl Polym Sci A, Polym Chem 87:1085
55. Furukawa Y, Yoneda T (2003) J Polym Sci A, Polym Chem 41:2704
56. Boutevin B, Guida-Pietrasanta F, Ratsimihety A (2000) J Polym Sci A, Polym Chem 38:3722
57. Abdellah L, Boutevin B, Guida-Pietrasanta F, Smaihi M (2003) J Membr Sci 217(1–2):295
58. Colomines G, André S, Andrieu X, Rousseau A, Boutevin B (2003) J Appl Polym Sci 90:2021
59. Boutevin B, Pietrasanta Y (1984) Fr Pat FR 8417279 (Atochem)
60. Loree LA, Brown ED (1971) US Pat US 3576020
61. Boutevin B, Pietrasanta Y, Sarraf L (1986) J Fluorine Chem 31:425
62. Boutevin B, Fleury E, Pietrasanta Y, Sarraf L (1986) J Fluorine Chem 31:437
63. Ameduri B, Boutevin B (1997) In: Chambers RD (ed) Topics in current chemistry: organofluorine chemistry. Springer, Heidelberg, pp 165–233
64. Ameduri B, Boutevin B (2000) J Fluorine Chem 102:253–268
65. Boutevin B, Boileau S, Pietrasanta Y, Lantz A (1984) FR PAT FR 2566401 (Elf Atochem)
66. Shashkova ZS, Frolova KS, Uelskaya NN (1970) USSR Pat SU 267910
67. Grindahl GA (1970) Fr Pat FR 2035608
68. Wu TC (1966) Fr Pat FR 1461933
69. Klebanskii AL, Yuzhelevskii YA, Kagan EG, Larionova ON, Kharlamova AV, Sergeeva EP (1970) USSR Pat SU 236006
70. Patwardhan GV, Zimmer H, Mark JE (1997) J Inorg Organomet Polym 7(2):93
71. Zhao Q, Mark JE (1990) Polym Prep 31(1):303
72. Patwardhan DV, Zimmer H, Mark JE (1996) Polym Prep 37:294
73. Giori C, Zerlaut GA (1973) J Polym Sci Polym Chem Ed 11(3):509
74. Zhao Q, Mark JE (1992) Macromol Rep A 29:221

75. Green JW, Rubal MJ, Osman BM, Welsch RL, Cassidy PE, Fitch JW, Blanda MT (2000) Polym Adv Technol 11:820
76. Zhou H, Venumbaka SR, Fitch JW III, Cassidy PE (2003) Macromol Symp 192:115
77. Manseri A, Ameduri B, Boutevin B, Caporiccio G (1997) J Fluorine Chem 81:103
78. Kim Y (1972) Siloxane Elastomers, US patent 3,542,830 (assigned to Dow Corning)
79. Riley MO, Kim YK, Pierce OR (1977) J Fluorine Chem 10:85
80. Loree L, Pierce O, Kim Y (1970) (Dow Corning), US 3647740
81. Kim YK (1974) US patent 3,818,064 (assigned to Dow Corning)
82. Ameduri B, Boutevin B (2004) Well architectured fluoropolymers; synthesis, properties and applications. Amsterdam, Elsevier
83. Modena M, Pianca M, Tato M, Moggi G (1989) J Fluorine Chem 43:15
84. Okawa T (2002) Eur Pat Appl 1,146,048 A2 (assigned to Dow Corning Toray Silicone)
85. Boutevin B, Caporiccio G, Guida-Pietrasanta F, Ratsimihety A (1999) Europ Patent Appl 1,097,958 (assigned to Daikin)
86. Thomas TH, Kendrick TC (1969) J Polym Sci A 7:537
87. Kim YK (1974) US patent 3,818,064 (assigned to Dow Corning)
88. Boutevin B, Caporiccio G, Guida-Pietrasanta F, Ratsimihety A (1997) Main Group Metal Chem 20:133
89. Boutevin B, Caporiccio G, Guida-Pietrasanta F, Ratsimihety A (1997) Recent Res Dev Polym Sci 1:241–248
90. Boutevin B, Caporiccio G, Guida-Pietrasanta F, Ratsimihety A (1998) Macromol Chem Phys 199:61
91. Maxson M, Norris AW, Owen MJ (1997) In: Scheirs J (ed) Modern Fluoropolymer. Wiley, Chichester, Chap 20:359
92. Legrand DG, Gaine GL (1969) J Colloid Interface Sci 31(2):162
93. Kobayashi H, Owen MJ (1995) Trends Polym Sci 3:10
94. Kobayashi H, Owen MJ (1993) Makromol Chem 194(6):1785
95. Grunlan MA, Lee NS, Weber WP (2005) Polym Prep 46(1):407
96. Owen MJ, Groh J (1990) J Appl Polym Sci 40:789
97. Shafrin EG, Zisman WA (1964) Adv Chem Ser 43:145
98. Owen MJ (1988) J Appl Polym Sci 35(4):895
99. Kobayashi H (1993) US 5300670 (Dow Corning Toray Silicone)
100. Hamada Y, Kobayashi H, Nishiumi W (1995) US 5578381 (Dow Corning Toray Silicone)
101. Kobayashi H, Honma H, Masatomi T (2000) US 6303675 (Dow Corning Toray Silicone)
102. Kobayashi H, Masatomi T (1996) US 5880227 (Dow Corning Toray Silicone)
103. Kobayashi H, Masatomi T (1996) US 5681914 (Dow Corning Toray Silicone)
104. Thünemann A, Kublicas R (2001) J Mater Chem 11(2):381
105. Bertolucci M, Galli G, Chiellini E, Wynne KJ (2004) Macromolecules 37:3666
106. Takago T, Inomata H, Sato S, Kinami H (1994) US 5342913 (Shinetsu Chemical Co)
107. Inomata H, Kishita H, Sato S, Koike N, Matsuda T (1993) US 5310846
108. Hamdani S, Longuet C, Perrin D, Lopez Cuesta JM, Ganachaud F (2009) Polym Degrad Stab 94:465
109. Battjes K (1995) Macromolecules 28:790
110. Kuo CM, Battjes K (1997) Rubber Chem Technol 70:769
111. Ameduri B, Boutevin B, Guida-Pietrasanta F, Manseri A, Ratsimehty A (1996) J Polym Sci A, Polym Chem 34:3077
112. Andre S, Guida-Pietrasanta F, Rousseau A, Boutevin B, Caporiccio G (2002) J Polym Sci Part A, Polym Chem 40:4485
113. Fox T, Flory P (1950) J Appl Phys 21:581
114. Fox T, Flory P (1954) J Polym Sci A, Polym Chem 14:315
115. Rizzo J, Harris FW, Fox T, Flory P (2000) Polymer 41:5125
116. Grassie N, Macfarlane IG, Francey KF (1979) Eur Polym J 15:415
117. Conrad MP, Shoichet MS (2007) Polymer 48:5333
118. Boutevin B, Caporiccio G, Guida-Pietrasanta F (2003) J Fluorine Chem 124:131

119. Boutevin B, Caporiccio G, Rousseau A (2001) EP 1097957 (Daikin Ind LTD)
120. Kim Y, O'Riley M (1976) US 3975362 (Dow corning)
121. Gomez-Anton MR, Masegosa RM, Horta A (1987) Polymer 28:2116
122. Strepparola E, Caporiccio G (1984) Ind Eng Chem Prod Res Dev 24:4
123. Evans ER (1981) US 4355121 (General Electric)
124. Bush RB, Evans ER (1983) US 4525528 (General Electric)
125. Evans E (1992) EP 520777 (General Electric)
126. Yerrick KB, Beck HN (1964) Rubber Chem Technol 37:261
127. Appetecchi G, Alessandrini F, Passerini S, Caporiccio G, Boutevin B, Guida-Pietrasanta F (2004) Electrochem Acta 50:149
128. Chaffee R, Siegel RA, Voci RJ (1992) EP 0542471 (Dow corning)
129. Singh N, Leman JT, Morgan JM (2002) EP 1176173 (General electric)
130. Irish PT, Maxson MT (1997) EP 0761762 Dow corning
131. Maxson MT (1988) Dow corning
132. Maxson MT (1991) US 5302632 Dow corning
133. Matsushita T, Shigehisa Y (1993) US 5378742 Dow corning toray silicone
134. Kobayashi H (1995) US 5428097 Dow corning toray silicone
135. Kobayashi H (1995) EP 0656391 Dow corning toray silicon
136. Kobayashi H (1995) EP 0636663 Dow corning toray silicon
137. Mize K, Takashi M, Kishita H, Oyama M (1993) US 5264522 Shin Etsu Chemical Co
138. Vaidya A, Chaudhury MK (2002) J Colloid Interface Sci 249:235
139. Hou A, Yu J, Shi Y (2008) Eur Polym J 44:1696
140. Tang C, Liu W, Ma S, Wang Z, Hu C (2010) Prog Org Coat 69:359
141. Suzuki H, Takeishi M, Narisawa I (2000) J Appl Polym Sci 78:1955
142. Baradie B, Lai PHM, Soichet M (2005) Can J Chem 83:553
143. Maraboti I, Morelli A, Orsini LM, Martinelli E, Galli G, Chiellini E, Lien EM, Pettitt ME, Callow ME, Callow JA, Conlan SL, Mutton RJ, Clare A, Kocijan A, Donik C, Jenko M (2009) Biofouling 25:481
144. Mielczarski JA, Mielczarski E, Galli G, Morelli A, Martinelli E, Chiellini E (2010) Langmuir 26:2871
145. Liang J, He L, Zhao X, Dong X, Luo H, Li W (2011) J Mater Chem 21:6934
146. Luo Z, He T, Yu H, Dai L (2008) Macromol React Eng 2:398
147. Zhang W, Zheng Y, Orsini L, Morelli A, Galli G, Chiellini E, Carpenter EE, Wynne KJ (2010) Langmuir 26:5848
148. Hung MH, Ameduri B (2010) World Pat WO2011/071599 and US2012/8,138,274 (CNRS–DuPont Performance Elastomers)
149. Boyer C, Ameduri B, Hung MH (2010) Macromolecules 43:3652
150. Darras V, Fichet O, Perrot F, Boileau S, Teyssie D (2007) Polymer 48:687
151. Scheirs J (1997) In: Scheirs J (ed) Modern fluoropolymers. Wiley, New York, p 435, Chap. 24
152. Yamaguchi H, Koike N, Takewaki K (2010) US 2010/0324250 (assigned to Shin Etsu)
153. Ato S, Arai M, Osawa Y, Sato M (2003) Europ Pat 1,288,243 A1 (assigned to Shin Etsu)
154. Uritani P (2002) High Performance Elastomers. In: Conference, November 13–14, Koln, Germany. Paper #14
155. Wilcek L (2011) WO 2011/011653 (DuPont de Nemours)
156. Ergengother A (1996) High Performance Polymers 55:787
157. Owens D, Wendt R (1969) J Appl Polym Sci 13:1741
158. Fowkes F (1962) J Phys Chem 66:382
159. Fowkes F (1964) Adv Chem Ser 43:99
160. Hauser R, Walkers CA, Kilbourne FL (1956) Ind Eng Chem 48:1202
161. Boyer R, Dow Chemical CO, Unpublished Data (Chemica Co)
162. Mangaraj D, Patra S, Rashid S (1963) Makromol Chem 65:39

Chapter 6
The Design of Non-wetting Surfaces with FluoroPOSS

Anish Tuteja and Joseph M. Mabry

6.1 Introduction

6.1.1 Non-wetting Surfaces

Non-wetting surfaces and materials that affect wetting resistance are desirable for a wide variety of military, commercial, and specialty applications. The simplest measure of wetting on a smooth surface is the equilibrium contact angle θ, given by Young's equation [1] as

$$\cos\theta = \frac{\gamma_{SV} - \gamma_{SL}}{\gamma_{LV}} \tag{6.1}$$

where γ refers to the interfacial tension and S, L, and V refer to the solid, liquid, and vapor phases, respectively. The solid–vapor interfacial tension (γ_{SV}) and the liquid-vapor interfacial tension (γ_{LV}) are also commonly referred to as the solid surface energy and the liquid surface tension, respectively. Smooth surfaces that display contact angles $\theta > 90°$ with water are considered hydrophobic, while smooth surfaces that display contact angles $\theta < 90°$ with water are considered hydrophilic. In recent years, a new class of '*superhydrophobic*' surfaces has emerged (see Chap. 4). These surfaces display contact angles greater than 150° and low contact angle hysteresis—the difference between the advancing and the receding contact angles (see

A. Tuteja (✉)
Department of Materials Science and Engineering, University of Michigan, Ann Arbor, MI 48109, USA
e-mail: ATuteja@umich.edu

J.M. Mabry (✉)
Space and Missile Propulsion Division, Air Force Research Laboratory, Edwards AFB, CA 93524, USA
e-mail: Joseph.Mabry@edwards.af.mil

M.J. Owen, P.R. Dvornic (eds.), *Silicone Surface Science*, Advances in Silicon Science 4,
DOI 10.1007/978-94-007-3876-8_6, © US Government 2012

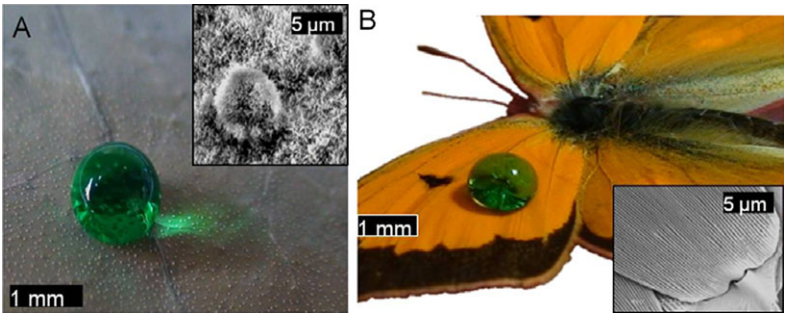

Fig. 6.1 (**A**) A droplet of water (*colored green*) on a superhydrophobic lotus leaf surface. The inset is an SEM image, highlighting the multiple scales of texture present on the lotus leaf surface. (**B**) A droplet of water (*colored green*) on top of a butterfly (*Colias fieldi*) wing. The *inset* is an SEM image illustrating the texture of the butterfly wing. Images adapted from Ref. [17] with kind permission of © Elsevier (2009)

Chap. 1) [2, 3]. Note that all superhydrophobic surfaces are textured (or rough), as the maximum water contact angle measured on a smooth surface is ∼125°–130° [4–6]. Superhydrophobicity is pervasive in nature (see Fig. 6.1) with various plant leaves [7–9], legs of the water strider [10–12], gecko's feet [13, 14], troughs on the elytra of desert beetles [15], and insect wings [16] displaying these water-repelling characteristics.

In a similar manner, based on their respective contact angles with oil, it is possible to classify surfaces as oleophilic ($\theta < 90°$), oleophobic ($\theta > 90°$), or superoleophobic ($\theta^* > 150°$). Here, θ^* refers to the apparent contact angles, i.e. the contact angle on a textured or rough surface. In spite of numerous natural superhydrophobic surfaces, there are no known naturally occurring oleophobic or superoleophobic surfaces. This is because oils possess significantly lower surface tension values than water and consequently spread on most natural and synthetic surfaces.

6.1.2 FluoroPOSS

Due to their low surface energy, fluorinated compounds are a logical choice for materials used in the creation of non-wetting surfaces. Polyhedral molecules may also contribute positively to wetting resistance by helping to increase roughness in the produced surfaces. For these reasons, fluorinated polyhedra are highly desired. Polyhedral Oligomeric SilSesquioxane (POSS) [18] compounds are comprised of a silicon–oxygen core that is surrounded by organic functionality. They have received much interest as robust nanometer-sized building blocks for the development of high performance materials and for use in several commercial, military, and specialty applications [19–21].

For the purposes of this chapter, FluoroPOSS (Fluorinated Polyhedral Oligomeric SilSesquioxanes), are described as POSS cages that are surrounded by fluoroalkyl

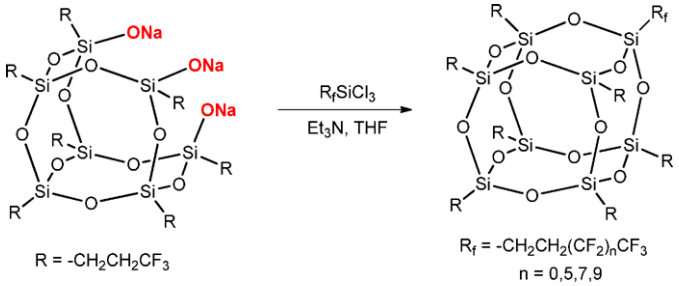

Scheme 6.1 The base-catalyzed "corner-capping" reaction of hepta(3,3,3-trifluoropropyl)tricycloheptasiloxane trisodium silanolate with fluoroalkyltrichlorosilanes of varying chain length to produce unsymmetrical, completely condensed FluoroPOSS compounds

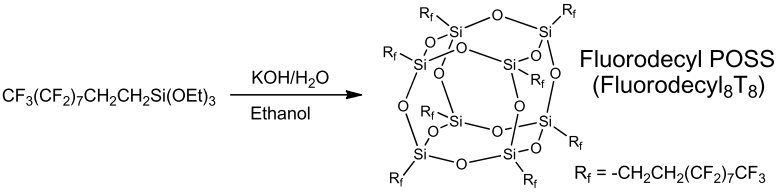

Scheme 6.2 The direct synthesis of symmetrical, completely condensed FluoroPOSS compounds via the single-step, base-catalyzed condensation of fluoroalkyltrialkoxysilanes in alcoholic solvent

functional groups with no surrounding hydrocarbon periphery, other than the methylene groups immediately adjacent to the silicon atoms. There are several possible methods to produce a range of different fluorinated POSS (FluoroPOSS) compounds [22–25]. In one case, hepta(3,3,3-trifluoropropyl)tricycloheptasiloxane trisodium silanolate was used as an intermediate for the preparation of FluoroPOSS compounds by "corner-capping" with fluoroalkyltrichlorosilanes (Scheme 6.1) [22]. Hepta(3,3,3-trifluoropropyl)tricyclohepta-siloxane trisodium silanolate was isolated as an intermediate and reacted with fluoroalkyltrichlorosilanes of varying chain length. Reaction with (3,3,3-trifluoropropyl)trichlorosilane produces octahedral (3,3,3-trifluoropropyl)$_8$Si$_8$O$_{12}$(Fluoropropyl POSS). Reaction with trichlorosilanes of longer fluoroalkyl chain length results in unsymmetrical, completely condensed FluoroPOSS compounds. Branched and ether-containing fluoroalkyl groups have also been attached using this method.

Another synthetic method was used to produce octameric FluoroPOSS cages directly from the starting silanes in nearly quantitative yields [24]. This method proceeds *via* the single-step, base-catalyzed condensation reaction of fluoroalkyltrialkoxysilanes. For example, synthesis of octameric (1H,1H,2H,2H-heptadecafluorodecyl)$_8$Si$_8$O$_{12}$ POSS (Fluorodecyl POSS or Fluorodecyl$_8$T$_8$) was achieved *via* condensation of (1H,1H,2H,2H-heptadecafluorodecyl)triethoxysilane in alcoholic solvent, as shown in Scheme 6.2. This method has been employed successfully to produce octahedral FluoroPOSS compounds possessing 3, 6, 8, 10, and 12 carbon atoms in each fluoroalkyl chain. Attempts to produce octahe-

dral (3,3,3-trifluoropropyl)$_8$Si$_8$O$_{12}$(Fluoropropyl POSS) *via* a similar condensation reaction of either (3,3,3-trifluoropropyl)trichlorosilane or (3,3,3-trifluoropropyl)-trimethoxysilane resulted in mixtures of completely condensed POSS cages possessing 8, 10, and 12 silicon atoms, respectively, which led to the use of the "corner-capping" method.

FluoroPOSS compounds are generally soluble in fluorinated solvents. Unlike most non-fluorinated POSS compounds, TGA analysis indicates that FluoroPOSS compounds tend to volatilize, rather than decompose, with no residue remaining after heating under nitrogen or dry air. Fluorodecyl POSS is the most stable compound, evaporating at ~325 °C. FluoroPOSS compounds are also very dense, high molecular weight materials. For example, the molecular weight and density of Fluorodecyl POSS are 3993.54 g/mol and 2.067 g/cc, respectively. Several groups have developed and examined theoretical models for the structure [26], miscibility [27], and wetting behavior [6, 28, 29] of these compounds and their surfaces.

Because of their interesting properties, FluoroPOSS compounds have been examined for use in a variety of applications, including non-wetting and antibacterial fabrics and meshes [30–33] and ice-phobic surfaces [34]. However, the majority of research involving FluoroPOSS has centered around the idea of non-wetting polymers and surfaces [6, 23, 29, 35–42]. Many groups have reported alternative compounds described as FluoroPOSS, Fluorinated POSS, F-POSS, or POSS-F, but these compounds are either hydrocarbon-surrounded POSS cages with a low number of fluoroalkyl groups [43–46], or non-fluorinated POSS compounds combined with fluorinated polymers [47–51], or both.

6.1.3 Design Parameters

The design of super-repellent surfaces typically involves the manipulation of two key surface parameters, the substrate surface energy (γ_{SV}) and the surface roughness or texture [52–57]. A droplet of liquid on a textured substrate can adopt one of the following two configurations to minimize its overall free energy [2, 55, 56, 58, 59]. In the first case, as shown in Fig. 6.2A and B, the contacting liquid droplet may completely cover all of the substrate surface asperities, forming the so-called 'fully wetted' interface. In this state, the apparent contact angles are calculated using the Wenzel relation [52], given as

$$\cos\theta^* = r\cos\theta \tag{6.2}$$

Here r is the surface roughness defined as actual surface area divided by projected surface area. On the other hand, for an extremely rough surface, a 'composite' interface may lead to a lower overall free energy. In this case, the rough surface is not fully wetted by a liquid, and pockets of air remain trapped underneath the liquid droplet (see Figs. 6.2C and D). In contrast to a fully wetted interface, the composite interface typically leads to low contact angle hysteresis and low roll-off angles

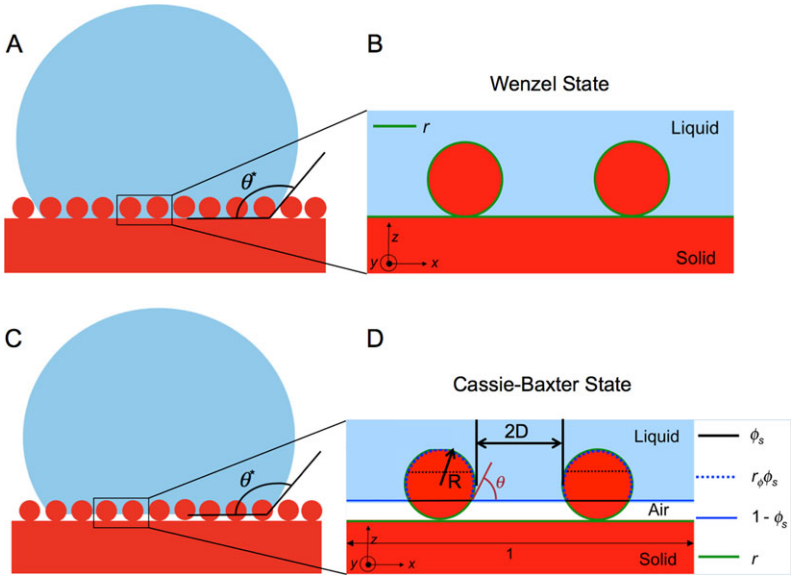

Fig. 6.2 (**A**) A schematic illustration of the Wenzel state with the liquid droplet filling in the various asperities present on the surface. (**B**) A magnified view of the schematic shown in (**A**). (**C**) A schematic illustration of the Cassie–Baxter state with the liquid droplets sitting partially on the solid substrate and partially on pockets of air, forming a composite interface. (**D**) A magnified view of the schematic shown in (**C**). Note that the local contact angle for the liquid on the solid substrate is equal to Young's contact angle θ

[3, 54, 60]. The apparent contact angle in this state is typically calculated using the Cassie–Baxter model [53], from the following equation:

$$\cos\theta^* = r_\phi \phi_s \cos\theta - 1 + \phi_s \tag{6.3}$$

Here ϕ_s is the fraction of the projected area wet by the liquid, and r_ϕ is the roughness of the wetted area. When $\phi_s = 1$ (fully wetted surface), $r_\phi = r$, and the Cassie–Baxter relation reduces to the Wenzel relation. Extremely non-wetting surfaces must be able to support a composite interface with various contacting liquids, as the Cassie–Baxter state typically yields both high apparent contact angles and low contact angle hysteresis. In recent work, we [6, 29, 32] and others [61–64] have explained how *re-entrant surface texture*, in conjunction with surface chemistry and roughness, can be used to support a composite interface, even with extremely low surface tensions liquids such as various oils and alcohols.

The systematic design of non-wetting surfaces with any contacting liquid requires the parameterization of two important physical characteristics for a composite interface: The magnitude of the observed apparent contact angle θ^*, and the magnitude of the breakthrough pressure, i.e., the external pressure which, when applied upon a contacting liquid, can force a transition from the composite Cassie–Baxter state to the fully wetted Wenzel state.

As mentioned earlier, the apparent contact angles for a composite interface are typically predicted using the Cassie–Baxter relation Eq. (6.2). In our recent work

[6, 29] we discussed a design parameter, the spacing ratio D^*, which provides a dimensionless measure of the surface porosity. For substrates possessing a predominantly spherical or cylindrical texture, $D^* = (R + D)/R$, where R is the radius of the cylinders (or spheres) and $2D$ is the inter-cylinder spacing (see Fig. 6.4D). Based on this definition of the spacing ratio, the Cassie–Baxter relation Eq. (6.2) may be re-written as

$$\cos\theta^* = -1 + \frac{1}{D^*}\left[\sin\theta + (\pi - \theta)\cos\theta\right] \tag{6.4}$$

Higher values of D^* correspond to a higher fraction of air in the composite interface. It is evident from Eq. (6.4) that θ^* increases with increasing values of D^*.

In our recent work [29, 32], we also discussed the robustness factor A^*, which is the ratio of the breakthrough pressure ($P_{\text{breakthrough}}$) to a reference pressure $P_{\text{ref}} = 2\gamma_{\text{LV}}/l_{\text{cap}}$. Here $l_{\text{cap}} = \sqrt{\gamma_{\text{LV}}/\rho g}$ is the capillary length for the liquid, ρ is the fluid density, and g is the acceleration due to gravity. P_{ref} is close to the minimum possible pressure differential across a millimeter sized liquid droplet or puddle. As a consequence, any substrate on which the robustness factor $A^* \leq 1$ for a given contacting liquid, cannot support a composite interface. On the other hand, values of A^* significantly greater than unity imply the formation of a robust composite interface able to support high breakthrough pressures. For surfaces possessing a cylindrical texture, the robustness factor is given by the relation

$$A^* = \frac{P_{\text{breakthrough}}}{P_{\text{ref}}} = \frac{Rl_{\text{cap}}}{D^2}\frac{(1 - \cos\theta)}{(1 + 2(R/D)\sin\theta)} \tag{6.5}$$

The optimal superhydrophobic or superoleophobic surfaces are expected to simultaneously display high contact angles and high breakthrough pressures with the contacting liquid, i.e. both $D^* \gg 1$ and $A^* \gg 1$.

6.2 Preparation of Materials

6.2.1 Fluorodecyl POSS Synthesis

This synthesis was performed as described previously in Refs. [24, 40] and [6]. 1H,1H,2H,2H-Heptadecafluorodecyltriethoxysilane (6.10 g), deionized water (0.27 g), and KOH (2.088 mg) were added to a 10 mL volumetric flask. The balance of the volume was filled with ethanol. Contents were transferred to a 25 mL round-bottomed flask with a Teflon covered magnetic stir bar and stirred at room temperature overnight. A fine white powder was formed. The product was rinsed with ethanol and dried. A 94.3 % yield of pure Fluorodecyl POSS was obtained. ^{29}Si NMR ($(CD_3)_2CO$, 59.6 MHz): $\delta = -67.0$ ppm.

6.2.2 FluoroPOSS Composite Preparation

6.2.2.1 Materials

Asahiklin AK-225G (1,3-dichloro-1,1,2,2,3-pentafluoropropane) was purchased from Asahi Glass Co. PMMA ($M_w = 540{,}000$, $PDI \approx 2.2$) was purchased from Scientific Polymer Products, Inc. Tecnoflon (BR9151), a commercial fluoroelastomer, was obtained from Solvay-Solexis. All other reagents were purchased from commercial sources and purified according to established procedures [65].

6.2.2.2 Spin-cast Surfaces

Both the polymer and fluoroPOSS were dissolved in a common hydrochlorofluorocarbon solvent, Asahiklin AK-225G, at a concentration of 5 mg/mL, and the rotation speed during spin-coating was set at 900 rpm.

6.2.2.3 Electrospun Surfaces

Both the polymer and fluoroPOSS were dissolved in Asahiklin AK-225G at a concentration of ∼5 wt.%. The solution was then electrospun using a custom-built apparatus with the flow rate, plate-to-plate distance and voltage set to 0.05 mL/min, 25 cm and 20 kV, respectively.

6.2.2.4 Dip-coated Surfaces

For the dip-coating process, a solution of fluorodecyl POSS (50 wt.%) and Tecnoflon in Asahiklin AK-225G was prepared at an overall solid concentration of 10 mg/mL. The use of Tecnoflon as a polymeric binder inhibits the crystallization of fluorodecyl POSS, and yields a more conformal and elastomeric coating. The substrate was then immersed in the fluorodecyl POSS-Tecnoflon solution. After 5 min, the substrate was removed from the solution and dried in a vacuum oven for 30 min at a temperature of 60 °C.

6.3 Characterization Techniques

6.3.1 Contact Angle Analysis

The contact angles for various liquids were measured using a contact angle goniometer, VCA2000 (AST Inc.). The advancing contact angle was measured by advancing a small volume of the probing liquid (typically 2–4 μL) on to the surface, using a syringe. The receding contact angle was measured by slowly removing the probing liquid from a drop already on the surface. For each sample a minimum of four different readings were recorded. Typical error in measurements was ∼2°.

6.3.2 Microscopy

6.3.2.1 Atomic Force Microscopy (AFM)

Atomic Force Microscopy (AFM) was conducted on a Nanoscope IV controller (3100 SPM Head) in tapping mode. Etched silicon probes of nominal spring resonance 300 kHz (spring constant approx. 0.3 mN m^{-1}) were used for light tapping (driving amplitude ca 1.1 V) of varying section size at 1–2 Hz collection times (512 points/line).

6.3.2.2 Scanning Electron Microscopy (SEM)

A JEOL-6060SEM (JEOL Ltd., Japan) Scanning Electron Microscope (SEM) was used for imaging. Before imaging, the electrospun surfaces were sputter-coated with a 5–10 nm layer of gold by use of a Desk II cold sputter/etch unit (Denton Vacuum LLC).

6.4 FluoroPOSS Material Properties

6.4.1 FluoroPOSS Compounds

Zisman demonstrated that the surface energy for organic molecules decreases with an increase in the degree of fluorination, and results in the surface energy for $–CH_3$ > $–CH_2F$ > $–CHF_2$ > $–CF_3$ [66]. The high concentration of perfluorinated carbon atoms in the alkyl chains surrounding each FluoroPOSS cage leads to extremely low surface energy values for these molecules [24, 66, 67]. As synthesized, fluorodecyl POSS molecules possess one of the lowest known solid surface energies ($\gamma_{SV} \approx$ 8 mN m^{-1}) [4–6]. In comparison, Teflon, has a surface energy of $\gamma_{SV} \approx 17$ mN m^{-1}. A film of fluorodecyl POSS, spin-coated on a Si wafer and having an rms roughness of 3.5 nm (this corresponds to a Wenzel surface roughness $r = 1.005$) displays an advancing (θ_{adv}) and receding (θ_{rec}) contact angle of $124.5 \pm 1.2°$. This is one of the highest water contact angles reported for a smooth substrate [5], and emphasizes the extremely low surface energy of the fluorodecyl POSS molecules.

6.4.2 FluoroPOSS Composites

The addition of fluorodecyl POSS molecules to different polymers leads to a rapid decrease in the overall surface energy of the synthesized composites, and also provides a facile route to systematically tune the surface energy of the produced composite over a very wide range. For example, we studied composites formed by blending fluorodecyl POSS molecules with a relatively hydrophilic polymer, poly(methyl

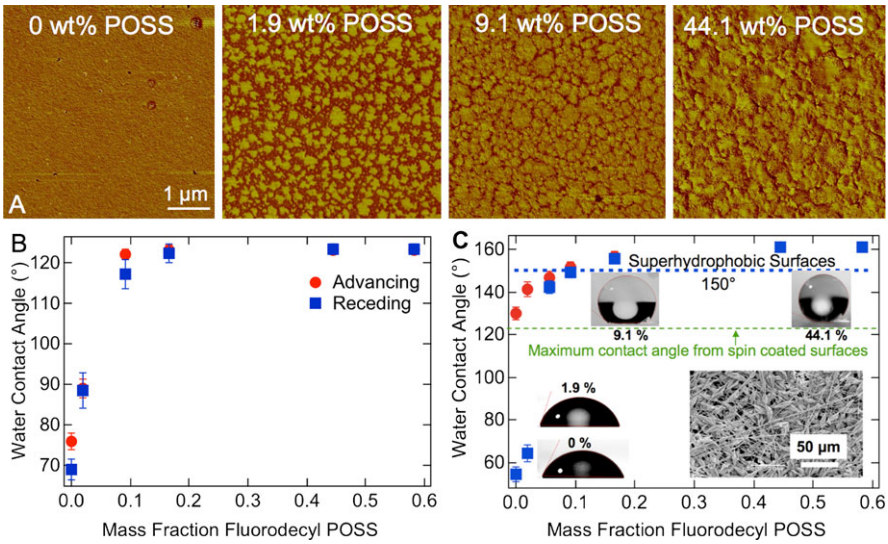

Fig. 6.3 (**A**) AFM phase images for neat PMMA and PMMA blends with fluorodecyl POSS. The phase angle scale on the AFM images is 0–10° for the 0, 9.1 and 44 wt.% POSS images and 0–90° for the 1.9 wt.% POSS image. (**B**) The advancing and receding contact angles for water on spin–coated surfaces composed of neat PMMA and its blends with fluorodecyl POSS. (**C**) The apparent advancing (*red dots*) and receding (*blue dots*) contact angles for water on various electrospun surfaces composed of PMMA and fluorodecyl POSS. The inset shows an SEM micrograph for an electrospun surface composed of PMMA + 9.1 wt.% fluorodecyl POSS. Adapted from Ref. [67] with kind permission of ©The American Association for the Advancement of Science (2007)

methacrylate) (PMMA). The addition of fluorodecyl POSS molecules allowed us to systematically tune the surface energy of the produced composites within the range $\gamma_{SV} = 9$–$35\ \mathrm{mN\,m^{-1}}$ [67, 68]. Figure 6.3A shows AFM phase images for various spin-coated blends of PMMA and fluorodecyl POSS. A comparison between the phase images for neat PMMA and for PMMA + 1.9 wt.% fluorodecyl POSS indicates significant surface segregation (or blooming) of fluorodecyl POSS molecules towards the air interface, due to their extremely low surface energy [6]. As a result, only a small amount of fluorodecyl POSS (∼10 wt.%) is needed to sufficiently cover the surface of the spin-coated blend. Figure 6.3B shows the advancing and receding contact angles for various spin-coated PMMA + fluorodecyl POSS blends. For fluorodecyl POSS, concentrations greater than ∼10 wt.%, both the advancing and receding contact angles reach a plateau at $\sim\theta_{adv} = \theta_{rec} = 123°$.

Figure 6.3C shows the corresponding contact angles on electrospun fabric surfaces possessing the so-called beads-on-a-string morphology. The insert shows the morphology of a typical electrospun mat, and highlights both the porosity and the re-entrant curvature present in the fabricated surfaces. It is clear that electrospun blend surfaces containing greater than ∼10 wt.% POSS are superhydrophobic, displaying both θ^*_{adv} and $\theta^*_{rec} > 150°$.

The re-entrant curvature inherently present in the electrospun fabric surface creates the potential to form a composite interface with any liquid with a Young's

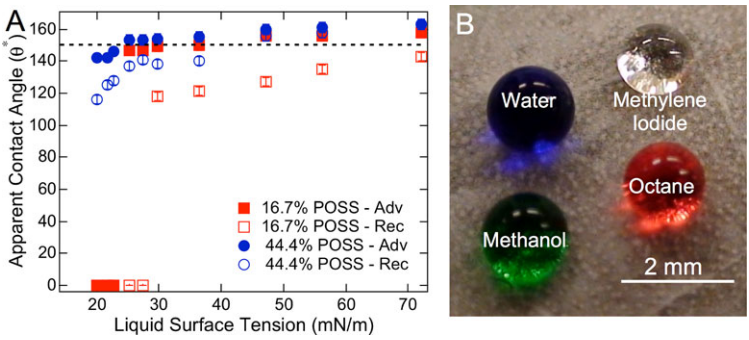

Fig. 6.4 (**A**) The apparent advancing (*filled symbols*) and receding (*open symbols*) contact angles as a function of the liquid surface tension for the electrospun surfaces possessing a beads-on-a-string morphology. The electrospun surfaces are composed of PMMA with either 16.7 wt.% or 44.1 wt.% fluorodecyl POSS. (**B**) Droplets of water ($\gamma_{LV} = 72.1$ mN m^{-1}), methylene iodide ($\gamma_{LV} = 50.1$ mN m^{-1}), methanol ($\gamma_{LV} = 22.7$ mN m^{-1}) and octane ($\gamma_{LV} = 21.7$ mN m^{-1}) on an electrospun surface composed of PMMA + 44 wt.% fluorodecyl POSS, possessing a beads-on-a-string morphology. The electrospun substrate is able to support a composite interface with all contacting liquids, as indicated by the presence of a reflective surface visible underneath all droplets [6]. Reported values are for undyed liquids. Adapted from Ref. [29] with kind permission of © The National Academy of Science (2008)

contact angle greater than 0°, provided the robustness factor $A^* > 1$ [29, 32]. Figure 6.4A shows the apparent advancing and receding contact angles on the electrospun surfaces containing 16.7 wt.% and 44.1 wt.% fluorodecyl POSS, for a series of liquids with surface tension values in the range of $\gamma_{LV} = 20.1$–72.1 mN m^{-1}. Due to the high porosity inherent in the electrospun mat ($D^* = 9$), the synthesized electrospun surfaces display extremely high apparent contact angles with a wide range of liquids (see Fig. 6.4B). For example, for hexadecane ($\gamma_{LV} = 27.5$ mN m^{-1}), $\theta^*_{adv} = 153°$ and $\theta^*_{rec} = 141°$. Further, due to their extremely small dimensions ($R \sim 500$ nm), the electrospun fibers also possess very high values of robustness factor [29]. For example, for the electrospun fibers containing 44.4 wt.% fluorodecyl POSS, $A^* = 40$ with hexadecane.

As mentioned previously, there are no naturally occurring oleophobic or superoleophobic surfaces. The insert in Fig. 6.5A shows droplets of rapeseed oil ($\gamma_{LV} = 35.7$ mN m^{-1}) on top of a lotus leaf. Evaluating the magnitude of the robustness factor ($A^* \ll 1$) helps explain why rapeseed oil spontaneously wets the leaf structure in spite of the presence of re-entrant texture [29]. To allow the leaf surface to support a composite interface with low surface tension liquids such as various oils, it is necessary to significantly increase the value of the robustness factor A^*. Based on Eq. (6.5), for a fixed substrate texture, it is clear that the magnitude of A^* is most easily increased by increasing the value for Young's contact angle θ. We use the dip-coating process to provide a conformal coating of fluorodecyl POSS molecules on top of the lotus leaf surface. This leads to a significant increase in the magnitude of Young's contact angle ($\theta = 86°$) and correspondingly the value of the robustness factor on the dip-coated lotus leaf ($A^* = 26$) [29]. As a result, the

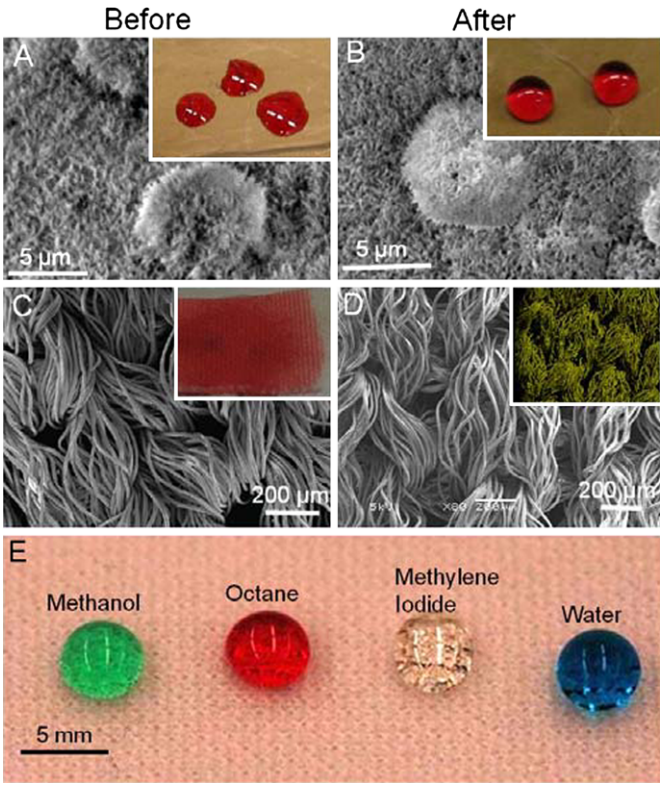

Fig. 6.5 (**A**) An SEM image of the lotus leaf surface before the dip-coating process. The insert shows the extremely low apparent contact angle ($\theta^* \sim 10°$) observed for rapeseed oil (*colored red*) on top of the lotus leaf surface. (**B**) An SEM image of the lotus leaf surface after the dip-coating process. The insert shows the high apparent contact angles observed for rapeseed oil on the dip-coated lotus leaf surface ($\theta^* = 145°$). (**C**) An SEM image illustrating the morphology of a commercially available polyester fabric. The insert shows that a droplet of hexadecane ($\gamma_{LV} = 27.5$ mN m^{-1}) readily wets the fabric surface. (**D**) An SEM image illustrating the morphology of the polyester fabric after the dip-coating process. The insert shows the elemental mapping for fluorine on the dip-coated fabric surface, obtained using EDAXS. (**E**) Droplets of water ($\gamma_{LV} = 72.1$ mN m^{-1}), methylene iodide ($\gamma_{LV} = 50.1$ mN m^{-1}), methanol ($\gamma_{LV} = 22.7$ mN m^{-1}) and octane ($\gamma_{LV} = 21.7$ mN m^{-1}) on the dip-coated fabric surface. Reproduced from Ref. [32] with kind permission of © John Wiley & Sons, Inc. (2009)

dip-coated lotus leaf is readily able to support a composite interface with rapeseed oil and display high apparent contact angles, as illustrated in the insert of Fig. 6.5B. Figure 6.5A and 6.5B compare the surface texture of the lotus leaf before and after the dip-coating process. It is clear that the dip-coating process preserves the inherent surface texture of the lotus leaf.

Recognizing the presence of re-entrant surface features in commercial fabrics, the dip-coating process was used to deliver a coating of fluorodecyl POSS molecules onto the fabric surface, bestowing superoleophobicity. Note that Tecnoflon, a fluoro-

elastomer binder, was added to the dip-coating solution to inhibit the formation of fluorodecyl POSS crystallites and yield a more conformal and elastomeric coating.

Figure 6.5C shows an SEM micrograph for a commercially available polyester fabric, and highlights both the porosity ($D^* = 6$) and the re-entrant curvature of the fabric surface. The insert in Fig. 6.5C shows that a drop of rapeseed oil readily wets the as-obtained fabric surface. Figure 6.5D illustrates the details of the polyester fabric surface after the dip-coating process. The inset in Fig. 6.5D shows the elemental mapping for fluorine on the dip-coated fabric surface, obtained using Energy Dispersive X-Ray Scattering (EDAXS). It is clear from this image that the dip-coating process allows for the complete and conformal coating of the fabric surface by the fluorodecyl POSS molecules. After the dip-coating process, as shown in Fig. 6.5E, the fabric surface is able to support a composite interface, and display extremely high apparent contact angles with a wide range of liquids including octane ($\gamma_{LV} = 21.7\ \text{mN m}^{-1}$; $A^* = 2.5$).

6.5 Conclusions

In the design of non-wetting surfaces, surface texture has been found to be of an importance equal to or greater than that of the surface free energy and surface roughness characteristics, which are considered critical for the creation of such surfaces. This is especially the case if the surface is desired to repel low surface tension liquids, such as different oils or alcohols. The low surface energy characteristics of fluorinated Polyhedral Oligomeric SilSesquioxanes (FluoroPOSS), as well as their octahedral structure, make them desirable compounds for use in the production of non-wetting surfaces. Wetting-resistant surfaces containing FluoroPOSS were produced by a variety of methods. Design parameters were also developed to aid the rational design of non-wetting surfaces. The spacing ratio, D^*, provides a dimensionless measure of surface porosity, while the robustness factor, A^*, is a measure of a surface's resistance to liquid breakthrough. The most favorable non-wetting surface would, therefore, possess high values of both D^* and A^* simultaneously, indicating high contact angles as well as high breakthrough pressures. Production of wetting-resistant surfaces may involve techniques that specifically incorporate all three factors critical for wetting resistance, such as electrospinning. Alternatively, substrates containing the desired surface texture may be modified to bestow wetting resistance, as seen in the dip-coating of commercial fabrics.

Acknowledgements We thank Dr. Charles Y.-C. Lee and the Air Force Office of Scientific Research (AFOSR) for financial support under grants FA9550-10-1-0523 and LRIR-92PL0COR. We also thank the Air Force Research Laboratory, Propulsion Directorate for their financial support. We also thank Prof. Robert E. Cohen, Prof. Gareth H. McKinley, and Prof. Wonjae Choi for their contributions to this work and helpful conversations.

References

1. Young T (1805) An essay on the cohesion of luids. Philos Trans R Soc Lond 95:65
2. Shuttleworth R, Bailey GLJ (1948) The spreading of a liquid over a rough solid. Discuss Faraday Soc 3:16–22. doi:10.1039/DF9480300016

3. Chen W, Fadeev AY, Hsieh MC, Oner D, Youngblood J, McCarthy TJ (1999) Ultrahydrophobic and ultralyophobic surfaces: some comments and examples. Langmuir 15(10):3395–3399
4. Genzer J, Efimenko K (2000) Creating long-lived superhydrophobic polymer surfaces through mechanically assembled monolayers. Science 290(5499):2130–2133. doi:10.1126/science.290.5499.2130
5. Nishino T, Meguro M, Nakamae K, Matsushita M, Ueda Y (1999) The lowest surface free energy based on –CF3 alignment. Langmuir 15(13):4321–4323
6. Tuteja A, Choi W, Ma ML, Mabry JM, Mazzella SA, Rutledge GC, McKinley GH, Cohen RE (2007) Designing superoleophobic surfaces. Science 318:1618–1622. doi:10.1126/science.1148326
7. Barthlott W, Neinhuis C (1997) Purity of the sacred lotus, or escape from contamination in biological surfaces. Planta 202(1):1–8
8. Herminghaus S (2000) Roughness-induced non-wetting. Europhys Lett 52(2):165–170
9. Neinhuis C, Barthlott W (1997) Characterization and distribution of water-repellent, self-cleaning plant surfaces. Ann Bot 79(6):667–677
10. Hu DL, Chan B, Bush JWM (2003) The hydrodynamics of water strider locomotion. Nature 424(6949):663
11. Hu DL, Bush JWM (2005) Meniscus-climbing insects. Nature 437(7059):733
12. Gao X, Jiang L (2004) Biophysics: water-repellent legs of water striders. Nature 432(7013):36
13. Autumn K, Liang YA, Hsieh ST, Zesch W, Chan WP, Kenny TW, Fearing R, Full RJ (2000) Adhesive force of a single gecko foot-hair. Nature 405(6787):681–685
14. Genzer J, Efimenko K (2006) Recent developments in superhydrophobic surfaces and their relevance to marine fouling: a review. Biofouling 22(5):339–360
15. Parker AR, Lawrence CR (2001) Water capture by a desert beetle. Nature 414(6859):33
16. Wagner T, Neinhuis C, Barthlott W (1996) Wettability and contaminability of insect wings as a function of their surface sculptures. Acta Zool 77(3):213–225
17. Choi W, Tuteja A, Mabry JM, Cohen RE, McKinley GH (2009) A modified Cassie–Baxter relationship to explain contact angle hysteresis and anisotropy on non-wetting textured surfaces. J Colloid Interface Sci 339(1):208–216
18. POSS is a registered trademark of Hybrid Plastics Inc., Hattiesburg, MS 39401
19. Pielichowski K, Njuguna J, Janowski B, Pielichowski J (2006) Polyhedral oligomeric silsesquioxanes (POSS)-containing nanohybrid polymers. In: Supramolecular polymers polymeric betains oligomers. Adv Polym Sci, vol 201. Springer, Berlin, pp 225–296. doi:10.1007/12_077
20. Lickiss PD, Rataboul F (2008) Fully condensed polyhedral oligosilsesquioxanes (POSS): from synthesis to application. In: Anthony FH, Mark JF (eds) Advances in organometallic chemistry, vol 57. Academic Press, San Diego, pp 1–116. Chapter 1
21. Cordes DB, Lickiss PD, Rataboul F (2010) Recent developments in the chemistry of cubic polyhedral oligosilsesquioxanes. Chem Rev 110(4):2081–2173. doi:10.1021/cr900201r
22. Iacono ST, Vij A, Grabow W, Smith JDW, Mabry JM (2007) Facile synthesis of hydrophobic fluoroalkyl functionalized silsesquioxane nanostructures. Chem Commun 47:4992–4994
23. Koh K, Sugiyama S, Morinaga T, Ohno K, Tsujii Y, Fukuda T, Yamahiro M, Iijima T, Oikawa H, Watanabe K, Miyashita T (2005) Precision synthesis of a fluorinated polyhedral oligomeric silsesquioxane-terminated polymer and surface characterization of its blend film with poly(methyl methacrylate). Macromolecules 38(4):1264–1270. doi:10.1021/ma047636l
24. Mabry JM, Vij A, Iacono ST, Viers BD (2008) Fluorinated polyhedral oligomeric silsesquioxanes (F-POSS). Angew Chem, Int Ed Engl 47(22):4137–4140
25. Xu J, Li X, Cho CM, Toh CL, Shen L, Mya KY, Lu X, He C (2009) Polyhedral oligomeric silsesquioxanes tethered with perfluoroalkylthioether corner groups: facile synthesis and enhancement of hydrophobicity of their polymer blends. J Mater Chem 19(27):4740–4745
26. Anderson SE, Bodzin DJ, Haddad TS, Boatz JA, Mabry JM, Mitchell C, Bowers MT (2008) Structural investigation of encapsulated fluoride in polyhedral oligomeric silsesquioxane cages using ion mobility mass spectrometry and molecular mechanics. Chem Mater 20(13):4299–4309. doi:10.1021/cm800058z

27. Zeng F-L et al. (2009) Molecular simulations of the miscibility in binary mixtures of PVDF and POSS compounds. Modelling and Simulation in. Mater Sci Eng 17(7):075002. http://www.scientific.net/AMR.138.107
28. Losada M, Mackie K, Osborne JH, Chaudhuri S (2010) Understanding nanoscale wetting using dynamic local contact angle method. In: Trasatti SPIJ (ed) Light weight metal corrosion and modeling for corrosion prevention, Life prediction and assessment. Advanced Materials Research, vol 138, pp 107–116. http://www.scientific.net/AMR.138.107
29. Tuteja A, Choi W, Mabry JM, McKinley GH, Cohen RE (2008) Robust omniphobic surfaces. Proc Natl Acad Sci USA 105(47):18200–18205. doi:10.1073/pnas.0804872105
30. Chhatre SS, Choi W, Tuteja A, Park K-C, Mabry JM, McKinley GH, Cohen RE (2009) Scale dependence of omniphobic mesh surfaces. Langmuir 26(6):4027–4035. doi:10.1021/la903489r
31. Chhatre SS, Tuteja A, Choi W, Revaux A, Smith D, Mabry JM, McKinley GH, Cohen RE (2009) Thermal annealing treatment to achieve switchable and reversible oleophobicity on fabrics. Langmuir 25(23):13625–13632. doi:10.1021/la901997s
32. Choi W, Tuteja A, Chhatre S, Mabry JM, Cohen RE, McKinley GH (2009) Fabrics with tunable oleophobicity. Adv Mater 21(21):2190–2195. doi:10.1002/adma.200802502
33. Vilcnik A, Jerman I, Såurca Vuk A, Kozåelj M, Orel B, Tomsåicå B, Simoncåicå B, Kovacå J (2009) Structural properties and antibacterial effects of hydrophobic and oleophobic sol–gel coatings for cotton fabrics. Langmuir 25(10):5869–5880. doi:10.1021/la803742c
34. Meuler AJ, Smith JD, Varanasi KK, Mabry JM, McKinley GH, Cohen RE (2010) Relationships between water wettability and ice adhesion. ACS Appl Mater Interfaces 2(11):3100–3110. doi:10.1021/am1006035
35. Chhatre SS, Guardado JO, Moore BM, Haddad TS, Mabry JM, McKinley GH, Cohen RE (2010) Fluoroalkylated silicon-containing surfaces, an estimation of solid-surface energy. ACS Appl Mater Interfaces 2(12):3544–3554. doi:10.1021/am100729j
36. Iacono ST, Budy SM, Mabry JM, Smith DW (2010) Polyhedral oligomeric silsesquioxane-functionalized perfluorocyclobutyl aryl ether polymers. In: Advances in silicones and silicone-modified materials. ACS symposium series, vol 1051. Am Chem Soc, Washington, pp 195–209. doi:10.1021/bk-2010-1051.ch016
37. Iacono ST, Budy SM, Mabry JM, Smith DW Jr. (2007) Synthesis, characterization, and properties of chain terminated polyhedral oligomeric silsesquioxane-functionalized perfluorocyclobutyl aryl ether copolymers. Polymer 48(16):4637–4645. doi:10.1016/j.polymer.2007.06.022
38. Iacono ST, Budy SM, Smith DW, Mabry JM (2010) Preparation of composite fluoropolymers with enhanced dewetting using fluorinated silsesquioxanes as drop-in modifiers. J Mater Chem 20(15):2979–2984
39. Iacono ST, Peloquin AJ, Dennis W, Smith J, Mabry JM (2011) Fluorinated polyhedral oligosilsesquioxane surfaces and superhydrophobicity. In: Hartmann-Thompson C (ed) Applications of polyhedral oligomeric silsesquioxanes, 1st edn. Springer, Berlin, p 392
40. Mabry Joseph M, Vij A, Viers Brent D, Grabow Wade W, Marchant D, Iacono Scott T, Ruth Patrick N, Vij I (2007) Hydrophobic silsesquioxane nanoparticles and nanocomposite surfaces. In: Science and technology of silicones and silicone-modified materials. ACS symposium series, vol 964. Am Chem Soc, Washington, pp 290–300. doi:10.1021/bk-2007-0964.ch018
41. Srinivasan S, Chhatre SS, Mabry JM, Cohen RE, McKinley GH (2011) Solution spraying of poly(methyl methacrylate) blends to fabricate microtextured, superoleophobic surfaces. Polymer 52(14):3209–3218. doi:10.1016/j.polymer.2011.05.008
42. Xue Y, Wang H, Zhao Y, Dai L, Feng L, Wang X, Lin T (2010) Magnetic liquid marbles: a “precise” miniature reactor. Adv Mater 22(43):4814–4818. doi:10.1002/adma.201001898
43. Dai L, Yang C, Xu Y, Deng Y, Chen J, Galy J, Gérard J-F (2010) Preparation of novel methyl methacrylate/fluorinated silsesquioxane copolymer film with low surface energy. Sci Chin Chem 53(9):2000–2005. doi:10.1007/s11426-010-4070-4
44. Dodiuk H, Rios PF, Dotan A, Kenig S (2007) Hydrophobic and self-cleaning coatings. Polym Adv Technol 18(9):746–750. doi:10.1002/pat.957

45. Kannan AG, Choudhury NR, Dutta N (2009) Fluoro-silsesquioxane-urethane hybrid for thin film applications. ACS Appl Mater Interfaces 1(2):336–347. doi:10.1021/am800056p
46. Rios PF, Dodiuk H, Kenig S, McCarthy S, Dotan A (2007) Transparent ultra-hydrophobic surfaces. J Adhes Sci Technol 21(5–6):399–408. doi:10.1163/156856107780474975
47. Gao Y, He C, Huang Y, Qing F-L (2010) Novel water and oil repellent POSS-based organic/inorganic nanomaterial: Preparation, characterization and application to cotton fabrics. Polymer 51(25):5997–6004. doi:10.1016/j.polymer.2010.10.020
48. Iacono ST, Budy SM, Mabry JM, Smith DW (2007) Synthesis, characterization, and surface morphology of pendant polyhedral oligomeric silsesquioxane perfluorocyclobutyl aryl ether copolymers. Macromolecules 40(26):9517–9522. doi:10.1021/ma071732f
49. Sawada H, Yoshioka H, Ohashi R, Kawase T (2002) Synthesis and properties of novel fluoroalkyl end-capped oligomers containing silsesquioxane segments. J Appl Polym Sci 86(14):3486–3493. doi:10.1002/app.10859. http://www.scientific.net/AMR.148-149.1212
50. Song L, Peng S, Shu Y (2011) Preparation of a novel functionated POSS nano-particle bearing the perfluoro aryl ether dendron. In: Liu XHJZYHJT (ed) Manufacturing processes and systems, Parts 1–2. Advanced materials research, vol 148–149, pp 1212–1216. doi:10.4028. http://www.scientific.net/AMR.148-149.1212
51. Vasilopoulou M et al. (2005) Characterization of various low- k dielectrics for possible use in applications at temperatures below 160¬∞C. J Phys Conf Ser 10(1):218
52. Wenzel RN (1936) Resistance of solid surfaces to wetting by water. Ind Eng Chem 28:988–994
53. Cassie ABD, Baxter S (1944) Wettability of porous surfaces. Trans Faraday Soc 40:546–551
54. Callies M, Quéré D (2005) On water repellency. Soft Matter 1(1):55–61
55. Marmur A (2003) Wetting on hydrophobic rough surfaces: to be heterogeneous or not to be? Langmuir 19(20):8343–8348
56. Nosonovsky M (2007) Multiscale roughness and stability of superhydrophobic biomimetic interfaces. Langmuir 23(6):3157–3161
57. Quéré D (2002) Rough ideas on wetting. Physica A, Stat Mech Appl 313(1–2):32–46
58. Johnson RE, Dettre RH (1964) Contact angle hysteresis. In: Contact angle, wettability and adhesion. ACS advances in chemistry series, vol 43. Am Chem Soc, Washington
59. Patankar NA (2003) On the modeling of hydrophobic contact angles on rough surfaces. Langmuir 19(4):1249–1253
60. Lafuma A, Quéré D (2003) Superhydrophobic states. Nat Mater 2(7):457–460
61. Ahuja A, Taylor JA, Lifton V, Sidorenko AA, Salamon TR, Lobaton EJ, Kolodner P, Krupenkin TN (2008) Nanonails: A simple geometrical approach to electrically tunable superlyophobic surfaces. Langmuir 24(1):9–14. doi:10.1021/la702327z
62. Cao L, Price TP, Weiss M, Gao D (2008) Super water- and oil-repellent surfaces on intrinsically hydrophilic and oleophilic porous silicon films. Langmuir 24(5):1640–1643. doi:10.1021/la703401f
63. Leng B, Shao Z, de With G, Ming W (2009) Superoleophobic cotton textiles. Langmuir 25(4):2456–2460. doi:10.1021/la8031144
64. Marmur A (2008) From hygrophilic to superhygrophobic: theoretical conditions for making high-contact-angle surfaces from low-contact-angle materials. Langmuir 24(14):7573–7579. doi:10.1021/la800304r
65. Armarego WLF, Chai CLL (2009) Purification of laboratory chemicals, 6th edn. Butterworth-Heinemann, Oxford. doi:10.1016/b978-1-85617-567-8.50004-4
66. Zisman WA (1964) Relation of the equilibrium contact angle to liquid and solid construction. In: Contact angle, wettability and adhesion. ACS advances in chemistry series, vol 43. Am Chem Soc, Washington
67. Tuteja A, Choi W, Ma ML, Mabry JM, Mazzella SA, Rutledge GC, McKinley GH, Cohen RE (2007) Designing superoleophobic surfaces. Science 318(5856):1618–1622
68. Tuteja A, Choi W, Mabry JM, McKinley GH, Cohen RE (2008) Engineering robust omniphobic surfaces. Proc Natl Acad Sci USA 105(47):18200–18205

Chapter 7
Langmuir Monolayers of Siloxanes and Silsesquioxanes

Alan R. Esker and Hyuk Yu

7.1 Introduction

Langmuir film formation at the air/water (A/W) interface by silicones has attracted research interest for more than sixty years. This chapter reviews the unique features of the surface pressure-area per repeat unit (Π-A) isotherm of polydimethylsiloxane (PDMS) and discusses the changes in surface viscoelastic properties determined by surface light scattering (SLS) associated with these features. The effects of molecular weight, end groups and non-methyl substituents on the isotherm are also considered. This discussion is then extended to another class of surface-active silicon containing materials, polyhedral oligomeric silsesquioxanes (POSSs). Trisilanolisobutyl-POSS and trisilanolcyclohexyl-POSS are discussed in terms of their Π-A isotherms and surface viscoelastic character and the chapter ends with a discussion of systems where POSS molecules are used as nanofillers within silicone monolayers.

7.2 Silicone Langmuir Films

Interesting chemistry, along with the unique flexibility and physical properties of the alternating Si-O backbone of silicone polymers, has led to intense study of this class of polymers [1–5]. The Si-O backbone, which is hydrophilic, along with two potentially hydrophobic substituents on the Si atom, R′ and R″, contributes to a

A.R. Esker (✉)
Department of Chemistry (0212), Virginia Tech, Blacksburg, VA 24061, USA
e-mail: aesker@vt.edu

H. Yu
Department of Chemistry, University of Wisconsin, 1107 University Avenue, Madison, WI 53706-1322, USA
e-mail: yu@chem.wisc.edu

M.J. Owen, P.R. Dvornic (eds.), *Silicone Surface Science*, Advances in Silicon Science 4,
DOI 10.1007/978-94-007-3876-8_7,

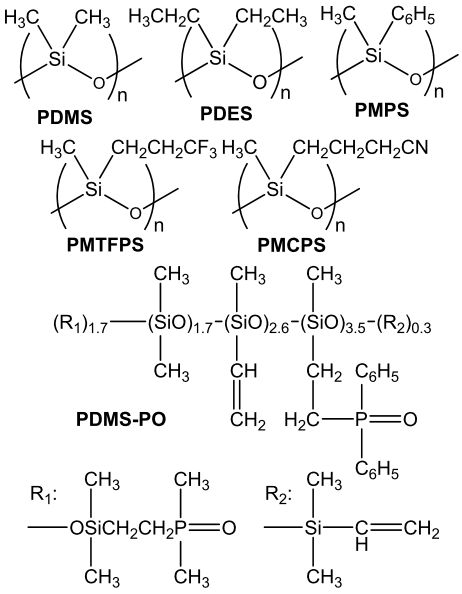

Fig. 7.1 Surface-active silicones used in this study

wide range of surface-active siloxanes [6, 7]. Figure 7.1 shows different surface-active silicones discussed in this chapter. All of these silicones form Langmuir films at the A/W interface, a topic of study that has been of interest since the first study of PDMS in 1947 [8].

7.2.1 Surface Pressure-Area per Repeat Unit (Π-A) Isotherms of PDMS Langmuir Films

In their seminal work [8] Fox et al. noted that the PDMS surface pressure-area per repeating unit (monomer for short) (Π-A) isotherm exhibits four distinct regimes. Figure 7.2 shows a representative Π-A isotherm for PDMS containing hydrophobic trimethylsilyl end groups and the four regimes Fox et al. attributed to complex structural transitions schematically depicted in Fig. 7.3.

The number average molecular weight (M_n) and polydispersity index (M_w/M_n) for the sample in Fig. 7.2 are $M_n = 3{,}260$, and $M_w/M_n = 1.62$, respectively, and the isotherm was obtained by making successive additions of PDMS in chloroform solution to the surface of the Langmuir trough. The studies used to discuss PDMS were part of a PhD thesis [9]. Hence, experimental details for the PDMS work are provided as Appendix A. In Regime A, PDMS chains would have a two-dimensional (2D) conformation in which all of the silicon and oxygen atoms adsorb onto the subphase. This regime could be homogeneous, such as a 2D analog to an ideal gas, or heterogeneous corresponding to the coexistence of gas and liquid-like or solid regimes. Brewster-angle microscopy (BAM) studies have

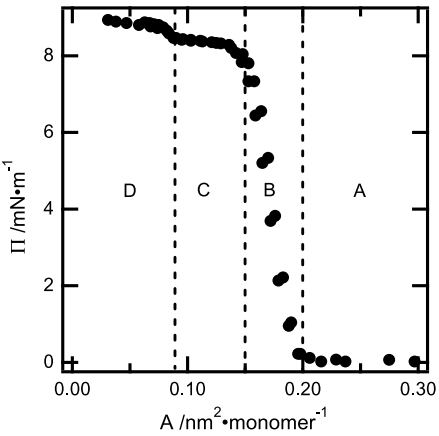

Fig. 7.2 Π-A isotherm for $M_n = 3{,}370$ PDMS at the A/W interface and 25.0 °C. The *vertical dashed lines* indicate the boundaries between the four regimes noted by Fox et al. [8]

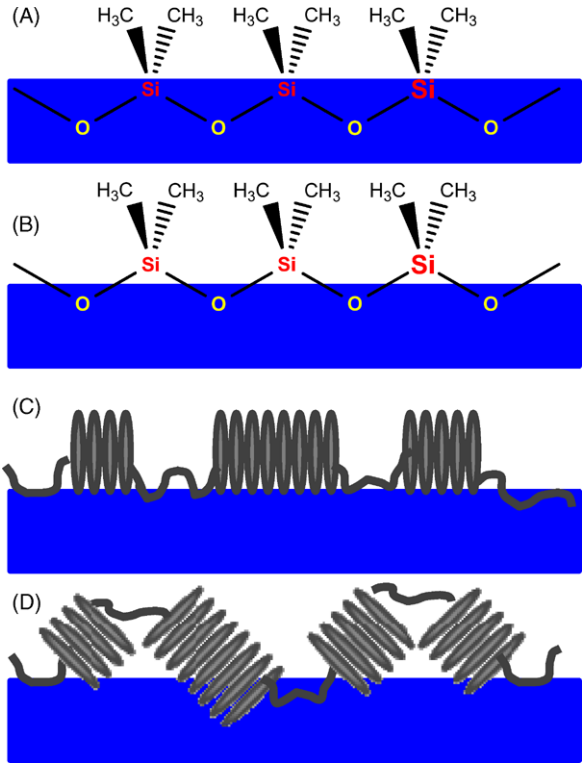

Fig. 7.3 Schematic depiction of the structural transitions proposed by Fox et al. [8] for the regimes in PDMS Π-A isotherms at the A/W interface: (A) all Si and O atoms adsorbed, (B) some Si and O atoms adsorbed (only shown as O), (C) helices parallel to the surface, and (D) helices oriented more perpendicular to the surface

shown heterogeneity in this regime ($\Pi \sim 0$) for some silicone systems [10]. As the monolayer forms (Regime B where Π increases from zero at a lift-off area of $A_{\text{lift-off}} \sim 0.2\ \text{nm}^2\ \text{monomer}^{-1}$), some of the silicon and oxygen atoms are squeezed out of the film (for simplicity, only the Si atoms are shown being squeezed out of the

monolayer in Fig. 7.3). Once the monolayer forms, the first plateau in Regime C of Fig. 7.2 at $\Pi_{\text{plateau1}} \sim 8.4\ \text{mN m}^{-1}$ is attributed to the successive coiling of PDMS into 6/1 helices. Once the helical monolayer forms, a second smaller rise in Π between Regime C and D is interpreted as the collapse of the helical monolayer as some helices could start standing on end leading to the second plateau in Regime D, $\Pi_{\text{plateau2}} \sim 9\ \text{mN m}^{-1}$. Figures 7.2 and 7.3 serve as a starting point for discussing the interest in silicone Langmuir films over the past 60 years.

While crystallographic [11] and solid state NMR studies [12] lend credence to the helical model proposed by Fox et al. for PDMS at the A/W interface [8], subsequent Langmuir film studies have provided alternative interpretations for the different regimes of PDMS isotherms like Fig. 7.2. Starting in the 1960s, Noll et al. systematically investigated silicone Langmuir films. In this work [13–15], speculation centers on water playing an important role in Regime B, the monolayer regime for PDMS. The new hypothesis being that compression of the monolayer squeezes water out of the film, along with silicon and oxygen atoms. Later, Granick [16] applied the scaling concepts of de Gennes [17], and treated the monolayer as a 2D semi-dilute polymer solution where Π scales with surface concentration ($\Gamma = 1/A$) as $\Pi \sim \Gamma^z$. The scaling exponent for PDMS of $z \sim 50$ [16], indicates that the A/W interface acts as a near theta (poor) solvent [18], i.e. 2D chain conformations correspond to the case where decreased polymer chain swelling arising from poor solvent quality exactly matches excluded volume effects. Noll et al. [13–15] also speculated that Regime C in Fig. 7.2 reflects bilayer formation rather than progressive coiling into helices. More recent BAM studies by Mann et al. [10] reveal film heterogeneity for some PDMS samples in Regime D, and both neutron reflectivity and ellipsometry studies [19] for PDMS Langmuir films favor a multilayer model for the transitions of PDMS Π-A isotherms rather than the more idealized model of Fig. 7.3. Other studies which may support the spreading of relatively "dry" PDMS on top of a hydrated PDMS monolayer are work by Runge and Yu [20] on Langmuir film blends of PDMS and poly(vinyl acetate) (PVAc) where a bilayer model was used to explain surface viscoelastic data, and Webster and Wightman [21] who showed that PDMS can spread on other polymers. Perhaps the most definitive study refuting the helical model comes from Kim et al. [22] using sum frequency generation vibrational spectroscopy (SFG) (see also Chap. 2). In SFG, only non-centrosymmetic vibrational stretches produce a signal. Vibrational signals associated with the methyl C-H stretch that are present in the monolayer, are unaffected by the collapse transition associated with Regime C. This observation supports the retention of a non-centrosymmetric monolayer with the formation of centrosymmetric multilayer domains. More recently, Bernardini et al. [23, 24] have combined Π-A isotherm, BAM, and self-consistent field (SCF) calculations to study the layering transitions associated with collapse of the PDMS monolayer. Nonetheless, there are still authors who have invoked the helical PDMS model to explain their observations for molecules in Langmuir [25, 26] and Langmuir–Blodgett (LB) films [26].

7.2.2 Viscoelastic Properties of PDMS Langmuir Films

Another area of interest for PDMS Langmuir films is their rheological properties. In 1966 [27], Jarvis used a surface canal viscometer and torsional surface viscometer to show that the surface shear viscosity of PDMS Langmuir films was on the order of 10^{-5} mN s m^{-1}, a nearly insignificant value. The next attempt by Garrett and Zisman [28] examined spatial damping coefficients of mechanically generated waves for PDMS as well as polymethylphenylsiloxane (PMPS) and polydiethylsiloxane (PDES). Interesting changes in the damping coefficients for the PDMS film occurred at transition points in the Π-A isotherms that are analogous to the variations in the temporal damping coefficients that will be discussed in this section. Later, Hård and Neuman [29] were the first to use surface light scattering (SLS) to study the propagation of spontaneously formed capillary waves in Regime A and B of Fig. 7.2. More discussion of their work appears later in this chapter. Runge and Yu [20] also used SLS to probe blends of PDMS and PVAc, and observed PDMS collapsed at even lower Π in the blend than as a single component film. Another technique for probing capillary wave propagation, electrocapillary wave diffraction (ECWD), was used by Mann and Langevin [19] and subsequently by Miller [30] to show that capillary wave techniques could also probe Regimes C and D of Fig. 7.2.

7.2.2.1 Limiting Viscoelastic Behavior in Langmuir Films

In a recent review by Esker et al. [31], the authors covered the analysis of SLS data for Langmuir monolayers of vinyl polymers at the A/W interface. In SLS, density fluctuations in the underlying subphase give rise to surface capillary waves or ripplons. These waves have amplitudes of ~0.5 nm [32] and, for typical experiments, wavelengths on the order of a few hundred microns. As these waves propagate along the surface they undergo temporal dampening. In contrast, the wave damping experiments of Garrett and Zisman [28] use mechanically generated waves and ECWD uses capillary waves generated through the electrocapillary effect to probe spatially damped waves of a fixed frequency. While these techniques cover different frequency domains, the propagation characteristics are governed by coupling of transverse wave motion to dilational and shear motion. Analysis of the data under most circumstances yields information about the surface dilational elasticity.

For SLS, heterodyne detection is used to obtain the frequency shift, f_s, and instrument corrected full-width at half-maximum intensity ($\Delta f_{s,c}$) of the power spectrum for the light scattered by capillary waves with different wavevectors (k). These in turn are related to the angular frequency ($\omega = 2\pi f_s$) and the temporal damping coefficient ($\alpha = \pi \Delta f_{s,c}$). These properties of the propagating capillary wave, along with the static surface tension (γ_s) which is normally measured simultaneously by the Wilhelmy plate technique, are used to solve the dispersion equation for capillary waves at an A/W interface covered with a thin surface film. The full dispersion

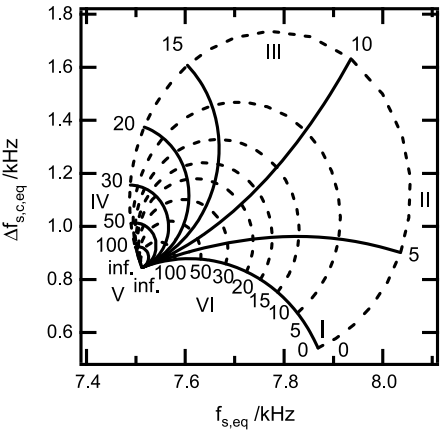

Fig. 7.4 $\Delta f_{s,c,eq} - f_{s,eq}$ deduced from Eq. (7.1). The *solid lines* on the figure correspond to constant ε_d in units of mN m^{-1}, while the *dashed lines* correspond to constant $\kappa \times 10^5$ in units of mN s m^{-1}. The roman numerals correspond to six cases of limiting dilational viscoelastic behavior for a reference state of water at 25 °C ($k_{\text{ref}} = 324.3$ cm^{-1})

equation for capillary waves at the A/W interface [33] is

$$\left[\eta\left(k - m^*\right)\right]^2 = \left(\frac{\varepsilon^* k^2}{i\omega^*} + \eta\left(k + m^*\right)\right)\left(\eta\left(k + m^*\right) + \frac{\gamma^* k^2}{i\omega^*} + \frac{g\rho}{i\omega^*} - \frac{\omega^* \rho}{ik}\right) \tag{7.1}$$

where g is acceleration due to gravity, η is the bulk viscosity of the subphase, ρ is the density of the subphase, and ε^*, γ^*, ω^*, and m^* correspond to the complex dilational modulus, complex surface tension, complex frequency, and the complex wavevector in the z-direction, respectively. These complex quantities correspond to Eqs. (7.2) through (7.5), respectively.

$$\varepsilon^* = \varepsilon_d + i\omega^* \kappa \tag{7.2}$$

$$\gamma^* = \gamma_d + i\omega^* \mu \tag{7.3}$$

$$\omega^* = \omega + i\alpha \tag{7.4}$$

$$m^* = \left(k^2 + \frac{i\omega^* \rho}{\eta}\right)^{1/2}, \qquad \text{Re}\left(m^*\right) > 0 \tag{7.5}$$

In Eqs. (7.2) through (7.5), ε_d is the dynamic dilational elasticity, κ is the dilational viscosity, μ is the transverse viscosity, γ_d is the dynamic surface tension, and g is acceleration due to gravity. In principle, ε_d and κ also contain a shear component, although this seems to be negligible in general [34] and especially for silicones [27]. The solution of Eq. (7.1) is complicated by the fact that only two quantities are measured, f_s and $\Delta f_{s,c}$, but four parameters, ε_d, κ, γ_d, and μ, need to be determined. Hence, during the analysis of the power spectra, μ is normally assumed to be zero [34] and γ_d is replaced by the γ_s [35]. Hence, ε_d and κ become the extractable parameters. This approach for acquiring dilational viscoelastic moduli is one of three analysis schemes used in this chapter.

The second approach is to compare experimental data with important theoretical limits of the dispersion equation [33]. Hård and Neuman [29] were the first to recognize that solutions of Eq. (7.1) can yield plots like Fig. 7.4, which clearly shows six important limiting cases for dilational viscoelastic behavior at the A/W interface (defined by the perimeter of the plot). One of these, (I), the pure liquid limit, corresponds to Eqs. (7.6) and (7.7):

$$\omega = 2\pi f_s = \sqrt{\frac{\gamma_d k^3}{\rho}}\left(1 - \frac{1}{2}y^{-3/4}\right) \tag{7.6}$$

$$\alpha = \pi \Delta f_{s,c} = \frac{2\eta k^2}{\rho}\left(1 - \frac{1}{2}y^{-1/4}\right) \tag{7.7}$$

where $y = \gamma_d \rho/(4k\eta^2)$. y in Eq. (7.6) represents a minor correction to the original work of Lord Kelvin [36], whereas it makes a more significant correction to the original work of Stokes [37] in Eq. (7.7). The Limits II, III, and IV all are associated with perfectly elastic surface films ($\mu = 0$ and $\kappa = 0$) and correspond to (II) the maximum velocity limit for a perfectly elastic surface film [31, 35, 38, 39]:

$$\omega = 2\pi f_s = \sqrt{\frac{\gamma_d k^3}{\rho}}\left(1 + \frac{1}{387}y^{21/64}\right) \tag{7.8}$$

$$\alpha = \pi \Delta f_{s,c} = \frac{\sqrt{2}}{2}\left(\frac{\gamma_d \eta^2 k^7}{\rho^3}\right)^{1/4}\left(1 - \frac{2}{25}y^{5/27}\right) \tag{7.9}$$

(III) the maximum damping coefficient for a perfectly elastic surface film [31, 35, 38–40]:

$$\omega = 2\pi f_s = \sqrt{\frac{\gamma_d k^3}{\rho}}\left(1 - \frac{10}{17}y^{-9/16}\right) \tag{7.10}$$

$$\alpha = \pi \Delta f_{s,c} = \frac{\sqrt{2}}{2}\left(\frac{\gamma_d \eta^2 k^7}{\rho^3}\right)^{1/4}\left(1 + \frac{4}{11}y^{-5/32}\right) \tag{7.11}$$

and (IV) the minimum velocity limit for a perfectly elastic surface film [31, 35, 41]:

$$\omega = 2\pi f_s = \sqrt{\frac{\gamma_d k^3}{\rho}}\left(1 - \frac{5}{14}y^{-19/64}\right) \tag{7.12}$$

$$\alpha = \pi \Delta f_{s,c} = \frac{\sqrt{2}}{4}\left(\frac{\gamma_d \eta^2 k^7}{\rho^3}\right)^{1/4}\left(1 + \frac{5}{3}y^{-25/121}\right). \tag{7.13}$$

Equations (7.8), (7.10), and (7.12), are all empirical fits assuming the functional form proposed by Lord Kelvin [36] for pure liquids is valid, as are Eqs. (7.14) and (7.16) discussed below. Equations (7.9) and (7.11) are also empirical with corrections to the functional form proposed by Dorrestein [38, 39] when he correctly

predicted the existence of a damping maximum at intermediate dilational elasticities. In contrast, Eq. (7.16) represents an empirical model that borrows the functional form for the damping coefficient proposed by Reynolds [41] for a film with an infinite dilational modulus. Another important limit (V) corresponds to a film with an infinite dilational modulus ($\varepsilon^* \to \infty$ and $\mu = 0$) [31, 35, 41]:

$$\omega = 2\pi f_s = \sqrt{\frac{\gamma_d k^3}{\rho}}\left(1 - \frac{1}{4}y^{-1/4}\right), \tag{7.14}$$

$$\alpha = \pi \Delta f_{s,c} = \frac{\sqrt{2}}{4}\left(\frac{\gamma_d \eta^2 k^7}{\rho^3}\right)^{1/4}\left(1 + \frac{1}{2}y^{-1/4}\right) \tag{7.15}$$

where Eq. (7.15) represents a minor correction to the earlier work of Reynolds [31]. One other limit worth noting (VI) is the case for a purely viscous surface film ($\mu = 0$ and $\varepsilon_d = 0$) [31, 35]:

$$\omega = 2\pi f_s = \sqrt{\frac{\gamma_d k^3}{\rho}}\left(1 - \frac{3}{25}y^{-2/11}\right), \tag{7.16}$$

$$\alpha = \pi \Delta f_{s,c} = \frac{\sqrt{2}}{4}\left(\frac{\gamma_d \eta^2 k^7}{\rho^3}\right)^{1/4}\left(1 + \frac{25}{22}y^{-8/25}\right). \tag{7.17}$$

Given the close proximity of Limit VI to Limit V, the functional form provided by Reynolds [41] was also used to obtain Eq. (7.17). These equations provide predictions for limiting dynamic viscoelastic data that can be directly compared to experimental f_s and $\Delta f_{s,c}$ data. In particular, Limits I through IV are the most important for silicone films.

The third and final approach is a "corresponding states approach" [31, 35]. As in the first analysis method, one obtains ε_d and κ from experimentally determined f_s and $\Delta f_{s,c}$, and γ_s values assuming $\gamma_s = \gamma_d$ and $\mu = 0$. Next, one defines a reference state. For this study, the reference state is water at 25 °C ($\eta_{\text{ref}} = 0.894$ cP, $\rho_{\text{ref}} = 0.997$ g cm^{-3}, $\gamma_{d,\text{ref}} = 71.97$ mN m^{-1}, and $\mu_{\text{ref}} = 0$) with a reference wavevector of $k_{\text{ref}} = 324.3$ cm^{-1}. Using the parameters of the reference state along with the deduced ε_d and κ, values of the equivalent frequency shift ($f_{s,eq}$) and instrument corrected full-width at half-maximum intensity ($\Delta f_{s,eq}$) at the reference state are determined. Once it is verified that ε_d and κ are independent of k, $f_{s,eq}$ and $\Delta f_{s,eq}$ values for different k are averaged with one standard deviation error bars for a given Π. Values of $\Delta f_{s,eq}$ vs. $f_{s,eq}$ for different Π are then graphed together on plots like Fig. 7.4, to determine the "viscoelastic paths" films take during monolayer formation and subsequent collapse transitions.

7.2.2.2 Limiting Viscoelastic Behavior of PDMS Langmuir Films

Figures 7.5 and 7.6 show f_s and $\Delta f_{s,c}$ obtained from SLS as a function of A for four different k using the same $M_n = 3{,}370$ PDMS sample used for the Π-A isotherm

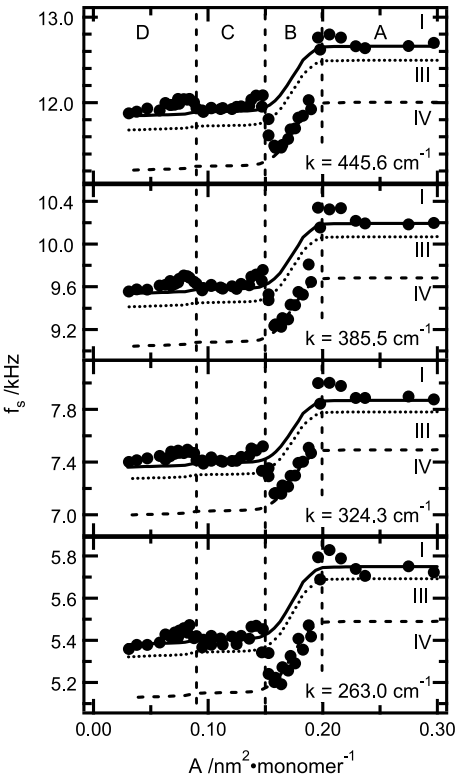

Fig. 7.5 f_s-A for $M_n = 3{,}370$ PDMS at the A/W interface and 25 °C for four different k. *Dashed vertical lines* and letters represent regimes in Fig. 7.2. *Solid* (I, (7.6)), *dotted* (III, (7.10)), and *dashed* (IV, (7.12)) *lines* represent limiting behavior

of Fig. 7.2. The vertical dotted lines highlight the regime boundaries of the isotherm defined for Fig. 7.2. As seen in Figs. 7.5 and 7.6, all four k show the same qualitative trends. The films in Regime A exhibit pure liquid dynamics (I) corresponding to the solid lines. At the end of Regime A, there is a slight upturn in f_s and $\Delta f_{s,c}$ relative to pure liquid dynamics (solid) lines. At the boundary between Regimes A and B, f_s and $\Delta f_{s,c}$ drop and rise precipitously, respectively. For Regime B, f_s shows a single minimum near the middle of the regime, whereas $\Delta f_{s,c}$ shows two maxima (at the start and end of the regime) and a local minimum at the same A where f_s exhibits a global minimum. The maxima approach the limiting behavior for (III), the maximum damping coefficient for a perfectly elastic surface film (dotted lines), while the minima in f_s and $\Delta f_{s,c}$ around $\mathrm{A} \sim 0.17\,\mathrm{nm^2\,monomer^{-1}}$ approach the limiting behavior for the minimum velocity limit of a perfectly elastic surface film (dashed lines). The two maxima in $\Delta f_{s,c}$ in Regime B indicate a film with intermediate elasticity, while the minima in f_s and $\Delta f_{s,c}$ indicate a film with larger viscoelastic moduli. As the film is compressed further into Regime C, one sees that pure liquid dynamics are observed again (solid lines). This observation indicates that independent of whether helix formation or collapse into multilayer structures is occurring, the film is no longer viscoelastic. At the boundary between Regime C and D, there is a temporary small increase in both f_s and $\Delta f_{s,c}$ indicating a recovery of at least some viscoelastic behavior before the film again behaves like a pure liquid of lower

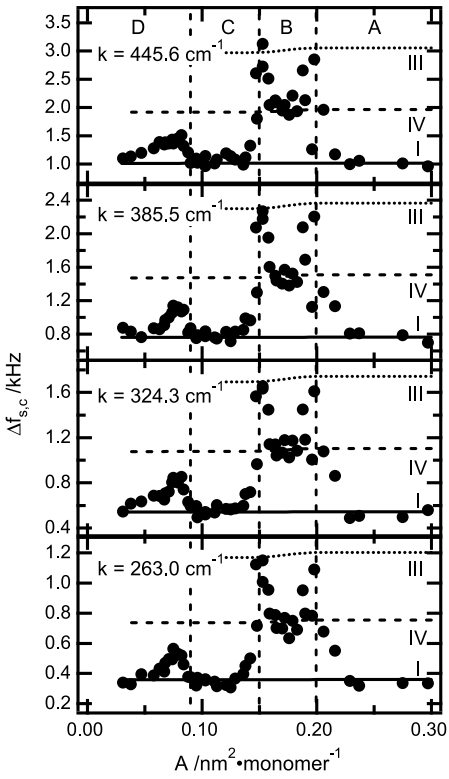

Fig. 7.6 $\Delta f_{s,c}$-A for $M_n = 3{,}370$ PDMS at the A/W interface and 25 °C for four different k. *Dashed vertical lines* and letters represent regimes in Fig. 7.2. *Solid* (I, (7.7)), *dotted* (III, (7.11)), and *dashed* (IV, (7.13)) *lines* represent limiting behavior

surface tension in Regime D. The trends in $\Delta f_{s,c}$ are qualitatively similar to spatial wave damping studies by Garrett and Zisman [28]. They are also consistent with the behavior reported by Runge and Yu [20].

From the isotherm in Fig. 7.2, along with the f_s and $\Delta f_{s,c}$ data in Figs. 7.5 and 7.6, it is possible to compute ε_d and κ. Figure 7.7 shows both ε_d and κ as a function of A along with the regime boundaries (vertical dashed lines) defined in Fig. 7.2. For Fig. 7.7a, the static dilational elastic moduli,

$$\varepsilon_s = -\mathrm{A}(\partial \Pi / \partial \mathrm{A})_T, \tag{7.18}$$

the 2D analogs to the 3D bulk modulus, are also plotted for comparison. As seen in Fig. 7.7, there is excellent agreement between ε_d and ε_s, except in Regime D, where ε_d is slightly but significantly larger than ε_s. Furthermore, there are maxima in ε_d in the middle of Regime B and at the boundary between Regimes C and D. Elsewhere, ε_s and ε_d are zero. These results are consistent with previously published studies [20]. In Fig. 7.7b, one sees that κ is essentially zero within experimental error ($\sim$100 % one standard deviation error bars have been omitted from Fig. 7.7b for clarity) except in the vicinity of the elasticity maximum in Regime B. These features are consistent with the discussion of Figs. 7.5 and 7.6. In Regimes A, C, and D, Figs. 7.5 and 7.6 were consistent with pure liquid dynamics, $\varepsilon^* = 0$. The

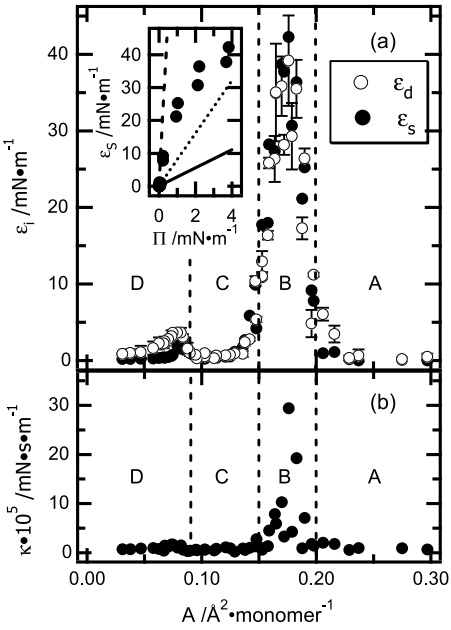

Fig. 7.7 (**a**) ε_i-A and (**b**) κ-A for $M_n = 3{,}370$ PDMS at the A/W interface and 25 °C. ε_d (with one standard deviation error bars) and κ are averages of four k. Error bars for κ (∼100 %) were omitted for clarity. The *dashed vertical lines* and letters indicate the regime boundaries of Fig. 7.2. The *inset* shows $\varepsilon_s - \Pi$ along with comparisons for scaling predictions for good $z = 2.76$ (*solid line*) and theta $z = 101$ (*dashed line*) to $z = 8$ (*dotted line*) solvent conditions

small κ values are consistent with shear viscosity studies [27] and previous SLS [20, 29, 42] and ECWD [19, 30] studies of dilational properties. Such low κ values indicate the film is essentially perfectly elastic during the viscoelastic transitions in Regime B and at the Regime C/D boundary.

The inset of Fig. 7.7a also contains a plot of ε_s vs. Π. Esker et al. [35] noted that $\varepsilon_s = z\Pi$ where z is the 2D scaling exponent. For a good solvent where the 2D chain conformation is swollen, $z = 2.76$ [43, 44] or 3 [45] for numerical or mean field treatments, respectively. In contrast, predictions for theta conditions range from 8 [46] to 101 [18]. For the case of a mean field treatment in 2D, z would be infinite. Dashed (largest slope) and dotted lines (intermediate slope) are used to highlight the range for theta solvent behavior, while the solid line (smallest slope) corresponds to the numerical prediction for the A/W interface behaving as a good solvent. As seen in the inset of Fig. 7.7a, the PDMS isotherm is consistent with the A/W interface being a poor (possibly theta) solvent as noted by Granick [16].

Once ε_d and κ are known, it is possible to calculate $f_{s,eq}$ and $\Delta f_{s,c,eq}$. Figures 7.8 and 7.9 are the analogous plots to Figs. 7.5 and 7.6, respectively. One advantage of Figs. 7.8 and 7.9 is that converting values from different k and Π to a single reference state allows one to average values from different k for frequency independent viscoelastic behavior (confirmed for PDMS over the range of k studied). Another advantage is that all of the limits of the dispersion equation (Eqs. (7.6) to (7.17)) are now constant (dotted horizontal lines on Figs. 7.8 and 7.9) for data obtained at different Π, thereby simplifying comparisons. Whereas Regimes A, C, and D look different on Figs. 7.5 and 7.6, one readily sees they are equivalent in that they exhibit pure liquid dynamics (I) in Figs. 7.8 and 7.9. Furthermore, it is now

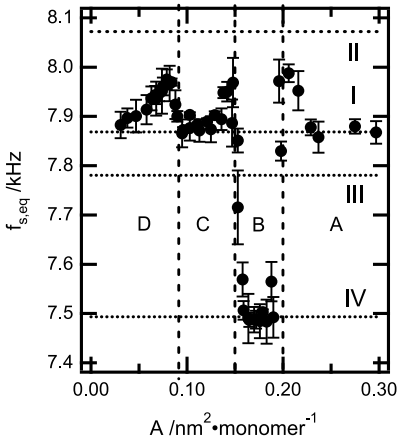

Fig. 7.8 Average $f_{s,eq}$-A from four k for $M_n = 3{,}370$ PDMS at the A/W interface and 25 °C with one standard deviation error bars. The reference state is water at 25 °C with $k = 324.3$ cm^{-1}. *Dashed vertical lines* and letters correspond to the regimes in Fig. 7.2. Relevant viscoelastic limits for PDMS (*dotted horizontal lines*) include (I, (7.6)) pure liquid dynamics, and the (II, (7.8)) maximum velocity, (III, (7.10)) maximum damping coefficient, and (IV, (7.12)) minimum velocity limit for a perfectly elastic surface film

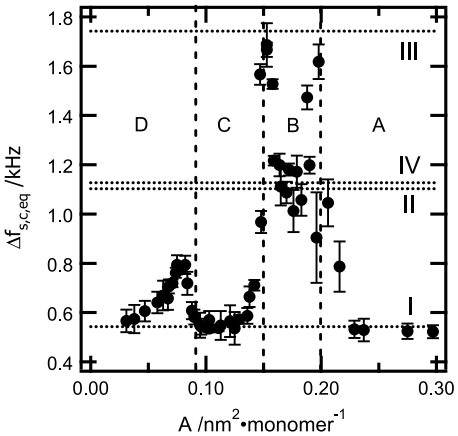

Fig. 7.9 Average $\Delta f_{s,c,eq}$-A from four k for $M_n = 3{,}370$ PDMS at the A/W interface and 25 °C with one standard deviation error bars. The reference state is water at 25 °C with $k = 324.3$ cm^{-1}. *Dashed vertical lines* and letters correspond to the regimes in Fig. 7.2. Relevant viscoelastic limits for PDMS (*dotted horizontal lines*) include (I, (7.7)) pure liquid dynamics, and the (II, (7.9)) maximum velocity, (III, (7.11)) maximum damping coefficient, and (IV, (7.13)) minimum velocity limit for a perfectly elastic surface film

possible to see that $f_{s,eq}$ increases toward the maximum velocity limit for a purely elastic surface film (II) as the monolayer forms (end of Regime A), the monolayer collapses (boundary between Regimes B and C), and at the bilayer to multilayer

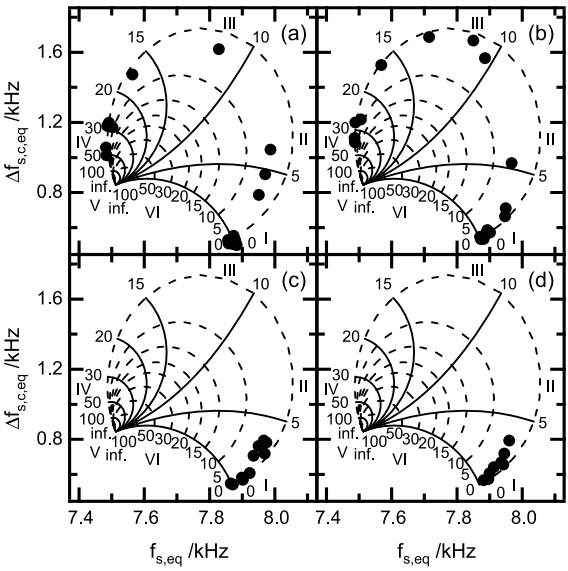

Fig. 7.10 $\Delta f_{s,c,eq}$–$f_{s,c,eq}$ for $M_n = 3{,}370$ PDMS at the A/W interface and 25 °C broken up by A and Π: (**a**) A > 0.17 nm^2 monomer^{-1} ($\Pi \leq 5$ mN m^{-1}, counterclockwise from I to IV), (**b**) 0.10 < A ≤ 0.17 nm^2 monomer^{-1} ($5 < \Pi < 8.4$ mN m^{-1}, clockwise from IV to I), (**c**) 0.07 < A < 0.10 nm^2 monomer^{-1} ($8.4 \leq \Pi < 8.8$ mN m^{-1}, counterclockwise from I), and (**d**) A ≤ 0.07 nm^2 monomer^{-1} (8.8 mN m^{-1} ≤ Π, clockwise towards I). Other features of the graph are defined in Fig. 7.4

transition (boundary between Regimes C and D). Likewise, one sees that the two maxima in $\Delta f_{s,c,eq}$ in Regime B are of identical magnitude (viscoelastically equivalent), a feature that may not be immediately apparent from Fig. 7.6. Looking at Figs. 7.8 and 7.9 together for the bilayer to multilayer transition (boundary between Regimes C and D), one also sees that local maximum $\Delta f_{s,c,\max}$ is more closely associated with the maximum velocity limit (II) than the maximum damping coefficient limit (III) of a perfectly elastic surface film. Similarly, it is possible to see that the positions of the maxima in Regime B for Fig. 7.9 with respect to A match the appropriate f_s behavior in Fig. 7.8. Finally, the position of the minima in the center of Regime B for $f_{s,eq}$ (global) and $\Delta f_{s,c,eq}$ (local) correspond to the minimum velocity limit for a perfectly elastic surface film (IV).

Figures 7.8 and 7.9 offer an improvement over Figs. 7.5 and 7.6, respectively, for understanding the limiting viscoelastic behavior relative to the Π-A isotherms for PDMS films. However, Fig. 7.4 is better able to relate $f_{s,eq}$, $\Delta f_{s,c,eq}$, and the corresponding ε_d and κ on the same graph. Plotting different ($f_{s,eq}$, $\Delta f_{s,c,eq}$) pairs for different Π as done in Fig. 7.10 allows one to see trends in changing viscoelastic behavior during compression of the film. The four plots in Fig. 7.10 do not exactly correspond to the regimes of the isotherm in Fig. 7.2. Changing the regimes more effectively captures the viscoelastic trends in the data during compression of the films.

In Fig. 7.10a ($f_{s,eq}$, $\Delta f_{s,c,eq}$) pairs are plotted from $\Pi = 0$ to the midpoint of Regime B ($\Pi \sim 5$ mN m^{-1} the maximum in ε_s or ε_d). During compression up to the maximum in ε_s or ε_d, the film follows an almost perfectly elastic path ($\kappa < 5 \times 10^{-5}$ mN s m^{-1} and an assumed $\mu = 0$). During this process the film approaches the maximum velocity limit (II at $\Pi \sim 0.1$ mN m^{-1}), and the maximum damping coefficient limit (III at $\Pi \sim 1$ mN m^{-1}), before reaching a maximum elas-

ticity that corresponds well with the minimum velocity limit (IV at $\Pi \sim 2$ mN m^{-1}) of perfectly elastic surface films along a counterclockwise trajectory. Further compression of the film results in a drop in the elasticity of the film as the film starts to collapse. Figure 7.10b shows this process for $\sim 5 < \Pi < \sim 8.4$ mN m^{-1}. Hence, Fig. 7.10b provides data from the midpoint of Regime B nearly to the end of Regime C. As seen in Fig. 7.10b, the film returns to pure liquid dynamics along the same "path" taken by the film during the formation of the monolayer (Fig. 7.10a) but along a clockwise trajectory. On its return, the film passes by the limit for the maximum damping coefficient (III at $\Pi \sim 7.5$ mN m^{-1}) and maximum velocity limit (II at $\Pi \sim 8$ mN m^{-1}) of a perfectly elastic film. This behavior is consistent with the observations of Hård and Neuman [29] who also saw the initial rise and fall for PDMS, although Figs. 7.10a and b more effectively establish the limiting behavior between pure liquid dynamics (I) and the maximum damping coefficient for a perfectly elastic surface film (III) during monolayer formation and collapse.

Figures 7.10c and 7.10d explore the viscoelastic behavior of the second transition in the Π-A isotherm between Regimes C and D. Figure 7.10c contains data from $\sim 8.4 < \Pi < \sim 8.8$ mN m^{-1} with a counterclockwise trajectory, corresponding to the midpoint of Regime C to the midpoint of the rise in Π between Regime C and Regime D. In contrast, Fig. 7.10d contains data as the elasticity that builds up during compression between Regimes C and D relaxes back to pure liquid dynamics (I) in Regime D along a counterclockwise trajectory. As seen in Figs. 7.10c, d, the increase in ε_d is small and the film approaches behavior that is consistent with the maximum velocity limit of a perfectly elastic surface film (II) before recovering pure liquid behavior (I) in Regime D.

The discussion of the dilational dynamics of PDMS monolayers clearly provides important limits for viscoelastic behavior and illustrates three different approaches for analyzing SLS data. These results serve as a "baseline" for understanding the effects that molar mass, endgroups, and bulkier substituents have on the properties of silicones at the A/W interface.

7.2.2.3 Molecular Weight Effects on the Dilational Viscoelastic Behavior of PDMS at the Air/Water Interface

Figure 7.11a shows Π-A isotherms for four different linear PDMS samples. In addition, a fifth sample, $M_n < 1{,}210$, failed to form stable monolayers ($\Pi \sim 0$ over the entire A range). The most obvious effect of molecular weight occurs in Regime A, where Π starts to rise from A ~ 0.30 nm^2 monomer^{-1} for $M_n = 1{,}210$ PDMS, whereas the three other samples have essentially identical isotherms in Regimes A and B. From the standpoint of scaling concepts [17, 35], this result indicates that the A/W interface is a slightly better solvent for the short oligomers of PDMS than the higher molecular weight samples (Figure 7.11b). As expected for a "semi-dilute" solution, the initial slope of Fig. 7.11b for the two higher molecular weight PDMS samples is independent of molecular weight and consistent with the A/W interface being a poor solvent for PDMS [16]. A more subtle difference in the Π-A isotherm

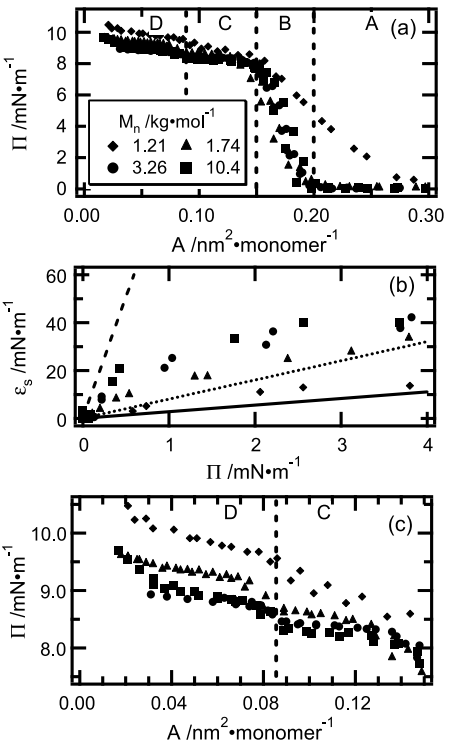

Fig. 7.11 (**a**) Π-A, (**b**) ε_s-Π, and (**c**) Π-A (expanded) for PDMS with different M_n at the A/W interface and 25.0 °C. The *vertical dashed lines* with letters indicate different regimes. Scaling predictions for good $z = 2.76$ (*solid line*) and theta $z = 101$ (*dashed line*) to $z = 8$ (*dotted line*) solvent conditions are provided on (**b**)

is highlighted in Figure 7.11c. As molecular weight decreases, the plateau Π values for Regimes C and D increase. This trend is similar to the one reported for cyclic polymers [47] and is consistent with multilayer formation.

Dynamic behavior for these systems is comparable to the discussion for the $M_n = 3{,}370$ PDMS of Figs. 7.5 to 7.10. The most important differences are best seen in plots of ε_d-A and κ-A. Figures 7.7–7.12a show ε_d-A for $M_n = 1{,}210$ PDMS plotted and Fig. 7.12b shows the three higher molecular weights plotted together. As expected from the isotherm, ε_s is different for the two cases, with smaller values for the more expanded $M_n = 1{,}210$ PDMS isotherm. Nonetheless, the maximum ε_d in Regime B for $M_n = 1{,}210$ PDMS of $\varepsilon_{d,\max} \sim 30$ mN m^{-1} is only slightly smaller than for the other three molecular weights which reach a maximum value of $\varepsilon_{d,\max} \sim 45$ mN m^{-1} for the $M_n = 10{,}400$ sample. Similar effects are observed for κ as well (Fig. 7.12c). In contrast, the other maximum in ε_d at the boundary between Regimes C and D does not show a systematic dependence on molecular weight as both the $M_n = 1{,}210$ and 10,400 samples have a local maximum of $\varepsilon_{d,\max} \sim 7$ mN m^{-1}. The other interesting difference is the appearance of viscoelastic behavior in Regime A for $M_n = 10{,}400$ PDMS with respect to ε_d for Fig. 7.12b. The coexistence of gas and liquid-like monolayer domains of PDMS on the micron scale can be detected by surface light scattering [35, 48–50]. For PDMS, Mann et al. [10] noted that domain formation in the gas/liquid coexistence region of the PDMS isotherm (Regime A) may be molecular weight dependent. The premise being that

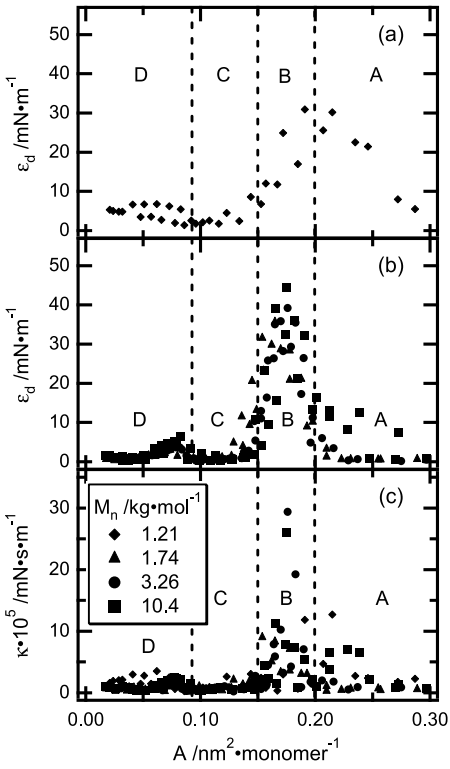

Fig. 7.12 (**a**) ε_d-A, (**b**) ε_d-A, and (**c**) κ-A for PDMS with different M_n at the A/W interface and 25.0 °C. The *vertical dashed lines* with letters indicate different regimes. The legend on (**c**) applies to all graphs

higher molecular weight PDMS may spread less efficiently than lower molecular weight PDMS leading to coexisting gas and liquid domains rather than a homogeneous gaseous monolayer.

7.2.2.4 Effects of Endgroups on PDMS Langmuir Films

In the previous section molecular weight was shown to influence the Π-A isotherms for small enough PDMS oligomers in Regimes A and B, with a more systematic effect on plateau pressures in Regimes C and D. The molecular weight dependent increases in the plateau pressures for PDMS films in Regimes C and D are also present for cyclic silicones as noted by Granick et al. [47]. The cyclic silicones exhibit substantially higher plateau pressures relative to linear PDMS in Regimes C and D. This enhancement in plateau pressure likely arises from the absence of hydrophobic endgroups. Nonetheless, the cyclic and linear silicones exhibit similar behavior in Regimes A and B.

The importance of endgroups on the Π-A isotherm can also be seen in Fig. 7.13 for a PDMS sample containing two silanol groups. This effect was first reported by Newig [51]. For this sample, Regime D is finite, and Π increases even further at even smaller A (labeled as Regime E on Fig. 7.13). This behavior is attributed to the

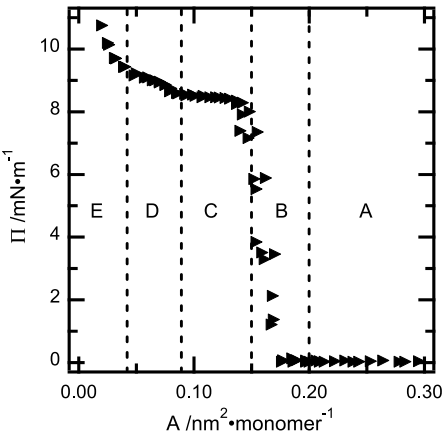

Fig. 7.13 Π-A isotherm for $M_n = 12{,}700$ PDMS (dihydroxy endgroups) at the A/W interface and 25.0 °C. The *vertical dashed lines* and letters indicate the boundaries between the regimes in Fig. 7.2 plus a new one

extra energy required to remove polar silanol groups from the A/W interface. Even more pronounced effects on the Π-A isotherm for PDMS samples containing amine, carboxylic acid, and epoxide terminal groups have been reported by Lenk et al. [52]. For these samples, the effects of the endgroups are most dramatic for small molecular weight and maximum achievable Π for samples of comparable molecular weight follow the general trend epoxide < hydroxyl < carboxylic acid < amine. More importantly, the high polarity of the end groups supports a more surfactant-like structure, which can interfere with the progressions seen in the PDMS Π-A isotherms of Figs. 7.2, 7.11 and 7.13. With decreasing molecular weight and strong polar end groups, Regime E will start to merge with Regime D, followed by Regimes E and D merging with C, etc. Yin et al. [42] also demonstrated the existence of Regime E for a PDMS sample containing a single tricarboxylic acid-terminal group. They also showed through SLS that there is an enhancement of both ε_d and κ in Regime E relative to PDMS with hydrophobic terminal groups which behaves like a pure liquid at these surface areas.

7.2.2.5 Effects Different Substituents on the Siloxane Backbone Have on Siloxane Langmuir Films

While both molecular weight and chain ends affect PDMS Π-A isotherms and dilational viscoelastic behavior, other changes in structure can have more profound effects. For example, if PDMS is capable of forming monolayers comprised of helices, the incorporation of bulky side groups should hinder rotation about the Si-O bond, thereby preventing helix formation. Fox et al. [8] reported two other siloxanes, whose isotherms they felt were consistent with the helical model: polymethylphenylsiloxane (PMPS) and polydiethylsiloxane (PDES). These two siloxanes, along with poly(methyl-3,3,3-trifluoropropylsiloxane) (PMTFPS) are briefly considered here in terms of their Π-A isotherms and by no means represent an exhaustive review of the wide range of surface-active silicones [6, 7] nor do they

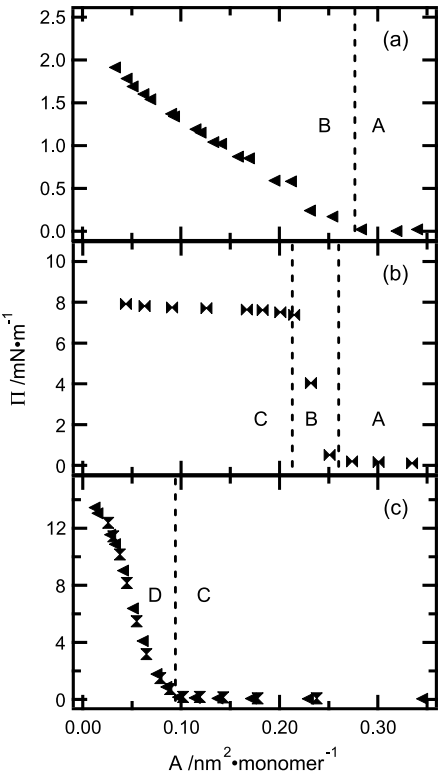

Fig. 7.14 Π-A isotherms for (**a**) PMPS, (**b**) PMTFPS, and (**c**) PDES at the A/W interface and 25.0 °C. The *vertical dashed lines* and letters indicate the boundaries between the regimes that occur for PDMS in Fig. 7.2 that may apply to these silicones

start to touch the area of hairy rod polymers with siloxane backbones (polyphthalocyaninatosiloxanes) whose LB-films have generated interest as conducting polymers [53]. In these systems, the phthalocyaninato groups negate the flexibility of the Si-O backbone leading to a rigid rod-like backbone which is very different from traditional silicones.

Figure 7.14 shows Π-A isotherms for (a) PMPS, (b) PMTFPS, and (c) PDES. It is interesting to note that the isotherms show a transition that occurs at an A consistent with either an A/B transition or C/D transitions in the PDMS isotherm but not both. In Figure 7.14a, the PMPS isotherm contains two key characteristics that are consistent with the work of Fox et al. [8]: $A_{\text{lift-off}} \sim 0.27\ \text{nm}^2\,\text{monomer}^{-1}$, and a maximum $\Pi \sim 2\ \text{mN}\,\text{m}^{-1}$. For the case of PMPS, Fox et al. [8] noted that molecular models could not be twisted into a helix because of steric hindrance. However, PMPS could be forced into a zig-zag conformation where both the methyl and phenyl groups are out of the water. This transition occurs at a larger A because of the larger size of the phenyl substituent.

For PMTFPS in Fig. 7.14b, $A_{\text{lift-off}} \sim 0.27\ \text{nm}^2\,\text{monomer}^{-1}$ with a sharp transition at the end of the monolayer regime at $A \sim 0.21\ \text{nm}^2\,\text{monomer}^{-1}$ ($\Pi \sim 7.5\ \text{mN}\,\text{m}^{-1}$) followed by a long featureless plateau (like Regime C). Likewise, Noll et al. [54] and Bernett and Zisman [55] both noted that PMTFPS, like PMPS, cannot readily form helices because of the bulky trifluoropropyl groups.

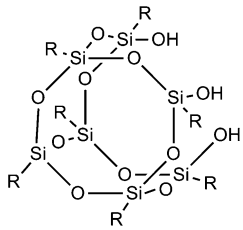

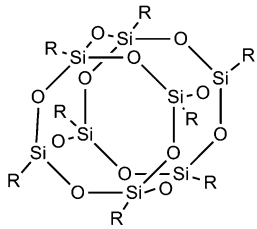

Fig. 7.15 POSS molecules used in this study

Indeed, Bernett and Zisman [55] speculated that the plateau in the isotherm corresponded to multilayer formation.

In contrast to PMTFPS and PMPS, PDES (Figure 7.14c) does not exhibit any transitions at A comparable to the A/B transition in PDMS. Instead, $A_{\text{lift-off}} \sim 0.09\ \text{nm}^2\ \text{monomer}^{-1}$ for PDES is comparable to the C/D transition in PDMS with maximum $\Pi \sim 14\ \text{mN m}^{-1}$. Fox et al. [8] noted that PDES molecular models could not be arranged into a zig-zag conformation where both ethyl substituents were out of the water if Si-O was bound to the surface. However, PDES can form a more compact conformation where some of the Si-O bonds lie on the A/W interface. This suggestion is consistent with work by Miller et al. [56] where PDES was modeled as a 5/1 helix in bulk. Perhaps more telling, Kalachev et al. [57] noted that PDES formed islands at the A/W interface after spreading that coalesced to form a film upon compression. In essence, the isotherms of PMTFPS, PMPS, and PDES, much like PDMS, are consistent with monolayer to multilayer transitions.

7.3 Polyhedral Oligomeric Silsesquioxane (POSS) Langmuir Films

While standard silicones are linear with a repeating structure of –(R′R″SiO)-, silsesquioxanes have a repeating unit structure of –($RSiO_{1.5}$)- [58, 59]. As a result, silsesquioxanes can be randomly branched, form ladder-like structures, or form highly organized cage-like molecules known as polyhedral oligomeric silsesquioxanes (POSSs) (see also Chap. 6). Structures of silsesquioxanes discussed in this chapter are shown in Fig. 7.15 and non-POSS silsesquioxanes will not be reviewed,

even though some are known to form Langmuir films [60]. POSS molecules are cube-like structures that can either be completely condensed (closed-cage POSS); bottom of Fig. 7.15 or partially condensed (open-cage POSS); top of Fig. 7.15. These molecules have $SiO_{1.5}$ cores that are a bit less than 1 nm along a diagonal. In most cases, they also have an organic corona that makes the overall size of the typical molecule 1 to 3 nm along a diagonal. In principle the inorganic core provides the thermal and oxidative stability of inorganic materials while the organic corona enhances processability. The nanometer sizes of the molecule have sparked intense research and technical interest [61] for things ranging from nanofillers [62], nanocomposites [63, 64], nanostructured polymers and copolymers [65], catalytic supports [66], space survivable materials [67], oleophobic surfaces [68] and more recently biomaterials [69].

Surprisingly, surface studies of POSS-based materials evolved more slowly than bulk studies even though the first POSS derivative [70] was known around the same time Fox et al. [8] reported the Π-A isotherm for PDMS. Knischka et al. coupled a POSS cage to an poly(ethylene glycol) (PEG) oligomer to create a water soluble amphiphile and determined its critical micelle concentration [71]. More recently, a similar concept was used to create POSS-based amphiphiles in which a carboxylic acid modified POSS-derivative served as the hydrophilic head, whereas polystyrene (PS) served as the hydrophobic tail [72].

It was not until 2002 that Deng et al. published the first study on Langmuir films of POSS derivatives [73]. In this study the authors reported that the open-cage trisilanolisobutyl-POSS (TiBuP) was amphiphilic and formed Langmuir films, whereas closed-cage octaisobutyl-POSS (OiBuP) was non-amphiphilic and formed heterogeneous films at all surface concentrations. A more detailed study of TiBuP followed [74]. Deng et al. [75] also reported a somewhat different Π-A isotherm for trisilanolcyclohexyl-POSS (TCyP). In contrast to TiBuP, TCyP formed intricate structures in the collapse state, including rod-like domains at very high Π. These features were attributed to dimerization which is commonly seen in the crystal structures of trisilanol-POSS derivatives and led to very rigid films [76]. This concept is reflected in the design of double-decker shaped POSS amphiphiles [77–79]. In 2007, Lee et al. [80] showed that the design concept of Knischka et al. [71] could also lead to insoluble Langmuir films, some of which even underwent LB-transfer. In 2009, Wen and Esker [81] also reported on the surface viscoelastic properties of TiBuP by SLS.

Some other studies of POSS films associated with A/W interfaces are worth noting. Several authors have made use of the fact that trisilanolphenyl-POSS (TPP) forms LB-films. Ferguson et al. [82, 83] used TPP films to study the interactions between silanol groups and simulants for chemical warfare agents. Paul et al. studied pattern formation associated with dewetting in bilayers where TPP LB-films were transferred onto films of poly(*t*-butyl acrylate) (PtBA) [84] or PS [85] and also used mixed LB-films of TPP and PtBA to study phase separation [86]. Huffer et al. also made use of the ability of TPP to form LB-films and interact with metal ions to study TPP layers as adhesion promoting layers [87]. In a somewhat different fashion, other authors looked at blends of POSS derivatives with silicones in Langmuir films. The

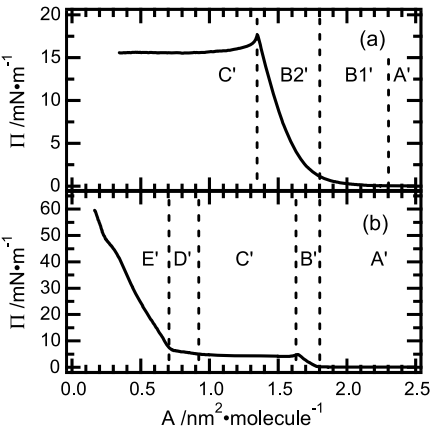

Fig. 7.16 Π-A isotherms for (**a**) TiBuP (data acquired under similar conditions to Ref. [74]) and (**b**) TCyP (data acquired unders similar conditions to Ref. [75]) at the A/W interface and 22.5 °C. The *vertical dashed lines* and letters indicate natural boundaries between regimes

first such study by Hottle et al. [88] looked at blends of TiBuP/PDMS and was followed by a study of OiBUP/PDMS [89]. Kim et al. followed up on the studies of TiBuP/PDMS by examining blends of TiBuP with polar functional silicones [90, 91]. These blend studies are discussed in greater detail next.

Three topics are addressed: comparisons of TiBuP and TCyP isotherms, studies of surface viscoelasticity for TiBuP and TCyP, and blends of silicones with POSS derivatives. The discussion focuses on general trends and features that are similar to factors that affected the Langmuir film properties of PDMS.

7.3.1 *Surface Pressure-Area per Molecule (Π-A) Isotherms of Trisilanolisobutyl-POSS (TiBuP) and Trisilanolcyclohexyl-POSS (TCyP) Langmuir Films*

Figure 7.16 shows Π-A isotherms for TiBuP [73, 74] and TCyP [75, 76]. Regimes are designated by letters with primes to distinguish them from PDMS. The isotherms were obtained by compression at a fixed rate. In Regime A′, BAM showed coexistence between condensed domains and gaseous monolayer for TCyP films, while Deng et al. [74] speculated that similar behavior may occur for TiBuP.

As the TiBuP and TCyP films are compressed, the monolayers form at the boundary to Regime B′ of Fig. 7.16, where Π increases from zero at a lift-off area of $A_{\text{lift-off}} \sim 2.3\ \text{nm}^2\,\text{molecule}^{-1}$ for TiBuP and $A_{\text{lift-off}} \sim 1.81\ \text{nm}^2\,\text{molecule}^{-1}$ for TCyP. In Regime B′ there are differences between TiBuP and TCyP. For TCyP, Π rises rapidly from $A_{\text{lift-off}}$ until a collapse pressure (Π_{collapse}) of $\sim$4.3 $\text{mN}\,\text{m}^{-1}$ where a kink in the Π-A isotherm corresponds to a collapse area (A_{collapse}) of $\sim$1.64 $\text{nm}^2\,\text{molecule}^{-1}$. Extrapolation of the Π-A isotherm in the sub-regime at smaller A back to the x-axis yields the experimental limiting area (A_o = 1.77 $\text{nm}^2\,\text{molecule}^{-1}$). This value is in excellent agreement with calculated cross-sectional area ($A_{o,c}$) of a POSS cage with a vertex-on conformation (one in which

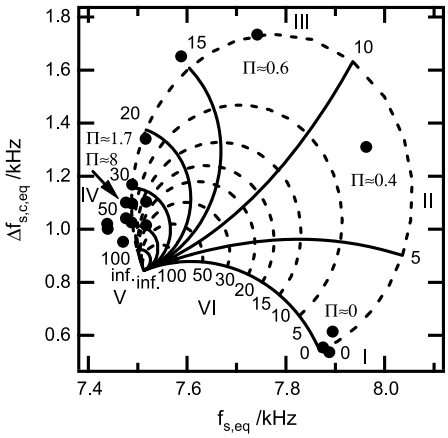

Fig. 7.17 $\Delta f_{s,c,eq} - f_{s,c,eq}$ for TiBuP at the A/W interface and 25 °C. Data were replotted from Ref. [81]

the POSS cube is standing on one corner, the trisilanol pocket), one finds $A_{o,c} \sim 1.78\ nm^2\,molecule^{-1}$. In the case of TCyP, $A_{o,c} \sim A_o \sim A_{lift\text{-}off}$. Regime B′ for TiBuP has two distinct sub-regimes: (B1′) $1.80 < A < 2.30\ nm^2\,molecule^{-1}$ and (B2′) $1.35 < A < 1.80\ nm^2\,molecule^{-1}$. In sub-regime B1′, the film is more compressible (surface isothermal compressibility $= \kappa_s = \varepsilon_s^{-1}$) than in sub-regime B2′. Extrapolation of the Π-A isotherm in sub-regime B2′ back to the x-axis yields $A_{o,c} \sim A_o = 1.77\ nm^2\,molecule^{-1}$. At the end of the monolayer regime (B′), collapse of the film is also signified by a kink in the isotherm at $A_{collapse} \sim 1.35\ nm^2\,molecule^{-1}$, $\Pi_{collapse} \sim 17\ mN\,m^{-1}$.

Several points about Regime A′ and B′ of Fig. 7.16 need to be emphasized before moving on to Regime C′: (1) qualitatively, the behavior exhibited by TiBuP and TCyP in Regimes A′ and B′ is completely analogous to Regimes A and B for PDMS in Fig. 7.2. More importantly, this behavior is consistent with any traditional amphiphile that forms stable Langmuir films; (2) the size differences for transitions in the isotherms between TiBuP and TCyP, reflect greater flexibility of the TiBuP groups and the larger overall size of TCyP; (3) the higher $\Pi_{collapse}$ for TiBuP relative to TCyP reflects a wrapping of the cyclohexyl substituents back around the cage that partially blocks the ability of the silanol groups to hydrogen bond. In this respect, it is similar to the effect polar functional end-groups have on the Π-A isotherm of PDMS; and finally, (4) the shape of the isotherms for TiBuP and TCyP at the collapse transition are consistent with Langmuir films that exist in a metastable state because the film is compressed at a rate faster than it can collapse (analogous to supercooling). If the isotherms are obtained by successive additions of spreading solution, the collapse pressures decrease to $\Pi_{collapse} = 13.2\ mN\,m^{-1}$ [74] and $2.6\ mN\,m^{-1}$ [76]. These values mean that in Regime B′ of Fig. 7.16, approximately the last third for TiBuP and last half for TCyP of the Π-A isotherm is in a non-equilibrium state. In contrast, the isotherms for PDMS are almost perfectly reversible over the entire range of A.

In the context of the discussion in Sect. 7.2.1, Regime C′ for TiBuP and TCyP is also analogous to Regime C for PDMS. Deng et al. speculated that both TiBuP

[73, 74] and TCyP [75, 76] collapsed through the formation of POSS dimers on the basis of the known dimeric unit cell of crystal structures for some of the trisilanol-POSS derivatives [92]. These studies confirmed collapse of the film through BAM where heterogeneous, bright structures were seen in Regime C′ for both TiBuP and TCyP. As seen in Fig. 7.16, Regime C′ is finite for TCyP, and terminal for TiBuP. The speculative explanation for this difference is that the enhanced flexibility of the isobutyl substituents hinders dimer formation and the ultimate formation of a well-ordered TiBuP film. In contrast, Regime C′ comes to an end around A ~ 0.91 nm^2 molecule^{-1} for TCyP. At this point, A is approximately half the area of the start of Regime B′. The small rise in Π associated with Regime D′ in Figs. 7.7–7.16 ends at A ~ 0.73 nm^2 molecule^{-1}, or $\sim 1/3$ the area at the start of Regime B′. If one does the same thing for the boundary between Regime C and D relative to the start of Regime B for PDMS in Fig. 7.2, the ratio is nearly identical. Simply on the basis of conservation of mass, an argument could be made for a trilayer state at this point for both PDMS and TCyP, with a monolayer against water, and a bilayer that hides hydrophilic moieties residing against air. Such a structure would be consistent with VSFS studies of PDMS [22].

To this point, the transitions in the TiBuP and TCyP Π-A isotherms are completely consistent with the transitions seen in PDMS, assuming the multilayer model for PDMS is correct. Looking at Regime E′ in Figs. 7.7–7.16 for TCyP, it is tempting to equate the behavior to Regime E for PDMS samples with polar functional end groups. However, the origin of the phenomenon is different. In Regime E for PDMS (like in Fig. 7.13), increasing Π reflects the energy required to remove polar functional groups from the interface. As seen in Fig. 7.16b, $\Pi_{\text{collapse}} < 5$ mN m^{-1} is all that is required in Regime B′ to remove TCyP from the A/W interface. Instead, Regime E′ in Fig. 7.16b reflects the formation of densely packed, thick ($\sim$6 TCyP molecules around A ~ 0.3 nm^2 molecule^{-1}) aggregates that form rigid, rod-like structures at $\Pi > 50$ mN m^{-1} [75]. In this respect, the successive formation of multilayer structures is more in line with the studies of successive multilayer formation in cyclolinear methylphenylsiloxane films at the A/W interface [93–97].

7.3.2 *Viscoelastic Properties of Trisilanolisobutyl-POSS (TiBuP) and Trisilanolcyclohexyl-POSS (TCyP) Langmuir Films*

In this section, two cases are considered, a study of TiBuP by SLS [81] and a study of TCyP by interfacial stress rheometry (ISR) [76]. The study of TiBuP can be directly compared to Sect. 7.2.2.2. Before discussing ISR results, it is worthwhile to briefly review the principle of the technique [98, 99]. In ISR, a Teflon-coated magnetic needle is placed at the A/W interface of a Langmuir trough situated inside an AC Helmholtz coil system. An oscillatory stress for angular frequencies (ω) of the order of 1 to 10 rad s^{-1} is applied through the coil system causing the needle at the interface to undergo translational motion. The motion of the needle is measured optically and the amplitude and phase are compared with the driving force. This information is used to determine the complex surface shear modulus ($G_s^* = G_s' + iG_s''$,

where G_s' and G_s'' are the shear elastic and shear loss modulus, respectively), loss tangent (tan $\delta = G_s''/G_s'$) and the complex shear viscosity ($\mu_s^* = [G_s'' - iG_s']/\omega$). As these experiments probe shear parameters, the most relevant comparison is to the work by Jarvis [27].

7.3.2.1 Limiting Viscoelastic Behavior in TiBuP Langmuir Films by SLS

Section 7.2.2.2 discussed the limiting viscoelastic behavior of PDMS Langmuir films through three different treatments of the data. Each treatment had different merits for bringing out the complex changes in dilational viscoelastic behavior that accompany the Π-A isotherm of PDMS in Fig. 7.2. The most remarkable feature of PDMS is how ε_d and κ return to zero as the PDMS monolayer collapses (the boundary between Regimes B and C) and after the multilayer transition between Regimes C and D to result in pure liquid dynamics in the plateaus (Regime C and D). Here, we simply consider the corresponding states approach for TiBuP, because the dilational viscoelastic behavior is far simpler [81]. Figure 7.17 is a plot of $\Delta f_{s,c}$ versus f_s for TiBuP. In Fig. 7.17, the boundaries for Regimes A′ correspond to Limit I and C′ corresponds to the points between Limits IV and V, while Regime B′ corresponds to the perimeter of the plot along a perfectly elastic ($\kappa = 0$) trajectory from (I) pure liquid dynamics until the maximum ε_d is reached somewhere near (V) the infinite dilational modulus limit. Values of Π on the graph help define the position within Regime B′. Upon film collapse, the films viscoelastic state remains unchanged in stark contrast to PDMS. In essence, Fig. 7.17, corresponds to Fig. 7.10a. Whereas ε_d in PDMS films started to decrease after the maximum ε_d was achieved at the midpoint of Regime B, the more rigid TiBuP films (larger maximum ε_d) exhibited no such relaxation in ε_d throughout the remainder of Regime B′ nor during collapse into multilayers in Regime C′. In this respect, the ability of PDMS to spread upon itself and inability to form solid-like collapsed domains like TiBuP play an important role in the unique dilational viscoelastic properties of PDMS films.

7.3.2.2 Shear Viscoelastic Behavior in TCyP Langmuir Films by ISR

Early on, Jarvis [27] used canal viscometry and a torsional surface viscometer to show that the surface shear viscosity of PDMS Langmuir films was on the order of 10^{-5} mN s m^{-1}. As these results were essentially at the detection limits of the technique, the values were insignificantly small and consistent with small values of κ seen in SLS experiments already discussed in this chapter. Deng et al. [76] applied ISR to study the shear viscoelastic properties of TCyP. It is possible to discuss their results in terms of the regimes defined in Fig. 7.16b. Measurements around the boundary between Regimes A′ and B′ yielded small G_s' and G_s'' (<0.001 mN m^{-1}), near the detection limit and were highly sensitive to hydrodynamic corrections for viscous drag on the floating needle. Such small values

are consistent with expectations from the work by Jarvis [27] for PDMS and the small molecule poorly packed TCyP film with small Π_{collapse}. From these values tan $\delta > 1$ were found indicating that viscous contributions were more important than elastic ones to the observed behavior. In Regime C′, three different types of response were observed. Near the boundary between Regimes B′ and C′, the films had slightly larger shear moduli (G_s' & $G_s'' \sim 0.001$ mN m^{-1}) than in the monolayer, a void region where measurements were not feasible, and much larger shear moduli (G_s' & $G_s'' \sim 0.02$ mN m^{-1}) near the boundary between Regimes C′ and D′. In essence, the three distinct responses in Regime C′ corresponded to monolayer-rich, approximately equal amounts of monolayer- and multilayer-rich domains, and multilayer-rich domains along the plateau. As G_s' and G_s'' of the monolayer-rich and multilayer-rich domains differed by more than an order of magnitude, ISR required different applied stresses to probe each type of domain which proved too difficult to do experimentally. Inside Regime D′, the larger G_s' and G_s'' of the films worked well, and the moduli increased systematically with decreasing A, however, G_s'' was still larger than G_s' leading to tan $\delta > 1$. Perhaps the most remarkable result was the dramatic increase in G_s' and G_s'' inside Regime E′. The value of G_s' (10 mN m^{-1}) had jumped by more than an order of magnitude from Regime D′ by $\Pi = 12$ mN m^{-1}, and between $12 < \Pi < 20$ mN m^{-1}, G_s' increased nearly linearly with A by another order of magnitude. More importantly, the films in Regime E′ were much more elastic with tan $\delta < 1$ as G_s' was more than an order of magnitude larger than G_s'' by $\Pi = 20$ mN m^{-1}. From these results, it was clear that rigid, solid-like domains were being formed, and they were consistent with the unique rod-like domains that form in TCyP at $\Pi > 50$ mN m^{-1} [75]. In essence, the transition of the TCyP Langmuir film from PDMS-like shear viscoelastic behavior in the monolayer to rigid, rod-like behavior is similar to the effect of adding rigid polyphthalocyaninatosiloxane to eicosanol Langmuir films [98].

7.3.3 *Blends of POSS Derivatives with Silicones as Langmuir Films*

An obvious extension of Langmuir film studies of POSS and PDMS is the study of blends, whereby POSS serves as a nanofiller with a dimension comparable to the thickness of the 2D film. Four such systems have been studied through Π-A isotherms and BAM. Three of these studies used TiBuP and PDMS (Figs. 7.1 and 7.15) that had non-polar endgroups (sec-butylsilyl and trimethylsilyl) (npPDMS) [88], polar phosphine oxide substituents (PDMS-PO) [90], or polar 3-cyanopropyl substituents (PMCPS) [91]. Π-A isotherms for these compounds are compared with Π_c for TiBuP in Fig. 7.18. Hottle showed that for npPDMS and TiBuP, the blends formed homogeneous films and were miscible for weight percentages (wt.%) POSS <80 %, the Π_{collapse} for the npPDMS component increased with increasing TiBuP, and that upon collapse of the TiBuP, POSS-rich aggregates formed. If the films were expanded from these collapsed states, network

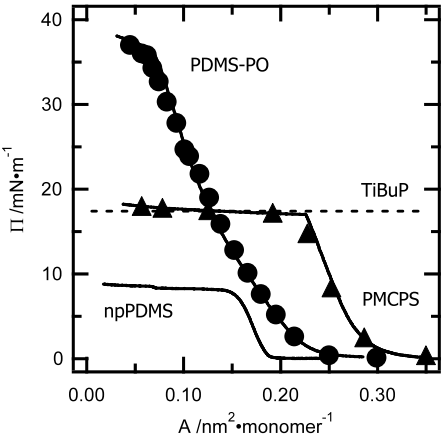

Fig. 7.18 Π-A isotherms for PDMS-PO (*circles*), PMCPS (*triangles*), and npPDMS (*solid line*) at the A/W interface and 22.5 °C (taken from Refs. [90] and [91]). The *horizontal dashed line* is the collapse pressure for TiBuP

structures were observed when the wt.% POSS was greater than 85 % (similar to neat TiBuP films [73, 74]), whereas only isolated POSS domains were observed for smaller wt.% POSS. These network domains are depicted in Fig. 7.19. In contrast, blends of npPDMS with PDMS-PO were miscible at all compositions, formed small round POSS aggregates for $\Pi > \Pi_{\text{collapse}}$ of TiBuP (like those depicted in Fig. 7.19), and these aggregates did not form network-like structures at any blend composition [90]. In essence, the morphology of the resulting blends upon expansion of the films (round domains vs. extended aggregation) was controlled by which component collapsed into multilayers first, the amphiphilic POSS or the silicone as depicted in Fig. 7.19. In a follow-up study by Kim et al. [91], TiBuP blends with PMCPS showed intermediate behavior. Extended aggregates only formed for POSS > 90 wt.%, but did not form complete networks. The authors attributed the inhibition of network formation to enhanced hydrogen bonding between the polar functional PDMS and the POSS cages.

The other study of blends to date [89] showed that the dispersion of octaisobutyl-POSS (OiBuP), a non-amphiphilic POSS derivative that forms large irregular aggregates, at the A/W interface improved in the presence of npPDMS. For these systems, the films were heterogeneous at all Π and A, but the morphologies fell into three regimes: (1) > 70 wt.% OiBuP, (2) ~ 40 to 70 wt.% OiBuP, and (3) < 40 wt.% OiBuP. In all regimes, the average thickness of the POSS-rich aggregates was reduced by at least 45 % relative to the neat OiBuP film. In Regime 1, POSS aggregates observed during compression were similar to neat OiBuP and upon expansion had a "shattered glass" appearance. For Regime 2, POSS domains in compressed films were smaller than Regime 1 and the morphologies were similar upon compression and expansion. As the amount of OiBuP decreased even further, the "heterogeneously homogeneous films" observed during compression gave rise to network-like structures that look similar to those seen for TiBuP blends with npPDMS. However, they occur at much smaller wt.% POSS.

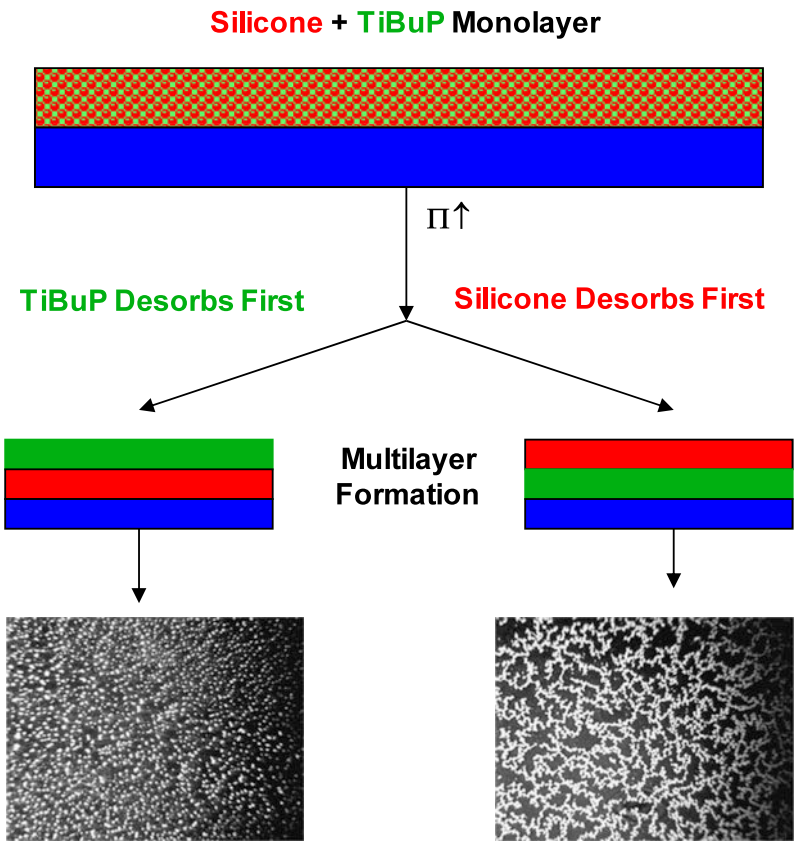

Fig. 7.19 Schematic depiction of layering for silicones with different collapse pressures like those in Fig. 7.18 (silicone denoted in *red*) blended with TiBuP (*green*) at the A/W interface. If the TiBuP collapses before the silicone with increasing Π, small isolated domains form in BAM images (4.8 mm × 6.4 mm), whereas intricate "network structures" are observed if the silicone collapses before the TiBuP

7.4 Summary

While the model of Fox et al. [8] for explaining the unique Π-A isotherm is now widely regarded as incorrect in light of data from new surface characterization techniques, it sparked intense interest in Langmuir films of silicones and broader surface studies of silicone surfactants and surface modifying agents. Over the past decade, this led researchers to look into analogous studies of POSS derivatives where the more rigid structure leads to more traditional Langmuir film behavior. Nonetheless, there is still much to learn about the intricacies of silicon containing materials in Langmuir films.

Acknowledgements The authors are grateful for financial support from the National Science Foundation (CHE-0239633) and the Virginia Tech Aspires Program and to Michael Owen from Dow Corning for providing the gel permeation chromatography data.

Appendix A: Experimental Details for PDMS Studies

A.1 Materials

Linear samples of trimethylsilyl-terminated PDMS were obtained from United Chemical Technologies. Gel permeation chromatography results obtained from Dr. Michael J. Owen at Dow Corning Corporation revealed the polymers had number average molecular weights (M_n) and polydispersity indices (M_w/M_n) of $(M_n, M_w/M_n) = (1{,}210, 1.46)$, $(1{,}740, 1.72)$, $(3{,}370, 1.55)$, and $(10{,}400, 2.47)$. Another linear sample with a viscosity of 5 cS corresponding to $M_n < 1{,}210$ failed to form a stable Langmuir film. A PDMS sample containing hydroxyl endgroups ($M_n = 12{,}700$, $M_w/M_n = 2.68$) was obtained from Scientific Polymer Products, Inc. PDES, PMPS, and PMFS with nominal molecular weights of 30,000 2,600, and 4,600 were also obtained from United Chemical Technologies. All of the commercial polymers were used as received. HPLC grade chloroform or dichloromethane (Aldrich) was used to prepare spreading solutions with nominal concentrations of $\sim$0.1 g L^{-1} for Π-A isotherm and SLS studies on Millipore-Q2 (18.2 MΩ cm) filtered distilled water subphases. The spreading solvent had no influence on the experimental results. For the case of the PDES system, a 1:1 by volume mixture of chloroform and hexane also yielded identical results.

A.2 Π-A Isotherm Measurements

A Teflon trough (28.5 $\times$ 11.0 $\times$ 1.25 cm) housed in a Plexiglas box to maintain high relative humidities (>70 %) was filled with Millipore water. The trough was cleaned before each experiment with a sulfuric acid/Nochromix (Godax Industries) mixture and was thoroughly rinsed with Millipore water. Temperature was maintained at 23.0 or 25.0 °C to $\pm$0.1 °C by circulating thermostated water (Lauda, RM6) through a glass coil in the bottom of the trough. Surface tension was measured by the Wilhelmy plate technique with a Cahn 2000 Model electrobalance and a platinum plate (2.64 $\times$ 1.12 $\times$ 0.01 cm) that was cleaned by overnight storage in a 1:1 by volume mixture of concentrated sulfuric and nitric acid followed by extensive rinsing with Millipore water. This approach allows for the determination of surface tension to $\pm$0.02 mN m^{-1}. After filling the trough with water to the brim, a Teflon barrier was used to sweep the surface and concentrate any surface-active impurities on the non-monolayer side of the barrier. A clean glass pipet was then used to suction off the surface. This process was repeated a minimum of three times, or until the correct surface tension for water was obtained. The quality of the water was also verified by SLS prior to spreading a monolayer. The surface concentration, expressed in terms of area per repeat unit (monomer for short) was controlled by making successive additions of spreading solvent. After adding a desired volume of spreading solvent, at least 15 minutes was allowed for the spreading solvent to evaporate with the exact time determined by the point where $d\Pi/dt < 0.04$ mN m^{-1} over a 5 min period.

A.3 SLS Measurements

All SLS and Π measurements were made simultaneously. The SLS instrument, see Sano et al. [100], incorporates the improvements of Hård and Neuman [101] and more recent descriptions of the instrument can be found elsewhere [31, 35]. The key feature for the SLS instrument is the use of a transmission diffraction grating [102] that allows for heterodyne detection of light scattered by spontaneously formed capillary waves that result from density fluctuations in the underlying subphase. For this study, fourth through seventh order diffraction spots were used to define the scattering angle. This range of diffraction orders corresponds to a spatial wave vector range of $k \sim 250$–$450\ \mathrm{cm}^{-1}$.

Instrument calibration was with water. Power spectra, obtained from water for each wave vector, were fit with a Lorentzian function to obtain f_s and the experimental full-width at half-maximum intensity ($\Delta f_{s,\mathrm{exp}}$). f_s is proportional to the angular frequency ($\omega = 2\pi f_s$). $\Delta f_{s,\mathrm{exp}}$ was corrected for Gaussian broadening of the laser beam profile [102]. For the ith diffraction order:

$$\Delta f_{s,c,i} = \Delta f_{s,\mathrm{exp},i} - \frac{\Delta f_{\mathrm{inst},i}^2}{\Delta f_{s,\mathrm{exp},i}} \tag{7.19}$$

where the instrumental broadening of the ith diffraction order is defined as

$$\Delta f_{\mathrm{inst},i} = \sqrt{2}\left(\frac{\Delta u_i \cos\theta}{R\lambda}\right)\left(\frac{d\omega}{dk}\right)_i. \tag{7.20}$$

The wavelength of the laser (λ), incident angle (θ), and distance from the interface to the detector (R) were 632.8 nm, 64.4°, and 3.64 m, respectively. Specific values of $(d\omega/dk)_i$, Δu_i, and k_i were obtained from an iterative solution of Eqs. (7.19) and (7.7), along with expressions for ω [47, 48] and the temporal damping coefficient ($\alpha = \pi \Delta f_{s,c}$) [37, 103] for pure liquids (Eqs. (7.6) and (7.7)). After calibrating with water, the validity of the calibration is tested with anisole and ethylbenzoate to ensure that Eqs. (7.6) and (7.7) yield σ_d and η values that agree with the literature to 3 %. This approach for monolayer studies yields overall errors of 0.5 % and 5 % for f_s and $\Delta f_{s,c}$, respectively.

References

1. Clarson SJ, Semlyen JA (eds) (1993) Siloxane polymers. PTR Prentice Hall, Englewood Cliffs
2. Clarson SJ, Fitzgerald JJ, Owen MJ, Smith SD (eds) (2000) Silicones and silicone-modified materials. ACS symposium series, vol 729. Am Chem Soc, Washington
3. Clarson SJ, Fitzgerald JJ, Owen MJ, Smith SD, Van Dyke ME (eds) (2003) Synthesis and properties of silicones and silicone-modified materials. ACS symposium series, vol 838. Am Chem Soc, Washington

4. Clarson SJ, Fitzgerald JJ, Owen MJ, Smith SD, Van Dyke ME (eds) (2007) Science and technology of silicones and silicone-modified materials. ACS symposium series, vol 964. Am Chem Soc, Washington
5. Clarson SJ, Fitzgerald JJ, Owen MJ, Smith SD, Van Dyke ME (eds) (2010) Advances in silicones and silicone-modified materials. ACS symposium series, vol 1051. Am Chem Soc, Washington
6. Owen MJ (1990) Siloxane surface activity. In: Ziegler JM, Fearon FWG (eds) Silicon-based polymer science: a comprehenseive resource. Advances in chemistry series, vol 224. Am Chem Soc, Washington
7. Owen MJ (1993) Surface chemistry and applications. In: Clarson SJ, Semlyen JA (eds) Siloxane polymers. Prentice Hall, Englewood Cliffs
8. Fox HW, Taylor PW, Zisman WA (1947) Polyorganosiloxanes—surface active properties. Ind Eng Chem 39:1401–1409. doi:10.1021/ie50455a607
9. Esker AR (1996) Molecular architecture and monolayer dynamics at the air/water interface by *s*urface light scattering, PhD thesis, University of Wisconsin, Madison, Wisconsin
10. Mann EK, Henon S, Langevin D, Meunier J (1992) Molecular layers of a polymer at the free-water surface—microscopy at the Brewster-angle. J Phys II (France) 2:1683–1704
11. Damaschun G (1962) Rontgenographische untersuchung der Struktur von silikongummi. Kolloid-Z Z Polymere 180:65–67. doi:10.1007/BF01499486
12. Schilling FC, Gomez MA, Tonelli AE (1991) Solid-state NMR observations of the crystalline conformation of poly(dimethylsiloxane). Macromolecules 24:6552–6553. doi:10.1021/ma00024a032
13. Noll W, Steinbach H, Sucker C (1963) Beitrage zur grenzflachen Chemie der Organopolysiloxanen. 1. Das Verhalten der Siloxankette bei der Spreitung von α-ω-trimethylsiloxy-dimethylpolysiloxanen. Ber. Bunsenges 67:407–415
14. Noll W, Steinbach H, Sucker C (1965) Beitrage zur Grenzflächenchemie der Organopolysiloxane. II Das Spreitungsverhalten von dimethyl- und methylhydrogenpolysiloxanen in abhängigkeit vom pH-wert. Kolloid-Z Z Polymere 204:94–101. doi:10.1007/BF01500384
15. Noll W, Steinbach H, Sucker C (1971) Monolayers of polyorganosiloxanes on water. J Polym Sci C Polym Symp 34:123–139. doi:10.1002/polc.5070340114
16. Granick S (1985) Surface pressure of linear and cyclic poly(dimethylsiloxane) in the transition region. Macromolecules 18:1597–1602
17. de Gennes PG (1979) Scaling concepts in polymer physics. Cornell University, Ithaca
18. Stephen M, McCauley J (1973) Feynman graph expansion for tricritical exponents. Phys Lett A 44:89–90. doi:10.1016/0375-9601(73)90799-8
19. Mann EK, Langevin D (1991) Poly(dimethylsiloxane) molecular layers at the surface of water and of aqueous surfactant solutions. Langmuir 7:1112–1117. doi:10.1021/la00054a016
20. Runge FE, Yu H (1993) Thin-films of a binary system—poly(vinyl acetate) poly(dimethylsiloxane) layers at the air-water-interface. Langmuir 9:3191–3199. doi:10.1021/la00035a071
21. Webster HF, Wightman JP (1991) Characterization of thin-films of poly(dimethylsiloxane) formed from surface-diffusion across defined polymer substrates. Langmuir 7:3099–3109. doi:10.1021/la00060a033
22. Kim C, Gurau MC, Cremer PS, Yu H (2008) Chain conformation of poly(dimethyl siloxane) at the air/water interface by sum frequency generation. Langmuir 24:10155–10160. doi:10.1021/la800349q
23. Bernardini C, Stoyanov SD, Stuart MAC, Arnaudov LN, Leermakers FAM (2010) Polymers at the water/air interface, surface pressure isotherms, and molecularly detailed modeling. Langmuir 26:11850–11861. doi:10.1021/la101003c
24. Bernardini C, Stoyanov SD, Stuart MAC, Arnaudov LN, Leermakers FAM (2011) PMMA highlights the layering transition of PDMS in langmuir films. Langmuir 27:2501–2508. doi:10.1021/la104285z
25. Ogarev VA (1997) Monomolecular films of poly(dimethyl siloxane) at liquid surfaces. Colloid J 59:625–634

26. Piwowar AM, Gardella JA (2008) Reflection-absorption Fourier transform infrared spectroscopic study of transferred films of poly(dimethylsiloxane) using the Langmuir–Blodgett technique. Macromolecules 41:2616–2619. doi:10.1021/ma702893d
27. Jarvis NL (1966) Surface viscosity of polydimethylsiloxane monolayers. J Phys Chem 70:3027–3033. doi:10.1021/j100882a001
28. Garrett WD, Zisman WA (1970) Damping of capillary waves on water by monomolecular films of linear polyorganosiloxanes. J Phys Chem 74:1796–1805. doi:10.1021/j100703a023
29. Hård S, Neuman RD (1987) Viscoelasticity of monomolecular films: a laser light-scattering study. J Colloid Interface Sci 120:15–29. doi:10.1016/0021-9797(87)90319-5
30. Miller ED (1994) 2-Dimensional and bulk viscoelastic properties of poly(dimethylsiloxane), PhD Thesis, University of Wisconsin–Madison, Wisconsin
31. Esker AR, Kim C, Yu H (2007) Polymer monolayer dynamics. Adv Polym Sci 209:59–110. doi:10.1007/12_2007_113
32. Braslau A, Pershan PS, Swislow G, Ocko BM, Als-Nielsen J (1988) Capillary waves on the surface of simple liquids measured by x-ray reflectivity. Phys Rev A 38:2457–2470. doi:10.1103/PhysRevA.38.2457
33. Lucassen-Reynders EH, Lucassen J (1970) Properties of capillary waves. Adv Colloid Interface Sci 2:347–395. doi:10.1016/0001-8686(70)80001-X
34. Langevin D (1981) Light-scattering study of monolayer viscoelasticity. J Colloid Interface Sci 80:412–475. doi:10.1016/0021-9797(81)90200-9
35. Esker AR, Zhang LH, Sauer BB, Lee W, Yu H (2000) Dilational viscoelastic behaviors of homopolymer monolayers: surface light scattering analysis. Colloids Surf A 171:131–148. doi:10.1016/S0927-7757(99)00564-6
36. Thomson W (1871) The influence of wind on waves in water supposed frictionless. Philos Mag 42:368–374
37. Stokes GG (1849) On the theories of the internal friction of fluids in motion, and of the equilibrium and motion of elastic solids. Cambridge Philos Soc Trans 8:287–319
38. Dorrestein RR (1951) General linearized theory of the effect of surface films on water ripples. I. Koninkl Ned Akad Wetenshap Proc B 54:260–272
39. Dorrestein RR (1951) General linearized theory of the effect of surface films on water ripples, II. Koninkl Ned Akad Wetenshap Proc B 54:350–356
40. Esker AR, Zhang LH, Olsen CE, No K, Yu H (1999) Static and dynamic properties of calixarene monolayers at the air/water interface. 1. pH Effects with p-dioctadecanoylcalix[4]arene. Langmuir 15:1716–1724. doi:10.1021/la970016b
41. Reynolds O (1880) On the effect of oil in destroying waves on the surface of water. Br Ass Rep 50:489–490
42. Yin W, Xie Q, Deng J, Goff JD, Vadala TP, Riffle JS, Esker AR (2010) Viscoelastic behavior of PDMS stabilized magnetite magnetic nanoparticle complexes. In: Clarson SJ, Fitzgerald JJ, Owen MJ, Smith SD, Van Dyke ME (eds) Advances in silicones and silicone-modified materials. ACS symposium series, vol 1051. Am Chem Soc, Washington
43. Le Guillou JC, Zinn-Justin J (1977) Critical exponents for the n-vector model in three dimensions from field theory. Phys Rev Lett 39:95–98. doi:10.1103/PhysRevLett.39.95
44. Le Guillou JC, Zinn-Justin J (1980) Critical exponents from field theory. Phys Rev B, Condens Matter 21:3976–3998. doi:10.1103/PhysRevB.21.3976
45. de Gennes PG (1979) Scaling concepts in polymer physics. Cornell University, Ithaca, p. 45
46. Duplantier B, Saleur H (1987) Exact tricritical exponents for polymers at the THETA point in two dimensions. Phys Rev Lett 59:539–542. doi:10.1103/PhysRevLett.59.539
47. Granick S, Clarson SJ, Formoy TR, Semlyen JA (1985) Studies of cyclic and linear poly(dimethylsiloxanes): 18. Surface pressures of the monolayers in the plateau region. Polymer 26:925–929. doi:10.1016/0032-3861(85)90139-9
48. Kawaguchi M, Sauer BB, Yu H (1989) Polymeric monolayer dynamics at the air/water interface by surface light scattering. Macromolecules 22:1735–1743. doi:10.1021/ma00194a039
49. Lee KY, Chou T, Chung DS, Mazur E (1993) Direct measurement of the spatial damping of capillary waves at liquid-vapor interfaces. J Phys Chem 97:12876–12878. doi:10.1021/j100151a039

50. Wang Q, Feder E, Mazur E (1994) Capillary wave damping in heterogeneous monolayers. J Phys Chem 98:12720–12726. doi:10.1021/j100099a041
51. Newing MJ (1950) The surface properties of polar silicones. Trans Faraday Soc 46:755–762. doi:10.1039/TF9504600755
52. Lenk TJ, Lee DHT, Koberstein JT (1994) End group effects on monolayers of functionally-terminated poly(dimethylsiloxanes) at the air–water interface. Langmuir 10:1857–1864. doi:10.1021/la00018a040
53. Wegner G (1993) Control of molecular and supramolecular architecture of polymers, polymer systems and nanocomposites. Mol Cryst Liq Cryst 234:283–316
54. Noll W, Steinbach H, Sucker C (1970) Beitr age zur Grenzflächenchemie der Polyorganosiloxane. III, Der Einflußvon Substituenten auf das Spreitungsverhalten kettenpolymerer Siloxane. Kolloid-Z Z Polymere 236:1–19. doi:10.1007/BF02084508
55. Bernett MK, Zisman WA (1971) Properties of poly[methyl(n-alkyl)siloxane] and poly[methyl(3,3,3-trifluoropropyl)siloxane] monolayers adsorbed on water. Macromolecules 4:47–53. doi:10.1021/ma60019a011
56. Miller KJ, Grebowicz J, Wesson JP, Wunderlich B (1990) Conformations of poly(diethylsiloxane) and its mesophase transitions. Macromolecules 23:849–856. doi:10.1021/ma00205a026
57. Kalachev AA, Litvinov VM, Wegner G (1991) Polysiloxanes at the air-water-interface and after transfer onto substrates. Makromol Chem, Macromol Symp 46:365–370. doi:10.1002/masy.19910460152
58. Baney RH, Itoh M, Skakibara A, Suzuki T (1995) Silsesquioxanes. Chem Rev 95:1409–1430. doi:10.1021/cr00037a012
59. Hanssen RWJM, van Santen RA, Abbenhuis HCL (2004) The dynamic status quo of polyhedral silsesquioxane coordination chemistry. Eur J Inorg Chem 675–683. doi:10.1002/ejic.200300412
60. Ogarev VA (2001) Silsesquioxane films on water surface. Colloid J 63:445–452. doi:10.1023/A:1016753805266
61. Hartmann-Thompson C (ed) (2011) Applications of polyhedral silsesquioxanes. Advances in silicon science, vol 3. Springer, Dordrecht
62. Joshi M, Butola BS (2004) Polymeric nanocomposites—polyhedral oligomeric silsesquioxanes (POSS) as hybrid nanofiller. J Macromol Sci, Polym Rev C44:389–410. doi:10.1081/MC-200033687
63. Gnansekaran D, Madhavan K, Reddy BSR (2009) Developments of polyhedral oligomeric silsesquioxanes (POSS) POSS nanocomposites and their applications: a review. J Sci Ind Res 68:437–464
64. Zhao JQ, Fu Y, Liu SM (2008) Polyhedral oligomeric silsesquioxane (POSS)-modified thermoplastic and thermosetting nanocomposites: a review. Polymers and Polymer Composites 16:483–500
65. Li GZ, Wang LC, Ni HL, Pittman CU (2001) Polyhedral oligomeric silsesquioxane (POSS) polymers and copolymers: a review. J Inorg Organomet Polym 11:123–154. doi:10.1023/A:1015287910502
66. Quadrelli EA, Basset JM (2010) On silsesquioxanes' accuracy as molecular models for silica-grafted complexes in heterogeneous catalysis. Coord Chem Rev 254:707–728. doi:10.1016/j.ccr.2009.09.031
67. Phillips SH, Haddad TS, Tomczak SJ (2004) Developments in nanoscience: polyhedral silsesquioxane (POSS)-polymers oligomeric. Curr Opin Solid State Mater Sci 8:21–29. doi:10.1016/j.cossms.2004.03.002
68. Tuteja A, Choi W, Ma ML, Mabry JM, Mazzella SA, Rutledge GC, McKinley GH, Cohen RE (2007) Designing superoleophobic surfaces. Science 318:1618–1622. doi:10.1126/science.1148326
69. Wu J, Mather PT (2009) POSS polymers: physical properties and biomaterials applications. Polymer Rev 49:25–63. doi:10.1080/15583720802656237
70. Scott DW (1946) Thermal rearrangement of branched-chain methylpolysiloxanes. J Am Chem Soc 68:356–358. doi:10.1021/ja01207a003

71. Knischka R, Dietsche F, Hanselmann R, Frey H, Mulhaupt R (1999) Silsesquioxane-based amphiphiles. Langmuir 14:4752–4756. doi:10.1021/la981594a
72. Yu XF, Zhong S, Li XP, Tu YF, Yang SG, Van Horn RM, Ni CY, Pochan DJ, Quirk RP, Wesdemiotis C, Zhang WB, Cheng SZD (2010) A giant surfactant of polystyrene-(carboxylic acid-functionalized polyhedral oligomeric silsesquioxane) amphiphile with highly stretched polystyrene tails in micellar assemblies. J Am Chem Soc 132:16741–16744. doi:10.1021/ja1078305
73. Deng JJ, Polidan JT, Hottle JR, Farmer-Creely CE, Viers BD, Esker AR (2002) Polyhedral oligomeric silsesquioxanes: a new class of amphiphiles at the air/water interface. J Am Chem Soc 124:15194–15195. doi:10.1021/ja027860v
74. Deng JJ, Hottle JR, Polidan JT, Kim HJ, Farmer-Creely CE, Viers BD, Esker AR (2004) Polyhedral oligomeric silsesquioxane amphiphiles: isotherm and brewster angle microscopy studies of trisilanolisobutyl-POSS at the air/water interface. Langmuir 20:109–115. doi:10.1021/la035240h
75. Deng JJ, Farmer-Creely CE, Viers BD, Esker AR (2004) Unique rodlike surface morphologies in trisilanolcyclohexyl polyhedral oligomeric silsesquioxane films. Langmuir 20:2527–2530. doi:10.1021/la035992b
76. Deng JJ, Viers BD, Esker AR, Anseth JW, Fuller GG (2005) Phase behavior and viscoelastic properties of trisilanolcyclohexyl-POSS at the air/water interface. Langmuir 21:2375–2385. doi:10.1021/la047568w
77. Mitsuishi M, Zhao F, Kim Y, Watanabe A, Miyashita T (2008) Preparation of ultrathin silsesquioxane nanofilms via polymer Langmuir–Blodgett films. Chem Mater 20:4310–4316. doi:10.1021/cm800067j
78. Kucuk AC, Matsui J, Miyashita T (2011) Langmuir–Blodgett films composed of amphiphilic double-decker shaped polyhedral oligomeric silsesquioxanes. J Colloid Interface Sci 355:106–114. doi:10.1016/j.jcis.2010.12.033
79. Kucuk AC, Matsui J, Miyashita T (2011) Effects of hydrogen bonding on the monolayer properties of amphiphilic double-decker-shaped polyhedral silsesquioxanes. Langmuir 27:6381–6388. doi:10.1021/la200604w
80. Lee W, Ni SL, Deng JJ, Kim BS, Satija SK, Mather PT, Esker AR (2007) Telechelic poly(ethylene glycol)-POSS amphiphiles at the air/water interface. Macromolecules 40:682–688. doi:10.1021/ma0618171
81. Yin W, Deng JJ, Esker AR (2009) Surface rheology of trisilanolisobutyl-POSS at the air/water interface. Langmuir 25:7181–7184. doi:10.1021/la900397r
82. Ferguson-McPherson MK, Low ER, Esker AR, Morris JR (2005) Sorption of dimethyl methylphosphonate within Langmuir–Blodgett films of trisilanolphenyl polyhedral oligomeric silsesquioxane. J Phys Chem 109:18914–18920. doi:10.1021/jp0521959
83. Ferguson-McPherson MK, Low ER, Esker AR, Morris JR (2005) Corner capping of silsesquioxane cages by chemical warfare agent simulants. Langmuir 21:11226–11231. doi:10.1021/la051477x
84. Paul R, Esker AR (2006) Pattern formation in dewetting poly(tert-butyl acrylate)/polyhedral oligomeric silsesquioxane (POSS) bilayer films. Langmuir 22:6734–6738. doi:10.1021/la060973y
85. Paul R, Karabiyik U, Swift MC, Hottle JR, Esker AR (2008) Morphological evolution in dewetting polystyrene/polyhedral oligomeric silsesquioxane thin film bilayers. Langmuir 24:4676–4684. doi:10.1021/la701625g
86. Paul R, Karabiyik U, Swift MC, Esker AR (2008) Phase separation in poly(tert-butyl acrylate)/polyhedral oligomeric silsesquioxane (POSS) thin film blends. Langmuir 24:5079–5090. doi:10.1021/la702065z
87. Huffer SM, Karabiyik U, Uzarski JR, Esker AR (2010) Ion effects on trisilanolphenyl-POSS as an adhesion promoter. In: Clarson SJ, Fitzgerald JJ, Owen MJ, Smith SD, Van Dyke ME (eds) Advances in silicones and silicone-modified materials. ACS symposium series, vol 1051. Am Chem Soc, Washington

88. Hottle JR, Kim HJ, Deng JJ, Farmer-Creely CE, Viers BD, Esker AR (2004) Blends of amphiphilic PDMS and trisilanolisobutyl-POSS at the air/water interface. Macromolecules 37:4900–4908. doi:10.1021/ma049511m
89. Hottle JR, Deng JJ, Kim HJ, Farmer-Creely CE, Viers BD, Esker AR (2005) Blends of amphiphilic poly(dimethylsiloxane) and nonamphiphilic octaisobutyl-POSS at the air/water interface. Langmuir 21:2250–2259. doi:10.1021/la047565j
90. Kim HJ, Deng JJ, Lalli JH, Riffle JS, Viers BD, Esker AR (2005) Blends of amphiphilic trisilanolisobutyl-POSS and phosphine oxide substituted poly(dimethylsiloxane) at the air/water interface. Langmuir 21:1908–1916. doi:10.1021/la0475674
91. Kim HJ, Hoyt Lalli J, Riffle JS, Viers BD, Esker AR (2007) Brewster angle microscopy studies of aggregate formation in blends of amphiphilic trisilanolisobutyl-POSS and nitrile substituted poly(dimethylsiloxane) at the air/water interface. In: Clarson SJ, Fitzgerald JJ, Owen MJ, Smith SD, Van Dyke ME (eds) Science and technology of silicones and silicone-modified materials. ACS symposium series, vol 964. Am Chem Soc, Washington
92. Feher FJ, Newman DA, Walzer JF (1989) Silsesquioxanes as models for silica surfaces. J Am Chem Soc 111:1741–1748. doi:10.1021/ja00187a028
93. Fang JY, Dennin M, Knobler CM, Godovsky YK, Makarova NN, Yokoyama H (1997) Structures of collapsed polysiloxane monolayers investigated by scanning force microscopy. J Phys Chem B 101:3147–3154. doi:10.1021/jp9633198
94. Buzin AI, Sautter E, Godovsky YK, Makarova NN, Pechhold W (1998) Influence of molecular weight on stepwise collapse of Langmuir monolayers of cyclolinear polyorganosiloxanes. Colloid Polym Sci 276:1078–1087. doi:10.1007/s003960050349
95. Buzin AI, Godovsky YK, Makarova NN, Fang JY, Wang X, Knobler CM (1999) Stepwise collapse of monolayers of cyclolinear poly(organosiloxane)s at the air/water interface: a Brewster-angle microscopy and scanning force microscopy study. J Phys Chem B 103:11372–11381. doi:10.1021/jp992708+
96. Jensen TR, Kjaer K, Brezesinski G, Ruiz-Garcia J, Mohwald H, Makarova NN, Godovsky YK (2003) Successive multilayer formation of cyclolinear polyorganosiloxanes floating at the air-water interface. A synchrotron X-ray reflectivity investigation. Macromolecules 36:7236–7243. doi:10.1021/ma034473c
97. Godovsky YK, Brezesinski G, Ruiz-Garcia J, Mohwald H, Jensen TR, Kjaer K, Makarova NN (2004) Stepwise collapse of cyclolinear polysiloxane langmuir monolayers studied by Brewster angle microscopy and grazing incidence X-ray diffraction. Macromolecules 37:4872–4881. doi:10.1021/ma049631u
98. Brooks CF, Fuller GG, Frank CW, Robertson CR (1999) An interfacial stress rheometer to study rheological transitions in monolayers at the air-water interface. Langmuir 15:2450–2459. doi:10.1021/la980465r
99. Naumann CA, Brooks CF, Fuller GG, Knoll W, Frank CW (1999) Viscoelastic properties of lipopolymers at the air-water interface: a combined interfacial stress rheometer and film balance study. Langmuir 15:7752–7761. doi:10.1021/la990261q
100. Sano M, Kawaguchi M, Chen YL, Skarlupka RJ, Chang T, Zografi G, Yu H (1986) Technique of surface-wave scattering and calibration with simple liquids. Rev Sci Instrum 57:1158–1162. doi:10.1063/1.1138620
101. Hård S, Neuman RD (1981) Laser light-scattering measurements of viscoelastic monomolecular films. Sci J Colloid Interface 83:315–334. doi:10.1016/0021-9797(81)90328-3
102. Hård S, Hamnerius Y, Nilsson O (1976) Laser heterodyne apparatus for measurements of liquid surface properties—theory and experiments. J Appl Phys 47:2433–2442. doi:10.1063/1.32295
103. Langevin D (1992) Simple liquids. In: Langevin D (ed) Light scattering by liquid surfaces and complementary techniques. Marcel Dekker, New York

Chapter 8
On the Interactions of Proteins with Silicon-Based Materials

Stephen J. Clarson, Kathy Gallardo, Siddharth V. Patwardhan, and Larry Grazulis

8.1 Introduction

Proteins and silicon-based materials have many combinations where the interactions are highly synergistic. These protein and silicon-based material combinations and interactions then result in applications that are highly useful to mankind. In the area of (bio)sensors, proteins may be incorporated into silicon-based devices giving unique sensing and detection capabilities. In the area of polymers, the protein may be incorporated into a variety of silicone systems. Here the protein can add functionality to the resulting polymeric material and the silicone may provide important long-term stability to the protein. In the area of ceramics and synthetic minerals, the protein can act as a catalyst, as a template and as a structure-directing agent during the preparation of a variety of bioinspired structures and forms. In this chapter we discuss some examples where the interactions of proteins and polypeptides with silicon-based materials are of importance.

8.2 Proteins, Biosilica and Silicon Biomaterial Surfaces

As stated by Brash [1]: "*Elimination of protein adsorption is not an easy task given that proteins are highly surface-active molecules due to their amphipathic nature*

S.J. Clarson (✉) · K. Gallardo
Department of Chemical and Materials Engineering and the Polymer Research Center, University of Cincinnati, Cincinnati, OH 45221, USA
e-mail: Stephen.Clarson@UC.Edu

S.V. Patwardhan
Department of Chemical and Process Engineering, University of Strathclyde, Glasgow, G1 1XJ, UK

L. Grazulis
University of Dayton Research Institute, 300 College Park, Dayton, OH 45469, USA

M.J. Owen, P.R. Dvornic (eds.), *Silicone Surface Science*, Advances in Silicon Science 4,
DOI 10.1007/978-94-007-3876-8_8,

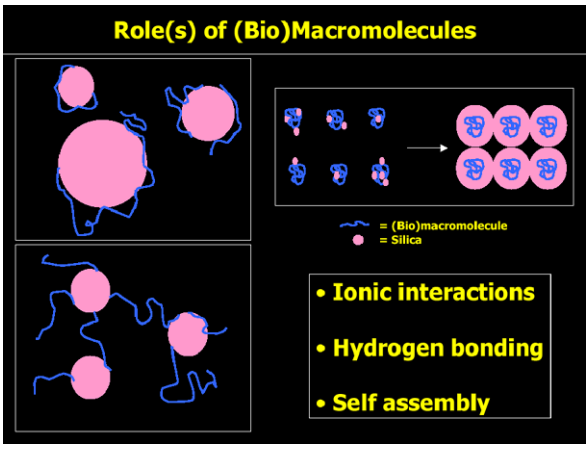

Fig. 8.1 The role(s) of (bio)macromolecules in biomineralization

and generally high molecular weights. Indeed it may be said that, along with a vacuum, Nature abhors a surface devoid of protein."

Brash has investigated quite extensively the modification of blood contacting materials with poly(ethylene oxide) (PEO) as a means of preventing the nonspecific adsorption of proteins [1].

Proteins can interact with colloidal silica particles (see Fig. 8.1) and such interactions can either disperse or flocculate the particles. As described below, the presence of proteins and/or functional biomacromolecules during biomineralization can lead to these molecules being entrapped within the resulting biomineral. In the case of biosilica, the selective chemical dissolution of the biosilica has allowed some of the entrapped proteins and biomacromolecules to be isolated and characterized.

8.2.1 On the Roles of Proteins in Biomineralization

Organisms of various kingdoms have been reported to deposit various biominerals through biomineralization. The synthesis of an ornate cell wall (frustule) through biosilicification in diatoms is one example [2, 3]. Biomineralization, which takes place under physiological conditions of temperature and pH, may be facilitated and controlled by proteins in each biological system. Investigations of these proteins and, in particular, the determination of their structure and functions is of interest for providing insights into biomineralization. Silaffin proteins isolated from the diatom *Cylindrotheca fusiformis* have been studied in detail [10]. It was found that key fragments (R1–R7 polypeptides) of silaffin-1A contained Lys–Lys and Arg–Arg clusters. Another noted feature of silaffins was their post-translational modification: in particular, the presence of N–CH_2-alkyl groups on the lysine residues and high levels of phosphorylation of the serine residues [10]. As these proteins are complex, difficult to isolate and to study, for the data that are presented in this chapter we have chosen the R5 polypeptide (a nineteen amino acid sequence) as

a model system that corresponds to the highly homologous repeating sequence of diatom silaffin proteins. We describe in detail the silica formation in vitro using this unmodified synthetic R5 polypeptide. The particulate bioinspired silica formed can be characterized by Atomic Force Microscopy (AFM) and Scanning Electron Microscopy (SEM) and the elemental analysis carried out using Energy Dispersive Spectroscopy (EDS).

The R5 polypeptide may self-assemble in solution and thus catalyze and scaffold the silica formation. We therefore propose that the silaffins may also be acting in a similar fashion during silica formation both in vitro and in vivo. As our understanding of biosilicification/biomineralization grows we will be able to design new biomimetic materials, new processes and new applications based on the aforesaid minerals prepared in vitro but in a bioinspired synthetic manner.

8.2.2 On the Mechanisms of Protein Mediated Biomineralization

The biominerals precipitated in Nature consist of various carbonates, phosphates, halides, oxides and oxalates in addition to (bio)silica [2]. Key features of biomineralization are the precise hierarchical control over the structural growth of the biominerals, the species-specificity of the biomineral morphology and the ambient conditions (temperature and pH) for their formation. The deposition of amorphous silica to form ornate cell walls (frustules) through biosilicification in diatoms is one example [3]. In addition, biomineralization may be facilitated and controlled by various characteristic proteins in each biological system [4]. Study of these proteins is therefore of great importance in our growing understanding of biomineralization. Furthermore, this understanding will help us in designing and preparing biomimetic materials in vitro.

As the proteins facilitating biomineralization can act as catalysts/templates/scaffolds (see Fig. 8.2) they can be isolated by the selective dissolution of the mineral phase in which they are incorporated. Indeed, such studies were undertaken for various biological systems to reveal the proteins associated with biominerals. The studies related to biosilicification (a process of silica deposition in vivo) are of particular interest.

The biological systems that have been investigated for biosilicification include grasses, diatoms and sponges [4]. Three plant materials that were silicified in various

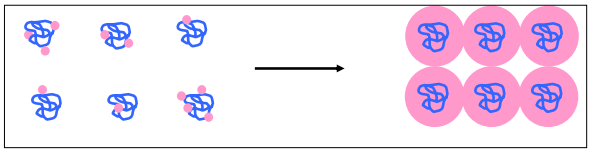

Fig. 8.2 Schematic representation of the role(s) of (bio)macromolecules/peptides as scaffolds for the (bio)silica structures. The coils in *blue* are the self-assembled (bio)macromolecules/polypeptides. The silica particles are shown in *pink*

amounts were analyzed for their protein content [5]. The amino acid compositions of these proteins were investigated and basic amino acid residues were found to dominate. It was concluded that these highly charged organic materials could be regulating the nucleation of biogenic silica. In addition, it was proposed that the amino acids that are capable of forming hydrogen bonds might govern the particle growth and thus control the structure and form of biosilica [5].

The marine sponge *Tethya aurantia* contains 75 % of its dry weight biosilica in the form of needle like spicules that act as structural elements, 1–2 mm in length and 30 μm in diameter and these were studied in order to isolate the proteins that facilitate biosilicification [6]. It was found that each spicule contained a central filament of protein (1–2 mm in length and 1–2 μm in diameter). After various treatments to dissolve the mineral silica from the sponge [6] three similar proteins were isolated and were named silicatein α, β and γ. Silicatein α was found in large quantities when compared to silicatein β and γ. It contained regular arrays of hydroxyl groups (serine, tyrosine and threonine clusters) and was found to be similar to members of the cathepsin L and papain family of proteases. In addition, it was found that the catalytic cysteine residues of the active sites in these proteases were replaced by serine in silicatein α. Using these and other findings, Morse and co-workers proposed a mechanism for the silicon ethoxide condensation and polymerization that was catalyzed by silicatein α and is based on the characteristic mechanism exhibited by the serine/histidine and the cysteine/histidine pairs of the active sites of the serine-based and cysteine-based proteases [7].

Proteins isolated from diatom *Cylindrotheca fusiformis* have also been studied in detail. An EDTA (ethylenediamine tetraacetate) extraction of purified cell walls of these diatoms revealed a family of proteins called frustulins [8]. Further treatment of these cell walls by HF led to the isolation of two sets of proteins. The high molecular weight proteins thus extracted were termed HEPs [9] and the low molecular weight (4,000–17,000) polycationic peptides were called silaffins due to their affinity towards biosilica [10]. The silaffins were studied in detail and their primary amino acid sequences determined. The sequence of 265 amino acids in silaffin-1A was divided into eight parts: an initial fragment (107 amino acids) containing higher amounts of acidic residues and a later part consisting of highly homologous repeating units (R1–R7) that were found to have a high content of basic amino acid residues [10]. It was also found that the later fragment (R1–R7) of silaffin-1A contained Lys–Lys and Arg–Arg clusters [10]. Another key feature of silaffins was their post-translational modification: the presence of N–CH_2-alkyl groups on the lysine residues [10] and the evidence of high degrees of phosphorylation [11]. In assay, a silicic acid solution (as the silica precursor) was treated with silaffins and in vitro the precipitation of 500–700 nm fused silica particles was observed over a wide range of pH [10]. It was proposed that the post-translational modifications might be key in silica formation facilitated by the silaffins [10].

Although the silaffin proteins, silicatein proteins and proteins extracted from grasses were able to facilitate silica formation in vitro, they have failed so far to produce silica structures that resemble the complex biosilica structures. In addition, as these proteins are complex, difficult to isolate and study, we have chosen to report

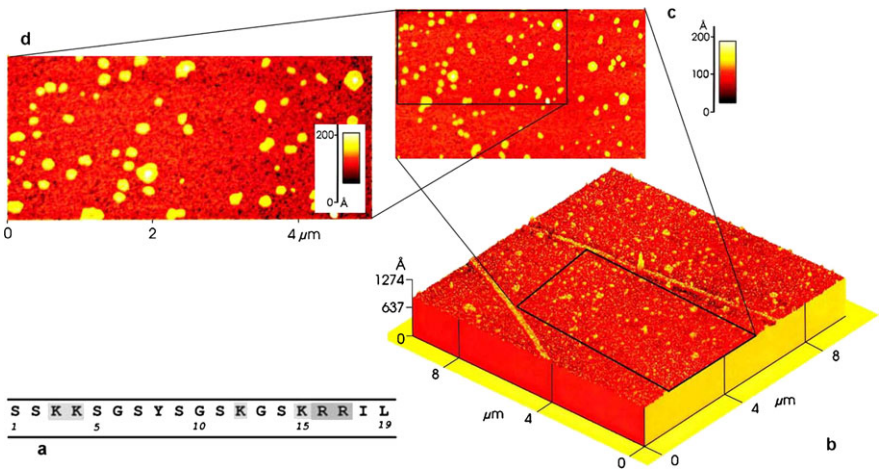

Fig. 8.3 Representative Atomic Force Microscopy (AFM) images of the precipitated silica. (**a**) The amino acid sequence of the unmodified synthetic R5 polypeptide used to facilitate the silica formation. (**b**) 3-D perspective AFM image of the precipitated silica particles. Base Size = 12 × 12 μm. (**c**) and (**d**) 2-D AFM images of silica particles at different magnifications. The R5 solution used was 20 mg/mL and the water glass was 0.1 M and the pre-hydrolysis was for 10 minutes in 1 mM HCl. The reaction time was 2 minutes

in this chapter investigations of the synthetic R5 polypeptide (a nineteen amino acid sequence) as a model system that corresponds to the highly homologous repeating sequence of diatom silaffin-1A protein, as discussed above. It is hoped that studies of the activity of the R5 polypeptide in vitro may provide insights into the role(s) of the silaffin proteins in vivo.

Elsewhere we have used the unmodified form of the synthetic R5 polypeptide (see Fig. 8.3a) to create nanopatterns of silica on an organic polymeric hologram by in vitro catalysis [12]. Furthermore, we have successfully used the unmodified synthetic R5 polypeptide to precipitate silica in vitro from an organosilicon precursor [13, 14]. Here we present results on silica formation in vitro using the unmodified synthetic R5 polypeptide.

8.3 Some Experimental Considerations

There are a wide variety of possible silica precursor molecules for these types of investigation. For all the data presented in this chapter we have chosen water glass as the silica precursor. The sodium trisilicate solution (namely water glass = $Na_2Si_3O_7$) containing 27 % SiO_2 by assay was purchased from Riedel-de Haën. The hydrochloric acid (HCl) used for water glass pre-hydrolysis was purchased from Fisher. The deionized ultra-filtered (DIUF) water, used for washing the samples, was obtained from Fisher. The potassium phosphate buffer was used to maintain the pH of the reaction mixture at 7.0 and was also purchased from

Fisher [15]. To avoid the effect of different ions in aqueous solution on the silicification, we used the same buffer (potassium phosphate) throughout. The custom synthesized unmodified R5 polypeptide (see Fig. 8.3a) of molecular weight of 2012 and amino acid sequence: SSKKSGSYSGSKGSKRRIL was supplied by New England Polypeptide Inc. All the reagents were used as received without any further purification. A stock solution of 1 mM HCl in DIUF water was prepared and was used for all the reactions. The water glass solution of desired concentration (0.1–3 M based on the water glass solution) in 1 mM HCl and the polypeptide solution in buffer (20 mg/mL) were always freshly prepared for each experiment, as the water glass solution was found to gel if left on the bench "as is". A typical reaction mixture contained 80 μL of the buffer, 20 μL of the polypeptide solution and 10 μL of the pre-hydrolyzed water glass solution. All the reactants were measured and added to micro sample polypropylene test tubes (1.5 mL). The tubes were then closed and shaken well to thoroughly mix the reactants in each case. All the reactions were carried out at 20 °C, atmospheric pressure and neutral pH. After the desired reaction time, the samples were centrifuged at 14,000 × *G* force for 3–5 minutes. It was observed that a white solid precipitated in the tubes. In control experiments without added polypeptide, gelation was observed rather than precipitation. The supernatant liquid was removed and DIUF water was added to the tubes. The precipitate was then re-dispersed in the DIUF water. This washing of samples was repeated three times in order to remove any free polypeptide and unreacted silicic acid, and therefore ensure that the reaction has been terminated. This dispersion was diluted further and 2–4 drops of this solution were placed on the respective sample holders. The substrates were then left to dry under ambient conditions overnight. The structure/morphology and sizes of the particulate silica formed was studied by AFM and SEM and the elemental analysis was carried out using EDS. In the case of SEM, a palladium-gold alloy was vacuum evaporated onto the dried samples. They were then investigated using a Hitachi S-4000 Field Emission Scanning Electron Microscope (FE-SEM). Samples for AFM were directly used without any sample coating. The AFM measurements were performed in ambient conditions, using a Park Scientific Instruments (PSI) AutoProbe CP research scanning probe microscope. The measurements were performed in intermittent contact (IC), non-contact (NC) and contact modes to check for artefacts. Scan artefacts were also minimized by using multiple scans, different scan directions, different size scans and sample rotations relative to the scan axes. The probes used were etched silicon ultralever probes from Thermomicroscopes with a nominal tip curvature of 10 nm. To maximize the lateral resolution, all images were taken in 512 × 512 mode with an image size (<5 × 5 mm). Zeroth order fit was used to flatten the images. Line profiles were formed by averaging several lines, which minimized any noise. Qualitative elemental analysis was obtained using EDS and was performed using an OXFORD ISIS system attached to the FE-SEM. The data obtained are presented in un-normalized form, meaning that the height of any peak does not correspond to the amount of element present in the sample.

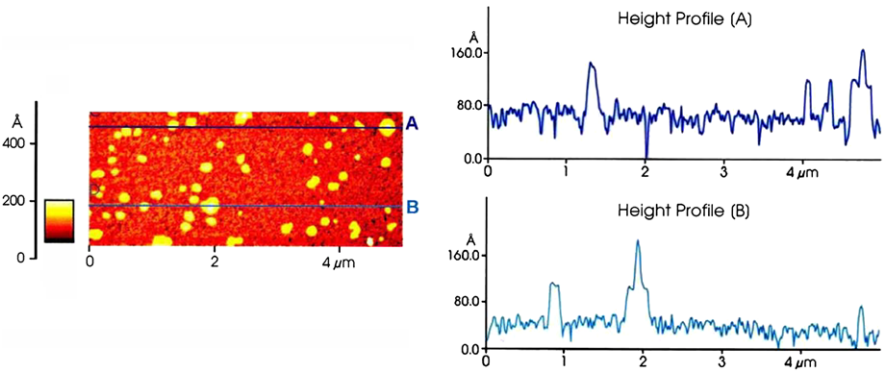

Fig. 8.4 Height profiles. AFM line scans at four different locations in the sample shown in Fig. 8.3c

8.4 On the Role of the Silaffin R5 in Biomineralization

Silaffin proteins have been shown to facilitate the formation of silica in vitro [10, 11]. It has been proposed to fulfil the same role in vivo [10, 11]. Next we discuss the role of the unmodified synthetic R5 polypeptide in silica formation in vitro.

8.4.1 On the Mechanism of the R5 Facilitated Biomineralization

Representative AFM images of the precipitated silica are shown in Fig. 8.3b–d. The lines seen in the AFM correspond to the surface irregularities of the sample holder. It can be seen that the particles formed are uniform in size ∼150–200 nm and that they aggregate to form clusters. The line profiles of these samples at various intersections are shown in Figs. 8.4 and 8.5. These line profiles confirm the sizes of the precipitated silica particles. The aggregation is also evident from Figs. 8.4 and 8.5.

The particle morphology was studied using SEM and is shown in Figs. 8.6a and 8.6b. Silica particles of sizes in the range ∼150–200 nm were formed. These particles were spherical in shape and it was confirmed that they form aggregates. Formation of a background material is also evident in the SEM micrographs. The AFM images have revealed that this background material is made up of smaller silica particles (∼50 nm) and that the larger silica particles are embedded in it. The elemental analysis as obtained from EDS is shown in Fig. 8.6c.

The sharp peaks at 0.5 keV and 1.74 keV are the signatures of oxygen K_α and silicon K_α, respectively. The peak around 0.23 keV corresponds to carbon K_α. The appearance of this peak confirms the incorporation of organic material (i.e. the R5 polypeptide) into the precipitated silica. Various other peaks correspond to the different salts present in the buffer. The SEM sample holders were made of aluminum, hence the aluminum peak.

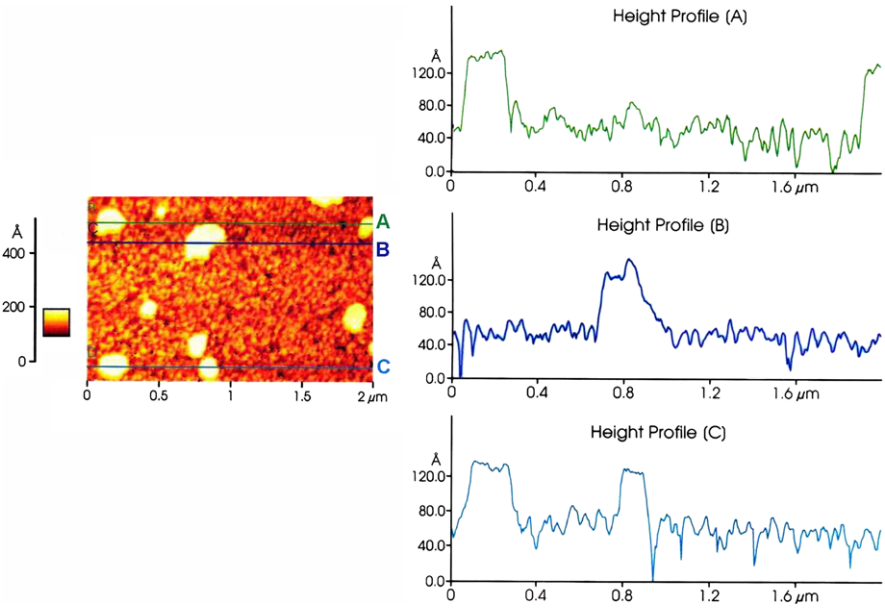

Fig. 8.5 Height profiles. AFM line scans at four different locations in the sample shown in Fig. 8.3d

Next we briefly describe biosilicification in diatoms and the polymerization of silicic acid and the chemistry of silica in order to clarify and understand the results presented in this chapter. Diatoms and other marine organisms that produce silica structures do so by selectively and actively up-taking and thus concentrating silicic acid as silica precursor. Soluble silicic acid is present in seawater at concentrations ~70–100 μM [20]. Due to this low concentration, it does not undergo polymerization and remains stable. In the case of diatoms, the silicic acid is actively transported using proteins and various ions into the intracellular pools called silicon transport vesicles (STV). The silicic acid remains unpolymerized in the STVs. This soluble and concentrated silicic acid is then transported to the silicon deposition vesicle (SDV) that is bound by silicalemma (a specialized membrane), wherein silica deposition to form ornate structures occurs by silicic acid polymerization [4]. The entire process of biosilicification occurs under physiological conditions of temperature and pH. The series of genetically controlled events taking place in diatom silica frustule morphogenesis from the silicon absorption into the cell to the daughter cell separation have been described by Sullivan [21] and are summarized here:

(i) Extracellular binding of silicon (as silicic acid or $SiO[OH]_3^-$) to a cell wall or plasmalemma.
(ii) Protein and ion mediated transmembrane active transport of silicon (which is not diffusion controlled as the extracellular concentration of silicon is higher) [22].

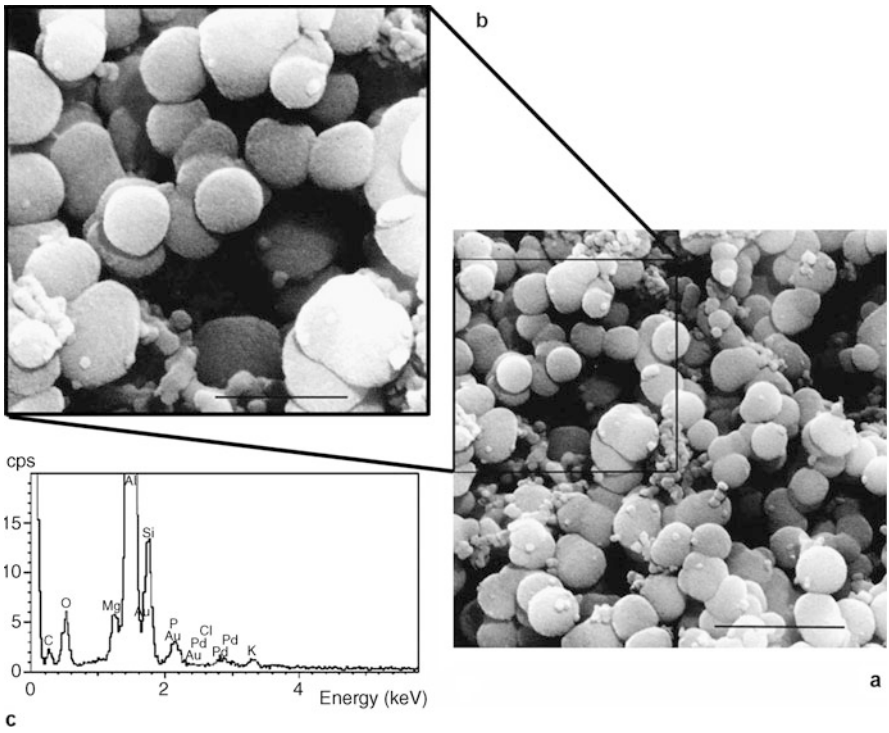

Fig. 8.6 Representative Scanning Electron Microscopy images and Energy Dispersive Spectroscopy spectrum. (**a**) and (**b**) SEM micrographs of the precipitated silica using 20 mg/mL R5 solution and 0.1 M pre-hydrolyzed water glass solution. (**c**) EDS spectrum of the same sample showing the silicon and oxygen K_α peaks

(iii) Storage of this soluble silicon in pools and inhibition of polymerization therein.
(iv) Active transport of this soluble silicon to the SDV and oligomerization of the silicic acid therein.
(v) Further polymerization, nucleation and particle growth followed by spatial organization of the silica. This is template directed in which the silicalemma may act as an organic matrix directing the growth.
(vi) Termination of the polymerization.
(vii) Extrusion of the valve through the plasmalemma.
(viii) Girdle band formation and daughter cell separation.

The reaction involved in silicic acid polymerization is the condensation of silanols into siloxanes:

Scheme 8.1 The (bio)silica condensation reaction

$$\text{-Si-OH + HO-Si-} \rightarrow \text{-Si-O-Si-} + H_2O$$

When a silica precursor (an alkoxysilane or a soluble silicate such as the water glass used here) is acidified in aqueous solution, silicic acid is formed and not colloidal silica [17]. Hence, the form of the precursor is of less importance once it is hydrolyzed and corresponds to the soluble silica observed in Nature [18, 19]. Perry [16] has reviewed the chemistry/biochemistry of silica and the process of silica precipitation from aqueous solution. In brief, a variety of precursors (alkoxysilanes or silicates) can be used to generate orthosilicic acid $Si(OH)_4$ in water which, at 25 °C, is thought to be stable at levels below *ca.* 100 ppm. At higher concentrations, polymerization is seen which involves three distinct stages [17]:

I. *Polymerization to form stable nuclei*: The polymerization of $Si(OH)_4$ via condensation of silanol groups (Si–OH) releasing water molecules (see Scheme 8.1) to produce discrete colloidal particles takes place. As observed, the polymerization of monosilicic acid in the aqueous phase is very different to the classical condensation polymerizations producing organic polymers. In the formation of colloidal particles, the siloxane (Si-O-Si) bond formation is maximized in this early stage of polymerization.

II. *Growth of the nuclei to form spherical particles*: The particles grow by further polymerization of discrete colloidal particles by nucleation. The particle growth follows either Ostwald ripening (in which, smaller, unstable particles dissolve and precipitate on the surfaces of the relatively larger, insoluble and stable particles) or condensation of intermediate sized particles. Particle bridging plays an important role in this as well as in the next stage of silica formation.

III. *Particle aggregation to form branched chains or other structures*: Aggregation of these particles to produce chains and networks then follows. The grown particles (nuclei) get bridged together with just a few new siloxane bonds formed.

The kinetics of the silica polymerization has been extensively studied using the colorimetric molybdosilicate method [5]. An important fact is that at circumneutral pH the silica particles bear a negative charge in solution.

As to the role of biomacromolecules in silicification/biosilicification, Tacke has described how the silaffin proteins from the diatom *Cylindrotheca fusiformis* and the silicatein proteins from the sponge *Tethya aurantia* have a catalytic/templating/scaffolding role in the formation of ordered silica structures [20] (see Fig. 8.2). Mizutani and co-workers [23] have reported that polyamines are able to catalyze the polymerization of sodium orthosilicate hydrate at pH 8.5. While they reported the incorporation of the polyamines into the silica product, such materials were described as gels and hence the role of the macromolecules as templates/scaffolds was not invoked. We have previously demonstrated that various synthetic macromolecules which are cationically charged at pH 7 are able to show the catalytic/templating/scaffolding behaviour for silica formation as exhibited by biomacromolecules [15, 24–31]. It is therefore clear that the notion of the cationic charge(s) of proteins facilitating biosilicification is of importance in the catalysis of silica formation.

Here we propose that the unmodified synthetic R5 polypeptide facilitates silica precipitation by a dual catalyzing and scaffolding role (see Fig. 8.2) under physiological conditions of temperature and pH. Furthermore, the results presented here

demonstrate that the post-translational modifications may not be necessary for the silica precipitation and hence may not be a key feature in the catalysis of silica precipitation facilitated by silaffin proteins in vivo. This is further supported by the fact that a series of synthetic macromolecules was identified that were able to facilitate silica precipitation in vitro [26, 28]. The modifications seen in the case of the silaffin proteins may be useful (i) in self-organization of these proteins in vivo as pointed out recently by Sumper, Kröger and their co-workers [11] and/or (ii) in simply amplifying the polycationic behaviour of the silaffin proteins. The incorporation of the (bio)macromolecules into the silica leads us to believe that the R5 polypeptide discussed here and the various aforesaid cationic macromolecules act as scaffolds by self-organization in addition to their role as catalysts. The self-organization of these macromolecules and their role in silicification and biosilicification are under investigation currently and the results will be reported in due course [32]. Another missing link in the silicification and biosilicification studies is the formation of various biomimetic structures that resemble the ornate structures seen in biological systems. This remains a major challenge to all working in this field.

8.5 Conclusions

In this chapter we have described silica precipitation using unmodified synthetic R5 polypeptide—a nineteen amino acid sequence corresponding to the homologous repeating sequence in silaffin-1A protein extracted from diatom *C. fusiformis*. The particle formation was investigated using modern materials characterization methods, namely AFM, SEM and EDS. It was found that silica particles of sizes ~150–200 nm were produced and that they formed aggregates. Furthermore, we propose that the R5 polypeptide self-organizes in solution and catalyzes and scaffolds the silica formation in vitro. We believe that silaffin proteins and other proteins facilitating silica formation in vivo behave in a similar fashion and this may provide insights into the role of proteins in biosilicification.

Acknowledgements We thank Dr. Srinivas Subramaniam (CME, UC) for help with the SEM analysis. The financial support for the work described in this chapter was kindly provided by DAGSI.

References

1. Brash JL (2000) Exploiting the current paradigm of blood-material interactions for the rational design of blood-compatible materials. J Biomater Sci Polym Ed 11(11):1135–1146
2. Lowenstam HA (1981) Minerals formed by organisms. Science 211:1126–1131
3. Round FE, Crawford RM, Mann DG (1990) The diatoms, biology and morphology of the genera. Cambridge University Press, Cambridge
4. Simpson TL, Volcani BE (1981) Silicon and siliceous structures in biological systems. Springer, New York

5. Harrison CC (1996) Evidence for intramineral macromolecules containing protein from plant silicas. Phytochemistry 41(1):37–42 (formerly Perry)
6. Shimizu K, Cha JN, Stucky GD, DE Morse (1998) Silicatein alpha: Cathepsin L-like protein in sponge biosilica. Proc Natl Acad Sci USA 95:6234–6238
7. Cha JN, Shimizu K, Zhou Y, Christiansen SC, Chmelka BF, Stucky GD, DE Morse (1999) Silicatein filaments and subunits from a marine sponge direct the polymerization of silica and silicones in vitro. Proc Natl Acad Sci USA 96:361–365
8. Kröger N, Bergsdorf C, Sumper M (1994) A new calcium-binding glycoprotein family constitutes a major diatom cell-wall component. EMBO J 13:4676–4683
9. Kröger N, Lehmann G, Rachel R, Sumper M (1997) Characterization of a 200-kDa diatom protein that is specifically associated with a silica-based substructure of the cell wall. Eur J Biochem 250:99–105
10. Kröger N, Deutzmann R, Sumper M (1999) Polycationic peptides from diatom biosilica that direct silica nanosphere formation. Science 286:1129–1132
11. Kröger N, Lorenz S, Brunner E, Sumper M (2002) Self-assembly of highly phosphorylated silaffins and their function in biosilica morphogenesis. Science 298:584–586
12. Brott LL, Pikas DJ, Naik RR, Kirkpatrick SM, Tomlin DW, Whitlock PW, Clarson SJ, Stone MO (2001) Ultrafast holographic nanopatterning of biocatalytically formed silica. Nature 413:291–293
13. Clarson SJ, Whitlock PW, Patwardhan SV, Brott LL, Naik RR, Stone MO (2002) Synthesis of silica nanostructures at neutral pH using catalytic polypeptides. Polym Mater Sci Eng 86:81
14. Patwardhan SV, Clarson SJ (2002) Silicification and biosilicification part 4. Effect of template size on the formation of silica. J Inorg Organomet Polym 12(3–4):109–116
15. Patwardhan SV, Mukherjee N, Clarson SJ (2002) Effect of process parameters on the polymer mediated synthesis of silica at neutral pH. Silicon Chem 1(1):47–55
16. Perry CC, Keeling-Tucker T (2000) Biosilicification: the role of the organic matrix in structure control. J Biol Inorg Chem 5:537–550
17. Iler RK (1979) The chemistry of silica: solubility, polymerization, colloid and surface properties and biochemistry. Wiley, New York, Chap 3
18. Coradin T, Livage J (2001) Effect of some amino acids and peptides on silicic acid polymerization. Colloids Surf B, Biointerfaces 21:329–336
19. Coradin T, Durupthy O, Livage J (2002) Interactions of amino-containing peptides with sodium silicate and colloidal silica: a biomimetic approach of silicification. Langmuir 18(6):2331–2336
20. Tacke R (1999) Milestones in the biochemistry of silicon: from basic research to biotechnological applications. Angew Chem, Int Ed Engl 38(20):3015–3018
21. Sullivan BE (1986) In: Silicon biochemistry. Wiley, Chichester, Chap 5
22. Hildebrand M, Volcani BE, Gassmann W, Schroeder JI (1997) A gene family of silicon transporters. Nature 385(6618):688–689
23. Mizutani T, Nagase H, Fujuwara N, Ogoshi H (1998) Silicic acid polymerization catalyzed by amines and polyamines. Bull Chem Soc Jpn 71:2017–2022
24. Patwardhan SV, Clarson SJ (2002) Silicification and biosilicification: Part 1. Formation of silica structures utilizing a cationically charged synthetic polymer at neutral ph and under ambient conditions. Polym Bull 48:367–371
25. Patwardhan SV, Durstock MF, Clarson SJ (2002) Silicification and biosilicification: Part 2. Silicification at pH 7 in the presence of a cationically charged polymer in solution and immobilized on substrates. In: Synthesis and Properties of Silicones and Silicone-Modified Materials. ACS Symposium Series, Vol 838, pp 366–374
26. Patwardhan SV, Clarson SJ (2002) Silicification and biosilicification: Part 3. The role of synthetic polymers and polypeptides at neutral pH. Silicon Chem 1(3):207–214
27. Patwardhan SV, Clarson SJ (2003) Silicification and biosilicification: Part 5. An investigation of the silica structures formed at weakly acidic pH and neutral pH as facilitated by cationically charged macromolecules. Mater Sci Eng C 23:495–499
28. Patwardhan SV, Clarson SJ (2003) Silicification and biosilicification: Part 6. Poly-L-histidine mediated synthesis of silica at neutral pH. J Inorg Organomet Polym 13(1):49–53

29. Patwardhan SV, Mukherjee N, Clarson SJ (2001) Formation of fiber-like amorphous silica structures by externally applied shear. J Inorg Organomet Polym 11(2):117–121
30. Patwardhan SV, Mukherjee N, Clarson SJ (2001) The use of poly-L-lysine to form novel silica morphologies and the role of polypeptides in biosilicification. J Inorg Organomet Polym 11(3):193–198
31. Patwardhan SV, Maheshwari R, Mukherjee N, Kiick KL, Clarson SJ (2006) Conformation and assembly of polypeptide scaffolds in templating the synthesis of silica: an example of a polylysine macromolecular "switch". Biomacromolecules 7(2):491–497
32. Clarson SJ (2012) A personal commentary on biological and bioactive silicon systems. Silicon 4(1):89–91

Chapter 9
Silicone Surfactants

Lenin J. Petroff and Steven A. Snow

9.1 Introduction

The energetic and commercially relevant topic of silicone surfactants was extensively reviewed by Hill in 1999 [1] with a series of follow-up, more specialized reviews between 2001–2011 by Henning et al. [2]; Hill [3]; Ruiz et al. [4]; Fleute-Schlachter and Feldmann-Krane [5]; Long and Wang [6]; Kamei [7]; Huang [8]; Hill [9]; Huang et al. [10]; O'Lenick and O'Lenick [11]; Han et al. [12]; Han et al. [13]; Huang et al. [14]; Somasundaran et al. [15]; Huang [16]; and Rodriguez-Abreu and Esquena [17]. With this in mind, and within the context of being part of the larger topic of silicon-based surface science, this chapter aims to carry out the following:

- Give an overview of the molecular structures, synthetic chemistry, interfacial activity and solution aggregation behavior of silicone surfactants.
- Make reference to the previously published reviews.
- Cover new developments in the field in the last twelve years.
- Discuss how these properties tie into the application science for these materials.

Silicone surfactants were first introduced into the marketplace in the 1950's as stabilizing agents for polyurethane foam [18]. This application was unusual in that more traditional surfactants, based on hydrocarbon residues as the "hydrophobic" portion of the molecule, did not act as effective stabilizers in this media. The experimental verity of surface activity in a non-aqueous media suggested that silicone surfactants would have some significant differences in physico-chemical behavior from their hydrocarbon analogues.

Over the next 60 years, both striking similarities and differences were observed between the behavior of silicone surfactants and their hydrocarbon analogues. Ta-

L.J. Petroff · S.A. Snow (✉)
Dow Corning Corporation, Midland, MI 48686, USA
e-mail: steven.a.snow@dowcorning.com

M.J. Owen, P.R. Dvornic (eds.), *Silicone Surface Science*, Advances in Silicon Science 4,
DOI 10.1007/978-94-007-3876-8_9,

Table 9.1 Similarities and differences between siloxane based and hydrocarbon based surfactants

Similarities between silicone and hydrocarbon-based surfactants	Differences between silicone and hydrocarbon-based surfactants
Surfactants are formed using most common hydrophilic moieties including non-ionic (polyether-based) and ionic (cationic/anionic/zwitterionic)	The great majority of commercial products containing silicone surfactants are based upon the non-ionic, polyether hydrophile
Aqueous surface activity including the marked reduction of aqueous surface tension	Silicone surfactants can routinely reduce the surface tension of water to values 10–20 % lower than measured with organic surfactants and display surface activity in organic media
Formation of a rich variety of aggregated structures in aqueous media including micelles and liquid crystalline phases	Silicone surfactants show a pronounced tendency to form bilayer-structured aggregates in aqueous dispersions including plate-like micelles, vesicles and lyotropic liquid crystalline phases
Stabilization of aqueous-based disperse systems such as foams and emulsions	Silicone surfactants can also stabilize dispersions in organic media
Wetting agents for aqueous mixtures	"Superwetting" of aqueous mixtures of specific silicone surfactants

ble 9.1 lists the similarities and differences between siloxane-based surfactants and hydrocarbon-based surfactants.

The physical behavior of silicone surfactants, as outlined in Table 9.1, has been the basis for a rich variety of commercial applications. Along with the foregoing example of the stabilization of polyurethane foams, the following applications have achieved significant commercial success:

- Process aids in fiber manufacturing.
- Spreading agents and emulsifiers in personal care and cosmetic formulations.
- Wetting agents, flow promoters, lubricants and foam control agents in paint and coating products/processes.

Therefore, this review of the field of silicone surfactants focuses on the following topics:

- The molecular structures of silicone surfactants and how they are synthesized.
- The interfacial activity of silicone surfactants.
- The aqueous aggregation behavior of silicone surfactants.
- The commercial applications of silicone surfactants.

This review also highlights areas of high activity which have begun in the last 12 years or have greatly intensified during this period:

- All aspects of research and product development of carbohydrate-functional silicone surfactants including synthesis, characterization, interfacial science, aggregation in aqueous solution and product conceptualization and development. This work is driven by environmental concerns, specifically the desire to work with

amphiphiles based on "natural" products, such as sugars/carbohydrates. This focus is highly relevant for the potential application of these materials into personal care, household care and health care markets.

- The intense work carried out on the bulk solution aggregation properties of silicone surfactants has yielded a number of exciting avenues of research and development. These areas lie in the exploding field of nanoscience and technology. For example:
  - The science and technology of nanoscale silicone surfactant vesicles has been extensively developed in the subsequent years. These materials are the first robust alternative to the highly established field of organic-surfactant-based vesicles/liposomes which are well-established in the personal care product and health care fields. By contrast to these organic materials, silicone vesicles are formed by a wide range of materials, under mild conditions and bring the benefit of silicone aesthetics to the skin care market.
  - The concentrated interest in and application of silicone emulsifiers in the personal care market has driven the discovery of novel methods of dispersion stabilization employing silicone surfactants. Specifically, a number of silicone surfactants act as nanoparticulate stabilizers at interfaces.
  - Silicone surfactant aggregates have been employed to "template" the formation of specific nanoscopic structures of metal oxides.

9.2 Molecular Structure

Silicone surfactants feature an amphiphilic molecular structure consisting of a non-polar/hydrophobic moiety, silicone, and various polar/hydrophilic moieties. The silicone moiety can vary from a linear to a highly branched (network) structure. The hydrophilic groups, including both non-ionic (polyether and carbohydrate) and ionic (cationic, anionic and zwitterionic) species can attach to the siloxanes in a wide variety of ways.

9.2.1 Silicone Structure

As discussed extensively in this book, "silicones" contain non-polar, hydrophobic groups composed of combinations of the monomer species $R^1R^2R^3SiO_{1/2}$, R^1R^2SiO, $RSiO_{3/2}$, and SiO_2. Common, minimally polar R groups bonded to silicon include methyl, longer chain alkyl, phenyl and γ,γ,γ-trifluoropropyl, with (by far) the most common R group being methyl. In order to satisfy the requirements of amphiphilicity, some of the R groups are highly polar and hydrophilic. These groups are discussed below.

9.2.1.1 Linear Silicone Structures

Many silicone surfactants are based upon a linear silicone structure featuring the oligomeric silicone group, -$(R_2SiO)_x$-. The typical R group is methyl and x can range from one to multiple hundreds. Hydrophilic groups can be attached to one (an "AB" structure) or both (an "ABA" structure) ends of this linear silicone. One can consider a linear structure BAB, where the hydrophilic group is in the middle. Examples of all three linear type structures are shown below, where the A group is a poly(oxyethylene) group. These have either a C-O-Si bond (hydrolytically unstable) or a O-C-C-C-Si bond (hydrolytically stable) as the linkage between the polyether portion and the silicone portion.

AB Structures:

$$HO(CH_2CH_2O)_y\text{-}(Me_2SiO)_x\text{-}SiMe_3$$

Structure 9.1

$$HO(CH_2CH_2O)_y\text{-}(CH_2)_3\text{-}(Me_2SiO)_x\text{-}SiMe_3$$

Structure 9.2

ABA Structures:

$$HO(CH_2CH_2O)_y\text{-}(Me_2SiO)_x\text{-}(CH_2CH_2O)_zH$$

Structure 9.3

$$HO(CH_2CH_2O)_y\text{-}(CH_2)_3\text{-}(Me_2SiO)_xSiMe_2\text{-}(CH_2)_3\text{-}(OCH_2CH_2)_zOH$$

Structure 9.4

BAB Structures:

$$Me_3SiO(Me_2SiO)_x(CH_2CH_2O)_y(Me_2SiO)_zSiMe_3$$

Structure 9.5

$$Me_3SiO(Me_2SiO)_xSiMe_2\text{-}[(CH_2)_3O(CH_2CH_2O)_y(CH_2)_3]\text{-}SiMe_2(Me_2SiO)_zSiMe_3$$

Structure 9.6

9.2.1.2 Branched Silicone Structures

Silicone branched structures can be further grouped according to the "degree" of branching. Examples with a lower degree of branching include "graft", "comb" or "rake" structures. Examples with higher degrees of branching usually feature some silicon atoms of the general formulas $RSiO_{3/2}$, and SiO_2, where R can be the hydrophilic moiety. These examples have been further grouped into the categories "resins", "dendrimeric structures" and "surface-active nanoparticles".

(a) "Graft", "Comb" or "Rake" branched silicone structures

The general representation of a "graft"- or "rake"-structured silicone surfactant is displayed in Structure 9.7. As in Structures 9.1–9.6, the hydrophilic group of choice is the poly(oxyethylene) group.

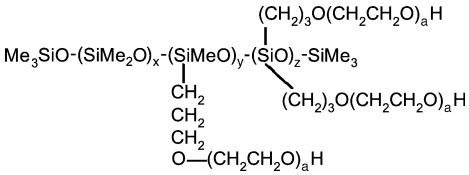

Structure 9.7

One specific case of the general formula in Structure 9.7 is worthy of further mention; specifically, the case where $x = 0$, $y = 1$ and $z = 0$. This specific example, often referred to as a "branched" trisiloxane structure, appears frequently in the literature on silicone surfactants.

Another variation of structure on the theme of "graft" structure is where the siloxane backbone is in a cyclic, rather than a linear form. This is shown as Structure 9.8.

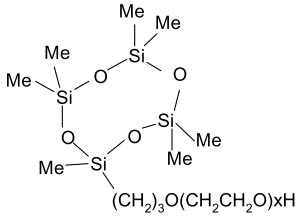

Structure 9.8

(b) Network silicone structures

The term "branching" within a silicone surfactant can also refer to materials containing $RSiO_{3/2}$ and/or SiO_2 units within their structure. The R group in the $RSiO_{3/2}$ unit can feature either a hydrophobic (typically methyl) or hydrophilic group. Gentle and Bassindale reported [19] a series of materials of the molecular formula $[(\text{polyether})SiO_{3/2}]_8$. These materials featured a cubic cage structure as depicted in Structure 9.9, also known as a polyhedral oligomeric silsesquioxane, POSS (see also Chaps. 6 and 7), where the polyether groups are the "R" groups attached to each corner of the cube. The interfacial activity of these compounds was not reported; however, interfacial activity was observed in cases where the R groups were a mixture of alkyl and polyether [20]. In a related study Deng and coworkers reported [21] that the species $[(\text{isobutyl})SiO_{3/2}]_8$ was not amphiphilic in behavior; however, they observed amphiphilic behavior in the case of the open cage species $[(\text{isobutyl})SiO_{3/2}]_4[(\text{isobutyl})SiO(OH)]_3$.

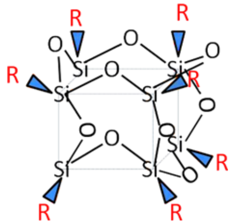

Structure 9.9

In Structure 9.9, R represents a polyether group. For simplicity of presentation, one vertex Si atom, the one behind the plane of paper, is not shown.

Most investigators consider the $[RSiO_{3/2}]_8$-based structures to be "molecular" surfactants. However, as the highly branched siloxane structure attains a much greater size and molecular weight, typically through incorporation of SiO_2 units, one might consider them to function as surface-active nanoparticles. Commercial materials are available which are best considered to be silica nanoparticles whose surfaces are covered with a mixture of organic and OH (silanol) groups. For example, amphiphilic behavior has been observed in the case where the organic group was methyl [22].

9.2.2 Silicon-Centered Hydrophobic Groups Other than Silicone

There are two such cases worthy of mention, both of which are structurally related to the siloxane (Si-O-Si-O-) backbone. The first example is a polysilane, where the backbone is Si-Si-Si and a carbosilane, where the backbone is Si-C-Si-C-. A small number of surfactants have been prepared from this backbone, as reviewed previously [23]. Since this review, one study reported [24] the synthesis and characterization of mixed fluoroalkyl/hydroxyl functional carbosilane dendrimers which demonstrated amphiphilic behavior. In a related study, Krska and Seyferth [25] reported the synthesis, characterization and amphiphilic behavior of carbosilane dendrimers decorated with a variety of hydrophilic groups. Kim et al. reported [26] the synthesis, characterization and amphiphilicity of dendrimers build around a cyclic siloxane core with silyl ether-based linkages (comprising the "generations" of the dendrimer structure) and capped with hydroxyl groups. For more detail about these and other silicon-containing dendrimers see Vol. 2 of this book series.

9.2.3 Hydrophilic Group Structure

Within the category of "silicone surfactants" one can also make distinctions based on the structural classification of the hydrophilic group. A first point of distinction would be between "non-ionic" and "ionic" hydrophilic groups. The two major categories of non-ionic groups are polyethers and carbohydrates. Within the category of ionic groups there are cationic, anionic and zwitterionic members.

9.2.3.1 Non-ionic Hydrophilic Groups

The vast majority of silicone surfactants feature the polyether group. Typically the polyether group is that of a poly(ethylene oxide)-PEO. However, a substantial number of silicone surfactants contain some poly(propylene oxide)-PPO in their polyether portion. PPO is generally used for non-aqueous applications of silicone surfactants [18] as it would be essentially a slightly polar hydrophobic material. For an alternative hydrophilic group, much work has been carried out on silicones containing hydrophilic carbohydrate moieties [27–49]. A small amount of work has also been carried out using phosphine oxides as the hydrophilic moiety [50].

9.2.3.2 Ionic Hydrophilic Groups

Although silicone surfactants containing ionic hydrophilic groups have not attained the commercial significance of their polyether-based, non-ionic cousins, there has been effort expended to synthesize, characterize and develop applications for these materials. A number of aspects of this field were covered in the afore-mentioned treatise on silicone surfactants [50]; however, this effort had a rather limited scope.

9.2.3.2.1 Cationic Silicone Surfactants

Silicone surfactants with a range of cationic hydrophilic moieties have been synthesized, characterized and their application potential assessed. The great majority of these materials have a quaternary ammonium moiety for the cationic group [51–60].

9.2.3.2.2 Anionic Silicone Surfactants

Silicone surfactants with a range of anionic hydrophilic moieties have been synthesized, characterized and their application potential assessed [61–66]. A wide variety of hydrophilic groups were investigated including sulfate, sulfonate, sulfosuccinate, carboxylate and phosphonate.

9.2.3.2.3 Zwitterionic Silicone Surfactants

A small number of silicone surfactants featuring zwitterionic hydrophilic groups have been prepared. Those reported included both betaine [67] and sulfobetaine [68] moieties.

$$Me_3SiCl + H_2O \rightarrow Me_3Si(OH) + HCl$$

Scheme 9.1 Hydrolysis of Methyltrichlorosilane

$$Me_2SiCl_2 + 2H_2O \rightarrow Me_2Si(OH)_2 + 2HCl$$

Scheme 9.2 Hydrolysis of Dimethyldichlorosilane

$$MeHSiCl_2 + 2H_2O \rightarrow MeHSi(OH)_2 + 2HCl$$

Scheme 9.3 Hydrolysis of Methylhydrogendichlorosilane

$$\begin{aligned} &2Me_3Si(OH) + xMe_2Si(OH)_2 + yMeHSi(OH)_2 \\ &\quad \rightarrow Me_3SiO(SiMe_2O)_x(SiMeHO)_ySiMe_3 + (1 + x/2 + y/2)H_2O \end{aligned}$$

Scheme 9.4 Condensation of Silanol Functionality

9.3 The Synthesis of Silicone Surfactants

Because of the amphiphilic nature of silicone surfactants, their hydrophobic and hydrophilic parts are usually separately synthesized and subsequently linked together. This section mirrors that logic as we cover (1) Silicone synthesis, and (2) Linkage of the hydrophilic group to the silicone. In some cases the hydrophilic group is directly linked to the siloxane in one step. In other cases, the silicone is converted to an intermediate organofunctional silicone, which is then converted into the surfactant via traditional organic chemistry routes.

9.3.1 Silicone Synthesis

The broad topic of silicone synthesis has been extensively reviewed in many publications and the reader is advised to consult some of the classic publications in this field [69–71]. Nevertheless, we briefly outline here some of the key steps:

- The key raw material for the synthesis of silicones is silicon metal. The metal is treated with mixtures of methyl chloride and hydrogen chloride producing chlorosilanes such as Me_3SiCl, Me_2SiCl_2, $MeSiCl_3$, $HSiCl_3$ and $MeSiHCl_2$.
- As can be seen in Schemes 9.1, 9.2 and 9.3, chlorosilanes readily hydrolyze producing silanol species such as $Me_3Si(OH)$, $Me_2Si(OH)_2$, $MeSi(OH)_3$ and $MeHSi(OH)_2$. As Scheme 9.4 shows, these silanol species, with the concurrent elimination of water, readily condense together to produce silicones. Within the silicone (Scheme 9.4), the Si-H functional group is introduced in order to provide an attachment point for a hydrophilic moiety.
- In some cases, in an intermediate step, an organic moiety is directly attached to the siloxane backbone via hydrosilylation reaction (the addition of an Si-H bond to an olefin). This moiety will be used as a synthon to link a hydrophilic

Scheme 9.5 Hydrosilylation of Allyl Amine

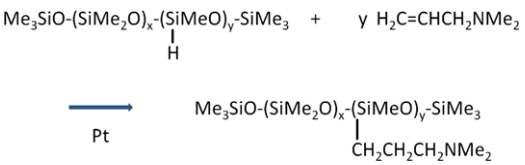

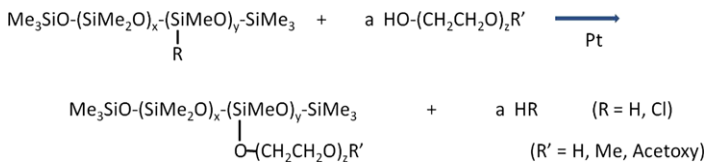

Scheme 9.6 Silylation of Hydroxy Terminated Polyether

group to the siloxane moiety. An example [72, 73] is shown in Scheme 9.5. This reaction, like the great majority of hydrosilylations, is catalyzed by a platinum-based catalyst.

9.3.2 Linkage of the Hydrophilic Group to the Silicone

In the final step to produce the silicone surfactant, there are two general synthetic approaches. First, one can directly convert an Si-X-functional silicone (X = H, Cl) to the surfactant (Schemes 9.6 and 9.7). Secondly, one can convert an organofunctional silicone in one step to the surfactant (Scheme 9.8).

9.3.2.1 Direct Linkage of the Hydrophilic Group to an Si-H Functional Silicone

There are two general methods to directly link a hydrophilic group to an Si-H functional silicone. First, as shown in Scheme 9.6, is the reaction between the hydroxyl group at the end of a polyether and the Si-R (R = H, Cl) group on a siloxane [74]. This silylation process is catalyzed by platinum compounds and yields H_2 gas as a by-product if R is H. Handling of the evolved hydrogen gas must be considered as part of the safety assessment of any material produced via this route. The resulting surfactants are typically used in non-aqueous applications as the Si-O-C linkage formed by the reaction is hydrolytically unstable.

The second method to directly link a hydrophilic group to a silicone is through hydrosilylation chemistry [74]. A seen in Scheme 9.7, an Si-H functional silicone is exposed to an olefin containing hydrophilic functionality, in this case an ethoxy polyether, in the presence of a platinum-based catalyst compound. This is a highly exothermic reaction (+28 kcal mole^{-1}), so in many cases care must be taken to ensure adequate dissipation of the heat generated. This can be done via external

Scheme 9.7 Hydrosilylation of Allylic Polyether

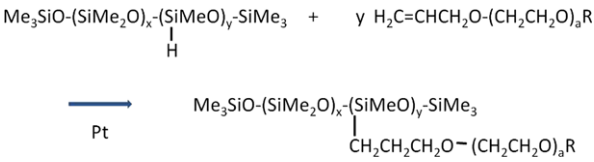

Scheme 9.8 Quaternization of Amino Functional Siloxane

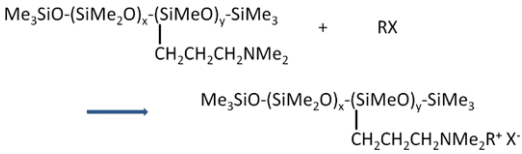

heat exchangers, or by the controlled/metered addition of one of the reactants. Additionally, the SiH groups can unintentionally react with terminal hydroxyl groups or water to liberate hydrogen gas. Care must be taken to minimize this during the reaction and with any residual SiH groups present after the reaction is deemed to be complete [75].

The resultant linkage, a propyl group, is hydrolytically stable; therefore, the product can function effectively as a surfactant in aqueous media. This strategy is particularly useful for the attachment of non-ionic hydrophilic groups, such as polyethers and carbohydrates, to the silicone backbone. The authors are not aware of any examples where ionic hydrophilic groups have been directly attached to the silicone backbone through this methodology. In those cases, the hydrophilic groups is usually generated by chemistry performed on an organofunctional silicone such as that seen in Scheme 9.5 and described in more detail below.

9.3.2.2 Conversion of an Intermediate Organofunctional Silicone into a Surfactant

A general method of converting organofunctional silicones (specifically amino-, phosphino- and sulfido-functional silicones) into surfactants is via traditional, carbon-based nucleophilic displacement types of chemistry. For example, as shown in Scheme 9.8, treatment of a tertiary aminofunctional silicone with standard quaternizing agents (R = alkyl, hydroxyalkyl, benzyl, alkylcarboxylate, alkylsulfonate or carbohydrate; X = halogen, alkylsulfonate, fluoroalkylsulfonate) results in the formation of cationic or zwitterionic silicone surfactants [76–83].

For cationic silicone surfactants, families of analogous species can be generated by standard anion exchange chemistries [84]. For example, as shown in Scheme 9.9, the chloride salt of the silicone surfactant can be converted into the nitrate salt. These anion exchanges produce surfactants with markedly different properties.

Anionic silicone surfactants have been synthesized by a variety of routes, most of which have their origins in the preparation of their hydrocarbon analogs. Many of the examples of anionic silicone surfactants are those containing sulfate or sulfonate anionic groups. For example, as shown in Scheme 9.10, the ring-opening of

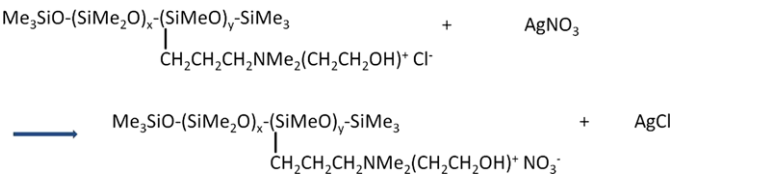

Scheme 9.9 Preparation of Cationic Silicone Surfactant

Scheme 9.10 Preparation of Sulfate Functional Silicone Surfactant

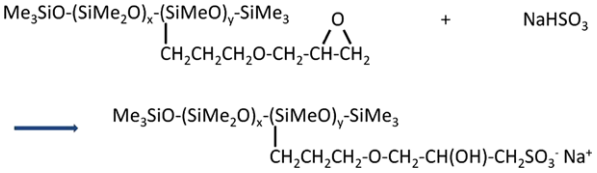

an epoxy-functional silicone by sodium bisulfate yields the sulfate-functional surfactant [85].

Although the authors are not aware of literature describing the synthesis of analogous anionic silicone surfactants, as generated by standard cation exchange chemistries, they postulate that this would be a feasible synthetic methodology.

9.4 Interfacial Behavior of Silicone Surfactants

Silicone surfactants are widely acclaimed for their exceptional activity at a wide range of interfaces. This activity is manifested by (1) the reduction of equilibrium surface tension, (2) the orientation of the surfactant at an interface, (3) interfacial viscosity, dispersion stability and lubrication, (4) dynamic interfacial tension, and (5) the "superwetting" behavior of silicone surfactant solutions.

9.4.1 The Reduction of Equilibrium Interfacial Tension

Regarding the activity of silicone surfactants at the air/water interface, a defining feature of this behavior is the extraordinarily low equilibrium/static surface tensions that are routinely measured. Many silicone surfactants can reduce the surface tension of water down to 21–30 mN m^{-1} [86–92]. This value is significantly lower (by *ca.* 10 mN m^{-1}) than those commonly achieved with hydrocarbon surfactants and is generally only bettered by fluorocarbon-containing surfactants.

To a first approximation, the minimal tension achieved by surfactants at the air/water interface reflects the nature of the cohesive forces existing between the hydrophobic portions of the molecule. The higher the cohesive forces, the higher the degree of tension at the interface (or, alternatively, the energy required to

stretch/extend the interface). As discussed extensively throughout this treatise silicones, particularly methyl silicones, have low intermolecular cohesive forces. Furthermore, the extraordinarily low energy barrier to rotation of the siloxane backbone allows the methyl groups of the silicone to adopt the lowest energy conformation possible [93]. This is also a reasonable explanation as to why methylated silicone surfactants with significant degrees of branching in the siloxane backbone generally have higher surface tension values than their linear analogs; the barrier to rotation of the siloxane network is much higher due to steric hindrance [93].

One result of the low interfacial tension of silicone surfactants is their vigorous adsorption at the organic/air interface [94–98].

9.4.2 The Orientation of Siloxane Surfactants at the Interface

As mentioned in the previous section, it has been well-established that silicone surfactants robustly adsorb at a variety of interfaces, including the following:

- Water/air.
- Organic liquid/air.
- Water/organic liquid.
- Many solid/liquid interfaces.

The adsorption of branched trisiloxane surfactants at the air/water interface has been extensively documented. A key principle underlying many of these studies is that the packing of the surfactant molecules at the air/liquid interface is a function of the nature of the hydrophilic group [99]. This principle is probably operative given that the siloxane moiety is relatively small in area. Within this category, one can separate the relative influences of ionic and non-ionic hydrophilic groups. For the ionic trisiloxane surfactants, the area per molecule at the interface is strongly determined by shielded electrostatic interactions between the solvated hydrophilic group and its counter ion. For non-ionic species, specifically the polyether-based trisiloxane surfactants, in the absence of strong electrostatic interactions, a much more complicated picture comes into play. Generally, the area/molecule scales with the length of the polyether chain [100]. For non-ionic carbohydrate-functional silicone surfactants the size of the carbohydrate groups strongly influences the area/molecule at the interface [101, 102]. Unlike for small trisiloxane surfactants, for polymeric silicone surfactants both the silicone and hydrophilic moieties have an effect on the area/molecule at the interface [103].

The case where the area per molecule at the interface is strongly determined by the dimension of the siloxane portion of the amphiphile is the general case for silicone surfactants based on $[RSiO_{3/2}]_4[RSiO(OH)]_3$ [104] or $(R_3SiO)_x(SiO_{3/2}OH)_y(SiO_2)_z$ [105] (R = short chain alkyl) molecules. In these cases, the hydrophilic group is OH, specifically the Si-OH (silanol) group. The $[RSiO_{3/2}]_4[RSiO(OH)]_3$ (R = isobutyl) species [a "pseudo-cube" (a cube missing one vertex) structure with Si atoms at each vertex of the pseudo-cube] was demonstrated to adsorb at the air/water interface with a near-saturation area/molecule of

1.35 nm^2 (approx. 180 $Å^2$) consistent with the size of the isobutyl-substituted POSS molecule.

9.4.3 Interfacial Viscosity, Dispersion Stability and Lubrication

Along with extraordinarily low liquid/air interfacial tensions, another result of the presence of the low energy cohesive forces between the methylated siloxane chains is *low interfacial (air/liquid) viscosity*. Measurements of the surface viscosity of spread polydimethylsiloxane monolayers put this value close to zero. In some cases, surface viscosity can be built up at a silicone surfactant-adsorbed interface by interactions of the hydrophilic groups with either the underlying liquid or with each other. However, typically the surface viscosity values are nevertheless quite low.

One example of this was observed in the stabilization of polyurethane foam. Model studies [106–108] of the stabilization process, employing free-standing silicone surfactant-containing polyol films ("soap films"), showed that the foam drainage process was governed by the processes of "marginal regeneration" and highly turbulent surface flows. These phenomena are signatures of a low surface viscosity film [109, 110].

Conversely, highly viscous surface films have also been produced employing silicone surfactants. For example, surface films of the $(R_3SiO)_x(SiO_{3/2}OH)_y(SiO_2)_z$ species. These films, featuring a highly packed surface layer of amphiphilic silica nanoparticles, have a high surface viscosity [109, 110]. In accordance, polyurethane foams produced using this material as a surfactant were extraordinarily stable.

In a related study, Hill and coworkers employed an interfacial stress rheometer to study the rheological properties of a silicone oil/water interface in the presence of siloxane surfactants that are used in the personal care industry as water-in-silicone-oil emulsifiers [111]. They appeared to stabilize water-in-silicone-oil emulsions in a fashion similar to that of Pickering emulsions, in which solid particles, such as silica or clay, accumulate at the oil/water interface forming a solid like "eggshell" that resists coalescence.

Regarding using silicone surfactants as dispersion stabilizers, along with the considerations of interfacial viscosity, one might consider the other traditional mechanisms of stabilization as well. These include bulk visco-elastic effects, electrostatic (double layer) stabilization and steric repulsion. Regarding bulk viscoelastic effects, Mehta and Somasundaran [112] studied the mechanism of emulsion stabilization where ionic silicone surfactants were employed as the stabilizer. Non-Newtonian behavior with viscosities an order of magnitude higher than that measured with non-ionic silicone emulsifiers was observed. This was explained by network formation at the droplet interface by weak interactions between the ionic functional groups. Bulk viscoelastic stabilization effects were also reported by Brook et al. in their investigation of the silicone surfactant stabilization of elastomeric silicone foams [113]. Liu and coworkers investigated the adsorption of "comb"-type silicone polyether (SPE) surfactants at the interface between water and a hydrophobic,

self-assembled monolayer [114, 115]. They concluded that SPEs showed significant oleophobic behavior and were therefore capable of stabilizing dispersions in organic media. They postulated that the stabilizing behavior was the result of a steric repulsion mechanism. This stabilization mechanism might also be operative in the case of castor oil-in-silicone emulsions stabilized by cyclomethicone/dimethicone copolyether surfactants [116] (see Chap. 13 for explanation of this therminology).

The adsorption and interfacial rheology of silicone surfactants adsorbed onto a solid surface is an active area of investigation, particularly in terms of the resulting lubricity of the solid surface. For example, Liu and coworkers [117] reported on interactions of an amphiphilic block copolymer of polyalkylene oxide-modified polydimethylsiloxane with thin films of polypropylene (PP), poly(ethylene terephthalate) (PET), and nylon, as well as with reference hydrophilic silica surfaces. They found that the silicone surfactant adsorbed following a Langmuir isotherm and that the adsorbed layers significantly improved fiber wettability and lowered friction.

9.4.4 Dynamic Interfacial Tension

Historically, the dynamic interfacial tension (air/water interface) or alternatively, the rate of interfacial tension reduction, has been a subject of intense interest in the silicone surfactant field. A likely reason for this interest is that dynamic interfacial tension plays a significant role in many processes and surfactant applications including wetting and dispersion stabilization, which are of special interest in the silicone surfactant field.

Generally, as expected, the rate of interfacial tension reduction of silicone surfactants scales inversely with the molecular weight (as expressed by the solvodynamic radius) of the surfactant. This conclusion is consistent with a model where the rate-determining step(s) of the interfacial adsorption process is the diffusion of the surfactant through solution or its rate of orientation at the interface. This has been recently confirmed in two independent studies [118, 119].

9.4.5 The "Superwetting" Behavior of Silicone Surfactant Solutions

For the last 30 years one of the most investigated phenomena regarding silicone surfactants has been that of "superwetting" of aqueous mixtures of certain low molecular weight, trisiloxane-based, silicone polyethers. This fascinating topic has been reviewed in a number of publications [120, 121]. "Superwetting" refers to the extraordinarily rapid wetting of low energy, hydrophobic surfaces (such as parafilm) by these aqueous surfactant mixtures. This phenomenon has been correlated to a number of the physical properties of the surfactant including:

- Low equilibrium interfacial tension. As seen below in Fig. 9.1.
- Low dynamic interfacial tension (high rate of interfacial tension lowering).

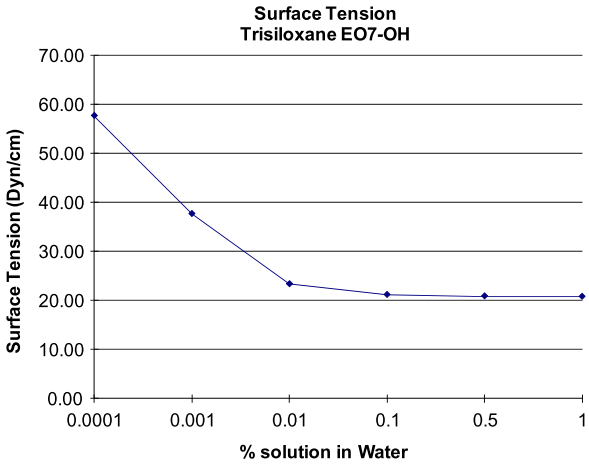

Fig. 9.1 Gibbs free energy plot of a trisiloxane-EO7-OH superwetter

- The presence of lamellar phases of surfactant bilayer aggregates (more information on surfactant aggregation is presented in Sect. 9.5.2).
- Marangoni flow.

Key to understanding superwetting is the assumption of rapid surfactant transport and surface reorientation. There is a strong correlation between a high rate of interfacial tension reduction (low dynamic surface tension) and superwetting [122]. Furthermore, in order to achieve a high rate of interfacial tension reduction, one should be using a relatively small surfactant, which as a result of its compact size will have high linear transport- and rotational-diffusion coefficients. This hypothesis has been quite robustly confirmed including in a recent study that demonstrated that for trisiloxane surfactants of the general formula $(Me_3SiO)_2Si(Me)\text{-}(CH_2)_3(EO)_xOH$ (where EO is $(CH_2)_2O$), the highest initial spreading rate and largest spreading area were measured for the $x = 6$ derivative [122].

Regarding the presence of lamellar phases of surfactant bilayer aggregates in superwetting, informal observations made in the authors' laboratories over 20 years ago showed that the superwetting solutions were often "cloudy", hinting at some type of two-phase system and the presence of lamellar surfactant aggregates [123]. More recently, a correlation between the ability of a silicone surfactant in aqueous media to aggregate into bilayer structures and a tendency to act as a "superwetter" was reported [124]. However, regarding this conceptual linkage of bilayer formation and superwetting, there is a significant amount of controversy with other authors disputing it [125, 126].

The role of surface tension gradient-stimulated flows (i.e. "Marangoni flows) in the superwetting phenomenon has also been discussed [127]. For example, the spreading front of the surfactant solution droplet causes the formation of a surface tension gradient which stimulates Marangoni flow. Furthermore, experiments [128] showed a correlation between the value of the gradient and the rate of flow.

9.5 Aqueous Solution Behavior—Hydrolysis and Aggregation

9.5.1 Hydrolytic Stability

An early and enduring observation about silicone surfactants was that they had a tendency to hydrolyze in aqueous solutions, a process that was quite slow at neutral pH and rapid at pH values below 4 and above 9. The hydrolysis process can be viewed as being the "reverse" chemical reaction to the siloxane condensation depicted in Scheme 9.4. The pH dependence of this phenomenon is explained by the consideration that acids and bases are catalysts for siloxane bond condensation and hydrolysis.

Hence, many studies and inventions in this field have been concerned with lessening the rate of hydrolysis of these surfactants. A common approach to this problem has been to consider the substitution of carbosilane (-Si-C-Si-)-based surfactants for their siloxane counterparts. However, carbosilane species are expensive and often do not have the favorable interfacial behavior of silicones.

Alternative approaches to diminish the rate of hydrolysis of silicone surfactants have been proposed by a number of authors. For example, Peng and coworkers demonstrated [129], while investigating the behavior of novel double-tail polyether-functional trisiloxanes, that some of the species were stable for more than 270 days in a neutral environment (pH 7.0). They concluded that the hydrolysis resistance of the double-tail trisiloxane surfactants can be improved by a weaker hydrophilicity of the surfactant molecule, and a larger volume of the hydrophobic groups. Another approach to lowering the rate of hydrolysis was reported by Pollicello and coworkers [130]. They claimed that the use of (presumably bulkier) alternative groups on both the siloxane backbone and the hydrophilic group achieved the purpose.

A less documented aspect of hydrolysis of silicone surfactants is the hydrolysis of silicone polyethers where the silicone-to-polyether linkage was a Si-O-C bond. Recently this hydrolytic "instability" was exploited by Lin and coworkers in order to prepare deliberately "cleavable" silicone surfactants [131–133]. The hydrolysis of these surfactants was, in some cases, accelerated by exposure to catalysts such as TiO_2, radiation or plasma sources. In these applications the siloxane fragment with silanol (Si-OH) functionality resulting from the cleavage, could be profitably applied as water-proofing and anti-bacterial coatings.

9.5.2 Aggregation

Due to the well-known "hydrophobic effect" [134], silicone surfactants exhibit a pronounced tendency, in aqueous media, to self-assemble into various aggregates including micelles, vesicles and liquid crystalline phases. An extraordinary number of these aggregates are characterized by the presence of surfactant bilayers. These aggregates include non-spherical, oblate-ellipsoidal, disk- or plate-like micelles [135–138], vesicles, lamellar liquid crystal phase [139] and microemulsion "middle" phase.

For example, since the original reports [140–147], many workers [148–153] have documented the ubiquitous tendency of silicone surfactants (different siloxane structures, different hydrophilic groups) to form bilayer vesicles in aqueous mixtures. This formation, properties and application potential of silicone vesicles has been extensively investigated and the following key features have been identified:

- In some cases, silicone vesicles spontaneously form upon the mixing of the specified silicone surfactant with the correct amount of water.
- The bilayers of silicone vesicles are quite fluid and do not show the gel-to-fluid phase transition ubiquitous to hydrocarbon-based vesicles/liposomes.
- A variety of materials can be encapsulated into silicone vesicles [154–158].
- The width of the bilayer corresponds to the length of the siloxane portion of the silicone surfactant [159, 160].

Other studies involving silicone surfactant bilayers include:

- The presence of an AB-structured silicone polyether surfactant, as a co-surfactant with an alkyl ethoxylate, in a surfactant/dodecane/water mixture, causes a striking increase in the solubilization power of either a lamellar liquid crystal (LC) phase or else a microemulsion "middle" phase [161]. This increase in solubilization capacity correlated with an increase in the structural length scale of the microemulsion.
- The bilayer-forming tendency of silicone surfactants has also been exploited in the fabrication of surfactant-templated, mesostructured metal oxide phases [162–168]. In a series of intriguing studies the investigators found that the templating process often leads to the formation of lamellar phases with long-range order. In one case, a silica mesophase was prepared featuring the largest lattice constant reported for lamellar materials to that date [169]. The authors concluded, consistent with other studies, that the lamellar structuring was the result of the virtually unrestricted chain mobility within the silicone surfactant.

This "flexibility factor" favoring the self-assembly of silicone surfactants into bilayer structures has been mentioned by a number of investigators in the field. For example, siloxane chain conformations with surfactant bilayer aggregates have been proposed including coiled (based on micelle aggregation numbers and small angle neutron scattering (SANS) data) [170], flexible [171], and folded ones (Hill and colleagues have also found that the bilayer thickness of vesicles formed by comb-type silicone surfactants is significantly smaller than their extended molecular length) [172].

Finally, we also wish to cite the following:

- As expected, the cloud point of SPE surfactants scales with the degree of hydration of the EO chain. This was confirmed in a recent study [173].
- For a series of AB-structured silicone polyether surfactants in water, a number of unusual aggregate structures were observed including reverse discontinuous cubic phase (I_2), reverse hexagonal phase (H_2), and discontinuous cubic (I_1) phases along with the common lamellar (L_α) and hexagonal (H_1) phases [174].

The authors rationalized the correlation of the appearance of these phases by considerations of the entropy gain/loss of the silicone chain. Specifically, the entropy loss of a long hydrophobic chain (such as the silicone chain) would be largely increased when it is stretched, and thus, long hydrophobic chains tend to be in a shrunk-bulky state. This shrinkage affects the surfactant parameter, which heavily influences the state of aggregation.

9.6 Applications

The unique combination of physical and surface properties of ethoxylated siloxane copolymers (or silicone polyethers (SPEs)) results in the specification of these materials in numerous industrial applications. Inherently the SPEs provide a means to deliver silicone properties to an aqueous system. These properties can be expressed in terms of surfactancy by delivering the low surface energies, as described earlier, to the end application. This can make the materials effective as emulsifiers, wetting agents, foam control agents, or surface modifiers. The flexibility in the product chemistries allows these properties to be tailored to specific end uses. Materials within the SPE family can be effective at emulsifying water in oil or oil in water emulsions. Alternatively the structure can be tailored to demulsify these same two-phase systems. Similarly, the SPEs can be designed to be pro-foaming and stabilize foam systems, or can be designed to be effective foam control agents.

However, the low surface energies are not the only feature that makes these materials of commercial interest in so many applications. The inclusion of polyether groups onto a siloxane backbone allows these materials to treat surfaces and render them hydrophilic. The functionality present on the terminal end of the polyethers can make the SPE copolymer reactive with other cure chemistries. The siloxane portion of the copolymer allows the delivery of silicone feel into aqueous systems. In total, the combinations of these properties offer multiple benefits to the individual application.

Each of these end uses for silicone surfactants is unique and is summarized in the next few sections of this chapter. Many of these applications have been reviewed in other publications. The intent of this portion of the chapter is not to further review, but to summarize these applications and how the surface behavior of the silicone surfactants enables them to provide benefits in these applications. In addition, new developments are also highlighted.

9.6.1 Personal Care

Silicone surfactants have been used in the personal care industry for a number of years, beginning primarily in the mid-1980s. Mainly, these have been silicone polyether copolymer-based products although many other functional compositions

have been developed and commercialized. The unique surface properties have allowed these products to be incorporated into a broad spectrum of personal care uses. These include antiperspirant formulations, skin care, facial care, as well as hair care applications. The primary functions of these materials are to provide emulsification, humectancy, and overall aesthetics to the personal care formulations.

Several review articles have been written on the use of silicone surfactants in personal care. Floyd described a range of silicone surfactant structures and their ties to specific applications and the resulting intellectual property in a review in Hill's book on silicone surfactants [175]. He describes the foundational patents for this application and considers specific segments which utilize these materials and the claims they provide in these segments. O'Lenick has also published extensively in this field. He has described the use of silicone surfactants in various personal care formulations [176]. He has also published a review that describes the nomenclature system used in this industry and summarizes many of the properties important to various personal care applications [177]. This review details his work not only with non-ionic silicone polyethers, but also with other amphiphilic silicone copolymers that he has developed. Many of the patents on these compositions are described in Floyd's review [181].

One of the major uses of silicone surfactants in personal care is in the area of emulsification. They have been used as emulsifiers for several years, beginning in the early 1980s. The initial work was in the antiperspirant segment where a series of unique silicone polyethers were utilized to stabilize water in silicone emulsions. Most specifically these were emulsions in which the external phase was based on cyclosiloxanes. The initial use of silicone surfactants as emulsifiers for water in silicone emulsions was described by Keil and Starch [178, 179]. The low surface energy of the siloxane external phase, as well as solubility parameters, did not allow the conventional hydrocarbon-based emulsifiers to stabilize this form of emulsion. The siloxane portion of a silicone surfactant is sufficiently low in surface energy, and is sufficiently compatible with the external phase to prevent coalescence of internal aqueous phase droplets. Key to this stabilization is managing the structural architecture of the silicone surfactant by balance of the dimethylsiloxane segments to the methyl/polyether siloxane segments of the copolymer. This provides the right solubility parameter of the silicone surfactant. Gruning and Bungard describe the use of hydrophile lipophile balance (HLB) methods to help predict the silicone surfactant composition best suited for stabilizing a water in silicone, as well as other types of emulsion (water-in-oil (W/O), oil-in-water (O/W), multiple emulsions) in their review article on silicone emulsifiers [180]. O'Lenick gives an additional perspective with a method called the three dimensional HLB system. This takes into account the consideration of the siloxane's unique solubility parameters and the fact that the silicones are hydrophobic, and yet not lipophilic [181]. Dahms and Zombeck collaborated on a series of papers in which they described how these molecular architectures are varied and used to prepare a range of personal care formulations, creams, and emulsions [182, 183].

Modifications of the basic structures of silicone oxyalkylene copolymers to include grafts of various alkyl functionalities and chain lengths have also been found

to stabilize water-in-oil emulsions, where the oil phase is hydrocarbon oil. Because of the non-lipophilic nature of the siloxane hydrophobe, there is little compatibility of the traditional silicone polyether graft copolymer with an oil phase, and these are not suitable for stabilizing W/O formulations. However, the added alkyl functionality to the composition provides for a proper solubility balance to effectively stabilize these systems [184].

Utilizing silicone surfactants as a primary surfactant in O/W formulations is not as common, as many organic-based surfactants are suitable for stabilizing these emulsions. Nevertheless, silicone surfactants can effectively perform in these formulations as well. Generally, the higher HLB silicone surfactants (HLB 10–18) are required to stabilize these formulations. More recently, non-polyether-based silicone modified carbonic acid surfactants have been shown to effectively stabilize O/W emulsions as well [185]. Further, efforts have shown how O/W emulsions containing pigment dispersants can be formed utilizing silicone surfactants with glycoside radicals as the key hydrophilic component in the surfactant composition. These are particularly useful in sun care products where the pigments help block harmful UV radiation [186].

Other recent developments in the field of silicone emulsifiers have focused on different architectures and improved understanding of emulsion fundamentals behind the preparations of various emulsions. Dimitrova et al. published two papers in which they describe the use of $(AB)_n$ type silicone polyether copolymers as emulsifiers for water in oil systems, and compare these with the more traditional graft or rake type structures [187]. These $(AB)_n$ materials are shown below as Structure 9.10 where the dimethylsiloxane block is the "A" component of the block copolymer and the "B" block is the combined EO and PO segments. These are prepared by the platinum catalyzed hydrosilylation of a silicon hydride end-blocked siloxane and an allyl end-blocked polyether. The EO/PO portion is prepared independently. The R1 simply signifies an end-blocking group.

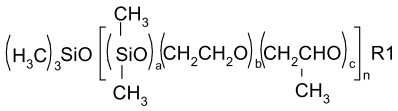

Structure 9.10

The data suggested that these $(AB)_n$ type emulsifiers require less shear energy to produce W/O emulsions vs. rake type SPEs of similar solubility parameters. These conclusions were further supported in a second paper in which a variety of personal care formulations were prepared and the fundamental stability studied [188]. Broader descriptions of how to use these fundamental properties in the preparation of stable formulations have also been described in a series of Society of Cosmetic Chemists papers [189, 190]. These papers describe how to prepare a range of formulations including glycerin in silicone, glycerin + water in silicone, and water in silicone emulsions and their stability and aesthetic properties.

Beyond the use as emulsifiers, the silicone-based surfactants have found utility as humectants, surface modifiers, and conditioning agents. In hair care applications,

a range of silicone surfactant structures has been shown to provide conditioning effects. The non-ionic polyether type surfactants confer a light conditioning. The lower HLB value silicone polyethers tend to be more effective in 2-in-1 conditioners [191]. In other cases, higher HLB surfactants improve conditioning on the hydrophilic portions of hair strands. Cationic silicone surfactants, like silicone quaternary amine compounds, give excellent conditioning properties as well as an improvement in hair body and curl retention [192]. The non-ionic polyether materials provide benefits to skin care and shave formulations by contributing humectancy and lubrication properties to the formulations [193].

9.6.2 Coatings

A second major application area for silicone-based surfactants is in the coatings industry. Here, they are primarily used as additives to various coating formulations to improve surface properties. The low surface energies provide for good leveling, wetting, spreading and gloss properties of the coating. The type of coatings where these materials are utilized is far reaching and includes: architectural, industrial protective coatings, wood, marine, cookware, and coil coatings. They are also used in many printing inks. The use of these additives significantly increased with the advent of more water borne systems which have inherently higher surface energies than solvent-based systems. Many of the desired coating properties were compromised with aqueous formulations without the use of additives. Easton provided an overview of silicone surfactants and their uses in waterborne coatings describing how they impacted the coating performance [194]. Perry published an updated review of these properties and discussed how dynamic surface tension and the rapid wet out provided by trisiloxane-based superwetters impact primarily aqueous-based coating formulations [195]. Her work also showed higher molecular weight copolymers tend to improve the slip and mar resistance of the coatings. This can be attributed to the orientation of the polysiloxane portion of the copolymer segments to the polymer/air interface yielding a lower energy surface. Ferritto et al. further developed this approach by extending the technology of branched silicone polyether copolymers into coatings [196]. These polymers utilized branched polyethers in the composition in place of pure linear ethoxylated or propoxylated ethers. The branching is derived from glycidol being utilized in the preparation of the polyether intermediates. These were shown to impact overall dirt pick up when formulated into wood coatings.

Another parameter that these materials provide is in reducing the propensity of these formulations to foam and to eliminate the appearance of microfoams in the resulting coatings, which can significantly impact end coating quality as well as processing when a coating is being applied. Semmler describes how the use of specialty silicone polyether additives in an overall formulation of a silicone antifoam helped to reduce the occurrence of microfoam when the coating was spray applied [197]. Van Dam describes the use of antifoams containing silicone polyether additives in printing inks [198]. These additives were more defoaming at the ink surface

and had good dynamic properties to eliminate foam build up during the printing process. Further, they had good durability and persistency in the process. O'Neil reviews the various mechanisms of foam destabilization by silicone surfactants and antifoam compounds. He describes differences between rake and ABA type silicone surfactants and their performance, as well as their uses in clear overprint varnishes, flexographic inks, wood parquet lacquers and automotive clear basecoats [199].

9.6.3 Household Care

The primary use of silicone surfactants in household care applications is again related to the control of foam. Unlike the applications in coatings where the target is to prevent the formation of foam, or to defoam a system in which foam has been created, the goal here is to control the foam to fit specific profiles. This is especially true in laundry applications. Fey has described the mechanism of foam control provided for with silicone fluids and silicone polyethers [200]. He suggested three main requirements for a material to behave as an effective antifoaming agent: (1) it must be insoluble in the foaming medium, (2) it must be readily dispersible in the foaming medium, and (3) it must have a lower surface energy than the foaming medium. This allows for the fluid to enter the air/liquid interface and spread over that interface. This allows for bridging of particles and eventual rupture (see Chap. 13).

In most cases, the silicone surfactant is used as part of an overall antifoam compound or composition. They are normally of the non-ionic polyether type and their role is to assist in the dispersion of the antifoam compound into the foaming media and to aid in the reduction and/or control of the foam. McGee et al. first showed this effect and described the impact of the incorporation of the silicone surfactant in combinations with silicone resins, fluids, silica particles and catalyst [201, 202].

Much of this knowledge has been applied to the development of antifoams specific for control of foam in liquid and powdered laundry detergents. In these products it has been found that branching in the polymer composition aids in the overall control of the foam. This branching can be introduced into the polymer chain by hydrosilylation of vinyl terminated polydimethylsiloxanes with a silicone polyether containing residual silicon hydride groups. Alternately, the crosslinking can be conducted in advance of the introduction of the allyl polyether to the polymer in the formation of the silicone polyether [203]. Elms et al. further developed this concept with formulated antifoam compounds containing linear and branched silicone polyether copolymers. These were shown to be more effectively dispersed in the detergent medium and to provide improved foam control profiles [204].

Beyond antifoaming there have been other uses of silicone surfactants in household care applications. Henning described the use of a range of silicone materials, especially silicone polyethers, in polishes and household cleaning products [205]. These included uses in car, furniture and shoe polishes, and in household and industrial cleaning applications. In some cases these uses are limited due to the inherent hydrolytic instability of silicone polyether copolymers under acidic or basic conditions. Panandiker described the use of low HLB type silicone polyethers in liquid

detergent formulations [206, 207]. These low HLB polymers were part of an overall formulation and were designed to deposit onto fabric in the washing cycle to improve fabric feel and hand.

9.6.4 Textiles

Silicone surfactants are used in numerous textile applications to impart hydrophilic properties to the textile. In this sense they are not specifically being utilized for their surfactancy properties; rather, their bulk structural properties allow them to orient at the interface of the textile to impact the feel. Often, these silicone materials contain amino groups to provide for excellent anchoring and hand to the fabric, and also polyether functionality to impart hydrophilicity [208]. More recently efforts have been focused on linear $(AB)_n$ type block copolymers containing both amino and polyether functionalities. Czech published the initial work in this area [215]. The polymers were block copolymers prepared from the addition of end-blocked diepoxysiloxane fluids to various amines and diepoxy end-blocked polyethers. They imparted good softening and hydrophilicity to cotton [209]. Favresse prepared versions of these via different routes based on grafting functional groups on to $(AB)_n$ block silicone polyether compounds utilizing free radical polymerizations. These showed improvements in hand on cotton, non-wovens, as well as synthetic fibers [210]. Kennan prepared different materials based on a process where an epoxy terminated $(AB)_n$ silicone polyether was initially prepared and then aminated. These too showed excellent hand and provided improved hydrophilicity [211].

Silicone polyethers and silicone polyether terpolymers with other functionalities have also been used to treat non-woven textiles. Non-woven fabrics are traditionally made from polypropylene and are very hydrophobic. They are used as backing on many textile substrates as well as synthetic leathers, feminine care products and baby diapers. Improving the hydrophilicity of these non-woven products can significantly improve end performance. Sabia discussed the use of standard graft silicone polyethers to improve the finish of non-woven fabrics [212]. One detriment has been the durability of the treatment. Since there is no reactive functionality on the silicone polyether copolymers, they tend to wash off if exposed to water and then render the fabric hydrophobic once again. This is particularly of concern in diaper applications where it results in leakage. To address this durability issue, multiple functionalities are often incorporated onto the silicone. Most common are epoxy groups and polyethers. The epoxy can open and provide for improved durability to the non-woven substrate.

Standard silicone grafts and ABA type silicone polyethers are also used as fabric treatments to aid ironing. For example, the use of these materials in iron spray solutions for cotton and synthetic fabrics has been shown to significantly reduce the difficulty in removing wrinkles from fabric [213].

9.6.5 Oil and Gas

Applications of silicone surfactants in the oil and gas industry primarily center on demulsification and foam control. One concern that dictates the type of silicone and application of silicones in the oil recovery, transportation and refining processes is the potential of silicones to foul the catalysts used in the hydrocracking process [214]. However, this is somewhat limited to more oil soluble silicones and not necessarily silicone surfactants. It is critical that the silicone does not enter the oil phase in the refinery where it can be converted into silica upon heating in the cracking process thereby impacting the catalyst activity.

Most of the references relating to the use of silicone foam control agents in the oil and gas industry are centered on pure polydimethylsiloxane- (PDMS) based technologies. Foams in the oil and gas industry are primarily non-aqueous foams stabilized by naturally occurring asphaltenes. The gas phases are generally low molecular weight hydrocarbons. High molecular weight PDMS fluids tend to lower surface energies and allow for coalescence of the gas phase droplets resulting in foam rupture [215]. Because of the need for high oil solubility, silicone surfactants are not generally utilized in foam control formulations in the oil and gas industry, although there have been some efforts with low HLB-based silicone polyethers, but this is not widely practiced [216].

Silicone surfactants are more broadly utilized in the field of crude oil demulsification. In the recovery and transportation of crude oils, there is an undesired formation of various emulsions of oil in water and water in oil. The exact type is dictated by many factors, but depends heavily on the type of crude, salinity of the aqueous/brine phase, level of stabilizing asphaltenes, age of the well, and extraction process. The emulsions are generally formed as part of the oil extraction due to high turbulence in the production process [217]. Before the recovered oil is sent to a refinery for further processing the emulsion must be broken, oil recovered, and the produced water treated and then generally re-injected back into the recovery process or treated/cleaned and released. Many types of surface-active material are used in this demulsification process. Most are organic and include polymers of EO, PO phenols, and nonylphenols. Oil service companies formulate demulsification cocktails and tailor them to specific field conditions. The demulsifiers are generally formulated into organic solvents such as aromatic naphtha. By far, the greatest volumes of demulsifiers utilized in the industry are of these types.

Silicone polyethers are also utilized and a wide range of product offerings and technologies are available. Early investigations and use in this application for silicone surfactants dates back to the early 1970s [218]. However, widespread use has not resulted, primarily due to cost considerations as the silicone materials typically have a higher in-use cost than organic-based options. In some cases efforts have been made to overcome this issue by blending or by the incorporation of solid particles such as silica [219, 220]. The silicone materials do find utility when the crude oil/water emulsions are difficult to break, such as heavy crudes, or under cold conditions [221]. This has not deterred further development of new silicone surfactant compositions and improved understanding of the mechanism of how they behave as

emulsion breakers. David et al. described efforts to better understand destabilization mechanisms and proposed two possible scenarios: dissolution of the stabilizing asphaltene aggregates thereby removing the natural occurring surfactant, and displacement of these asphaltenes with a more surface-active silicone component. Further, these components are inherently not designed to be stabilizing, thereby allowing coalescence [222]. More recently, Phukan et al. described a new composition type of a silicone demulsifier that contains multiblocks of silicone and polyether with amino groups in the backbone that introduce further silicone branching sites [223].

9.6.6 Pulp and Paper Applications

Within the pulp and paper industry silicone surfactants are used as various process aides. These applications include pulp drainage, pulp digestion, antifoaming/defoaming, cleaning, and paper deinking. Silicone polyethers are used in many of these applications either directly or as part of an overall formulation component.

One of the first steps in the papermaking process is cooking which liberates the cellulosic fibers from the wood chips. This is done under highly alkaline conditions and is referred to as the Kraft process. In a simplified description of this process the wood chips are hydrated and impregnated with pulping chemicals (mainly highly alkaline sodium hydroxide and sodium sulfide) called white liquor. These are cooked to remove the lignin and recover the individual cellulosic fibers [224]. The used white liquor is referred to as the 'black liquor'. It is separated from the fibers by washing and recycled. The fibers are then screened and the resulting brownstock pulp is washed and bleached before the final conversion to paper. Process aids, surfactants, and additives are added throughout this process to aid in the paper production.

In the first part of this cooking, digester additives are commonly added to aid delignification. Silicone polyethers have been used in this process to reduce the digestion/cook time, to increase the yield of the pulp, and to reduce the level of undigested fibrous materials [225]. The low surface energies provided by the inclusion of the silicone surfactant allow the cooking chemicals to better impregnate the wood chips, thereby increasing their effectiveness.

Silicone defoaming agents are used in the washing of the brownstock. During delignification, many types of surface-active agent are formed. This causes severe foam control issues downstream during the pulp washing steps. Silicone-based defoaming agents are highly effective due to their inherent low surface activity and spreadability at the air/liquid interface. They exhibit good foam knock-down and persistence and are used at very low concentrations [226]. Silicone polyethers are included in many of these antifoam formulations to aid in the delivery of the primary silicone active, or to act as secondary antifoam fluids. The low surface energies have also been shown to aid in pulp drainage [227]. Compositions with branching in the siloxane backbone have also shown effectiveness in this application [228].

Silicone polyethers aid in the process of treating paper making equipment which helps to eliminate the need for frequent shut-down and cleaning of the equipment.

In this stage of the paper making process, dilute cleaned pulp is applied to a forming fabric and begins to drain and dry. The resulting paper web comes into contact with felt presses to further dry the pulp web to the desired moisture content. These felts become fouled with various deposits from the pulp drying process which can significantly decrease the process on-line time as a result of frequent cleaning. Solutions of silicone polyethers have been shown to reduce the amount of time required to clean when spray applied on these press felts [229].

Another segment in the pulp and paper industry that is growing in significance is in the area of paper deinking as part of the overall paper recycling process. Existing technologies often lead to inferior quality pulp that limits the applications for the recycled pulp to low value forms of paper or cardboard. Hence, removal of the ink from the recycled paper is critical in achieving a high quality recycled pulp that can be used for higher end paper products. Silicone polyethers have been shown to be effective in deinking flotation processes [230]. In this process the ink is removed utilizing more mild conditions vs. caustic treatments. SPEs help to emulsify the ink and are then skimmed off from the deinking bath [231].

9.6.7 Other Foam Control Applications

In addition to the foam control applications that are described in the sections on detergent foam control, pulp and paper, and in defoaming and antifoaming of coating formulations, silicone polyethers are also used in other foam control applications such as defoaming of diesel fuel. Silicone polyether copolymers that had the terminal carbinol functionality present on the polyether capped with succinic anhydride provide for excellent foam control in diesel and jet fuels. These polymers had good stability in the hydrocarbon liquid and retained their defoaming ability during storage [232]. Adding branching or crosslinking to the siloxane portion of the silicone polyether was also shown to impart improved foam control properties [233].

9.6.8 Agriculture

The use of silicone surfactants in the agricultural industry is mainly based on the wetting and penetration behavior of the trisiloxane-based silicone polyethers. As described earlier, the trisiloxane polyether copolymers are commonly referred to as superwetters. The unique, spontaneous wetting achieved by the use of these materials allows them to be very effective wetting agents and adjuvants in aqueous-based pesticide formulations. Penner et al. provided a comprehensive review of this application in Hill's book on silicone surfactants [234]. They described how the ultra low surface tension allows the aqueous pesticide solution to spontaneously wet the surface of leaves and aids in the penetration of the pesticide solution through the leaf cuticle into the active cell structure. This can impact the rate of pesticide applied

and can also provide for the pesticide to be resistant to wash off by rain, as the rate of pesticide uptake is significantly increased.

A common issue with trisiloxane-based superwetters is the inherent hydrolytic instability of the siloxane bond when solubilized into acidic or basic formulations. Under these conditions the siloxane bond will rearrange and surfactancy and superwetting behavior is lost. To combat this issue, non-siloxane-based Si containing materials have been suggested. Letherman et al. proposed a series of M–M′ disiloxanes modified with ionic functionalities to combat the hydrolysis [235]. Additionally, they also proposed *t*-butyl substitutions on the terminal silicon groups to stabilize the trisiloxane groups to hydrolysis [236]. Klein et al. also addressed this issue by developing polyether-modified trimethylsilanes [237].

9.6.9 Polyurethane Foams

The final application in this review is the use of silicone surfactants as stabilizers for polyurethane foams. This was the original use of these materials and was the initial reason for their development. It still remains today the largest use of silicone surfactants although other applications discussed in this review are of growing importance. The primary functions these materials play in this application is to compatibilize the polyol and isocyanate intermediates, blowing agents and catalysts, and then to aid in the stabilization of the bubbles/cells during the foam formation until the final cure of the foam. This prevents coalescence of the cells and provides for the desired foam density and cell structure. Snow and Stevens have provided a thorough review of the types of silicone surfactant used to stabilize flexible, rigid and molded foams [18].

9.7 Conclusions

Silicone surfactants are a broad class of surface-active silicone compounds. The unique surface properties contributed by the siloxane structure are the result of the siloxane bonds and the free rotation of functional groups grafted onto the silicon atoms. This allows these materials to uniquely orient at interfaces, drive surface energies to very low values, and to form structured systems in aqueous formulations and solutions. This gives them a set of unique properties that allows them to be utilized in a diverse set of end applications ranging from polyurethane foam stabilization to personal care emulsifiers. The structural variations are many and will continue to develop and expand as new applications continue to evolve.

References

1. Hill RM (1999) Silicone surfactants. Surfactant science series, vol 86. Marcel Dekker, New York

2. Henning J, Muller F, Peggau J (2001) Silicone surfactants—multitalented with backbone. SOFW J 127(1/2):38–43
3. Hill R (2002) Silicone surfactants-new developments. Curr Opin Colloid Interface Sci 7(5/6):255–261
4. Ruiz MA, Hernandez A, Llacer JM, Gallardo V (2003) The development of silicone chemistry II Hydrophilic silicones. J Appl Cosmetol 21(4):147–157
5. Fleute-Schlachter I, Feldmann-Krane G (2003) Silicone surfactants. In: Novel surfactants. Surfactant science series, vol 114. Marcel Dekker, New York, pp 585–622
6. Long B, Wang H (2004) Synthesis and application of polysiloxane-polyether surfactant. Xiangliao Xiangjing Huazhuangpin 2:31–35
7. Kamei M (2005) High performance trend of silicone surfactants. Fragr J 33(6):28–34
8. Huang W (2005) Silicone surfactant with special structure (continued). Youjigui Cailiao 19(3):48–51
9. Hill RM (2006) Other types of surfactants—silicone surfactants. In: Farn RJ (ed) Chemistry and technology of surfactants. Blackwell Publishing, Oxford
10. Huang L, Yang J, Lu B, Li G, An Q (2008) Development of amino polyether organic silicone surfactants. Riyong Huaxuepin Kexue 31(9):21–24
11. O'Lenick AJ, O'Lenick KA (2008) Silicone amphiphiles; getting the best of all worlds. Househ Pers Care Today 2:xxiv–xxvii
12. Han F, Liu Z, Zhou Y, Xu B (2009) Special surfactants and functional surfactants (III)—preparation and properties of organic silicone surfactants. Riyong Huaxue Gongye 39(2):133–137
13. Han F, Liu Z, Zhou Y, Xu B (2009) Special surfactants and functional surfactants (IV)—application of organic silicone surfactants. Riyong Huaxue Gongye 39(3):200–206, 212
14. Huang L, Hao L, Yuan J, Liu Y, An Q (2010) Research progress on preparation and application of silicone surfactants for pesticide adjuvants. Youjigui Cailiao 24(1):59–64
15. Somasundaran P, Purohit P, Gokarn N, Kulkarni R (2010) Silicone emulsions: interfacial aspects and applications. Househ Pers Care Today 3:35–39, 42
16. Huang W (2010) Silicone nonionic surfactant. Youjigui Cailiao 24(1):65–66
17. Rodriguez-Abreu C, Esquena J (2011) Preparation of mesoporous materials with nonhydrocarbon surfactants. In: Tadros TF (ed) Self-organized surfactant structures. Wiley, Weinheim, pp 213–238
18. Snow S, Stevens R (1999) The science of silicone surfactant application in the formation of polyurethane foam. In: Hill RM (ed) Silicone surfactants. Surfactant science series, vol 86. Marcel Dekker, New York, Chap 5
19. Bassindale AR, Gentle TE, Taylor PG, Watt A (1996) Octopus molecules based on silsesquioxane cores Tailor-made silicon-oxygen compd. In: Corriu R, Jutzi P (eds) Lect workshop, meeting date 1995. Vieweg, Wiesbaden, pp 171–176
20. Gentle TE, private communication
21. Deng J, Polidan JT, Hottle JR, Farmer-Creely CE, Viers BD, Esker AR (2002) Polyhedral oligomeric silsesquioxanes: a new class of amphiphiles at the air-water interface. J Am Chem Soc 124(51):15194–15195
22. Snow SA, Pernisz UC, Nugent BM, Stevens RE, Braun RJ, Naire S (2001) Modeling the stabilizing behaviour of silicone surfactants during the processing of polyurethane foam: the use of thin liquid films. In: Klempner D, Frisch KC (eds) Advances in urethane science and technology. In this document the material of interest is referred to as the Trimethylsilyl Capped Polysilicate (TCP), Chap 5
23. Hill RM (1999) Siloxane surfactants. In: Hill RM (ed) Silicone surfactants. Surfactant science series, vol 86. Marcel Dekker, New York, Chap 1
24. Omotowa BA, Shreeve JM (2003) Preparation, characterization, and thermal and surfactant studies of polyfluorinated amphiphilic carbosilane dendrimers. Macromolecules 36(22):8336–8345
25. Krska SW, Seyferth D (1998) Synthesis of water-soluble carbosilane dendrimers. J Am Chem Soc 120(15):3604–3612

26. Kim C (2009) Silyl ether containing dendrimers with cyclic siloxane cores. In: Dvornic PR, Owen MJ (eds) Silicon-containing dendritic polymers. Springer, Berlin, Chap 6
27. Jonas G, Stadler R (1991) Polysiloxanes with statistically distributed glucose and galactose units. I. Synthesis and thermal characterization. Makromol Chem, Rapid Commun 12(11):625–632
28. Jonas G, Stadler R (1994) Carbohyrate modified polysiloxanes. II. Synthesis via hydrosilylation of mono-, di- and oligosaccharide allylglycosides. Acta Polym 45(1):14–20
29. Akimoto T, Kawahara K, Nagase Y, Aoyagi T (2000) Preparation of oligodimethylsiloxanes with sugar moiety at a terminal group as a transdermal penetration enhancer. Macromol Chem Phys 201:2729–2734
30. Loos K, Jonas G, Stadler R (2001) Carbohydrate modified polysiloxanes, 3 solution properties of carbohydrate-polysiloxane conjugates in toluene. Macromol Chem Phys 202(16):3210–3218
31. Boysen MMK, Lindhorst TK (2003) Sugaring' carbosilane dendrimers via hydrosilylation. Tetrahedron 59(22):3895–3898
32. Ogawa T (2003) Simplified synthesis of carbohydrate-functional siloxanes via transacetalation. I. Glucose-functional siloxanes. J Polym Sci A Polym Chem 41(21):3336–3345
33. Ogawa T (2003) Simplified synthesis of amphiphilic siloxanes with methyl gluconyl glycinate functionalities via transacetalation. Macromolecules 36(22):8330–8335
34. Brandstadt KF, Gross RA, Lane TH (2004) New organosilicon carbohydrate compound for use in forming gels, fibers, films, or coatings. US Patent 7,078,519
35. Gross RA, Kalra B, Kumar A (2004) Enzymatic condensation polymerization used to prepare polyester-containing polymers, comprises combining enzyme, compound consisting of diols and polyols, and diacid in reaction vessel, and heating vessel to preselected temperature. US Patent 6,972,315
36. Henkensmeier D, Abele BC, Candussio A, Thiem J (2004) Synthesis and characterization of terminal carbohydrate modified poly(dimethylsiloxane)s. Macromol Chem Phys 205(14):1851–1857
37. Sahoo B, Brandstadt KF, Lane TH, Gross RA (2005) Sweet silicones: biocatalytic reactions to form organosilicon carbohydrate macromers. Organic Lett 7(18):3857–3860
38. Henkensmeier D, Abele BC, Candussio A, Thiem J (2005) Synthesis of carbohydrate-segmented polydimethylsiloxanes by hydrosilylation. J Polym Sci A Polym Chem 43(17):3814–3822
39. Racles C, Hamaide T (2005) Synthesis and characterization of water-soluble saccharide functionalized polysiloxanes and their use as polymer surfactants for the stabilization of polycaprolactone nanoparticles. Macromol Chem Phys 206:1757–1768
40. Carillo FV, Costello M, Creutz SFA, Deklippel L, Henault B, Joffre EJ, McAuliffe JC, O'Neil VK, Simon C (2006) Surface treatment composition use as fabric treatment composition, comprises saccharide-siloxane copolymer(s), which is reaction product of functionalized organosiloxane polymer and hydroxyfunctional saccharide(s). Patent applications WO2006127882, US0683589, US0915007
41. Joffre EJ, Johnson BK, Starch MS, Swanton BJ (2006) Personal care composition for personal care product for hair, and skin, i.e. antiperspirant, comprises saccharide-siloxane copolymer(s) having a saccharide component and an organosiloxane component and linked by linking group. Patent applications WO2006127883, US0683590, US0915051
42. Joffre EJ, McAuliffe JC (2006) New ionically-modified saccharide siloxane copolymer useful in e.g. personal care product comprises saccharide and organosiloxane component, and is prepared by reaction of saccharide siloxane copolymer with ionic monomer/oligomer. Patent applications WO2006127924, US0683718 US0915077
43. Joffre EJ, Kollar C, McAuliffe JC (2006) Cross-linkable composition for use as adhesive release coatings on paper, as wood water repellents or as wound dressings, comprises saccharide-siloxane copolymer, cross-linking agent and optionally solvent. Patent applications WO2006071772, US0638871, US0793067

44. McAuliffe JC, Smith WC, Starch MS (2006) Saccharide compound for cosmetic and personal care formulations comprises ester derivative of ascorbic acid or 2-keto acid saccharide, where ester has been introduced by ester bond formation between ascorbic acid or 2-keto acid saccharide. Patent applications WO2006066227, US0636567, US0636567, US0792460
45. Canfield L, Debdi N, Lavaux V, Starch MS, Van Reeth I (2006) Cosmetic, veterinary, pharmaceutical or therapeutic composition comprises ionic cross-linked polymer as thickening agent, water-in-oil emulsifying agent, silicone material, active agent, water and silicone-based emulsifying agent. Patent GB2422605
46. Racles C, Hamaide T, Ioanid A (2006) Siloxane surfactants in polymer nanoparticles formulation. Appl Organomet Chem 20:235–245
47. Wang GY, Du ZP, Li QX, Zhang W (2010) Carbohydrate modified siloxane surfactants and their adsorption and aggregation behavior in aqueous solution. J Phys Chem B 114:6872–6876
48. Han F, Zhang G (2003) New family of siloxane surfactants having glucosamide. Tenside Surfactants Deterg 40(6):332–337
49. Haupt M, Knaus S, Rohr T, Gruber H (2000) Carbohydrate modified polydimethylsiloxanes. Part 1. Synthesis and characterization of carbohydrate silane and siloxane building blocks. J Macromol Sci, Part A, Pure Appl Chem A37(4):323–341
50. Schmaucks G (1999) Novel siloxane surfactant structures. In: Hill RM (ed) Silicone surfactants. Surfactant science series, vol 86. Marcel Dekker, New York, Chap 3
51. Maki H, Horiguchi Y, Suga T, Komori S (1970) Syntheses and properties of surfactants containing organometallic compounds. VI. Syntheses and properties of surfactants with three-chained hydrophobic groups containing organotin and organosilicon compounds. Yukagaku 19(4):245
52. Maki H, Horiguchi Y, Suga T, Komori S (1970) Syntheses and properties of organometallic surfactants. VII. Cationic surfactants containing polydimethylsiloxane. Yukagaku 19(11):1029
53. Azechi S, Meguriya N, Tanaka M (1989) Cationic silicone surfactant and method of its manufacture. US Patent 5,124,466
54. Schmaucks G, Sonnek G, Wuestneck R, Herbst M, Ramm M (1992) Effect of siloxanyl groups on the interfacial behavior of quaternary ammonium compounds. Langmuir 8(7):1724
55. Snow SA (1993) Synthesis and characterization of cationic siloxane surfactants $(Me_3SiO)_2Si(Me)$-$(CH_2)_3NMe_2(CH_2)_2OR^+$ X. Langmuir 9(2):424
56. Hill RM, Snow SA (1993) Cationic diquaternary ammonium salt functional silicones. US Patent 5,235,082
57. Wagner R, Sonnek G (1994) Dicyclopentadienyl units containing silicone surfactants. In: Auner N, Weis J (eds) Organosilicon chem. VCH, Weinheim, pp 267–268
58. Kuo P-L, Hou S-S, Teng C-K, Liang W-J (2001) Function and performance of silicone copolymer (VI). Synthesis and novel solution behavior of water-soluble polysiloxanes with different hydrophiles. Colloid Polym Sci 279(3):286–291
59. Cheng J, Wang X, Wu Q, Gan G (2002) Synthesis of polyether-modified silicone quaternary ammonium salt and its properties. Youjigui Cailiao 16(2):10–13
60. Coo-Ranger JJ, Zelisko PM, Brook MA (2004) Ionic silicone surfactants in water-in-silicone oil emulsions containing proteins. Papers Present Meet - Am Chem Soc, Div Polym Chem 45(1):674–675
61. Klein KD, Schaefer D, Lersch P (1994) Anionic silicone surfactants. Tenside Surfactants Deterg 31(2):115–119
62. Renauld F, Colas AR (1988) Organosilicon sulfosuccinate(s) preparation by reaction of organosilicon compounds with base and sodium bisulfite, useful as surfactants. US Patent 4,777,277
63. Renauld F, Colas AR, Sawick GC (1988) Surface active silicon compound. GB Patent 2,203,152

64. Renauld F, Colas AR (1988) Preparation of organo-silicon compounds having sulphoxide-containingt hydrocarbon groups from sodium periodate and silane or organo-siloxane, used for textile softeners and antistatic treatments. GB Patent 2,223,232
65. Azechi S, Meguriya N, Tanaka M (1989) Anionic silicone surfactant and method of its manufacture. US Patent 5,068.380
66. Huang W (2005) Silicone surfactant with special structure. Youjigui Cailiao 19(3):48–51
67. Snow SA, Fenton WN, Owen MJ (1991) Zwitterionic organofunctional siloxanes as aqueous surfactants: synthesis and characterization of betaine functional siloxanes. Langmuir 7(5):868
68. Snow SA, Fenton WN, Owen MJ (1990) Synthesis and characterization of zwitterionic silicone sulfobetaine surfactants. Langmuir 6(2):385
69. Eaborn C (1960) Organosilicon compounds. Butterworth Publications. The authors were able to obtain a copy form the service. "Out of Print Books on Demand" from University Microfilms International
70. Noll W (1968) Chemistry and technology of silicones
71. Brook MA (2000) Silicon in organic, organometallic and polymer chemistry
72. Snow SA, Fenton WN, Owen MJ (1990) Synthesis and characterization of zwitterionic silicone sulfobetaine surfactants. Langmuir 6(2):385
73. Pricop L, Hamciuc V, Marcu M (2002) Siloxane surfactants. Mater Plast 39(4):213–216
74. LeGrow GE, Petroff LJ (1999) Silicone polyether copolymers: synthetic methods and chemical compositions. In: Hill RM (ed) Silicone surfactants. Surfactant science series, vol 86. Marcel Dekker, New York, Chap 2
75. The silicones environmental, health and safety council of north America, materials handling guide: hydrogen-bonded silicon compounds (http://www.sehsc.com/PDFs/SiHManual Revised 01 Aug 07.pdf)
76. Maki H, Horiguchi Y, Suga T, Komori S (1970) Syntheses and properties of surfactants containing organometallic compounds. VI. Syntheses and properties of surfactants with three-chained hydrophobic groups containing organotin and organosilicon compounds. Yukagaku 19(4):245
77. Maki H, Horiguchi Y, Suga T, Komori S (1970) Syntheses and properties of organometallic surfactants VII. Cationic surfactants containing polydimethylsiloxane. Yukagaku 19(11):1029
78. Snow SA, Fenton WN, Owen MJ (1990) Synthesis and characterization of zwitterionic silicone sulfobetaine surfactants. Langmuir 6(2):385
79. Snow SA, Fenton WN, Owen MJ (1991) Zwitterionic organofunctional siloxanes as aqueous surfactants: synthesis and characterization of betaine functional siloxanes. Langmuir 7(5):868
80. Schmaucks G, Sonnek G, Wuestneck R, Herbst M, Ramm M (1992) Effect of siloxanyl groups on the interfacial behavior of quaternary ammonium compounds. Langmuir 8(7):1724
81. Snow SA (1993) Synthesis, characterization of cationic siloxane surfactants $(Me_3SiO)_2Si(Me)$-$(CH_2)_3NMe_2(CH_2)_2OR^+$ X. Langmuir 9(2):424
82. Schmaucks G (1999) Novel siloxane surfactant structures. In: Hill RM (ed) Silicone surfactants. Surfactant science series, vol 86. Marcel Dekker, New York, Chap 3
83. Cheng J, Wang X, Wu Q, Gan G (2002) Synthesis of polyether-modified silicone quaternary ammonium salt and its properties. Youjigui Cailiao 16(2):10–13
84. Snow SA (1993) Synthesis, characterization of cationic siloxane surfactants $(Me_3SiO)_2Si(Me)$-$(CH_2)_3NMe_2(CH_2)_2OR^+$ X. Langmuir 9(2):424
85. Colas AR, Renauld FA (1988) Organosilicon sulfosuccinate(s) preparation by reaction of organosilicon compounds with base and sodium bisulfite, useful as surfactants. US Patent 4,777,277
86. Hoffmann H, Ulbricht W (1999) Surface activity and aggregation behavior of siloxane surfactants. In: Hill RM (ed) Silicone surfactants. Surfactant science series, vol 86. Marcel Dekker, New York, Chap 4

87. Kuo P-L, Hou S-S, Teng C-K, Liang W-J (2001) Function and performance of silicone copolymer (VI). Synthesis and novel solution behavior of water-soluble polysiloxanes with different hydrophiles. Colloid Polym Sci 279(3):286–291
88. Wang G, Qu W, Du Z, Cao Q, Li Q (2011) Adsorption and aggregation behavior of tetrasiloxane-tailed surfactants containing oligo(ethylene oxide) methyl ether and a sugar moiety. J Phys Chem B 115(14):3811–3818
89. Wang GY, Du ZP, Li QX, Zhang W (2010) Carbohydrate modified siloxane surfactants and their adsorption and aggregation behavior in aqueous solution. J Phys Chem B 114:6872–6876
90. Kim D, Lim C, Choi J, Noh S (2004) Surface active properties and LCST behavior of oligo(propylene oxide-blockethylene oxide) allyl ether siloxane surfactants in aqueous solution. Bull Korean Chem Soc 25(8):1182–1188
91. Kim D, Noh S, Jo B (2006) Effect of salt and pH on surface active properties of comb rake-type polysiloxane surfactants. Colloids Surf A 287(1–3):106–116
92. Wang W, Lu Y, Cai Z (2010) Surface characters of methylsiloxane-oxyalkylene copolymers. Jingxi Huagong 27(3):229–233
93. Owen MJ (1980) The surface activity of silicones: a short review. Ind Eng Chem Prod Res Dev 19:97
94. Owen MJ (1980) The surface activity of silicones: a short review. Ind Eng Chem Prod Res Dev 19:97
95. Hoffmann H, Ulbricht W (1999) Surface activity and aggregation behavior of siloxane surfactants. In: Hill RM (ed) Silicone surfactants. Surfactant science series, vol 86. Marcel Dekker, New York, Chap 4
96. Snow SA, Stevens RE (1999) The science of silicone surfactant application in the formation of polyurethane foam. In: Hill RM (ed) Silicone surfactants. Surfactant science series, vol 86. Marcel Dekker, New York, Chap 5
97. Snow SA, Pernisz UC, Braun RJ (2006) Tying up loose ends silicone surfactants as stabilizing agents for flexible polyurethane foam. Silicon Chem 3(1/2):1–10
98. Fawcett AS, So HY, Brook MA (2010) Silicone foams stabilized by surfactants generated in situ from allyl-functionalized PEG. Soft Matter 6:1229–1237
99. Hoffmann H, Ulbricht W (1999) Surface activity and aggregation behavior of siloxane surfactants. In: Hill RM (ed) Silicone surfactants. Surfactant science series, vol 86. Marcel Dekker, New York, Chap 4
100. Gentle TE, Snow SA (1995) Adsorption of small silicone polyether surfactants at the air/water interface. Langmuir 11:2905–2910
101. Wang G, Qu W, Du Z, Cao Q, Li Q (2011) Adsorption and aggregation behavior of tetrasiloxane-tailed surfactants containing oligo(ethylene oxide) methyl ether and a sugar moiety. J Phys Chem B 115(14):3811–3818
102. Wang GY, Du ZP, Li QX, Zhang W (2010) Carbohydrate modified siloxane surfactants and their adsorption and aggregation behavior in aqueous solution. J Phys Chem B 114:6872–6876
103. Kuo P-L, Hou S-S, Teng C-K, Liang W-J (2001) Function and performance of silicone copolymer (VI). Synthesis and novel solution behavior of water-soluble polysiloxanes with different hydrophiles. Colloid Polym Sci 279(3):286–291
104. Deng J, Polidan JT Hottle JR, Farmer-Creely CE, Viers BD, AR Esker (2002) Polyhedral oligomeric silsesquioxanes: a new class of amphiphiles at the air/water. Interface (J Am Chem Soc) 124(51):15194–15195
105. Snow SA, Pernisz UC, Nugent BM, Stevens RE, Braun RJ, Naire S (2001) Modeling the stabilizing behaviour of silicone surfactants during the processing of polyurethane foam: the use of thin liquid films. In: Klempner D, Frisch KC (eds) Advances in urethane science and technology. In this document the material of interest is referred to as the trimethylsilyl capped polysilicate (TCP). Chap 5
106. Snow SA, Pernisz UC, Nugent BM, Stevens RE, Braun RJ, Naire S (2001) Modeling the stabilizing behaviour of silicone surfactants during the processing of polyurethane foam: the

use of thin liquid films. In: Klempner D, Frisch KC (eds) Advances in urethane science and technology. Chap 5
107. Snow SA, Pernisz UC, Braun RJ (2006) Tying up loose ends silicone surfactants as stabilizing agents for flexible polyurethane foam. Silicon Chem 3(1/2):1–10
108. Snow SA, Pernisz UC, Stevens RE (1998) Thin liquid model polyurethane films. In: Polyurethanes world congress, pp 1–10
109. Braun RJ, Snow SA, Naire S (2002) Models for gravitationally-driven free-film drainage. J Eng Math 43:281–314
110. Mysels KJ, Shinoda K, Frankel S (1959) Soap films and studies of their thinning. Pergamon, Elmsford
111. Anseth JW, Bialek A, Hill RM, Fuller GG (2003) Interfacial rheology of graft-type polymeric siloxane surfactants. Langmuir 19(16):6349–6356
112. Mehta SC, Somasundaran P (2007) Modification in rheological properties due to charged network of ionic silicone surfactants at water-oil interface. Abstracts of papers. In: 233rd ACS national meeting, Chicago, IL, United States
113. Fawcett AS, So HY, Brook MA (2010) Silicone foams stabilized by surfactants generated in situ from allyl-functionalized PEG. Soft Matter 6(6):1229–1237
114. Wang A, Jiang L, Mao G, Liu Y (2001) Direct force measurement of comb silicone surfactants in alcoholic media by atomic force microscopy. J Colloid Interface Sci 242(2):337–345
115. Wang A, Jiang L, Mao G, Liu Y (2002) Direct force measurement of silicone and hydrocarbon-based ABA triblock surfactants in alcoholic media by atomic force microscopy. J Colloid Interface Sci 256(2):331–340
116. Suitthimeathegorn O, Jaitely V, Florence T (2005) Novel anhydrous emulsions: formulation as controlled release vehicles. Int J Pharm 298(2):367–371
117. Liu X, Song J, Wu D, Genzer J, Theyson T, Rojas OJ (2010) Surface and friction behavior of a silicone surfactant adsorbed on model textiles substrates. Ind Eng Chem Res 49(18):8550–8557
118. Snow SA, Pernisz UC, Nugent BM, Stevens RE, Braun RJ, Naire S (2001) Modeling the stabilizing behaviour of silicone surfactants during the processing of polyurethane foam: the use of thin liquid film. In: Klempner D, Frisch KC (eds) Advances in urethane science and technology. Chap 5
119. Kuo P-L, Hou S-S, Teng C-K, Liang W-J (2001) Function and performance of silicone copolymer (VI). Synthesis and novel solution behavior of water-soluble polysiloxanes with different hydrophiles. Colloid Polym Sci 279(3):286–291
120. Stoebe T, Hill RM, Ward MD, Scriven LE, Davis HT (1999) Surfactant-enhanced spreading. In: Hill RM (ed) Silicone surfactants. Surfactant science series, vol 86. Marcel Dekker, New York, Chap 11
121. De Ruijter MJ (2000) The role of surfactants in dynamic wetting. Annu Surfactants Rev 3(Surface Active Behaviour of Performance Surfactants):169–188
122. Wagner R, Wu Y, Czichocki G, Berlepsch HV, Weiland B, Rexin F, Perepelittchenko L (1999) Silicon-modified surfactants and wetting: I. Synthesis of the single components of Silwet L77 and their spreading performance on a low-energy solid surface. Appl Organomet Chem 13(9):611–620
123. Unpublished data of the Dow Corning Corporation
124. Venzmer J, Wilkowski SP (2000) Trisiloxane surfactants-mechanisms of wetting and spreading. In: Auner N, Weis J (eds) Organosilicon chem IV lect poster contrib muenchner silicontage meeting 1998. Wiley-VCH, Weinheim, pp 690–698
125. Nikolov AD, Wasan DT, Chengara A, Koczo K, Policello GA, Kolossvary I (2002) Superspreading driven by Marangoni flow. Adv Colloid Interface Sci 96(1-3):325–338
126. Wagner R, Wu Y, Berlepsch HV, Rexin F, Rexin T, Perepelittchenko L (1999) Silicon-modified surfactants and wetting: III. The spreading behavior of equimolar mixtures of nonionic trisiloxane surfactants on a low-energy solid surface. Appl Organomet Chem 13(9):621–630
127. Peng Z, Lu C, Xu M (2010) Influence of substructures on the spreading ability and hydrolysis resistance of double-tail trisiloxane surfactants. J Surfactants Deterg 11(1):75–81

128. Nikolov AD, Wasan DT, Chengara A, Koczo K, Policello GA, Kolossvary I (2002) Superspreading driven by Marangoni flow. Adv Colloid Interface Sci 96(1-3):325–338
129. Peng Z, Lu C, Xu M (2010) Influence of substructures on the spreading ability and hydrolysis resistance of double-tail trisiloxane surfactants. J Surfactants Deterg 13(1):75–81
130. Policello GA, Leatherman MD, Peng W, Rajaraman SK, Xia Z (2007) Hydrolysis-resistant organo modified trisiloxane surfactants and aqueous emulsion incorporating surfactants. US Patent Application, Publ 17 pp
131. Lin L, Chen K (2006) Surface activity and water repellency properties of cleavable-modified silicone surfactants. Colloids Surf A 275(1–3):99–106
132. Lin L, Wang C, Chen K (2006) Water-repellency and antibacterial activities of plasma-treated cleavable silicone surfactants on nylon fabrics. Surf Coat Technol 201(3–4):674–678
133. Lin L, Wang C, Chen C, Chen K (2006) Water-repellency and antibacterial activities of plasma-treated cleavable silicone surfactants on nylon fabrics. Surf Coat Technol 201(3–4):674–678
134. Tanford C (1980) The hydrophobic effect. Wiley, New York
135. Soni SS, Sastry NV, Aswal VK, Goyal PS (2002) Micellar structure of silicone surfactants in water from surface activity, SANS and viscosity studies. J Phys Chem B 106(10):2606–2617
136. Soni SS, Sastry NV, Joshi JV, Seth E, Goyal PS (2003) Study on the effects of nonelectrolyte additives on the phase, thermodynamics, and structural changes in micelles of silicone surfactants in aqueous solutions from surface activity, small angle neutron scattering, and viscosity measurements. Langmuir 19(17):6668–6677
137. Soni SS, Sastry NV, George J, Bohidar HB (2003) Dynamic light scattering and viscosity studies on the association behavior of silicone surfactants in aqueous solutions. J Phys Chem B 107(22):5382–5390
138. Lin Y, Alexandridis P (2003) Association of siloxane polymeric surfactants in aqueous solution. In: Synthesis and properties of silicones and silicone-modified materials. ACS symposium series, vol 838, pp 222–234
139. Ahn S, Alexandridis P (2001) Phase behavior and structural characterization of trisiloxane surfactant—water-silicone oil systems. Papers Present Meet - Am Chem Soc, Div Polym Chem 42(1):169–170
140. Lin Z, He M, Scriven LE, Davis HT, Snow SA (1993) Vesicle formation in electrolyte solutions of a new cationic siloxane surfactant. J Phys Chem 97:3571
141. Hill RM, Lin Z, He M, Scriven LE, Davis HT (1993) Lyotropic liquid crystal phase behavior of polymeric siloxane surfactants. Langmuir 9(11):2789–2798
142. Lin Z, He M, Scriven LE, Davis HT, Snow SA (1994) Aggregation behavior and microstructures of cationic trisiloxane surfactants in aqueous solutions. J Phys Chem 98:6148
143. Hoffmann H, Munkert U, Thunig C, Valiente M (1994) Altering the rheological properties of silicone surfactant vesicles. J Colloid Interface Sci 163:217
144. Hill RM, Lin Z, He M, Scriven LE, Davis HT, Talmon Y (1994) Cryo transmission electron microscopy study of vesicles and micelles in siloxane surfactant aqueous solutions. Langmuir 10(4):1008–1011
145. Hill RM, Lin Z, He M, Scriven LE, Davis HT (1994) Comparison of the liquid crystal phase behavior of four trisiloxane superwetter surfactants. Langmuir 10(6):1724–1734
146. Hill RM, Snow SA (1994) Silicone vesicles and entrapment. US Patent 5,364,633
147. Hill RM, Snow SA (1995) Silicone vesicles and entrapment. US Patent 5,411,744
148. Kickelbick G, Bauer J, Huesing N, Andersson M, Holmberg K (2003) Aggregation behavior of short-chain PDMS-b-PEO diblock copolymers in aqueous solutions. Langmuir 19:10073–10076
149. Kickelbick G, Bauer J, Husing N, Andersson M, Palmqvist A (2003) Spontaneous vesicle formation of short-chain amphiphilic polysiloxane-b-poly(ethylene oxide) block copolymers. Langmuir 19:3198–3201
150. Yao D, Bender T, Gerroir PJ, Sundararajan PR (2005) Self-assembled vesicular nanostructures of perylene end-capped poly(dimethylsiloxane). Macromolecules 38(16):6972–6978

151. Yan Y, Hoffmann H, Drechsler M, Talmon Y, Makarsky E (2006) Influence of a hydrocarbon surfactant on the aggregation behavior of a silicone surfactant: observation of intermediate structures in the vesicle-micelle transition. J Phys Chem B 110(11):5621–5626
152. Wang GY, Du ZP, Li QX, Zhang W (2010) Carbohydrate modified siloxane surfactants and their adsorption and aggregation behavior in aqueous solution. J Phys Chem B 114:6872–6876
153. Wang G, Qu W, Du Z, Cao Q, Li Q (2011) Adsorption and aggregation behavior of tetrasiloxane-tailed surfactants containing oligo(ethylene oxide) methyl ether and a sugar moiety. J Phys Chem B 115(14):3811–3818
154. Postiaux S, Lin S (2005) Preparation of vesicle composition comprises combining organopolysiloxane, water miscible volatile solvent, optionally silicone or organic oil and personal care or health care active with water and mixing the obtained aqueous dispersion. World Patent Filing # WO2005102248
155. Lin S (2005) Preparing vesicle composition useful for personal and health care product involves mixing organopolysiloxane, water miscible volatile solvent and water to form vesicles, and optionally removing the solvent from the vesicles. World Patent Filing # WO2005103157
156. Lin S, Nguyen K (2005) Aqueous composition for use in making personal, household, and health care composition used in, e.g. antiperspirants, deodorants, comprises dispersed particles with block silicon polyether copolymer. World Patent Filing WO2005103118
157. Lin S, Leaym T (2006) Polyoxyalkylene-alkyl functional siloxane resin for manufacturing aqueous dispersion, vesicle composition, and aqueous composition for entrapment and delivery of personal, household, and healthcare composition, comprises siloxy units. World Patent Filing WO2006091295
158. Lin S, Newton J, Postiaux S, Thompson J (2007) Preparation of vesicle composition useful in personal care product e.g. deodorant involves mixing dispersions of organopolysiloxane having hydrophilic substituent with hydrophilic active and hydrophobic active component and mixing water. World Patent Filing WO2007053424
159. Kickelbick G, Bauer J, Huesing N, Andersson M, Holmberg K (2003) Aggregation behavior of short-chain PDMS-b-PEO diblock copolymers in aqueous solutions. Langmuir 19:10073–10076
160. Kickelbick G, Bauer J, Husing N, Andersson M, Palmqvist A (2003) Spontaneous vesicle formation of short-chain amphiphilic polysiloxane-b-poly(ethylene oxide) block copolymers. Langmuir 19:3198–3201
161. Kumar A, Uddin MH, Kunieda H, Furukawa H, Harashima A (2001) Solubilization enhancing effect of A-B-type silicone surfactants in microemulsions. J Disp Sci Tech 22(2&3):245–253
162. Xu A, Yu JC, Zhang H, Zhang L, Kuang D, Fang Y (2003) Continuous formation of supported unusual mesostructured silica films by sol–gel dip coating. Langmuir 18(24):9570–9573
163. Xu A (2002) Novel surfactants for the synthesis of unusual highly ordered lamellar oxides. J Phys Chem B 106(45):11713–11715
164. Xu A (2002) Synthesis of highly ordered long-range lamellar silica composites. Chem Lett 9:878–879
165. Xu A, Cai Y, Zhang H, Zhang L, Yu JC (2002) Hierarchically ordered silica mesophases using mixed surfactant systems as templates. Angew Chem, Int Ed Engl 41(20):3844–3848
166. Xu A (2002) Synthesis of mesostructured silica using nonionic copolymers as the templates. Chem Lett 10:982–983
167. Xu A, Yu JC, Cai Y, Zhang H, Zhang L (2002) The preparation of a highly ordered long-range lamellar silica structure with large interlayer spacings. Chem Commun 15:1614–1615
168. Xu A (2002) Highly ordered lamellar silica/surfactant composites templated from nonionic amphiphilic copolymer. Chem Mater 14(9):3625–3627
169. Xu A, Yu JC, Zhang H, Zhang L, Kuang D, Fang Y (2003) Continuous formation of supported unusual mesostructured silica films by sol–gel dip coating. Langmuir 18(24):9570–9573

170. Gradzielski M, Hoffmann H, Robisch P, Ulbricht W, Gruning B (1990) The aggregation behaviour of silicone surfactants in aqueous solutions. Tenside Surfactants Deterg 27:366–379
171. Schmaucks G, Sonnek G, Wfistneck R, Herbst M, Ramm M (1992) Effect of siloxanyl groups on the interfacial behavior of quaternary ammonium compounds. Langmuir 8:1724–1730
172. Hill RM, He M, Lin Z, Davis HT, Scriven LE (1993) Lyotropic liquid crystal phase behavior of polymeric siloxane surfactants. Langmuir 9:2789–2798
173. Iwanaga T, Kunieda H (2000) Effect of added salts or polyols on the cloud point and the liquid-crystalline structures of polyoxyethylene-modified silicone. J Colloid Interface Sci 227(2):349–355
174. Kunieda H, Uddin MH, Horii M, Furukawa H, Harashima A (2001) Effect of hydrophilic- and hydrophobic chain lengths on the phase behavior of A–B-type silicone surfactants in water. J Phys Chem B 105(23):5419–5426
175. Floyd DT (1999) Silicone surfactants: Applications in the personal care Industry. In: Hill RM (ed) Silicone surfactants. Surfactant science series, vol 86. Marcel Dekker, New York, Chap 7
176. O'Lenick AJ, O'Lenick K (2010) Formulating with surfactant silicones. Cosmet Toilet 125(1):44–49
177. O'Lenick AJ (2001) PEG/PPG dimethicone: a new name for an old friend. Cosmet Toilet 116(7):49–52
178. Keil JW (1979) US Patent 4,265,878 and 4,268,499 antiperspirant stick compositions and antiperspirant emulsion compositions
179. Starch MS (1979) US Patent 4,311,695, Personal care emulsions comprising a siloxane-oxyalkylene copolymer, December
180. Gruning B, Bungard A (1999) Silicone surfactants: Emulsification. In: Hill RM (ed) Silicone surfactants. Surfactant science series, vol 86. Marcel Dekker, New York, Chap 8
181. O'Lenick AJ (1979) Applying the three dimensional HLB system. Cosmet Toilet 112(11):59–60, 65
182. Zombeck A, Dahms G (1996) Novel formulations based on non-aqueous emulsions of polyols in silicones. In: 19th IFSCC Congress, Sydney
183. Dahms G, Zombeck A (1995) New formulation possibilities offered by silicone co-polyols. Cosmet Toilet 110(3):91–100
184. Keil J (1985) US Patent 4,532,132
185. Araki et al. (2009) In: 9th ASCS conference, Oral Presentation #148
186. Koini T, Dahms G (2003) O/W Emulsions US Patent Pub No 2003/0202948 A1
187. Dimitrova T, Saulnier L, Verhelst V, Van Reeth I (2011) Silicone polyethers as stabilizers of water-in-oil emulsions. In: Morgan S, Lochhead R (eds) Polymeric delivery of therapeutics. ACS symposium series, vol 1053. Am Chem Soc, Washington
188. Dimitrova T, Saulnier L, Van Reeth I, Verhelst V (2008) Stabilization of cosmetic formulations by silicone polyethers. In: 25th ISSCC congress, Barcelona, October 2008
189. Van Reeth I, Bao X, Durand B, Vervier I, Yasuhiro K, Devalle C (2010) Silicone emulsifiers: new developments and formulation concepts. In: 26th IFSCC congress, Buenos Aires, poster 0050
190. Van Reeth I, Van Oycke S, Kondo H (2006) New developments in water-in-silicone and water-in-oil silicone based emulsifiers. In: 24th IFSCC congress, Osaka, PC-070
191. Yahagi K (1992) Silicones as conditioning agents in shampoos. J Soc Cosmet Chem 43(5):275–284
192. Ostergaard T, Gomes A, Quackenbush K, Johnson B (2004) Silicone quaternary microemulsions: a multifunctional product for hair care. Cosmet Toilet 119(11):45–48, 50, 52
193. Philip A (1988) Formulating for a close shave. Cosmet Toilet 59(10):53–59
194. Easton T, Stephens D (1995) Silicone surfactants as performance enhancers in waterborne coatings. Polym Paint Colours J 185(4371):26, 28–30
195. Perry D (2001) Glorious speed. Polym Paint Colours J September:16–19
196. Ferritto M, Fornier F, Stanga M, Verineau P, Whitmarsh R, Witucki G (2007) WO patent 2007075927

197. Semmler H, Heilen W (2000) Silicones fight foam formation. Polym Paint Colours J 190(4431):16–18
198. Van Dam P (2001) Ending bubble trouble. Polym Paint Colours J 191(4441):30–33
199. O'Neil V, Zeng J Perry D (2003) New silicone foam control agents for waterborne coatings. Paint and Coatings Industry, BNP Media, October
200. Fey R, Hill RM (1999) Silicone polymers for foam control and demulsification. In: Hill RM (ed) Silicone surfactants, surfactant science series, vol 86. Marcel Dekker, New York, Chap 6
201. McGee J, Petroff L, Aizawa K, Shoji H (1995) Silicone foam control compositions. US patent 5,380,464
202. McGee J, Petroff L, Brecht D, Ollinger W (1996) Silicone foam control compositions, US patent 5,543,082
203. Tonge L, Kidera H, Okada R, Noro T, Harkness B (2003) US patent application 20030013808 A1
204. Elms R, Lin F, Severance M (2004) Silicone based foam control compositions stable in detergents EP 1 167 502 A1
205. Henning J, Muller F, Peggau J (1999) Novel applications of silicone surfactants in cleansers and polishes. Commun J Comm Esp Deterg 29:235–246
206. Panandiker RJ, Rajan K, Vetter K, Barnabas F, Delplancke P (2009) Fabric care compositions and systems comprising organosilicone microemulsions and methods employing same. US patent 7,608,575 B2
207. Panandiker R, Vetter K, Combs M, Gladney D, Sheets C (2010) Fabric care composition comprising organosilicone microemulsion and anionic/nitrogen containing surfactant system. US patent 7,678,752 B2
208. Achwal W (2002) Hydrophilic silicone based softeners. Colourage 49(6):58–59
209. Czech A (2002) Block, non-$(AB)_n$ silicone polyalkyleneoxide copolymers with tertiary amino links. US patent 6,475,568
210. Schwab P, Favresse P, Maurer T, Pascaly M (2010) Silicone containing graft copolymers of blockwise structure. US patent 7,838,603 B2
211. Kennan J, Lewis K, Vazquez F (2010) Silicone polyether block copolymers having organofunctional endblocking groups. US patent publication US 2010.0048795 A1
212. Sabia A, Metzler R (1983) The role of silicones in nonwoven fabric applications. Nonwovens Ind 14(9):16–22
213. Casado-Dominguez A, Goossens E, Hubesch B (2003) Process for preparing an organomodified-silicone by hydrosilylation reaction. US patent application 20030232947 A1
214. Robinson P, Dolbear G (2006) Hydrotreating and hydrocracking: fundamentals. In: Hsu C, Robinson P (eds) Practical advances in petroleum processing, vol 1. Springer, Berlin, pp 177–217, Chap 7
215. Hill RM, Fey KC (1999) Silicone polymers for foam control and demulsification. In: Hill RM (ed) Silicone surfactants. Surfactant science series, vol 86. Marcel Dekker, New York, Chap 6
216. Callagahan I, Gould C, Grabowski W (1987) Method for the separation of gas from oil. US patent 4,711,714
217. Dalmazzone Noik C (2005) Mechanism of crude-oil/water interface destabilization by silicone demulsifiers. SPE J March:44–53
218. Owen MJ (1972) Siloxane surfactants as demulsifiers. In: Proc VI int cong surf act, Switzerland, pp 623–630
219. Theile H, Hoffman H, Rossmy G, Koerner G, Zaske P (1980) Use of demulsifying mixtures for breaking petroleum emulsions. US Patent 4,183,820
220. Fink H, Koerner G, Rossmy G (1977) De-emulsifier for breaking petroleum emulsions. US Patent 4,029,596
221. Graham D, Lidy W, McGrath P, Thompson R (1986) Demulsification process. US patent 4,596,653

222. David D, Le Folletec A, Pezreon I, Dalmazzone C, Noik C, Barre L, Komunjer L (2008) Destabilization of water in crude oil emulsions by silicone copolymer demulsifiers. Oil Gas Sci Technol Rev IFP 63(1):165–173
223. Phukan M, Koczo K, Falk B, Palumbo A (2010) New silicon copolymers for efficient demulsification. SPE paper 128553, SPE oil and gas conference, Mumbai, India
224. Alen R (2000) Basic chemistry of wood delignification. In: Gullichsen J, Paulapuro H, Stenium P (eds) Forest products chemistry. Papermaking science and technology, vol. 3, pp 59–103. Tappi Fapet Oy, Chap 2
225. Burger W, Beubig O, Lappalainen K, Wahlberg H (2003) Chemical digestion process using organosilicone compounds. US Patent 6,521,084
226. Habermehl J (2005) Silicone processing. Pulp paper technol, summer:59–62
227. Wilson D (2005) Silicone's applications. Pulp paper technol, summer:37–40
228. Ikeda T, Takewaki K (2006) Defoaming composition. Japan patent 2006320837
229. Pease J, McKendree G (2009) Felt and equipment surface conditioner. US patent 7,534,324
230. Nellesen B, Northfleet C (2006) Method of deinking. US patent publication 2006/0102298
231. Nellesen B (2006) Practical experience with the use of silicone derivatives for the detachment and removal of ink. In: Proceedings of 12th PTS/CTP deinking symposium, Leipzig, 25–17 April 2006
232. Battice D, Fey K, Petroff L, Stanga M (1998) Silicone foam control agents for hydrocarbon liquids—displays consistent compatibility and miscibility with other frequently present fuel additives, especially in diesel or jet fuels. US patent 5,767,192
233. Fey KC, Combs CS (1995) Middle distillate hydrocarbon foam control agents from crosslinked organopolysiloxane-polyoxyalkylenes. US patent 5,397,367
234. Penner D, Burow R, Roggenbuck F (1999) Use of organosilicone surfactants as agricultural adjuvants. In: Hill R (ed) Silicone surfactants. Surfactant science series, vol 86. Marcel Dekker, New York, Chap 9
235. Leatherman M, Policello G, Peng W, Zheng L, Wagner R, Rajaraman S, Xi Z (2009) Hydrolysis resistant organomodified disiloxane ionic surfactant. US patent publication 2009/0173913
236. Leatherman M, Policello G, Peng W, Zheng L, Wagner R, Rajaraman S, Xia Z (2009) Mixtures of hydrolysis resistant organomodified trisiloxane ionic surfactants. US Patent Publication 2009/0173912
237. Klein K, Wilkowski S, Selby J (1995) Silane surfactants, novel adjuvants for agricultural applications. In: Gaskin R (ed) 4th international symposium on adjuvants for agrichemicals, Oct 3–6, Melbourne, Aus. NZ Forest Research Institute Bulletin, vol 193, pp 27–31

Chapter 10
Silanes and Siloxanes as Coupling Agents to Glass: A Perspective

Janis G. Matisons

10.1 Composites and Coupling Agents

Silicate glass-reinforced composites, based on synthetic resins such as phenolics, ureas, epoxies, melamines, and unsaturated polyesters, generally became available in the 1940s. The importance of such products in a number of areas, such as aircraft and marine applications, was soon realized, as these products offered high strength and modulus at a reduced weight. However, it was soon uncovered that such products were very susceptible to the effects of ambient humidity. Although the specific dry strength and modulus of these reinforced composites exceeds that of aluminum or steel, upon prolonged exposure to humidity, a dramatic decrease in these properties is seen in such environments [1, 2].

Furthermore, the coefficient of thermal expansion for the glass fiber is very much lower than that of the polymer resin. Thus, if the resulting polymer composite is exposed to extreme temperature cycling, the difference between these thermal expansion coefficients results in stresses at the interface between the organic polymer and the inorganic glass. Such stresses at the interface may even exceed the strength of the composite [1, 2].

Commercial glass fibers used in reinforced composites are almost always pretreated with a coupling agent, which is capable of interacting with both the organic polymer resin and inorganic oxide substrate. Such a coupling agent must not only ensure that the physical properties of the reinforced material remain relatively unaffected by moisture or humidity, but must also reduce the stress at the interface during excessive thermal cycling. Trialkoxysilanes, which contain organic groups compatible with the polymer resin, are the most commonly used coupling agents. The addition of almost any trialkoxysilane coupling agent to the glass fiber surface, will improve the water resistance of the resulting reinforced composite. However, it is important to note that such silanes are usually applied from aqueous solution, where

J.G. Matisons (✉)
Gelest Inc., 11 East Steel Road, Morrisville, PA 19067, USA
e-mail: jmatisons@gelest.com

M.J. Owen, P.R. Dvornic (eds.), *Silicone Surface Science*, Advances in Silicon Science 4,
DOI 10.1007/978-94-007-3876-8_10,

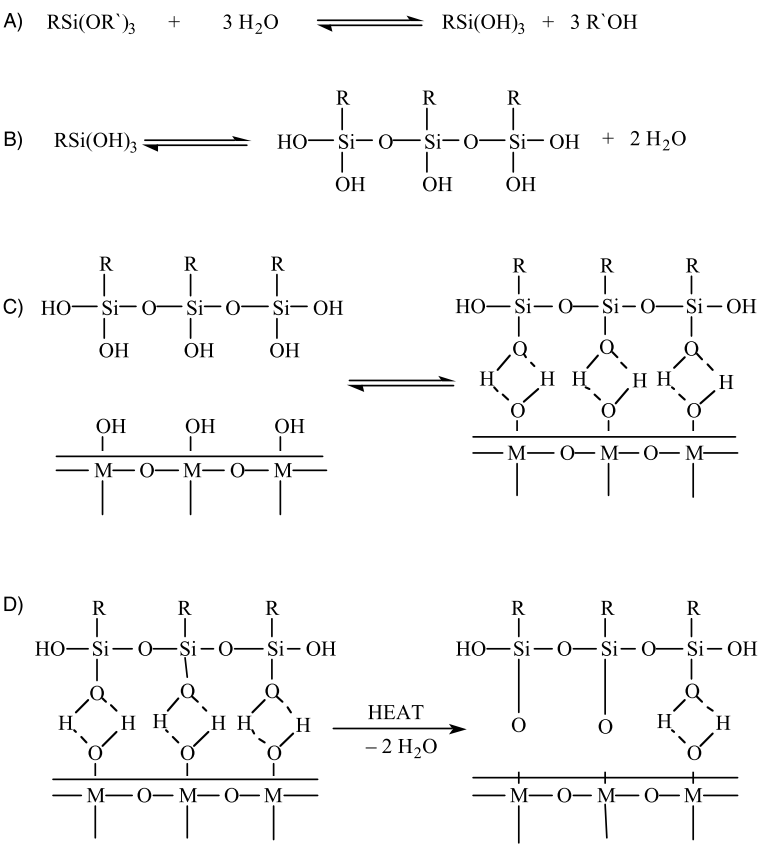

Fig. 10.1 Mechanism of silane coupling to surfaces. M is a mineral element (Si for glass)

both hydrolysis and condensation of the silane coupling agent occur (see Fig. 10.1), resulting in the formation of oligomeric siloxane materials (oligomerization takes place in solution several hours prior to the silane being applied to the glass). Such oligomers may well be what is actually adsorbed onto the glass surface, given that the silane may stand awaiting application for several days. Application of silane coupling agents from an aqueous solution therefore represents a dynamic process, which is highly dependent on the age of the solution being applied. Thus, there are a number of factors affecting the reproducibility of the coupling agent application, and so affecting the final properties of the composite (its physical properties and water resistance). For a particular silane coupling agent, the main factors affecting its final properties relate to its degree of oligomerization and cross-linking.

These properties are more easily controlled in the glass fiber industry if the silane is supplied very shortly after manufacture, and thus is not partially oligomerized and/or cross-linked prior to use. Coupling agents, as supplied to the glass fiber industry, can undergo varying degrees of oligomerization and cross-linking. There is a need for an aqueous coupling agent solution which remains stable, or at least

constant with respect to its state of oligomerization, no matter how much time has lapsed since its manufacture.

10.2 The Glass–Polymer Interface

The deleterious effects of water on the mechanical properties of many metal oxide or glass-reinforced composites are well documented [1–5]. Diffusion of and interaction with water at the filler-polymer interface is responsible for the delamination between the glass fiber and the polymer matrix. To overcome such problems, coupling agents are used to generate a water resistant interface between the polymer and the glass or for that matter, any inorganic filler [1, 2, 6–8]. These coupling agents must be able to react or interact with both the glass surface and the polymer, to improve the overall performance of the final reinforced composite materials [1, 2, 8–12]. It has been established that if only a small amount of silane coupling agent is added to an inorganic filler, the performance of the resultant composite will improve [1, 2]. The site-selective adsorption of silanes and their oligomers at predefined positions on solid surfaces is a key fabrication step, and a major challenge in many applications.

There have been several theories proposed to explain how silane coupling agents improve composite performance. The variety of applications for the trialkoxysilane coupling agents precludes any single theory used to explain their effectiveness in improving the composite properties. The chemical bonding theory, where a silane coupling agent formed covalent bonds with both the polymer resin and the inorganic substrate, was proposed independently by Arkles [13] and Plueddemann [14]. Investigating some 142 silanes in epoxy- and polyester glass laminates, Plueddemann [14] found that the overall composite properties greatly improved when a silane was used that could chemically react with both the resin and the substrate.

A conventional glass fiber sizing solution always contains more than just the silane coupling agent. In fact the silane coupling agent is not even the major active component of such a sizing solution. Many sizing solutions contain more than a dozen different active chemicals. In such complex formulation chemistry, generally resident to the patent literature, it is often difficult to unravel what is really important in making sizing formulations effective.

Basically a sizing agent for glass fibers *must* contain at minimum the following active ingredients:

- 4–7 % film forming agents (polymers)
- <1 % silane coupling agents
- $\sim$0.1 % lubricant or mixture of synergistic lubricants
- <0.1 % electrostatic agent
- remainder is water (generally as an emulsion, and considered an ‘inactive’ ingredient)

As the molten glass is drawn from the furnace into fibers it cools rapidly. On cooling, the glass sizing solution (containing the silane coupling agent) is sprayed onto the cooling fibers in a confined space. The fibers in this space move at several tens of

meters per second, and without the addition of a film former, the fibers are brittle and can rupture. While the hydrolysis and condensation of the silane takes place the film former maintains the integrity of the cooling fiber. Clearly, in these circumstances, the picture of the hydrolysis and condensation of a sole coupling agent to the glass fiber surface (Fig. 10.1) is a simplification of a more complex system. Nevertheless, this is the mechanism for surface treating such fibers. It provides an initial approach to understanding the mechanism for surface treating such fibers as well as simpler (in terms of monitoring the surface chemistry), non-heterogeneous surfaces such as silica.

10.2.1 Silane Hydrolysis and Condensation

Trialkoxysilanes, with the general formula $RSi(OR')_3$, where R is a functional group similar to, or compatible with, the polymerizing functional group of the polymer resin, and R′ is a hydrocarbon radical (usually methyl or ethyl), are generally used in composites manufacture. Alkoxysilanes are applied from dilute aqueous solutions, as partial hydrolysates, or from organic solvents (generally alcohols) [1, 2, 15]. All such silane coupling agent solutions undergo initial hydrolysis and some oligomerization, prior to interacting with glass substrates. Initially, such silane coupling agents may interact with glass surfaces through hydrogen bonding with the glass-surface hydroxyl groups. Subsequently condensation of these initial surface structures generates siloxane bonds to the surface (Fig. 10.1). It is also possible that some lateral polymerization occurs without the formation of bonds to the surface [16]. Irrespective of how such a siloxane film is formed on the substrate, it generally consists of multiple siloxane layers [17–19].

Siloxanes are generated from chloro- or alkoxysilanes under hydrolytic conditions, which involve silanols as reactive intermediates [9]. To selectively obtain a specific siloxane-surface structure, it is crucial to control the competition between silanol formation and silanol condensation [6]. The presence of a sterically demanding group on the silane can successfully slow down the condensation reaction, and thus permit the formation of stable silanols, silanediols, and silanetriols [20–24]. The primary condensation products of di- or tri-functional silanols such as disiloxane 1,3-diols or disiloxane 1,2,3-triols are in fact functionalized oligomeric siloxanes themselves [25, 26].

Organosilanes containing various organic groups, such as alkyl [27–30], perfluoroalkyl [31], phenyl [32], and vinyl [33] groups, have been used for the surface modification of layered silicates. Silylation is now also common for the immobilization of organosilyl groups onto layered titanates [34, 35]. Such diversity, however, is not apparent when it comes to glass surfaces, where traditionally used silanes still occupy >99 % of the commercial applications. Of these silanes, γ-aminopropyltrialkoxysilane is used in well over 60 % of the treated glass fiber market; while γ-glycidoxypropyltrialkoxysilane and methacryloxypropyltrialkoxysilane also maintain significant use.

Oxane bonds (see Fig. 10.1) that form between silane coupling agents and any inorganic substrate are easily hydrolyzed [36, 37]. However, this hydrolysis and bond re-formation remain in true equilibrium, and hydrolyzed oxane bonds will readily re-form [36, 37]. Improved composite properties occur where hydrolysis and condensation reactions are in equilibrium. It has been suggested that these hydrolysis and condensation reactions provide a mechanism for stress relief at the interface [1, 2]. As a consequence, a silane/siloxane interphase forms at the surface.

10.2.2 Factors Affecting Silane Adsorption

There are a number of factors which influence the structure of the silane coupling agent interphase. Firstly, the pH of the aqueous silane solution is important, since basic or acidic conditions affect the relative rates of silane hydrolysis and condensation [9]. The condensation of neutral alkoxysilanes with glass and silica is catalyzed by the addition of aliphatic amines [18]. The tensile strengths of the composites made from these catalyzed silanes are greatly improved [1, 10, 18]. Acidic or basic conditions are also found to increase the amount of silane adsorbed [10, 18]. The surface potential of the oxide substrate also varies with the pH of the applied solution, affecting the orientation of the adsorbed silane layers [19]. This effect of pH upon surface potential is more complex on mixed-oxide substrates, such as glass, where surface micro-heterogeneities exist, such that the resultant surface potential is not a simple average of the component oxide potentials [19].

The selection of the trialkoxysilane coupling agent may, in fact, contribute to the poor water resistance properties of the composite, as the treated substrate is still hydrophilic [37–40]. This is certainly the case for amino-functional silanes, where excess amine still exists at the interface. Such hydrophilicity has been countered by either (i) using very-dilute silane solutions, or (ii) by washing the treated surface with solvent (water or the appropriate organic solvent) to remove any excess, non-covalently bound (or physisorbed) silane [41–48]. Alternatively, a mixture of amino-functional silane and phenyltrimethoxysilane can be used to impart a high degree of hydrophobicity to the resultant surface [37, 38].

Basic functional groups such as amines will self-catalyze the hydrolysis reaction leading to more aggressive monolayer formation as compared to non-animated silanes [44]. The initial hydrolysis step can occur either in solution or at the substrate surface depending on the amount of water present in the system. An overabundance of water will result in excessive polymerization in the solvent phase, while a deficiency of water will result in the formation of an incomplete monolayer.

The drying conditions used for the silane treated substrate also affect the structure of the adsorbed silane [49, 50]. The temperature and duration of the drying procedure will influence the number of siloxane bonds formed between adjacent silanes (siloxane formation) as well as with the surface [49, 50]. The generation of a siloxane coating with multiple surface bonds results in improved composite performance [41, 43, 44, 49, 50]. This is because the probability of all the siloxane-surface bonds

being hydrolyzed at the same instant in time is remote. Solvent, concentration, reaction time, and reaction temperature all have an effect on the attachment kinetics, but most studies only examine one or two of these parameters, and so often a consistent picture of silane adsorption remains missing.

10.2.3 Silane–Polymer Interactions

The oligomeric silanols formed from the hydrolyzed silanes, and attached to the substrate, must retain some degree of solubility/compatibility in order to interact with the polymer resin [41, 43]. If both the oligomeric siloxane layer and the polymer resin are compatible, a copolymer can result upon cure. However, if the oligomeric siloxane and polymer resin are only partially compatible, the resin and the siloxane will cure separately, generating an interpenetrating polymer network of the coupling agent residing on the substrate and within the polymer matrix [7, 49, 50]. Pseudo-interpenetrating polymer networks result from the weak secondary bonding interactions between the oligomeric siloxanes and pre-formed thermoplastic polymer resins, as here only the silane can cross-link through the formation of condensed siloxane bonds [7, 50].

Silane coupling agents lower the surface tension of a substrate, wet it and make its surface energy higher, and hence accessible for effective bonding [13]. Thus, a hydrophobic matrix (resin composite) can adhere to hydrophilic surfaces, It is now well established that more than a monolayer of silane coupling agent is required on the substrate in order to optimize the strength of the resultant composite [1, 2, 7]. In fact, an optimum thickness of coupling agent must be achieved in order to obtain optimal overall performance of the composite [1, 7, 49]. The amount of γ-methacryloxypropyltrimethoxysilane adsorbed upon E-glass fibers, affects the curing process of a vinylester resin at a far greater distance than the thickness of the silane interphase [45, 50, 51]. Previous work has shown that excessive amounts of a silane at the interface resulted in a reduction in the composite fracture toughness, due to the final resin becoming brittle [51].

The highly flexible polymeric siloxane backbone, arising from the silane hydrolysis, enables the interphase to adjust to steric constraints imposed by the oxide filler surface. Furthermore, the ratio of hydrophobic to hydrophilic groups may be adjusted, by either using more than one silane, or by using a hydrophobic hydrocarbon chain to adjust the distance that a polar hydrophilic group maintains from the silicon atom. In this way the number of polar group interactions with the polymer resin can be optimized, such that the polymer "sees" a continuous reactive surface on the fiber or filler, which results in maximum dry strength and durability in the resultant composite [7, 50, 52]. It is, therefore, necessary to control the hydrolysis and oligomerization rates very carefully, if controlled and reproducible silane modified surfaces are to be produced. It is also necessary to control the degree of silane cross-linking (through condensation) and size of the polymeric siloxane segments, to ensure that their interpenetration into the polymer matrix results in optimum composite properties [8, 45, 50].

Usually, the surface treatment is carried out with a silane water–alcohol solution in concentrations of 0.5–2 % by weight. These conditions offer several advantages, in particular

(i) an increase of silane solubilization,
(ii) better control of the surface film thickness, and
(iii) more uniform surface coverage.

10.2.4 Acid-Base Perspectives

Fowkes and coworkers first described the interaction between polymers, fillers and silane coupling agents in terms of their respective acid-base properties [53–55]. Using the principles first described by Drago [56], they characterized these materials as either Lewis acids or bases, from calorimetric and/or spectroscopic measurements. Such information was then used to explain the interactions between the materials produced, which affected their solubility, wettability, adsorption and adhesion properties [53–55]. For example, the acid-base nature of various silane treated fillers affects their dispersion in a range of polymers, as well as the viscosity of the final mixtures. The orientation of some silane coupling agents on the surface has similarly been explained in terms of the respective acid-base properties of the silane and the substrate. Employing angle-resolved X-ray photoelectron spectroscopy (XPS) and zeta-potential measurements, Fowkes found the methacryl functional group in γ-methacryloxypropyltrimethoxysilane, and the amino-functional group in γ-aminopropyltrimethoxysilane were both oriented towards the surface of a magnesium aluminum silicate glass powder [53–55].

The role of acids or bases in the adsorption of silanes or siloxane polymers, especially if applied from organic solvents, cannot be overlooked. Leyden and coworkers [57, 58] investigated the interactions between trimethoxysilane, $HSi(OMe)_3$, and Cab-O-Sil in toluene, in the presence of various amines. They concluded that all amines catalyze the interaction between the silane and the surface silanols of silica; however, amines with exchangeable protons do have an additional catalytic effect.

The presence of boron on silica surfaces is known to enhance the reactivity of surface silanol groups [60]. Elevated levels of boric oxide in E-glass formulations were found to enhance silane adsorption on such surfaces [61]. Similarly, silica surfaces treated with boron trichloride, followed by washing with water, produce B-OH surface groups on silica [61]. These B-OH groups are more reactive, than Si-OH groups towards trialkoxysilanes [60].

The structure and dynamics of alkoxysilane chemisorption onto metal oxides and glass was studied by many techniques including nuclear magnetic resonance (NMR), Fourier-transform infrared spectroscopy (FTIR), XPS, streaming zeta-potential and secondary ion mass spectrometry (SIMS) [42, 50, 53–55, 62–66]. The nature of the substrate selected helps determine whether the nature of the chemisorption process is easily identified. Also, the silane-substrate system under study determines which spectroscopic technique will reveal the most about the chemisorption

process. It is often useful to attach "identifying groups" to the silane, or ensure that the silane selected is likely to undergo chemical reactions with the surface which may be followed spectroscopically, in order to achieve a better understanding of the chemisorption processes. Unfortunately, the chemistries of the most industrially useful silanes and substrates are not always amenable to such spectroscopic techniques.

10.3 Surface Structure and Adsorption Processes

There has been little theoretical treatment of real surfaces, which are both non-uniform and non-planar. The impact of such surfaces on polymer physisorption has usually been left up to experimentalists. There have also been relatively few systematic studies of the effects of chemical heterogeneity [65, 66]. Physical heterogeneity, and in particular the geometry of the surface, has received more attention.

Although most theoretical treatments assume planar geometry, there have been some investigations on the adsorption of polymers on spherical particles [9, 40, 50, 60]. It is predicted that the effect of the curvature of the surface is more pronounced as the radius of the particles approaches that of the polymers (i.e. the radius of gyration, r_g). The thickness of a layer of poly(vinyl alcohol) ($M_w = 67{,}000$, $r_g = 11.7$ nm), adsorbed from water onto polystyrene latex particles decreased by a factor of two, when the size of the latex particles decreased from 250 to 50 nm [40]. The effects of pore size on polymer adsorption were examined and it was concluded that adsorption also increased with pore size [40].

10.3.1 Adsorption on Silica Surfaces

Pure silica surfaces dominate the studies of adsorption. There are a number of reasons why the majority of work on adsorption has been conducted using silica as the substrate. This homogeneous substrate's surface properties have been well characterized, to the extent that it is possible to quantitatively follow adsorption by a number of spectroscopic as well as non-spectroscopic techniques [37, 38]. For example, there are two main types of surface silanol groups on silica, the isolated and the vicinal (which are those within close proximity to one another), which are easily distinguished by FTIR spectroscopy [38]. The surface area of the various types of silica, and the numbers of isolated and vicinal silanol groups per 10 nm^2, have also been well established by numerous techniques [38, 39]. It has, therefore, been possible to follow silane adsorption and to detect if it will occur at the isolated silanol functional group, as the FTIR band of this group decreases proportionally with the degree of silane adsorption [38]. FTIR studies of pyridine and ammonia adsorption also confirm that the isolated silanol is the adsorption site for such small molecules [38]. Furthermore, infrared analysis of the exchange between D_2O and the surface

silanol groups on silica identifies the vicinal silanol groups as sites for water adsorption.

XPS is able to very precisely determine the elemental composition on the substrate surface, and so remains an important technique for determination of the extent of surface coverage on glass, as the minor elements in the glass can reveal incomplete silane surface coverage. Sum frequency generation (SFG) (see Chap. 2) has proved a new and exciting addition to monitoring surface silane treatments. SFG spectroscopy is a second-order nonlinear vibrational technique, with an intrinsic surface selectivity and sub-monolayer sensitivity [58], known to be more effective than conventional vibrational techniques, such as infrared and Raman [38, 59], for revealing the structural ordering, arrangement, and composition in the organic monolayers adsorbed on various substrates, including oxide surfaces [58]. Furthermore, SFG offers the only means to study the interfacial water structure.

Shafrin and Zisman investigated the effects of relative humidity on silicate glass surfaces by contact angle measurements using methylene iodide (a non-hydrogen bonding organic liquid) [93]. They measured a contact angle of 13° at 1 % relative humidity (RH), and a contact angle of 36° at 95 % RH [93], similar to the contact angle of 37° for methylene iodide on water. These results may be better understood when compared with that observed for methylene iodide on a clean silica surface, where in an ultra-high vacuum (i.e., where silica has only surface silanol groups), a contact angle of ∼10° is measured [93]. If water vapor is slowly admitted into the vacuum chamber containing the silica sample, the fractional monolayer coverage of molecular water gradually increases, and contact angles from 11°–20° are successively measured. Above 20°, however, adsorbed water forms multilayers on the silica sample. Therefore, Shafrin and Zisman concluded that at high RH, multilayers of water are adsorbed on the silicate glass surface; whereas at low RH, only residual amounts of adsorbed water are present. Subsequent adsorption isotherm studies have confirmed this conclusion.

A composite isotherm was produced from a number of studies in different pressure regions [93–95]. Silicate glasses subjected to RH levels between 1–50 % gradually form a monolayer of adsorbed molecular water. Above 50 % RH, multilayers of water adsorb until a thick film forms. Placing the monolayer films under low pressure (between 10^{-3} to 10^{0} Torr, which corresponds to 0.005–5 % RH), the resulting isotherms indicate that only a small fraction of an original water monolayer remains. It is, however, unclear whether this residual moisture is due to molecular water, or surface silanols, which may be thought of as chemisorbed water.

10.3.2 Adsorption on Heterogeneous Surfaces

The adsorption processes on other homogeneous metal and metal oxide surfaces have also been studied, and often the nature of the interaction was identified as being similar to that of silica [37, 38, 69–71]. The only extensively examined heterogeneous surface is glass. In particular, the chemisorption of silane coupling agents

onto E-glass fibers has received great attention because of its industrial relevance [1, 2, 19, 95, 96]. In what follows, the main problems associated with all studies of chemisorption upon heterogeneous surfaces are pointed out.

First of all, the existing chemical heterogeneity may not only vary from manufacturer to manufacturer, but also with the history of the substrate, i.e. how it was cleaned and stored. Thus, in making comparisons between studies of chemisorption on similar substrates, such as E-glass fibers, it is important to know the exact surface chemistry of the substrates being compared. There is also the possibility that chemical micro-heterogeneities may exist, which complicate the matter further [19]. Adding sodium, boron, calcium, and alumina to glass shifts the surface isoelectric point of a quartz glass or pure silica to a higher pH. The consequences in terms of absorption are dramatic. For instance, carboxylic acids will not absorb on silica, but will on E-glass fibers that have trace amounts of boron and alumina.

Secondly, there are a number of geometric forms in which the same sample may be presented, for instance plates (microscope slides), cylinders (fibers) and spheres (powder), and chemisorption of silanes on a substrate may be substantially different between them. Furthermore, chemisorption may also be affected by differences in diameters for the same geometry [40]. The surface area of the substrate is of vital importance. This will influence not only the chemical interaction of the surface (as more surface functional groups promote better interaction with adsorbed molecules), but also the sensitivity required by the analytical technique employed to monitor the chemisorption process (the smaller the surface area the greater the sensitivity required). For these reasons, studies of chemisorption of small molecules, such as silane coupling agents, have generally focused on large surface area, homogeneous particles, such as silica.

When considering the adsorption of polymers onto surfaces, there is always the possibility of patch-wise adsorption. This type of adsorption process has been examined using a multifractal approach [72]. Chemical and/or physical heterogeneities on the surface may be responsible for patch-wise adsorption, which is thought to proceed in a multi-step growth process. Each step occurs with smaller and smaller probability, but results in bigger and bigger patches. The interplay between these two events results in fractal behavior, a fractal being defined as a geometrical structure with an irregular or fragmented appearance. A multifractal approach is required when the interplay between the chemical and physical heterogeneities of the surface is considered.

10.4 Glass Surfaces

The composition of a glass will vary with its intended application [73–76]. Sodalime glass (see Table 10.1), composed primarily of oxides of silicon, sodium and calcium, is commonly used for bottles and containers. Pyrex, a borosilicate glass, has high resistance to thermal shock due to the presence of boron oxide, making it suitable for laboratory and kitchen glassware. E-glass fibers, the most common type of glass employed in textiles or reinforced composites, are also borosilicates. S-glass

Table 10.1 Constituents of commercial glasses by weight %

Component	Sodalime glass (%)	Pyrex (%)	E-glass (%)	S-glass (%)
SiO_2	70–75	80–86	52–56	64–66
CaO	7–10	–	16–25	0–0.3
Al_2O_3	0–1.5	0–2	12–16	24–26
B_2O_3	–	6–18	5–10	–
MgO	0–4	–	0–5	9–11
Na_2O	10–13	2–8	0–2	0–0.3
K_2O	0–1	–	0–2	0–0.3
TiO_2	–	–	0–0.8	–
Li_2O	–	0–1	–	–
SO_3	0–0.5	–	–	–
Fe_2O_3	0–0.2	–	0.05–0.4	0–0.3
F	–	–	0–1.0	–

fibers, however, are alumino-silicates, and are used primarily for high performance materials which require fibers with very high tensile strength. Some minor oxide ingredients are added not only for economic and production purposes, but also to control and modify certain glass properties. Calcium and aluminum oxides control or improve the expansion, durability and chemical resistance of the glass [73–76]. Alkali metal/alkaline earth oxides are added to reduce the melting temperature and viscosity of the glass, by disrupting the continuity of the silica network (i.e. breaking some of the Si-O bonds). However, alkali oxides also lower the chemical resistance of the glass. The silica network is retained upon formation of the multi-component silicate glass, and the non-bridging oxygen atoms are there to provide the necessary charge balance for the added cations.

The surface concentrations of the various oxides, which comprise the glass, will vary from the bulk composition, depending on the thermal history of the glass, the relative humidity, and the surface treatment to which it was subjected after melting and cooling [75–80]. The strength of a glass fiber is influenced by the nature of its surface. Components which lower the surface free energy will diffuse towards the glass surface (surface segregation), while the glass being formed is in its molten state. Hydrolysis and leaching of the alkali and alkali earth metal silicates, and volatilization of the alkali oxides (such as Na_2O and B_2O_3) during glass melting and cooling to room temperature, also affect the surface composition [77–83].

Immediately after glass manufacture, optical measurements have detected a lower refractive index from a thin surface film. This very fine silica film is between 1–35 nm thick, and is due to the loss of alkali oxides by both volatilization, and the hydrolysis/leaching of the alkali and alkali earth metal silicates [73–75]. Such thin surface films have different chemical and physical properties from those of the bulk glass, and help retard further bulk glass hydrolysis or leaching, by acting as a barrier for component ion diffusion. Both thickness and density of the surface film vary with glass composition, time, temperature and pH. A less durable glass produces a

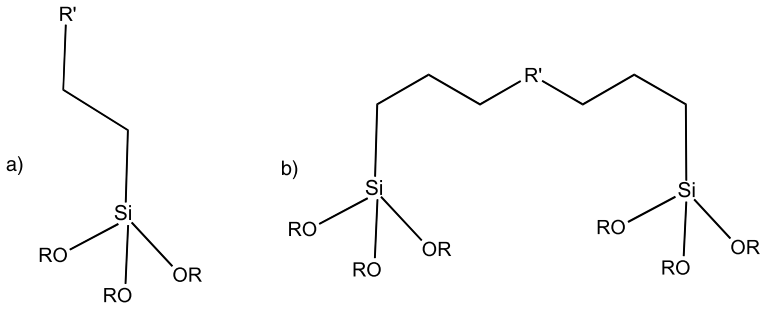

R = Me or Et; R' = Organofunctional Group

Fig. 10.2 (**a**) Conventional silane coupling agent and (**b**) Dipodal silane coupling agent (Matisons and Kempson—unpublished data (1997))

thicker film than a more durable glass [73–75]. Studies in this author's laboratories [66] of the streaming potential of water sized E-glass revealed an acidic isoelectric point (pH = 3) which, while consistent with that established for silica surfaces (pH = 2.3), also indicated a shift to higher pH arising from the presence of added alkaline components in the glass.

The drying conditions used for the silane treated glass also affect the structure of the adsorbed silane/siloxane interphase. The temperature and duration of the drying procedure influence the number of siloxane bonds formed between adjacent silanes (siloxane formation) as well as with the surface. Such 'siloxane coatings' with multiple surface bonds (see Fig. 10.2) generally give improved composite performance. The use of dipodal silanes has proved important in this respect.

Silanes are available in many forms, but two distinct structural types, the mono and the *bis*, or dipodal silanes are most commonly used. Mono-silanes are of the type R'-$(CH_2)_n$-$Si(OR)_3$, and *bis*- or dipodal silanes are of the type, $(RO)_3Si$-$(CH_2)_n$-R-$(CH_2)_m$-$Si(OR)_3$ (see Fig. 10.2). Mono-silanes are commonly used for the organic functionalization of inorganic surfaces via condensation of hydrolyzed silanols onto hydroxylated surfaces. These self-assembled monolayers (SAMs) do not form highly cross-linked structures as silanols are mostly attached to the surface and unavailable for the formation of siloxane bonds above the interface. Dipodal silanes, however, with twice as many hydrolyzable alkoxy groups as mono-silanes, form denser interfacial layers and stronger structures above the interface through the formation of highly cross-linked siloxane networks.

Dipodal silanes are a new type of adhesion promoter because of their commercial success in applications such as plastic optics, circuit boards, and on metallic surfaces. These coupling agents are hydrolytically far more stable than conventional silane coupling agents, yet have a significant impact on substrate bonding and composite mechanical strength. Dipodal silanes show improved wet adhesion, improved chemical resistance, good corrosion protection and improved composite processing. Importantly, dipodal silanes also enhance film formation at the interface, where such film formation is desired, as in corrosion protection. Film thickness is then related to

silane concentration and time of exposure to the silane solution. Dipodal silanes can be readily mixed with conventional silane coupling agents to suit particular applications. The resulting siloxane film thickness that forms by introducing such dipodal silanes depends mainly on the silane concentration and the substrates residence time in the silane solution.

10.5 Sizing Formulations

It is well established that more than a monolayer of silane coupling agent is required on the oxide substrate in order to optimize the strength of the resultant composite. Only in this way is it possible to generate an interpenetrating network of the coupling agent (resident on the fiber) within the polymer matrix. There is, however, an optimum thickness of coupling agent which, if not achieved, results in a substantial decline in the overall performance of the composite. A large flexible polymeric backbone will enable the interphase to adjust to the steric constraints imposed by the oxide surface and display a continuous reactive surface to the polymer matrix. Furthermore, by using a mixture of silanes, the ratio of hydrophobic to hydrophilic groups can be adjusted so as to optimize the number of polar group interactions (which may also act as sites for water ingress) for maximum dry strength and durability [1]. Arkles [13] reported that it is necessary to control the hydrolysis and oligomerization rates very carefully, if controlled and reproducible silane modified surfaces are to be produced. It is also necessary to control the degree of cross-linking and size of the polymeric silane segments, to ensure their interpenetration into the polymer matrix for optimum composite properties.

Preformed siloxanes, like the silane products of hydrolysis and condensation, are also capable of adhering to a variety of surfaces [39–45, 86–88]. They are strongly water resistant polymers and should, in principle, also be able to give water resistant interfaces between glass fibers and organic resins in composite materials. They display considerable backbone flexibility, so that they may also adjust to the availability of the reactive sites on glass surfaces. Siloxanes may be synthesized with a variety of functional groups attached, and the molecular weight distribution may be readily controlled. The investigation of siloxanes bearing appropriate functional groups may then lead to a whole new class of coupling agents, with all the advantages of silanes, but with greater control and reproducibility of the surface modification procedure. Importantly, siloxanes offer the prospect of combining the properties of a polymeric film former (see Sect. 10.2) with that of a coupling agent in the one molecule.

A number of factors affect the adsorption of polymers onto surfaces: these include the type of solvent; the polymer's molecular weight and polydispersity index; the concentration; the time allowed for an interaction; the number of reactive groups per molecule, the functionality of reactive groups on polymers; the reaction temperature; the pH in aqueous systems; the type of post-treatment; and the nature of the substrate.

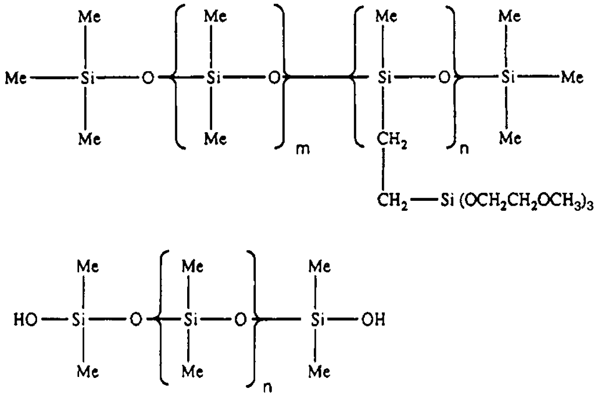

Fig. 10.3 Siloxane-based coupling agent (*top*) Conventional siloxane—PDMS (*bottom*) (Matisons and Kehoe—unpublished data (1994))

Our group's past research focused on siloxanes, which, like silanes, are strongly water resistant polymers capable of binding tenaciously to a variety of surfaces, including glass. Preformed siloxanes exhibit remarkable backbone flexibility enabling them to be used as film formers, surfactants as well as coupling agents linking polymers (having the appropriate functional groups) to glass surfaces. Their inherent backbone flexibility, results from both the electronic and structural properties of the Si-O and Si-C bonds, which permit unhindered rotation about the siloxane backbone in the case of PDMS. The freedom of rotation gives ideal screening for the polar Si-O-Si backbone, by the non polar methyl groups, thereby giving the polymer excellent film forming properties. As a result, siloxanes have very low surface tensions usually between 20 and 25 $mN\,m^{-1}$, which promote their use as surfactants in personal care products and in the textile industry.

Earlier studies in this author's laboratories examined the attachment of a number of functionalized siloxanes onto E-glass fibers, and compared them to commercial silane coupling agents [41–45, 86–88]. XPS and diffuse reflectance Fourier transform infrared spectroscopy (DRIFT) were employed to establish the presence of the siloxane on the glass surface; and to semi-quantitatively compare the modified surfaces. It was found that not only did siloxanes bearing trialkoxy-functional groups (see Fig. 10.3) adsorb to glass fiber surfaces as effectively as a common coupling agent, vinyltris(methoxyethoxy)silane; but, surprisingly, that other siloxanes bearing a variety of functional groups (e.g. amino, aminohydroxy, hydrido, and methacryl) also strongly adsorbed [41–45, 86–88].

The initial results with functionalized siloxanes prompted the synthesis and examination of a siloxane "coupling agent analog" bearing a large number of alkoxy groups to E-glass fibers. This allows a comparison to be made among this siloxane coupling agent analog (Fig. 10.3 top), the vinyltris(2-methoxyethoxy) silane used in the earlier study, and a hydroxy-terminated poly(dimethylsiloxane) (Fig. 10.3 bottom). DRIFT and XPS were again used to analyze the treated E-glass fibers [41, 43, 87]. However, the scanning electron microscopy (SEM) pictures in Figs. 10.4a and 10.4b contrasting conventional sizing formulations (in aqueous solution) with that of the pure siloxane coupling agent analog, applied in the case of the latter from

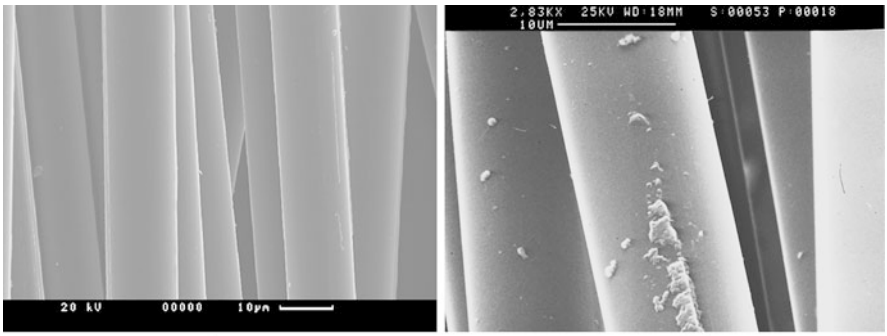

Fig. 10.4 (**a**): SEM of E-glass fibers sized with formulation containing film former, silane coupling agent, lubricant, and antistatic agent (Matisons, J. and Kempson, S.—unpublished data (1997)). (**b**): SEM of hydroxy-terminated PDMS sizing solution (Matisons and Le Huy—unpublished data (1996))

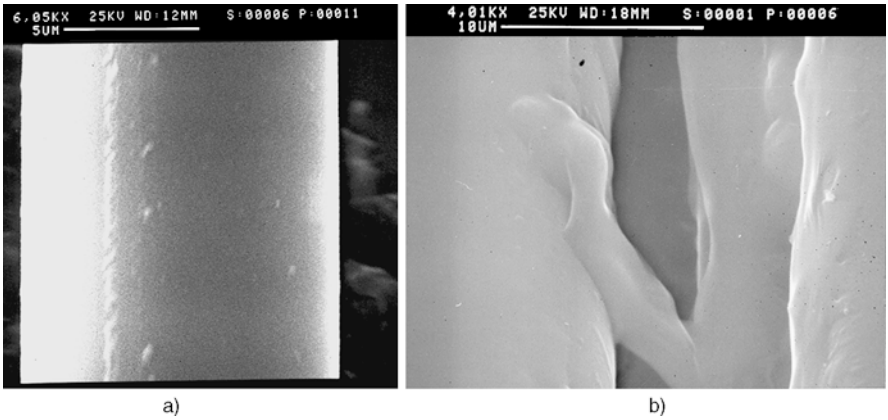

Fig. 10.5 (**a**): Siloxane coupling agent (Fig. 10.3 *top*; $m = 195$; $n = 3$) applied from toluene Solution (Matisons and Le Huy—unpublished data (1996)). (**b**): Siloxane coupling agent (Fig. 10.3 *top*; $m = 175$; $n = 23$) applied from toluene solution (Matisons and Le Huy—unpublished data (1996))

toluene solution, illustrate more than anything else that such siloxanes can be used to treat glass fibers.

An interpenetrating polymer network, IPN, that is formed between the glass fibers and the siloxane coupling agent analogs when the pendant alkoxy groups are increased and the siloxane film that forms is shown in Fig. 10.5a. Activated alkoxy groups on the siloxane in this case turn to silanols that deposit onto the glass fibers and during cross-linking not only form a siloxane film, but form polymeric bridges between glass fibers as shown in Fig. 10.5b. Such cross-linked siloxanes have a significant impact on bonding and mechanical strength.

While the static mechanical performance benefits of fiber-reinforced composites are often the reason for their selection in structural applications, it is generally accepted that the response of the fiber–matrix interphase region can contribute to impact resistance and damage tolerance. The effect of the interphase on impact performance is largely determined by the choice of sizing components applied during glass fiber production. Published results indicate that the impact response of a fiber-reinforced composite can be tailored towards high energy absorption by engineering weak fiber–matrix interfacial interactions; or, conversely, high damage tolerance (e.g., residual strength after impact) can be produced by promoting strong fiber–matrix interfacial interactions. These siloxane coupling agents uniquely lend themselves to not only protecting glass fiber integrity (i.e. damage tolerance), but also to being able to absorb high energy impacts. As the fiber–matrix bond strength is increased, energy absorption during impact decreases. Furthermore, the fiber-siloxane coupling agent bond strength can now be tailored by adjusting the number of alkoxy side groups on the siloxane backbone. A final note of caution should be added; making siloxanes with alkoxy groups resident on each silicon atom along the siloxane backbone is possible, but the utility of such siloxanes is very limited, as they gel rapidly on contact with trace amounts of moisture, such as is resident on common laboratory glassware.

In summary, pre-formed functionalized siloxanes containing alkoxy side groups can be made to serve as effective sizing agents that combine the film forming properties of polymers, together with the coupling properties of conventional silane coupling agents. It remains to optimize the molecular weight and the number of alkoxy side groups on such siloxane coupling agents to generate the best possible sizing results in commercial applications.

References

1. Plueddemann E (1990) Silane coupling agents, 2nd ed. Plenum Press, New York
2. Plueddemann E (1991) J Adhes Sci Technol 5:261
3. Bader MG, Bailey JE, Bell I (1972) In: Kriegel WW, Palmour H (eds) Ceramics in severe environments. Material science research, vol 5. Plenum Press, New York
4. Atkins AG (1975) J Mater Sci 10:819
5. Outwater JO (1975) J Adhes 2:242
6. Brook MA (2000) Silicon in organic, organometallic, and polymer chemistry. Wiley, New York
7. Angst DL, Simmons GW (1991) Langmuir 7:2236
8. Pantano CG, Wittberg TN (1990) Surf Interface Anal 15:498
9. Schubert U, Husing N (2000) Synthesis of inorganic materials. Wiley-VCH, Weinheim
10. Wang D, Jones FR, Denison P (1992) J Adhes Sci Technol 6:79
11. Allen KW (1992) J Adhes Sci Technol 6:23
12. Drown EK, Moussawi H, Drzal LT (1991) J Adhes Sci Technol 5:865
13. Arkles B (1977) Chemtech 7:766
14. Pleuddemann E, Clark H, Nelson L, Hoffmann K (1962) Mod Plast 39:136
15. Blum FD, Meesiri W, Kang H-J, Gambogi J (1991) J Adhes Sci Technol 5:479
16. Tripp CP, Hair ML (1991) Langmuir 8:1120
17. Arkles B, Steinmetz JR, Zazyczny J, Mehta P (1992) J Adhes Sci Technol 6:193

18. Hair ML (1986) In: Leyden DE (ed) Silane surfaces and interfaces, vol 1. Gordon & Breach, New York
19. Ishida H (1983) In: Mittal KL (ed) Adhesion aspects of polymeric coatings. Plenum Press, New York, pp 45–106
20. Jutzi P, Strassburger G, Schneider M, Stammler H-G, Neumann B (1996) Organometallics 15:2842
21. Simons R, Galat KJ, Rapp BJ, Tessier CA, Youngs WJ (2000) Organometallics 19:5799
22. Winkhofer N, Roesky HW, Noltemeyer M, Robinson WT (1992) Angew Chem 104:670
23. Ishida H, Koenig JL, Gardner KC (1982) J Chem Phys 77:5748
24. Al-Juaid SS, Buttrus NH, Damja RI, Derouiche Y, Eaborn C, Hitchcock PB, Lickiss PD (1989) J Organomet Chem 371:287
25. Unno M, Alias SB, Saito H, Matsumoto H (1996) Organometallics 15:2413
26. Walawalkar MG (2003) Organometallics 22:879
27. Ogawa M, Okutomo S, Kuroda K (1998) J Am Chem Soc 120:7361
28. Ruiz-Hitzky E, Rojo JM (1980) Nature 287:28
29. Yanagisawa T, Kuroda K, Kato C (1998) React Solids 5:167
30. Okutomo S, Kuroda K, Ogawa M (1999) Appl Clay Sci 15:253
31. Ogawa M, Miyoshi M, Kuroda K (1998) Chem Mater 10:3787
32. Yanagisawa T, Kuroda K, Kato C (1988) Bull Chem Soc Jpn 61:3743
33. Isoda K, Kuroda K, Ogawa M (2000) Chem Mater 12:1702
34. Ide Y, Ogawa M (2003) Chem Commun 1262
35. Ide Y, Ogawa M (2005) Chem Lett 360
36. Abbenhuis HCL (2000) Chem Eur J 6:25
37. Lickiss PD (2001) In: Rappoport Z, Apeloig Y (eds) Chemistry of organic silicon compounds, vol 3. Wiley, Chichester, pp 695–744
38. Iler R (1979) The surface chemistry of silica. Wiley Science, New York
39. Hariharan A, Kumar S, Russel T (1990) Macromolecules 23:3584
40. Cohen SM, Cosgrove T, Vincent B (1986) Adv Colloid Interface Sci 24:143
41. Britcher LG, Kehoe DC, Matisons JG, Netting AKO, Smart RStC, Swincer AG (1993) Langmuir 9:1609
42. Britcher LG, Kehoe DC, Matisons JG, Swincer AG (1995) Macromolecules 28:3110
43. Britcher LG, Kehoe DC, Matisons JG (2001) Polym Preprints 42:178
44. Arora PS, Matisons JG, Provatas A, Smart RStC (1995) Langmuir 11:2009
45. Britcher LG, Kehoe DC, Matisons JG, Arora PS, Smart RStC (1996) In: High performance coating materials. Silicones in coatings, vol 1. Paint Research Association, New York, p 16
46. Jokinen AE, Matisons JG, Rosenholm JB (1997) J Colloid Interface Sci 194:263
47. Watson H, Jokinen AE, Mikkola P, Matisons JG, Rosenholm JB (1997) Prog Colloid Polym Sci 105:80
48. Jokinen AE, Matisons JG, Rosenholm JB (1998) J Mater Sci Lett 17:149
49. Matisons JG (1998) In: High performance coating materials. Silicones in coatings, vol 2. Paint Research Association, New York, p 5
50. Le-Huy CC, Britcher LG, Matisons JG (2002) Silicon Chem 1:195
51. Ikuta N, Suzuki Y, Maekawa Z, Hamada H (1961) Polymer 34:2445
52. Bell JP, Schmidt RG, Malofsky A, Mancini D (1992) J Adhes Sci Technol 5:927
53. Fowkes F, Dwight D, Manson J, Lloyd T (1988) Mater Res Soc Symp Proc 119:223
54. Dwight D, Fowkes F, Cole D, Kulp M, Sabat P, Salvati L Jr, Huang T (1990) J Adhes Sci Technol 4:619
55. Dwight D, Fowkes F, Cole D, Kulp M, Sabat P, Salvati LJr, Huang T (1990) J Adhes Sci Technol 4:690
56. Drago R (1973) Struct Bond 15:73
57. Blitz J, Murthy R, Leyden D (1987) J Am Chem Soc 109:7141
58. Shen YR (1984) The principles of nonlinear optics. Wiley, New York
59. Eggers PK, Da Silva P, Darwish NA, Zhang Y, Tong Y, Ye S, Paddon-Row MN, Gooding JJ (2010) Langmuir 26:15665

60. Pantano C, Carman L, Warner S (1992) J Adhes Sci Technol 6:49
61. Nitzsche S, Burkhardt J, Wegehaupt K (1971) Wacker-Chemie GmbH, German Patent, DE 1,955,514
62. Watson H, Mikkola PJ, Matisons JG, Rosenholm JB (2000) Colloids Surf 161:183
63. Watson H, Mikkola PJ, Matisons JG, Rosenholm JB (2001) Colloid Polym Sci 279:1020
64. Watson H, Norstrom AE, Matisons JG, Root A, Rosenholm JB (2001) J Adhes Sci Technol 15:1103
65. Britcher LG, Kehoe DC, Matisons JG (2000) In: Mittal K (ed) Silanes and other coupling agents, vol 2. VSP, Utrecht, pp 99–114
66. Kempson SD, Matisons JG (1997) Chem Australia 12:3
67. Embery CJ, Clarke SR, Matisons JG (2003) In: Clarson S, Fitzgerald J, Owen M, Van Dyke M (eds) Synthesis and properties of silicones and silicone-modified materials. ACS symp., vol 838. Amer Chem Soc, Washington, p 26
68. Matisons JG, Graser S, Britcher LG (2001) In: Mittal K (ed) Acid–base interactions—relevance to adhesion, vol 2. VSP, Utrecht, p 601
69. Danner J, Vohs J (1992) Appl Surface Sci 62:255
70. van Ooij W, Sabata A (1993) Surf Interface Anal 20:475
71. Porro T, Pattacini S (1992) J Adhes Sci Technol 6:73
72. Vlad M (1993) J Colloid Interface Sci 159:21
73. Doremus R (1973) Glass science. Wiley, New York
74. Holland L (1964) The properties of glass surfaces. Chapman & Hall, London
75. Rosington D (1972) In: Pye L, Stevens H, La Course W (eds) Introduction to glass science. Plenum Press, New York, p 101
76. Kruger A (1988) In: Nowotuy J, Du Four L-C (eds) Surface and near surface chemistry of oxide materials. Materials science monographs, vol 47, Chap. 9, Amsterdam
77. Prabakar S, Mueller KT (2004) J Non-Cryst Solids 349:80
78. Fry R, Tsomaia N, Pantano CG, Mueller KT (2003) J Am Chem Soc 125:2378
79. Van Ginhoven RM, Jónsson H, Corrales LR (2005) J Phys Chem B 109:10936
80. Hall MM, Clare AG (2007) J Sol-Gel Sci Technol 41:107
81. Pedone A, Malavasi G, Menziani MC, Cormack AN, Segre U (2006) J Phys Chem B 110:11780
82. Kister S (1962) J Am Ceram Soc 45:59
83. Varshneya AK (1994) Fundamentals of inorganic glasses. Academic Press, London
84. Haaland D (1986) Appl Spectrosc 40:1152
85. Davydov V, Kislev A, Zhuravlev L (1964) Trans Faraday Soc 60:2254
86. Matisons JG, Provatas A (1998) Langmuir 14:1656
87. Ma R, Le-Huy CC, Britcher LG, Matisons JG (2001) Polym Preprints 42:248
88. Matisons JG, Provatas A (1994) Macromolecules 27:3397
89. Watson H, Norstrom AE, Mikkola PJ, Matisons JG, Rosenholm JB (2000) J Colloid Interface Sci 232:149
90. Ooi K, Miyatake M (1992) J Colloid Interface Sci 148:303
91. Huang K, Balazs AC (1993) Macromolecules 26:4736
92. Kuksenok O, Yeomans JM, Balazs AC (2001) Langmuir 17:7786
93. Shafrin E, Zisman W (1967) J Am Ceram Soc 50:478
94. Paul AJ (1977) Mater Sci 12:2246
95. Clare AG (2007) In: Groza JR, Shackelford JF, Lavernia EJ, Powers MT (eds) Materials processing handbook. CRC Press, Boca Raton, p 23/1
96. Matinlinna JP, Dahl JE, Lassila LVJ, Vallitu PK (2007) In: Mittal KL (ed) Silanes and other coupling agents, vol 4. VSP/Brill, Leiden, p 82

Chapter 11
Oxidative Surface Treatment of Silicone Rubber

Henrik Hillborg and Ulf W. Gedde

11.1 Introduction

Silicone rubber exhibits hydrophobic surface properties with excellent long-term durability. The material is also very responsive to environmental stimuli, which opens the way to a tailoring of the surface properties. The underlying molecular processes are complex and it is therefore important to 'understand' the material structure and structural changes in order to fully utilize its potential. The generic low surface energy of silicone rubber can be raised by various types of oxidative surface treatment, usually plasma, corona or combined UV and ozone treatment. However, the oxidized surfaces are not stable with time and the hydrophobicity is gradually regained. This is referred to as a hydrophobic recovery, and it is utilized in high-voltage outdoor insulation applications. During severe weather conditions, electrical discharges may occur along the insulator surface. Such discharges temporarily reduce the hydrophobicity of the insulator, but after a discharge period, the hydrophobicity is regained. In addition, when the insulator surface becomes polluted with e.g. dust or salt, low molar mass siloxanes migrate from the silicone rubber onto the pollutant layer restoring the hydrophobicity of the insulator surface. It is important to have a hydrophobic insulator surface so that any water present on the surface is prohibited from forming a continuous path, bridging the high-voltage electrode and the ground, thereby maintaining a low leakage current and avoiding the risk of

H. Hillborg (✉) · U.W. Gedde
Fibre and Polymer Technology, School of Chemical Science and Engineering, Royal Institute of Technology, 100 44 Stockholm, Sweden
e-mail: henrik.hillborg@se.abb.com

U.W. Gedde
e-mail: gedde@polymer.kth.se

H. Hillborg
Corporate Research, ABB AB, 72178 Västerås, Sweden
e-mail: henrik.hillborg@se.abb.com

M.J. Owen, P.R. Dvornic (eds.), *Silicone Surface Science*, Advances in Silicon Science 4,
DOI 10.1007/978-94-007-3876-8_11,

a fatal electrical surface flashover. Hydrophobicity thus enhances the performance of the insulation, making it more reliable even during severe weather conditions. This raises a question: will the low molar mass siloxanes, inherent to most silicone rubber compositions, become depleted, and finally leave a permanently hydrophilic, oxidized, surface? The general experience from a number of scientific studies is that hydrophobic recovery occurs even after extended periods of service over decades.

In other industrial applications, silicone rubber is banned due to its dynamic surface properties, for example in the coating industry. Volatile siloxanes can readily adsorb onto high-energy surfaces causing problems with wetting when the coating is applied. Bonding silicone rubber is a challenge due to its low-energy surface. The low surface energy which is beneficial for water repellency results in weak adhesion to other substrates. Even though good bonding between silicones can be obtained without primers, these are usually required when attaching silicones to other substrates. The primers contain active components such as triethoxysilanes, orthosilicates, or titanates. These systems commonly require the presence of surface hydroxyl groups where a condensation reaction can take place. The surface hydroxyl groups can be introduced by oxidative surface treatment of the silicone rubber. In many applications it is desirable to have a silicone rubber with hydrophilic surface properties. Examples are soft lithography, microfluidics and medical implants, where readily wettable surfaces in aqueous environments are required. In these applications, the hydrophobic recovery is usually not desired. Instead much research has been devoted to the development of permanently hydrophilic silicone rubber surfaces. This issue has also been addressed in applications where strong adhesion between silicone rubber and some other substrate is desired.

The following section of this chapter starts by addressing the origin of the dynamic surface properties of silicone rubber. The effects of different oxidative surface treatments are summarized in Sect. 11.3. This section also describes an emerging research field based on the spontaneous surface wrinkling patterns occurring on silicone rubbers after oxidative treatment. The mechanisms of hydrophobic recovery are discussed in Sect. 11.4. A few selected applications in which oxidative surface treatments are commonly used are covered in Sect. 11.5. A summary and outlook are presented at the end of the chapter.

11.2 Surface Properties of Silicone Rubber

The dynamic surface properties of silicone rubber originate from the structural characteristics of polysiloxanes. Even though a large variety of polysiloxanes is available, polydimethylsiloxane (PDMS) is by far the most commonly used polysiloxane in commercial applications. The surface properties are the result of four structural characteristics: (1) the low *inter*molecular forces between the methyl groups, (2) the uniquely high flexibility of the siloxane backbone, (3) the high strength of the siloxane bond, and (4) the partial ionic nature of the siloxane bond (see also Chap. 1) [1]. The high segmental flexibility of PDMS is demonstrated by its very low glass transition temperature ($-127\,^{\circ}\mathrm{C}$). The low surface free energy ($20\ \mathrm{mJ\,m^{-2}}$) towards

gases, such as air, is due to closely packed methyl groups located at the surface. If the material is exposed to a polar environment such as water, the methyl groups are reoriented towards the bulk, exposing the siloxane backbone which has a more polar character. Exposure to an oxidizing treatment results in the formation of polar groups as well as oxidative cross-linking reactions of the polymer network. Both processes lead to a reduction in hydrophobicity. Scission of the polymer chains can also occur, generating linear or cyclic siloxane oligomers. Oxygen-free conditions facilitate chain scission whereas oxygen-containing media lead to a combination of oxidative cross-linking and chain scission [2, 3]. The balance between cross-linking and chain scission is also influenced by the presence of other species, such as benzoic acid [4], or acids or bases [5, 6]. The oligomers exhibit a lower surface energy (15–19 mJ m^{-2}) than silicone rubber (20–25 mJ m^{-2}). The silicone rubber exhibits higher surface energy compared to PDMS due to the addition of fillers, as well as cross-linking systems. As a result these oligomers readily migrate to the interface between silicone rubber and air. Since silicone rubber is manufactured by the condensation of mainly cyclic PDMS oligomers, a certain amount of these remain in the rubber. A typical concentration of extractable oligomers is of the order of 1 to 5 wt.%. After removal of the extractable part, there is also a certain regeneration of these species, since the condensation process is slightly reversible. It is thus very difficult to manufacture a silicone rubber which contains no free oligomers.

11.3 Effects of Oxidative Surface Treatments

11.3.1 Introduction

The surface treatment of choice is often dependent on the application and tradition. Milder treatment facilitates specific surface functionalization by the formation of silanol groups, which can then be used for further grafting of desired functionalities. UV/ozone (UVO), corona or short plasma treatments are commonly used. Corona treatment under ambient conditions is usually used to improve the adhesion of larger objects, e.g. the use of a corona knife. The drawback of surface treatments in ambient conditions is the influence of humidity and temperature, which affects both the corona discharge intensity and the oxidation of the silicone rubber. Corona discharges have also been used to understand the ageing of silicone rubber outdoor insulation. Plasma-treatment is commonly used in soft lithography, microfluidics, or medical applications to reduce hydrophobicity. Plasma treatment can be powerful and can rapidly create a brittle silica-like surface layer, which is prone to cracking and wrinkling (see Chap. 3).

11.3.2 Surface Functionalization

During the initial stage of oxidation of silicone rubber, surface silanol groups are mainly formed. The flexible chain dynamics are maintained, allowing molec-

ular relaxation processes to occur. This can be readily observed by measuring the contact angle of water on silicone rubber at this stage of oxidation. The advancing contact angle is essentially the same, whereas the receding contact angle is significantly reduced, i.e. the contact angle hysteresis is increased. The advancing contact angle is unchanged because of the methyl groups oriented towards the surface, whereas the receding contact angle is reduced as a result of the reorientation of the introduced polar groups towards the surface as a response to the changing environment [7, 8]. A partially oxidized surface exhibiting a high water contact angle hysteresis is a typical result after a few minutes of UV/ozone or corona treatment, or after a plasma treatment using a low intensity and a short exposure time (typically a few seconds). Only minor changes in surface composition are observed at this stage. Using X-ray photoelectron spectroscopy (XPS) typically a few percent reduction in carbon content and a corresponding increase in oxygen is detected whereas the silicon content remains unchanged. The ideal atomic surface composition of pristine PDMS is 50 at.% carbon, 25 at.% silicon and 25 at.% oxigen. The same trend can be observed by reflection infrared spectroscopy, where the hydrocarbon absorption peaks are slightly reduced and a broad but weak absorption peak originating from hydroxyl-groups is introduced. Primary amino groups can be introduced directly using an ammonia-plasma treatment in combination with a short treatment time. Primary amino groups can also be introduced by exposure to oxygen plasma followed by a silanization of the formed surface hydroxyl groups using 3-aminopropyltriethoxysilane [9].

UV-irradiation of silicone rubber under ambient conditions leads to a rapid and controllable polymer oxidation. The formation of ozone generated by the UV in combination with oxygen leads to the formation of an oxidized surface layer [10, 11]. UV-irradiation alone results in a significantly slower oxidation rate than combined UV-ozone treatment [10, 12]. The hydrophobicity of the silicone rubber was lost after 20 min of combined UV/ozone treatment (UVO), whereas samples exposed to UV alone remained hydrophobic (ca. 90° advancing water contact angle) even after a 60 min. treatment (Fig. 11.1). The surface energy of the silicone rubber increased from an initial value of 20 mJ m^{-2} to 70 mJ m^{-2} after 20 min of combined UV/ozone treatment, whereas it remained low at 25 mJ m^{-2} after 60 min of UV irradiation. The contact angle hysteresis increased from an initial value of 15° to 35° for the combined UV/ozone-treated samples, typical for the introduction of polar groups in the surface which reorientate readily depending on the environment. Further treatment resulted in a significantly reduced contact angle hysteresis, down to only a few degrees, indicating the formation of an immobilized surface structure. X-ray reflectivity measurements showed an increase in electron density, shifting from that of PDMS to a silica-like structure of the surface region after both types of treatment. The combined UV/ozone-treated surfaces reached a maximum conversion of 50 % silica within the top 5 nm followed by a gradual reduction in silica content over the next 30–60 nm. Materials exposed to UV alone reached a silica content of only 25 % at the immediate surface and gradually approached the PDMS structure during the next 70 nm. The conversion from organically to inorganically bound silicon was thus significantly higher in the presence of ozone.

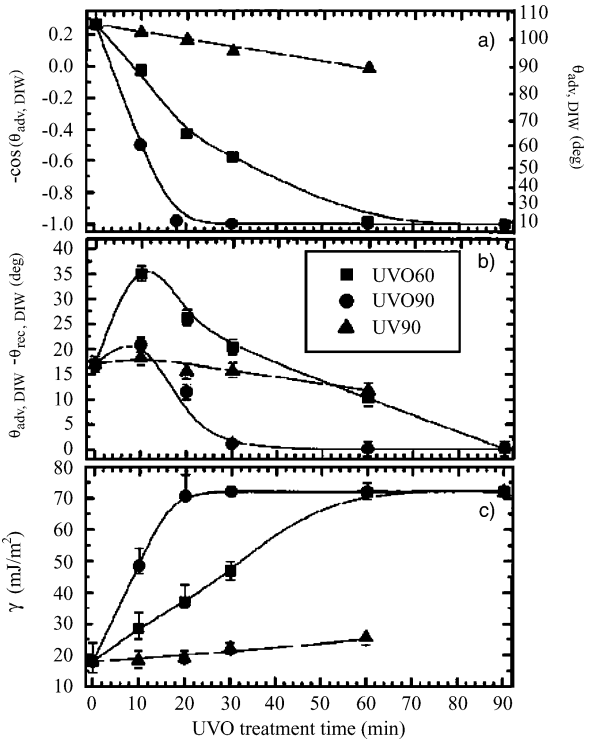

Fig. 11.1 Dependence of (**a**) the advancing contact angle of deionized water ($\theta_{adv,DIW}$), (**b**) the contact angle hysteresis of deionized water ($\theta_{adv,DIW} - \theta_{rec,DIW}$), and (**c**) the surface energy on the UVO treatment time for silicone rubber exposed to UVO60 (*squares*), UVO90 (*circles*), and UV90 (*up-triangles*). UV-lamps with 60 % (UVO 60) and 90 % (UVO90 and UV90) of the radiation at 184.9 nm were used. Reprinted from Ref. [10] with kind permission of © Elsevier (2002)

The structure of the oxidized surface of combined UV/ozone-treated silicone rubber was further characterized on a sub-micrometer level using chemically modified atomic force microscopy, AFM [13]. During the initial 30 min of combined UV/ozone treatment, a homogeneously (on a <50 nm scale) hydrophilic surface with a higher normalized surface-specific modulus was created. Contact angle measurements with water showed a large hysteresis, indicating that the polar groups introduced could readily reorientate. Longer treatment times (1 h) led to the formation of a hydrophilic structure with a high normalized surface-specific modulus. The surface-specific modulus increased linearly with treatment time, from 1 for the pristine silicone to 5–15 after 1 h corona treatment. Contact angle measurements with water showed that these samples exhibited a slow and incomplete hydrophobic recovery, in combination with a low hysteresis. In addition ToF-SIMS studies confirmed that surface silanol groups were primarily formed by the combined UV/ozone treatment, and that their concentration increased with increasing exposure time [14]. Pull-off force and stiffness mapping using hydroxyl-functionalized AFM tips in an aqueous environment revealed a gradual surface reconstruction within the silica-like layer after the treatment (Figs. 11.2 and 11.3). Hydrophilic silica-rich domains with a diameter less than 100 nm gradually formed, surrounded by a more hydrophobic matrix phase with a lower elastic modulus. The silica-like layer is thus heterogeneous on a sub-micrometer scale and not a homogeneous glass-like structure. The effective surface pKa value of the silica-like layer was in the

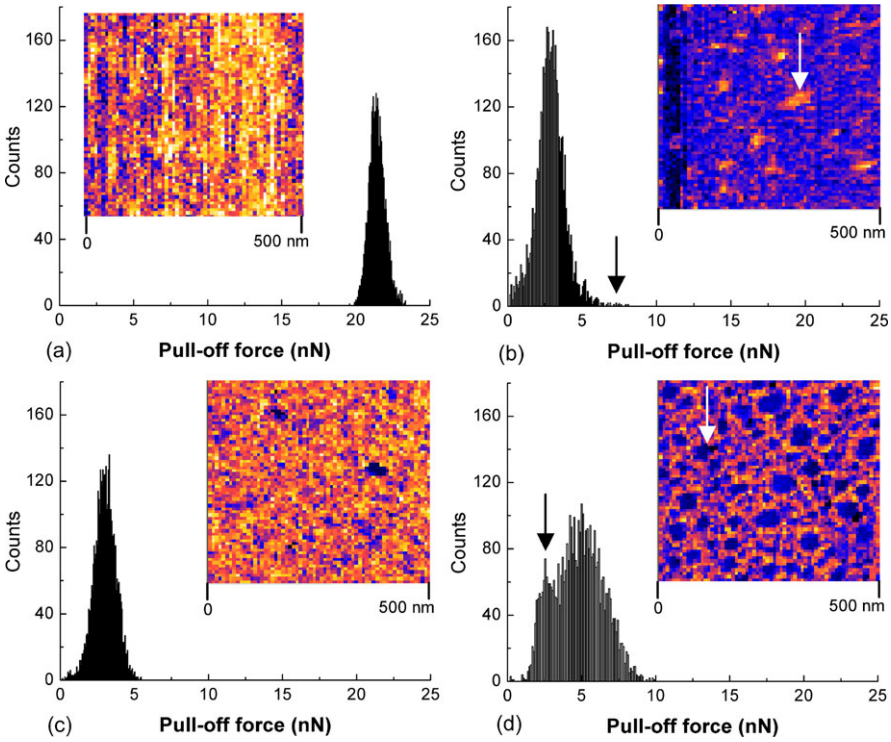

Fig. 11.2 Histograms of AFM pull-off forces and corresponding adhesion images of (**a**) pristine silicone rubber, and of oxidized silicone rubber after (**b**) 0.1, (**c**) 8, and (**d**) 40 days after 60 min combined UV/ozone treatment. In the adhesion images, the colour scales are individually scaled from dark (low pull-off force) to light (high pull-off force). Reprinted from Ref. [13] with kind permission of © The American Chemical Society (2004)

range of 4.5–5.5, determined by AFM pull-off force measurements using hydroxyl-functionalized tips in aqueous buffer solutions at different pHs [14]. This is higher than the corresponding values of surface silanol groups, homogeneously distributed on a silica surface (pKa $\sim$ 4). It was suggested that the shift in pKa was due to the heterogeneous nature of the silica-like layer, where more hydrophobic regions had a stabilizing effect on the surface ionization of the silica-like patches [14]. The stability of the silica-like layer formed after 60 min combined UV/ozone treatment was further verified on the meso-scale using JKR contact mechanics (see Chap. 1) [15]. The higher elastic modulus of the oxidized surfaces was retained during storage after exposure, whereas a hydrophobic recovery was observed both on the continuum scale by an increasing contact angle with water and on the meso-scale by a decreasing work of adhesion according to the JKR theory. The recovery of the surface-specific modulus observed 40 days after UVO treatment is probably caused by migration of PDMS oligomers to the surface (see Sect. 11.4).

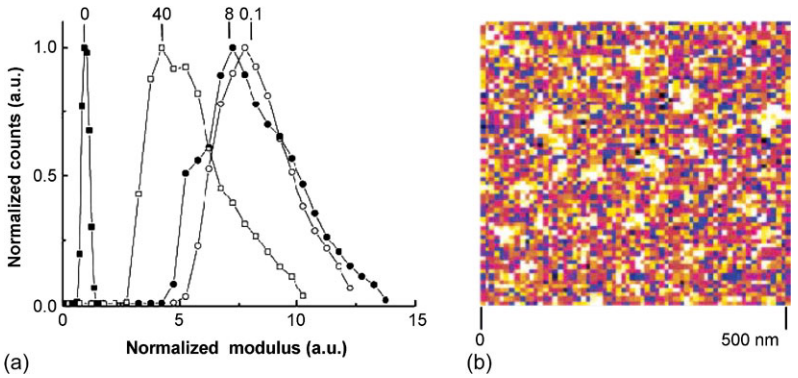

Fig. 11.3 (**a**) Change in the normalized surface-specific modulus after 60 min of combined UV/ozone treatment obtained from AFM indentation mapping. Times after treatment in days are indicated above the distributions. The peak indicated by 0 corresponds to pristine silicone rubber (normalized modulus = 1). (**b**) Example of modulus mapping, 40 days after the UV/ozone exposure; the colour scale corresponds to a normalized modulus from 2 (*darkest*) to 10 (*lightest*). Reprinted from Ref. [13] with kind permission of © The American Chemical Society (2004)

11.3.3 Formation of a Silica-Like Surface Layer

The structural effects of the oxidative treatment of silicone rubber using either a corona discharge at atmospheric pressure or a plasma treatment at low pressures have been thoroughly studied. Silicone rubbers with different cross-link densities were exposed to corona discharges in dry air or in GHz air plasma [16]. The oxidation induced by the GHz air plasma proceeded at a higher rate than that induced by a corona treatment. For example, the carbon to oxygen ratio (C/O) in the surface region after 10 s air-plasma treatment, determined by XPS, was comparable to that obtained after 30 min air corona (C/O decreased from an initial ratio of 2.2 to 1.2–1.3). The oxidation rate also increased with increasing initial cross-link density of the silicone rubber, indicating that the carbon-carbon cross-links are sensitive to oxidation. The mechanical properties of the silica-like layers formed were characterized in terms of onset of cracking and subsequent fragmentation length upon stretching of the oxidized rubber films. The brittleness of the layers increased with increasing exposure time and increasing initial cross-link density of the rubber. Samples oxidized by corona discharges showed a lower fracture strain than samples oxidized by plasma due to a higher layer thickness after corona treatment (Fig. 11.4).

It is reasonable to assume that extensive oxidation would result in a full conversion of the surface from silicone to silica, SiO_2. The atomic surface composition would then change from the previously stated ideal composition of 50 at.% carbon, 25 at.% silicon and 25 at.% oxygen to 33 at.% silicon and 66 at.% oxygen, using XPS. However, even after 200 h of continuous corona exposure 14 % carbon remained [17]. Further information on the changes occurring in the surface region can be obtained from high-resolution spectra of the Si 2p orbital. For PDMS, the po-

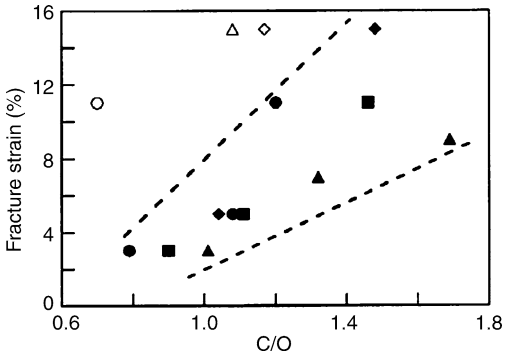

Fig. 11.4 Fracture strain of silica-like surface layers on silicone rubber with different cross-link density, as a function of carbon-to-oxygen (C/O) ratio by XPS, after exposure to corona (*solid symbols*) and air plasma (*open symbols*). Reprinted from Ref. [16] with kind permission of © Elsevier (2001)

sition of the peak in the high-resolution spectrum is at 102.1 eV. On conversion to a silica-like structure, the bond energy is shifted toward higher energies. There are several different ways to define this shift, but a rather straightforward way is to fit a new peak at 103.6–103.8 eV, associated with an inorganic silica-like phase [18, 19]. It is also possible to resolve the high-resolution spectrum of the Si 2p peak to give three components: silicon bound to two oxygen atoms at 102.1 eV, silicon bound to three oxygen atoms at 102.8 eV and silicon bound to four oxygen atoms at 103.4 eV [20]. A large fraction of the silicon bonded to two oxygen atoms (PDMS) remains even after extended corona or plasma treatment [12, 17, 19].

The observation that a full conversion into SiO_2 is not reached can be explained by the gradual decrease in segmental mobility during the oxidative cross-linking. Polymers oxidize more rapidly above their glass transition temperature than in the glassy state, primarily due to the faster rate of diffusion of oxygen and to the so-called cage effect, i.e. recombination of nearby radicals [21]. It has also been shown that the quantum yield for chain scission induced by UV radiation of a range of fully amorphous polymers decreased markedly when reaching the glass transition temperature [22]. This implies that the oxidized and unoxidized components must be mixed on a sub-micrometer scale. If they formed separate, larger (micrometer-size) domains, the segmental mobility of the molecules within the unoxidized domains would be unaffected, and they would be available for further oxidation. Thus once vitrification of the surface layer has occurred, further oxidation is impossible. This explains the observed heterogeneity on the nanometre scale of the silica-like layer, where the silica-like and silicone-like species are intimately mixed on a very fine scale (Figs. 11.2 and 11.3). Another reason for the incomplete conversion observed by XPS is the presence of silicone oligomers. These must be extracted before the XPS analysis, otherwise they will be adsorbed onto the oxidized surface layer. This can be readily observed by performing surface analysis using a different angle of incidence between the X-ray beam and the surface, thereby assessing different thickness. Using this technique, it was found that the top 2 nm layer had a lower oxygen content and higher carbon content than the top 8–10 nm after air-plasma or corona treatment of silicone rubber [17, 19].

The thickness of the silica-like layer on oxidized silicone rubber has been characterized by several methods. Neutron reflectometry showed a thickness of the order of 130–160 nm, which did not increase with increasing exposure time to RF-plasma [23]. Cryo-microtomed sections of oxygen-RF plasma-treated PDMS was characterized by transmission electron microscopy (TEM), and the silica-like layer ranged between 9 and 65 nm, depending on the plasma-treatment conditions [24]. A sharp transition in surface densification and chemical modification showed that the use of a gradient-based mechanical analysis was not needed for mechanical calculation of the composite structure, i.e. the silica-like layer and silicone rubber bulk [24]. This was in contrast to previously published work based on neutron reflectometry measurements where the layer thickness was not of uniform composition but was either fitted with a model based on two layers and an asymmetric interface [23], or by applying a four-layer model, using three layers of differently oxidized PDMS and one layer of natural silicon oxide on the silicon wafer [25].

The limited thickness of the silica-like layers can be explained by the diffusion of reactive species into the silicone rubber [26]. The rate-limiting process for preparing oxide films on silicon surfaces is the diffusion of molecular oxygen into the silicon. By analogy, when silicone rubber is exposed to plasma, reactive species and UV radiation are both created, and this then oxidizes the surface region. The formation of the silica-like layer retards diffusion of the reactive species into the bulk, gradually reducing the oxidation rate. The primary reactant responsible for the conversion is atomic oxygen produced by the photo-dissociation of the formed ozone by UV radiation [12]. The atomic oxygen is too short-lived and must be generated in situ within a region of unconverted PDMS in order to continue the oxidation process. After a certain thickness of the silica like layer all of the generated ozone will photo-dissociate before it reaches the pristine PDMS. Since the penetration depth of the UV radiation (<180 nm wavelength) into polymers is generally less than a few hundred nanometres, this will result in a limited layer thickness, which is consistent with the published experimental data.

AFM and micro-indentation measurements of the elastic modulus of silica-like layers on silicone rubber usually give values below 0.2 GPa after combined UV/ozone- or plasma-treatment [13, 14, 27–29]. Other techniques for determining the elastic modulus of thin films on elastomeric substrates are based on analysis of the strain-induced buckling patterns of the films. The modulus of the silica-like layer on oxygen-plasma-treated silicone rubber was estimated to be 0.8 GPa, which is significantly higher than that given by the indentation-based techniques [30]. The modulus of the silica-like layers can also be determined from the buckling patterns induced by oxidation of pre-strained PDMS films. Under sufficiently strong plasma conditions, but below the occurrence of spontaneous surface micro-cracks, the elastic modulus was found to be in the range of 1.5 GPa [24]. These results show that the silica-like layer cannot be regarded as true silica, but rather as a highly cross-linked thermoplastic close to or below its glass transition temperature. Cracking of the silica-like layer occurs spontaneously during longer oxidative surface treatment at high intensity (Fig. 11.5). This is caused by the reduction in specific volume compared to that of PDMS, leading to a build-up of tensile stresses. Surface cracking can also

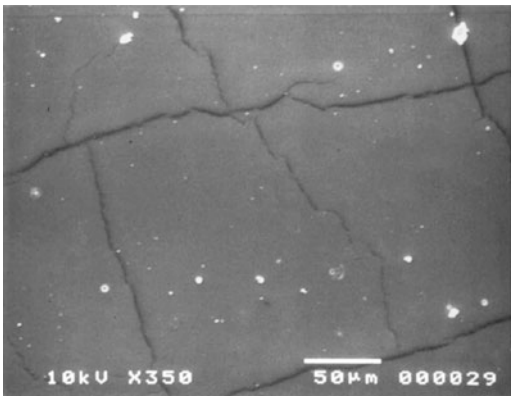

Fig. 11.5 Spontaneous surface cracking of the silica-like layer after exposure to a corona discharge in dry air for 3 h. Reprinted from Ref. [23] with kind permission of © Elsevier (2000)

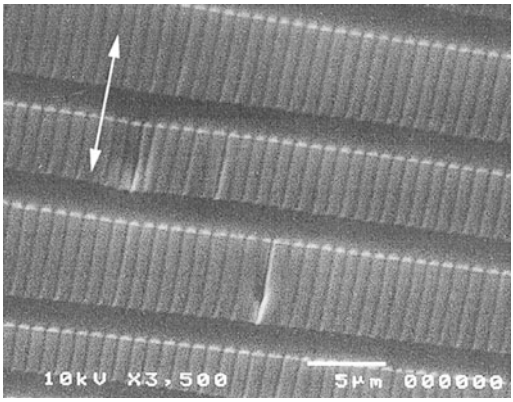

Fig. 11.6 Uniaxially stretched (along the *white arrow*) oxidized silicone rubber showing distinct perpendicular cracks through the silica-like surface layer. A regular buckling pattern appears between the cracks. The buckling process is reversible. Reprinted from Ref. [16] with kind permission of © Elsevier (2001)

occur during sample handling after the treatment. Surface buckling patterns appear due to the modulus mismatch between the surface layer and the bulk [17, 31]. An example of reversible buckling pattern, seen between the surface cracks created by extending an oxidized silicone rubber is shown in Fig. 11.6. The pattern is a result of a compressive stress on the material between the cracks, whereas the material below the cracks is readily elongated in the axial direction. Such buckling patterns have received significant attention during recent years and are further discussed in the next section (see also Chap. 3).

11.3.4 Hierarchical Surface Patterning of Silica-Like Layers

The buckling of a silicone surface as a result of the formation of silica-like layers has opened up a variety of new applications such as tunable gratings, biocompatible topographic matrices for cell alignment, microfluidic sieves, stretchable conductors and integrated stress sensors [28, 32, 33]. They all involve the creation of complex

patterns on silicones utilizing the difference in modulus or thermal expansion coefficient between the silica-like layer and the bulk silicone rubber. The instability is generally generated by a pre-stretch release or a temperature change, creating surface undulations in the form of buckles with defined wavelengths. The patterns on combined UV/ozone-treated silicone rubber have exhibited hierarchical buckles or folds, from a few nanometres up to one millimeter in wavelength spanning almost five orders of magnitude in dimension [28] (see also Chap. 3). The wavelength of the buckling increases linearly with increasing oxidation time. Surfaces with an anisotropic hydrophobicity can be obtained, which is promising for applications requiring directional variation of physical properties, such as controlled wetting, adhesion and friction [34].

Superhydrophobic properties can be obtained by deposition of fluorocarbons on the formed patterns [35]. Also two-dimensional buckling patterns can be generated using biaxially pre-stretched silicone rubber. The morphological characteristics of the buckling pattern (i.e. wavelength and amplitude) can be controlled by treatment conditions and stretch release rate [36]. Vapor deposition of metals onto thermally expanded silicone rubber also yielded ordered structures after cooling, when the compressive stress in the metal film was relieved by buckling with a uniform wavelength of 20 to 50 μm [37]. Not only oxidative treatment in the gas phase can be used for surface patterning. Micro-scale buckling patterns on silicone rubber were introduced by immersion of silicone rubber samples into H_2SO_4/HNO_3 solutions [38]. The periodicity could be tuned by adjusting the immersion time and by adjusting the concentration of H_2SO_4/HNO_3 in the solution. Recent work strives to identify the parameters determining the technologically important, pure buckled, crack-free topography [39]. By systematic variation of plasma dose and oxygen pressure, four different topographies were obtained: flat, cracked, buckled and cracked and crack-free buckled. The fourth topography is desired for the preparation of large surfaces with highly perfect periodicity, with wavelengths down to 250 nm. These materials are used as feedback resonators of organic lasers [39].

11.4 Hydrophobic Recovery

After the end of the oxidative treatment, the hydrophobicity starts to recover towards the initial state. As example, the hydrophobic recovery of a peroxide-crosslinked silicone rubber, filled with aluminum trihydrate and silica, after exposure to 1 h of corona discharges is shown in Fig. 11.7. Directly after exposure the advancing and receding contact angles are reduced to 40° and 27°, respectively; but gradually increase with storage time. The advancing contact angle did not recover completely during the time frame of the experiment. Both the corona exposure and the subsequent hydrophobic recovery were performed in dry air conditions at ambient temperature. The hydrophobic recovery in this instance can be explained by the reorientation of silanol groups from the surface towards the bulk and/or by the condensation of silanol groups during removal of water [7], a characteristic reaction unique to siloxanes. The recovery is also influenced by migration of silicone

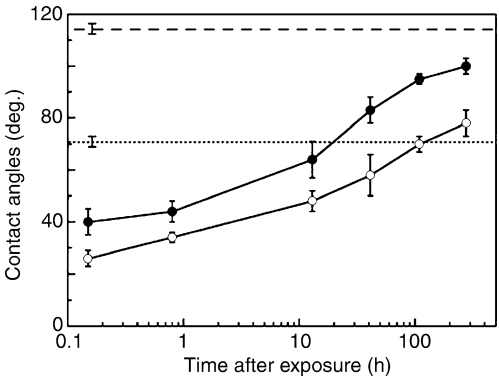

Fig. 11.7 Hydrophobic recovery of silicone rubber after exposure to 1 h corona discharges. Advancing (*filled circles*) and receding (*open circles*) water contact angles. The initial values are indicated by the *dotted lines*

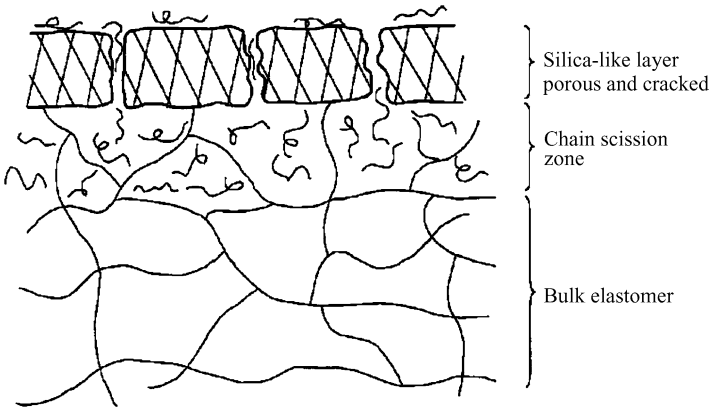

Fig. 11.8 Schematic cross-section showing the different zones that are produced on a silicone rubber as a result of exposure to an oxidizing surface treatment. The uppermost surface is affected mostly, and it is converted into a silica-like layer. Beneath this layer, scission of polymer chain occurs, induced by UV radiation and migrating reactive species. The silica-like layer is porous, or cracked, and thus silicone oligomers (produced in situ or as residues from the polymerization) can migrate through it and be adsorbed at the air-polymer interface. Reprinted from Ref. [41] with kind permission of © Elsevier (2000)

oligomers from the bulk. The similarity in hydrophobic recovery rate of oxidized silicone rubber aged in different atmospheres [23] and aged in a clean room environment [40] excluded contamination through adsorption from the atmosphere as a cause.

Once the silica-like layer is formed, the situation (sketched in Fig. 11.8) becomes more complex [17, 27, 41]. Direct contact with reactive species and oxygen results in the formation of the hydrophilic silica-like top layer, as previously discussed. Beneath this layer, a zone of chain scission is present. Siloxane oligomers formed in this zone, or already present from the manufacturing process, slowly migrate through pores in the silica-like layer or diffuse rapidly through cracks to the surface where they are adsorbed at the air-polymer interface and restore the initial

hydrophobicity. This proposed recovery process has later been supported by theoretical work where the effects of diffusion of migrating siloxanes onto the oxidized surface were considered [42]. These results indicate that the faster hydrophobic recovery observed on fluorinated silicone rubber was due to the faster rate of diffusion of fluorinated oligomers than of PDMS oligomers. The mechanical properties of the silica-like layer acting as a diffusion barrier are thus an important factor determining the hydrophobic recovery rate. Once cracking occurs, a rapid transport of oligomers through these cracks follows, resulting in an instantaneous recovery of hydrophobicity [16, 17]. Since this cracking can be a rather stochastic process, this is one of the complicating factors in the design of a silicone rubber with slow, or at least reproducible, hydrophobic recovery.

The activation energy of the hydrophobic recovery has been calculated by a number of researchers. The activation energy decreased from 40 to 31 kJ mol^{-1} when the corona discharge density was increased from 6 to 12 kV [41], and from 57 to 36 mol^{-1} when the corona exposure time was increased from 0.3 to 200 h at constant voltage of 20 kV [17]. By increasing discharge intensity or exposure time, the activation energy of the recovery is thus reduced. This has been attributed to regeneration of migrating siloxanes. Similar rates of hydrophobic recovery, even after extraction of the mobile silicone oligomers, showed that the in-situ generation of these is sufficient for hydrophobic recovery [41]. It has been suggested that the hydrophobic recovery can be reduced by grafting the plasma-treated silicone rubber with e.g. methacrylate copolymer or poly(ethylene glycol) [43–45]. However, the low surface tension of the migrating silicone oligomers means that they have a tendency to adsorb on top of the grafted-polymers during storage under ambient conditions, thereby increasing the hydrophobicity.

11.5 Applications

11.5.1 Soft Lithography

Soft lithography is a collection of techniques involving printing, molding and embossing using elastomeric stamps allowing the rapid prototyping of micro-scale and nano-scale structures on planar, curved, flexible and soft substrates [46, 47]. In these applications, silicone rubber offers a number of attractive features such as low shear modulus and low tensile modulus that enable it to conform easily to surfaces and achieve atomic-level contact, non-toxicity and optical transparency at a relatively low cost, whilst intrinsic hydrophobicity can be reduced by exposure to partial discharges [48]. Thus, after surface oxidation, PDMS adheres and seals reversibly in its intrinsic state as well as irreversibly to many substrates. In combination with the ease of processing, it was foreseen that the use of PDMS in these applications will shift from the demonstration of components and devices to the development of fully functional structures [49]. By using composite stamps consisting of a more densely cross-linked PDMS layered on a softer elastomeric PDMS, the capability

of soft lithography was extended down to the 50–100 nm range [50]. Since the oxidation and hydrophobic stability of such stamps are controlled by the degree of cross-linking (i.e. the amount of vinyl-groups and hydro-silane used in RTV formulations), this can be useful for the control of both loss and recovery of hydrophobicity, as well as for sealing quality. However, plasma-oxidation should be used with care in order to avoid both the deformation of the fine regular patterns during the build-up of the silica-like layer and the surface cracking. The transfer of silicone oligomers from the silicone rubber stamp to the substrate should also be considered in microcontact printing, since they can adversely affect the chemical homogeneity of the patterned areas, which may in turn influence their intended function [51]. The free oligomers which are transferred onto the surface of the stamp can also act as an ink in conventional microcontact printing [52]. The transferred monolayer is then oxidized into a silica-like structure which is etch-resistant. The patterns can thus be transferred to the substrate via wet or dry etching. A 'Marathon test' showed that the stamp could be repeatedly used for transfer. The recommended setting for microcontact printing of proteins using oxygen-plasma treatment (13.56 MHz) was at 0.26 mbar of oxygen and 40 W of power for 1 min [47].

11.5.2 Microfluidics

Silicone rubber has a long history in a large variety of biological and medical applications, such as microfluidic devices, thanks to its biocompatibility and low toxicity [53]. However, the hydrophobic surface makes it difficult to transfer aqueous solutions, or to transport such solutions through capillaries. A reduction of hydrophobicity improves its wettability by aqueous solutions and reduces the risk of nucleation of air bubbles in the micro-channels [54]. This can be accomplished by exposing the silicone rubber surfaces to an oxidizing treatment, usually RF or MW plasmas in oxygen, argon, air or nitrogen. The hydrophilicity can be maintained for several weeks if the material is stored in deionized water after plasma treatment [55]. The hydrophilic stability after surface oxidation can also be improved by chemical derivatization with (aminopropyl)triethoxy silane [56]. The oxidized silicone rubber surface showed significant ageing. Within 24 h the electro-osmotic flow rate dropped by 75 % compared to that of the freshly oxidized surface. The amine-modified surfaces also showed ageing effects, but they were much less. After 24 h, the migration rate decreased by only 5 %, demonstrating that amine modification greatly reduced the rate of hydrophobic recovery. Permanent adhesion between silicone rubber and other silica-like materials, such as glass, silicon and silicone, is essential for microfluidic devices. Ideally, fluctuations in the plasma-treatment conditions should not significantly influence the quality of the adhesion under industrial-scale conditions. The influence of process parameters, such as power and treatment time on the quality of the adhesion between glass and air-plasma-treated silicones has been systematically evaluated [57] as illustrated in Fig. 11.9.

The best quality of adhesion ($QA = 2$) was obtained after creation of sufficient functional groups but before the formation of the brittle silica-like layer which could

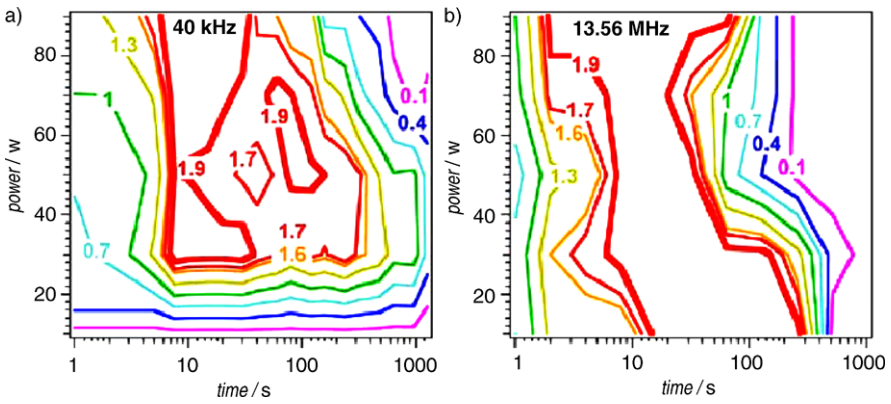

Fig. 11.9 Contour plots showing the quality of adhesion (QA) as a function of applied power and treatment-time of an air-plasma at 0.35 mbar pressure. RF plasmas were generated at (**a**) 40 kHz or (**b**) 13.56 MHz. Maximal adhesion at $QA = 2$; no permanent adhesion at $QA = 0$. Reprinted from Ref. [57] with kind permission of © Springer (2011)

result in a lack of permanent adhesion ($QA = 0$). The stability of the treatment could then be optimized with respect to treatment time, power, and the type of plasma used. The best adhesion was obtained using 13.56 MHz-plasma at an intermediate time and intermediate power. The contours corresponding to $QA = 1.7$–1.9 in Fig. 11.9 indicate conditions that are feasible for fabrication procedures. These settings are similar to those used by Qin et al. [47].

11.5.3 Outdoor Insulation

Silicone rubber is used as a high-voltage outdoor insulation material, as an alternative to porcelain [3, 58, 59]. The most common use is as housing material on a load-bearing structure of e.g. glass-fibre-reinforced epoxy in composite insulators. The main benefits of the composite insulators, compared to those of porcelain, are their lower weight and their hydrophobic surface properties. On hydrophilic porcelain, water readily forms a continuous film. In the presence of contamination, leakage currents develop, which may lead to a flashover of the insulator. The hydrophobic surface properties of silicone rubber prevent the formation of these continuous water films, and thus reduce the leakage currents and the risk of surface flashover. During severe weather conditions, partial discharges may still be initiated, thereby reducing the hydrophobicity. However, the hydrophobicity is gradually restored, provided that sufficient time elapses without further electrical discharge activities.

Hydrophobicity can also be lost by the heavy and rapid deposition of pollutants on the insulator surface, but a hydrophobic recovery will also be observed in such cases (Fig. 11.10). The most important recovery mechanism is the migration of mobile siloxane oligomers from the rubber to the surface of the insulator, impregnating

Fig. 11.10 Silicone rubber outdoor insulation after 10 years of service in a high-voltage substation located close to the sea. The pollution has been impregnated by mobile siloxanes rendering a hydrophobic surface

the pollution layer. A temporary reduction in hydrophobicity under winter conditions has been reported [60], with a combination of continuous pollutant deposition, low ambient temperature and poor washing by precipitation. This increases the risk of partial discharges. A suitable amount of flame-retarding filler (aluminum trihydrate) is commonly used to protect the silicone rubber during these critical periods when the hydrophobicity is reduced.

The effect of an electrical discharge on the silicone rubber depends on the intensity. Low-intensity corona results in the formation of silica-like surface layers, as discussed in previous sections. High-energy discharges lead to surface erosion, as well as to thermal depolymerization of the PDMS [61]. If the silicone rubber is filled with aluminum trihydrate, mullite ($3Al_2O_3{\cdot}2SiO_2$) is formed, together with amorphous silica [62, 63]. Amorphous silica is both a decomposition product of PDMS and a reinforcing filler in the silicone rubber. Electrical discharges in air also lead to production of acids like NO_x, HNO_2 and HNO_3 that can dissolve in any water present on the silicone rubber surface. These acids may accelerate the degradation processes, for example by hydrolysis of the polymer in the surface layer [64].

The influence of UV radiation, originating from the sunlight, on hydrophobicity is still under discussion. Silicone rubber line insulators were energized in a field test in a coastal environment in Sweden [65, 66], and it was observed that the insulators were less hydrophobic during cold/wet conditions (winter, autumn) than in the summer. In addition, the silicone rubber sheds were less hydrophobic on the parts that were shielded from direct sunlight [66]. Thus a positive effect of UV radiation on the hydrophobicity was observed. In another study, silicone rubber composite insulators were removed after a 15-year service on a 400 kV transmission line in a coastal region in the UK [67], with no indication of any reduction in performance in service. Contact angle measurements using water showed that these insulators were mainly hydrophobic with contact angles between 70 and 100°. The side of the insulators that faced the sun and prevailing winds from the sea aged more rapidly, as shown by a higher degree of surface oxidation and a lower hydrophobicity. However, no cracks were observed on the rubber surfaces, indicating the absence of a brittle silica-like layer. Electrical testing showed that aged insulators exhibited higher leakage currents over the surfaces during wet conditions than unaged insu-

lators. The average ac flashover/resistance voltage was reduced by 5 % and 10 % after service. These reductions were not, however, considered significant given the scatter of the results. Based on these results, the role of solar radiation appears to be critical for the non-uniform ageing and should be taken into consideration in the prediction of long-term operational performance [67].

11.6 Outlook

In this chapter we described the mechanisms behind the loss and recovery of hydrophobicity of silicone rubber after exposure to oxidative surface treatments, such as UV irradiation, corona or plasma. These treatments are commonly used to reduce the hydrophobicity or may occur during high-voltage applications where silicone rubber is used as an outdoor insulation material. In the initial step, polar groups are introduced into the surface region, mainly in the form of silanol (Si-OH) groups. The high segmental mobility of the network readily allows reorientation of these groups, depending on the environment. This initial state is desirable for further surface functionalization reactions. The oxidation then proceeds towards a vitrified silica-like surface layer.

During recent years, the properties of these silica-like surface layers have been intensively studied. The formation of complex buckling patterns, formed by the mechanical stress difference between the silica-like layer and the rubbery bulk opens the way to a wide range of new applications, such as gratings and flexible electronics (see Chap. 3). The silica-like layer is heterogeneous on a nanometer scale, where harder, more hydrophilic, silica-rich domains are surrounded by a softer, more hydrophobic matrix. This opens the way to new potential applications, where control of hydrophobicity on a nanometer scale is desirable. The main challenge is to address the hydrophobic recovery process after an oxidative surface treatment. In some applications, such as high-voltage outdoor insulation materials, this recovery is desired but in most other cases the hydrophobic recovery is undesirable. The most difficult task is to control or totally prevent the diffusion of mobile siloxane oligomers from the rubber to the oxidized hydrophilic surface. These species remain in the silicone rubber from the manufacturing process, and are also formed during the degradation/oxidation process. The most common methods of inhibiting hydrophobic recovery are careful extraction of the silicone rubber, which removes the extractable oligomers, the storage of oxidized silicone rubber in water directly after the treatment, or the grafting of polar species onto the oxidized surface. It is also desirable to avoid cracking of the silica-like surface layer, since cracks will promote the migration of silicone oligomers to the surface.

References

1. Owen MJ (1990) In: Ziegler J, Fearon FWG (eds) Silicon-based polymer science, a comprehensive resource. Advances in Chemistry Series, vol 224. Am Chem Soc, Washington

2. Thomas TH, Kendrick TC (1969) Thermal analysis of polydimethylsiloxanes. 1. Thermal degradation in controlled atmospheres. J Polym Sci 7:537–549
3. Hillborg H, Gedde UW (1999) Hydrophobicity changes in silicone rubbers. IEEE Trans Dielectr Electr Insul 6:703–717
4. Doyle CD (1958) Logarithmic thermal degradation of a silicone rubber in air. J Polym Sci 31:95–104
5. Kucera M, Jelinek M, Lankova J, Vesely K (1961) Termination in anionic polymerization of octamethylcyclotetrasiloxane. Formation of stable complexes on active sites. J Polym Sci 53:311–320
6. Kucera M, Lanikova J, Jelinek M (1961) Neutralization of residual catalyst in polydimethylsiloxane. Effect of neutralization on the thermal stability of the polymer. J Polym Sci 53:301–310
7. Morra M, Occhiello E, Marola R, Garbassi F, Humphrey P, Johnson D (1990) On the aging of oxygen plasma-treated polydimethylsiloxane surfaces. J Colloid Interface Sci 137:11–24
8. Fritz JL, Owen MJ (1995) Hydrophobic recovery of plasma-treated polydimethylsiloxane. J Adhes 54:33–45
9. Roth J, Albrecht V, Nitschke M, Bellman C, Simon F, Zschoche S, Michel S, Luthmann C, Grundke K, Voit B (2008) Surface functionalization of silicone rubber for permanent adhesion improvement. Langmuir 24:12603–12611
10. Efimenko K, Wallace WE, Genzer J (2002) Surface modification of Sylgard-184 poly(dimethyl siloxane) networks by ultraviolet and ultraviolet/ozone treatment. J Colloid Interface Sci 254:306–315
11. Graubner VM, Jordan R, Nuyken O, Schnyder B, Lippert T, Kötz R, Wokaun A (2004) Photochemical modification of cross-linked poly(dimethylsiloxane) by irradiation at 172 nm. Macromolecules 37:5936–5943
12. Quyang M, Yuan C, Muisener RJ, Boulares A, Koberstein JT (2000) Conversion of some siloxane polymers to silicon dioxide by UV/ozone photochemical processes. Chem Mater 12:1591–1596
13. Hillborg H, Tomczak N, Oláh A, Schönherr H, Vancso GJ (2004) Nanoscale hydrophobic recovery: a chemical force microscopy study of UV/Ozone-treated cross-linked poly(dimethylsiloxane). Langmuir 20:785–794
14. Song J, Duval JFL, Stuart MAC, Hillborg H, Gunst U, Arlinghaus HF, Vancso GJ (2007) Surface ionization and nanoscale chemical composition of UV-irradiated poly(dimethylsiloxane) probed by chemical force microscopy, force titration, and electro kinetic measurements. Langmuir 23:5430–5438
15. Oláh A, Hillborg H, Vancso GJ (2005) Hydrophobic recovery of UV/ozone treated poly(dimethylsiloxane): adhesion studies by contact mechanics and mechanism of surface modification. Appl Polym Sci 239:410–423
16. Hillborg H, Sandelin M, Gedde UW (2001) Hydrophobic recovery of polydimethylsiloxane after exposure to partial discharges as a function of crosslink density. Polymer 42:7349–7362
17. Hillborg H, Gedde UW (1998) Hydrophobic recovery of polydimethylsiloxane after exposure to corona discharges. Polymer 39:1991–1998
18. Beamson G, Briggs D (1992) High resolution XPS of organic polymers: the Scienta ESCA300 database. Wiley, Chichester
19. Tóth A, Bertóti I, Blazsó M, Bánhegyi G, Bognár A, Szaplonczay P (1994) Oxidative damage and recovery of silicone rubber surfaces. I. X-ray photoelectron spectroscopic study. J Appl Polym Sci 52:1293–1307
20. Alexander MR, Short RD, Jones FR, Michaeli W, Blomfield CJ (1999) A study of HMDSO/O_2 plasma deposits using a high sensitivity and -energy resolution XPS instrument. Curve fitting of the Si 2p core level. Appl Surf Sci 137:179–183
21. Grassie N, Scott G (1985) Polymer degradation and stabilization. Cambridge University Press, Cambridge
22. Dan E, Guillet JE (1973) Photochemistry of ketone polymers. X. Chain scission reactions in the solid state. Macromolecules 6:230–235

23. Hillborg H, Ankner JF, Gedde UW, Smith GD, Yasuda HK, Wikström K (2000) Crosslinked polydimethylsiloxane exposed to oxygen plasma studied by neutron reflectometry and other surface specific techniques. Polymer 41:6581–6863
24. Béfahy S, Lipnik P, Pardoen T, Nascimento C, Patris B, Bertrand P, Yunus S (2009) Thickness and elastic modulus of plasma treated PDMS silica-like surface layer. Langmuir 26:3372–3375
25. Graubner VM, Clemens D, Gutberlet T, Kötz R, Lippert T, Nuyken O, Schnyder B, Wokaun A (2005) Neutron reflectometry and spectroscopic ellipsometry studies of cross-linked poly(dimethylsiloxane) after irradiation at 172 nm. Langmuir 21:8940–8946
26. Mirley CL, Koberstein JT (1995) A room temperature method for the preparation of ultrathin SiO_x films from Langmuir–Blodgett layers. Langmuir 11:1049–1052
27. Bar G, Delineau L, Hafele A, Whangbo MH (2001) Investigation of the stiffness change in the indentation force and the hydrophobic recovery of plasma-oxidized polydimethylsiloxane surfaces by tapping mode atomic force microscopy. Polymer 42:3627–3632
28. Efimenko K, Rackaitis M, Manias E, Vaziri A, Mahadevan L, Genzer J (2005) Nested self-similar wrinkling patterns in skins. Nat Mater 4:293–297
29. Mills KL, Zhu X, Takayama S, Thouless MD (2008) The mechanical properties of a surface-modified layer on polydimethylsiloxane. J Mater Res 23:37–47
30. Bowden N, Huck WTS, Paul KE, Whitesides GM (1999) The controlled formation of ordered sinusoidal structures by plasma oxidation of an elastic polymer. Appl Phys Lett 75:2557–2559
31. Roucoules V, Ponche A, Geissler A, Siffer F, Vidal L, Ollivier S, Vallat MF, Marie P, Voegel JC, Hemmerlé J, Schaaf P (2007) Changes in silicone elastomeric surface properties under stretching induced by three surface treatments. Langmuir 23:13136–13145
32. Huck WTS, Bowden N, Onck P, Pardoen T, Hutchinson JW, Whitesides GM (2000) Ordering of spontaneously formed buckles on planar substrates. Langmuir 16:3497–3501
33. Huck WTS (2005) Artificial skins-Hierarchical wrinkling. Nat Mater 4:271–272
34. Chung JY, Youngblood JP, Stafford CM (2007) Anisotropic wetting on tunable micro-wrinkled surfaces. Soft Matter 3:1163–1169
35. Tsougeni K, Tserepi A, Boulousis G, Constantoudis V, Gogolides E (2007) Control of nanotexture and wetting properties of polydimethylsiloxane from very hydrophobic to superhydrophobic by plasma processing. Plasma Process Polym 4:398–405
36. Moon MW, Vaziri A (2009) Surface modification of polymers using a multi-step plasma treatment. Scr Mater 60:44–47
37. Bowden N, Brittain S, Evans AG, Hutchinson JW, Whitesides GM (1998) Spontaneous formation of ordered structures in thin films of metals supported on an elastomeric polymer. Nature 393:146–149
38. Wang JH, Chen CF, Ho JR, Shih TK, Chen CC, Whang WT, Yang JY (2009) One-step fabrication of surface-relief diffusers by stress-induced undulations on elastomers. Opt Laser Technol 41:804–808
39. Görn P, Wagner S (2010) Topographies of plasma-hardened surfaces of poly(dimethylsiloxane). J Appl Phys 108:093522
40. Owen MJ, Gentle M, Orbeck T, Williams DE (1988) Dynamic wettability of hydrophobic polymers. In: Andrade JD (ed) Polymer surface dynamics. Plenum Press, New York
41. Kim J, Chaudhury MK, Owen MJ (2000) Hydrophobic recovery of polydimethylsiloxane elastomer exposed to partial electrical discharge. J Colloid Interface Sci 226:231–236
42. Kim J, Chaudhury MK, Owen MJ (2006) Modeling hydrophobic recovery of electrically discharged polydimethylsiloxane elastomers. J Colloid Interface Sci 293:364–375
43. Donzel C, Geissler M, Bernard A, Wolf H, Michel B, Hilborn J, Delamarche E (2001) Hydrophilic poly(dimethylsiloxane) stamps for microcontact printing. Adv Mater 13:1164–1167
44. Pinto S, Alves P, Matos CM, Santos AC, Rodriques LR, Teixeira JA, Gil MH (2010) Poly(dimethylsiloxane) surface modification by low pressure plasma to improve its characteristics towards biomedical applications. Colloids Surf B, Biointerfaces 81:20–26
45. Roth J, Albrecht V, Nitschke M, Bellman C, Simon F, Zschoche S, Michel S, Luthmann C, Voit B, Grundke K (2011) Tailoring the surface properties of silicone elastomers to improve adhesion of epoxy topcoat. J Adhes Sci Technol 25:1–26

46. Xia Y, Whitesides GM (1998) Soft lithography. Angew Chem, Int Ed Engl 37:551–575
47. Qin D, Xia Y, Whitesides GM (2010) Soft lithography for micro- and nanoscale patterning. Nature Protocols 5:491–502
48. Semlyen JA, Clarson SJ (1993) Silicone polymers. Prentice-Hall, Englewood
49. Whitesides GM (2006) The origins and the future of microfluidics. Nature 442:368–373
50. Odom TW, Love JC, Wolfe DB, Paul KE, Whitesides GM (2002) Improved pattern transfer in soft lithography using composite stamps. Langmuir 18:5314–5320
51. Langowski BA, Uhrich KE (2005) Oxygen plasma-treatment effects on silicone transfer. Langmuir 21:6366–6372
52. Kim JH, Hwhang HS, Hahm SW, Khang DY (2010) Hydrophobically recovered and contact printed siloxane oligomers for general-purpose surface patterning. Langmuir 26:13015–13029
53. Makamba H, Kim JH, Lim K, Park N, Hahn JH (2003) Surface modification of poly(dimethylsiloxane) microchannels. Electrophoresis 24:3607–3619
54. Martin BD, Brandow SL, Dressick WJ, Schull TL (2000) Fabrication and application of hydrogel stamps for physisorptive micro contact printing. Langmuir 16:9944–9946
55. Tan SH, Nguyen NT, Chua YC, Kang TG (2010) Oxygen plasma treatment for reducing hydrophobicity of a sealed polydimethylsiloxane microchannels. Biomicrofluidics 4:032204
56. Wang B, Chen L, Abdulali-Kanji Z, Horton JH, Oleschuk RD (2003) Aging effects on oxidized and amine-modified poly(dimethylsiloxane) surfaces studied with chemical force titrations: effects on electroosmotic flow rate in microfluidic channels. Langmuir 19:9792–9798
57. Chau K, Millare B, Lin A, Upadhyayula S, Nuñez V, Xu H, Vullev VI (2011) Dependence of the quality of adhesion between poly(dimethylsiloxane) and glass surfaces on the composition of the oxidizing plasma. Microfluid Nanofluid 10:907–917
58. Vlastós A, Gubanski SM (1991) Wettability of naturally aged silicone and EPDM insulators. IEEE Trans Power Deliv 5:1527–1535
59. Kim SH, Cherney EA, Hackam R (1990) Loss and recovery of hydrophobicity of RTV silicone rubber insulator coatings. IEEE Trans Power Deliv 5:1491–1500
60. Li C, Zhao L, Xiong J, Zhang S, Yao J (2008) Influence of seasons on hydrophobicity of silicone rubber insulators in semi-wet warm-temperature zone of China. IEEE Trans Dielectr Electr Insul 15:1081–1088
61. Gustavsson TG, Gubanski SM, Hillborg H, Karlsson S, Gedde UW (2001) Ageing of silicone rubber under ac and dc voltages in a coastal environment. IEEE Trans Dielectr Electr Insul 8:1029–1039
62. Kumagai S, Yoshimura N (2004) Polydimethylsiloxane and alumina trihydrate system subjected to dry-band discharges or high temperature. Part 1. Chemical structure. IEEE Trans Dielectr Electr Insul 11:691–700
63. Kumagai S, Yoshimura N (2004) Polydimethylsiloxane and alumina trihydrate system subjected to dry-band discharges or high temperature. Part 2. Electrical insulation. IEEE Trans Dielectr Electr Insul 11:701–707
64. Sigmond RS, Sigmond T, Goldman A, Goldman M (1991) On the role of water in the ageing of polymers in air-insulated electrical systems. IEEE Trans Electr Insul 26:770–775
65. Gubanski SM, Vlastós AE (1990) Wettability of naturally aged silicone and EPDM composite insulators. IEEE Trans Power Deliv 5:1527–1535
66. Sörqvist T, Vlastós AE (1997) Outdoor polymeric insulators long-term exposed to HVDC. IEEE Trans Power Deliv 12:1041–1048
67. Rowland SM, Robertson J, Xiong Y, Day RJ (2010) Electrical and material characterization of field-aged 400 kV silicone rubber composite insulators. IEEE Trans Dielectr Electr Insul 17:375–383

Chapter 12
Surface Analysis of Silicones

Stuart Leadley, Lesley-Ann O'Hare, and Christopher McMillan

12.1 Introduction

Many of the desirable performance characteristics of silicones may be related to their surface properties (see Chap. 1). For example, information on the chemistry and structure of silicone surfaces is essential to understanding their behavior in the areas of adhesion/release, bio-compatibility, wetting, mixing and packaging. Although a surface is defined as the boundary of a solid, for many, if not most practical applications, the "surface" extends to some limited depth below the outermost layer of atoms. In applied studies, the problem at hand defines where the surface ends and the bulk begins. Thus, the "surface" can be as little as a few angstroms thick or as many as several microns, depending on the information required or the analysis methods available.

In many cases, an analytical technique routinely used for bulk analysis may be employed for surface analysis when applied in a suitably constrained operating regime. This may be achieved through grazing incidence of the probe or signal (grazing incidence X-ray scattering, Fourier transform—reflection absorption infrared spectroscopy etc.), a surface-enhanced signal (surface-enhanced Raman spectroscopy) or through the ability to differentiate the signal/chemistry of the surface from that of the bulk (solid-state nuclear magnetic resonance spectroscopy, sum frequency generation vibrational spectroscopy). The analyst who sees a wide variety of materials and systems will typically apply multiple techniques to gather the information needed through the depth required. Frequently, it is a combination of surface and bulk analysis techniques that provides greater understanding of the behaviors of silicone systems.

S. Leadley
Dow Corning Europe, Seneffe, Belgium

L.-A. O'Hare · C. McMillan (✉)
Dow Corning Corporation, Midland, MI, USA
e-mail: chris.mcmillan@dowcorning.com

M.J. Owen, P.R. Dvornic (eds.), *Silicone Surface Science*, Advances in Silicon Science 4,
DOI 10.1007/978-94-007-3876-8_12,

Surface chemical and structural probes have been created from particle beams (photons, electrons, ions and neutrals) and from fields (thermal, electric, magnetic and acoustic). The detected signals arise from transmission, scattering or emission of particles or physical deflections caused by force fields. The growing breadth of techniques available for surface analysis is indicated by schematics and tables of methods and by the increase in chapters that have been assembled by reviewers [1–5]. One of the most comprehensive lists of surface analysis techniques has been compiled by the UK Surface Analysis Forum [6], which lists over eighty techniques and their various acronyms. Many of the techniques are quite specialized, requiring equally specialized probe sources, detection and environment control equipment. These can entail constraints that make them expensive and/or difficult to access, or difficult to apply to the range of surfaces an analyst may be asked to investigate. In addition, many are best suited to a limited range of materials and are not commonly applied to silicones. There are few laboratories that can afford the high cost of maintaining enough techniques to completely characterize a surface, but fortunately a limited selection of broadly applicable techniques can supply a sufficient amount of information to solve many problems faced by a surface analyst confronting silicones.

Surface analysis techniques can provide information regarding structure (morphology), chemical composition and surface physical properties. Although many of the surface analytical techniques would provide one of these types of information, there are some overlaps; e.g. chemical probes may reveal structure. Thus, it is useful to have some reference providing the information accessible by surface analysis. As a result, surface analysis techniques have been organized in a variety of different ways, using various methods to illustrate their basic mechanisms, strengths and limitations as well as how they are commonly applied. For example:

- simple schematics that organize techniques according to the input probe vs. output signal [1];
- by sampling depth of the technique or surface sensitivity [3, 7];
- by the type of information obtained [3, 5, 8] (elemental, structural, molecular, chemical state);
- by typical application or problem to be solved [9].

The graphic in Fig. 12.1 is one example, which illustrates the detection range (elemental detection limit) plotted against analytical spot size for a range of commercially available analytical techniques. This shows that the mass spectrometry-based analysis techniques are orders of magnitude more sensitive than others for a given analysis spot size, while electron beam-based probe techniques lead in spatial resolution.

Another example, shown in Fig. 12.2 [10], illustrates the relationship between spatial resolution and the surface chemical information available.

Despite the wide range of surface analytical techniques available, the subset of techniques that is typically applied to silicone polymers is defined by its ability to analyze generally non-conductive, amorphous materials comprised of low atomic number elements. The higher atomic number of silicon allows some techniques that

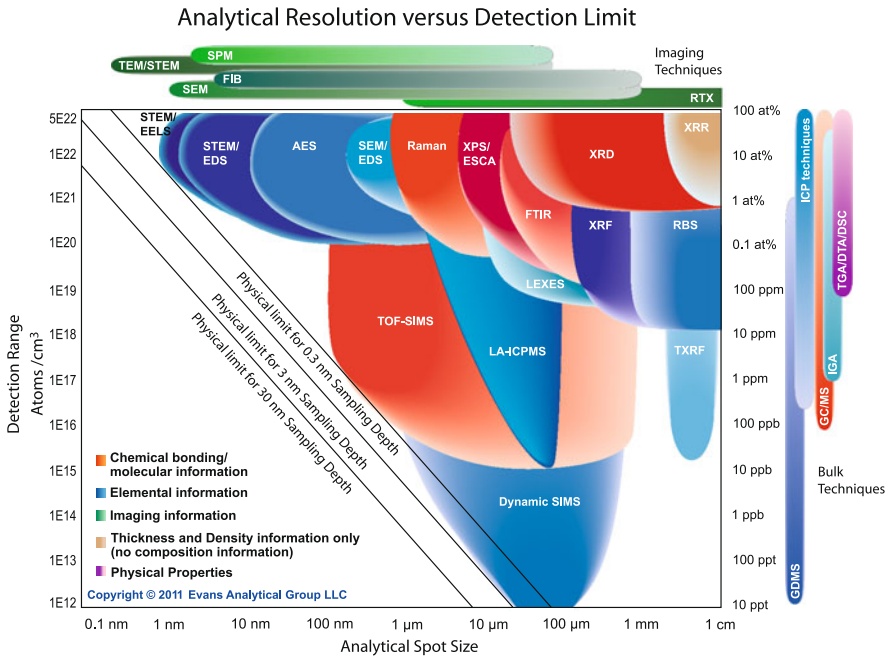

Fig. 12.1 Chart of analysis spot size vs. detection range by technique. Reproduced from Ref. [7] with kind permission of © Evans Analytical Group (2011)

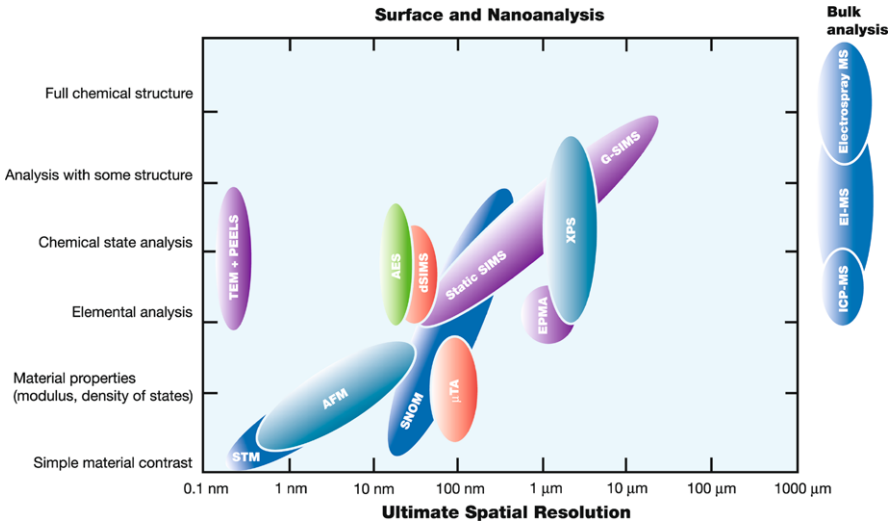

Fig. 12.2 Chemical functionality versus spatial resolution compiled for a range of surface analytical techniques. Reproduced from Ref. [10] with kind permission of the controller of HMSO and the Queen's Printer for Scotland—© Crown (2011)

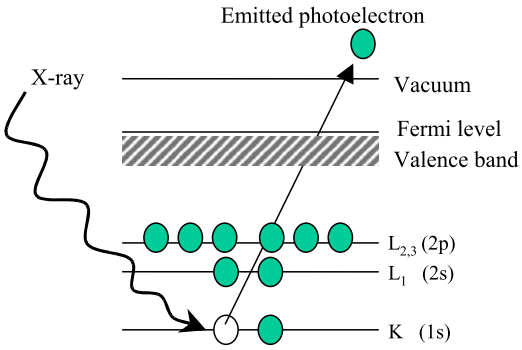

Fig. 12.3 Schematic indicating emission of a photoelectron from an atom irradiated with X-ray photon. The energy of the ejected electron identifies the chemical nature and environment of the atom

differentiate on that basis to be used a little more effectively than they might be for general organic polymers. Even within this subset there are many more techniques than can be done justice to in this chapter. For example, infrared (IR) spectroscopy is an outstanding method for obtaining molecular information that is widely used in the surface analysis of silicone-based materials. IR reflection modes probe from one to several microns into the surface depending on the sample, substrate, wavelength and angle of incidence. While this is orders of magnitude less surface sensitive than X-ray photoelectron spectroscopy (XPS) or secondary ion mass spectrometry (SIMS), sub-monolayers of adsorbates can be identified. For more information on IR spectroscopy methods we refer the reader to references [11–16], with specific application of IR spectroscopy to silicones being discussed here [17].

The focus of this chapter, however, is on a limited number of techniques that provide structural and chemical information.

12.2 X-ray Photoelectron Spectroscopy

Chemical information about the top few nanometers of silicone surfaces is provided most extensively through X-ray photoelectron spectroscopy (XPS). XPS, also known as ESCA (Electron Spectroscopy for Chemical Analysis) identifies the atoms comprising the top few nanometers of a surface. This is done by measuring the kinetic energy and intensity of electrons emitted on absorption of an X-ray photon, as shown schematically in Fig. 12.3.

The greatest strength of XPS is its very high surface sensitivity. Additionally, the energy resolution obtained in XPS is sufficient not only to provide the elemental identification of atoms at the surface, but also their chemical states—an invaluable advantage when there is a need to differentiate siloxanes from silica. Matrix effects on signal yields are moderate and semi-quantitative results can be routinely obtained. Imaging modes of operation in modern instruments permit mapping of elements and bond states with spatial resolutions on the order of a few microns. Elemental concentration vs. depth profiles can be obtained by sputtering surfaces with an ion beam and analyzing the newly exposed surface in repeated cycles. In this way, the near-surface concentration profile of an adhesion promoter in a silicone

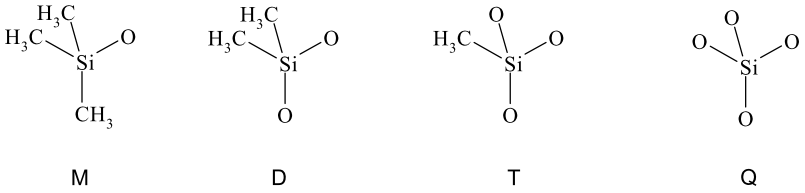

Fig. 12.4 Representations of various siloxy units encountered in polysiloxanes

sealant might be determined based on elemental differences. Until fairly recently, sputter depth profiling has incurred a loss of chemical information due to destruction of sub-surface bonds from high energy ion impacts. Recent advances in ion guns based on heavy cluster ions have seen the achievement of deep sputtering profiles of organic materials where the bonding information is maintained in nearly pristine form throughout [18, 19]. Details of XPS instrument design and operation will not be discussed here, but the reader is directed to the book by Watts and Wolstenholme [20] for a general overview. However, the application of XPS to silicones and fluorosilicones is specifically discussed in greater detail in this chapter.

In a manner similar to the chemical shift in NMR, an electron binding energy shift in XPS can identify the atoms or functionalities attached to the atom under investigation, with the added benefit of analyzing only the surface of the material. The application of XPS in the study of silicones has been mentioned in the literature as far back as the mid 1970s [21]. In the 1980s, it was used to try to provide understanding around the relationship between surface energy and elemental composition [22], but it was not until the 1990s that fundamental understanding of how the silicon chemistry varied with processing parameters was studied more systematically [23]. Since the initial reference in the frequently used XPS spectrum database of Beamson and Briggs [24], where the high-resolution C 1s, O 1s and Si 2p core level spectra of polydimethylsiloxane (PDMS) and polymethylphenylsiloxane (PMPS) were presented, progress has been made on defining the Si 2p binding energy values for the different 'oxidation states' of silicon in silicones.

When discussing 'oxidation states' of silicon in silicone materials it is useful to use notation to identify silicon atoms. A useful notation and abbreviation of complex silicone structures takes advantage of the number of oxygen atoms around the silicon atom in a *siloxy* unit [25]. This notation uses the letters M (mono), D (di), T (tri) and Q (quaternary) to represent siloxy units where the silicon atom is linked to one $[(CH_3)_3SiO_{1/2}]$, two $[(CH_3)_2SiO_{2/2}]$, three $[(CH_3)SiO_{3/2}]$, or four $[SiO_{4/2}]$ oxygen atoms, respectively (Fig. 12.4). Fractions are used in this notation to take into account an equal share of an oxygen atom with adjacent siloxy monomeric units.

Identification of chemical environment can be relatively straightforward for carbon, where the C 1s core level often has clearly defined features. This is due to binding energy shifts occurring over a relatively wide binding energy range. However, in the case of silicon, the range of siloxy chemical environments often makes it difficult to resolve distinct features by curve fitting the Si 2p core level. In addition, the binding energy shift for the substitution of each methyl group with an

oxygen atom (i.e. each new Si-O group) is estimated at 0.65 eV. By comparison, the effect of each additional C-O bond is to increase the binding energy shift by 1.5 eV. Therefore, with the exception of elemental silicon and its oxide having very clearly defined components, it is often difficult to obtain detailed information about the chemical environment of silicon atoms in a material. However, it is usually possible to distinguish silicon in 'organic' silicone polymers from 'inorganic' silicate forms [26, 27]. In the first of these papers, although discussing PDMS as the substrate, even the 'as received' substrate contained a second component, at higher binding energy than for PDMS, suggesting the presence of a more oxidized silicon form. The binding energy of this component has been reported as 103.4 eV, in the relevant range for a silicate.

Curve fitting the Si 2p core level is further complicated by the presence of two signals for each chemical state, whereas carbon has only one. In Si 2p, these are associated with Si $2p^{3/2}$ and Si $2p^{1/2}$ electron spin states. Beamson and Briggs [24] fitted a doublet to the Si 2p core level obtained from analysis of PDMS and PMPS D siloxy units. However, no literature was found that described fitting both the Si $2p^{3/2}$ and Si $2p^{1/2}$ spins to a system containing all the M, D, T and Q components. In general, curve fitting of the Si 2p core level acquired from silicon oxides (siloxy units) typically fits the peak using four components, with an increase in binding energy for the replacement of each methyl group by an additional oxygen atom [28].

Alexander et al. [29] fitted one synthetic peak for each of the M, D, T, Q components of a film obtained by plasma deposition of hexamethyldisiloxane. In their work, the positions of D (polydimethylsiloxane) and Q (quartz) were measured. The positions of M and T were estimated to be shifted by half the distance between D and Q, with full width at half-maximum (FWHM) constrained to be equal. Similarly, Hillborg et al. [30] resolved the Si 2p peak into D, T and Q components, although in this work the FWHM does not appear to have been constrained, nor is it possible to determine peak positions from the data provided in the publication. Roualdes et al. [31] used a fifth component (representing SiC_4), in curve fitting the Si 2p core level of polysiloxane deposits formed using 'soft plasma polymerization' of octamethyltrisiloxane, where a low energy per unit mass of monomer condition was employed.

Until the work described by O'Hare et al., in 2004 [32], and later refined in 2007 [33], a method for curve fitting XPS core levels for silicone compounds, using model systems with known chemistry, had not been reported. The first of these papers described the use of model compounds to unambiguously determine the binding energy position for the Si 2p core level components, depending on the number of oxygen atoms bonded to the silicon atom. For the sake of brevity, the reader is directed to the short communication [32] or thesis [34] for details of the procedure used. It was initially assumed that the binding energy positions of the C-Si bonds in the C 1s core level would be equal. However, on examination of a resinous material comprising D and T siloxy environments, the surface chemistry found by XPS was not in agreement with that obtained by ^{29}Si NMR. While minimizing the surface energy through orientation of the D siloxy species at the surface may be used to explain this, the possibility of the carbon in D, T and Q siloxy environments having

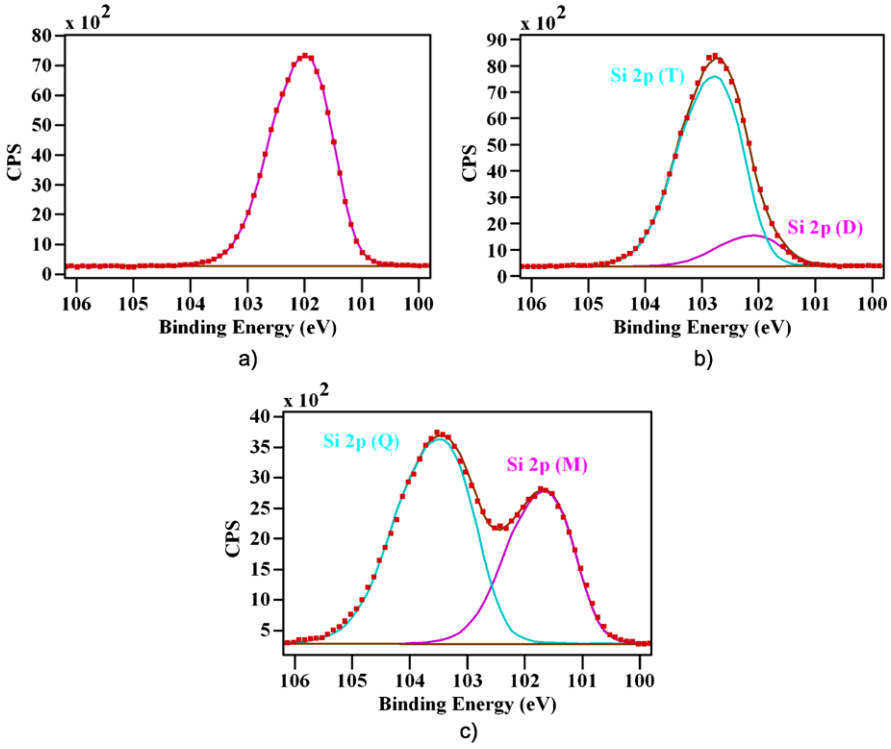

Fig. 12.5 Curve-fits for Si 2p core level spectra acquired from: (**a**) high molecular weight linear PDMS homopolymer (D Gum), (**b**) DT resin [$D_{0.14}$-$DOH_{0.12}$-$T_{0.74}$], and (**c**) MQ resin [$M_{0.47}$-$TOH_{0.15}$-$Q_{0.38}$]

different binding energy positions was investigated in the second paper [33]. An iterative method linking the relative concentration of each Si species with the number of associated carbon atoms, allowed for the differentiation between carbon atoms in the various siloxy environments.

The Si 2p core level spectra obtained for each material are presented in Fig. 12.5.

A summary of the binding energies of M, D, T and Q siloxy components of the O 1s, C 1s and Si 2p core levels determined from XPS analysis of the model compounds is presented in Table 12.1.

This work has confirmed experimentally, using model compounds of known composition, that the binding energy positions of Si $2p^M$, Si $2p^D$, Si $2p^T$ and Si $2p^Q$ are in good agreement with the estimated values presented in the literature. It has also demonstrated that binding energy shifts for components of the O 1s, and particularly C 1s core levels, can be assigned for siloxanes containing a range of siloxy environments.

In a recent review of the literature, this work is frequently cited in studies where the specific chemistry of multiple-oxidation state siloxanes needs to be understood. Further progress has been documented by Roth et al. [35], where Ag L_α radiation

Table 12.1 Binding energies for various siloxy units in the O 1s, C 1s and Si 2p core levels

	Binding energy (eV)		
	O 1s	C 1s	Si 2p
$M[(CH_3)_3SiO_{1/2}]$	532.0 ± 0.1	284.2 ± 0.1	101.4 ± 0.1
$D[(CH_3)_2SiO_{2/2}]$	532.0 ± 0.1	284.5 ± 0.1	102.0 ± 0.1
$T[(CH_3)SiO_{3/2}]$	532.5 ± 0.1	284.7 ± 0.1	102.8 ± 0.1
$Q[SiO_{4/2}]$	532.6 ± 0.1	na	103.2 ± 0.1

was used to gain access to the Si 1s core level. In this work, a PDMS reference material was used to determine the binding energy of this chemical environment, while for a PDMS sample modified by oxygen plasma, the remainder of the experimental envelope was curve-fitted by the addition of a component assigned to silicon in the Q siloxy form. No additional chemical states were estimated or determined, and it was not clear if silica had been analyzed to confirm the position assigned to Q units. However, the majority of works in the literature do not discuss siloxy chemistry in detail, instead they report the elemental composition of the surface under examination, details of the carbon chemistry (when relevant), or assignments to generic 'organosilicon' versus 'inorganic' silicon types. Specific examples follow in a later section.

Fluorosilicones are a very useful class of siloxanes comprised of fluorocarbon and siloxane groups from which polymers may be created that have exceptionally low surface energy and good performance at low and high temperatures. Most fluorosilicones are constructed such that the flexibility of a siloxane backbone enhances the low temperature performance of fluoropolymers. Since the surface energy of polymers is related to the size and packing of the hydrophobic groups, the increased size of CF_2 and CF_3 groups and their lower intermolecular interactions typically result in lower surface energies than can be achieved by non-fluorinated siloxanes (CH_3– pendant groups), which in turn are lower than alkanes (–CH_2–) [36, 37]. Thus, the already low surface energy and good solvent resistance of a siloxane are enhanced by appending fluorocarbon side chains. Hybrid fluorosilicones, defined as polymers with alternating siloxane and fluorinated components in the backbone, and reverse fluorosilicones, where the siloxane moiety is pendent to a fluorocarbon backbone (see Chap. 5), have been synthesized and characterized [38], but are not commercially employed at this time. Due to their unique material properties, fluorosilicones are employed to form fuel- and solvent-resistant seals with good low- and high-temperature performance for aerospace and automotive applications. Other applications include electronics (potting), anti-fouling, anti-grafitti and anti-smudge coatings, cosmetics and release liners for use with silicone pressure sensitive adhesives.

XPS analysis of fluorocarbon materials goes back at least to the early 1970's [39, 40], but the most definitive data were obtained later and published within a general database of XPS spectra of organic polymers from Beamson & Briggs [24]. Although the original book is out-of-print, this extensive database is available on compact disk [41] and comprises one of the most useful resources available for the interpretation or the XPS spectra of polymeric materials. The first commercialized

Fig. 12.6 Chemical structure of polymethyltrifluoropropyl-siloxane (PMTFPS)

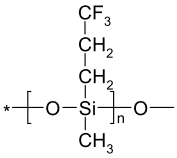

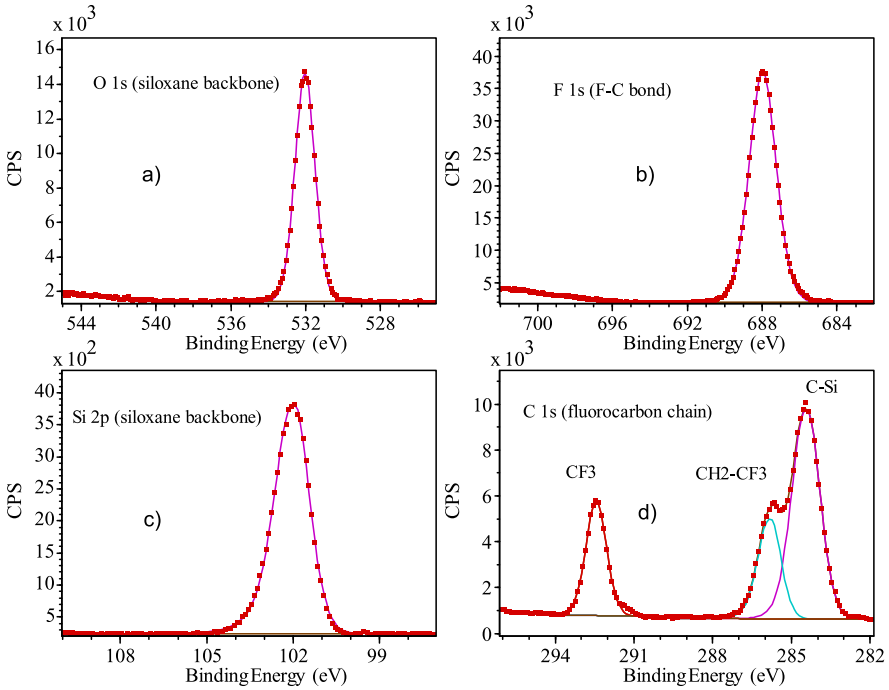

Fig. 12.7 High-resolution spectra of PMTFPS: (**a**) oxygen 1s, (**b**) fluorine 1s, (**c**) silicon 2p and (**d**) carbon 1s. Spectra have been charge corrected to position the C 1s (CH3-Si) at 284.4 eV. (Images courtesy of Dow Corning Corp.)

fluorosilicone, polymethyltrifluoropropylsiloxane (PMTFPS), is perhaps one of the most structurally similar to PDMS (as shown in Fig. 12.6), in that it contains a very small fluorocarbon segment. The XPS spectra of fluorosilicones are a combination of siloxane and fluorocarbon spectra. High-resolution XPS oxygen 1s, fluorine 1s, carbon 1s and silicon 2p spectra acquired from PMTFPS are shown in Fig. 12.7.

The notable features of the carbon 1s spectrum of PMTFPS are the C-Si component at 284.4 eV, the very high binding energy component from the terminal CF_3 group (~292.4 eV) and the equally intense "bridging" CH_2 component that has a binding energy of approximately 286 eV. The bridging CH_2 is chemically shifted to a higher binding energy (cf. with CH_2-Si) due to the influence of the fluorine atoms of adjacent CF_3. Such secondary chemical shifts are typically modest ($\leq$0.5 eV) for a single contributing secondary atom, but are cumulative if there are multiple contributions (e.g. CF_2 or CF_3). The C-Si component is roughly twice the intensity

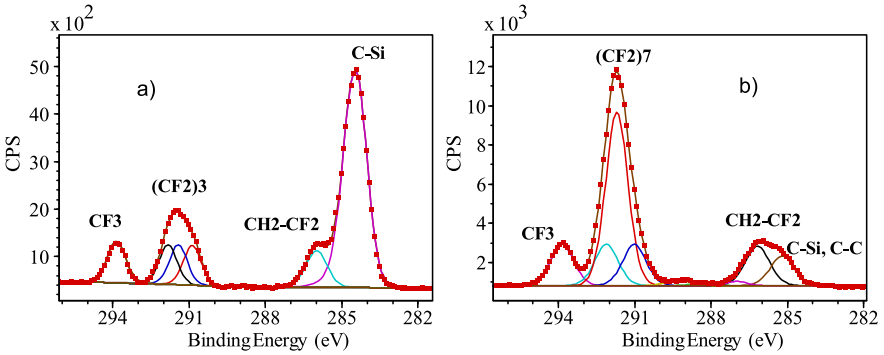

Fig. 12.8 Carbon 1s spectra of: (**a**) polymethylnonafluorohexyl siloxane (PMNFHS) with PDMS and (**b**) 1H,1H,2H,2H-heptadecafluorodecyl-POSS (fluorodecyl POSS) spun-on film on Si wafer. (Fluorodecyl-POSS sample courtesy of A. Tuteja and J. Mabry)

of the CF_3 group and bridging CH_2, reflecting the CH_3 and CH_2 groups bound to each silicon atom. The C 1s component assigned to the lone CF_3 group has a similar binding energy to the $(CF_2)_n$ of polytetrafluoroethylene (PTFE), but PMTFPS has a much lower F 1s binding energy (688 eV vs. 689.7 eV of PTFE). The Si 2p and O 1s spectra of the siloxane backbone match those of PDMS.

As the length of the fluorocarbon branch is extended to further lower the surface energy in other fluorosilicones such as polymethylnonafluorohexylsiloxane (PMNFHS), CF_2 components appear at binding energies >290.8 eV. This can be seen in Fig. 12.8a, which shows the C 1s spectrum of PMNFHS mixed with PDMS. The range of CF_2 binding energies reflects the influence of different secondary chemical shifts arising from bonding to CF_3 or CH_2 groups at opposite ends of the CF_2 chain. As with PMTFPS, the similar magnitude of the bridging CH_2 and the terminal CF_3 components (Fig. 12.8a), supports the identification of a fluorosilicone, rather than a mixture of fluorocarbon and siloxane at the surface. The bridging CH_2 component binding energy lies close to that of C-O components of alcohols and ethers, but is slightly lower.

Some recent work by Tuteja and Mabry on superoleophobic surfaces (see also Chap. 6) has involved the combination of highly re-entrant surface-curvature textures and fluorocarbon-substituted polyhedral oligomeric silsesquioxanes (fluoro-POSS) materials [42, 43]. As can be seen in Fig. 12.8b, the carbon 1s spectra of 1H,1H,2H,2H-heptadecafluorodecyl-polyhedral oligomeric silsesquioxane (referred to as fluorodecyl POSS) is quite similar to that of PMNFHS though with a much larger CF_2 component. Note that the bridging methylene group (i.e., the methylene group attached to the first CF_2) is chemically shifted by about 1.1 eV from the saturated hydrocarbon reference binding energy (285 eV) due to the electron withdrawing nature of the CF_2 groups. Note also that the CF_2 groups have slightly different chemical shifts depending on the nature of the adjacent carbon groups (CF_3 vs. CF_2 vs. CH_2).

Perfluoroethersiloxanes constitute another interesting class of siloxanes used to make rubber parts, adhesives, coatings and pottants. They possess the low surface

energy and fuel resistance of fluorocarbons with somewhat greater flexibility at low temperature due to their lower glass transition temperature. Chemically they are identified through the OCF_2 groups. The C 1s binding energy of OCF_2 is roughly equivalent to that of CF_3 groups, but the oxygen 1s has a uniquely high binding energy of ~536 eV which offers an excellent way to identify perfluoroether siloxanes.

12.3 Applications of XPS to Analysis of Silicones and Fluorosilicones

The following section discusses the main areas where XPS has been used to analyze the surfaces of silicone and fluorosilicone materials. These can be generally classified as follows: surface reorientation studies, modification with siloxanes, modification of siloxanes, adhesion, and biomaterials.

An interesting study on polymer reorganization was carried out by Chen et al. [44]. The surface chemistry of an amphiphilic siloxane copolymer was investigated in dry and hydrated states, through the use of cryo-XPS. In the dry state, PDMS was determined to have segregated to the surface by determining the elemental composition; in the hydrated state, the surface was enriched with hydrophilic poly(2-hydroxyethyl methacrylate) (PHEMA). However, in either condition, the PDMS concentration always exceeded that found in the bulk, and conversely the PHEMA concentration was lower. This reorganization was found to be much more apparent when angle resolved XPS was carried out, at low take off angles (TOAs) with respect to the sample surface. When the copolymer was retained in the hydrated state, the intensity of the C 1s core level components assigned to C-O and O-C=O were noted to increase. This effect was found to increase with hydration time. In this work, no differentiation was made in binding energy between C-C and C-Si: both were reported at 285.0 eV. This reorientation phenomenon could be of interest in applications such as contact lens manufacturing: taking advantage of the oxygen permeability of PDMS in combination with the higher wettability of the surface delivered by PHEMA when in an aqueous environment.

In another study the effect of process parameters (such as spin-coating speeds) was reported by Ponjée et al. [45]. In this poly(3-hexylthiophene) (P3HT) system, a low concentration of siloxane material was added, and the elemental composition analyzed with varying conditions. The concentration of silicon at the surface was found to be less for samples prepared with faster spin-coating speeds, and samples prepared from lower solution concentration in toluene.

There are numerous papers in the literature which describe how various substrates are modified by siloxanes, with a number of different approaches taken to make the modification. A significant area of surface modification is through plasma deposition of silicones. For example, the initial work on deposition from hexamethyldisiloxane (HMDS)/oxygen plasmas by Alexander et al. [23] provided a quantitative indication of the changes in the chemistry of deposited coating, related to the process parameters. It was reported that as the flow of oxygen was increased,

the ratio of C/O decreased, with a corresponding increase in O/Si ratio. This was supported by a shift of the Si 2p core level to a higher binding energy, indicating silicon in a more oxidized environment. When HMDS was deposited in the absence of oxygen, the resulting deposit had a chemistry similar to that of the starting material. This work was carried out using a Mg K_α anode, and was later expanded to use a higher-sensitivity and higher-energy resolution anode to facilitate curve fitting of the Si 2p core level [29]. As pointed out earlier in this review, the absence of features in this core level hinders this possibility, and as such, a systematic method was used, with constrained binding energies. The work demonstrated that as the oxygen flow increased, the contribution of Si in a more highly oxidized form also increased.

Similarly, a mechanistic study on the preparation of polysiloxane membranes by plasma-enhanced chemical vapor deposition was carried out by Roualdes et al. [31]. From this work, mechanistic differences in deposits were elucidated, depending on the use of a cyclic or linear siloxane starting material. It was also found that under conditions of the lowest plasma composite factor (V/FM where V is voltage, F is precursor flowrate and M is precursor molecular weight) retention of the precursor chemistry could be best achieved.

In another study, Vycor™ glass was modified by deposition of tetraethoxysilane (TEOS) using atmospheric pressure plasma liquid deposition (APPLD) [46]. Relationships were drawn between the process parameters and coating thickness, surface energy, surface chemistry and surface roughness. In addition, it was intended to evaluate the thermal stability of such materials at elevated temperatures, for potential future applications such as gas separation. Consistent with previous work, as the plasma exposure was increased, the resultant surface was more oxidized. Subsequently, the surface energy increased, as did the coating thickness. Thermal annealing was found to further decrease the carbon content of the films (which was supported by FT-IR data), and led to a reduction in coating thickness (ascribed to an increase in film density), and reduction in surface particulates and the roughness of the film. This work was carried out on a reel-to-reel parallel plate deposition system (Dow Corning SE-1100 *LabLine*™). The same group also reported similar conclusions for work carried out on a plasma-jet type deposition tool (Dow Corning SE-2100 *PlasmaStream*™) [47]. Here, an increase in plasma power and a decrease in precursor flow rate led to the most highly oxidized coatings.

Boscher et al. [48] deposited thin films of hexamethyldisiloxane (HMDS) onto aluminum foil. The purpose of the investigation was to evaluate the potential use of nitrogen as the gas to generate plasmas, to reduce costs compared with helium and argon, which are typically used. The aim was to prepare smooth, defect-free, well-polymerized films, and to relate these properties to the process gas parameters, specifically the concentration of oxygen added. The electrical performance of the deposited films was also investigated. Decreasing the ratio of N_2/O_2 during deposition was found to lead to the formation of more highly oxidized species. As the concentration of oxygen increased, the intensity of Q siloxy species increased. Films prepared in the absence of oxygen were found to have particulate defects, although they were pinhole-free. Furthermore, the film growth rate was related to the gas composition. The brittleness of the film increased with increasing inorganic character, as did the dielectric constant and the film's barrier performance.

An example of surface modification that does not use plasma processing is the modification of cellulose fibers using aminosiloxanes for enhanced softening and improved mechanical performance [49]. Here, Xu et al. used XPS to follow the appearance of silicon and nitrogen following modification, which are absent from the cellulose substrate. Examination of the C 1s core level spectra indicated a change in shape indicating an increase in the component assigned to C-Si. This was also linked to a decrease in surface energy and in roughness, occurring as a result of the modification process. In another study Cao et al. reported on the preparation and characterization of a novel silicone biomaterial [50]. This involved grafting of vinylmethyltrisiloxane to poly(methyl methacrylate) particles. XPS characterization was limited to a survey spectrum with small peaks assigned to Si 2s and 2p core levels. The presence of the silicone layer was linked to a small increase in water contact angle, and to increasing protein adsorption with increasing concentration of silicone monomer.

As for modification of substrates *with* silicones, there is an abundance of work in the literature on modification *of* silicones, which is covered in more detail in a previous chapter. For the sake of continuity, a limited selection of papers is presented here.

For example, the effect of UV/Ozone treatment on PDMS is reported by Egitto et al. [51]. They documented an increase in oxygen concentration at the surface with exposure to UV/Ozone, and that the depth of modification was related to the substrate thickness; for 2.5 nm thick PDMS substrates, the entire material was transformed to SiO_x, while for a 48 nm thick substrate, the conversion from PDMS to SiO_x was limited approximately to the top 10 nm.

A relationship between plasma treatment time and hydrophobic recovery of silicones was made by Morra et al. [52]. They observed that an increase in oxygen concentration led to a decrease in the advancing contact angle of water. They proposed that oxygen incorporation occurs more on the Si atom than on the C atom, supported by a shift in the binding energy of the Si 2p core level, versus the addition of only minor components to the C 1s core level.

In some early work, Fakes et al. [27] compared the extent of surface modification by plasma discharge of an alkylacrylate, with that of a similar polymer which also contained silicone. They found that the extent of modification (as determined by curve fitting of the C 1s core level spectra) was much less for the material which contained no silicone. Additionally, curve fitting of the Si 2p core level spectra was used to quantify the organosilicon versus silicate component of the silicone-containing material. These results were related to the treatment time at constant power. A rapid increase in the intensity of the SiO_x component was noted, followed by a plateau of constant chemistry, irrespective of treatment time.

Modification of silicones can also be used to lead to improved adhesion performance. Roth et al. investigated how adhesion of silicone rubber could be improved by functionalization of its surface [53]. Two methods of modification were discussed: oxygen plasma, and ammonia plasma. Samples created by each method were further functionalized by poly(ethylene-*alt*-maleic anhydride) (PEMA) to provide adhesion to an epoxy resin. The oxygen plasma treated sample required an intermediate step to react the newly created functional groups with

3-aminopropyltriethoxysilane (γ-APS), which provides the necessary amino groups for the PEMA to react with. The samples were also derivatized with trifluoromethylbenzaldehyde to facilitate quantitation of the $–NH_2$ groups on the surface. The extent of surface modification following the initial oxygen plasma treatment was investigated by examination of the C 1s core level spectra. The Si 2p core level spectra were not used, although formation of silanol was proposed indirectly by the reduction of isoelectric point, determined by zeta potential. The adhesion between the modified siloxane and epoxy resin was found to be higher than for an untreated silicone rubber. However, since failure of the adhesion test pieces was found to be cohesive in the silicone rubber, it was not possible to further relate specifically the adhesion to the surface modification.

Due to their inherently low surface energy, adhesion of silicones can be enhanced by modification of a substrate. For example, O'Neill et al. [54] described a novel route to improved adhesion between silicone sealants and poly(butyl terephthalate) (PBT) or stainless steel using deposition of a primer layer via plasma. XPS data were used to relate the process parameters (composition of polyhydrogenmethylsiloxane (PHMS) and tetraethoxysilane (TEOS) precursors) to the exhibited adhesion. Adhesion was improved in all cases, when compared with a non-primed system, and the surface chemistry suggested an enrichment of Si-H containing species at the surface. Similarly, Nwankire et al. [55] plasma deposited a siloxy primer layer to enhance adhesion of a siloxane elastomer to stainless steel. They linked a decrease in water contact angle and an increase in oxygen concentration determined by XPS, with an increasing plasma:substrate gap. Examination of the Si 2p core level showed a transformation from D to T siloxy groups. Adhesion was found to be inversely related to this change, with a reduction in adhesion fracture energy.

In the report of Ahn et al. [56] the C-O component of the C 1s core level spectra was used to provide understanding of enrichment and reactivity of a titanate catalyst with the adhesion of a polycarbonate:siloxane elastomer system. A thermal gradient had been used to examine the development of the composition of the interface. Enrichment of the titanate was apparent at cure temperatures below that required for optimal adhesion, while loss of organic ligands occurred before cohesive failure was observed.

The effect of the chain length of the siloxane component on the adhesion of a poly(imide siloxane) copolymer was evaluated by Mahoney et al. [57]. They used XPS to provide the elemental composition of a series of samples with constant silicon concentration (10 %), but varying chain length combinations. They found that the incorporation of siloxane components with both long (9 repeat units) and short (1 repeat unit) segments, led to the same surface chemistry as materials containing only long segments. Adhesion was found to follow the same trend: it was better when only short segments were present, which resulted in less silicon detected at the surface. When the siloxane components comprised mixed 'intermediate' (5 repeat units) versus long segments, the surface chemistry was found to vary as the long segment percentage was increased from 0 to 3 %; above 3 % long units resulted in the same surface chemistry as when the siloxane was entirely comprised of long segments. Extraction of all samples in toluene reduced the silicon detected at the surface, and resulted in improved adhesion.

The analysis of fluorosilicone surfaces is focused on a few specific areas. These include surface contamination, surface modification, copolymerization, surface segregation and adhesion science. Answers to questions in these areas are often found through the application of multiple techniques. High-resolution XPS spectra of fluorosilicones have been published relating the effects of gas plasma treatments on the wettability of PMTFPS [58] and fluorosilicone acrylate contact lens materials [59, 60], the morphology and mechanical performance of plasma-deposited fluorosilicone/silicone mixtures [61], and also for characterization of new fluorosilicone triblock copolymers [62] and perfluoroether-modified siloxane surfaces [63].

An example of the application of XPS to study surface modification with a fluorosilane is provided by N. Ghosh et al. [64]. They studied fluorosilane modification of bio-mimetic silicone surfaces and uncovered incidental cross-contamination as a source of anomalous contact angle results through the use of XPS, SEM, contact angle measurement and optical microscopy. Unexpectedly enhanced oil-repellency at the surface of a positive copy of a bio-mimetic PDMS replica of a colocasia leaf surface was determined via XPS to be due to cross-contamination of the positive copy with a fluorocarbon release agent. Subsequent oxidation of the surface and reaction with $CF_3(CF_2)_7CH_2SiCl_3$ created a much higher concentration of fluorocarbon groups at the surface. This resulted in a superhydrophobic and highly oil-repellent surface (receding θ_{water} 142° and advancing θ_{water} 155°, receding θ_{oil} 102° and advancing θ_{oil} 120°). SEM was used extensively to show the protuberances of the dry colocasia leaf, the quality of the positive and negative replications and the effects of wet chemical treatments used to oxidize the surface of the replicas. Contact angle analyses were used to illustrate the effects of chemical modifications and varying roughness on the water and oil repellency.

Guan et al. [65] characterized the surfaces and morphologies of novel fluorosilicone triblock copolymers synthesized via reversible addition-fragmentation chain transfer polymerization using XPS, static water contact angle measurement, AFM and transmission electron microscopy (TEM). The high-resolution C 1s spectrum of the triblock copolymer has a uniquely high C-O binding energy that arises from the secondary chemical shift effect of adjacent CF_2 groups $–OCH_2(CF_2)_2CF_3$.

Nwankire et al. [60] examined how precursor type and deposition conditions for an atmospheric plasma-jet system (Dow Corning SE-2100 *PlasmaStream*™) influence the morphology, adhesion and coating durability of superhydrophobic coatings deposited from tetramethylcyclotetrasiloxane (TMCTS), HMDS and a mixture of TMCTS and fluorosilicone. They found the latter yielded a substantial enhancement in coating adhesion and mechanical durability compared to the super-hydrophobic coatings obtained with either TMCTS or HMDS precursors alone. They employed optical profilometry, AFM, SEM, ellipsometry, XPS, water contact angle and FTIR to evaluate the surface roughness, morphology, thickness and chemical functionality of the coatings, and mechanical properties were evaluated using the Nano tribometer, Nano Scratch, Ultra Nanoindentation and ultrasonic abrasion tests.

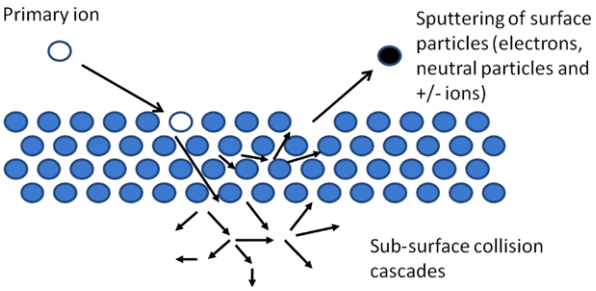

Fig. 12.9 Schematic representation of the SIMS process

12.4 Secondary Ion Mass Spectrometry (SIMS)

Another very powerful technique for obtaining surface chemical information is secondary ion mass spectrometry (SIMS). This is an analytical technique used to analyze the chemical composition of solid surfaces. The SIMS process is shown schematically in Fig. 12.9, in which the sample is bombarded by a beam of primary ions under ultra-high vacuum (UHV) conditions [66]. The primary ions penetrate the surface to a depth of 30 to 100 Å, and their kinetic energy is dissipated by a cascade of collisions [66]. This collision cascade results in the formation of neutral species and secondary ions that are removed from the surface under investigation. The secondary ions are then analyzed in terms of their mass to charge ratio by a mass spectrometer detector, yielding positive and negative ion spectra. As with conventional mass spectrometry, the SIMS spectra can be analyzed to determine the elemental and molecular composition of the surface under investigation. It is worth noting that the secondary ion yields are strongly influenced by the make-up of the surface and the nature of the primary ion beam, making the technique very sensitive, but generally non-quantitative. This is useful to remember, particularly when analyzing surfaces where silicones are suspected of playing an undesired role. The appearance of an intense peak in a SIMS spectrum can make the insignificant appear important.

There are three types of SIMS experiment possible, dynamic SIMS, static SIMS and imaging SIMS, each experiment using different primary beam parameters [67]. Dynamic SIMS uses a high flux density of primary ions to obtain a very high yield of secondary ions. The surface is eroded rapidly to give a depth profile yielding elemental analysis [67]. Static SIMS uses a relatively low energy, low flux primary beam [67]. These conditions will hopefully give surface monolayer life-times in excess of the time taken for spectral acquisition. Imaging SIMS is performed in the static mode by raster scanning a microfocused primary ion beam across the sample surface [67]. By collecting the secondary ions at each point a chemical image can be generated [67]. Of the three types of SIMS experiment, static and imaging SIMS are the most beneficial to the surface analysis of silicones due to their capacity for negligible damage to the sample surface, and ability to study its chemical structure. Therefore further discussion is limited to SIMS experiments performed in the static mode.

Static SIMS has been used to analyze a wide variety of different polymers and the secondary ion spectra are usually most intense in an m/z range considerably

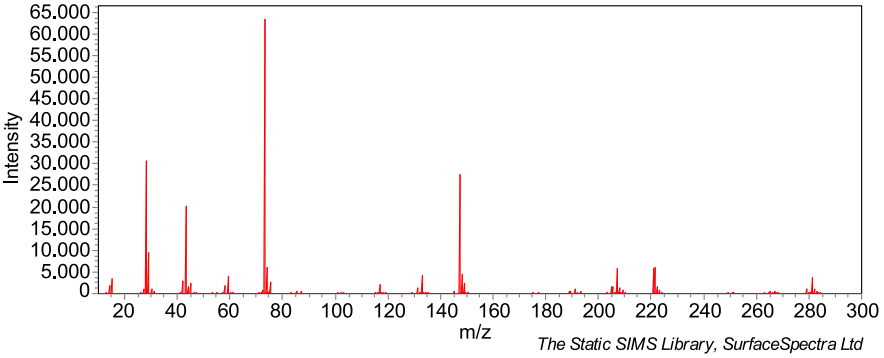

Fig. 12.10 Example of the positive ion spectrum acquired from polydimethylsiloxane (PDMS). Reproduced from Ref. [71] with kind permission of ©The SurfaceSpectra Static SIMS Library

lower than the molecular weight of the polymer. Therefore, it is useful to have a terminology that can describe static SIMS spectra in terms of fragmentation and ion formation processes. Dong et al. [68] proposed such a terminology that will be used henceforth: *fragment* is a segment cut from a polymer chain; *cluster* is a group of peaks corresponding to ions from a particular fragment; *pattern* is a repeating sequence of clusters; *Rn* will refer to a cyclic fragment containing a number of repeat units (n) and *nR* will refer to a linear fragment containing a number of repeat units (n).

Due to the low surface energy of silicone materials they are a common source of contamination on surfaces. Static SIMS is sensitive to silicones at very low surface coverage since the positive ion yield is high and the fragmentation pattern very distinctive [69]. This high sensitivity to PDMS, makes the positive ion SIMS spectrum of silicones instantly recognizable [70], as shown in Fig. 12.10 [71].

Some of the characteristic peaks in these spectra are believed to be due to secondary ions with the linear or cyclic structures shown below [70]:

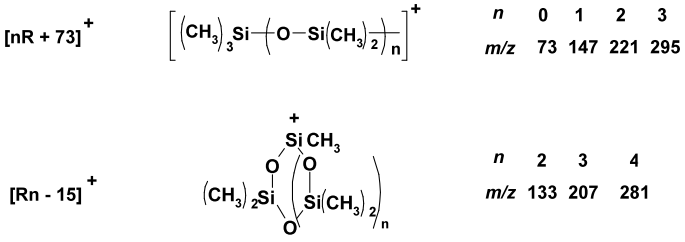

Dong et al. used static SIMS to study the fragmentation mechanisms of PDMS [68]. They proposed that because the characteristic spectra of silicone materials contain cyclic secondary ions, cleavage of the siloxane (Si-O) bond (799.6 kJ/mol) must occur in preference to the silicon-carbon (Si-C) bond (451.5 kJ/mol) of the pendant group. It was also proposed that during the fragmentation process two new siloxane bonds are formed to produce a four-membered ring

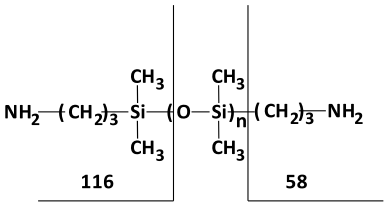

Fig. 12.11 Static SIMS fragmentation pathways proposed for aminopropyldimethylsiloxane [69]

intermediate. This allows two siloxane bonds to be broken simultaneously, which results in no net energy change during the ion formation process. Four-membered ring intermediates may be formed by either intermolecular or intramolecular mechanisms [68]. The intermolecular mechanism forms two linear ions, while the intramolecular mechanism can form a linear ion and a cyclic ion.

The same authors also used static SIMS to study the fragmentation of PDMS terminated by different end groups [68]. They proposed that although the polymer is terminated at both ends with the same group, the mass of the ion derived from the terminal group depends on whether fragmentation is caused by cleavage of a Si-O or a Si-C bond [68]. As an example the two fragmentation pathways for (aminopropyl)dimethylsiloxane are shown in Fig. 12.11. They also observed that in the low mass range, terminal group cleavage occurs at the Si-O bond with charge transfer to silicon atom [68]. This is counter-intuitive as the Si-O bond energy is greater than the Si-C bond energy.

Before the introduction of new polyatomic primary ion sources, gaining static SIMS spectra in mass ranges greater than 1000 was difficult. This meant that determining the presence of oligomers and the molecular ion structure of high molecular weight polymers with static SIMS was challenging. However, it was shown that static SIMS could detect oligomers using a method called *cationization* [70]. This method originally involved depositing a dilute solution of the polymer onto an etched silver substrate. This results in distinctive fragmentation patterns with each peak representative of an $[M_n + Ag]^+$ species where M_n is the mass of the intact oligomeric component and the peak separation reveals the monomer mass [70].

Dong et al. used this silver cationization method to analyze the fragmentation patterns of a series of trimethylsilyl-terminated PDMS with different molecular weights [68]. In the high mass range (>1000 Da), clear patterns were observed, corresponding to linear and cyclic fragments. They noticed that the relative intensity of cyclic fragments increases with increasing molecular weight and that there was an effect of the end group on silver cationized fragmentation patterns of PDMS [68]. They also observed that the formation of cyclic fragments may be more difficult in PDMS terminated by nitrogen containing end group, causing preferential cleavage of the Si-C bond. It was also noted that the effects of end group chemistry tend to become smaller with increasing PDMS chain length.

It is not always practical to deposit the silicone from solution, in order to perform cationization. An alternative method that has been used is the deposition of a silver pattern on the surface of the material under investigation. This method has been used by Inoue et al. for the SIMS analysis of trisilyl terminated PDMS, PHMS and polymethylphenylsiloxane (PMPS) [72]. They observed that intervals in the

silver cationized fragmentation patterns could be used to determine the monomer structure of each siloxane. For example, the interval of the PDMS fragments was $m/z = 74$, the interval of the PHMS fragments was $m/z = 60$, and the interval of the PMPS fragments was $m/z = 136$. They also observed that the end groups could be determined based on the silver cationized linear fragments [72].

12.5 Applications of SIMS to Analysis of Silicones

Because PDMS contamination is a common problem in SIMS analysis, the deliberate introduction of silicones into a SIMS instrument is often avoided by practitioners of this analytical method. Nevertheless, there is a body of work that has used SIMS to analyze this important class of materials and this is discussed with some examples below.

PDMS is common material used in micro-contact printing due to its elastomeric and mold making properties. In micro-contact printing the patterned PDMS stamp is "inked" with a molecule/species of interest and then brought into contact with a substrate [73]. The molecules are then transferred to the substrate at the raised points of the stamps that are making contact. However, there is a risk of the transfer of molecules or fragments from the stamp material to the patterned surface. Such transfer could contaminate the surface resulting in changes in the wetting and adhesion properties. Due to its high sensitivity to PDMS, SIMS analysis is ideally suited for analyzing whether material is being transferred from the micro-contact stamp. Yang et al. investigated the extent of PDMS transfer onto a series of surfaces with a wide range of hydrophobicities [73]. In this study the relationship between the amount of PDMS detected in SIMS spectra and the surface tensions of initial surfaces was investigated. It was observed that PDMS preferentially transfers onto more hydrophilic surface features during stamping, with little being transferred onto very hydrophobic surface features [73]. This led to the hypothesis that it is the free energy of the surface that plays a major role in determining the degree of PDMS transfer during micro-contact printing.

Therefore, efforts have been made to minimize the transfer of silicone during micro-contact printing. For example, Glasmaster et al. have looked at the effect of UV/ozone treatment of the PDMS stamps on silicone transfer to gold substrates [74]. It was observed that the UV/Ozone treatment reduced the amount of silicone transfer from flat stamps. SIMS images of an untreated patterned stamp showed, as expected, transfer of silicone in the regions of contact. However, after UV/ozone treatment of the stamp surface, the SIMS images showed transfer of silicone in the regions of non-contact. This observation is consistent with silicone transfer to an aluminum surface from patterned PDMS stamps [75]. In the study by Hale et al. it was observed that curing the PDMS at elevated temperatures minimized the amount of silicone transferred [76]. It was also observed that subsequent plasma treatment of the PDMS to make it more hydrophilic had a detrimental effect on the transfer of an aminosilane to a PTFE substrate. Graham et al. used SIMS in combination with principal component analysis to study micro-contact printing of

thiol self-assembled monolayers (SAMs) [77]. They observed that scatter in the data was related to the presence of PDMS contamination from the stamp. This contamination was seen to be random between samples but increased with decreasing thiol ink concentration [77]. They concluded that to minimize or eliminate the presence of PDMS contamination from micro-contact printed thiol SAMs it is preferable to use an exhaustive pre-cleaning procedure for the stamp in combination with a higher thiol ink concentration.

Silicones have been widely used in the field of medicine as implant materials; as either temporary implants such as catheters, or in more permanent augmentive applications in the field of plastic surgery. Despite its material benefits, the lack of bio-compatibility of these materials still represents a major problem; i.e. protein adsorption and cell adhesion is low [78]. In order to enhance cell adhesion, Hausner et al. deposited collagen coatings on silicone surfaces [78]. They observed, using SIMS analysis to detect amino acid groups, that it was necessary to plasma treat the silicone implant material prior to collagen deposition. The in vitro tests showed that the collagen coating led to a significant increase in cell adhesion and cell viability [78]. Delcorte et al. have investigated deposition of metal coatings on silicone in order to improve their compatibility [79]. They used SIMS in conjunction with gold cationization to determine that short PDMS chains were present at the untreated silicone surfaces. A combination of argon ion bombardment and hexane cleaning of the silicone removed this oligomer overlayer and, thus, led to a significant adhesion improvement of a titanium coating [79].

Another approach to improve the bio-compatibility of silicones is through copolymerization with other materials, such as urethanes. Zhuang et al. used SIMS to study the surface segregation behavior of poly[dimethylsiloxane-urethane] (PU-DMS)-segmented copolymers [80]. When investigating surface segregation in copolymer systems it is important to understand the quantitative nature of the SIMS spectra. In this study Zhuang et al. used SIMS to determine that the molecular weights and molecular weight distribution of PDMS homopolymers were in good agreement with those values determined from GPC measurement [80]. They then used SIMS to observe that the distribution of PDMS segment lengths segregated at the surface was nearly identical with that in the bulk for the PU-DMS copolymer.

Silicone materials are commonly used as additives in coatings and engineering polymers, to impart a low energy surface. A small amount of the silicone is added to the coating formulation or added to the molten engineering plastic. During solidification or drying process, the silicone migrates to the surface of the coating or polymers, which leaves the bulk-phase properties of the material essentially unchanged [81]. However, the concentration of the additive and the processing conditions can have an impact on the surface segregation phenomena. The affinity of SIMS toward detection of silicones, plus its small sampling depth, makes it an ideal analytical method for investigating surface segregation. For example Chen et al. have used SIMS to investigate the effects of solvents on the surface segregation behavior of poly(dimethylsiloxane-*co*-polystyrene)/polystyrene blends [81]. In this study they used SIMS to reveal that surface segregation of the silicone was influenced by the solvent used for casting polymer films. When chloroform was used

a complete surface layer of PDMS was not observed as secondary ions related to polystyrene were still detected. Whereas when toluene and cyclohexanone were added to the chloroform an increase in the amount of PDMS present at the surface was observed, with complete surface PDMS layer being formed when using cyclohexanone. It is also possible to use SIMS to monitor silicone segregation phenomena in more complex multilayer coatings. For example Hinder et al. used SIMS to investigate segregation of a silicone flow agent used in a polyester/polyurethane coil coating primer [82]. SIMS was used to confirm that, as expected, the silicone flow agent segregates to the primer's air/coating surface. Characterization of a poly(vinylidene difluoride) topcoat, after application and curing over the silicone-containing primer, revealed the presence of the silicone flow agent at the air/top coating surface [82].

Hair is known to be easily damaged by a variety of mechanisms including environmental exposure, mechanical abrasion and chemical processing [83]. To alleviate the symptoms of damaged hair, conditioners or conditioning treatments that include silicones are often used [83]. Due to their low surface energy it is expected that the silicone spreads uniformly over the hair surface forming a uniform thin coating on the fiber. However, the effectiveness of this conditioning effect is dependent on the deposition efficiency of the silicone, which varies depending on the initial condition of the hair; i.e. colored, bleached, damaged etc. Because of the high spatial resolution of SIMS and its molecular specificity it is ideally suited for analyzing the effectiveness of shampoos and conditioners. Berthiaume et al. used SIMS to determine whether silicone does penetrate through the cuticle of a hair fiber [83]. In this study the level of silicone deposited on the exterior of hair fiber and just below the cuticle was investigated using SIMS dot map images. It was observed that the level of penetration below the cuticle was directly related to the droplet size of a silicone emulsion. There was a fourfold increase in penetration from treatment with a micro-emulsion compared to a macro-emulsion [83]. In this study, cross-sections of hair fibers treated with different silicone emulsions were also analyzed by SIMS. The SIMS images of the cross-sections clearly showed significant penetration of the silicone into the hair fiber. Brown et al. used SIMS positive ion images to visualize the deposition of silicone conditioning agents on hair from two shampoo formulations [84]. They semi-quantitatively imaged the hair surfaces by creating a two dimensional image with a complete positive ion SIMS spectrum at each pixel.

12.6 Scanning Electron Microscopy (SEM)

Structural information about silicones is provided through a variety of microscopies, optical microscopy often being the first applied because of the relatively low expense and ease of use. Advantages of optical microscopy include useful color information, the ability to examine the sample surface within its native environment without inducing changes that would occur when placing the sample in a vacuum environment and an ability to examine relatively large scale morphology. Some limitations of most optical microscopes used in air include modest spatial resolution

(ca. 0.5 μm) and a relatively shallow depth of field, which decreases with increasing magnification and numerical aperture. This results in a practical magnification limit of around 2000×. With regard to silicones, optical microscopy is most often used in bright field mode as an enhancement to the naked eye in an initial assessment of a surface and for fine manipulation or preparation of the sample. Other modes of optical imaging can provide information about the surface that may be difficult to perceive in the typical bright field image. Dark field imaging of a metal-coated surface may enhance the appearance of surface roughness. The phase contrast mode can increase the visibility of interfaces and show changes in local thickness or refractive index, and interference microscopy provides a means of measuring sample height. In depth information on optical microscopy is available through many excellent resources [85–89] and the applications are not further discussed here.

A large increase in surface structure resolution, and arguably one of the most powerful and widely used techniques for surface structural analysis, is founded on moving from the limits of photon optics to electron optics. Scanning electron microscopy (SEM) provides an enormous increase in magnification, resolution and depth of field over optical microscopy. SEM instruments typically include additional detectors that emphasize chemical information to supplement the structural information; i.e. topographical and near-surface elemental information are commonly obtainable. Under ideal conditions, the SEM can resolve features under 1 nm in size and has a magnification range of 10×–500,000×. A great deal of reference material on SEM theory and application is available to the general reader, so the scope of this discussion will be brief so as to cover a few essential aspects while pointing the interested reader to a few useful references. Useful general references on SEM and its application to the analysis of polymers include books by J. Goldstein et al. [90], G.H. Michler [91] and Sawyer et al. [89]. There are many online resources available at this time including general tutorials from Michigan State University [92] and the Materials Science and Engineering Department at Iowa State University [93], and more detailed single-topic tutorials available from Microscopy and Analysis (Wiley Online Library) [94].

The basic concept of SEM is that a primary electron beam is focused on and scanned across a solid material within a vacuum, producing signals that reveal surface structure and elemental identity. As the primary beam electrons penetrate the solid surface some of them lose their energy through inelastic scattering. The transfer of energy during inelastic scattering produces secondary and Auger electrons, characteristic X-rays and continuum X-rays. Primary beam electrons may also be scattered back out of the sample surface through a series of collisions, primarily with atomic nuclei. These retain much of the primary beam energy and are referred to as back-scattered electrons. SEM instruments may detect any of these electrons and X-rays when fitted with appropriate detectors. Correlation of the signal with the scanning of the primary beam position results in a corresponding image of the surface.

Secondary electron emission depends on variation in the sample surface topography, as well as the degree to which the electrons can diffuse back to the surface and escape with sufficient energy to be detected. The yield of elastically back-

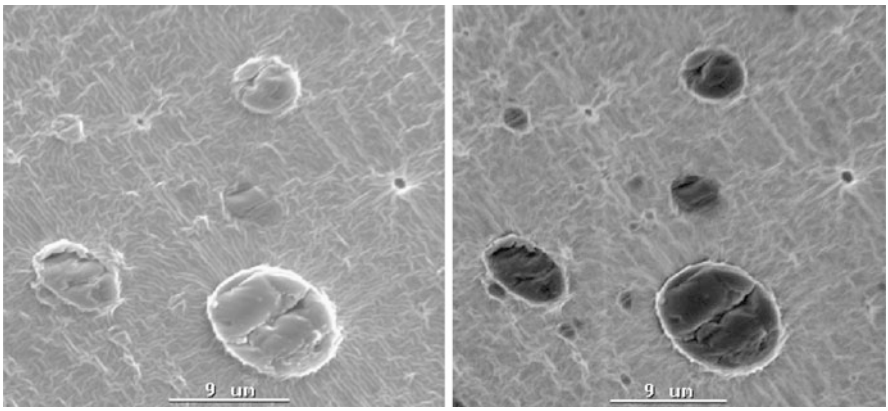

Fig. 12.12 SEM secondary electron image: (*left*) and back-scattered electron image (*right*) of silicone cross-linked PMMA domains in a PDMS matrix (Images courtesy of Ginam Kim and Michael J. Watson of Dow Corning Corp.)

scattered electrons increases sharply with increasing atomic number. For heavy elements back-scattering is efficient, occurs at a shallow depth and the electrons retain most of their kinetic energy. For light elements, such as carbon and oxygen, back-scattering is not so efficient, scattering occurs deeper in the sample and about half of the beam energy may be lost [89]. Because of the atomic number dependence, back-scattered electrons produce images that can reveal domains of different elemental composition. A comparison of images produced from secondary electrons versus back-scattered electrons of silicone cross-linked poly(methyl methacrylate) (PMMA) domains in a PDMS matrix is shown in Fig. 12.12. The secondary electron image shows the surface details a little more clearly and does not reveal some of the smaller, slightly sub-surface PMMA domains that stand out in the back-scattered electron image.

Electron interactions with surfaces also produce X-rays, whose intensity and energy can be determined by energy dispersive (EDS or EDX) or wavelength dispersive (WDS or WDX) X-ray detectors. The differences between EDS and WDS are due to the means by which the X-ray energy (and thus the originating element) is determined. The energy of the detected X-ray provides elemental identification of the originating atom and ultimately a semi-quantitative measure of near-surface composition. Characteristic X-rays can also provide structural information when EDS or WDS are used in a mapping mode, as illustrated in Fig. 12.13. This shows oxygen, carbon and silicon maps corresponding to the secondary and back-scattered electron images of Fig. 12.12.

Another very useful modification of SEM instruments is a cold stage for analyzing samples at cryogenic temperatures. Cryo-fixed samples are preserved such that fragile, moisture or temperature sensitive materials are frozen in place and can be imaged, often in face-on view after fracturing of the frozen sample. This method can be used to analyze silicone emulsions (Fig. 12.14) and hydrated materials such as contact lenses [95].

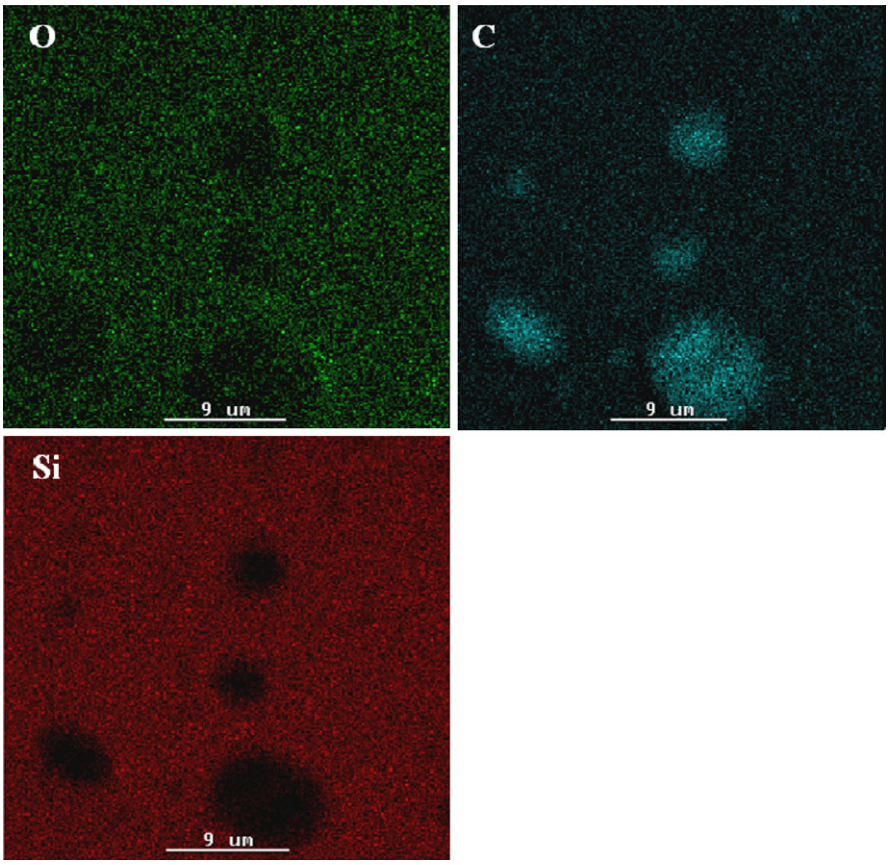

Fig. 12.13 EDS maps of oxygen (*upper left*), carbon (*upper right*) and silicon (*lower left*) of silicone cross-linked PMMA domains in a PDMS matrix corresponding to the areas imaged in Fig. 12.12. (Images courtesy of Ginam Kim and Michael J. Watson of Dow Corning Corp.)

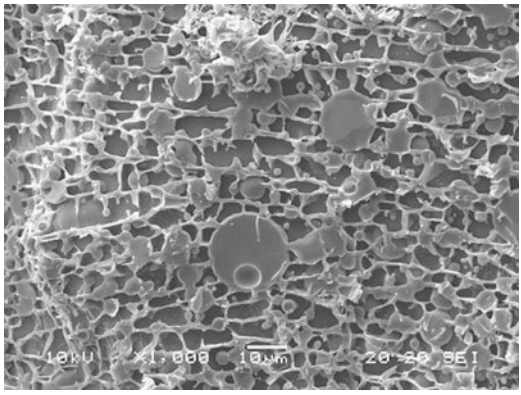

Fig. 12.14 Secondary electron image showing the internal structure of a silicone emulsion with a fluid core and silica shell. (Images courtesy of Dow Corning Corp.)

12.7 Applications of SEM to Analysis of Silicones

Microscopy techniques in general are essential for depicting and understanding the organization of surfaces and three dimensional structure of any material. SEM is arguably the most powerful and the second most widely used microscopy technique for imaging surfaces after optical microscopy. SEM has a vast range of application, for example providing information about the role of surface roughness in adhesion studies [96] and superhydrophobic materials (see Chap. 4) [97], the distribution of functionality in chemical patterning [98] and the presence of diatoms in marine biofouling [99], to name an arbitrary few. Examples of the application of SEM and associated techniques to the characterization of a silicone surface are illustrated below.

Silicone analysis by SEM and EDS has an extensive history going back notably to early studies of silicone implant surfaces [100, 101] and silicone migration within the body from implanted materials [102]. Other early studies included cosmetic application [103], copolymer model systems in bioadhesion [104], paper coatings [105] and surface degradation of electrical insulators [106].

In more recent work, Polizos et al. [97] relied on SEM to estimate the fractal dimension of constructed PDMS surfaces. Analysis of SEM images provided an estimate of the fractional coverage of PDMS spherulites, which together with the contact angles of smooth and constructed PDMS allowed an estimate of the fractal dimension by the method of Feng [107]. By creating a fractal-like surface using an imprint method, which relied on hydrophobic-hydrophilic interactions in a polymer blend of PDMS and polyethylene glycol, they raised the water contact angle from 100° to 160°. In another study Ghosh et al. [108] used SEM in a more qualitative manner to monitor the retention of the surface pattern of a PDMS bio-mimetic replica of a lotus leaf surface as it was modified structurally with nanoscale silica and then chemically with heptadecafluorodecyltrichlorosilane, ultimately becoming superoleophobic.

As well as morphological studies, SEM can be used to gain structural information. For example, Longley and Chaudhury [109] were able to obtain absolute sol-gel film thicknesses on PDMS using SEM and establish a linear relationship between buckling wavelength and thickness, allowing the determination of the elastic modulus of the thin sol-gel film. The buckling instability technique permits the rapid determination of elastic modulus of thin films as a function of various chemical and processing parameters. In another study Kanamori et al. [110] found that competition between phase separation (spinodal decomposition) and wetting in a confined space resulted in a unique pillar structure rather than a bicontinuous structure for methylsiloxane gel when the distance between supporting surfaces (groove width in support) was below the characteristic length of the bulk gel.

12.8 Scanning Probe Microscopy (SPM)

An additional step in surface sensitivity if not spatial resolution is achieved by using scanning probe microscopies (SPM) such as atomic force microscopy (AFM). The

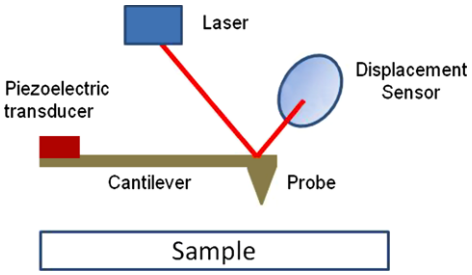

Fig. 12.15 Schematic of an SPM system

spatial (horizontal) resolution may fall a little short of that achieved by a SEM in most modes of use, but the AFM height sensitivities are on the order of 1 Å. Besides an ability to reveal the shortest physical features, modifications to the AFM mode of operation or probe tip enable mapping of different material phases, magnetic or charge domains, changes in physical properties such as friction, surface energy and hardness, and imaging of chemical changes. The relatively modest price, surface sensitivity and environmental flexibility of AFM instruments has made them a popular addition to the arsenal of surface analysis instruments, despite some limitations on the physical forms and textures that can be analyzed.

SPM works on the principle of a sharp probe being moved in close proximity to a sample surface. The probe tip is situated at the end of a cantilever, which is typically manufactured from silicon or silicon nitride. The probe and sample are moved relative to each other in a raster pattern, which makes it possible to record the probe-sample interaction point-by-point. The collection of these data points is then converted to an SPM image. Moving the probe tip relative to the sample surface is usually achieved using piezoelectric actuators in the x and y plane. These actuators can either move the sample relative to a fixed cantilever or vice versa. The schematic in Fig. 12.15 shows the set up of a cantilever and probe in a typical SPM system.

The original mode of operation for SPM maintained the probe tip in constant contact with the sample surface. In order to reduce damage to samples due to applied load and lateral forces experienced in imaging, intermittent contact mode of operation was developed. Intermittent contact between the probe tip and the sample surface is achieved by oscillating the probe's cantilever at or near its resonance frequency. This oscillation is most often achieved through the use of a piezoelectric transducer in contact with the fixed end of the cantilever. When the cantilever is in close proximity to the sample surface the oscillating probe tip touches the surface for only short periods of time. This led to this mode of intermittent contact being commonly referred to as "Tapping Mode", which is a trade mark of Digital Instruments. A significant advantage of SPM over the other surface analysis methods described in this chapter is the ability to operate under ambient conditions; i.e. not in a vacuum. In addition to this, it is also possible to conduct SPM experiments in a liquid environment.

During SPM imaging, any interaction between the probe tip and the sample are monitored by displacement of the free end of the cantilever. The most common method for measuring this displacement is through movement of a reflected laser beam across a segmented photodetector. In most SPM imaging modes the probe is

maintained at a fixed distance above the sample surface or at a fixed force when in constant contact with the sample surface. This is achieved by using a feed-back system to control a piezoelectric actuator in the z plane during the rastering process. Monitoring the change in the position of the z actuator at each $x-y$ coordinate in the raster pattern will generate a map of surface topography, which is commonly referred to as a height image. This is useful for understanding the surface topography of materials at small dimensions in a similar manner to SEM. However, the great advantage of SPM is mapping the forces of interaction between the probe tip and the sample, which can provide information relating to material properties at sub-micron spatial resolution. This has led to the development of numerous different SPM modes of operation, designed to measure specific tip-sample interactions.

While there are many different SPM modes, they can be classified into two groups; those where the probe tip is in constant contact with the sample and those where the sample is in intermittent contact. Examples of contact modes of operation include "lateral force microscopy" for mapping the variations in the friction properties of a surface, and "force modulation mode" that maps changes in the elastic properties of a sample. Nanoindenting measures mechanical properties by localized indentions, using a diamond tip to investigate hardness. AFM can also perform nano-scratching and wear testing to investigate film adhesion and durability. The intermittent contact mode of operation most commonly used to image changes in material properties is "phase imaging". This mode of operation maps the phase lag between the signal that drives the cantilever and the oscillations of the cantilever. Changes in the phase lag often indicate changes in the properties of the sample surface. It has been proposed that phase imaging can detect variations in composition, adhesion, friction, and viscoelasticity. However, the phase images are often a combination of material properties, such as adhesion and modulus.

12.9 Applications of SPM to Analysis of Silicones

Due to their good mold forming characteristics silicone materials have been considered for micro-lithographic patterning and the development of micro-fluidic devices. However, for many of these applications it is an advantage to have hydrophilic properties in discrete areas of the surface. For example, a popular method for making the surface of a silicone material hydrophilic is through conversion of the surface to a silicate structure. Due to SPM having the capability to measure changes in sample height on the nanometer scale it has been adopted to investigate the effects of these surface modifications. Takao et al. investigated the modification of silicone surfaces using laser irradiation, using SPM to monitor the changes that occur in surface morphology [111]. Orhan et al. used SPM to monitor changes in surface roughness resulting from bonding a borosilicate coating to micro-fluidic channels in PDMS [112].

Similarly, the low surface energy and hydrophobic nature of PDMS inhibit its bioactivity [113]. In order to improve cell adhesion several approaches have been

made to modify the surfaces of silicone materials. For example, Parito et al. deposited thin aluminum films onto PDMS through a patterned mask in the presence of a gaseous plasma [113]. After etching away the aluminum, it was observed that fibroblast cells adhered to the modified PDMS. Contact mode AFM analysis observed sinusoidal ripples present in the areas exposed to the aluminum deposition process. However, it was determined that the oxygen enrichment at the surface of the PDMS was responsible for the improved bioactivity rather than the changes in surface topography. In another example, Voelcker et al. graft copolymerized acrylates on plasma treated silicone surfaces to generate a hydrophilic layer [114]. The covalent attachment of fibronectin to these modified surfaces resulted in improved cell adhesion. Contact mode AFM was used to observe that the plasma treatment removed the molding features from the silicone surface and introduced fissures of about 200 nm width and 30 nm depth. Grafting of the acrylates resulted in the filling of the fissures to provide an even layer.

While the examples above have focused on the improvement of cell adhesion, the prevention of cell adhesion is equally important to reduce biofouling. It was for this aim that Barrios et al. incorporated zosteric acid in silicone coatings to deter bacterial attachment [115]. In this study, SPM was used to determine the surface roughness of silicone coatings with and without zosteric acid incorporated. It was observed that the surface roughness of the coating increased with the presence of zosteric acid. However, it was concluded that it was the presence of zosteric acid rather than increased surface roughness that reduced bacterial adhesion.

The adjustment of the material properties of silicone materials can also be achieved through copolymerization with other monomers. For example, Viville et al. investigated the preparation of PDMS-polycaprolactone and PDMS-trimethyleneoxydimethylenyl propionate materials [116]. Using AFM phase imaging they were able to monitor the dispersion of these materials in polycaprolactone, showing the changes in spherulite structure of the different materials. Yan et al. investigated the preparation of PDMS-acrylate latexes using emulsion copolymerization [117]. AFM analysis of films formed with varying PDMS content showed differences in surface roughness, and phase images indicated changes in modulus. In another study Keüpczyn'ski et al. used SPM to analyze the morphology of the silicone nanocapsules [118]. They synthesized silicone hollow particles inside the membrane of an equilibrated surfactant vesicle using cross-linking/polymerization processes of 1,3,5,7-tetramethylcyclotetrasiloxane. Tapping mode AFM was used to analyze the structure of the nanocapsules in their dry state. The height images showed hemispherical structures with a polydisperse distribution of lateral sizes (30–90 nm).

In order to improve the mechanical properties of silicones, filler materials are commonly added. A common filler material used for this purpose is fumed silica nanoparticles. Ogashi et al. used tapping mode and phase images to investigate the effect of cure conditions of a condensation cured silicone on the surface distribution of fumed silica filler [119]. They observed that under certain cure conditions the near-surface fumed silica nanoparticles seemed to "disappear". Le et al. used AFM phase imaging to investigate the macro- and micro-dispersion of carbon black filler in silicone rubber [120]. They then used these phase images to distinguish large carbon black agglomerates observed in optical micrographs from smaller aggregates

detected as a micro-dispersion between the agglomerates. These results were then related to conductivity measurements of the silicone rubber, which led to the observation that the conductivity is related to the micro-dispersion of small carbon black aggregates, rather than the macro-dispersion of larger agglomerates.

Silicones can provide surface properties such as softness, bounciness and anti-wrinkle behavior to fabrics and related materials [121]. They are typically applied to a fabric via an emulsion, from which droplets of silicone are deposited on the fabric surface. Purohit et al. used tapping mode AFM to show changes in the morphology of textile fibers after treatment with an amino-functional silicone. From this analysis it was concluded that silicone treatment modified the microstructural properties of the fiber.

Hair conditioners are complex mixtures of materials designed to improve the sensory perception of the hair. Silicones are often used in hair conditioners to improve the dry feel of hair after washing [122]. La Torre et al. used SPM to investigate the nano-tribological effects of silicones on hair fibers, using lateral force microscopy to determine the coefficient of friction on hair cuticles. They observed that the deposition of silicones from the hair conditioner reduced the coefficient of friction of hair cuticles, which was consistent with the sensory perception.

The surface of a contact lens can be a key factor in determining ocular surface tolerance [123]. This is particularly important with the advent of some modern contact lens materials whose surfaces are treated to improve their wettability as in first generation silicone-hydrogel materials. The advantage of SPM being able to operate in a liquid environment allows the monitoring of surface roughness in worn and unworn silicone-hydrogel contact lenses in their hydrated state. In this study it was observed that for the majority of silicone-hydrogel contact lenses analyzed the surface roughness increased significantly after they had been worn. SPM has been used to quantify the surface roughness of contact lenses at a nanometric level with high resolution.

12.10 Concluding Remarks

As many of the desirable performance differences of silicones are related to their surface properties, it is important to be able analyze their surfaces effectively. This chapter presents an overview of key surface analysis techniques that can provide information on the surface morphology, chemical composition and surface physical properties of silicone materials. It will have been observed through the use of key examples that in many cases it is a combination of these analytical techniques that provides a clearer picture of the surface properties of silicones.

References

1. Lichtman D (1975) Comparison of the methods of surface analysis and their applications. In: Czanderna AW (ed) Methods of surface analysis. Elsevier, Amsterdam, p 42

2. Riviere JC (1982) Surface-specific analytical techniques. Philos Trans R Soc Lond A 305:545
3. Seah MP, Briggs D (1990) A perspective on the analysis of surfaces and interfaces. In: Briggs D, Seah MP (eds) Practical surface analysis, 2nd edn. Auger and X-ray photoelectron spectroscopy, vol 1. Wiley, New York, pp 1–18
4. Campbell D, Pethrick RA, White RR (2000) Polymer characterization: physical techniques, 2nd edn. CRC Press, Boca Raton, p 417
5. Vickerman JC, Gilmore IS (2009) Surface analysis: the principal techniques, 2nd edn. Wiley, New York
6. http://www.uksaf.org/tech/list.html. Accessed 26 July 2011
7. http://www.eaglabs.com/techniques/analytical_techniques/. Accessed 26 July 2011
8. Czichos H, Saito T, Smith LM (2006) Springer handbook of materials measurement methods. Springer, Berlin, pp 153–158
9. http://www.eaglabs.com/solutions/application/materialcharacterization.php. Accessed 26 July 2011
10. Gilmore IS, Seah MP, Johnstone JE (2003) Quantification issues in ToF-SSIMS and AFM co-analysis in two-phase systems, exampled by a polymer blend. Surf Interface Anal 35:888–896
11. Aroca RF, Ross DJ, Domingo C (2004) Surface enhanced infrared spectroscopy. Appl Spectrosc 58:324A
12. Chen Z, Shen YR, Somorjai GA (2002) Studies of polymer surfaces by sum frequency generation vibrational spectroscopy. Annu Rev Phys Chem 53:37–465
13. Griffiths P, De Haseth JA (2007) Fourier transform infrared spectrometry, 2nd edn. Wiley, New York
14. Colthrup NB, Daly LH, Wilberley SE (1990) Introduction to infrared and raman spectroscopy, 3rd edn. Academic Press, San Diego
15. Burns DA, Ciurczak EW (2007) Handbook of near-infrared analysis, 3rd edn. CRC Press, Boca Raton
16. http://www.spectroscopynow.com/coi/cda/home.cda?chId=2. Accessed 26 July 2011
17. Lipp ED, Smith AL (1991) Infrared, raman, near-infrared and ultraviolet spectroscopy. In: Smith AL (ed) The analytical chemistry of silicones. Wiley-Interscience, New York
18. Sakai Y, Iijima Y, Asakawa D, Hiraoka K (2010) XPS depth profiling of polystyrene etched by electrospray droplet impact. Surf Interface Anal 42:658–661
19. Miyayama T, Sanada N, Suzuki M, Hammond JS, Si S-QD, Takahara A (2010) X-ray photoelectron spectroscopy study of polyimide thin films with Ar cluster ion depth profiling. J Vac Sci Technol, A, Vac Surf Films 28:L1
20. Watts JF, Wolstenholme J (2003) An introduction to surface analysis by XPS and AES. Wiley, Chichester
21. Clark DT, Dilks A, Peeling J, Thomas RH (1975) Applications of ESCA to studies of structure and bonding in polymers. Faraday Disc Chem Soc 60:183–195
22. Duel LA, Owen MJ (1983) ESCA studies of silicone release coatings. J Adhes 16:49–59
23. Alexander MR, Short RD, Jones FR, Stollenwerk M, Zabold J, Michaeli W (1996) An X-ray photoelectron spectroscopic investigation into the chemical structure of deposits formed from hexamethyldisiloxane oxygen plasmas. J Mater Sci 31:1879–1885
24. Beamson G, Briggs D (1992) High resolution XPS of organic polymers—the scienta ESCA300 database. Wiley, Chichester
25. Noll W (1968) Chemistry and technology of silicones. Academic Press, New York
26. Morra M, Ochiello E, Marola R, Garbassi F, Humphrey P, Johnson DJ (1990) On the ageing of oxygen plasma-treated polydimethylsiloxane sufaces. J Colloid Interface Sci 137:11
27. Fakes DW, Newton JM, Watts JF, Edgell MJ (1987) Surface modification of a contact lens co-polymer by plasma-discharge treatments. Surf Interface Anal 10:416–423
28. Ward LJ, Schofield WCE, Badyal JPS, Goodwin AJ, Merlin PJ (2003) Atmospheric pressure glow discharge deposition of polysiloxanes and SiO_x films. Langmuir 19:2110–2114

29. Alexander MR, Short RD, Jones FR, Michaeli W, Blomfield CJ (1999) A study of HMDSO/O2 plasma deposits using a high-sensitivity and -energy resolution XPS instrument: curve-fitting of the Si 2p core level. Appl Surf Sci 137:179–183
30. Hillborg H, Ankner JF, Gedde UW, Smith GD, Yasuda HK, Wilkström K (2000) Crosslinked polydimethylsiloxane exposed to oxygen plasma studied by neutron reflectometry and other surface specific techniques. Polymer 41:6851
31. Roualdes S, Berjoan R, Durand J (2001) 29Si NMR and Si 2p XPS correlation in polysiloxane membranes prepared by plasma enhanced chemical vapour deposition. Sep Purif Technol 25:391
32. O'Hare L-A, Parbhoo B, Leadley SR (2004) Development of a methodology for XPS curve-fitting of the Si 2p core level of siloxane materials. Surf Interface Anal 36:1427–1434
33. O'Hare L-A, Hynes A, Alexander MR (2007) A methodology for curve-fitting of the XPS Si 2p core level from thin siloxane coatings. Surf Interface Anal 39:926–936
34. O'Hare L-A (2005) Surface characterization of atmospheric pressure plasma-modified and -deposited polymers. Dow Corning Ltd and the Open University
35. Roth J, Albrecht V, Nitscke M, Bellman C, Simon F, Zscoche S, Michel S, Luhmann C, Grundke K, Voit B (2011) Tailoring the surface properties of silicone elastomers to improve adhesion of epoxy topcoat. J Adhes Sci Technol 25:1–26
36. Owen MJ (2010) Fluorosilicones in advances in silicones and silicone-modified materials. In: Clarson S (ed) ACS symposium series. Am Chem Soc, Washington, Chap 9
37. Zisman WA (1964) Contact angles, wettability and adhesion. In: Fowkes FM (ed) Advances in chemistry series, vol 43. Am Chem Soc, Washington
38. Conrad MPC (2009) Synthesis, characterization and thermal decomposition of hybrid and reverse fluorosilicones. Dissertation. University of Toronto
39. Clark DT, Kilcast D, Musgrave WKR (1971) J Chem Soc, Chem Commun 4:517
40. Clark DT, Kilcast D, Musgrave WKR (1973) J Polym Sci Polym Chem Ed 11:389
41. Beamson G, Briggs D (2000) The XPS of Polymers Database, SurfaceSpectra Ltd. (Manchester UK) © 2000 http://www.surfacespectra.com
42. Tuteja A, Choi W, Ma M, Mabry JM, Mazzella SA, Rutledge GC, McKinley GH, Cohen RE (2007) Science 318:1618
43. Mabry JM, Vij A, Iacono ST, Viers BD (2008) Angew Chem, Int Ed Engl 47:4137–4140
44. Chen L, Hook DJ, Valint PL, Gardella JA (2008) X-ray photoelectron spectroscopy studies of water-induced surface reorientation of amphiphilic poly(2-hydroxyethylmethacrylate-g-dimethylsiloxane) copolymers using cryogenic sample handling techniques. J Vac Sci Technol, A, Vac Surf Films 26:616–623
45. Ponjée MWG, Reijme MA, Denier van der Gon AW, Brongersma HH, Langeveld-Voss BMW (2002) Intermolecular segregation of siloxane in P3HT: surface quantification and molecular surface-structure. Polymer 43:77–85
46. Ramamoorthy A, Rahman M, Mooney DA, MacElroy JMD, Dowling DP (2008) Thermal stability studies of atmospheric plasma deposited siloxane films deposited on VycorTM+ glass. Surf Coat Technol 202:4130–4136
47. Ramamoorthy A, Rahman M, Mooney DA, MacElroy JMD, Dowling DP (2009) The influence of process parameters on chemistry, roughness and morphology of siloxane films deposited by an atmospheric plasma jet system. Plasma Proces Polym 6:S530–S536
48. Boscher ND, Choquet P, Duday D, Verdier S (2010) Chemical compositions of organosilicone thin films deposited on aluminium foil by atmospheric pressure dielectric barrier discharge and their electrochemical behavior. Surf Coat Technol 205:2438–2448
49. Xu Y, Yin H, Yuan S, Chen Z (2009) Film morphology and orientation of amino silicone adsorbed onto cellulose substrate. Appl Surf Sci 255:8435–8442
50. Cao S, Deng X, Liu B, Luo R, Chen J (2006) The preparation and characterization of a novel siloxane biomaterial. Polym Compos 14:833–840
51. Egitto FD, Matienzo LJ (2006) Transformation of poly(dimethylsiloxane) into thin surface films of SiO_x by UV/Ozone treatment. Part I: factors affecting modification. J Mater Sci 41:6362–6373

52. Morra M, Occhiello E, Marola R, Garbassi F, Humphrey P, Johnson D (1990) On the ageing of oxygen plasma-treated polydimethylsiloxane surfaces. J Colloid Interface Sci 137:11–24
53. Roth J, Albrecht V, Nitscke M, Bellman C, Simon F, Zscoche S, Michel S, Luhmannm C, Grundke K, Voit B (2008) Surface functionalization of silicone rubber for permanent adhesion improvement. Langmuir 24:12603–12611
54. O'Neill L, Shephard N, Leadley SR, O'Hare L-A (2008) Atmospheric pressure plasma polymerized primer to promote adhesion of silicones. J. Adhes 84:562–577
55. Nwankire CE, Dowling DP (2010) Influence of atmospheric plasma deposited coatings on the adhesion of silicone elastomer to stainless steel. J Adhes Sci Technol 24:1291–1302
56. Ahn D, Shephard NE, Olney PA, McMillan CS (2007) Thermal gradient enabled XPS analysis of PDMS elastomer adhesion to polycarbonate. Macromolecules 40:3904–3906
57. Mahoney CM, Gardella JA, Rosenfeld JC (2002) Surface characterization and adhesive properties of poly(imidesiloxane) copolymer containing multiple siloxane segment lengths. Macromolecules 35:5256–5266
58. Perz SV, McMillan CS, Owen MJ (2001) Wettability of fluorosilicone surfaces. In: Castner DG, Grainger DW (eds) Fluorinated surfaces, coatings and films. ACS symposium series. Am Chem Soc, Washington
59. Ren L, Yin S, Zhao L, Wang Y, Chen H, Qu J (2008) Appl Surf Sci 255:473–476
60. Yin S, Ren Y, Zhao L, Juang T, Chen H, Qu J (2008) Appl Surf Sci 255:483–485
61. Nwankire CE, Favaro G, Duong Q-H, Dowling DP (2011) Enhancing the mechanical properties of superhydrophobic atmospheric pressure plasma deposited siloxane coatings. Plasma Proces Polym 8:305–315
62. Guan G-M, Lo Z-H, Qiu J-J, Tang P-P (2010) Eur Polym J 46:1582–1593
63. Thanawala SK, Chaudhury MK (2000) Langmuir 16:1256–1260
64. Ghosh N, Bajoria A, Vaidya AA (2009) ACS Appl Mater Interfaces 1:2636–2644
65. Guan C-M, Luo Z-H, Qiu J-J, Tang P-P (2010) Eur Polym J 46:1582–1593
66. Davies MC, Lyn RAP (1990) Crit Rev Biocompat 5:297
67. Vickerman JC (1987) Chemistry in Britain, October, 969
68. Dong X, Proctor A, Hercules DM (1997) Characterization of poly(dimethylsiloxane)s by time-of-flight secondary ion mass spectrometry. Macromolecules 30:63–70
69. Briggs D (1992) Static SIMS—surface analysis of organic materials. In: Briggs D, Seah MP (eds) Practical surface analysis, 2nd edn. Ion and neutral spectroscopy, vol 2. Wiley, New York, pp 367–423
70. Briggs D (1998) Surface analysis of polymers by XPS and static SIMS. Cambridge University Press, Cambridge
71. Henderson A, Briggs D, Vickerman JC (eds) (2006) The SurfaceSpectra static SIMS library: version 4, SurfaceSpectra Ltd
72. Inoue M, Murase A, Sugira M (2004) Molecular weight evaluation of poly(dimethylsiloxane) on solid surfaces using silver deposition/TOF-SIMS. Anal Sci 20:1623–1628
73. Yang L, Shirahata N, Saini G, Zhang F, Pei L, Asplund MC, Kurth DG, Ariga K, Sautter K, Nakanishi T, Smentkowski V, Linford MR (2009) Effect of surface free energy on PDMS transfer in microcontact printing and its application to TOF-SIMS to probe surface energies. Langmuir 25:5674–5683
74. Glasmaester K, Gold J, Andersson A-S, Sutherland DS, Kasemo B (2003) Silicone transfer during microcontact printing. Langmuir 19:5475–5483
75. Yunus S, de Crombrugghe de Looringhe C, Poleunis C, Delcorte A (2007) Diffusion of oligomers from polydimethylsiloxane stamps on microcontact printing: surface analysis and possible applications. Surf Interface Anal 39:922–925
76. Hale PS, Kappen P, Prissanaroon W, Brack N, Pigram PJ, Liesegang J (2007) Minimizing silicone transfer during micro-contact printing. Appl Surf Sci 253:3746–3750
77. Graham DJ, Price DD, Ratner BD (2002) Solution assembled and microcontact printed monolayers of dodecanethiol on gold: a multivariate exploration of chemistry and contamination. Langmuir 18:1518–1527

78. Hauser J, Zietlow J, Koeller M, Esenwein SA, Halfmann H, Awakowicz P, Steinau HU (2009) Enhanced cell adhesion to silicone implant material through plasma surface modification. J Mater Sci, Mater Med 20:2541–2548
79. Delcorte A, Befahy S, Poleunis C, Troosters M, Bertrand P (2004) Improvement of metal adhesion to silicone films: a TOF-SIMS study. In: Mittal KL (ed) Adhesion aspects of thin films, vol 2, VSP, pp 1–12
80. Zhuang H, Gardella JA, Hercules DM (1997) Determination of the distribution of poly(dimethylsiloxane) segment lengths at the surface of poly[(dimethylsiloxane)-urethane]-segmented copolymers by time-of-flight secondary ion mass spectrometry. Macromolecules 30:1153–1157
81. Chen J, Gardella JA (1998) Solvent effects on the surface composition of poly(dimethylsiloxane)-co-polystyrene/polystyrene blends. Macromolecules 31:9328–9336
82. Hinder SJ, Lowe C, Maxted JT, Watts JF (2005) Migration and segregation phenomena of a silicone additive in a multilayer organic coating. Prog Org Coat 54:104–112
83. Berthiaume MD, Merrifield JH, Riccio DA (1995) Effects of silicone pretreatment on oxidative hair damage. J Soc Cosmet Chem 46:231–245
84. Brown MA, Hutchins TA, Garmsky CJ, Wagner MS, Page SH, Marsh JM (2010) Liquid crystal colloidal structures for increased silicone deposition efficiency on colour-treated hair. Sci Int J Cosmetic 32:193–203
85. Davidson MW, Abramowitz M (2011) Optical microscopy, online at http://micro.magnet.fsu.edu/primer/pdfs/microscopy.pdf. Accessed 26 July 2011
86. Microscopy Resource Center (2011) Olympus America, online resource at http://www.olympusmicro.com/primer/anatomy/anatomy.html. Accessed 26 July 2011
87. MicroscopyU, Nikon, online resource available at http://www.microscopyu.com/articles/digitalimaging/. Accessed 26 July 2011
88. Murphy D (2001) Fundamentals of light microscopy and electronic imaging. Wiley, New York
89. Sawyer L, Grubbs D, Meyers G (2008) Polymer microscopy, 3rd edn. Springer, Berlin
90. Goldstein J, Newbury D, Joy DC, Lyman CE, Echlin P, Lifshin E, Sawyer L, Michael JR (2003) Scanning electron microscopy and x-ray microanalysis, 3rd edn. Springer, Berlin
91. Michler GH (2008) Electron microscopy of polymers. Springer Laboratory
92. http://www.chems.msu.edu/resources/tutorials/SEM. Accessed 26 July 2011
93. http://mse.iastate.edu/microscopy/home.html. Accessed 26 July 2011
94. http://www.microscopy-analysis.com/electron/learn-develop/tutorials
95. Guryca V, Hobzova R, Pradny M, Sirc J, Michalek J (2007) Surface morphology of contact lenses probed with microscopy techniques. Contact lens anterior eye. J Br Contact Lens Assoc 30:215–222
96. Critchlow GW, Litychfield RE, Sutherland I, Grandy DB, Wilson S (2006) A review and comparative study of release coatings for optimized abhesion in resin transfer moulding applications. Int J Adhes Adhes 26:577–599
97. Polizos G, Tuncer E, Qiu X, Aytug T, Kidder M, Messman JM, Sauers I (2011) Nonfunctionalized polydimethylsiloxane superhydrophobic surfaces based on hydrophobic–hydrophilic interactions. Langmuir 27:2953–2957
98. Lin M-H, Chen C-F, Shiu J-W, Chen C-H, Gwo S (2009) Multilength-scale chemical patterning of self-assembled monolayers by spatially controlled plasma exposure: nanometer to centimeter range. J Am Chem Soc 131:10984–10991
99. Arce FT, Avci R, Beech IB, Cooksey KE, Wigglesworth-Cooksey B (2006) Modification of surface properties of a poly(dimethylsiloxane)-based elastomer, TRV11, upon exposure to seawater. Langmuir 22:7217–7225
100. Allwork SP, Norton R (1976) Surface ultrastructure of silicone rubber aortic valve poppets after long-term implantation. A scanning electron microscope study of four poppets. Thoirax 31:742–752

101. Freeman HA, Henrich RT (1991) Evaluation of silicone breast implant surfaces by transmission and scanning electron microscopy. In: Microbeam analysis, San Francisco 26th, pp 19–20
102. Wickham MG, Rudolph R, Abraham JL (1978) Silicon identification in prosthesis-associated fibrous capsules. Science 27:437–439
103. Sauermann G, Duesing HJ, Kopplow HJ, Roemling E, Wittern W (1979) Effect of silicone oil-containing skin products. Aerztliche Kosmetologie 9:110–112, 114, 116
104. Ratner BD, Hoffman AS (1980) Surface characterization of hydrophilic-hydrophobic copolymer model systems. I. A preliminary study. Polymer Science and Technology (Plenum), 12B (Adhes Adsorption Polym, Part B) 691–706
105. Wilson JE, Freeman HA (1981) Analysis of silicone-coated papers with the scanning electron microprobe. Tappi J 64:95–97
106. Vlastos A, Gubanski S (1991) Surface structural changes of naturally aged silicone and EPDM composite insulators. IEEE Trans Power Deliv 6:888–890
107. Feng L, Li S, Li Y, Li H, Zhai J, Song Y, Liu B, Jiang L, Zhu D (2002) Super-hydrophobic surfaces: from natural to artificial. Adv Mater 14:1857–1860
108. Ghosh N, Bajoria A, Vaidya AA (2009) Surface chemical modification of poly(dimethylsiloxane)-based biomimetic materials: oil repellant surfaces. ACS Appl Mater Interfaces 1:2636–2644
109. Longley JE, Chaudhury MK (2010) Determination of the modulus of thin sol-gel films using buckling instability. Macromolecules 43:680–681
110. Kanamori K, Nakanishi K, Hirao K, Jinnai J (2003) Interface-directed web-to-pillar transition of microphase-separated siloxane gels. Langmuir 19:9101–9103
111. Takoa H, Okoshi M, Inoue N (2004) Swelling and modification of silicone surface by F2 laser irradiation. Appl Phys A 79:1571–1574
112. Orhan J-B, Parashar VK, Flueckiger J, Gijs MAM (2008) Internal modification of poly(dimethylsiloxane) microchannels with borosilicate glass coating. Langmuir 24:9154–9161
113. Patrito N, McCague C, Norton PR, Petersen NO (2001) Spatially controlled cell adhesion via micropatterned surface modification of poly(dimethyl siloxane). Langmuir 23:715–719
114. Voelcker N, Klee D, Hoecker H, Langefeld S (2001) Functionalization of silicone rubber for the covalent immobilization of fibronectin. J Mater Sci, Mater Med 12:111–119
115. Barrios CA, Qingwei X, Cutright T, Newby BZ (2005) Incorporating zosteric acid into silicone coatings to achieve its slow release while reducing fresh water bacterial attachment. Colloids Surf B, Biointerfaces 41:83–93
116. Vilville P, Lazzaroni R (2003) Impact of silicone-based block copolymer surfactants on the surface and bulk microscopic organization of a biodegradable polymer, poly(e-caprolactone). Biomacromolecules 4:696–703
117. Yan P, Qiu L (2009) Preparation and characterisation of polysiloxane-acrylate latexes with MPS-PDMS oligomer as macromonomer. J Appl Polym Sci 114:760–768
118. Keüpczyn'ski M, Lewandowska J, Romek M, Zapotoczny S, Ganachaud F, Nowakowska M (2007) Silicone nanocapsules templated inside the membranes of catanionic vesicles. Langmuir 23:7314–7320
119. Ogoshi T, Fujiwara T, Bertolucci M, Galli G, Chiellini E, Chujo Y, Wynne KJ (2004) Tapping mode AFM evidence for an amorphous reticular phase in a condensation-cured hybrid elastomer: alpha, omega-dihydroxypoly(dimethylsiloxane)/poly(diethoxysiloxane)/fumed silica nanoparticles. J Am Chem Soc 126:12284–12285
120. Le HH, Ilisch S, Radusch H-J, Steinberger H (2008) Macro- and microdispersion of carbon black in liquid silicone rubbers. Plast Rubber Compos 37:367–375
121. Purohit P, Somasundaran P, Kulkarni R (2006) Study of properties of modified silicones at solid-liquid interface: fabric–silicone interactions. J Colloid Interface Sci 298:987–990
122. La Torre C, Bhushan B, Yang J-Z, Torgersen PM (2006) Nanotribological effects of silicone type, silicone deposition level and surfactant type on human hair using atomic force microscopy. J Cosmet Sci 57:37–56

123. Gonzales-Meijome JM, Lopez-Alemany A, Almeida JB, Parafita MA (2008) Surface AFM microscopy of unworn and worn samples of silicone hydrogel contact lenses. J Biomed Mater Res, Part B, Appl Biomater 88B:75–82

Chapter 13
Surface Applications of Silicones

Michael J. Owen and Petar R. Dvornic

13.1 Introduction

Applications of silicones that exploit their surface properties derive from their fundamental characteristics as outlined in Chapter 1 and further detailed throughout this volume. However, there are thousands of different silicone products and industrial applications so considerable simplification and focus on a small number of representative major applications is necessary to meaningfully relate the characteristics of silicones to their uses. Part of this focus is to concentrate almost exclusively on polydimethylsiloxane (PDMS), still the mainstay of the silicone industry for over sixty years. Accordingly, in what follows we offer two manageable lists for consideration of the structure/property/use relationship of PDMS; some important characteristics of this parent polymer of the polysiloxane family, and some significant applications of the same. Our aim is to offer a general overview that can meaningfully wrap up this discussion of the surface science of silicones and not to engage in a detailed examination of each use. More information, however, can be obtained from the chapter in Silicon-Based Inorganic Polymers devoted to Silicones in Industrial Applications [1].

The characteristics of silicones list is a familiar one. The first five listed items are the most fundamental set, already considered in Chapter 1. The list of applications (List 2) is somewhat more subjective. Detailed information on market segment sizes is difficult to come by outside of expensive surveys aimed at distributors and producers. There are also regional differences. For example, the market forecast issued by the Freedonia Group for the US industry [2] tells us that silicone fluids remain the leading product type in 2009, accounting for over 40 % of the market. Conversely, the earlier Centre Européen des Silicone information [3] suggests only half

M.J. Owen (✉) · P.R. Dvornic
Michigan Molecular Institute, 1910 W, St. Andrews Rd., Midland, MI 48640, USA
e-mail: michaelowen01@chartermi.net

P.R. Dvornic (✉)
e-mail: dvornic@mmi.org

M.J. Owen, P.R. Dvornic (eds.), *Silicone Surface Science*, Advances in Silicon Science 4,
DOI 10.1007/978-94-007-3876-8_13,

that amount at most. Nevertheless, we are confident that each of the chosen applications in our list is a well-established use that represents at least 5 % of the output of the silicone industry or, as is the case for high-voltage insulation, is a high-growth area that is rapidly approaching that level. In total, these selected applications taken together account for well over half of all silicone usage.

Another factor in these choices is to address apparent paradoxes such as why the same material can be both a foam stabilizer and an antifoam agent or why it can be an adhesive sealant material as well as a release coating for other adhesives. Also note that there is an inevitable overlap between some of these categories. For example, some silicone surfactants are used as emulsifiers in personal care products while clearly part of the attraction of silicone encapsulants to some microelectronic applications must derive from its water repellency as well as its electrical properties. Furthermore, silicone surfactants comprise both polyurethane foam additives and the so-called "superwetter" surfactants. It should also be borne in mind that these applications come from three broad use categories; bulk, coating and additive, and that bulk applications have surface aspects and vice versa.

List 1: Some Important Characteristics of PDMS

- Low intermolecular forces between methyl groups
- Compact size of the methyl group
- High siloxane backbone flexibility
- High siloxane bond energy
- Partial ionic nature of the siloxane bond
- Low surface energy
- Hydrophobic/oleophilic nature
- Low solubility parameter
- High free volume
- Low glass transition temperature
- High gas permeability
- Liquid nature to high molecular weight
- Presence of low molecular weight cyclic and linear species
- Low toxicity
- UV stability
- High thermal/oxidative stability
- Low dielectric constant
- Low electrical conductivity

List 2: Some Selected Surface Applications of PDMS

- Elastomers/sealants
- Personal care products
- Antifoams
- Surfactants
- Pressure-sensitive adhesive release coatings
- High-voltage insulation
- Water-repellent coatings

Fig. 13.1 Many of these products can be found in the average household, sometimes very obviously such as the brightly colored silicone baking utensils but more often as an unseen additive in such items as hair conditioners and hand creams

Much of the general population is unaware of how prevalent many of these products are in the average household and our daily lives. To illustrate the point, Fig. 13.1 shows a miscellany of such items, both all silicone (e.g. baking trays) and those in which silicones are used only as additives (e.g. personal care products).

13.2 Elastomers/Sealants

Sealants are available as one or two part, room temperature or heat curing systems depending on the cross-linking chemistry. The variety of cross-linking reactions available is one of the significant characteristics of silicone chemistry which includes systems based on hydrosilylation, free radical formation and coupling, acetoxy, oxime, alkoxy, amine, and aminoxy reagents. Condensation cure materials, particularly those producing acetic acid as an in situ etchant, have excellent adhesion to a variety of substrates. Others, such as those based on hydrosilylation cure, might require incorporation of adhesion promoters such as silane coupling agents.

Three broad classes of siloxane elastomers are available: room temperature vulcanized (RTV), high temperature vulcanized (HTV) and liquid silicone rubbers (LSR). RTV products are based on polymers in the 10^4 to the 10^6 molecular weight range. In addition to elastomers and sealants, silicone materials are also available as adhesives, encapsulants, foams, coatings, and glazing and mold-making materials. HTV products cover a wide range of molded, extruded, calendered, or fabric-coated rubber parts including insulators, gaskets, seals, belting, air bags and tubing. These products are usually formed by vulcanizing high-molecular weight ($>3 \times 10^5$) linear PDMS using compression molding at elevated temperatures. The LSR materials

Table 13.1 Mechanical properties of typical commercial silicone elastomers [4]

Property	PDMS	PMTFPS
Specific gravity (g cm^{-3})	1.04–1.51	1.35–1.65
Hardness (Shore A)	30–80	20–80
Tensile strength (MPa)	1.55–9	5.55–11.7
Elongation (%)	430–725	100–600
Compression set (%) (22h/177 °C)	*ca* 10	10–40
Tear strength, die B (kN m^{-1})	4.9–37.7	10.5–46.6
Bashore resilience (%)	30–65	10–40

are made from low-viscosity polymers that are pumpable and can be cured in molds similar to those used for injection molding.

Although the emphasis of this volume is on surface properties the importance of bulk properties in elastomeric space-filling products cannot be forgotten. These depend on the base formulation (molecular weight, degree of cross-linking, filler type and quantity) and the final compounding ingredients. Representative mechanical property data ranges for PDMS and polymethyltrifluoropropylsiloxane (PMTFPS) elastomers are given in Table 13.1. It is usually possible to match the bulk properties of the two systems when needed with the marked exception of swelling and permeability behavior.

Sealants and elastomers are widely used in the automotive and aerospace industries and in other machinery and construction applications. Other significant uses are in textile coatings, biomedical materials (e.g. tubing) and in the protection and packaging of electronic and photovoltaic assemblies. Silicone coatings and encapsulants show considerable promise in the growing light-emitting diodes (LED) industry and emerging photonics applications. In terms of fundamental requirements for an elastomer, apart from the restrictions imposed by the cross-links, the macromolecular segments must be free to move reversibly relative to each other, providing for rubber-like elasticity. The combination of low intermolecular forces between methyl groups, their small size, large free volume and the high siloxane backbone flexibility readily satisfies these conditions. Easy rotation about skeletal bonds is also advantageous in maximizing configurations; for PDMS the energy of such rotation is almost zero [5].

Silicones are often used at higher and lower temperatures where other organic materials do not perform adequately [6, 7]. This ability to be used over a wide temperature range from −100 °C to 300 °C is a key feature of silicone elastomers and sealants. It results from the high thermal/oxidative stability which is derived in large measure from the high siloxane bond energy and the retention of flexibility at low temperature arising from the high siloxane backbone flexibility and compact size of the methyl group [6, 7]. Note that some commercial sealants have much lower thermal stability, even as low as 130 °C. The largest contributing factor to such degradation is the presence of impurities which catalyze the oxidative decomposition of silicones. These often come from the various initiators used in the polymer synthe-

sis, fillers incorporated into the elastomer/sealant formulation as well as residual cure catalysts, either acidic or basic, that have not been fully neutralized [8].

Other applicational advantages include a low viscosity of many products before curing and facile displacement of leaving groups due to the high permeability of PDMS which is a consequence of its high free volume. The first step in good adhesion is good wetting of the substrate and the low surface tension certainly promotes this. Another benefit accruing from the low surface energy is water repellency of great importance for applications such as building sealants. For outdoor applications of silicone elastomers and sealants, their long service life in adverse environments is vital. They are virtually unaffected by rain, snow, humidity and ozone. Their UV stability also adds to their ability to withstand environmental exposure for many years.

The main shortcoming of silicone elastomers and sealants is the oleophilic nature of PDMS. This can lead to problems such as swelling of elastomers by organic fuels, oils and solvents. Consequently, solving this drawback was the main driving force behind the development of PMTFPS elastomers which were originally designated "LS" (low swell) materials [9]. Other consequences of the oleophilic nature of PDMS are staining and fungal growth on construction sealants. One solution to the former difficulty is to use a fluorosilicone elastomer instead (see Chapter 5), while problems with fungal growth can be avoided by the incorporation of fungicides.

The very fundamental character that makes it easy for PDMS to wet many substrates makes it difficult to be wetted by many organics. Thus, silicone sealants cannot be painted by water-based paints or even some solvent-based ones and incorporation of fluorocarbon-based wetting agents is a potential solution. PDMS is not the best silicone to resist γ-radiation; phenyl containing siloxanes such as polymethylphenylsiloxane (PMPS) are considerably superior under such conditions. Aqueous stability of PDMS at extremes of pH can also be a limitation. The pH of acid rain is usually not low enough to detract from the environmental stability of PDMS where serious surface degradation occurs in the 1.5–2.5 pH range. For more details about silicone elastomers and sealants, the reader is referred to "Silicone Elastomers" by Jershow [10] and "Sealants in Construction" by Klosowski [11]. The websites of the silicone manufacturers are also an increasingly rich source of information on products and applications.

13.3 Personal Care Products

When used as a cosmetic or personal care product ingredient PDMS is known as "Dimethicone". Note that the similar term "Simethicone" is limited to PDMS antifoam products incorporated into anti-flatulence preparations. This type of labeling of silicones is the nomenclature authorized by the Food and Drug Administration in the USA to describe ingredients on package labels [12]. It is referred to as the INCI(CTFA) nomenclature: i.e. International Cosmetic Ingredient (Cosmetic, Toiletries and Fragrance Association). Organofunctional silicones are also used in personal care products, for example, amino, amido, or quaternary ammonium functional PDMS enhance substantivity to hair in shampoos and conditioners.

Each polymer type has its own INCI(CTFA) name, such as "Amodimethicone" for amine functional silicones.

The use of silicones in this application is ubiquitous; the Dow Corning Corporation website [13] informs that approximately half of all makeup, hair, skin care, and underarm products introduced today contain silicones. Note that some of the usage is of low molecular weight cyclics such as decamethylcyclopentasiloxane (known as D5) serving as a quick-drying solvent. In such products the cyclic may be more precisely identified on the label as cyclopentasiloxane rather than cyclomethicone. Our emphasis in this chapter is on polymeric silicones but it would be remiss of us not to mention the current concern regarding the accumulation in the environment of cyclic volatile methylsiloxanes. There is no doubt about the global dispersion of these cyclics [14] but whether or not this presents a risk to human health or the environment is a subject of considerable current debate.

A variety of beneficial functions have been reported for silicone polymers in cosmetic and personal care products. The following list shows such benefits along with an example of the silicone conferring it. The list is compiled from information on the cosmeticsinfo.org website [15].

List 3

- Antifoaming agent — Dimethicone
- Corrosion inhibitor — Stearylamidopropyl Dimethicone
- Film former — Stearylamidopropyl Dimethicone
- Hair conditioning agent — Aminopropyl Dimethicone
- Skin conditioning agent — Dimethicone
- Skin protectant — Dimethicone
- Surface modifier — Methicone
- Viscosity increasing agent — Alkyl Methicone

Perceived benefits of silicone incorporation into cosmetics and personal care products can be difficult to quantify, particularly the sensory impressions of enhanced softness, silkiness and smoothness. Human test panels are often employed in such evaluations. Response to touch is clearly, at least partially, a surface phenomenon and in some cases reasonably quantitative data are available from such sources. Taking just one example of skin conditioning agents, the primary function of an oil in these products is to improve emolliency (from the French *emollire*, to soften) which can be viewed as having two more quantifiable components, spreadability and lubrication. Based on panel evaluations, Brand and Brand-Garnys [16] report that silicone fluids show significantly greater emolliency than mineral oil with Dimethicone 350 cS having the highest spreadability of the oils tested; more spreadable by a factor of ten compared to mineral oil 150 cS. Using a skin friction device these authors report a friction factor for Dimethicone three times lower than that of mineral oil. Combing force relationships to silicone polymer composition with hair tresses is another quantifiable laboratory test that has become an important tool in evaluating performance of hair conditioning formulations.

One intriguing trend is that polydiethylsiloxane is now often mentioned in personal care product patents and is commercially available from Gelest Inc. who

cite [17] its improved compatibility with commonly used cosmetic waxes and oils compared to PDMS. Polydiethylsiloxane has long been an established silicone polymer in the Russian Federation but has had little impact so far in the West.

13.4 Antifoams

There is a very wide variety of applications for antifoaming agents or defoamers as they are also known. List 4 shows some of the areas where such products are used. Their purpose is to improve the efficiency of a particular process or to increase the quality or performance of products when they are subsequently used. Given the breadth of applications it is not the object of this section to analyze in detail any specific applications; but rather to relate the mode of silicone antifoam action to its fundamental characteristics. More details on particular applications are available in encyclopedia articles [18], books [19, 20] and silicone manufacturers websites [13]. Note also that there are a multitude of antifoam types and products available and very few applications are solely reliant on only silicone materials. One area which is very dependent on silicone antifoam products is oil and petroleum processing. This is because competitive materials based on hydrocarbons are too soluble, those based on polyethers are insufficiently surface active, and those based on fluoropolymers are rare, with the exception of fluorosilicones, and expensive. The use of silicones as Simethicone (see Section 13.3) in anti-flatulence preparations is another example where silicones dominate as a consequence of the inertness and non-toxic character of PDMS.

List 4: Antifoam Applications

- Adhesives and sealants
- Agricultural chemicals
- Asphalt manufacture
- Chemical processing
- Coatings, paints and inks
- Construction industry
- Detergents and other cleaning compounds
- Distillation systems
- Fermentation processes
- Fertilizer production
- Food and beverages
- Leather processing
- Lubricating oils
- Medical products
- Metal working
- Oil and petrochemicals
- Polymer manufacture and processing
- Pulp and paper production
- Textile dyeing and finishing

Table 13.2 Surface tensions of surfactants and antifoams

Material	Surface tension ($mN\,m^{-1}$)
$C_{12}H_{25}SO_4Na$	39.5
$C_{12}H_{25}C_6H_5NBr$	41.2
$C_{12}H_{25}(OCH_2CH_2)_nOH$	36.3
$(CH_3)_3C(CH_2)_4(OCH_2CH_2)_nOH$	33.5
Surfynol 104	31.4
Pluronic L62	42.8
Polyoxypropylene [MW 3000]	31.2
PDMS [MW 3900]	20.2
Kerosene	27.5
Mineral oil (MWP paraffin)	28.8
Corn oil	33.4
Peanut oil	35.5
Tributyl phosphate	25.1

- Wastewater treatment

The three fundamental requirements of a potential antifoam are:

- It must be insoluble in the foaming medium
- It must be readily dispersible in the foaming medium
- It must have a lower surface energy than the foaming medium

PDMS-based antifoams are likely to be most useful in aqueous systems where concentrated solutions of efficient organic surfactants are used and also in hydrocarbon and other non-aqueous systems. Less efficient aqueous surfactants may be readily defoamed by less surface-active antifoams based on polyethers and hydrocarbons. An example of an aqueous system that utilizes high concentrations of powerful organic surfactants is in detergents where antifoams are encapsulated into the formulation to prevent excessive foaming when used. The high thermal stability of PDMS is another factor that can make it the preferred choice in an application such as a distillation process. Table 13.2 contains some surface tension data for selected surfactants and antifoam oils. Most organic surfactants and aqueous media have surface tensions in the 30–50 mN/m range whereas the oils' surface tension values range from 20 to 40 mN/m. Being near the lower end of these surface tension ranges has much to do with the wide applicability of PDMS antifoams.

Although there is still considerable debate regarding aspects of antifoam theory, at its simplest it is agreed that they function by entering and spreading into the foam lamellae thereby displacing the foam stabilizer. Entering and spreading occur when the Entering Coefficient (E) and the Spreading Coefficient (S) are positive:

$$E = \gamma_F + \gamma_{AF} - \gamma_A \tag{13.1}$$

$$S = \gamma_F - \gamma_{AF} - \gamma_A \tag{13.2}$$

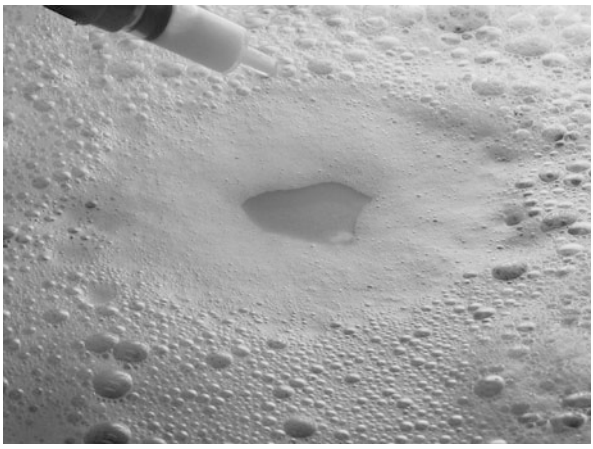

Fig. 13.2 A picture of a silicone antifoam in action on an aqueous foam. The antifoam droplet is at the lower right of the clear area where defoaming is already complete. Around this is a region where spreading has occurred but where defoaming is incomplete or not yet commenced. Reproduced with permission of © Dow Corning Corporation

where γ_F is the surface tension of the foaming system, γ_A that of the antifoam, and γ_{AF} is the interfacial tension between them. The advantage of low antifoam surface tension is obvious. With regard to the other two fundamental criteria mentioned earlier, insolubility is necessary for efficiency by focusing the action at the interface and avoiding dilution into the bulk, and dispersibility serves to help the antifoam droplet get to those interfaces. To aid in dispersion in aqueous media, silicone antifoams are often provided in oil-in-water emulsion form. An example of a silicone antifoam in action on an aqueous foam is shown in Fig. 13.2.

Values in Table 13.2 are all measured at room temperature (20–30 °C range). The first four entries are frequently encountered surfactants and the value quoted is at the critical micelle concentration (CMC). Surfynol 104 is an acetylenic glycol, 2,4,7,9-tetramethyl-5-decyne-4,7-diol from Air Products and Chemicals, Inc. Pluronic L62 is a polyoxyethylene-polyoxypropylene copolymer from BASF AG. Both products are marketed for surfactant and antifoam usage. The surface tension values listed are at 0.1 %. The last seven entries are typical antifoam oils. The table is taken from Ref. [18], which also contains the original citations for these data.

For most aqueous foaming challenges another key component is required—hydrophobic particles such as hydrophobized silica, usually in the 0.2–30 μm particle size range and incorporated into the silicone in the 1–20 % content range. Such an antifoam is known in the industry as an antifoam compound. Hydrophobic solids have been used in hydrocarbon-based antifoams as well as silicone antifoams for over 40 years. They are at least as active a component of the antifoam compound as the hydrophobic oil is. Such solids will break foams when sprinkled onto them. The evident synergy between oil and solid in an antifoam compound is still not fully explained but is generally ascribed to the bridging and dewetting steps that follow entering and spreading at the foam interfaces and lead to film rupture. Bridging occurs when the same antifoam compound droplet or hydrophobic particle occupies both sides of a foam film. Subsequent dewetting of the particle on both sides of the film can then cause rapid collapse of the film. One valid view of antifoam compound action is thus that the oil delivers the solids to the point where it can have

its optimum effect. Because of its low surface tension deriving from the low intermolecular forces and the lack of other foam stabilizing features such as a very low surface viscosity, PDMS is one of the best oils to use in antifoams. The same can be said of solids such as silica which have been hydrophobized by silane or siloxane chemistry.

Antifoams for non-aqueous foams do not need hydrophobic solids to be effective. This is because they do not form the very stable, well-drained foam lamellae common in aqueous foams so the need for bridging and dewetting mechanisms from a hydrophobic solid is not as great. Displacement of the foam stabilizer and the mechanical disruption caused by the spreading are sufficient to destabilize the foam. As most non-aqueous foaming systems are essentially oleophilic, in many cases it is necessary to use an oleophobic oil such as a fluorosilicone. Generally, if PDMS is soluble in an oil at low concentration it will promote foaming and antifoaming effects will not appear until the solubility limit is passed.

13.5 Silicone Surfactants

Chapter 9 is devoted to a broad survey of silicone surfactants so only a very short synopsis is added here for reasons of completeness. Two of the largest use categories for silicone surfactants are as polyurethane foam additives (PUFAs), and the so-called "superwetters". Both these applications depend on the ability of silicone surfactants to lower surface tension of both aqueous and non-aqueous systems to the level of *ca* 20 $mN\,m^{-1}$, significantly below the *ca* 30 $mN\,m^{-1}$ value that can generally be achieved by hydrocarbon-based surfactants. There are some important low-energy surfaces in the 20–30 $mN\,m^{-1}$ range that silicone surfactants would be expected to wet including a number of plastics and polymers, human skin and hair, and a variety of plant surfaces. In addition to surface activity the other essential for surfactancy is solubility in or compatibility with the selected medium; otherwise we would anticipate defoaming tendencies as opposed to foam stabilizing behavior. As silicones such as PDMS are insoluble in water, the desired solubility has to come from hydrophilic entities attached to the PDMS. As explained in Chapter 9 this most commonly comes from polyoxyethylene chains although other hydrophiles similar to those found in other classes of surfactants are utilized such as sulfates, quaternary ammonium salts, betaines and saccharides. Fluorocarbon surfactants also achieve low surface tensions in solution and are used in spreading and wetting applications although for some reason, presumably that of cost, they have never achieved any significance in the urethane foam arena.

The molecular origin of the difference between silicone and hydrocarbon surfactants can be traced directly to the unusual flexibility of the siloxane backbone allowing the methyl groups with their low intermolecular forces to dominate the outermost surface as opposed to the alkyl or alkylaryl hydrophobes of most hydrocarbon surfactants that contain mostly $–CH_2–$ groups and pack loosely at the surface. This last tendency is related to the fact that most hydrophiles occupy a

larger area than the cross-section of an alkyl chain so packing is dominated by hydrophile/hydrophile contact rather than that of terminal methyl groups. Apart from this dominant difference, silicone surfactants share much common behavior with hydrocarbon surfactants, including a break in the surface tension versus log concentration plots indicative of micelle formation (CMC). They also show similar patterns of self-aggregation including liquid crystal formation that can be related to surfactant structural trends in the same manner as is seen with hydrocarbon-based surfactants. Their principal defect is instability at extremes of pH, a result of hydrolytic cleavage of the siloxane bond, limiting their use to the 4–9 pH range.

13.6 Pressure-Sensitive Adhesive Release Coatings

Most simply, a silicone fluid can be wiped or sprayed onto a substrate to provide a non-stick surface. This type of release agent functions as a weak boundary layer and results in significant transfer to the released surface causing subsequent wetting and adhesion problems. Here we are concerned with the more advanced release liner products that carry and protect pressure-sensitive adhesives (PSAs) until the moment of application. This PSA use is by far the largest single use of silicone release liners but there are numerous other uses including carriers for oily or sticky masses, interleaving sheets in rubber processing, casting sheets for plastic films, food processing aids and packaging materials. Although a vital component of a PSA construction, the release coating is a very minor part, less than 1 % by weight. Its thickness is usually of the order of 1–2 μm but can be as low as 0.1 μm, whereas the adhesive layer is often over 20 μm in thickness and the supporting substrates for the release coating and the adhesive thicker still. Both of these substrates can be very different; as, for example, in the case of the release liners where they can be papers of many sorts, both coated and uncoated, plastics, or various metals.

Kinning and Schneider [21], who have provided an excellent review of release coatings for PSAs, give the primary requirements for such a coating as:

- Provision of the correct level of release force for the intended application.
- Stability of the release force under any environmental conditions the PSA product will experience.
- Adequate anchoring to the backing supporting the release liner.
- No transfer of labile components from the liner to the PSA.

In the case of silicone release liners, which dominate this application, the release force provided is often inherently adequate with problems arising from too low a release force in some cases. Such instances are addressed by the use of high release additives, which are discussed later in this section.

To obtain a non-migratory release surface the polymer chains must be tied together in a coherent film. This requires the use of cross-linking or curing chemistry and is the crux of silicone release coating development. The act of peeling an adhesive tape away from its release liner involves viscoelastic responses in both the adhesive and the silicone coating as well as interfacial effects. Release force is modified

Table 13.3 Adhesion of a PSA on low-energy surfaces

Release substrate	Surface energy (mJ m^{-2})	Release force (J m^{-2})
Fluorocarbon monolayer	11	29
PTFE	16	22
Crystalline hydrocarbon monolayer	21	11
PDMS	22	1
Liquid-like hydrocarbon monolayer	23	8
Polystyrene	40	63

not by alterations in surface energy but by changes in the silicone network. Cross-link density, i.e. degree of polymerization between cross-links, has a major impact; longer chains give higher release forces at a given peel rate as more work is required to stretch such compositions compared to those with the shortest chains which are more brittle and have no measurable elongation at break. In principle, any of the chemistries used to cross-link silicone elastomers and sealants can be employed, but in practice two types have become dominant: the tin-catalyzed silanol/alkoxysilicon condensation cure and the platinum-catalyzed hydrosilylation addition cure. Suppliers offer a choice between solvent-based, emulsion, or solventless coating depending on processing variables and desired product performance with the majority of users today opting for solventless addition cure products. These products eliminate environmental emissions, solvent cost and flammability issues but it is more difficult to control coat weights and coverage than it is with solvent-based products.

The low surface energy of PDMS with its low intermolecular force between the methyl groups is clearly part of the reason for its success as a release liner. Most adhesives have higher surface energies and have negative spreading coefficients on PDMS. However, its low glass transition appears to be at least as important in this application. It is well-recognized that low surface energy alone does not guarantee a good release surface. In particular, a number of comparisons between PDMS and fluorinated release surfaces have shown that even though they have lower surface energies than PDMS, these fluorinated materials do not exhibit lower release forces. Some data of this type, taken from the work of Chaudhury's group [22], are shown in Table 13.3. In these studies a PSA release coating was slowly (velocity of 100 μm s^{-1}) peeled from an acrylic adhesive.

The authors [22] have demonstrated by visual inspection that the peel front of the tape as it is being peeled away differs considerably with pronounced fingering of the front with the fluorinated layers, less so with the hydrocarbon substrates and least of all in the case of PDMS. Using fluorescent marker particles placed at the adhesive/release coating interface and in the bulk of the adhesive, they were able to unequivocally demonstrate that interfacial slippage occurs at the interface in the PDMS case, thereby preventing the fingering of the adhesive and the higher release forces associated with it. The fundamental characteristic of PDMS that seems to be significant in this phenomenon is its high degree of backbone flexibility. Hence low T_g would seem to be as important as low surface energy in this application.

Table 13.4 Surface resistance and flashover voltage of selected insulator materials

Material	Minimum surface resistance (kΩ)	Flashover voltage (kV rms)
Porcelain	262	16.5
Ethylene-propylene rubber (EPR)	270	21
PDMS rubber	2820	35

Interfacial slippage has also been shown important in the mode of action of high release additives (HRA). The main type of HRA is the so-called MQ resins, being based on M ($Me_3SiO_{1/2}$) and Q (SiO_2) units and having in some cases functionality such as vinyl or silanol. These methylated resins raise the T_g of the release system, reduce segmental mobility of the PDMS chain, and increase viscoelastic properties such as storage modulus and loss modulus. Although the use of the HRA resins does not markedly affect surface energy except at the highest loadings, they have a pronounced effect on interfacial behavior. Only silicone coatings with no HRA exhibit interfacial slippage. The added resins "freeze out" surface slippage not by raising surface energy but by modifying the viscoelastic response to peeling of the silicone coating [23].

13.7 High-Voltage Insulation

PDMS has a variety of characteristics pertaining both to bulk and surface behavior that make it particularly suitable for outdoor high-voltage (HV) insulation applications in comparison to competitive materials such as porcelain, glass and other polymers. The chief advantages of polymeric insulators are light weight, superior vandal resistance and better contamination performance. Lightness of weight is a considerable bonus, particularly in remote areas where installation and servicing is carried out by helicopter. Even in conventional installations breakage rates of up to 30 % can be experienced with glass and porcelain. Some silicone insulators can provide electrical equivalence to porcelain at one tenth of the weight. Vandal resistance is self-evident; bullets can be accommodated with little effect on performance whereas glass and porcelain can shatter and fail catastrophically.

Contamination by airborne particles that settle on the insulators is a major problem. It can be natural such as salt deposits from sea fog and spray, or from industrial, agricultural and transport sources. In the presence of moisture, an electrolytic film is created which leads to corona discharges, surface deterioration by erosion from dry-band arcing, and ultimately flashover. Some illustrative comparative data are given in Table 13.4 [24]. The electrical measurements were made under identical contamination conditions (equivalent salt deposit density of 0.07 mg cm^{-2} and non-soluble salt deposit density of 0.1 mg cm^{-2}) and sample geometry (rods of diameter 25 mm and length 250 mm).

For this reason, water repellency has been a key design feature accounting for the preponderance of hydrophobic polymers evaluated for this application, notably silicones, ethylene-propylene rubbers (EPR) such as ethylene-propylene diene monomer (EPDM), polyethylene and other polyolefins, polyurethanes, epoxies and polytetrafluoroethylene (PTFE). There are bulk property reasons for favoring the use of silicone apart from the good electrical resistance feature. These include resistance to UV exposure and high thermal stability which is not only advantageous at elevated temperatures in the natural environment but also at the extremely high temperatures experienced when arcing occurs.

However, it is not simply water repellency and environmental stability that matter but also how that repellency is recovered after surface damage from arcing. Hydrophobic recovery is a critically desirable feature in a polymer insulator; the more rapidly it occurs, the better. Corona exposure produces a more wettable silica-like surface on the silicone and it is this aspect and the subsequent recovery of hydrophobicity once the corona exposure is interrupted or ceases that has been the impetus for much of the corona and plasma treatment studies reviewed in Chapter 11. The highly mobile surface of PDMS, reflected in the low T_g and flexible backbone, facilitates the two principal mechanisms of hydrophobic recovery, surface reorientation and diffusion of low molecular weight species from the bulk to the surface. It is not only pre-existing low molecular weight species in the formulation that participate in this hydrophobic recovery but they are also produced in situ by polymer degradation when the corona discharge energy is sufficient.

In common with other applications considered in this chapter, silicone high-voltage materials are available in a variety of types and formulations. In the simplest form, silicone greases were spread on conventional porcelain insulators to resist discharges and flashovers, particularly in salt fog conditions. Greases are little used nowadays but a more substantive alternative, an elastomer designed for spray applications that cross-links on the insulators is still in use by electrical utilities to extend the utility of porcelain arrestors. However, to realize the full benefit of using silicones in high-voltage applications such as lightness of weight, a third type of product made mostly of silicone to completely replace the glass or porcelain insulator has been introduced. Typically such an insulator consists of a central solid fiberglass/resin rod for strength surrounded by the PDMS elastomer housing. A longitudinal cross-section of such an insulator is shown in Fig. 13.3.

As with other elastomer applications, a wide variety of compositions is available with different molecular weight base polymers, various cross-linking strategies, fillers, stabilizers and other additives. Conventional fillers such as silica are used to confer strength but other fillers such as alumina trihydrate (ATH) are also incorporated. ATH is a very significant component of most HV silicone elastomer formulations. It provides improved arc resistance by conducting heat from discharges rapidly away from the surface. Note that the silicone rubber used to obtain the data shown in Table 13.4 contained both silica and ATH. A good, practical source of more information on high-voltage insulation is the guide by Vosloo and co-workers [25].

Fig. 13.3 A portion of a silicone high-voltage insulator is shown on the right of this picture. The design maximizes possible leakage path length along the insulator and facilitates water run-off as well as maintaining dry regions. To the left is a cross-section of a smaller insulator exposing its internal fiberglass/resin strengthening rod

13.8 Water-Repellent Coatings

A considerable variety of silicone water-repellent products is available, both from the original polymer manufacturers and from numerous formulators. In this regard the water-repellent product market is similar to the antifoam situation. Typical applications include treatments of industrial and clothing textiles and fabrics, leather, components of cosmetic and personal care products, and treatment of finished roofs, masonry walls etc.

These products come in two main forms, those designed to cross-link to an elastomeric coating on or near the substrate surface and those intended to penetrate more deeply into porous substrates and bond chemically with them. The elastomer forming coatings have prepolymers of similar molecular weight to conventional silicone elastomers and sealants and in principle any of the commonly available cure systems can be employed but one-part systems that cure on exposure to the air are preferred for simplicity. The penetrating water-repellent systems are based on lower molecular weight reactive silanes and silicone resins with cross-linking side-chains and bearing reactive functionalities. These can be tailored to specific materials with reactive entities such as amino, alkoxy, hydroxyl and hydrido groups. A broad range of substrates can be penetrated including concrete, gypsum, bricks, tiles, wood, and rocks such as sandstone, limestone, granite and marble.

Both types of products are available in solvent or aqueous emulsion form and can be sprayed or painted onto substrates as desired. For example, a one-part, water-based, 100 % silicone weathersealing product is available for exterior surfaces. Such products are available in a considerable variety of pigmented colors as it is difficult to coat them with conventional organic paints. On the other hand, the disadvantage

Fig. 13.4 The Cape Race lighthouse being treated with a protective, water-repellent, elastomeric coating. Courtesy of Ross Noel

of being difficult to spread upon silicones becomes an advantage in the wetting and spreading of silicones on low-energy surfaces. In particular, such silicone coatings have the ability to coat over silicone joint sealants. An example of such a coating in use in a harsh environment, the seashore, is shown in Fig. 13.4.

Other beneficial properties include resistance to UV radiation, retention of flexibility at extremes of high and low temperatures, and good adhesion to most substrates so that primers and adhesion promoters are not usually needed. The big drawback is the oleophilic nature of PDMS. For example, this can lead to staining by deposition of organic materials in the environment onto building surfaces or from oily products used on silicone treated fabrics. Obvious solutions are to use fluorosilicones instead of PDMS but this is not often done because of expense considerations except in special cases such as camera lens treatments. One can also incorporate fluorochemical surfactants that can concentrate in the outermost surface of the silicone layer and provide oleophobicity without compromising other silicone benefits.

One advantageous feature of silicone treated fabrics, particularly for outerwear applications is the ability of silicone elastomer networks to “breathe”. Because of the backbone flexibility and openness of the network structure, individual water molecules can readily diffuse through the coating making the treated article more

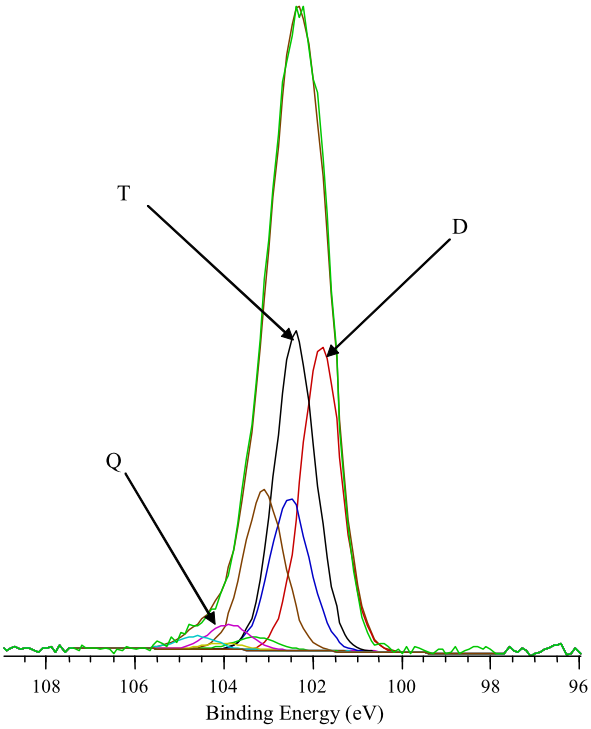

Fig. 13.5 A Si_{2p} XPS spectrum of octamethylcyclotetrasiloxane-treated cotton applied in an atmospheric pressure plasma deposition process. Reprinted from Ref. [27] with kind permission of ©CSIRO Publishing (2005)

comfortable for the wearer whereas larger assemblies of water molecules, i.e. raindrops, are too large to enter the network and remain beaded on the water-repellant low-energy surface or roll off it. Fabrics can now be treated by a significant recent advance in plasma polymerization at ambient pressure [26]. An XPS spectrum of octamethylcyclotetrasiloxane-treated cotton is shown in Fig. 13.5 [27].

Much of the dimethylsiloxane nature is retained after the plasma treatment (Me_2SiO, D in Fig. 13.5) although some monomethylsiloxane ($MeSiO_{3/2}$, T units) are present but with a very low silica-like content (SiO_2, Q units). Without the treatment water wets the fabric immediately, with the treatment an apparent water contact angle of *ca* 140° is sustained.

13.9 Conclusions

In this chapter we presented only a somewhat brief survey of each of the application areas of silicone polymers that deal with their unique surface properties. Our aim was to provide sufficient, but not excessive, information to relate the practical uses of silicone products to the fundamental characteristics of the parent polymer. Our focus was on PDMS as it remains the dominant mainstay of the silicone industry. In this way we attempted to extend the structure/property relationships of this versatile

polymer which underlie a great deal of the preceding chapters into its commercial practice arena. For those readers requiring more extensive information on silicone surface applications we recommend as an excellent starting point the chapter on Silicones in Industrial Applications by 22 Dow Corning professionals in the book Inorganic Polymers [28].

Central to the seven broad applicational areas considered in this chapter are the low intermolecular forces between the PDMS methyl groups which result in the low surface energy of this polymer. This is aided by the compact size of the methyl group and high siloxane backbone flexibility resulting in a low glass transition temperature important to most of these areas with the exceptions of antifoams and silicone surfactants. Many of the uses are at higher temperatures than organic equivalents can withstand because high siloxane bond energy permits this and is hence critical to most of these applications. Notable exceptions to this are personal care and PSA release liners where the stability of the substrates is the limiting factor in heat exposure. Partial ionic nature of the siloxane bond does not seem to play an important role in the majority of these applications. Its relevance is much more to the chemistry of silicones than to their physical properties and surface behavior. However, it is a key limiting factor in the use of silicone surfactants at extremes of pH.

Although each application is unique in its requirements, there are a couple of generalizations that can be made from these considerations. Firstly, no application is solely dependent on any one fundamental characteristic of the silicones but each derives from a combination of several of these factors that are generally both surface and bulk related. For example, an additive application such as antifoaming that might at first glance appear to be a purely surface phenomenon requires not only low surface tension but also insolubility in the foaming medium. Likewise, a coating application such as PSA release liners requires not only the familiar low surface energy but also a low glass transition temperature to promote interfacial slippage. Secondly, it is clear that PDMS, versatile as it is, rarely provides all the features that a given application demands. For instance, the PDMS antifoam could not function against stable aqueous foams without hydrophobic silica being compounded into it, and the PSA release coatings could not offer the full range of release forces required by the fabricators without MQ resin high release additives. Silicone chemists will be heartened by the observation that the non-PDMS components used in these two examples are based on organosilicon chemistry but, of course, this need not necessarily be the case. The aqueous solubility of silicone surfactants, for example, must come from very different species to PDMS. Likewise, HV insulation materials benefit considerably from incorporation from non-silicaceous fillers such as ATH. Recognize also that no consumer personal care product is 100 % silicone and all elastomers and sealants contain fillers and other additives as well as pigments in many cases. Similarly, water-repellent coatings are rarely supplied neat but come in solvent or emulsion form.

In conclusion, we would like to emphasize that the silicone future is shaping up to be at least as exciting as its past. With over 60 years of industrial innovation PDMS is a mature material with a plethora of new opportunities for it. Examples of developing new areas where surface properties and behavior will

dominate include; microemulsions, biofouling release coatings, electrically conductive adhesives, wound dressings, microcontact printing, polyhedral oligomeric silsesquioxanes, silicon-containing dendrimers and hyperbranched polymers, optoelectronic coatings and encapsulants, antifouling coatings and polyfluoroether-functional PDMS and copolymers. A confident conclusion can be made that the future will need polymers with the combination of low intermolecular forces and high chain flexibility provided by PDMS and related organosilicon polymers at least as much as it has benefited from them in the past.

References

1. Owen MJ (2000) Surface properties and applications. In: Jones RG, Ando W, Chojnowski J (eds) Silicon-containing polymers. Kluwer Academic, Dordrecht, pp 213–231
2. http://www.freedoniagroup.com. Accessed 23 March 2011
3. http://www.silicones-europe.com. Accessed 23 March 2011
4. Owen MJ (2001) Elastomers: siloxane. In: Brown H (ed) Encyclopedia of materials: science and technology. Elsevier, Amsterdam
5. Tobolsky AV (1960) Properties and structure of polymers. Wiley, New York, p 67
6. Dvornic PR, Lenz RW (1990) High temperature siloxane elastomers. Huthig and Wepf
7. Dvornic PR (2000) Thermal properties of polysiloxanes. In: Jones RG, Ando W, Chojnowski J (eds) Silicon containing polymers. Kluwer Academic, Dordrecht, pp 185–212
8. Owen MJ, Klosowski JM (1988) Durability of silicone sealants. In: Lee L-H (ed) Adhesives, sealants, and coatings for space and harsh environments. Plenum, New York, pp 281–291
9. Kim YK (1980) In: Grayson M (ed) Kirk-Othmer encyclopedia of chemical technology, vol 11, 3rd edn. Wiley, New York, pp 74–81
10. Jershow P (2002) Silicone elastomers. In: RAPRA review reports
11. Klosowski JM (1988) Sealants in construction. CRC Press, Boca Raton
12. Floyd DT (1999) Silicone surfactants: applications in the personal care industry. In: Hill RM (ed) Silicone surfactants. Dekker, New York, pp 181–207
13. For example, http://www.dowcorning.com. Accessed 23 March 2011
14. Gunualdi S, Harner T, Cheng Y, MacLeod M, Hansens KM, van Egmond R, Shoeib M, Lee SC (2011) Global distribution of linear and cyclic volatile methyl siloxanes in air. Environ Sci Technol Article ASAP. doi:10.1021/es200301j, March 25, 2011
15. http://www.cosmeticsinfo.org. Accessed 23 March 2011
16. Brand HM, Brand-Garnys EE (1992) Cosmet Toiletries 107:93
17. http://www.gelest.com. Accessed 23 March 2011
18. Owen MJ (1993) Defoamers. In: Kirk-Othmer encyclopedia of chemical technology, vol 7, 4th edn, pp 928–946
19. Hill RH (1999) Silicone surfactants. Surfactant science ser, vol 86. Dekker, New York
20. Garrett PR (1993) Defoaming: theory and industrial applications. Surfactant science ser, vol 45. Dekker, New York
21. Kinning DJ, Schneider HM (2002) Release coatings for pressure sensitive adhesives. In: Chaudhury MK, Pocius AV (eds) Surfaces, chemistry and applications. Elsevier, New York, pp 535–571
22. Newby BZ, Chaudhury MK (1997) Langmuir 13:1805
23. Gordon GV, Leaym TM, Owen MJ, Owens MS, Perz SV, Stasser JL, Tonge JS, Chaudhury MK, Vorvolakas KA, She H (2000) Adhes Age 43(4):41
24. Goudie JL, Owen MJ, Orbeck T (1998) In IEEE Electrical insulation and dielectric phenomena annual report, vol 1, pp 120–127
25. Vosloo WL, Macey RE, de Tourreil C (2004) The practical guide to outdoor high voltage insulators. Crown Publications, Johannesburg

26. Leadley S, Goodwin A, Lord G (2007) Ambient plasma processing a revolution in surface engineering. Surf Coat Int 90(3):128–130
27. Owen MJ (2005) Plasma/corona treatment of silicones. Aust J Chem 58:433–436
28. Andriot M, DeGroot JV, Meeks R, Gerlach E, Jungk M, Wolf AT, Cray S, Easton T, Mountney A, Leadley S, Chao SH, Colas A, de Buyl F, Dupont A, Garaud JL, Gubbels F, Lecomte JP, Lenoble B, Stassen S, Stevens C, Thomas X, Shearer G (2007) Silicones in industrial applications. In: De Jaeger R, Gleria M (eds) Inorganic polymers. Nova Sciences Publisher, New York, pp 61–161

ERRATUM

Silicone Surface Science

Michael J. Owen and Petar R. Dvornic

Erratum to: ***Silicone Surface Science***, **Advances in Silicon Science 4**
DOI 10.1007/978-94-007-3876-8

Due to an error by Springer, the sequence of the editors appeared incorrectly on the cover and front matter of Silicone Surface Science. This error has now been corrected.

M.J. Owen, P.R. Dvornic (eds.), *Silicone Surface Science*, Advances in Silicon Science 4,
DOI 10.1007/978-94-007-3876-8_14,

Index

M.J. Owen, P.R. Dvornic (eds.), *Silicone Surface Science*, Advances in Silicon Science 4,
DOI 10.1007/978-94-007-3876-8, © Springer Science+Business Media Dordrecht 2012